University of Nottingham
UK | CHINA | MALAYSIA

Combinatorial Application of Tocotrienols and Chemotherapeutic Drugs Enhances Apoptosis and Autophagy in Colorectal Cancer Cells

Tham Shiau Ying

Thesis submitted to the University of Nottingham for the degree of

Doctor of Philosophy

October 2019

Abstract

Chemotherapy remains a cornerstone among the cancer treatment modalities but the therapeutic effectiveness of most conventional chemotherapeutic drugs is often limited by their dose-related toxicity. Tocotrienols, a class of vitamin E analogues, have been widely recognised as promising anti-cancer candidates due to their anti-proliferative, apoptotic, anti-invasive and anti-metastatic properties. Given that the multi-targeted actions of tocotrienols are suitable to be used as an adjunct treatment, a combinatory application with chemotherapeutic drugs in the cancer treatments may offer a synergism that provides augmented therapeutic effects and reduces high dose toxicities associated with chemotherapeutic drugs. Despite many combination studies with tocotrienols were conducted previously, the combined treatments of δ-tocotrienol (δT3) and conventional chemotherapeutic drugs, namely 5-fluorouracil (5FU) and doxorubicin (Dox) have not been reported in colorectal cancer cells. Hence, the current study aimed to study the therapeutic effects of δT3 + 5FU and δT3 + Dox combined treatments as an enhanced cancer therapeutic approach on Caco-2 and SW48 colorectal cells.

A high-throughput screening was initially conducted to identify synergistic combinations between tocotrienols and chemotherapeutic drugs. The selection of combination treatments was based upon the combination index (CI), drug reduction index (DRI), selectivity index (SI) and/or the capacity for inhibiting of clonogenic survival. Current study identified that synergisms are present on Caco-2 (CI= 0.45, DRI= 16.25, SI=21.88) and SW48 (CI=0.72, DRI=3.54, SI=5.58) colorectal cancer cells receiving δT3 + 5FU combined treatment. Meanwhile, δT3 + Dox combined treatment resulted a synergism on Caco-2 (CI=0.75, DRI, 2.80, SI=21.44) and a slight antagonism on SW48 (CI=1.50, DRI=0.95, SI=56.55). Nonetheless, both

combinations exerted significant anti-clonogenic survivals on Caco-2 and SW48 cells, which warrants further investigations.

The ideal combined treatments were identified and subjected to various assays in order to investigate for their apoptosis-inducing properties, which include phosphatidylserine externalisation, DNA damage, cell cycle perturbation and DNA fragmentation. The presence of apoptosis was confirmed morphologically by the presence of cell shrinkage, membrane blebbing, nuclear condensation and fragmentation. Enhanced apoptosis and DNA fragmentation were detected in both cell lines receiving δT3 + 5FU and δT3 + Dox combined treatments as compared to their individual single treatments. The cellular apoptotic effect induced by δT3 + 5FU combined treatment was mediated through enhanced single-stranded DNA breaks and S-phase arrest. In contrast, δT3 + Dox combined treatment caused enhanced single-stranded and double-stranded DNA breaks and G2/M phase arrest.

To study the underlying apoptosis mechanism, several apoptosis-related proteins family such as caspases, inhibitor of apoptosis (IAP) and B-cell lymphoma 2 (Bcl-2) were evaluated. The combined treatments resulted in significantly higher caspase-3 activation than the individual single treatments, accompanied by the downregulation of IAP proteins (e.g., cIAP1, survivin and XIAP), suggesting the occurrence of a chemosensitisation effect toward apoptosis. Despite clear caspase-8 and -3 activations in response to δT3 + 5FU combined treatment was found, only SW48 but not Caco-2 cells exhibited caspase-3 dependent apoptosis, suggesting an additional cell death pathway was involved. The upregulation of Bax and/or downregulation in Bcl-2 have suggested an involvement of mitochondrial outer membrane permeabilisation. The findings of cyclosporine A inhibited the mitochondrial permeability transition and successfully prevented cell death, signify

the importance of mitochondria in shaping cell death induced by the combined treatments. The results collectively suggest an involvement of caspase-dependent apoptosis and caspase-independent cell death.

In order to detect the autophagy manifestation induced by the combined treatments, acridine orange and monodansylcadaverine (MDC) staining methods were performed. The autophagy-related proteins namely microtubule-associated protein light chain 3 (LC3)-II and beclin-1 were also studied. Pharmacological inhibition of autophagy was performed using 3-methyladenine (3-MA) and bafilomycin A1 (Baf-1) autophagy inhibitors to delineate the role of autophagy in relation to cell death. An enhanced autophagy was also detected in the combined treatments as evidenced by significantly higher MDC intensity and elevated LC3-II protein. Inhibition of autophagy by 3-MA and Baf-1 successfully prevented cell death for Caco-2 and SW48 cell lines, could be an indication that an autophagic cell death has been involved.

In conclusion, both δT3 + 5FU and δT3 + Dox combined treatments in the study have been shown executing multi-targeted actions in killing the colorectal cancer cells. Therefore, it could potentially offer valuable therapeutic effects for the colorectal cancer treatment in a near future. Yet, further mechanistic, *in vivo* and clinical investigations of these combined treatments are still necessary to materialize its cancer treatment application.

Acknowledgements

First and foremost, I would like to thank my principal supervisor, Professor Dr Sandy Loh Hwei San for her continual support throughout my PhD study. I am grateful to be supervised by her who always selflessly shares her knowledge and experience with me. I truly appreciate the freedom she gave me to attempt new ideas that have deeply shaped my interest in science. Her encouragement, constructive feedbacks, and professional advice are crucial elements that enriched my academic experience. Without her guidance and help, this thesis would not be made possible.

I would like to extend my gratitude to Dr Mai Chun Wai (IMU) and Dr Fu Ju Yen (MPOB). They are extraordinary co-supervisors, who have always been helpful and supportive to me and my research. I appreciate their constant financial and technical supports, as well as the insightful knowledge in making this research fruitful.

To my friends at the International Medical University and University of Nottingham Malaysia (especially Won Ting and Fei Kean), thank you for lending me a helping hand when I needed the most. All the good times we spent had made my research journey a valuable and memorable experience which I will cherish for a lifetime.

My sincere gratitude is also extended to the Ministry of Higher Education Malaysia and Malaysia Toray Science Foundation, for the financial supports via MyPhD scholarship and Science and Technology Research Grant, respectively.

I am also truly indebted to my parents, Mr Tham Choong Chuan and Mrs Ng Bee Peng. Thanks for being the pillars of my life and supportive of every decision I have made in my life thus far. Special thanks also go to Yu Sheng, for his presence and love to share all my ups and downs in this PhD journey.

Table of Contents

List of Abbreviations

3-MA	3-methyladenine
5FU	5-fluorouracil
ABCG2	ATP-binding cassette subfamily G member 2
ACC	Acetyl-coa carboxylase
AIF	Apoptosis-inducing factor
Akt	Protein kinase B
ALDH	Aldehyde dehydrogenase
AMPK	AMP-activated protein kinase
ANOVA	Analysis of variance
AO	Acridine orange
Apaf-1	Apoptotic protease activating factor-1
APC	Adenomatous polyposis coli
ATF	Activating transcription factor
ATG	Autophagy-related protein
ATM	Ataxia telangiectasia mutated
ATP	Adenosine triphosphate
ATR	Ataxia Telangiectasia and Rad3-related
ATST	Atorvastatin
AVD	Apoptotic volume decrease
AVO	Acidic vesicular organelles
Bad	Bcl-2-associated death promoter
Baf-1	Bafilomycin A1
Bak	Bcl-2 homologous antagonist/killer
Bax	Bcl-2-associated X protein
Bcl-2	B-cell lymphoma 2
Bcl-w	Bcl-2-like protein w
Bcl-xL	B-cell lymphoma-extra large
Bid	BH3 interacting-domain death agonist
Bik	Bcl-2 interacting killer
Bim	Bcl-2-like protein 11
BiP/ GRP78	Glucose-regulated protein
BIR	Baculoviral IAP repeat

Bmf	Bcl-2-modifying factor
Bok	Bcl-2 related ovarian killer
BSA	Bovine serum albumin
CAD	Caspase-activated dnase
cAMP	Cyclic adenosine monophosphate
CDK	Cyclin-dependent kinase
CDKIs	Cell-dependent kinases inhibitors
Chk1	Checkpoint kinase 1
Chk2	Checkpoint kinase 2
CHOP	CCAAT-enhancer-binding protein homologous protein
CI	Combination index
cIAP	Cellular inhibitor of apoptosis protein 1
CICD	Caspase-independent cell death
Cl-	Chloride ions
CO_2	Carbon dioxide
COX-2	Cyclooxygenase -2
CVD	Cardiovascular disease
CXB	Celecoxib
CXCR4	C-X-C motif chemokine receptor 4
CYP450	cytochrome P450 enzyme
DAPI	4, 6-Diamidino-2-phenylindole
DC	Dendritic cells
DHA	Docosahexanoic acid
DISC	Death-inducing signalling complex
DNA	Deoxyribonucleic acid
Dox	Doxorubicin
DR	Death receptor
DRI	Drug reduction index
DSBs	Double-stranded breaks
ECM	Extracellular matrix
EGCG	Epigallocatechin gallate
EGF	Epidermal growth factor
EGFR	Epidermal growth factor receptor

EGR	Early growth response
eIF2-α	Eukaryotic initiation factor 2 alpha
ELISA	Sandwich enzyme-linked immunosorbent assay
EMT	Epithelial-mesenchymal transition
Endo G	Endonuclease G
ER	Endoplasmic reticulum
ERK1/2	Extracellular signal-regulated kinase 1/2
ERO1α	Endoplasmic reticulum oxidation 1
ETK1	Epithelial and endothelial tyrosine kinase
FADD	Fas-associated protein with death domain
FDFT1	Farnesyl-diphosphate farnesyltransferase 1
FITC	Fluorescein isothiocyanate
FLIP	FLICE-inhibitory protein
G1	Gap 1
G2/M	Gap 2/ mitosis
GAPDH	Glyceraldehyde 3-phosphate dehydrogenase
GSK-3a/b	Glycogen Synthase Kinase 3 alpha/beta
GSK-β	Glycogen synthase kinase 3 beta
GST	Glutathione S-transferase
Hes-1	Hairy and enhancer of split-1
HGF	Hepatocyte growth factor
HMG-CoA	3-hydroxy-3-methyl-glutaryl-coa reductase
Hrk	Harakiri
HRP	Horseradish peroxidase
HSP	Heat shock protein
hTERT	Human telomerase reverse transcriptase
HTS	High-throughput screening
HUVEC	Human umbilical vein endothelial
IAP	Inhibitor of apoptosis
IC_{50}	Half maximal inhibitory concentration
ICAD	Inhibitor of CAD
ICAM-1	Intercellular adhesion molecules-1
Id-1	Inhibitor of differentiation/DNA binding

IGF	Insulin-like growth factor
IKKα/β	Iκb kinase alpha/beta
IL-6	Interleukin 6
IRE-1	Inositol-requiring enzyme 1
IκBα/β	Inhibitor of kappa B alpha/beta
JAK	Janus kinase
JC-1	5,5',6,6'-Tetrachloro-1,1',3,3' tetraethylbenzimidazolocarbocyanine
JNK	C-Jun N-terminal kinase
JNK	C-Jun N-terminal kinase
K+	Potassium ions
KRAS	Kirsten-ras
LC3	Microtubule-associated protein 1A/1B light chain 3
LEF	Lymphoid enhancer-binding factor
MAPK	Mitogen-activated protein kinase
MC1R	Melanocortin 1 receptor
Mcl-1	Myeloid cell leukemia 1
MDC	Monodansylcadaverine
MDR	Multi drug resistance
MDR1	multidrug resistance protein-1
MEK	Mitogen-activated protein kinase
MIC-1	Macrophage inhibitory cytokine 1
MITF	Melanogenesis associated transcription factor
MLKL	Mixed lineage kinase domain-like
MMP	Mitochondrial membrane permeabilisation
MMP-9	Matrix metalloproteinase 9
MOMP	Mitochondrial outer membrane permeabilisation
MPTP	Mitochondria permeability transition pore
mTOR	Mammalian target of rapamycin
Na+	Sodium ions
NF-κB	Nuclear transcription factor-kappa B
NQO1	NAD(P)H dehydrogenase quinone 1
Nrf2	Nuclear factor erythroid 2–related factor 2

NVI	Necrotic volume increase
Oct-4	Octamer-binding transcription factor 4
p27Kip1	Cyclin-dependent kinase inhibitor 1B
p53	Tumour suppressor p53
p62	Ubiquitin-binding protein p62
PARP	Poly ADP ribose polymerase
PBS	Phosphate buffered saline
PBST	Phosphate buffered saline-Tween 20
PCD	Programmed cell death
PCNA	Proliferating cell nuclear antigen
PDK1	Phosphoinositide-dependent protein kinase-1
PERK	PKR-like ER-localized eif2α kinase
PGD2	Prostaglandin D2
PGDS	Prostaglandin synthase
PI	Propidium iodide
PI3K	Phosphoinositide 3-kinase
PI3P	Phosphatidylinositol 3-phosphate
PPARγ	Peroxisome proliferator-activated receptor gamma
PS	Phosphatidylserine
PSP	Polysaccharopeptide
PTEN	Phosphatase and tensin homologue deleted on chromosome 10
Puma	P53 upregulated modulator of apoptosis
PVDF	Polyvinylidene difluoride
PXR	pregame-X-receptor
Rb	Retinoblastoma-associated
RIPK	Receptor-interacting serine-threonine kinase
RM	Malaysian ringgit
RNA	Ribonucleic acid
ROS	Reactive oxygen species
S	Synthesis
SAPK/JNK	Stress-activated protein kinase/c-Jun NH2-terminal kinase
SDS-PAGE	Sodium dodecyl sulphate polyacrylamide gel electrophoresis

SELECT	Selenium Vitamin E and Prostate Cancer Chemoprevention Trial
SHP2	Src homology phosphatase 2
SI	Selectivity index
Smac/DIABLO	Second mitochondria-derived activator of caspase/ direct inhibitor of apoptosis-binding protein with low pi
Sox-2	Sex determining region Y-box 2
SSBs	Single-stranded breaks
STAT2	Signal transducer and activator of transcription factor 2
STAT3	Signal transducer and activator of transcription factor 3
SXR	steroid and xenobiotic receptor
T3	Tocotrienols
TBARS	Thiobarbituric acid reactive substances
TERT	Telomerase reverse transcriptase
TGFβ	Transforming growth factor β
TGF-β1	Transforming growth factor beta 1
TIMP	Tissue inhibitor of metalloproteinase
TL	Tumour lysate
TNF	Tumour necrosis factor
TNFRSF	Tumour necrosis factor receptor superfamily
TNF-α	Tumour necrosis factor alpha
Tocomin	Mixed tocotrineols with tocopherols
TP	Tocopherols
TRADD	TNF receptor-associated death domain
TRAF	TNF-receptor-associated factor
TRAIL	TNF-related apoptosis-inducing ligand
TRF	Tocotrienol- rich fraction
TRITC	Tetramethylrhodamine
TSP-1	Thrombospondin-1
TUNEL	Terminal deoxynucleotidyl transferase dutp nick end labelling
TYRP	Tyrosinase-related proteins
UGT1A1	glucuronosyltransferase 1A1

ULK1	Unc-51-like kinase 1
uPA	Urokinase-type plasminogen activator
US	United States
VEGF	Vascular-endothelial growth factor
VEGF-A	Vascular-endothelial growth factor-A
Vps	Vacuolar protein sorting
WHS	Women health study
Wnt	Wingless/integrase
XBP	X-box binding protein
XIAP	X-linked inhibitor of apoptosis protein
Zeb1	Zinc finger E-box binding homeobox 1
α	Alpha
α-SMA	Alpha-smooth muscle actin.
αT3	Alpha-tocotrienol
α-TPP	Alpha tocopherol transfer protein
β	Beta
βT3	Beta-tocotrienol
γ	Gamma
γT3	Gamma-tocotrienol
δ	Delta
δT3	Delta-tocotrienol
ΔΨm	Mitochondrial membrane potential

List of Figures

List of Tables

Chapter One: Introduction

1.1 Cancer and current treatment strategies

Cancer is a group of chronic diseases characterised by uncontrollable proliferation of aberrant cells that eventually spread and invade other organs. In 2018 alone, it was predicted that cancer would cause 9.6 million deaths according to the World Health Organisation (Thun et al., 2010). By the year 2030, new cancer cases are projected to ascend to about 26 million and cause 17 million deaths of human lives per year (Thun et al., 2010). The high morbidity and mortality rates of this disease highlight the urgent need for new and effective chemotherapeutic drugs.

Recent advances in molecular biology, genomics and bioinformatics have enabled a deeper understanding of cancer, which led to an emergence of 'targeted' therapy, 'personalised' or 'precision' medicine. These therapeutic strategies help to identify and rectify the specific mutation(s) in the patients. Seemingly, these therapeutic approaches provide only little benefits to patients. The molecular target drugs that aim at one or two specific mutations of growth factors, receptors, or enzymes, would maximally constitute to 1–3% of therapeutic success (Maeda and Khatami, 2018). One of the major reasons for the repetitive failures lies within an infinite number of genetic mutations and enormous variations across different patients (inter-tumour heterogeneity) or same tumour (intra-tumour heterogeneity). These molecular targets derived from mutated genetic components could only be an isolated molecular entity from a highly heterogeneous and chaotic landscape in cancer biology (Maeda and Khatami, 2018). As a result, the underlying unique mutations contribute to differential drug responses in patients (White Al-Habeeb et al., 2016).

Traditional treatments such as surgery, radiotherapy and chemotherapy remain the standard options used for cancer treatment (Abbas and Rehman, 2018). Surgical

procedure and radiation therapy are considered as ‘local treatment’ options limited to site-confined tumours. On the contrary, chemotherapy is a mainstay ‘systemic treatment’ for metastasised tumours that spread to other parts of the body (Hanahan and Weinberg, 2011). A few groups of conventional chemotherapeutic drugs that are commonly incorporated into chemotherapy are (but not limited to) anthracyclines, alkylating agents, anti-metabolites and mitotic inhibitors (Palumbo et al., 2013). These conventional chemotherapeutic drugs which are referred to as cytotoxic agents kill rapidly proliferating cancer cells by causing damage or stress, imparting interference in cell proliferation and precipitating cell death. Adhering to this mechanistic principle, chemotherapy is essentially non-selective because it targets both the active-growing healthy cells and fast-replicating cancer cells equally well. This phenomenon means that patients will inevitably have to endure some common side effects such as alopecia (hair loss), loss of appetite and nausea during chemotherapy which can significantly impact their quality of life. Severe toxicities e.g. cardiotoxicity may also be lethal to the patients. Hence, a solution is needed to reduce the toxicities while improve the efficacy of chemotherapeutic drugs.

1.2 Tocotrienols as potential anti-cancer candidates

Tocotrienols are minor constituents of the Vitamin E family. There are four isomeric forms, namely alpha (α), beta (β), gamma (γ) and delta (δ)-tocotrienols, which can be differentiated by the degree of saturation in their chromanol head structure. Tocotrienols are commonly found in rice bran, palm oil, annatto seeds and barley (Miyazawa et al., 2008). Tocotrienol-rich fraction (TRF) is most commonly available form of vitamin E oral supplement containing a mixture of α-, β-, γ-, δ-tocotrienols and α-tocopherol. Despite the early discovery of tocotrienols in 1922, their contributions toward human health improvement have only been appreciated

after the growing disappointments from tocopherols (the major constitutes of the vitamin E family) in clinical trials. To date, publications of tocotrienols only made up of less than 3% out of all vitamin E publications (Peh et al., 2016). Therefore, the current state of knowledge about tocotrienols deserves further investigations.

Tocotrienols have been recognised as prospective anti-cancer candidates because they are selective towards cancer without causing much harm to normal cells (Shah and Sylvester, 2005; Srivastava and Gupta, 2006). Additionally, tocotrienols were reported to efficiently target cancer via multiple pathways and mechanisms. The anti-cancer ability of tocotrienols was found to be associated with multifaceted mechanisms such as anti-proliferation, promotion of apoptosis, anti-angiogenesis and invasion (Kwang et al., 2007) via modulation of various molecular targets (Figure 1.1).

Despite the enormous potential of tocotrienols in cancer treatment, tocotrienols suffer from limited oral bioavailability as compared to α-tocopherol. This is due to the low affinity of α-tocopherol transfer protein (α-TTP) towards tocotrienols and instead, it binds preferentially to α-tocopherol. As an example, the binding affinity of α-tocotrienol to α-TTP is 8.5-fold lower than α-tocopherol (Hosomi et al., 1997). Tocotrienols which are not bound to α-TPP will remain in the liver and are susceptible to catabolism via P450 cytochrome (Abe et al., 2007). Due to this constraint, oral application of high dose tocotrienols was deemed a futile approach as tocotrienols are prone to metabolic degradation under high dose administration (Brigelius-Flohé, 2005). Hence, it is suggested that tocotrienols are more suitable to be used in adjunct treatments at lower doses (Abubakar et al., 2016; Shirode and Sylvester, 2010; Wali et al., 2009a; Ye et al., 2015).

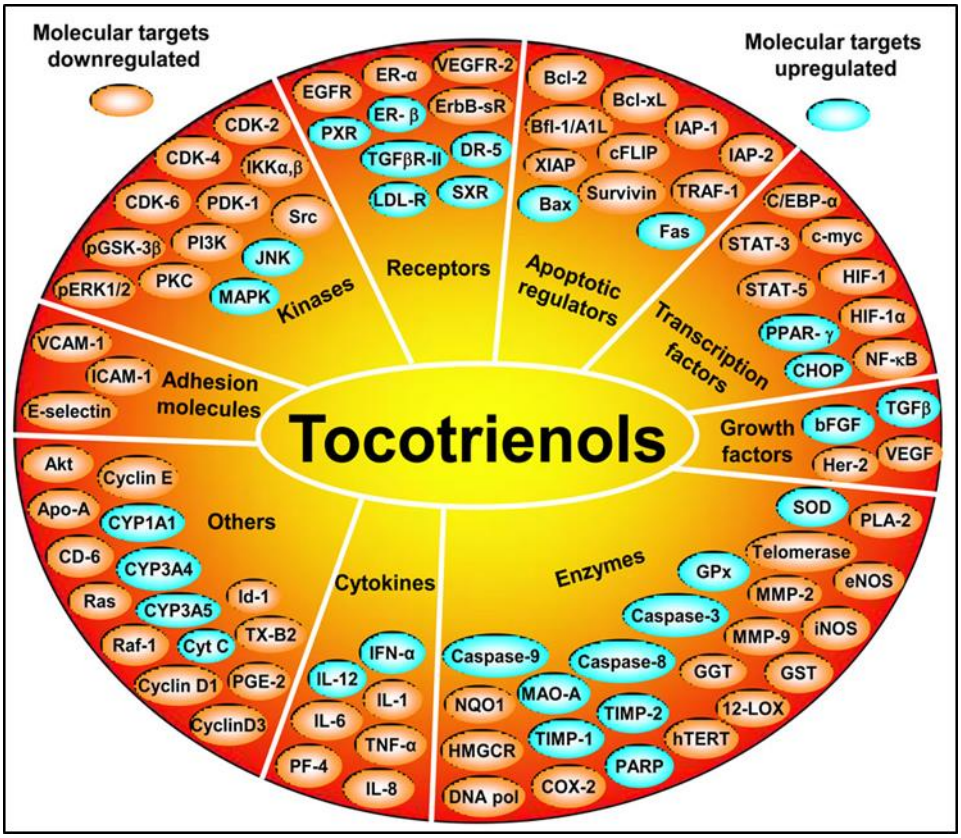

Figure 1.1 Molecular targets of tocotrienols. The diagram was adapted from Aggarwal et al. (2010).

1.3 Research problems

The battle with cancer began in 1971 after President Nixon from the United States declared "war on cancer". Yet, the pace of new cancer drug discovery is unable to keep up with the rate of life lost to cancer. Generally, a cancer drug discovery journey can be summarized by the "3D" realities which are delayed (in time), deluxe (in cost) and discouraging (in effectiveness). For instance, a new cancer drug takes about 6-12 years from discovery to approval before it is available on the market (Van Norman, 2016). If the time taken for drug approval is shortened by one year, as much as 79,920 life-years per drug could have been saved (Stewart et al., 2018). The excessive cost incurred by using new cancer drugs can too be problematic. For example, as many as 12 out of 13 newly-approved cancer drugs in 2012 were priced above USD100,000 annually, which made these drugs unaffordable to most patients

and healthcare systems (Stewart et al., 2018; Workman et al., 2017). A recent research found that most of the new cancer drugs failed to show a clear evidence of extending or improving the quality of life in patients (Davis et al., 2017). This research was based on indications of 68 cancer drugs approved by European Medicines Agency (EMA) during 2009-2015; as much as 39 (57%) drugs were released into the market even without evidence of survival and quality of life benefit overactive treatment, placebo or as an 'add-on' treatment (Davis et al., 2017). Collectively, these issues have posed an urgent need for affordable, effective and immediate treatment options for cancers.

1.4 Rationale of study

New treatments are not necessarily better, old treatments are not necessarily outdated. While much attention has been devoted to the development of new cancer drugs; the therapeutic success, availability, and affordability still remain uncertain. Despite their dose-limiting toxicity, these chemotherapeutic drugs are still clinically relevant and accessible. Their established mechanisms, predictable safety and pharmacokinetics profiles harnessed through a long clinical history are *de facto* valuable for the optimisations of combinations involving these chemotherapeutic drugs. On the other hand, cancer selectivity and multi-targeted actions offered by tocotrienols are deemed worthy to be incorporated into the chemotherapy regimen. To circumvent high dose associated limitations of chemotherapeutic agents, adopting a combination therapy using their respective lower effective doses has proven to be a viable approach.

A combination treatment represents a promising platform, which offers an immediate, effective and affordable solution that benefits a greater patient population. By definition, combination therapy is a treatment modality which comprises two or more therapeutic agents (Mokhtari et al., 2017). Synergy is commonly defined as the

effect of two or more agents working in combination that is greater than the expected additive effect of the single agents (Greco et al., 1996). The amalgamation consisting of various anti-cancer drugs could enhance the therapeutic efficacy when compared to the monotherapy approach by targeting key pathways in a synergistic manner. This approach could potentially reduce drug resistance, arrest actively proliferating cells, induce apoptosis or cell death, reduce metastatic potential and target cancer stem cell population (Mokhtari et al., 2017).

Given that the chemotherapeutic drugs had been approved for clinical use and the tocotrienols were recognised as Generally Recognised As Safe (GRAS) status by Food and Drug Administration (FDA), these positions have granted them a 'green light' for human use. Combined treatments are deemed a cost effective approach as low doses of chemotherapeutic drugs will be used as compared to current high dose chemotherapy. In addition, promising cytotoxic properties of chemotherapeutic drugs and multi-targeted actions of tocotrienols have been recorded previously. Hence, commencement on this project was justifiable for exploring and studying the effectiveness of the tocotrienol-chemotherapeutic drug combinations on cancer cells. The potential contribution of this study towards finding an immediate, affordable and effective solution for cancer management in the near future is indeed significant.

Despite many tocotrienols combination studies were reported previously, most of the studies reported on γ-tocotrienol and breast cancers. Little research attention was given to δ-tocotrienol combined treatment and colorectal cancers. Current study represents the first study attempted on δ-tocotrienol and conventional chemotherapeutic drugs combination on colorectal cancer cells, underscoring the room for research and potential to be unveiled through embarking on this novel study.

1.5 Scope of study

Current study covers identification of synergistic tocotrienol-chemotherapeutic drug combinations (Chapter Three), characterisation of the induced apoptosis (Chapter Four), delineation of the underlying apoptosis mechanisms (Chapter Five) and examination on the role of the induced autophagy (Chapter Six).

In Chapter Three, a high-throughput screening was employed to study the individual anti-proliferative effects of α-, γ-, and δ-tocotrienols, TRF, conventional chemotherapeutic drugs, namely doxorubicin, cisplatin, 5-fluorouracil and vinblastine across three cancer types (lung, colorectal and nasopharyngeal cancers). The anti-proliferative and cancer selective effects of tocotrienols were analysed in order to identify the most potent tocotrienol candidate for combination. Effects of combined treatments were then assessed based upon the combination index (CI), drug reduction index (DRI) and selectivity index (SI). Clonogenic survival assay was employed to study the effects on long-term cell survival of the selected combinations.

Following the identification of synergistic combinations, Chapter Four pursued a characterisation on the induced cell death response, primarily in assessing apoptosis. The concentrations of individual single agents used in the combination were included for a fair comparison to demonstrate the potential boon and bane effects derived from the combined treatments. Cancer cells were firstly evaluated morphologically (qualitative) upon treatments to identify the presence of apoptosis. Secondly, the detections of apoptosis and DNA fragmentation (quantitative) were conducted. DNA damage profiles and associated cell cycle arrests were also studied to understand the cytotoxic effects of the combined treatments.

In Chapter Five, the activations of intrinsic (caspase-9) and extrinsic (caspase-8) pathways of apoptosis were studied. The presence of apoptosis was determined

through caspase-3 activation. Also, the effect of treatments on inhibitor of apoptosis (IAPs) was studied to identify a potential chemosensitisation. Lastly, pharmacological inhibitors of apoptosis were applied to investigate the pathway dependency through caspase activation and/or mitochondrial permeability transition.

In Chapter Six, the study ventured into the involvement of autophagic cell death, which is an emerging cell death modality. Autophagy was assessed qualitatively through fluorescence microscopy aided by acridine orange (AO) or quantitatively through monodansylcadaverine (MDC). Markers of autophagy in an early (beclin-1) and late (microtubule-associated proteins 1A/1B light chain 3A, LC3) phases were assessed. An involvement of autophagy-related survival pathway was studied by assessing the level of protein kinase B (PKB/Akt) and its activation by kinase phosphoinositide-dependent kinase-1 (PDK-1). Lastly, the 3-methyladenine and bafilomycin A1, autophagy inhibitors at early and late phases, respectively were added to confirm the role of autophagy whether it is destined for cell death.

1.6 General aim and specific objectives

The current research envisioned and advocated a drug combination approach comprising lower concentrations of tocotrienols and chemotherapeutic drugs as an augmented therapeutic strategy in cancers. In general, this research aims to develop a combination therapeutic approach consisting of tocotrienols and conventional chemotherapeutic drugs to effectively combat cancers. To materialize this aim, the current study thus embarked the following specific objectives:

i. a. To identify synergistic anti-proliferative combinations of tocotrienols and chemotherapeutic drugs.

b. To study the cytotoxic effects of δ-tocotrienol, 5-fluorouracil and doxorubicin single and combined treatments on Caco-2 and SW48 colorectal cancer cells.

ii. To characterise the apoptotic cell death response induced by the δ-tocotrienol, 5-fluorouracil and doxorubicin single and combined treatments on Caco-2 and SW48 colorectal cancer cells.

iii. To study the underlying apoptosis mechanism(s) provoked by the δ-tocotrienol, 5-fluorouracil and doxorubicin single and combined treatments on Caco-2 and SW48 colorectal cancer cells.

iv. To investigate the role of autophagy induced by the δ-tocotrienol, 5-fluorouracil and doxorubicin single and combined treatments on Caco-2 and SW48 colorectal cancer cells.

Chapter Two: Literature Review

2.1 Continual fight against cancer

The word ‘cancer’ originated from Hippocrates (460-370 BC), a Greek physician who is universally recognised as the ‘Father of Medicine’. He termed carcinoma (*karkinoma*), a Greek word for crab, to describe non-ulcer-forming tumours. With the resemblance of this disease to a crab’s outgrowing finger-like projections, the Roman physician, Celsus (28-50 BC) then translated the term into *cancer*, which is a Latin word for crab (American Cancer Society, 2016).

Presently, cancer is a collective term to describe a disease when abnormal cells proliferate uncontrollably with the invasive potential to spread to other parts of the body. Most of the cancers grow into tissue masses that form solid tumours; however, blood cancer such as leukaemia does not. In fact, not every tumour is cancerous. A malignant tumour that can spread to other parts of the body is cancerous, conversely, a benign tumour which does not carry the spreading is non-cancerous.

Cancer has been long associated with human life. Some of the earliest evidences of cancer were discovered in ancient Egyptian mummies, fossilized bone tumours and ancient manuscripts. The oldest written record about cancer was found in an Egyptian textbook on trauma surgery (named Edwin Smith Papyrus) dated back to 3000 BC. At that time, the writing described cancer as a disease with no treatment (American Cancer Society, 2016). In fact, not much progress has been achieved for curing cancer since then until the discovery of chemotherapeutic drugs in the 1940’s, in which human won a short celebration over the war against cancer. However, the success rate of chemotherapy is essentially low in the advanced stage of cancers (Maeda and Khatami, 2018). Therefore, the quest for effective anti-cancer treatments has to be continued vigorously.

2.1.1 Cancer- the silent killer

Cancer remains as one of the leading causes of death worldwide. In 2016, cancer overtook cardiovascular disease (CVD) as the top killer in at least 12 European countries, including Belgium, Denmark, France and Italy. Unsurprisingly, it may continue to strike CVD as the first morbidity and mortality cause in more countries in the coming decades (Cao et al., 2017). In the United States (US), approximately 40% of the population will be diagnosed with cancer at some point during their lifetime (White et al., 2014). Globally, it is predicted that new cancer cases will soar to about 26 million and claim 17 million lives per annum, by the year 2030 (Thun et al., 2010). In Malaysia, one out of four people will develop cancer by the age of 75 (Lim, 2006). In the most recent Malaysian National Cancer Registry Report 2007-2011, the six most popular cancer types affecting Malaysian residents were breast, lung, colorectal, breast, lymphatic and nasopharyngeal cancers (Abdul-Manan et al., 2016).

Notably, colorectal cancer is considered as one of the clearest indicators for the epidemiological transition of cancer. Nowadays, countries undergoing rapid societal and economic changes show more rapid increases in cancers than the high-income countries (Arnold et al., 2016). It was reported that processed meat, alcohol drinks, and body fatness can increase the risk of colorectal cancer (World Cancer Research Fund/American Institute for Cancer Research, 2018). Although colorectal cancer predominantly occurs in the older population with a median age of 72, there is a sharp rise of colorectal incidence in young adults (<55 years old) in the US (Mitchell, 2012). In other words, colorectal cancer is ‘getting younger’ by affecting population which is in their most productive years.

2.1.2 The study focus: colorectal cancer

Colorectal cancer refers to the cancer type which originates from colon or rectum. Colorectal cancer develops when healthy cells in the lining of the colon or rectum begin to proliferate uncontrollably into a malignant tumour. Due to high similarity between colon and rectal cancers, they are often being referred as colorectal cancer. Most of the colorectal cancer belongs to a tumour type called adenocarcinoma, a type of cancer that starts in mucous glands.

Globally, it was estimated that there would be more than 1.8 million and 0.8 million new cancer cases and deaths for colorectal cancer in 2018 alone. It ranks third in terms of incidence while second in terms of mortality (Bray et al., 2018). In Malaysia, colorectal cancer is the second and third most commonly occurring cancer in men and women respectively, at the prevalence of 13.2% as reported in Malaysian National Cancer Registry Report (2007 – 2011) (Abdul-Manan et al., 2016). Moreover, the GLOBOCAN project reported that the overall incidence and mortality of colorectal cancer in Malaysia is the third highest in South East Asia as reviewed by Hassan et al. (2016).

Furthermore, a study conducted in 2012 reported that the mean cost of treating colorectal cancer per year in the central region of Malaysia using conventional chemotherapy, enumerated in Malaysian Ringgit (RM) were RM13,622 for Stage 1, RM19,752 for Stage 2, RM24,972 for Stage 3, and RM27,377 for Stage 4 (Natrah et al., 2012). As such, the estimated cost of colorectal cancer management of new cases in Malaysia in 2012 was approximately RM108 million per year.

Indeed, colorectal cancer has posed an increasing burden globally and locally, necessitating improvements in treatment options which are more effective and accessible.

2.2 Hallmarks of cancer

Hanahan and Weinberg (2011) have denoted six hallmarks of cancer as a logical framework for understanding of the remarkable and diversified disease. Self-stimulating proliferative signalling, overcoming tumour suppressors, resisting cell death, enabling replicative immortality, inducing angiogenesis, activating tissue invasion and metastasis are the six common hallmarks of cancer that contribute to the complexity of this disease. Understanding of these cancer hallmarks is of a prime importance to develop effective anti-cancer strategies via rational drug designs.

2.2.1 Self-stimulating proliferative signalling

Growth-promoting signals are carefully coordinated in normal cells to ensure tissue homeostasis. In cancer cells, these signals are dysregulated by producing growth factor ligands to achieve autocrine proliferation or stimulating normal cells to supply cancer cells with various growth factors. Specifically, cancer cells may have an elevated level of surface receptor protein to hypersensitively responsive to a limiting growth factor ligands pool. Alternatively, the receptor is structurally altered enabling ligand-independent constitutive downstream activation of signalling pathways. One of the renowned examples is Ras, a growth-controlling signal transducer which activates the mitogen-activated protein kinase (MAPK) pathway. In addition, phosphoinositide 3-kinase (PI3K)/ protein kinase B (Akt)/ mammalian target of rapamycin (mTOR) pathway is one of the most frequently dysregulated signalling conduits associated with human malignancies (Dienstmann et al., 2014). Mutations in PI3K cause hyperactivation of the signalling circuitry, including Akt signal transducer, leading to constitutive cell proliferation state. Additionally, a loss-of-function mutation in phosphatase and tensin homologue deleted on chromosome 10 (PTEN), a negative regulator of PI3K signalling further promotes the proliferation of cancer cells.

2.2.2 Overcoming tumour suppressors

Normal cells are governed by a number of tumour suppressors to negatively regulate cell proliferation. For instance, retinoblastoma-associated (Rb) protein and tumour protein p53 proteins play central roles in deciding cell proliferation or senescence and apoptosis. Rb guards cell cycle progression, in which without its presence will result in persisting cell proliferation. Rb protein is responsible for G1 checkpoint to block the unready cells from entering into S phase and cell growth (Giacinti and Giordano, 2006). On the other hand, p53 is known as the 'guardian of genome'. More than half of all human cancers are associated with p53 malfunction; either completely lost or mutated (Muller et al., 2011). In response to a wide range of stress signals, activated p53 can influence cell cycle checkpoint controls and induce apoptosis. The p53 is the most frequent type of gene-specific alterations in human cancer leading to tumour progression and increased resistance to treatment (Oren and Rotter, 2010). Furthermore, mutations in p53 lead to cell migration and invasion, enabling cancer to metastasise (Muller et al., 2011).

2.2.3 Resisting cell death

Attenuation in apoptosis is closely associated with progression into higher-grade of malignancy and resistance to therapy. Losing p53 tumour suppressor as a critical damage sensor is the most common event that impedes apoptosis. At the same time, some cancers prevent apoptosis by upregulating anti-apoptotic regulators or survival signals and/or downregulating pro-apoptotic regulators. Apoptosis machinery is orchestrated by two major mechanisms: extrinsic death receptor pathway and intrinsic mitochondrial pathway. Briefly, the extrinsic pathway is activated through extracellular ligand binding whereas the intrinsic pathway is activated intracellularly through 'stress sensors' such as mitochondria and endoplasmic reticulum. Both

activation pathways engage the cysteine-aspartic proteases known as caspases to convey cell death signal and precipitate apoptosis (refer more details in Section 2.3.1). Another cell death program is autophagy. It is a catabolic process that recycles cellular materials by delivering cytoplasmic content to lysosome for degradation (refer more details in Section 2.3.2). However, it is regarded as a double-edge sword when comes to cancer. Autophagy can promote cell survival by eliminating damaged organelles and defective protein aggregates as well as serving as a backup mechanism when apoptosis was disabled (Thorburn et al., 2014). It was argued that autophagy plays different roles at different stages in cancer development; autophagy is crucial for tumour suppression at early cancer development but confers a protection role during tumour progression (Bhutia et al., 2013). Therefore, the role of autophagy in the context of cancer therapy remains elusive.

2.2.4 Enabling replicative immortality

Telomeres are hexanucleotide repeats that protect the ends of chromosome from erosion during DNA replication. In normal cells, this sequence limits the replicative potential to a finite number before the onset of senescence. Quite the reverse, cancer cells are able to maintain telomeric DNA sufficiently long to avoid triggering senescence and apoptosis. The state where cells have evolved from a limited replicative capacity into an infinite replicative potential is known as immortalisation, a featured trait for most of the established cancer cell lines. In cancer cells, the telomerase, a RNA-dependent DNA polymerase that synthesises telomeric DNA sequences is commonly (~90%) upregulated in order to pursue longevity. It was discovered that the telomerase reverse transcriptase (TERT), a protein subunit of telomerase exerts a proliferative effect by some novel telomere-independent functions such as serving as a cofactor of β-catenin/ lymphoid enhancer-binding factor (LEF)

transcription factor to amplify Wnt signalling pathway (Park et al., 2009). Moreover, non-canonical roles of telomerase such as enhance cell proliferation, resistance to apoptosis, involvement in DNA damage repair and RNA-dependent RNA polymerase could also be associated with the unlimited replicative potential in cancer.

2.2.5 Inducing angiogenesis

To address the necessity of evacuating metabolic waste and sufficient oxygen and nutrients intake, tumours initiate angiogenesis to develop neovasculature to support these demands. In fact, assembly of endothelial cells into tubes (vasculogenesis) and vessels sprouting (angiogenesis) were only active during embryogenesis. Since then, normal vasculatures are mainly quiescent unless transient activation by physiological events such as wound healing or female reproductive cycle. However, this 'angiogenesis switch' is turned on during tumour progression. In fact, angiogenesis is a process regulated by counterbalance between inducers and inhibitors such as vascular-endothelial growth factor-A (VEGF-A) and thrombospondin-1 (TSP-1), respectively. VEGF is an important growth factor for vascular endothelial cells during sprouting of new blood or lymph vessels. It can remain latent in extracellular matrix and subjects to release and activation by extracellular matrix-degrading proteases such as matrix metalloproteinase 9 (MMP-9). On the other hand, TSP-1 is an adhesive glycoprotein that can bind and sequester various proteins, including VEGF (Margosio et al., 2003), hence it is served as suppressive signals of angiogenesis. Of note, oncogenes such as *Ras* and *Myc* expressions could also serve as an inductive signal to angiogenesis (Bajaj et al., 2010; Gabay et al., 2014).

2.2.6 Activating invasion and metastasis

Progression of carcinomas into a higher grade of malignancy is associated with local invasion and distant metastasis. In fact, invasion and metastasis involve multiple sequences known as invasion-metastasis cascade. Initially, the tumour becomes locally invasive and enters the nearby blood and lymphatic vessels (intravasation). Subsequently, cancer cells transit systemically through lymphatic vessels and haematogenous systems. Next, the cancer cells escape from the lumina into parenchyma of distant tissues (extravasation). Eventually, small nodules of cancer cells (micrometastases) form macroscopic tumours (colonisation) (Hanahan and Weinberg, 2011).

It is widely accepted that detachment and mobility of cancer cells from the primary tumour site mimic epithelial-mesenchymal transition (EMT), a crucial process for developmental plasticity. Briefly, epithelial cells lose their cell polarity and cell-cell adhesion, and gain migratory and invasive properties to become mesenchymal stem cells (Franzen et al., 2015). Cancer acquires this multifaceted EMT program during the course of invasion and metastasis. EMT is characterised by the loss of epithelial cell junction proteins, such as E-cadherin, α-catenin, claudins, occluding, ZO-1 and (mostly) coincide with the elevated expression of mesenchymal markers, including N-cadherin, vimentin and fibronectin (Jiang et al., 2015). EMT is initiated with the inception of growth factors including epidermal growth factor (EGF), transforming growth factor β (TGFβ) and hepatocyte growth factor (HGF). Following that, the downstream transcription factors, for instances, Snail, Slug, Twist and zinc finger E-box binding homeobox 1 (Zeb1) are activated. These transcription factors can directly or indirectly repress E-cadherin expression, thus depriving the key suppressor in the EMT related migratory processes. Apart from that, the loss of adherens junction,

changing the polygonal/epithelial to spindly/fibroblastic morphology, expressing matrix-degrading enzymes, increased motility and resistance to apoptosis are also the transcription factors' resultants (Peinado et al., 2004). Upon reaching at a new metastatic site, tumour cells reverse the EMT process.

2.3 Mechanisms of cancer cell death

Programmed cell death (PCD) is an evolutionary conserved cellular mechanism which is important for maintaining body homeostasis. There are two common types of PCD, namely apoptosis (Type I) (Figure 2.1) and autophagy (Type II) (Figure 2.3). Necrosis although is more popularly known as an accidental cell death, accumulating evidence proposed an existence of regulated form of necrosis, known as necroptosis (Type III PCD). Often, dysregulation of these pathways is captured during cancer development, rendering an enhanced cell survival in cancer cells (Fulda, 2013a). Therefore, understanding on the molecular mechanisms of PCD is crucial to identify the opportunities in the cancer therapeutics development.

2.3.1 Apoptosis

Apoptosis is one of the regulatory mechanisms to regulate cell homeostasis. Damaged cells that cannot be recovered or repaired eventually undergo apoptosis. Unlike necrosis (sudden cell death), it is a subtle cell killing mechanism that allows the body to eliminate the unwanted cells with minimal burden, is a major aspiration of any of the cancer drugs. Generally, apoptosis can be triggered by different biochemical routes either via extrinsic cell death receptor-mediated or intrinsic mitochondria-mediated pathways (Elmore, 2007).

2.3.1.1 Extrinsic pathway of apoptosis

The extrinsic pathway is also known as death receptor-mediated pathway. The death stimulus begins outside of a cell involving the binding of extracellular death ligands to their respective transmembrane death receptors from the tumour necrosis factor receptor superfamily (TNFRSF) (see Table 2.1). For instance, FasL binds to Fas receptor, leading to activation of caspase-8 (initiator caspase) and recruitment of the Fas-associated protein with death domain (FADD) adapter molecule to form death-inducing signalling complex (DISC). It transduces a downstream signalling cascade to caspase-8, leading to the proteolytic activation of caspase-3. In fact, the extrinsic pathway can cause amplification of cascade via intrinsic mitochondrial pathway whereby caspase-8 cleaves Bid to promote mitochondrial outer membrane permeabilisation (MOMP) and execution of the intrinsic pathway of apoptosis (Kantari and Walczak, 2011).

Table 2.1 TNFRSF receptors, their ligands, adapted from (Vanamee and Faustman, 2018).

TNFRSF receptor (TNFRSF#, other names)	TNFSF ligand (TNFSF#, other names)
TNFR1 (1a, CD120a)	TNF (2, TNF-α), LTα (1, TNF-β), LTβ (3)
Fas (6, CD95)	FasL (6, CD178)
TRAILR1 (10A, DR4, CD261)	TRAIL/Apo2L (10, CD253)
TRAILR2 (10B, DR5, CD262)	TRAIL/Apo2L (10, CD253)
NGFR (16, p75NTR, CD271)	NGF (not a TNFSF member)
DR3 (25 or 12, TRAMP)	TL1A (15, VEGI), TWEAK (12)
DR6 (21, CD358)	N-APP (not a TNFSF member)

2.3.1.2 Intrinsic pathway of apoptosis

The intrinsic pathway was initiated by internal stimuli such as DNA damage, growth factor deprivation, hypoxia, oxidative stress and flux of Ca^{2+} (Wong, 2011). The stimuli then perceive cell death signals via the mitochondria, which represent the

metabolic status of a cell. The MOMP is often regarded as the primary step required for activation of caspases. Pro-apoptotic and anti-apoptotic Bcl-2 family proteins regulate the permeability of mitochondrial membrane (see Figure 2.1) (Brentnall et al., 2013; Harris and Thompson, 2000). When an apoptotic stimulus causes MOMP to take place, cytochrome *c* will be released from intermembrane space. In the cytoplasm, cytochrome *c* engages apoptotic protease activating factor-1 (Apaf-1) and procaspase-9 to form a macromolecular complex (apoptosome), eventually leads to the activation of caspase-9 (initiator caspase). Following that, caspase-9 activates executioner caspases such as caspase-3-, -6, -7, and causes downstream biochemical events (Brentnall et al., 2013).

Of note, caspase-3 specifically activates the endonuclease caspase-activated DNase (CAD) by cleaving the inhibitor of CAD (ICAD). Then, CAD degrades the chromosomal DNA within the nuclei and causes its condensation. Caspase-3 also induces cytoskeletal reorganisation and disintegration of cells into apoptotic bodies. The execution caspases activate cytoplasmic endonuclease, which leads to degradation of nuclear and cytoskeletal protein. The poly (ADP-ribose) polymerase (PARP) is also a substrate of execution caspases, in which its cleavage disables the DNA repair. The ultimate outcomes at the end of execution pathway include cell shrinkage, chromosomal condensation, nuclear and chromosomal DNA fragmentation, and blebbing (Elmore, 2007; He et al., 2009; Kiraz et al., 2016).

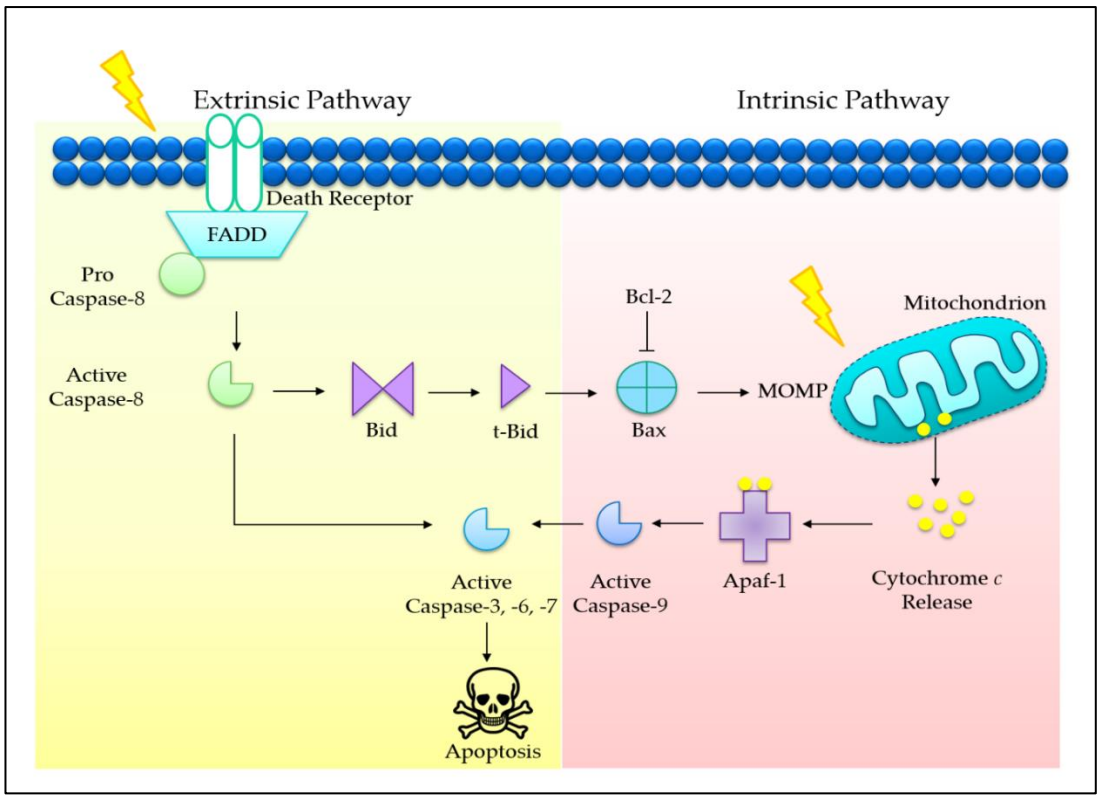

Figure 2.1 Extrinsic and intrinsic pathways of apoptosis.

Table 2.2 Bcl-2 family, adapted from Kale et al. (2018).

Bcl-2 family member	Abbreviation	Apoptosis regulator nature
Bcl-2	B-cell lymphoma 2	Anti-apoptotic
Bcl-xL	B-cell lymphoma-extra large	Anti-apoptotic
Bcl-w	Bcl-2-like protein w	Anti-apoptotic
Mcl-1	Myeloid Cell Leukemia 1	Anti-apoptotic
Bax	Bcl-2-associated X protein	Pro-apoptotic
Bak	Bcl-2 homologous antagonist/killer	Pro-apoptotic
Bok	Bcl-2 related ovarian killer	Pro-apoptotic
Bad	Bcl-2-associated death promoter	Pro-apoptotic (BH3 only protein)
Bid	BH3 interacting-domain death agonist	Pro-apoptotic (BH3 only protein)
Bik	Bcl-2 interacting killer	Pro-apoptotic (BH3 only protein)
Bim	Bcl-2-like protein 11	Pro-apoptotic (BH3 only protein)
Bmf	Bcl-2-modifying factor	Pro-apoptotic (BH3 only protein)

Hrk	Harakiri	Pro-apoptotic (BH3 only protein)
Noxa	-	Pro-apoptotic (BH3 only protein)
Puma	p53 upregulated modulator of apoptosis	Pro-apoptotic (BH3 only protein)

2.3.2 Autophagy

Autophagy is a highly conserved eukaryotic cellular recycling process. It is known for its role in facilitating cell survival and maintenance through recycling the metabolic precursors from damaged organelles or aggregated proteins (Das et al., 2012). Generally, there are three defined types of autophagy, namely macroautophagy, microautophagy and chaperone-mediated autophagy. However, the most prevalent form of autophagy is macroautophagy (henceforth referred to as 'autophagy') (Glick et al., 2010). Under unrecoverable cellular stress, autophagy can cause cell death (Type II PCD). During autophagy, double membrane vesicles (autophagosomes) are formed to engulf the cytoplasmic content. Following that, a fusion with lysosome degrades the content and recycles the nutrients to fuel the cellular deficiency.

As illustrated in Figure 2.2, autophagy begins with phagophore formation which is driven by unc-51-like kinase 1 (ULK1) complex and vacuolar protein sorting (Vps) 34 complex. The expansion of phagophore is facilitated by Atg5-12/Atg16L complex to uptake cargos from the cytoplasm into a double-membraned autophagosome. The loaded autophagosome then fuses with lysosome to allow the degradation of cargo by lysosomal proteases while microtubule-associated protein light chain 3 (LC3-I) will be recycled back to cytosol. The endogenous LC3-I presents in the cytoplasm, is conjugated to phosphatidylethanolamine to form LC3-phosphatidylethanolamine conjugate (LC3-II), which are bound to the autophagosome during autophagy. Therefore, the ratio of LC3-I (water soluble) and LC3-II (lipidated)

is often used as a marker to assess autophagy. Then, the lysosomal permeases and transporters export amino acids and other by-products of degradation back to the cytoplasm, where they can be re-used for building macromolecules and for metabolism (Glick et al., 2010).

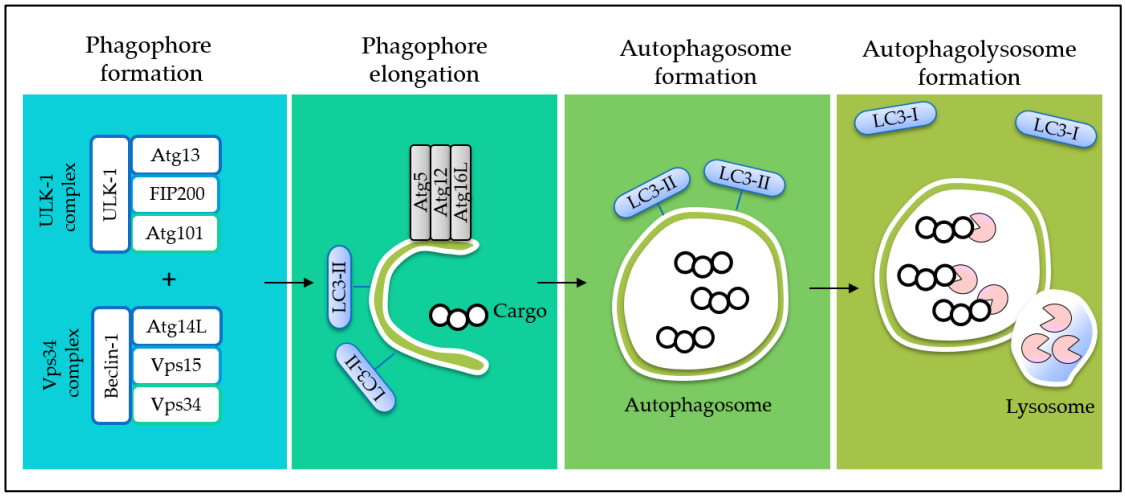

Figure 2.2 The process of autophagy.

2.3.3 Necroptosis

For many years, necrosis was known as a form of accidental cell death. However, it is gaining attention that necrosis may exist in a programmed manner, known as necroptosis (Fulda, 2013b). The activation of necroptosis primarily depends on receptor-interacting serine-threonine kinase 3 (RIPK3) and mixed lineage kinase domain-like (MLKL). Morphologically, cells exhibited similar features as necrosis such as rupture of plasma membrane, swelling of cytoplasm and organelles and release of cellular constituents into microenvironment. Accumulating evidence has suggested that necroptosis could be an alternative cell death mechanism for apoptosis-deficient cancer cells (Galluzzi et al., 2017).

The best characterised signal transduction cascade is initiated by TNFR1 ligation. Upon ligation, the receptor oligomerises and recruits various proteins including TNF receptor-associated death domain (TRADD), RIPK1, cellular inhibitor

of apoptosis (cIAP) protein, TNF-recetor-associated factor (TRAF) 2, TRAF 5 to form multi-protein complex, namely necrosome (Galluzzi et al., 2017). Subsequently, the RIPK3 phosphorylates MLKL, leading to MLKL oligomerisation. As a result, MLKL translocates to the plasma membrane and causes its permeabilisation (Weber et al., 2018).

2.4 Chemotherapy as a cornerstone of cancer treatment

Conventional treatment options that are available for cancer include surgery, radiotherapy and chemotherapy (Abbas and Rehman, 2018). Surgical removal of tumour is considered as a preferred treatment option if the tumour mass is located at easily accessible site and can be removed with minimal harm to the surrounding tissues. The purposes of surgical procedure are to remove the entire tumour, debulk a tumour or ease symptoms caused by a large tumour. Radiotherapy utilises ionizing radiation to attack cancer cells. As such, the ionizing energy can either kill the cells directly, or, harm the cells so that they accede cell death indirectly (Abbas and Rehman, 2018). As compared to surgery and radiotherapy, chemotherapy is one of the widely used systemic approaches to treat cancer. Chemotherapeutic drugs used are served as a cytotoxic agent that halts tumour progression by stopping cancer cell proliferation and enforcing apoptosis.

2.4.1 Types of chemotherapeutic drugs

There are several classes of chemotherapeutic drugs, categorised by the mechanisms of action, chemical structures and interactions with other drugs. Generally, chemotherapeutic drugs such as anthracyclines, alkylating agents, anti-metabolites and mitotic inhibitors are the common drugs used in existing treatment regimens. Understanding on the mechanisms of action to propel cancer cell death is

of particular importance in order to identify the strengths and weaknesses in clinical applications.

2.4.1.1 Anthracyclines

Anthracyclines are a group of anti-tumour antibodies that commonly used in chemotherapy regimen. Doxorubicin is the first anthracycline drug extracted from *Streptomyces peucetius var. caesius* in the 1970s and is still actively being used clinically for treating a variety of cancers such as haematological cancers (leukaemia and lymphoma), carcinoma (solid tumours) and soft tissue sarcomas (Thorn et al., 2011).

There are three potential mechanisms of doxorubicin mediated cell death, namely topoisomerase II poisoning, DNA adduct formation and oxidative stress production (Yang et al., 2014). Topoisomerase II is an enzyme that is important for DNA transcription. Doxorubicin traps and stabilises the topoisomerase II complex after it has broken the DNA chain for replication, preventing the DNA double helix from being resealed thus stopping the process of replication (Kumar et al., 2014). Secondly, it intercalates into DNA at guanine base and form a DNA-doxorubicin adducts to prevent topoisomerase II's activity for DNA synthesis. Thirdly, doxorubicin contains a quinone structure which can readily be oxidised to semiquinone and formed reactive oxygen species when react with oxygen. The doxorubicin-induced release of oxidative radicals result in DNA damage, further contributing to its cytotoxicity (Kumar et al., 2014; Yang et al., 2014).

2.4.1.2 Alkylating agents

Alkylating agents refer to a group of cytotoxic drug which can attach an alkyl group to the guanine base of DNA, thereby imposing direct DNA damage to cancer cells. One classical example is the mustard gas that was used in World War I. Later

on, safer alternatives such as platinum-based agents were derived. For examples, cisplatin, carboplatin and oxaliplatin are the several drugs under this category, with cisplatin being the oldest and most potent agent amongst them. Platinum-based agents are commonly used to treat various cancer types, for instances, leukemia, multiple myeloma, hodgkin disease and sarcoma including breast, lung and ovary (Dasari and Tchounwou, 2014).

Upon entering the cells, cisplatin is activated at cytoplasm whereby chloride atoms on it are displaced by water molecule. It then becomes a potent electrophile that can attack nucleophiles on protein or DNA. Cisplatin can bind to the N7 reactive centre on the purine residues and cause DNA damage in cancer cells by crosslinking the purine bases. As such, the DNA repair mechanisms are triggered and apoptosis is induced (Dasari and Tchounwou, 2014).

2.4.1.3 Anti-metabolites

Anti-metabolites represent a group of anti-cancer agents that resemble to naturally occurring substances which can interfere with cell metabolism, for instance by interfering DNA and RNA synthesis. There a few examples of anti-metabolites namely 5-fluorouracil, 6-mercaptopurine, capecitabine, cytarabine and gemcitabine. These drugs are commonly used to treat leukemia, cancers in breast, ovary and colon. Notably, 5-fluorouracil remains a popular choice for treating colon cancer, therefore is selected for further review in the following paragraph (Mhaidat et al., 2014).

The 5-fluorouracil structure mimics an analogue of uracil by having a fluorine atom at the C-5 position instead of a hydrogen; it rapidly enters the cell using the same facilitated transport mechanism as uracil. There are two primary mechanisms of actions rendering the 5-fluorouracil's cytotoxicity. Intracellularly, 5-fluorouracil is converted to fluorouridine triphosphate and subsequently to fluorouridine triphosphate

by phosphorylation. The formation of fluorodeoxyuridine monophosphate inhibits thymidylate synthase, depleting intracellular levels of thymidine monophosphate and thymidine triphosphate, which are essential for DNA synthesis (Dobson et al., 2008). On the other hand, fluorouridine triphosphate is incorporated in RNA as a fraudulent nucleotide to inhibit RNA synthesis (Dobson et al., 2008). Not only that, the incorporation of 5-fluorouracil can result in toxicity to RNA at several levels including pre-RNA, mature RNA, tRNA, snRNA and pre-mRNA (Longley et al., 2003).

2.4.1.4 Mitotic inhibitors

Mitotic inhibitors are anti-cancer drugs that inhibit mitosis or cell division. Examples of the mitotic inhibitors are vinblastine, vincristine, and vinorelbine. These drugs are commonly used to treat lymphomas, myelomas, and leukaemia, breast and lung cancers. It was reported that vinblastine was able to induce higher oxidative DNA stress than vincristine and vinorelbine (Mhaidat et al., 2016).

Vinblastine is an alkaloid derived from Madagascar periwinkle plant, namely *Catharanthus roseus* (Thirumaran and Gilman, 2007). Vinblastine is known as a mitotic inhibitor because it binds to the building blocks of a protein called tubulin, inhibiting the assembly of tubulins into microtubules (that form mitotic spindles) (Sajó, 1977). These microtubules provide cells with both the structure and flexibility they need to divide and replicate. Without microtubules, cells cannot undergo cell division and eventually cell death would occur.

2.4.2 Challenges of chemotherapy

Despite being the central pillar of cancer treatments, chemotherapy is undeniably restricted by manifold limitations, such as poor selectivity, dose-associated toxicities and drug resistance.

Poor selectivity of chemotherapeutic drugs harms the actively growing normal cells as much as cancer cells. The fast-growing normal cells which are likely to be targeted by chemotherapy include blood-forming cells (in bone marrow), hair follicles and epithelial cells (in mouth, digestive tract and reproductive system). As a result, patients undergoing chemotherapy have been reported to experience anaemia, alopecia (hair loss due to medical treatment), nausea, loss of appetite, constipation and diarrhoea.

The more serious complications that may develop over time such as heart and kidney problems, nerves damage as well as infertility. For instance, dose-dependent cardiotoxicity remains as the major concern of oncologists for using doxorubicin in clinical practice. Excessive generation of reactive oxygen species is a primary mechanism leads to cardiac toxicity. As such, there is a lifetime cumulative dose limit for doxorubicin at 450-550mg/m^2 (Barrett-Lee et al., 2009). Not only that, toxic side effects for cisplatin are nephrotoxicity, hepatotoxicity, allergic reaction, decreased immunity, gastrointestinal disorders, haemorrhage and hearing loss in young patients (Dasari and Tchounwou, 2014). Due to high dose associated toxicity, chemotherapy is always given intermittently to allow the recovery of normal cells. During this time, surviving cancer cells may develop an acquired resistance to overcome the treatment.

The resistance remains one of the major hurdles in effective chemotherapy. Sometimes, recurrent cancer may develop multi-drug resistance (MDR) to a wide range of medicines which could be structurally or mechanistically distinct from the previous chemo-drugs, hampering the efficacy of subsequent salvage therapies. Commonly, the mechanisms of MDR involve a reduction of the drug concentration intracellularly due to high expression of efflux pumps (e.g., P-glycoprotein), enhanced drug-metabolising enzyme (e.g., glutathione S-transferase (GST)) and altered

expression of apoptosis-related proteins (AbuHammad and Zihlif, 2013; Bernig et al., 2016; Housman et al., 2014).

With reference to the abovementioned aspects, a more effective chemotherapy should focus on decreasing the dose and increasing the efficacy. As such, the side effects of chemotherapy could be reduced while cell death could be enhanced to reduce the risk of drug resistance development.

2.5 Vitamin E as a source for cancer treatment

Vitamin E is a group of fat-soluble and anti-oxidative compounds, consisting of two main groups of members, namely tocopherols and tocotrienols. The first discovery of Vitamin E happened in 1922 which was first identified as a dietary fertility factor in rats (Evans and Bishop, 1922). With respect to its function in fertility improvement, it was scientifically named as 'tocopherol', which was adapted from Greek words, *tokos* (childbirth) and *phero* (to bear). In 1938, the chemical structure of vitamin E was elucidated (Sen et al., 2006). For many years, α-tocopherol had been synonymous with vitamin E, until the discovery of tocotrienols in 1964 by Pennock and Whittle. Tocotrienol's contribution to human health was only discovered in the early 1980s for its cholesterol lowering properties (Qureshi et al., 1986), while the anti-cancer benefits were recognised during 1990s (Guthrie et al., 1997).

Structurally, the two groups of Vitamin E family members share a similar chromanol head and a side chain at the C-2 position (Figure 2.3). The major dichotomous between the two groups lies within the degree of saturation in the side chain; tocopherols contain a saturated phytyl tail whereas tocotrienols contain an unsaturated isoprenoid tail. Both of the Vitamin E groups exist in four isomeric forms, namely alpha-(α), beta-(β), gamma-(γ) and delta-(δ), depending on the position and number of methyl group in the chromanol head. Tocopherols exist mainly in

vegetables and nut, while tocotrienols are commonly found in oils extracts of rice bran, oil palm, annatto seeds and barley (Miyazawa et al., 2008; Yoshida et al., 2003). Tocotrienol-rich fraction (TRF) is the most commonly available form of vitamin E oral supplement containing a mixture of α-, β-, γ-, δ-tocotrienols and α-tocopherol.

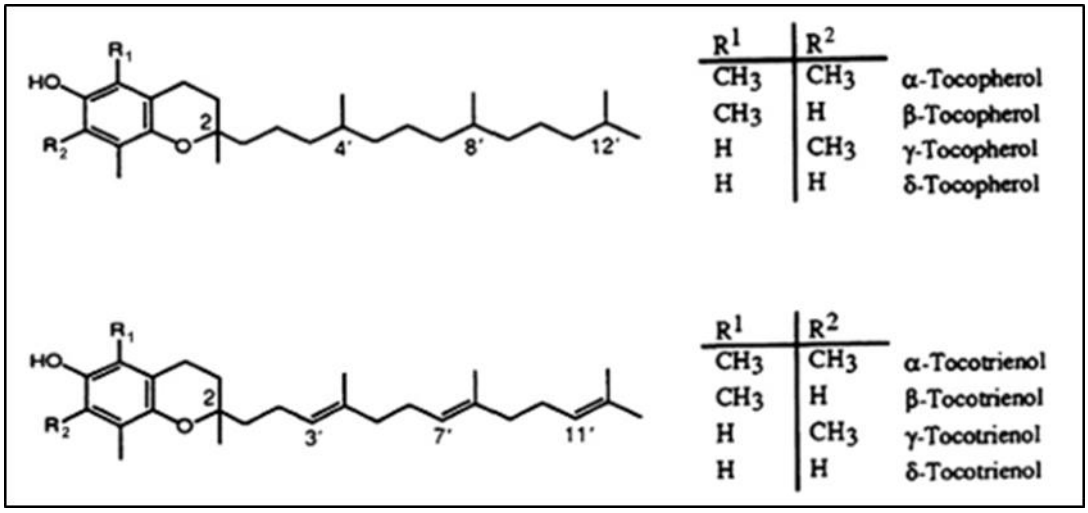

Figure 2.3 Structure of the Vitamin E analogues. Adapted from Miyazawa et al., (2008).

2.5.1 Tocotrienols are superior to tocopherols

The Vitamin E family members are well-known as powerful anti-oxidants. They exhibit anti-oxidative properties by donating hydrogen from the chromanol ring to neutralise free radicals (Peh et al., 2016). Of note, tocotrienols have been reported to offer superior anti-oxidant activity as compared to tocopherols. For instance, α-tocotrienol was reported to have 40-60 times greater potency than that of α-tocopherol in preventing lipid peroxidation in rat liver microsomal membrane (Serbinova et al., 1991) and 6-7 times greater activity in preventing cytochrome P-450 oxidative damage (Sylvester and Shah, 2005). It was proposed that the superiority of tocotrienols over tocopherol in terms of anti-oxidant properties could be due to several possible mechanisms: i) uniform distribution in the cell membrane lipid bilayer, ii) flexible

isoprenoid side chain that allows effective interaction with lipid radical, and iii) high chromanoxyl radical recycling efficiency as reviewed by Peh et al., (2016).

Other than anti-oxidative properties, tocotrienols were proven to be more superior to tocopherols in terms of cholesterol-lowering, neuroprotection, anti-inflammation and anti-cancer (Sailo et al., 2018; Sen et al., 2006). Several lines of evidence delineated that tocotrienols abrogated various cancer-promoting pathways involving cyclooxygenase (COX), nuclear transcription factor-kappa B (NF-κB) and signal transducer and activator of transcription factor 3 (STAT3), which are closely associated with inflammation (Nesaretnam and Meganathan, 2011).

Despite enormous potentials of tocotrienols in health promotion, publications of tocotrienols only made up of less than 3% out of those reported for tocopherols (Peh et al., 2016). Tocotrienols have started to gain attention after disappointment of α-tocopherol in two clinical trials, namely the Women Health Study (WHS) trial and the Selenium Vitamin E and Prostate Cancer Chemoprevention Trial (SELECT). Neither trial showed a significant effect of α-tocopherol against lung, breast and colon cancers in women and prostate cancer in men (Ye et al., 2015). Since then, different tocotrienol isomers have evoked more research attention recently, owing to their potential application as a non-toxic dietary anti-cancer agent.

2.5.2 Molecular targets and multi-targeted anti-cancer effects of tocotrienols

Both the tocopherols and tocotrienols are potent anti-oxidants; however, only tocotrienols are effective in inhibiting tumour growth and viability. The anti-cancer effect of tocotrienols was first discovered in a comparative study on biological activities of α-tocopherol, α-tocotrienol and γ-tocotrienol in tumour bearing mice (Komiyama et al., 1989). The studies showed that the tocotrienols were more effective against the transplantable murine tumours as compared to α-tocopherol. Subsequently

in a different study, it was discovered that palm oil intake inhibited carcinogen-induced mammary tumour (Nesaretnam et al., 1992). However, palm oil with tocotrienols stripped off did not exhibit the same protective effect, suggesting that the tocotrienols but not tocopherols in the palm oil are responsible for the growth inhibition of cancer (Nesaretnam et al., 1992). Since then, increasing attention has been given to anti-cancer benefits of tocotrienols. Herein, the molecular targets of tocotrienols elucidated from *in vitro* cancer cell lines (Table 2.3), anti-cancer outcomes from *in vivo* studies in mouse (Table 2.4) and human clinical trials (Table 2.5) were summarised.

Table 2.3 Exemplar *in vitro* studies for elucidating the molecular targets of tocotrienols-induced cell death. Adapted from Tham et al. (2019) and the cited references.

Cancer Type	Cell Line(s)	Molecular Target(s)	Reference(s)
Bladder	T24 5637 J82 UMUC-3	↑ p21, p27, Bax, caspase-3, cleaved PARP, SHP-1 ↓ cyclin D1, Bcl-2, Bcl-xL, Mcl-1, ETK phosphorylation, STAT3	(Ye et al., 2015)
Brain	U87MG	↑ caspase-8, Bid, cytochrome *c*, Bax	(Abubakar et al., 2016; Lim et al., 2014b)
Breast	MDA-MB-231	↑ caspase-8, caspase-9, caspase-7, caspase-3, cleaved PARP, DR5, DR4, p-JNK, p-c-Jun, p-p38, BiP, ATF3, ATF4, p-PERK, p-IRE1α, p-eIF2α, CHOP, LC3-II/I, Beclin-1, Bax, Profilin-1 ↓ NF-κB, cyclin D1, cyclin D3, CDK4, Bcl-2, PI3K, p-AKT, p-mTOR, XIAP, Serpine1, Cathepsin D	(Marchi et al., 2014; Patacsil et al., 2012; Ramdas et al., 2019; Tiwari et al., 2015; Wang et al., 2015b)
	MCF-7	↑ caspase-8, caspase-9, caspase-7, caspase-3, Bax, cleaved PARP, ATF3, BiP, CHOP, p-PERK, p-IRE1α, p-EIF2α, ATF4, LC3-II/I, Beclin-1, DR5, p-JNK, p-c-Jun, p-p38, MIC-1, EGR-1, and cathepsin D ↓ cyclin D1, cyclin D3, CDK4, NF-κB, Bcl-2, PI3K, p-AKT, p-mTOR	(Comitato et al., 2016, 2010; Park et al., 2010; Patacsil et al., 2012; Tiwari et al., 2013; Wang et al., 2015b)
	+SA	↑ LC3-II/I, Beclin-1, Bax, cleaved PARP, cleaved caspase-3 ↓ Bcl-2, PI3K, p-AKT, p-mTOR	(Tiwari et al., 2013)

	SKBR3	↓ p-ERK1/2	(Viola et al., 2013)
	MDA-MB-435	↑ cleaved PARP, p-JNK-1, JNK1, p-c-Jun, c-Jun, TGFβRII, TGFβRI	(Shun et al., 2004)
Cervix	HeLa	↑ Bax, cytochrome *c*, caspase-12, caspase-9, caspase-8, caspase-3, IL-6, XBP-1, p-IRE-1α, BiP, CHOP, XBP-1, cleaved PARP ↓ PCNA, cyclin D3, p16, CDK6	(Hasani et al., 2008; Wu and Ng, 2010; Xu et al., 2017; Yamasaki et al., 2014)
	CaSki	↑ p53, Bax, caspase-3 ↓ MEK-2, ERK	(Hasani et al., 2011, 2008)
Colon	HT29	↑ p21, Bax, caspase-9, caspase-3 ↓ Bcl-2, NF-κB p65, β-catenin, cyclin D1, c-Myc, survivin	(Shibata et al., 2010; Xu et al., 2009, 2012; Yang et al., 2010)
	SW620	↑ E-cadherin, PARP ↓ Wnt-1, β-catenin, cyclin D1, c-Jun, MMP-7, MMP-9, NF-κB, VGEF	(Husain et al., 2019; Zhang et al., 2013, 2011)
	HCT116	↑ p21, PARP, E-cadherin ↓ cIAP1, cIAP2, survivin, cyclin D1, c-Myc, MMP-9, VEGF, ICAM-1, CXCR4, NF-κB, β-catenin, vimentin	(Husain et al., 2019; Prasad et al., 2016; Shibata et al., 2010)
	DLD-1	↑ p21, p27, caspase-7, caspase-9 ↓ hTERT	(Eitsuka et al., 2016, 2006; Shibata et al., 2010)
Gastric	SGC-7901	↑ Bax, caspase-3, caspase-9, cleaved PARP ↓ Bcl-2, c-Myc, p-ERK1/2, Raf-1	(Sun et al., 2009, 2008)
	SNU-5	↓ NF-κB	(Manu et al., 2012)
	SNU-16	↑ cleaved PARP ↓ cyclin D1, Bcl-2, MMP-9, CXCR4, VEGF, NF-κB	(Manu et al., 2012)
Leukemia	ED40515	↑ caspase-3, caspase-6, caspase-7, caspase-9, PARP, Bcl-2, Bcl-xL, XIAP ↓ FDFT1, NF-κB	(Yamasaki et al., 2014)
	HL-60	↑ cleaved Bid, cytochrome *c* release, caspase-8, caspase-9, caspase-3	(Inoue et al., 2011)
	NB-4	↑ cleaved Bid, cytochrome *c* release, caspase-8, caspase-9, caspase-3	(Inoue et al., 2011)
Lung	A549	↑ caspase-3, caspase-8, Bid, cytochrome *c*, Bax, cleaved PARP ↓ Notch-1, Hes-1, Bcl-2, NF-κB, uPA, survivin, Bcl-xL, MMP-9	(Ji et al., 2012; Lim et al., 2014b;

			Rajasinghe et al., 2018)
	H520	↑ PARP, caspase-3 ↓ Notch-1, Hes-1, Bcl-2, NF-κB, survivin, Bcl-xL	(Rajasinghe et al., 2018; Rajasinghe and Gupta, 2017)
	H1299	↓ Notch-1, Hes-1, uPA, MMP-9	(Rajasinghe et al., 2018)
Pancreas	MIA PaCa-2	↑ E-cadherin, EGR-1, Bax, p27Kip1 ↓ NF-κB, Bcl-2, cIAP1, survivin, cyclin D1, c-Myc, COX-2, VEGF, MMP-9, ICAM-1, CXCR4, N-cadherin, vimentin, p-MEK, p-AKT, p-GSK-β	(Hodul et al., 2013; Husain et al., 2017; Kunnumakkara et al., 2010; Wang et al., 2015a)
	L3.6pl	↑ E-cadherin ↓ N-cadherin, vimentin, VEGF, MMP-9	(Husain et al., 2017)
	BXPC3	↑ p27Kip1 ↓ p-MEK, p-AKT, p-ERK	(Hodul et al., 2013)
	SW1990	↑ p27Kip1 ↓ p-MEK, p-AKT, p-ERK	(Hodul et al., 2013)
	PANC-1	↑ p21	(Eitsuka et al., 2014)
	Pancreatic cancer stem cell	↑ cleaved PARP ↓ Nanog, Sox-2, Oct-4, Notch-1, p-AKT, pERK	(Husain et al., 2017)
Prostate	PC-3	↑ caspase-9, cytochrome *c*, cleaved PARP, LC3-II, CHOP, p-eIF2α, ATF4, BiP, IRE1α, p62, p-JNK, p38 ↓ p-Akt, β-catenin, Id-1, Bcl-2, Angiopoietin-1	(Fontana et al., 2019; Jiang et al., 2012; Tang et al., 2019; Yap et al., 2008)
	PC-3 (stem cell-like)	↑ caspase-3, cleaved PARP ↓ Id-1	(Luk et al., 2011)
	LNCaP	↑ caspase-9, caspase-8, caspase-7, caspase-3, cytochrome *c*, cleaved PARP, LC3-II ↓ Id-1, p-Akt	(Jiang et al., 2012; Yap et al., 2008)
	DU145	↑ CHOP, p-eIF2α, ATF4, BiP, IRE1α, p-JNK, p38	(Fontana et al., 2019)
Skin	G361	↑ cleaved PARP, caspase-7, caspase-9, caspase-3, E-cadherin, β-catenin, γ-catenin ↓ Snail, vimentin, α-SME, Twist	(Chang et al., 2009)
	C32	↑ cleaved PARP, caspase-7, caspase-9, caspase-3, IκB, p-ATF2, p-c-Jun, p-SAPK/JNK	(Chang et al., 2009)

		↓ PI3K p85, p-IKKα/β, IκBα/β, NF-κB p65, EGFR, Id-1, Id-3	
	A375 (stem cell-like)	↓ ABCG2	(Marzagalli et al., 2018)
	BLM	↑ caspase-3, caspase-4, cleaved PARP, Bax, BiP, PERK, p-eIF2α, IRE1α, ATF4, CHOP ↓ Bcl-2	(Marelli et al., 2016)
	A375	↑ caspase-3, caspase-4, cleaved PARP, BiP, PERK, p-eIF2α, IRE1α, ATF4, CHOP, ERO1α ↓ Bcl-2, CDK4, Ras, caspase-3	(Fernandes et al., 2010; Marelli et al., 2016)
	A2058	↓ CDK4, Ras, caspase-3	(Fernandes et al., 2010)
	B16	↑ p-ERK ↓ Tyrosinase, MC1R, MITF, TYRP-1, TYRP-2, p-p38	(Ng et al., 2014)

Note: ↑ upregulation; ↓ downregulation; p-, phosphorylated state

Abbreviations: ABCG2, ATP-binding cassette subfamily G member 2; Akt, or PKB, protein kinase B; ATF, activating transcription factor; ATP, adenosine triphosphate; Bcl-xL, B-cell lymphoma-extra large; BiP, or GRP78, glucose-regulated protein; CDK, cyclin-dependent kinase; CHOP, CCAAT-enhancer-binding protein homologous protein; cIAP, cellular inhibitor of apoptosis; COX-2, cyclooxygenase-2; CXCR4, C-X-C motif chemokine receptor 4; DR, death receptor; EGR, early growth response; eIF2-α, eukaryotic initiation factor 2 alpha; ERK1/2, extracellular signal-regulated protein kinase 1/2; ERO1α, endoplasmic reticulum oxidation 1; ETK1, epithelial and endothelial tyrosine kinase; FDFT1, farnesyl-diphosphate farnesyltransferase 1; GSK-β, glycogen synthase kinase 3 beta; Hes-1, hairy and enhancer of split-1; hTERT, human telomerase reverse transcriptase; ICAM-1, intercellular adhesion molecules-1; Id-1, inhibitor of differentiation/DNA binding; IκBα/β, inhibitor of kappa B alpha/beta; IKKα/β, IκB kinase alpha/beta; IL-6, interleukin 6; IRE-1, inositol-requiring enzyme 1; JNK, c-Jun N-terminal kinase; LC3, microtubule-associated protein 1A/1B-light chain 3; MC1R, melanocortin 1 receptor; Mcl-1, myeloid cell leukemia 1; MEK, mitogen-activated protein kinase; MIC-1, macrophage inhibitory cytokine 1; MITF, melanogenesis associated transcription factor; MMP, matrix metalloproteinases; mTOR, mammalian target of rapamycin; NF-κB, nuclear factor kappa B; Oct-4, octamer-binding transcription factor 4; p27Kip1, cyclin-dependent kinase inhibitor 1B; p62, ubiquitin-binding protein p62; PARP, poly(ADP-ribose) polymerase; PCNA, proliferating cell nuclear antigen; PERK, PKR-like ER-localized eIF2α kinase; PI3K, phosphoinositide 3-kinase; ROS, reactive oxygen species; SAPK/JNK, stress-activated protein kinase/c-Jun NH2-terminal kinase; Sox-2, sex determining region Y-box 2; TGF-β1, transforming growth factor beta 1; TYRP, tyrosinase-related proteins; VEGF, vascular endothelial growth factor; uPA, urokinase-type plasminogen activator; Wnt, wingless/integrase; XBP, X-box binding protein; XIAP, X-linked inhibitor of apoptosis protein; α-SMA, alpha-smooth muscle actin.

Table 2.4 Exemplar *in vivo* studies of tocotrienols for various cancer treatments using mouse models.

Cancer Type	Tocotrienol(s)	Anti-cancer Effect(s) / Molecular Target(s)	Reference(s)
Colon	δT3	δT3 significantly inhibited the formation of colorectal polyps by 70% and colorectal cancer by almost 99% in azoxymethane-induced colorectal carcinogenesis model.	(Husain et al., 2019)
	TRF or δT3-enriched diet	δT3-enriched diet decreased the number of colorectal tumours in an animal model, but not in TRF-fed group. δT3-enriched diet suppressed COX-2 protein levels in colorectal mucosa.	(Wada et al., 2017)
	TRF	TRF inhibited xenografts in mice by a regulation of Wnt pathways. TRF increased expression of Wnt pathways related factors, i.e., Axin-2, GSK-3β, APC and decreased the protein expression of Wnt-1, β-catenin and β-catenin target genes, i.e., *cyclin D1*, *c-Myc* and *survivin* in the xenografts.	(Zhang et al., 2015)
Gastric	γT3	γT3 inhibited > 50% of tumour growth. γT3 downregulated microvessel density indicator CD31. γT3 downregulated NF-κB and NF-κB-regulated cyclin D1, COX-2, survivin, Bcl-xL, XIAP, ICAM-1, MMP-9 and VEGF.	(Manu et al., 2012)
Pancreas	γT3	γT3 inhibited cancer cell proliferation in tumour tissues. γT3 inhibited constitutive activation of NF-κB. γT3 significantly downregulated the expression of proinflammatory marker COX-2, suppressed the expression of invasion biomarker MMP-9, and inhibited the angiogenic biomarker VEGF in the tissues. γT3 reduced Bcl-2, cIAP1, CXCR4, NF-κB, c-Myc.	(Kunnumakkara et al., 2010)
	δT3	δT3 inhibited pancreatic tumour growth and metastasis. δT3 inhibited epithelial-to-mesenchymal transition in pancreatic tumours as E-cadherin was	(Husain et al., 2017)

		upregulated, N-cadherin, vimentin, VEGF, MMP-9 and CD44 were downregulated. δT3 inhibited cancer cell proliferation and increased cleaved caspase-3.	
	δT3	δT3 inhibited cancer cell proliferation, decreased phosphorylated MAPK expression and induced expression of p27Kip1.	(Hodul et al., 2013)
	δT3	δT3 significantly enhanced the survival of mice. δT3 decreased levels of p-AKT, p-MEK, p-ERK, NF-κB and Bcl-xL and increased levels of p27Kip1, Bax, CK18 and activated caspase-3.	(Husain et al., 2013)
Prostate	γT3	γT3 inhibited tumourigenicity of PC-3 cells in mice.	(Luk et al., 2011)
	γT3	γT3 inhibited xenograft growth in nude mice.	(Jiang et al., 2012)
	γT3	γT3 inhibited the growth of xenograft. γT3 reduced PCNA, Ki-67 and Id1 in tumour tissues. γT3 increased cleaved PARP and cleaved caspase-3. γT3 increased expression levels for the tumour suppressor gene (*E-cadherin*) and its repressor (Snail).	(Yap et al., 2010a)
	Tocomin	Mixed-tocotrienols (Tocomin)-fed groups had a lower incidence of tumour formation. Tocomin significantly reduced the levels of high-grade neoplastic lesions. Tocomin associated with modulating cell cycle regulatory proteins and increasing expression of pro-apoptotic proteins.	(Barve et al., 2010)
Skin	δT3	δT3 treatment disabled the formation of melanospheres completely in mice.	(Marzagalli et al., 2018)
	δT3	δT3 inhibited the growth and progression of melanoma xenografts in nude mice.	(Marelli et al., 2016)

Despite several completed clinical trials were recorded in ClinicalTrials.gov website, only three clinical trials outcomes were published. All the three clinical trials reported positive effects for using tocotrienols for combined treatment. The first

clinical trial that involved 248 women showed that TRF in combination with tamoxifen improved breast-cancer-specific survival compared to the tamoxifen group (NCT01157026) (Nesaretnam et al., 2010). The second clinical trial conducted on pancreatic ductal neoplasia patients reported that δ-tocotrienol was well tolerated by patients at 200-1600mg/day for two weeks. The δ-tocotrienol was able to achieve bioactive level in blood and caused an elevated caspase-3 activity in the tumour samples, suggesting an enhanced apoptosis due to δ-tocotrienol intervention (NCT00985777) (Springett et al., 2015). A recent clinical study on recurrent ovarian cancer patients with δ-tocotrienol and bevacizumab demonstrated a prolonged lifespan without negative influence on quality of life (Thomsen et al., 2019). Of note, a number of clinical trials are currently in progress to study the anti-cancer effects of tocotrienols and/or in combination with other therapeutic agents (Table 2.5). These studies could provide a better understanding of clinical applications of tocotrienols with optimal benefits.

Table 2.5 Recent clinical trials conducted using tocotrienols for various cancer treatments.

Cancer Type	Target Application(s) of Tocotrienols	Drugs Involved	Phase: Status	ClinicalTrials.gov Identifier
Breast	Adjunct cancer treatment	TRF and Tamoxifen	Pilot trial: Completed in 2010	NCT01157026
	Health supplement	Gamma-Delta Tocotrienols and TRF	1: Completed in 2013	NCT01571921
	Neoadjuvant treatment	Epirubicin, Cyclophosphamide, Docetaxel, Paclitaxel, Trastuzumab, Pertuzumab and Tocotrienols	2: Ongoing	NCT02909751
Colon	Adjunct cancer treatment	Irinotecan, Oxaliplatin, Calcium Folinate, 5-	2: Ongoing	NCT02705300

		Fluorouracil and Tocotrienols		
Lung	Adjunct cancer treatment	Cisplatin, Vinorelbine, Carboplatin and Tocotrienols	3: Ongoing	NCT02644252
Ovary	Adjunct cancer treatment	Bevacizumab and Tocotrienols	2: Completed in 2018	NCT02399592
	Cancer treatment	Cabazitaxel and / or Tocotrienols	2: Ongoing	NCT02560337
Pancreas	Cancer treatment	δT3	1: Completed in 2016	NCT00985777
	Health supplement	δT3	1: Completed in 2016	NCT01450046
	Health supplement	δT3	1: Completed in 2016	NCT01446952

Note: Examples of clinical studies that are registered at https://clinicaltrials.gov showing status as accessed on 29th May 2019.

Having known that tocotrienols are capable of affecting enormous molecular targets, the underlying anti-cancer signalling pathways with respect to cancer hallmarks are hence presented. The anti-cancer properties of tocotrienols are found to be associated with multifaceted mechanisms such as anti-proliferation, apoptosis, anti-angiogenesis and anti-invasion.

2.5.2.1 Anti-proliferation

In cancer, the cell proliferation mechanism is subverted in such a way that the mitogenic signalling is hyperactive, leading to uncontrolled cell population expansion. For instance, the epidermal growth factor receptor (EGFR), namely ErbB receptor tyrosine kinases are overexpressed in some cancers. The ErbB receptors then signal through mitogenic pathways such as MAPK cascade consisting extracellular receptor kinase (ERK), c-Jun N-terminal kinase (JNK) or p38. Other signalling pathways such

as PI3K/Akt and Janus kinase (JAK)/ signal transducer and activator of transcription (STAT) could also be intricately related to proliferation.

A study revealed that TRF did not reduce the level of ErbB receptor in preneoplastic CL-S1 mouse mammary epithelial cells, but targeted at post-receptor event involving cyclic adenosine monophosphate (cAMP) production. As a result, the activation of downstream mitogenic signallings (PI3K/Akt and MAPK) were reduced, as evidenced by reduction in activated Akt and ERK1/2 (Sylvester et al., 2002).

On the contrary, another study found that the anti-proliferative effects of γ-tocotrienol on neoplastic +SA mouse mammary epithelial cells were associated with the reduction in ErbB3 (but not ErbB1 or ErbB2) receptor tyrosine phosphorylation, subsequently leading to a reduced PI3K/ phosphoinositide-dependent protein kinase-1(PDK-1)/Akt mitogenic signalling (Samant and Sylvester, 2006). Other than blocking ErbB receptor tyrosine kinase activation, γ-tocotrienol was reported to inhibit Met receptor tyrosine kinase activation in +SA cells via downregulation of Met expression at both transcriptional and post-transcriptional levels (Ayoub et al., 2011). It was later discovered that the anti-proliferative effect of γ-tocotrienol on mouse +SA and human MCF-7 mammary was directly associated with suppression of c-Myc, resulting from the increment in GSK-3a/b-dependent ubiquitination and degradation. Correspondingly, the reduction of Myc decreased in PI3K/Akt/mTOR and Ras/ mitogen-activated protein kinase kinase (MEK)/ERK mitogenic signalling (Parajuli et al., 2015a).

In pancreatic cancer cells, γ- and δ-tocotrienols were reported to disturb cancer cell proliferation via both PI3K/Akt and ERK/MAPK pathways (Shin-Kang et al., 2011). The tocotrienols caused a reduction in phosphorylated Akt and upregulation of c-Jun. The suppression of Akt led to downregulation of p-GSK-3β and upregulation

accompanied by nuclear translocation of Foxo3. On the other hand, a reduction in total ERK and phosphorylated ERK was observed after treatment with γ- and δ-tocotrienols. The authors found that activation of PI3K/Akt and ERK/MAPK pathways were mediated by a downregulation of Her2/ErbB2 expression at post-transcriptional level (Shin-Kang et al., 2011).

Mitogen-dependent cell cycle regulation is another crucial part of cell proliferation. It is a series of tightly-controlled events to prepare for cell division. There are several checkpoints when a cell progresses from G1 to G2/M phase of the cell cycle, which are regulated by cyclin-dependent kinases (CDKs) and cell-dependent kinases inhibitors (CDKIs). To further illustrate, cyclin D and E expressions are increased during early G1. Then, cyclin F activates CDK4/6 complex while cyclin E activates CDK2. These cyclin/CDK complexes phosphorylate to inactivate the cell cycle restriction protein, i.e., Rb protein. As a result, E2F transcription factors are released and cause the transcription of genes required for cell cycle progression from G1 to S. On the other hand, p21 and p27 are CDKIs that inactivate cyclin/CDK complexes to block cell cycle progression (Parajuli et al., 2015b). Evidence showed that γ-tocotrienol significantly diminishes cyclin D1, CDK4, CDK2 and CDK6 levels and elevates the p27 protein expression. The study has suggested that the potential anti-proliferative effect of γ-tocotrienol could induce G1 cell cycle arrest (Samant et al., 2010). Correspondingly, CDK4, cyclin D1, phosphorylated Rb, and E2F1 were reduced while p27 increased in +SA and MCF-7 mammary tumour cells after γ-tocotrienol treatment. Likewise, the anti-cancer effect of TRF in prostate cancer cells was also found to associate with cell cycle arrest at G0/G1 phase (Srivastava and Gupta, 2006). On the other hand, δ-tocotrienol induces G1 cell cycle arrest in pancreatic cancer cells (Shin-Kang et al., 2011) and melanoma

cells (Fernandes et al., 2010). Lim et al. (2014a) reported G0/G1 cell cycle arrest of A549 lung and U87MG brain cancer cells after individually treated with δ- and γ-tocotrienols. The arrest was postulated to be induced by the suppression of cyclin D1, the key regulator of the G1 to S phase progression, partly if not all (Wada, 2009). Of note, tocotrienols showed no effect on the cell cycle of normal cells (Wada, 2009).

2.5.2.2 Apoptosis

Tocotrienols have been shown to initiate apoptosis via both intrinsic and/or extrinsic pathway(s) of apoptosis, depending on cancer cell types. TRF induced apoptosis via mitochondria-mediated mechanism through activation of caspase-9 and increased Bax/Bcl-2 ratio in RKO human colon carcinoma cell line (Agarwal et al., 2004). Similarly in SKBR3 human breast cancer cell line, δ-tocotrienol was reported to induce reactive oxygen species (ROS) generation, downregulation of Bcl-2 and disruption of mitochondrial membrane potential, collectively supportive to the involvement of redox-dependent activation of the intrinsic pathway of apoptosis (Viola et al., 2013).

On the other hand, the involvement of the extrinsic pathway of apoptosis was either death receptor independent, or, coupled to the intrinsic pathway. For instance, γ-tocotrienol caused caspase-8 activation with a decrease in FLICE-inhibitory protein (FLIP) level, which is an anti-apoptotic protein that negatively regulates caspase-8 activation. However, the study showed that the caspase-8 activation was independent of death receptor apoptotic signalling in +SA cells (Shah and Sylvester, 2004). In A549 lung and U87MG brain cancer cells, δ- and γ-tocotrienols were reported to cause apoptosis via caspase-8 activation coupled to the disturbance of mitochondrial potential, suggesting engagement of both apoptotic pathways (Lim et al., 2014a). Correspondingly in Hep3B human hepatoma cells, γ-tocotrienol elevated the activities

of caspase-8, -9, -3 and accompanied by the upregulation of truncated Bid, Bax and PARP cleavage, proving a concurrent activation of intrinsic and extrinsic pathways (Sakai et al., 2006). In addition, co-elicitation between intrinsic pathway by inducing Ca^{2+} release, loss of mitochondrial membrane potential and increase in Bax/Bcl-2 ratio, and extrinsic pathway via upregulating surface expression of Fas and FasL in γ-tocotrienol-treated human T-cell lymphoma (Jurkat cells) was reported. Eventually, apoptosis was induced via the activation of caspase-8, -9, and -3 and PARP cleavage (Wilankar et al., 2011).

2.5.2.3 Anti-angiogenesis

Angiogenesis is a process of new blood vessels formation from pre-existing vessels. In the context of cancer, this process is crucial for transporting blood-borne nutrients to the tumour for its growth and survival (De Silva et al., 2016). *In vitro*, δ-tocotrienol inhibited the stimulatory effects of colorectal adenocarcinoma (DLD-1) on human umbilical vein endothelial (HUVEC) tube formation and migration (Miyazawa et al., 2008). To further elaborate, the inhibition of HUVEC adhesion was partly related to ROS generation in HUVEC (Miyazawa et al., 2008). Besides, δ-tocotrienol also significantly hindered *in vivo* tumour angiogenesis via the inhibition of endothelial cell invasion and neovessel formation (Miyazawa et al., 2008). γ-tocotrienol-inhibited angiogenesis in HUVECs was reported to associate with the downregulations of β-catenin, cyclin D1, CD44, phospho-VEGFR-2 and MMP-9 which has thus suggested a regulation of Wnt signalling (Li et al., 2011).

2.5.2.4 Anti-invasion and anti-metastasis

Metastasis begins with the local invasion that tumour cells adhere to the adjacent cells and extracellular matrix (ECM), followed by the proteolytic degradation

of basement membrane for permitting the invasion into vessels. Hence, preventing cell adhesion and membrane degradation represent prospective approaches for suppressing tumour invasion and metastasis. It was reported that γ-tocotrienol caused a dose-dependent inhibition of human gastric cancer cells attachment to fibronectin and laminin, the principal constituents of the ECM (Liu et al., 2010). Furthermore, γ-tocotrienol-treated prostate cancer cells also led to the suppression of mesenchymal markers and restoration of E-cadherin and γ-catenin expression, which was associated with the suppression of cell invasion capability (Yap et al., 2008). Another study conducted on human gastric adenocarcinoma SGC-7901 cell line reported that γ-tocotrienol caused a significant reduction in invasion capability through the downregulation of MMP-2 and MMP-9 and upregulation of tissue inhibitor of metalloproteinase-1 (TIMP-1) and TIMP-2, suggesting a potential γ-tocotrienol-mediated anti-metastasis activity (Liu et al., 2010).

2.5.3 Benefits of combined treatment with tocotrienols

Combination therapy is defined as a disease treatment involving two or more drugs to achieve the desired efficacy with lower doses or lower toxicity of drugs; chemosensitise cells so that an additional compound can be more potent, gain additive or synergistic effects; or combat expected acquired resistance or minimise the possibility for development of drug resistance (Karjalainen and Repasky, 2016). It is a promising approach whereby two or more drugs with compatible and complementary mode of actions are combined to give a beneficial synergy or additive effect (Mokhtari et al., 2017). Moreover, a synergistic combination would be able to (i) reduce the effective dose of the drugs without compromising the effectiveness, (ii) lessen the risk of adverse reaction associated with single high dose treatment, (iii)

target cancer stem cells, and (iv) lower the risk of drug resistance (Bell, 2013; Chang et al., 2017).

In fact, combined treatments with tocotrienols have been widely conducted previously. The reported benefits include (but not limited) modulating the apoptosis, reducing the side effects, targeting the cancer stem cells and activating chemosensitisation thereby inferring a prospective therapeutic avenue towards an enhanced treatment.

2.5.3.1 Modulation of apoptosis sensitivity

Cellular response towards apoptosis dictates a successful therapeutic outcome of a therapy. In fact, apoptosis commitment relies on a balance between pro-apoptosis and anti-apoptosis signals that make up the apoptotic threshold. In an analogy, pro-apoptosis signals can be regarded as an 'acceleration pedal' while anti-apoptosis signals as 'brake pedal'. For apoptosis to take place, the acceleration pedal must be engaged while the brake pedal disengaged. A comparative magnitude between the pro-death and pro-survival signals would dictate the degree of apoptosis.

Several studies demonstrated that tocotrienols combination treatment leads to the enhanced cell death via apoptosis. For instance, a combined treatment of tyrosine kinase inhibitors (erlotinib and gefitinib) with γ-tocotrienol resulted an enhanced apoptosis as demonstrated by more prominent expression in caspase-3 and cleaved PARP (Bachawal et al., 2010a). Combined treatment of δ-tocotrienol with jerantinine B induced a synergistic apoptosis via enhanced caspase-8 and caspase-3 activations in U87MG glioblastoma and HT29 colorectal adenocarcinoma (Abubakar et al., 2016). *In vivo*, combined treatment of γ-tocotrienol with capecitabine showed a prominent reduction in tumour volume. The xenografted-tumour treated with combined treatment showed the lowest expressions of anti-apoptotic proteins, including cIAP1, cIAP2,

Bcl-2, Bcl-xL and survivin, has suggested that apoptosis is enhanced as a result of the reduction in apoptotic threshold (Prasad et al., 2016).

2.5.3.2 Reducing side effects of the treatment

Conventional chemotherapeutic drugs remain as a mainstay in current cancer treatment modalities. However, those drugs could cause detrimental side effects on the patients who receive the drugs. Some of the side effects can be life-threatening. For example, cardiotoxicity could lead to heart failure in patients receiving doxorubicin. Hence, novel approaches are imperative to cope with the side effects being generated during chemo-treatment.

A study demonstrated that hepatocyte-targeted nanoparticles consisting of epirubicin when co-administrated with tocotrienols, exhibited both anti-tumour activity and higher protection against oxidative stress and inflammation as compared to epirubicin nanoparticle alone in mice. The cardioprotection function was found to associate with a decrease in glutathione and superoxide dismutase levels as well as the thiobarbituric acid reactive substances (TBARS), nitrate/nitrite and tumour necrosis factor alpha (TNF-α) (Nasr et al., 2014). Another studies showed that γ-tocotrienol prevents 5-fluorouracil-induced ROS production in human oral keratinocytes through the activation of nuclear factor erythroid 2-related factor 2 (Nrf2), suggesting that the combined treatment could improve mucositis, the side effect of 5-fluorouracil treatment (Takano et al., 2015). Therefore, combined treatment could be feasible to alleviate the side effects and is hoped to improve patient performance during chemotherapy.

2.5.3.3 Targeting cancer stem cell population

Characterized by high CD44+ surface receptor, cancer stem cells are a subpopulation of cancer cells sharing similar characteristics as normal stem cells such as self-renewal and multi-lineage differentiation (Ayob and Ramasamy, 2018). The cancer stem cells can remain in quiescent and toxic exclusion (efflux). Due to its high resistant nature, it represents a crucial player in metastasis and recurrence. Challengingly, most of the conventional cancer treatments only target at debulking the tumour while leaving behind cancer stem cells which could potentially contribute to the cancer recurrence.

Promising research outcome reported that γ-tocotrienol could serve as an effective agent in targeting prostate cancer stem cell-like population (Luk et al., 2011). In addition, γ-tocotrienol inhibited colon and cervical mammospheres and spheres formation in a dose-dependent manner (Gu et al., 2015). Further analysis showed that γ-tocotrienol targets tyrosine phosphatase SHP2 and causes cell death via RAS/ERK pathway (Gu et al., 2015). More recently, δ-tocotrienol was reported to target melanoma stem cells (Marzagalli et al., 2018). Gopalan et al. (2013) showed that a combination of simvastatin and γ-tocotrienol can eliminate drug resistant breast cancer stem-like cells via the suppression of STAT-2 signalling mediators. Another study of combining γ-tocotrienol with simvastatin successfully eliminated breast cancer stem-like cells via the suppression of STAT-3 signalling (Gopalan et al., 2013).

2.5.3.4 Chemosensitisation

By definition, chemosensitisation means a process in which a previously ineffective chemotherapeutic drug is enhanced to become effective treatment by altering the susceptibility of a tumour. It is a strategy to overcome drug resistance by

enhancing the activity of another through the modulation of one or more mechanisms of resistance. In fact, using dietary agents to sensitize tumours to the chemotherapeutics remains one of the possibilities since natural products render attractive properties such as multiple targeting, relatively low toxicity and immediate availability (Gupta et al., 2011).

One of the promising criteria of opting tocotrienols to combine with chemotherapeutic drugs is its ability to chemosensitise the tumour cells to the chemo-treatment. It was reported that δ-tocotrienol induces chemosesitisation through the inhibition of STAT3 pathway in human bladder cancer cell (Ye et al., 2015). In the study, bladder cancer cells co-treated with δ-tocotrienol and low-dose gemcitabine exhibited an enhanced apoptosis with decreased colony formation capacity and induction of Bax, proving that the presence of δ-tocotrienol has potentiated the apoptotic effect.

Moreover, γ-tocotrienol sensitises gastric cancer to capecitabine *in vitro* and in a xenograft mouse model (Manu et al., 2012). The study showed that γ-tocotrienol potentiated the apoptotic effects of capecitabine by inhibiting the activation of NF-κB and suppressed its regulated gene expressions such as COX-2, cyclin D1, Bcl-2, C-X-C Motif Chemokine Receptor 4 (CXCR4), VEGF and MMP-9. Additionally, the combination of γ-tocotrienol and capecitabine at minimal doses showed an enhanced apoptosis.

On the other hand, a combination of γ-tocotrienol and celecoxib synergistically inhibited the growth of neoplastic +SA mouse mammary epithelial cells mediated by COX-2-dependent mechanism (Shirode and Sylvester, 2011). The combination resulted in a significant reduction of COX-2 expression as compared to either agent

alone, suggesting COX-2 could be a factor of sensitising the cancer cells to cancer drugs.

Combination of γ-tocotrienol and statin treatments synergistically acted on anti-proliferative mechanism with a large reduction in MAPK, JNK, p38 and Akt intracellular levels (Wali and Sylvester, 2007). Triple combination study of atorvastatin, γ-tocotrienol and celecoxib also showed that human colon cancer HT29 and HCT116 exhibited a synergism via the induction of G0/G1 phase cell cycle arrest and apoptosis (Yang et al., 2010).

Taken together, these evidences have suggested that tocotrienols could be a chemosensitiser to cancer drugs via various mechanisms including STAT3, NF-κB, COX-2, MAPK, JNK, and p38 signalling pathways. Notably, while many studies have reported the benefits of γ-tocotrienol combined treatments, only a few studies were reported in δ-tocotrienol (Table 2.6). The anti-cancer effect of δ-tocotrienol is comparable to even more potent that γ-tocotrienol (Husain et al., 2019; Kaneko et al., 2018; Nesaretnam et al., 2012; Pierpaoli et al., 2010). Therefore, this underlines the importance of the study on the unexplored potential of δ-tocotrienol in the combined treatments of current research.

2.5.4 Challenges of tocotrienols

Despite the promising anti-cancer effects of tocotrienols, poor oral bioavailability remains the main hurdle which limits the therapeutic efficacy *in vivo*. The initial tissue distribution via α-tocopherol transfer protein (α-TPP) in the liver represents the major obstacle (Aykin-Burns et al., 2019; Sen et al., 2006). This hepatic protein has a higher affinity for tocopherols than tocotrienols as the unsaturated isoprenoid side chains obstruct the binding pocket of α-TPP. The binding affinity of α-tocotrienol to α-TTP is 8.5-fold lower than α-tocopherol (Hosomi et al., 1997). The

saturable uptake in the transport mechanism within intestine and bloodstream has therefore conferred low bioavailability, leading to compromised efficacy and potency of tocotrienols via oral intake (Sen et al., 2006).

Additionally, it has been widely reported that the administration of high dose tocotrienols is a futile manoeuvre due to high metabolic degradation *in vivo* (Abubakar et al., 2018). Prominently, the hypomethylated forms of tocotrienols, i.e., δ-tocotrienol and γ-tocotrienol, show the highest cellular metabolism. The high metabolism of tocotrienols is associated with the induction of drug metabolizing enzymes, such as CYP450 cytochrome and glucuronosyltransferase 1A1 (UGT1A1) as well as the induction of multidrug resistance protein-1 (MDR1) via pregame-X-receptor (PXR) and steroid and xenobiotic receptor (SXR). These enzymes appear to deliver positive cytotoxic effects to cancer cells; however, co-administration of high dose tocotrienols with other drugs may potentially interfere the metabolism, thereby affecting the therapeutic efficacy of these drugs (Brigelius-Flohé, 2005; Viola et al., 2012; Zhou et al., 2004).

Based on the above-mentioned challenges, it is plausible to propose that synergistic combinations of tocotrienols with other anti-cancer agents at low doses can augment the therapeutic efficacy and potency (both bioactives) as well as reduce the dose-limiting toxicities (i.e., chemotherapeutic agents). Moreover, a combined treatment approach could potentially reduce the risk of developing drug resistance in cancer cells. As "one drug one target"-based targeted therapy (e.g., tyrosine kinase inhibitors) is inclined to drug resistance (Chen and Zhang, 2015), the combinatorial application of tocotrienols that concurrently targets multiple signalling pathways deemed a viable approach to effectively eradicate cancer cell population (Melisi et al., 2013).

Table 2.6 Drug combinations studies of tocotrienols.

Types of cancer	Types of tocotrienols	Combined agents	Study cell line/ model	Effects	Reference
Bladder Cancer	δT3	Gemcitabine	T24 5637	Low concentration of δT3 (25μM) enhanced the anti-cancer effects of gemcitabine via reducing cell growth, increase apoptosis and inhibit STAT3 activation.	(Ye et al., 2015)
Breast Cancer	δT3	Curcumin	MCF-7	The δT3/curcumin nanoemulsion showed superior cytotoxicity, suppressed constitutive NF-κB activation and significantly induced apoptosis.	(Steuber et al., 2016)
	γT3	Docosahexaenoic acid (DHA)	MDA-MB-231 SUM 159 SUM 149	The combined treatment significantly reduced mammosphere formation, upregulated SHP-1 protein and suppressed STAT3 signalling.	(Xiong et al., 2016)
	γT3	Oridonin	+SA	The combined treatment synergistically induces autophagy with suppression Akt/mTOR mitogenic signalling and corresponding increase in apoptosis.	(Tiwari et al., 2015)
	γT3	PPARγ antagonist	+SA	The anti-cancer effect is associated with a mediated through PPAR γ -independent mechanisms via downregulation in COX-2, PGDS, and PGD2 synthesis.	(Malaviya and Sylvester, 2014)
	γT3	Met inhibitor (SU11274)	+SA MCF-7 MDA-MB-231	The combined treatment induced synergistic inhibition of cell growth, reduction in Akt STAT1/5 and NFκB activation and suppression of epithelial-to-mesenchymal transition.	(Ayoub et al., 2013)

	γT3	Sesamin	+SA MCF-7 MDA-MB-231	Combined treatment with sub-effective doses of γT3 and sesamin was found to induce synergistic anti-proliferation in a cytostatic, not cytotoxic effect, via G1 cell cycle arrest.	(Akl et al., 2013)
	γT3	PPARγ antagonist (GW9662 or T0070907)	MCF7 MDA-MB-231	Combined low-dose treatment of γT3 and PPARγ antagonists act synergistically to inhibit cell proliferation, mediated through reduction in PPARγ expression and corresponding decrease in PI3K/Akt mitogenic signalling	(Malaviya and Sylvester, 2014)
	γT3	Simvastatin	Doxorubicin resistant MCF-7 Tamoxifen resistant MCF-7	Combination of simvastatin and γT3 at low doses enhanced the suppression of STAT3 signalling via the inhibition of mevalonate pathway to eliminate cancer stem-like cells.	(Gopalan et al., 2013)
	γT3	Sesamin	+SA	The combined treatment of sub-effective doses of γT3 and sesamin caused a synergistic inhibition of cancer cell growth, which is associated with the suppression of EGF-dependent mitogenic signalling.	(Akl et al., 2012)
	γT3	Met inhibitor (SU11274)	+SA	Combined treatment with sub-effective doses of γ-tocotrienol and SU11274 resulted in significant inhibition of cancer cells in a cytostatic manner with a reduction in Met signalling.	(Ayoub et al., 2011)

	γT3	Celecoxib	+SA	The synergistic anti-cancer effects of combined celecoxib and γT3 therapy are mediated by COX-2 dependent and independent mechanisms.	(Shirode and Sylvester, 2011)
	γT3	Tyrosine kinase inhibitor (erlotinib or gefitinib)	+SA	Combined treatment with sub-effective doses of erlotinib or gefitinib with γT3 significantly inhibited the growth and induced apoptosis with a large decrease in ErbB3 and ErbB4 receptor level.	(Bachawal et al., 2010a)
	γT3	Gefitinib or erlotinib	+SA	Combined treatment of γT3 with erlotinib or gefitinib prevents ErbB receptor heterodimer cooperation and inhibits EGF-dependent mitogenic signalling.	(Bachawal et al., 2010b)
	γT3	Simvastatin	+SA	Combined treatment of γT3 with statins induced cell cycle arrest in G1 marked by increase p27 and decrease in cyclin D1, CDK2, and hypophosphorylation of Rb protein.	(Wali et al., 2009b)
	γT3	Epigallocatechin gallate (EGCG) and/or resveratrol	MCF-7	γT3 combined with either EGCG or resveratrol caused a significant additive effect in reducing cyclin D1 and bcl-2 expression. Functional synergism among the three phytochemicals was due to the induction of quinone reductase NQO1.	(Hsieh and Wu, 2008)
	γT3	Simvastatin or lovastatin or mevastatin	+SA	γT3 with individual statins resulted in a synergistic anti-proliferative effect and large decrease in intracellular levels of phosphorylated (activated) MAPK, JNK, p38, and Akt.	(Wali and Sylvester, 2007)

	Tocomin®	3-methyladenine (3-MA)	MDA-MB 231	The autophagy inhibitor, 3-MA, potentiated the apoptosis induced by Tocomin®.	(Tran et al., 2015)
	TRF	Dendritic cell and tumour lysate	*In vivo*	The combined therapy of using dendritic cell (DC) and tumour lysate (TL) injections and TRF supplementation (DC+TL+TRF) significantly inhibited tumour growth and metastasis	(Abdul-Hafid et al., 2013)
Colorectal Cancer	δT3	Jerantinine B	HT29	Synergistic inhibition of cancer cell growth via disruption of the microtubule networks.	(Abubakar et al., 2016)
	γT3	Capecitabine	*In vivo*	Oral administration of γ-T3 inhibited tumour growth and enhanced the anti-tumour efficacy of capecitabine indicated by reduced expressions of Ki-67, cyclin D1, MMP-9, CXCR4, NF-κB/p65, and VEGF in the tumour.	(Prasad et al., 2016)
	γT3	Capecitabine	HCT116	γT3 enhanced the anti-cancer effects of capecitabine by downregulating survival, proliferation and metastasis proteins.	(Prasad et al., 2016)
	γT3	Atorvastatin (ATST)	HT29 HCT116	γT3 and atorvastatin combination caused cell cycle arrest and apoptosis via modulation of HMG-CoA reductase and small G-protein geranylgeranylation	(Yang et al., 2010)
	γT3	ATST and celocoxib	HT29 HCT116	Triple combination of ATST, γ-TT, and CXIB synergistically induced G0/G1 phase cell cycle arrest and apoptosis.	(Yang et al., 2010)
Gastric Cancer	γT3	Capecitabine	SNU-5 MKN45 SNU-16	Enhancement of apoptosis when used in combination.	(Manu et al., 2012)

	γT3	Capecitabine	*In vivo*	γT3 potentiated the anti-tumour effects of capecitabine in a xenograft gastric cancer model in nude mice. The combined treatment effectively downregulated various gene products regulated by NF-κB	(Manu et al., 2012)
Glioblastoma	δT3	Jerantinine B	U87MG	Synergistic inhibition of cancer cell growth and upregulation of caspase activities.	(Abubakar et al., 2016)
	γT3	Hydroxychavicol	1321N1 SW1783 LN18	Synergistic inhibition of cell proliferation through the induction of apoptosis	(Abdul-Rahman et al., 2014)
Leukemia	γT3	Lovastatin	HL-60	γT3 enhanced the apoptotic effect of lovastatin through the down-regulation of GLO1 and HMG-CoA reductase.	(Chen et al., 2015)
Liver cancer	γT3	Doxorubicin or paclitaxel	HepG2	γT3 significantly potentiated the apoptotic effect of doxorubicin and paclitaxel in HCC cells	(Rajendran et al., 2011)
	T3 mixture	Epirubicin (nanoparticle)	*In vivo*	Combined therapy of epirubicin nanoparticles with tocotrienols further enhanced apoptosis and reduced VEGF level. Tocotrienols provided both anti-tumour activity and higher protection against oxidative stress and inflammation.	(Nasr et al., 2014)
Lung Cancer	δT3	Cisplatin	A549 H1650	Treatment with a combination of δT3 and cisplatin resulted significant inhibition of cell growth, migration, invasiveness, and induction of apoptosis, as compared to the single agents.	(Ji et al., 2012)

Skin	δT3	Lovastatin	*In vivo*	δT3 potentiated lovastatin-mediated growth suppression.	(McAnally et al., 2007)
Mesothelioma	γT3	Atrovastatin or simvastatin	MSTO H2452	Statin + γT3 combination induced greater cell growth inhibition more than each single treatment via inhibition of mevalonate pathway.	(Tuerdi et al., 2013)
	TRF	Cisplatin	H28	Enhanced cytotoxicity by the combination treatment which was closely related to the inhibition of phosphatidylinositol 3-kinase (PI3K)-AKT signalling.	(Nakashima et al., 2010)
Oral Cancer	γT3	Docetaxel	B88	γT3 enhanced the chemosensitivity of human oral cancer cells to docetaxel through the downregulation of the expression of NF-κB-regulated anti-apoptotic gene products associated with the inhibition of apoptosis.	(Kani et al., 2013)
Ovarian Cancer	δT3	Curcumin	OVCAR-8	The δT3/curcumin nanoemulsion showed superior cytotoxicity, suppressed constitutive NF-κB activation and significantly induced apoptosis.	(Steuber et al., 2016)
Pancreatic Cancer	δT3	Ferulic acid	PANC-1	The combined treatment synergistically inhibit cancer cell growth via G1 cell cycle arrest. The synergy was associated with increased δT3 cellular concentration.	(Eitsuka et al., 2014)
	δT3	Gemcitabine	*In vivo*	δT3 augmented gemcitabine activity with a significant suppression of NF-κB activity and the expression of NF-κB transcriptional targets.	(Yap et al., 2010b)

	δT3	Gemcitabine	MiaPaCa-2 AsPc-1	δT3 significantly enhanced the efficacy of gemcitabine to inhibit pancreatic cancer growth and survival via suppression of NF-κB activity and the expression of NF-κB transcriptional targets.	(Husain et al., 2011)
	γT3	Gemcitabine	*In vivo*	γT3 potentiated the effects of gemcitabine in downregulating the expression of NF-κB–regulated gene products with an enhancement of tumour apoptosis caspase activation.	(Kunnumakkara et al., 2010)
Prostate Cancer	γT3	Polysaccharopeptide (PSP)	PC3	The combined treatment induced a drastic activation of AMP-activated protein kinase (AMPK) accompanied by inactivation of acetyl-CoA carboxylase (ACC).	(Liu et al., 2014)
	γT3	PSP	*In vivo*	PSP and γT3 treatments significantly reduced the growth of prostate tumour *in vivo*.	(Liu et al., 2014)
	γT3	Docetaxel	*In vivo*	The combined treatment decreased cell proliferation, increased in the rate of cancer cell apoptosis.	(Yap et al., 2010)

Note: ACC- acetyl-CoA carboxylase; ALDH- Aldehyde dehydrogenase; AMPK-AMP-activated protein kinase; ATST- atorvastatin; COX-2-Cyclooxygenase2; CXB-Celecoxib; DC- dendritic cells; DHA- docosahexanoic acid; EGCG-Epigallocatechin gallate; EGF - Epidermal growth factor; G1- Gap1; HMG-CoA- 3-hydroxy-3-methyl-glutaryl-CoA reductase; JNK - Jun amino-terminal kinases; MAPK- Mitogen-activated protein kinases; mTOR- mechanistic target of rapamycin; NF-κB- nuclear factor kappa-light-chain-enhancer of activated B cells; NQO1- NAD(P)H dehydrogenase quinone 1; PGD2-prostaglandin D2; PGDS -prostaglandin synthase; PI3K -phosphoinositide 3-kinase; PPARγ- Peroxisome proliferator-activated receptor gamma; PSP-Polysaccharopeptide; STAT3-Signal transducer and activator of transcription 3; T3- Tocotrienol; TL-Tumour lysate; Tocomin- Mixed tocotrineols with tocopherols; TRF- Tocotrienol rich fraction; VEGF- Vascular endothelial growth factor

Chapter Three: Anti-proliferative and anti-survival effects of individual tocotrienols, chemotherapeutic drugs and combined treatments on cancer cell lines

3.1 Introduction

Chemotherapy remains as one of the most widely used systemic treatments for cancers. However, the effectiveness of these drugs is limited by several shortcomings such as unspecific killing activity, dose-associated toxicities and development of drug resistance by cancer (Alberts et al., 2002; Ayalew Sisay, 2015). Of note, the median time to develop a single new cancer drug is around 7.3 years at a median cost of $648.0 million (Prasad and Mailankody, 2017). Taking the time and capital constraints of developing new cancer drugs into consideration, therapeutic options arise from novel drugs combination could serve as the most plausible approach and an immediate solution to address the critical medical need.

Despite tremendous development in 'omics' technologies that have led to identification of aberrant molecular targets in cancers and venture into targeted drugs, however, many targeted drugs showed limited efficacy in clinical trials mostly due to variability in treatment responses and often rapidly emerging resistance (He et al., 2018). Hence, immense research attention has been devoted towards multi-targeted drugs or drug combinations, which can potentially inhibit the growth of tumour, reduce toxicity and resistance of cancers via distinct mechanisms (He et al., 2018; Pemovska et al., 2018). In these aspects, tocotrienols appear as a potential candidate to be used in combination with chemotherapeutic drugs. The tocotrienols may offer several advantages to current chemotherapy regimen due to the cancer-selective,

apoptosis-inducing and multi-targeting properties (Aggarwal et al., 2010; Fernandes et al., 2010; Sylvester and Shah, 2005; Yap et al., 2008).

In this chapter, a high-throughput screening (HTS) was performed to study the anti-proliferative effects of tocotrienols and chemotherapeutic drugs combinations in colorectal, lung and nasopharyngeal cancer cell lines. In a 384-well plate setting, arrays of cancer cell lines were seeded and treated concurrently on the same plate, enabling minimal plate-to-plate variations which usually occur when a 96-well plate format is used. Conventionally, cell viability is estimated based upon the ability of cells in reducing the tetrazolium. The MTT (3-(4,5-dimethylthiazol-2-yl)-2,5-diphenyltetrazolium bromide) is one of the most popular tetrazolium reduction assays (Riss et al., 2016). One of the major limitations of MTT is interference by tocotrienols, which can cause self-reduction of tetrazolium to formazan crystals without the presence of cells (Lim et al., 2015). Hence, current HTS employing an adenosine triphosphate (ATP)-based luminescence assay to estimate cell viability is deemed more suitable. This assay is sensitive (can detect as few as 15 cells/well in the 384-well format), rapid (minimal incubation time) and less prone to artefact (not affected by tocotrienols) (Riss et al., 2016).

Generally, a drug pharmacological interaction can be classified as synergistic, antagonistic or additive. The additive effect must first be identified in order to provide a basis for assessing the synergism and antagonism. To further illustrate, a drug combination is considered synergy when the combined effect is significantly greater than the expected additive effect. On the other hand, antagonism is meant to describe the combined effect which is lesser than the additive effect (Tallarida, 2011). This project adopted a combination index (CI) calculation based on Loewe additivity model, a well-established and widely used method for analysing drug-drug interaction in

previous tocotrienol combination studies (Abdul-Rahman et al., 2014; Shirode and Sylvester, 2011; Steuber et al., 2016). In addition, isobologram analysis evaluates and depicts the nature of interaction of two drugs at a given effect level graphically (Zhao et al., 2010). Other informative parameters such as drug reduction index (DRI) and selectivity index (SI) further describe the valuable pharmacological impacts in the combined treatments. As such, various aspects of the combined treatments can be fully explored.

It was suggested that only certain drugs embracing complementary mechanisms of actions would produce a synergistic effect in the combination with tocotrienols (Sylvester et al., 2011). Grounding from the available literatures, current research has taken additional factors into consideration in determining the synergism of the combined treatment. It has been widely reported that tocotrienol isomers display differential biopotencies across various types of cancer (Wada, 2009). For instance, pure tocotrienol isomers or mixture tocotrienols might lead to diverse reactions in a cell. As such, current study involved three pure tocotrienol (T3) isomers, namely alpha (α)-, gamma (γ)-, delta (δ)-T3, one T3 mixture of tocotrienol rich fraction (TRF). Similarly, different classes of chemotherapeutic drugs possess diverse anti-cancer mechanisms which could contribute to different pharmacological interactions. Current study incorporated four distinct classes of chemotherapeutic drugs (anthracycline, alkylating agent, anti-metabolite and mitotic inhibitor), represented by doxorubicin (Dox), cisplatin (Cis), 5-fluorouracil (5FU) and vinblastine (Vin) (reviewed in Section 2.4.1). These drugs were selected based on the application in existing chemotherapy regimens for three of the most commonest cancers in Malaysia, namely lung, nasopharyngeal and colorectal cancers (Abdul-Manan et al., 2016).

As the ATP-based anti-proliferative assay is a short-term screening assay (terminated at 72 hours), the clonogenic assay was employed to study the long-term effects on cell survival. The treatments were withdrawn after 72-hour treatment followed by a prolonged incubation (1-2 weeks) for assessing the cell ability to undergo sufficient proliferation to form colony (Menyhárt et al., 2016). Guided by HTS results, the selected combined treatments were subjected to clonogenic assay to further evaluate their anti-survival capabilities.

In order to elucidate the combinatorial effects of tocotrienols and conventional chemotherapeutic drugs, the current study specifically embarked the following objectives:

i. To determine the *in vitro* anti-proliferative effects (IC_{50}) induced by the individual tocotrienols (αT3, γT3, δT3 and TRF) and chemotherapeutic drugs (Dox, Cis, 5FU, Vin) on lung (H1299, A549, H23, Calu-1), colorectal (Caco-2, HCT116, SW48, HCC2998) and nasopharyngeal (SUNE-1, HK-1, TW01, CNE-1) cancer cell lines.
ii. To determine the *in vitro* anti-proliferative effects (IC_{50}) induced by the tocotrienols (δT3 and TRF) and chemotherapeutic drugs (Dox, Cis, 5FU, Vin) on lung (H1299, A549, H23, Calu-1) and colorectal (Caco-2, HCT116, SW48, HCC2998).
iii. To identify the types of interaction resulted from the combined treatments in term of synergism, additive effect and antagonism by quantitative combination index (CI) and qualitative isobologram analyses.
iv. To determine the dose reduction of chemotherapeutic drugs induced by the combined treatments based on dose reduction index (DRI).

v. To determine the therapeutic selectivity of the combined treatments via selectivity index (SI).

vi. To evaluate the anti-survival effect (clonogenicity) of selected groups of combined treatments on Caco-2 and SW48 colorectal cancer cell lines.

3.2 Materials and Methods

The flowchart below illustrates an overview of the HTS used in the current study (Figure 3.1). The half-maximal growth inhibitory concentrations (IC_{50}) for tocotrienols (e.g., αT3, γT3-, δT3, TRF) and chemotherapeutic drugs (e.g., Dox, Cis, 5FU, Vin) were firstly determined. Following that, sub-effective concentrations of tocotrienols were combined with varying concentrations of chemotherapeutic drugs, the IC_{50} values were then be determined. The effects of combined treatments were evaluated by combination index (CI), dose reduction index (DRI), selectivity index (SI) and isobologram based on the previously reported methods (Wali and Sylvester, 2007).

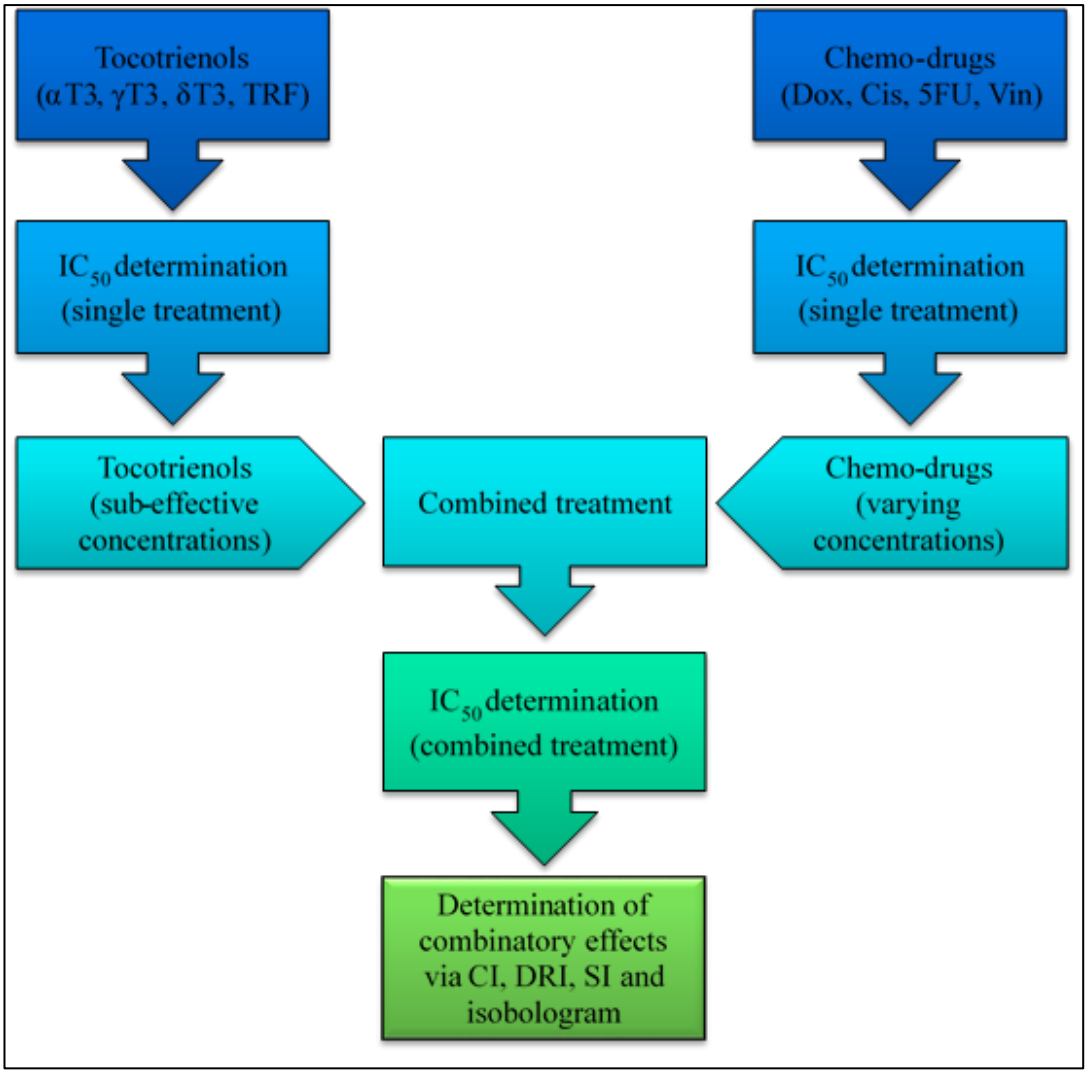

Figure 3.1 Overview of the workflow of high-throughput screening (HTS).

3.2.1 Preparation of stock solution

The tocotrienols and chemotherapeutic drugs used in this chapter were prepared according to the manufacturer's recommendation as enlisted in Table 3.1. The constituted stock solutions were kept in -20°C until further use.

Table 3.1 Preparation of tocotrienols and chemotherapeutic drugs involved in HTS.

Compound	Chemical name	Manufacturer	Solvent	Stock concentration
αT3	Alpha-tocotrienol	Davos Life Science, Singapore	DMSO	100mM

δT3	Delta-tocotrienol	Davos Life Science, Singapore	DMSO	100mM
γT3	Gamma-tocotrienol	Davos Life Science, Singapore	DMSO	100mM
TRF	-	Carotech (M) Sdn. Bhd, Malaysia	DMSO	100μg/ml
Dox	Doxorubicin hydrochloride	Sigma-Aldrich, USA	DMSO	10mM
Cis	cis-diaminedichloroplatinum (II)	Merck Millipore, USA	PBS	100mM
5FU	2,4-Dihydroxy-5-fluoropyrimidine	Merck Millipore, USA	DMSO	100mM
Vin	Vinblastine sulphate	Merck Millipore, USA	DMSO	10mM

Note: DMSO, dimethyl sulfoxide; PBS, phosphate buffered saline.

3.2.2 Culture and maintenance of cell lines

A total of 15 cell lines (Table 3.2) were cultured in appropriate medium conditions (Table 3.3). All cell lines were incubated in a 37°C humidified carbon dioxide (CO_2) incubator (ESCO Life Sciences, Singapore). Routinely, subculture was performed whenever cells reached 80-90% confluence in a 100mm culture dish (Corning Life Sciences, USA). Briefly, culture medium was aspirated and added with 2ml of 0.05% trypsin solution (Corning Life Sciences, USA) to sufficiently cover the surface of the culture dish. Then, the cells were returned to the incubator for about 5 minutes to facilitate cell detachment. Two millilitres of complete medium was added to inactivate the trypsin before subjecting the cells to centrifugation at 1,500rpm for 5 minutes. The cell pellet was resuspended in 2ml of complete medium and an appropriate ratio of cells was added into a new 100mm culture dish.

Table 3.2 Cell lines that were involved in the current study.

Lung cancer type	Colorectal cancer type	Nasopharyngeal cancer type
H1299 (epidermoid carcinoma)	HCT116 (carcinoma)	HK-1 (squamous carcinoma)
A549 (adenocarcinoma)	HCC2998 (carcinoma)	TW01 (carcinoma)
H23 (adenocarcinoma)	Caco-2 (adenocarcinoma)	SUNE1 (carcinoma)
Calu-1 (epidermoid carcinoma)	SW48 (adenocarcinoma)	CNE-1 (carcinoma)
MRC5 (immortalized fibroblast)	CCD-841-CoN (colon epithelial cells)	NP460 (nasopharyngeal epithelial cells)

Table 3.3 Culture medium conditions for the respective cell lines.

Medium	Supplement	Manufacturer	Cell line
RPMI-1640	10% fetal bovine serum (FBS) 100 units/ml of penicillin 100 µg/ml of streptomycin	Corning Life Science, USA	All cell lines except those are mentioned below
DMEM	10% FBS 100 units/ml of penicillin 100 µg/ml of streptomycin	Thermo Fisher Scientific, USA	Calu-1
DMEM	20% FBS 100 units/ml of penicillin 100 µg/ml of streptomycin	Thermo Fisher Scientific, USA	CCD-841-CoN
EpiLife ^{TM}	1x EpiLife Defined Growth Supplement (EDGS)	Thermo Fisher Scientific, USA	NP460

3.2.3 Cell seeding

Cells at 70-90% confluence were collected by trypsinisation procedure as described in the Section 3.2.2. Then, the cells were counted using Countless II FL automated cell counter (Invitrogen, USA). The cells were seeded at a density of 2000

cell/well in 20µL in opaque 384 well plates (Thermo Scientific, USA). The plates were incubated overnight in a CO_2 incubator at 37°C to facilitate cell attachment.

3.2.4 Experimental treatments

3.2.4.1 Treatment with individual tocotrienols and chemotherapeutic drugs

To determine IC_{50} based on the dose-response curve, the range of final drug concentrations were set within 0.1-100µM for all the compounds. The treatment solutions were prepared in 10x higher concentration than that of the final concentration in a 96-well plate. All drugs were diluted to which the highest concentration of DMSO did not exceed 0.1%. A vehicle control containing DMSO 0.1% was included in the assay. On the treatment day, cells were replenished with 18µl/well of appropriate serum free medium and kept in the incubator until treatment solution was added. Using a multichannel pipette, two microliters of treatment solution (10x) was added into the well (containing 18µl of medium) and eventually diluted into the desired final concentration (1x). All cancer cells lines were exposed to 72 hours of individual compound treatments. This experiment was repeated three times independently (n = 3).

3.2.4.2 Treatment with tocotrienols and drugs combination

On the treatment day, cells were replenished with appropriate medium containing the respective sub-effective concentration of δT3 (10µM) or TRF (5µg/ml). Then, treatment solutions containing variable concentrations were added (Table 3.4). All cells were exposed to the combined treatments for 72 hours. A total of three independent experiments were conducted (n = 3).

Table 3.4 Final concentrations of the chemotherapeutic drugs that were combined with sub-effective concentrations of δT3 (10μM) or TRF (5μg/ml) in the dilution series tested.

Dox (μM)	Cis (μM)	5FU (μM)	Vin (μM)
100	100	100	10
50	50	50	1
10	10	10	0.1
5	5	5	0.01
1	1	1	0.001
0.5	0.5	0.5	0.0001
0.1	0.1	0.1	0.00001
1% DMSO	1% PBS	1% DMSO	1% DMSO

3.2.5 CellTiter-Glo® luminescent cell viability assay

CellTitre-Glo® luminescent cell viability assay (Promega, USA) is a method of determining the number of viable cells based upon ATP quantification, which serves as an indicator of metabolically active cells. In principles, the ATP that is contained in viable cells will convert luciferin (present in CellTiter-Glo reagent) to oxyluciferin and light (luminescence) with the aid of Ultra-Glo™ rluciferase enzyme (present in CellTitre-Glo reagent). The luminescent signal can be measured by a luminometer.

After 72 hours of either individual or combined treatment, the media were removed; and followed by the addition of 40μl of 1x CellTitre-Glo® reagent (Promega, USA) into the wells. The plates were gently shaken for 2 minutes to induce cell lysis. Then, the plates were subjected to data acquisition using SpectraMax M3 luminometer (Molecular Devices, USA).

3.2.6 Determination of IC_{50} values

Dose-response curves were plotted using Excel 2016 (Microsoft, USA), with the x-axis representing the drug concentration (dose) while y-axis representing the cell viability (response). A linear equation was fit into data points that span 50% of the cell

viability. The IC_{50} value of each independent experiment was calculated based on the equation generated. The IC_{50} values of three independent experiments were presented as mean IC_{50} ± standard deviation (S.D.)

3.2.7 Determination of combination, selectivity and drug reduction indices

The level of interaction between tocotrienols and chemotherapeutic drugs was determined by combination index (CI) and isobologram methods (Wali and Sylvester, 2007). The CI method is a quantitative representation of pharmacological interaction between two drugs. The CI values were calculated at 50% cell growth inhibition, as:

$$CI = Tc/T + Dc/D$$

where T and D represent IC_{50} of tocotrienols and chemotherapeutic drugs, respectively; Tc and Dc are IC_{50} of tocotrienols and chemotherapeutic drugs in a combination. Based on CI values, the extent of synergism/antagonism was determined. In brief, CI values between 0.85 and 0.9 suggest a moderate synergy, whereas those values which are in the range of 0.3 to 0.7 indicating a strong synergistic interaction between the drugs. CI values in the range of 0.9 to 1.10 suggest a near additive effect (Abdul-Rahman et al., 2014). CI values beyond 1.10 indicate an antagonistic effect.

Additionally, isobologram is a graphical presentation of pharmacological interaction of a two-drug combination. The straight line in each isobologram was formed by plotting the individual IC_{50} values of tocotrienols and chemotherapeutic drugs on x- and y-axes, respectively. A data point locates on the line suggests an additive effect, whereas, below and above the line suggest synergistic and antagonistic effects of the combined treatment respectively.

On the other hand, dose reduction index (DRI) values represent fold changes of each individual agent in a combination from its alone application at a given effect level. The DRI values for chemotherapeutic drugs were calculated as below:

$$DRI = D/Dc$$

where D represents the drug concentration when is applied individually to kill 50% of cancer cells; Dc represents the drug concentration in a combination used to achieve the same killing response.

Selectivity index (SI) is a parameter that measures the window between cytotoxicity towards the cancer cells and normal cells. To quantify this parameter, SI was calculated as the average IC_{50} value in the normal cell line divided by the IC_{50} value in the cancer cell lines (Calderón-Montaño et al., 2018), as simplified in the equation:

$$SI = IC_{50}^{\ normal} / IC_{50}^{cancer}$$

where 'normal' represents normal cell lines and 'cancer' represents cancer cell lines.

3.2.8 Clonogenic assay

Clonogenic assay is a gold standard to assess the survival of cancer cells after exposure to ionizing radiation or therapeutics (Citrin, 2016). In this study, clonogenic assay was performed on selected combinations identified in HTS (Table 3.5). Firstly, Caco-2 and SW48 cells were seeded at a density of 800 and 2,000, respectively into each well of a 6-well plate followed by overnight incubation to facilitate attachment. The cells were exposed to 72 hours of single and combined treatments. Guided by the IC_{50} values obtained from HTS, the combinations with 5FU were performed at 2-fold dilution series from respective original concentrations while combinations with Dox were performed at 10-fold dilution series. A vehicle control containing the respective

amount of DMSO in the drug was included. Then, the medium was removed and replenished with complete medium. The cells were allowed to grow for another 7-14 days to form visible colonies which contained at least 50 cells. Upon colonies formation, the culture media were aspirated from 6-well plate and rinsed with 1x PBS. Next, 1ml of fixative solution containing methanol and acetic acid (4:1 ratio) was added and incubated for 5 minutes. Then, the fixative solution was removed and 2ml of 0.5% crystal violet solution was added to the well (LabChem Sdn Bhd, Malaysia) for 30 minutes. After that, the crystal violet solution was removed and subjected to rinsing under running tap water until purple colonies were visible. The colonies formed were enumerated and the percentage of colony formed was calculated based on (Colony number of treated cell/ Colony number of vehicle control) x 100%. One way analysis of variance (ANOVA) test was followed by Dunnett's multiple comparisons to identify the statistical significance levels between the mean percentages of treated groups and untreated vehicle control using GraphPad Prism 7 software (GraphPad Prism, USA). The mean percentage was considered as statistically significant if p-value is less than 0.05 (*) or 0.01 (**).

Table 3.5 Concentrations of selected combined treatments and their respective single treatments.

Treatment groups	Final concentration	
	Caco-2	SW48
Vehicle control	1% DMSO (v/v)	1% DMSO (v/v)
δT3	10μM	10μM
5FU	3.5μM	18μM
*δT3 + 5FU	10μM + 3.5μM	10μM + 18μM
Dox	2μM	1μM
*δT3 + Dox	10μM + 2μM	10μM + 1μM

* denotes selected combined treatment groups.

3.3 Results

3.3.1 Anti-proliferative effect of single treatments

3.3.1.1 IC_{50} values

The individual anti-proliferative effects of αT3, δT3, γT3, TRF, Dox, Cis, 5FU and Vin were tested against a panel of lung (H1299, A549, H23, Calu-1), nasopharyngeal (SUNE-1, HK-1, TW01, CNE-1) and colorectal (Caco-2, HCT116, SW48, HCC2998) cancer cell lines. The normal cell lines in lung (MRC5), nasopharyngeal (NP460) and colon (Con-841) were also included. Each respective half-maximal inhibitory concentration (IC_{50}), which is a parameter to indicate anti-proliferative potency (Griffiths and Sundaram, 2011) was then determined. A lower IC_{50} value represents a higher potency.

Tocotrienol isomers displayed differential anti-proliferative activities across different types of cancers (Table 3.6). Generally, the IC_{50} ranges of δT3 and γT3 were 18.46 - 31.24μM and 17.12 - 32.08μM, respectively, demonstrating a similar anti-proliferative potency to each other. In comparison, the IC_{50} range of αT3 was higher (28.25 - 66.53μM), indicating a lower anti-proliferative potency. The anti-proliferative potencies of δT3 and γT3 were higher in colorectal than lung and nasopharyngeal cancer cell lines. The specific biopotency orders of tocotrienol isomers for each cell line were summarised (Table 3.7).

Table 3.6 IC_{50} values of tocotrienols under single treatment on various cell lines. The values are presented as mean ± SD, (n = 3).

Cell line	αT3 (μM)	δT3 (μM)	γT3 (μM)	TRF (μg/ml)
Lung				
MRC5	34.06 ± 4.97	39.68 ± 3.66	40.05 ± 5.99	39.67 ± 5.10
H1299	47.91 ± 0.04	27.80 ± 2.76	29.20 ± 2.57	27.11 ± 3.02
A549	50.20 ± 6.37	30.24 ± 0.77	32.08 ± 2.14	27.77 ± 3.08

H23	31.60 ± 1.73	28.28 ± 4.18	27.96 ± 1.48	8.97 ± 0.52
Calu-1	32.91 ± 1.72	31.24 ± 3.10	17.20 ± 9.09	44.96 ± 2.64
Nasopharyngeal				
NP460	51.52 ± 1.20	32.44 ± 5.62	30.16 ± 0.55	30.25 ± 2.47
SUNE-1	34.63 ± 8.57	18.46 ± 7.67	17.12 ± 3.85	31.88 ± 3.42
HK-1	28.25 ± 1.98	25.58 ± 3.14	31.31 ± 0.77	30.56 ± 0.97
TW01	66.53 ± 3.44	27.40 ± 1.90	25.90 ± 1.36	26.81 ± 2.17
CNE-1	40.14 ± 4.29	29.51 ± 2.47	31.93 ± 3.45	32.31 ± 1.00
Colorectal				
Con-841	75.04 ± 2.42	65.76 ± 1.33	48.04 ± 0.98	42.38 ± 1.24
Caco-2	32.75 ± 2.50	25.46 ± 1.20	20.24 ± 2.90	24.01 ± 1.93
HCT116	29.44 ± 2.49	25.84 ± 3.64	27.40 ± 2.75	24.22 ± 2.73
SW48	29.66 ± 3.00	22.78 ± 3.36	18.62 ± 4.81	17.98 ± 0.73
HCC2998	33.16 ± 1.89	25.03 ± 5.62	23.97 ± 5.99	8.28 ± 0.17

Table 3.7 Biopotency ranking orders of tocotrienols on each cancer cell line.

Cell line	first	order	second	order	third
Lung					
H1299	δ	≈	γ	>	α
A549	δ	≈	γ	>	α
H23	γ	>	δ	>	α
Calu-1	γ	>	δ	≈	α
Nasopharyngeal					
SUNE-1	γ	≈	δ	>	α
HK-1	δ	≈	α	>	γ
TW01	γ	≈	δ	>	α
CNE-1	δ	≈	γ	>	α
Colorectal					
Caco-2	γ	>	δ	>	α
HCT116	δ	≈	γ	≈	α
SW48	γ	≈	δ	>	α
HCC2998	γ	≈	δ	>	α

The chemotherapeutic drugs, Dox and Vin displayed higher anti-proliferative potencies (lower IC_{50} values), ranging from 0.54μM to 8.99μM and from 0.007μM to 24.8μM, respectively. The IC_{50} values of Cis ranged from 4.78μM to 56.53μM, which potency is considered moderate as compared to 5FU (IC_{50} values ranged from 8.14μM to >100μM) (Table 3.8). 5FU showed differential potencies in the four colorectal cell lines, which the potencies were ranked in a descending order (increasing IC_{50} values) as: HCT116 > HCC2998 > Caco-2 > SW48. Similarly, the potencies of Dox and Cis on the four lung cancer cell lines were ranked in a descending order (with increasing IC_{50} values) as: H23 > A549 > Calu-1 > H1299.

Table 3.8 IC_{50} values of chemotherapeutic drugs under single treatment on various cell lines. The values are presented as mean ± SD, (n = 3).

Cell line	Dox (μM)	Cis (μM)	5FU (μM)	Vin (μM)
Lung				
MRC5	3.55 ± 2.92	41.69 ± 4.79	>100	7.00 ± 3.60
H1299	3.35 ± 0.41	46.14 ± 2.90	43.27 ± 6.02	0.064 ± 0.01
A549	1.73 ± 0.75	22.43 ± 3.76	15.09 ± 0.12	0.39 ± 0.01
H23	0.66 ± 0.09	20.44 ± 1.25	>100	0.061 ± 0.01
Calu-1	2.60 ± 0.01	24.28 ± 1.91	>100	24.8 ± 1.44
Nasopharyngeal				
NP460	29.64 ± 11.68	7.29 ± 1.37	>100	0.08 ± 0.01
SUNE-1	8.99 ± 0.33	56.53 ± 0.94	>100	1.45 ± 0.11
HK-1	2.57 ± 0.17	26.82 ± 1.57	59.46 ± 15.36	1.92 ± 0.12
TW01	0.54 ± 0.068	8.85 ± 6.29	8.14 ± 0.11	0.07 ± 0.02
CNE-1	0.72 ± 0.054	4.78 ± 1.24	33.96 ± 0.71	0.05 ± 0.00
Colorectal				
Con-841	34.5 ± 7.64	14.55 ± 0.15	>100	4.68 ± 1.26
Caco-2	5.67 ± 0.75	24.66 ± 3.23	54.37 ± 0.63	0.07 ± 0.01
HCT116	1.76 ± 0.45	27.72 ± 1.98	15.70 ± 3.84	0.06 ± 0.01
SW48	0.73 ± 0.09	24.29 ± 3.93	63.50 ± 8.06	0.007 ± 0.01

HCC2998	2.80 ± 0.17	32.76 ± 2.61	21.68 ± 1.39	0.05 ± 0.01

Note: >100 = beyond tested range <0.1 = below tested range

3.3.1.2 SI values

SI demonstrates the differential cytotoxicity of a pure compound; the greater the index, the more selective the anti-cancer drug is. It was suggested that SI value less than 2 indicates general toxicity of a pure compound (Badisa et al., 2009). Hence, SI values equal to or greater than 2 were bolded (Table 3.9 & 3.10). Of note, in referring Table 3.9, tocotrienols display two-fold selectivity in all colorectal cancer cell lines, but only two in lung and none in nasopharyngeal cancer cell lines. In particularly, αT3 and δT3 exhibited SI > 2 on all the colorectal cancer lines tested in this study, whereas lower selectivity of γT3 and TRF was observed on Caco-2 (SI = 1.77) and HCT116 colorectal cell lines (SI = 1.75).

Based on Table 3.10, the SI values of Dox were above 2 in all tested cancer cell lines, except H1299 and Calu-1 lung cancer cell lines. The SI values of Vin were remarkably high on all the colorectal cancer cells tested (in a range of SI > 67-670). Being the first line chemotherapeutic drug for colorectal cancer, 5FU displayed selectivity only on HCT116 (SI = 6.37) and HCC2998 (SI = 4.67) cell lines. On the other hand, Cis is the first line chemotherapeutic drug for lung cancer exhibited a general selectivity only on H23 cell line (SI = 2.04).

Table 3.9 SI values of tocotrienol isomers and TRF on various cancer cell lines.

Cell line	αT3 (μM)	δT3 (μM)	γT3 (μM)	TRF (μg/ml)
Lung				
H1299	0.71	1.43	1.37	1.46
A549	0.68	1.31	1.25	1.43
H23	1.08	1.40	1.43	**4.42**
Calu-1	1.03	1.27	**2.33**	0.88
Nasopharyngeal				

SUNE-1	1.49	1.76	1.76	0.95
HK-1	1.82	1.27	0.96	0.99
TW01	0.77	1.18	1.16	1.13
CNE-1	1.28	1.10	0.94	0.94
Colorectal				
Caco-2	**2.29**	**2.58**	**2.37**	1.77
HCT116	**2.55**	**2.54**	1.75	1.75
SW48	**2.53**	**2.89**	**2.58**	**2.36**
HCC2998	**2.26**	**2.63**	**2.00**	**5.12**

Note: SI > 2 indicates general selectivity (in bold)

Table 3.10 SI values of chemotherapeutic drugs on various cancer cell lines.

Cell line	Dox (μM)	Cis (μM)	5FU (μM)	Vin (μM)
Lung				
H1299	1.06	0.90	**2.31**	**115.63**
A549	**2.05**	1.86	**6.63**	**18.97**
H23	**5.38**	**2.04**	NA	**121.31**
Calu-1	1.37	1.72	NA	0.30
Nasopharyngeal				
SUNE-1	**3.30**	0.13	NA	0.06
HK-1	**11.53**	0.27	1.68	0.04
TW01	**54.89**	0.82	**12.29**	1.14
CNE-1	**41.17**	1.53	**2.94**	1.60
Colorectal				
Caco-2	**6.08**	0.59	1.84	**67.00**
HCT116	**19.60**	0.52	**6.37**	**78.17**
SW48	**47.26**	0.60	1.57	**670.00**
HCC2998	**12.32**	0.44	**4.67**	**93.80**

Note: SI > 2 indicates general selectivity (in bold)

3.3.2 Anti-proliferative effect of combined treatments

3.3.2.1 IC_{50} values

The tables below summarise the IC_{50} values of the combined treatments with δT3 (Table 3.11) and TRF (Table 3.12). In lung cancer cell lines, there were a consistently higher relative IC_{50} values of H1299 and Calu-1 when compared to H23 and A549 across all the combined treatments with δT3 and TRF (Table 3.11 & 3.12). The decreasing potencies of the combined treatments in the four lung cancer cell lines were ordered as: H23 > A549 > H1299 ≥ Calu-1. Generally, the combined IC_{50} values with δT3 were lower as compared to TRF, signifying a higher potency in δT3. For instance, the combined IC_{50} values of Dox ranged between 0.26 – 3.28μM in δT3, which was lower than 0.54 - >10μM in TRF. In Cis, combined treatment with δT3 showed the lowest IC_{50} value of 10.23μM versus 23.34μM in TRF. In 5FU, the lowest combined IC_{50} values of δT3 and TRF were 3.35μM and 6.37μM respectively.

Table 3.11 IC_{50} values of the combined treatments on selected cancer cell lines.

Cell line	δT3 + Dox	δT3 + Cis	δT3 + 5FU	δT3 + Vin
Lung				
MRC5	0.83 ± 0.04	19.54 ± 3.61	>100	0.87 ± 0.44
H1299	3.06 ± 0.38	>100	>100	0.20 ± 0.01
A549	0.67 ± 0.15	37.39 ± 2.13	67.22 ± 2.01	0.06 ± 0.03
H23	0.26 ± 0.02	24.83 ± 0.70	49.20 ± 1.73	<0.0001
Calu-1	3.28 ± 0.14	>100	>100	>100
Colorectal				
Con-841	43.43 ± 8.25	91.74 ± 2.45	>100	>10
Caco-2	2.03 ± 0.25	10.23 ± 1.76	3.35 ± 0.22	0.08 ± 0.01
HCT116	0.93 ± 0.19	35.55 ± 2.25	15.02 ± 0.14	0.73 ± 0.26
SW48	0.77 ± 0.03	47.50 ± 4.28	17.93 ± 1.81	0.99 ± 0.18
HCC2998	1.02 ± 0.07	27.64 ± 3.32	27.81 ± 3.97	0.38 ± 0.12

Note: >100 / >10 = beyond tested range <0.0001 = below tested range

Table 3.12 IC_{50} values of the TRF combined treatments on selected cancer cell lines.

Cell line	TRF + Dox	TRF + Cis	TRF + 5FU	TRF + Vin
Lung				
MRC5	3.88 ± 0.12	65.84 ± 11.88	>100	3.12 ± 0.89
H1299	3.38 ± 0.16	>100	>100	0.15 ± 0.03
A549	2.03 ± 0.76	34.89 ± 3.95	63.53 ± 5.42	0.067 ± 0.03
H23	0.54 ± 0.09	28.80 ± 2.03	66.88 ± 15.14	<0.0001
Calu-1	>10	>100	>100	>10
Colorectal				
Con-841	12.04 ± 1.31	58.03 ± 18.35	>100	>10
Caco-2	2.51 ± 0.26	27.63 ± 2.53	>100	0.85 ± 0.02
HCT116	1.55 ± 0.33	32.45 ± 1.56	6.37 ± 1.47	4.93 ± 1.21
SW48	2.04 ± 0.71	30.09 ± 3.31	21.41 ± 2.87	2.32 ± 1.69
HCC2998	2.35 ± 0.25	23.34 ± 0.56	37.88 ± 3.58	0.68 ± 0.34

Note: >100 / >10 = beyond tested range <0.0001 = below tested range

3.3.2.2 CI values

CI value less than 0.9 indicates a synergism, a range between 0.85 - 1.10 suggests an additive effect and more than 1.10 designates an antagonism. δT3 + Dox combined treatment resulted mostly synergistic interactions in all the cancer cell lines tested, except for H1299 (CI = 1.27), Calu-1 (CI =1.58) and SW48 (CI = 1.50) (Table 3.13). δT3 + Cis combined treatment resulted mostly antagonistic interactions except in Caco-2 (CI = 0.81). δT3 + 5FU combined treatment showed synergisms in H23 (CI = 0.81), Caco-2 (CI = 0.45) and SW48 (CI = 0.72) cell lines. δT3 + Vin combined treatment exhibited synergisms only in A549 (CI = 0.49) and H23 (CI = 0.37) cell lines. In total, ten combined treatments involving δT3 were detected with synergistic effects.

Table 3.13 CI values of δT3 combined treatment on selected cancer cell lines.

Cell lines	δT3 + Dox	δT3 + Cis	δT3 + 5FU	δT3 + Vin
Lung				
H1299	1.27	2.53	2.67	3.53
A549	0.72*	2.00	3.82	0.49*
H23	0.75*	1.57	0.85*	0.37*
Calu-1	1.58	ND	1.32	ND
Colorectal				
Caco-2	0.75*	0.81*	0.45*	48.20
HCT116	0.91[#]	1.67	1.34	12.62
SW48	1.50	2.39	0.72*	142.07
HCC2998	0.76*	1.24	1.70	8.01

Note: *synergistic effect [#]additive effect ND = not determined

For drugs combination with TRF, fewer synergisms were detected (Table 3.14). TRF + Dox combined treatment resulted in a synergism only in Caco-2 (CI = 0.65). TRF + Cis combined treatment showed an antagonism in all the cell lines tested. In addition, the TRF + 5FU combined treatment showed synergisms in HCT116 (CI = 0.66) and SW48 (CI = 0.62). TRF + Vin combined treatment demonstrated mostly antagonistic interactions, except for A549 (CI = 0.49) and H23 (CI = 0.37). In total, there were five combined treatments involving TRF identified with synergistic effects.

Table 3.14 CI values of TRF combined treatment on selected cancer cell lines.

Cell lines	TRF + Dox	TRF + Cis	TRF + 5FU	TRF + Vin
Lung				
H1299	1.19	ND	ND	2.55
A549	1.35	1.76	1.65	0.35*
H23	1.38	1.97	1.23	0.57*
Calu-1	1.48	ND	ND	ND
Colorectal				

Caco-2	0.65*	1.33	2.05	12.29
HCT116	1.13	1.53	0.66*	82.38
SW48	3.09	2.23	0.62*	331.68
HCC2998	1.36	1.37	2.29	14.10

Note: *synergistic effect [#]additive effect ND = not determined

3.3.2.3 Isobologram profiles

Herein, the isobologram profiles of combined treatments with δT3 on a panel of lung (Figure 3.2) and colorectal (Figure 3.3) cancer cell lines were generated. The isobologram profiles of combined treatments with TRF are presented in Figures 3.4 and 3.5 for lung and colorectal cancer cell lines, respectively.

Regardless of types of tocotrienols, there was a collective of ten synergisms (below the line of additivity) detected in colorectal cancer cell lines, but only seven synergistic effects were found in lung cancer cell lines. When types of tocotrienols were taken into consideration, the combined treatments with δT3 (Figures 3.2 & 3.3) generated two-fold more synergistic combination (below the line of additivity) than that of TRF (Figures 3.4 & 3.5). The combination effects depicted in isobologram in fact were consistent to findings generated in the CI findings (as summarised in Tables 3.15 & 3.16)

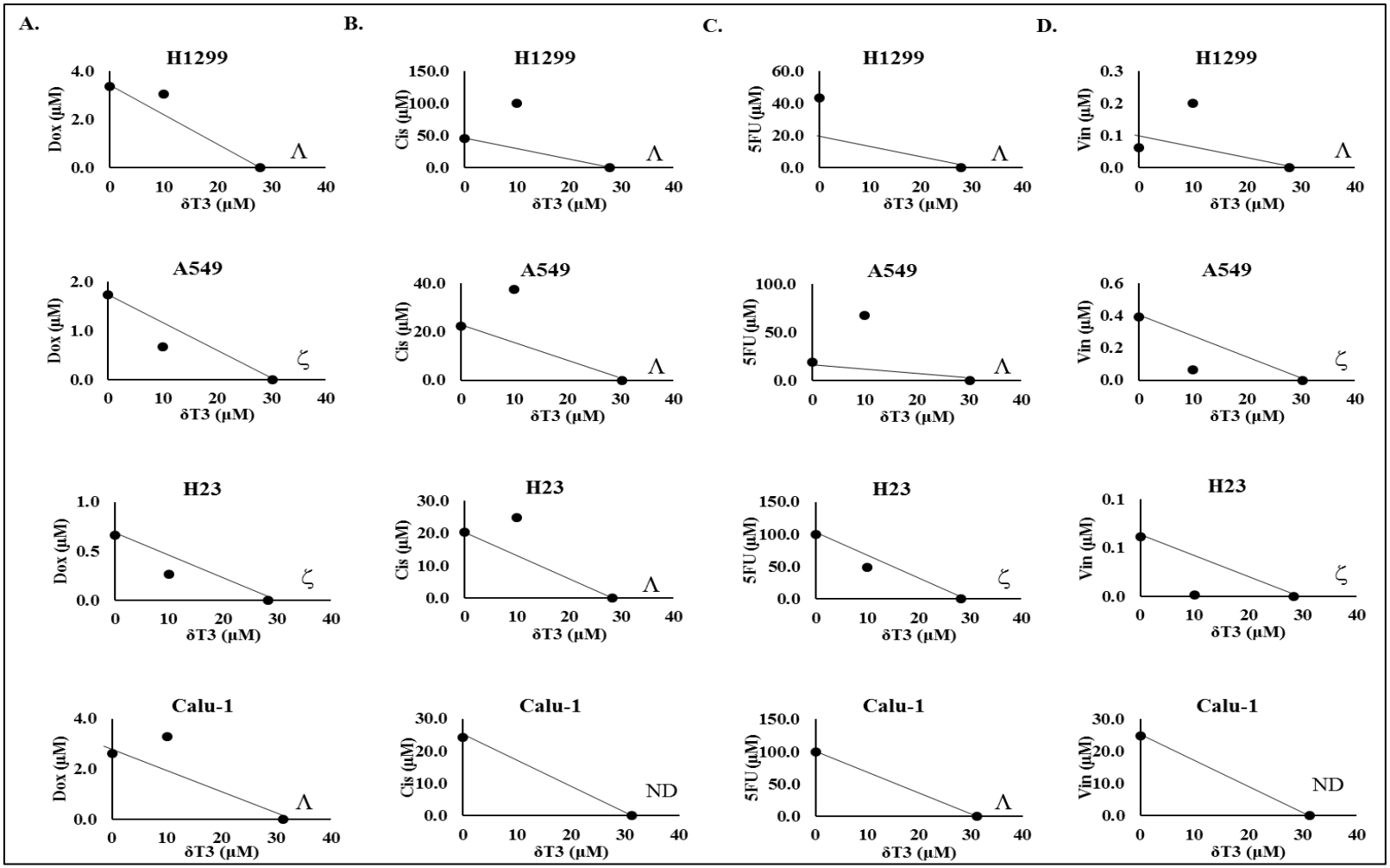

Figure 3.2 Isobologram profiles of δT3 combined treatments with A, Dox; B, Cis; C, 5FU; D, Vin on lung cancer cell lines. Data points appearing below, above and on top of the diagonal line indicate synergistic (ζ), antagonistic (Λ) and additive (⊕) effects of the combined treatments, respectively. ND denotes not determined.

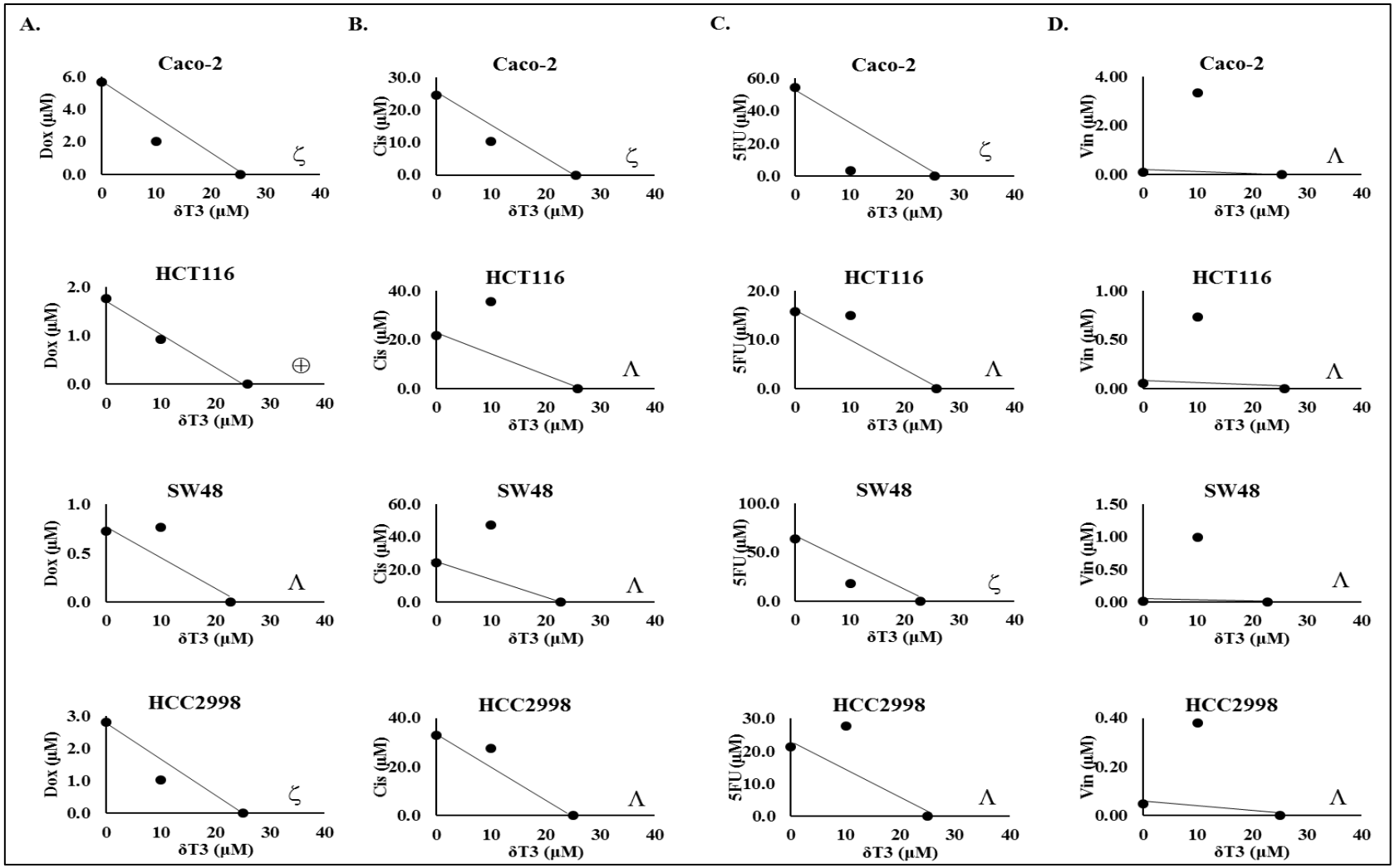

Figure 3.3 Isobologram profiles of δT3 combined treatments with A, Dox; B, Cis; C, 5FU; D, Vin on colorectal cancer cell lines. Data points appearing below, above and on top of the diagonal line indicate synergistic (ζ), antagonistic (Λ) and additive (⊕) effects of the combined treatments, respectively. ND denotes not determined.

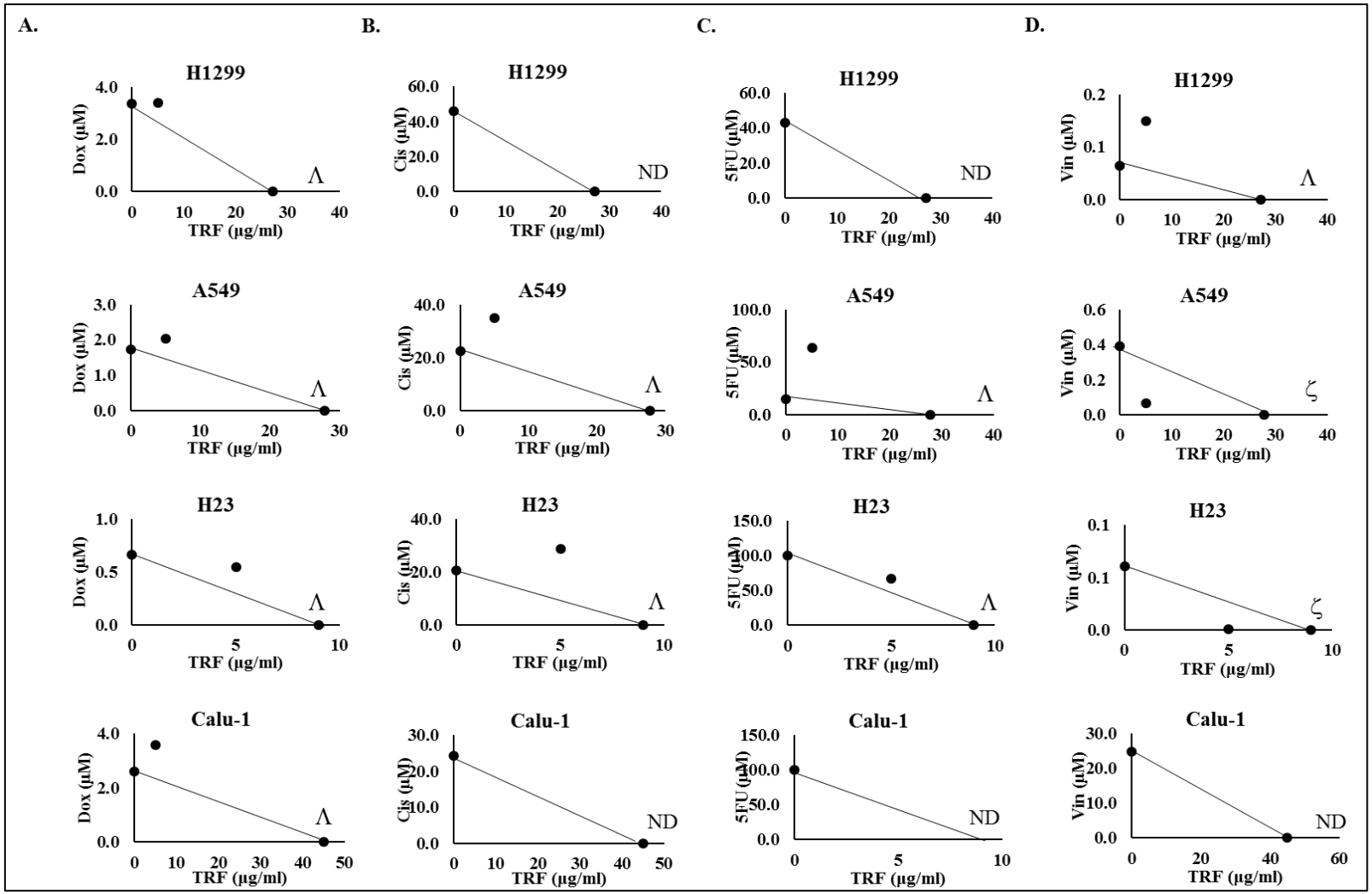

Figure 3.4 Isobologram profiles of TRF combined treatments with A, Dox; B, Cis; C, 5FU; D, Vin on lung cancer cell lines. Data points appearing below, above and on top of the diagonal line indicate synergistic (ζ), antagonistic (Λ) and additive (⊕) effects of the combined treatments, respectively. ND denotes not determined.

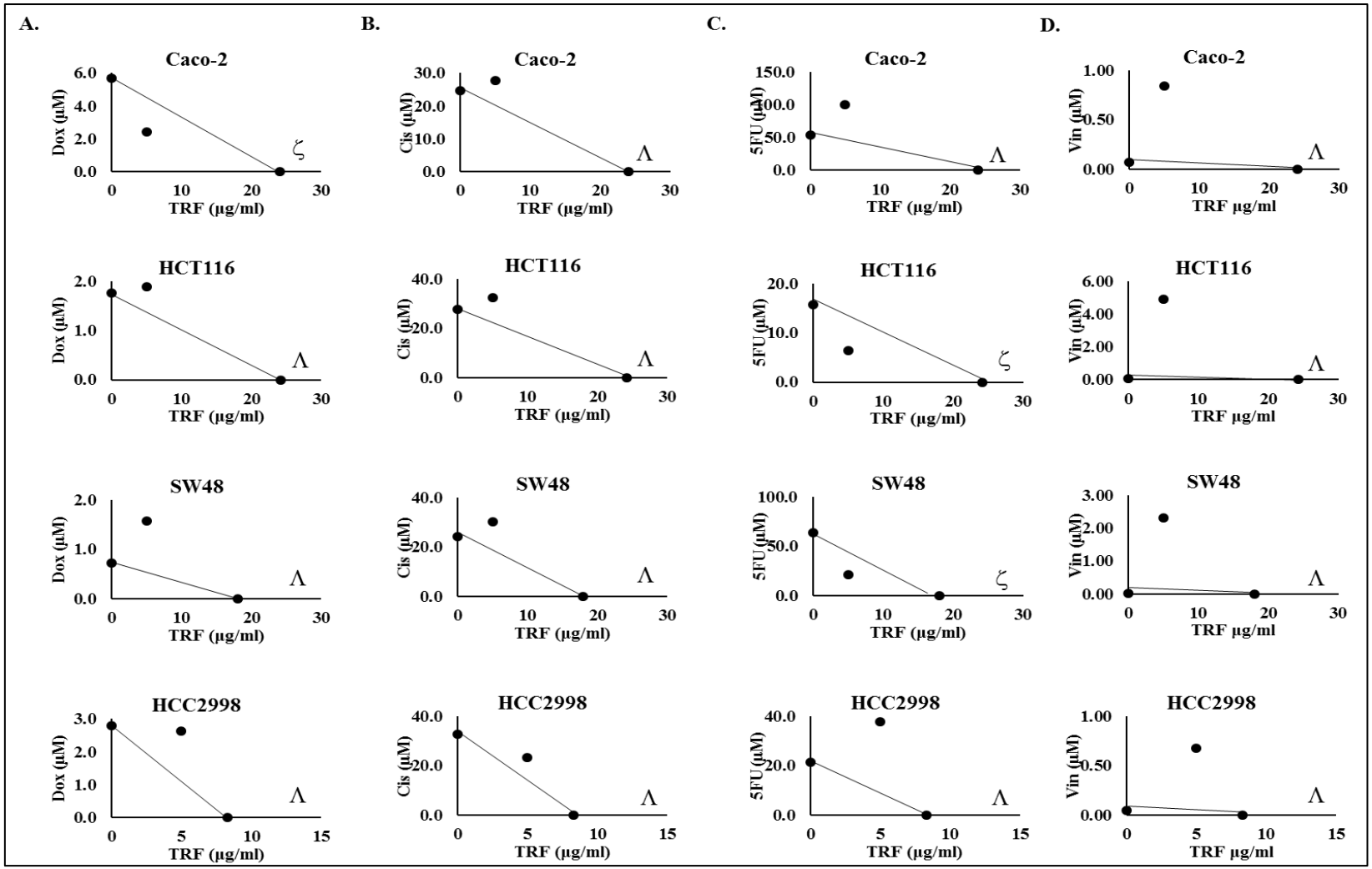

Figure 3.5 Isobologram profiles of TRF combined treatments with A, Dox; B, Cis; C, 5FU; D, Vin on colorectal cancer cell lines. Data points appearing below, above and on top of the diagonal line indicate synergistic (ζ), antagonistic (Λ) and additive (⊕) effects of the combined treatments, respectively. ND denotes not determined.

Table 3.15 A summary of δT3 combination effects on lung and colorectal cancer cell lines.

Cell lines	δT3 + Dox		δT3 + Cis		δT3 + 5FU		δT3 + Vin	
Lung	CI	Isobologram	CI	Isobologram	CI	Isobologram	CI	Isobologram
H1299	1.27	Λ	2.53	Λ	2.67	Λ	3.53	Λ
A549	0.72*	ζ	2.00	Λ	3.82	Λ	0.49*	ζ
H23	0.75*	ζ	1.57	Λ	0.85*	ζ	0.37*	ζ
Calu-1	1.58	Λ	ND	ND	1.32	Λ	ND	ND
Colorectal								
Caco-2	0.75*	ζ	0.81*	ζ	0.45*	ζ	48.20	Λ
HCT116	0.91#	⊕	1.67	Λ	1.34	Λ	12.62	Λ
SW48	1.50	Λ	2.39	Λ	0.72*	ζ	142.07	Λ
HCC2998	0.76*	ζ	1.24	Λ	1.70	Λ	8.01	Λ

CI values of <0.9 denote a synergistic effect*; CI values of 0.9-1.10 represent an additive effect#; while CI values of >1.1 represent an antagonistic effect; combination effects of isobologram were marked ζ for synergistic, Λ for antagonistic and ⊕ for additive effects of the combined treatments. ND denotes not determined.

Table 3.16 A summary of TRF combination effects on lung and colorectal cancer cell lines.

Cell lines	TRF + Dox		TRF + Cis		TRF + 5FU		TRF + Vin	
Lung	CI	Isobologram	CI	Isobologram	CI	Isobologram	CI	Isobologram
H1299	1.19	Λ	ND	ND	ND	ND	2.55	Λ
A549	1.35	Λ	1.76	Λ	1.65	Λ	0.35*	ζ
H23	1.38	Λ	1.97	Λ	1.23	Λ	0.57*	ζ
Calu-1	1.48	Λ	ND	ND	ND	ND	ND	ND
Colorectal								
Caco-2	0.65*	ζ	1.33	Λ	2.05	Λ	12.29	Λ
HCT116	1.13	Λ	1.53	Λ	0.66*	ζ	82.38	Λ
SW48	3.09	Λ	2.23	Λ	0.62*	ζ	331.68	Λ
HCC2998	1.36	Λ	1.37	Λ	2.29	Λ	14.10	Λ

CI values of <0.9 denote a synergistic effect*; CI values of 0.9-1.10 represent an additive effect[#]; while CI values of >1.1 represent an antagonistic effect; combination effects of isobologram were marked ζ for synergistic, Λ for antagonistic and ⊕ for additive effects of the combined treatments. ND denotes not determined.

3.3.2.4 DRI values

DRI measures fold reduction of IC_{50} in combinations as compared to the individual dose to achieve the same therapeutic effect level. DRI equals to 1 indicates no dose reduction, whereas DRI >1 or <1 suggests a favourable and unfavourable dose reduction, respectively. The IC_{50} values of δT3 + Dox combined treatment were reduced in two lung cancer cell lines (A549 and H23) and two colorectal cancer cell lines (Caco-2 and HCC2998) by 2.55 - 2.80 folds. On the other hand, δT3 + 5FU combined treatment showed a great concentration reduction of 16.25 and 3.54 folds in Caco-2 and SW48 colorectal cancer cells, respectively (Table 3.17). Generally, δT3 + Cis displayed poor DRI with only HCC2998 displayed a slight increase of DRI at 1.19. δT3 + Vin combined treatment reduced its dose by 6.14 and 61 folds, respectively in A549 and H23 lung cancer cell lines.

The DRI values of TRF combined treatments were tabulated in Table 3.18. As compared to δT3 combinations, the magnitude of dose reduction in combined treatment with TRF was smaller, ranging from 1.14 to 5.86 folds. Dox, Cis, 5FU and Vin showed the highest reductions of 2.26-fold (Caco-2 cell line), 1.4-fold (HCC2998 cell line), 2.97-fold (SW48 cell line) and 5.86-fold (A549 cell line), respectively when combined with TRF.

Table 3.17 DRI values of δT3 combined treatments on selected cancer cell lines.

Cell lines	δT3 + Dox	δT3 + Cis	δT3 + 5FU	δT3 + Vin
Lung				
H1299	1.10	0.46	ND	0.32
A549	2.56	0.60	0.64	6.14
H23	2.55	0.82	0.39	61.00
Calu-1	0.79	ND	ND	ND
Colorectal				

Caco-2	2.80	0.89	16.25	0.021
HCT116	1.90	0.78	1.05	0.082
SW48	0.95	0.51	3.54	0.0071
HCC2998	2.76	1.19	0.77	0.13

Note: ND denotes 'not determined' by which the IC_{50} values of normal cells and cancer cells were beyond detection range, hence, it is impossible to estimate the DRI.

Table 3.18 DRI values of TRF combined treatments on selected cancer cell lines.

Cell lines	TRF + Dox	TRF + Cis	TRF + 5FU	TRF + Vin
Lung				
H1299	0.99	0.46	ND	0.42
A549	0.85	0.64	0.68	5.86
H23	1.21	0.71	0.29	ND
Calu-1	0.73	ND	ND	ND
Colorectal				
Caco-2	2.26	0.89	0.54	0.83
HCT116	1.14	0.85	2.47	0.01
SW48	0.36	0.81	2.97	0.01
HCC2998	1.19	1.40	0.57	0.07

ND denotes 'not determined' by which the IC_{50} values of normal cells and cancer cells were not detected, hence, it is impossible to estimate the DRI.

3.3.2.5 SI values

In terms of SI, combined treatments of δT3 with Dox, Cis and 5FU showed an improved selectivity on all the tested colorectal cancer cell lines except HCC2998 receiving δT3 + 5FU treatment (Table 3.19). Of note, δT3 + Vin did not improve selectivity in all the tested colorectal cancer cell lines. In comparison, SI values for TRF combined treatments were lesser in terms of the degree of reduction (Table 3.20).

Table 3.19 SI values of combined treatments with δT3 on various cancer cell lines.

Cell line	δT3 + Dox	δT3 + Cis	δT3 + 5FU	δT3 + Vin
Lung				
H1299	0.27	0.20	ND	**4.32**
A549	1.23	0.52	1.49	**13.71**
H23	**3.21**	0.79	**2.03**	ND
Calu-1	0.25	ND	ND	ND
Colorectal				
Caco-2	**21.44** ↑	**3.32** ↑	**29.88** ↑	**2.99**
HCT116	**46.92** ↑	**2.58** ↑	**6.66** ↑	**13.62**
SW48	**56.55** ↑	1.93 ↑	**5.58** ↑	**10.09**
HCC2998	**42.74** ↑	**3.32** ↑	**3.60**	**26.28**

Note: SI > 2 indicates general selectivity (in bold). The improved SI values in combined treatments as compared to the individual chemotherapeutic drug treatments are marked with ↑. ND denotes 'not determined' by which the IC_{50} values of normal or cancer cells were not detected, hence, it is impossible to estimate the SI.

Table 3.20 SI values of combined treatment with TRF on various cancer cell lines.

Cell line	TRF + Dox	TRF + Cis	TRF + 5FU	TRF + Vin
Lung				
H1299	1.15	0.66	ND	**20.77**
A549	1.92	1.89	1.57	**46.84**
H23	**7.13** ↑	**2.29**	1.50	ND
Calu-1	1.09	0.66	ND	ND
Colorectal				
Caco-2	**4.80**	**2.10** ↑	ND	**118.20** ↑
HCT116	**7.76**	1.79	**15.70** ↑	**2.03**
SW48	**5.88**	1.93	**4.67** ↑	**4.31**
HCC2998	**5.12**	**2.49** ↑	**2.64**	**14.73**

SI > 2 indicates general selectivity (in bold). The improved SI values in combined treatments as compared to the individual chemotherapeutic drug treatments are marked with ↑. ND denotes 'not determined' by which the IC_{50} values of normal or cancer cells were not detected, hence, it is impossible to estimate the SI.

3.3.3 Anti-survival effect of single and combined treatments

The treated cells which retain the capacity to proliferate into visible colonies signify the survived cells. Generally, the cells treated by single and combined treatments at their original (1x) concentrations showed inhibited clonogenicity (Figures 3.6 - 3.9). When serial dilutions were performed, δT3 + 5FU combined treatment prominently inhibited colonies formation in Caco-2 (Figure 3.6) and SW48 (Figure 3.8) cells, as compared to their individual single treatments.

Caco-2	1x	0.5x	0.25x
Vehicle control	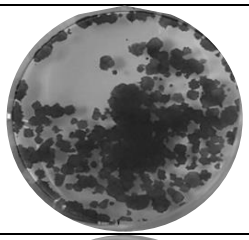	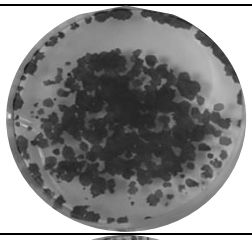	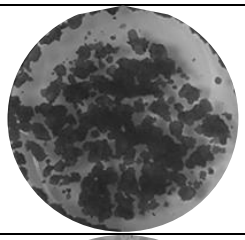
δT3 (10μM)	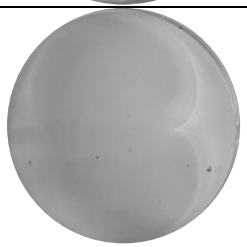	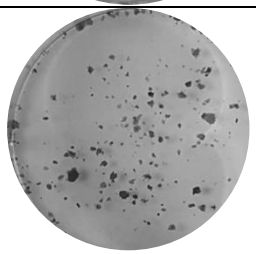	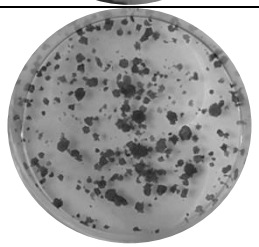
5FU (3.5μM)		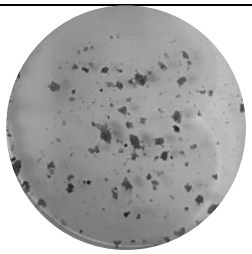	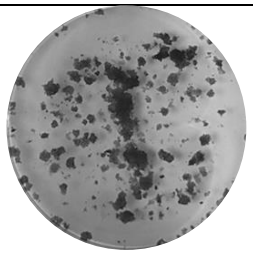
δT3 + 5FU (10μM + 3.5μM)	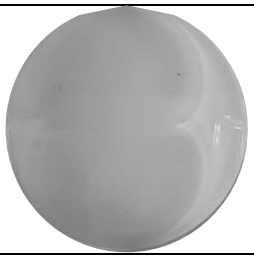	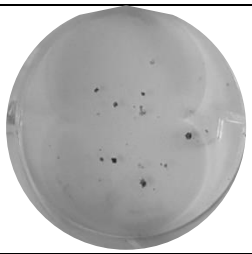	

Figure 3.6 Representative images of colonies formation of Caco-2 cells at 2-fold dilutions of single and combined treatments of δT3 and 5FU.

SW48	1x	0.5x	0.25x
Vehicle control	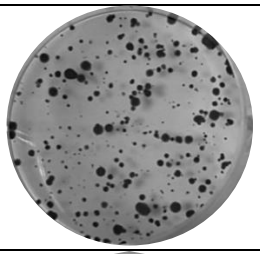	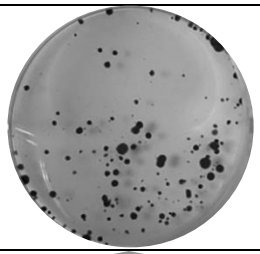	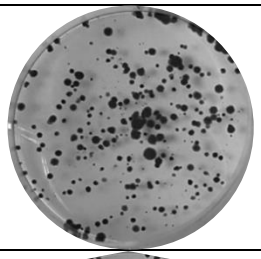
δT3 (10μM)		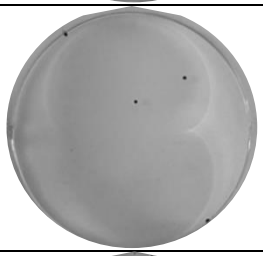	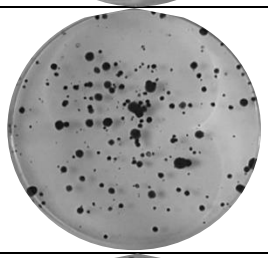
5FU (18μM)	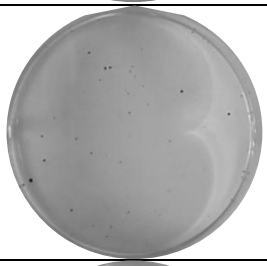	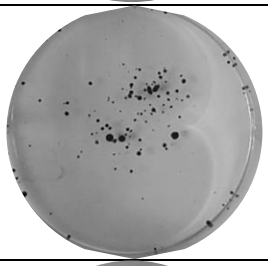	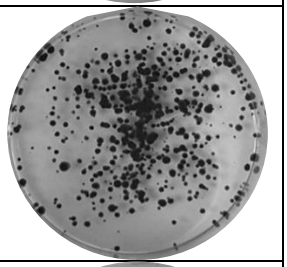
δT3 + 5FU (10μM + 18μM)			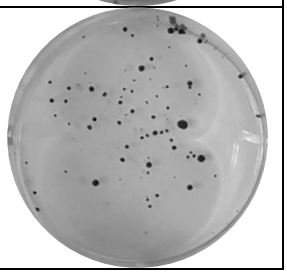

Figure 3.7 Representative images of colonies formation of SW48 cells at 2-fold dilutions of single and combined treatments of δT3 and 5FU.

Likewise, δT3 + Dox combined treatment exhibited a notable effect in inhibiting colonies formation in Caco-2 (Figure 3.8) and SW48 (Figure 3.9) cells, as compared to their individual treatments alone.

Caco-2	1x	0.1x	0.01x
Vehicle control	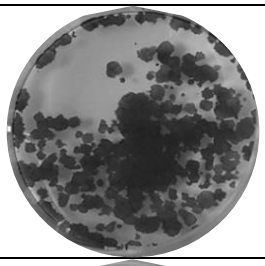	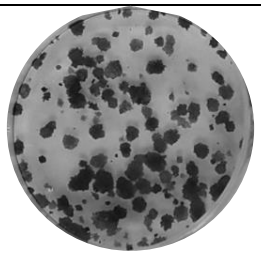	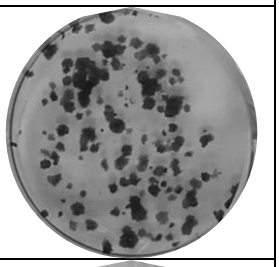
δT3 (10μM)	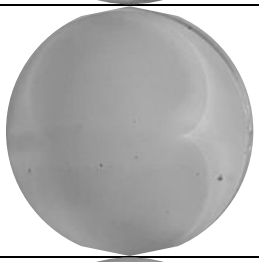	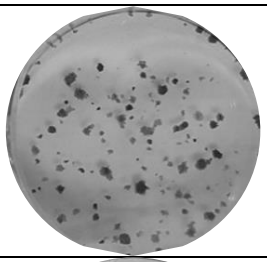	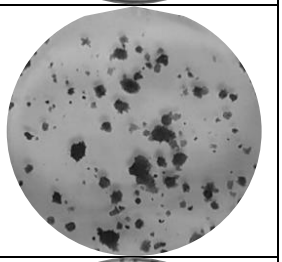
Dox (2μM)	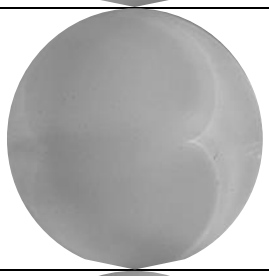	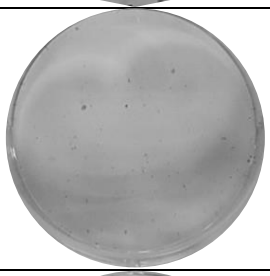	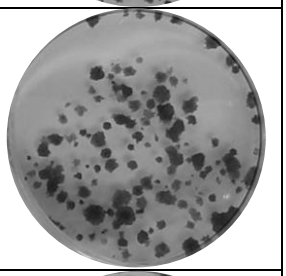
δT3 + Dox (10μM + 2μM)	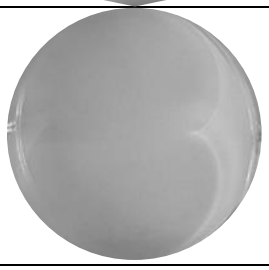	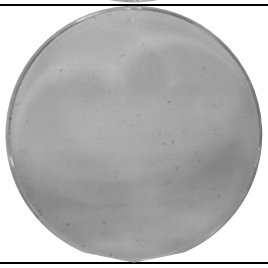	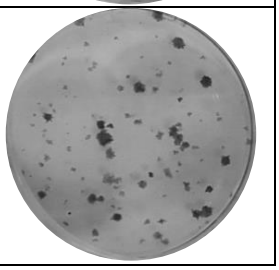

Figure 3.8 Representative images of colonies formation of Caco-2 cells at 10-fold dilutions of single and combined treatments of δT3 and Dox.

SW48	1x	0.1x	0.01x
Vehicle control	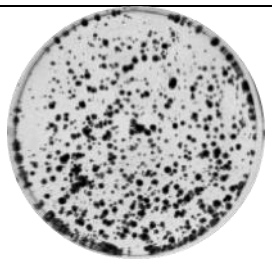	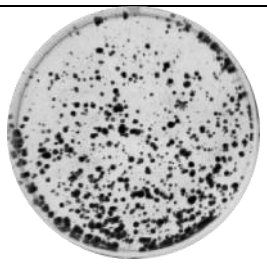	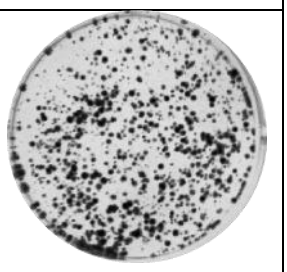
δT3 (10μM)		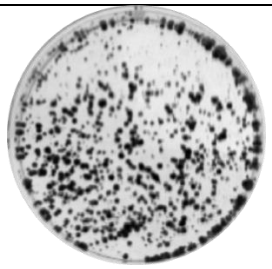	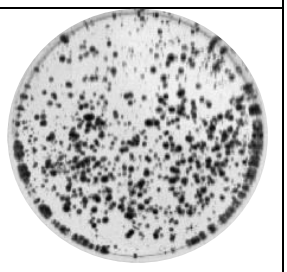
Dox (1μM)		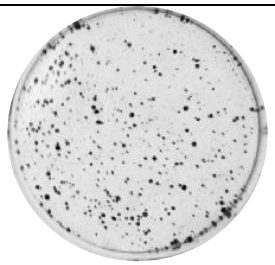	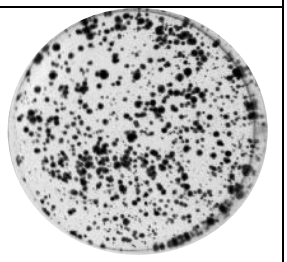
δT3 + Dox (10μM + 1μM)		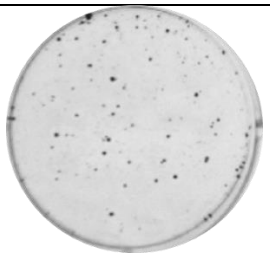	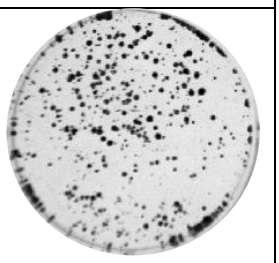

Figure 3.9 Representative images of colonies formation of SW48 cells at 10-fold dilutions of single and combined treatments of δT3 and Dox.

The inhibition of colonies formation induced by δT3 + 5FU combined treatment (Figure 3.10) was statistically significant ($p < 0.01$) over the vehicle control in both Caco-2 and SW48 cells. On the other hand, the δT3 + Dox combined treatment (Figure 3.11) also induced a significant inhibition of clonogenicity in Caco-2 ($p < 0.05$) and SW48 ($p < 0.01$) cells, as compared their respective vehicle control.

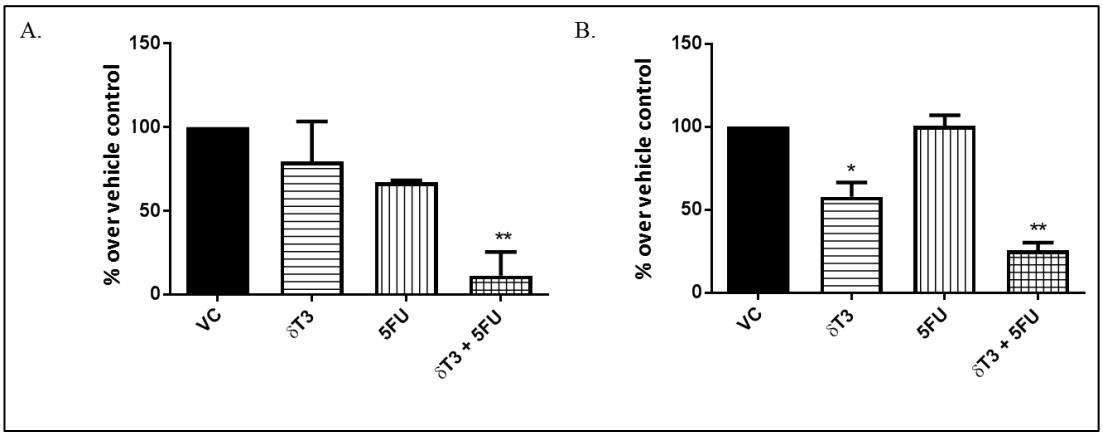

Figure 3.10 Clonogenic survival percentage after receiving single and combined treatments of δT3 and 5FU. Panel A, Caco-2 cells; Panel B, SW48 cells. VC, vehicle control; δT3, δ-tocotrienol; 5FU, 5-fluorouracil. * $p < 0.05$; ** $p < 0.01$.

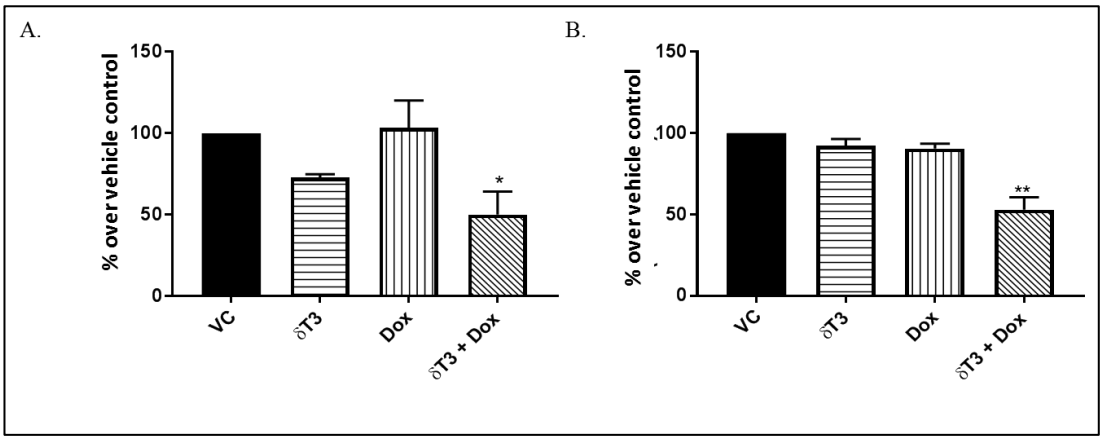

Figure 3.11 Clonogenic survival percentage after receiving single and combined treatments of δT3 and Dox. Panel A, Caco-2 cells; Panel B, SW48 cells. VC, vehicle control; δT3, δ-tocotrienol; Dox, doxorubicin * $p < 0.05$; ** $p < 0.01$.

3.4 Discussion

There is a compelling need for affordable, effective and immediate cancer therapeutic options. In fact, tocotrienols can offer valuable anti-cancer benefits but the therapeutic effects are hindered by low oral bioavailability. Chemotherapeutic drugs although is effective when used at high dose, the corresponding side effects and toxicities are relatively higher to endure. Hence, the combined treatment of tocotrienols and chemotherapeutic drugs at lower doses of their respective effective concentrations may offer an augmented therapeutic effectiveness while reducing the high dose associated limitations. As such, the current project embarked on elucidating the combinatorial effects of tocotrienols and chemotherapeutic drugs as the first manoeuvre towards exploring the potential anti-cancer effects in combination.

In this study, three tocotrienols isomers (i.e., αT3, γT3, δT3), one tocotrienol mixture (i.e., TRF), four distinct classes of chemotherapeutic drugs (i.e., Dox, Cis, 5FU and Vin) and three different types of cancers (i.e., lung, colorectal and nasopharyngeal cancers) were involved. Based on the cancer types involved in this study, the corresponding chemotherapeutic drugs were carefully selected according to existing chemotherapy regimens for lung, nasopharyngeal and colorectal cancers (Table 3.21). This selection is to ensure the applicability and reflectivity of current work to the actual clinical practice.

Unlimited proliferation is a predominant characteristic of cancers, hence the evaluation of the anti-proliferative potential of anti-cancer candidates is seen as the highest priority. To study the anti-proliferative effect, the metabolic status of treated cells was determined using an ATP-based assay, namely the CellTitre-Glo® assay. This assay is deemed a more sensitive and higher reliability platform as compared to

the conventional MTT assay (Menyhárt et al., 2016). In fact, MTT assay should be avoided due to the interference by tocotrienols, which will contribute to error in estimating the cell viability (Lim et al., 2015). In embracing the trustworthiness of this research through selecting an appropriate assay platform, the associated parameters such as combination index (CI), drug combination index (DRI) and selectivity index (SI) can be generated with higher reliability. Following an affirmative (short-term) anti-proliferative effect as suggested by ATP-based assay, clonogenic assay was performed to assess the long-term anti-proliferative (or survival) effect of the selected combined treatments.

Table 3.21 Chemotherapeutic drugs used in the existing chemotherapy regimen.

Cancer type	Drugs	Acronym
Lung	Cyclophosphamide, **doxorubicin**, vincristine	CAV
	Cisplatin, vinorelbine	NP
Colorectal	Mitomycin**, vinblastine, cisplatin**	MVP
	5-fluorouracil, folinic acid, oxaliplatin	FOLFOX
	5-fluorouracil, leucovorin	FL
	5-fluorouracil, folinic acid, irinotecan	FOLFIRI
Nasopharynx	**Cisplatin**, **5-fluoruracil**	CF

The IC_{50} values generated by the CellTitre-Glo® assay infer the potencies of anti-cancer agents, in such a way that the lower the IC_{50} is, the higher the drug potency will be and *vice versa*. On the other hand, high SI also infers a high selectivity for cancers over normal cells. Hence, it is imperative to understand the potency and selectivity of the individual tocotrienols and chemotherapeutic drugs before proceeding into the combination study.

Out of the three tocotrienols isomers, current results on the anti-proliferative effects demonstrated that δT3 and γT3 were more potent (lower IC_{50}) than αT3 on most of the cell lines tested (Table 3.7). In fact, this result is in agreement with many previous studies (Constantinou et al., 2009; Parker et al., 1993; Pierpaoli et al., 2010; Wada, 2009). For instance, δT3 and γT3 were reported to have stronger anti-cancer effects as compared to αT3 and α-tocopherol in HER-2/neu breast cancer cells (Pierpaoli et al., 2010). From the structure-function perspective, the stronger anti-proliferative effects of δT3 and γT3 could be attributed to their hypomethylated chroman ring. The decreased methylation in chroman ring therefore allows the molecule to be easily incorporated into the cell membrane (Palozza et al., 2006). In cancer cells, these hypomethylated forms of tocotrienols showed a higher uptake rate (Viola et al., 2012), suggesting a cellular concentration-dependent effect. In addition, higher number of hydroxyl groups in the hypomethylated chroman ring rendering a greater anti-oxidant capacity and potential interactions with biomolecules (i.e. proteins and lipids). As a result, an array of biochemical reactions and signalling routes can be triggered. Of note, δT3 and γT3 demonstrated higher potencies in colorectal as compared to lung and nasopharyngeal cancer cell lines (Table 3.6). Although the underlying reason is currently unknown, it is postulated that the colon cells may have better absorption of tocotrienols than lung and nasopharyngeal cancers.

Apart from tocotrienol isomers, TRF also exhibited a consistent trend to tocotrienol isomers in which a greater potency was observed in colorectal cancer cell lines than lung and nasopharyngeal cancer cell lines (Table 3.6). Typically, TRF contains approximately 70% of αT3, δT3 and γT3 mixtures and 30% of α-tocopherol. This anti-proliferative effect could solely be attributed to the tocotrienol mixtures contained in TRF as α-tocopherol does not possess anti-cancer properties (Yu et al.,

2009). The multiple compounds when existing together, could act differently as a new bioactive, therefore the potential of TRF is worthwhile to be further explored. Moreover, taking the market availability of TRF as an added advantage, it is treasured to investigate its potency under combinatorial application with chemotherapeutic drugs.

Other than anti-proliferative potency, selective toxicity is another concern in drug discovery. Several lines of evidence reported that tocotrienols display selective toxicity towards cancer cells without affecting normal cells (Comitato et al., 2017; Har and Keong, 2005; Lim et al., 2014a). Specifically, δT3 and γT3 were accumulated in *in vivo* tumour but not the normal tissue, inferring that selective accumulation of tocotrienols is a critical factor for anti-tumour activity (Hiura et al., 2009). In a human clinical study, δT3 was proven safe when consumed at 3,200mg per daily intake without causing any adverse effect (Mahipal et al., 2016). Additionally, tocotrienols had been recognised as Generally Recognised As Safe (GRAS) by FDA (Schauss et al., 2008). Current study conformed to previous studies that tocotrienols exhibited a varying degree of selectivity, where the IC_{50} values of normal cells were higher than cancer cells (SI > 1) (Table 3.9). However, guided by the general guideline of selectivity, SI < 2 is considered as poor selectivity. Tocotrienols appeared to have better selectivity (SI > 2) in colorectal cancer cells and lung than nasopharyngeal cancers. Despite the anti-proliferative potency of γT3 and δT3 is comparable, the selectivity of δT3 is better than γT3. Hence, δT3 was chosen as the combination candidate for the subsequent combined treatment study.

The chemotherapeutic drugs, Dox and Vin exhibited a greater anti-proliferative potency (lower IC_{50}) than that of Cis and 5FU (Table 3.8). The

differential drug potency could be attributed by their respective mechanisms of actions. For instance, both Dox and Vin target G2/M phase of the cell cycle by inhibiting DNA replication and division machinery, namely the topoisomerase II and tubulin respectively (Kumar et al., 2014; Sajó, 1977; Thorn et al., 2011). In contrast, Cis and 5FU target S-phase of the cell cycle by directly intercalating the DNA to block DNA biosynthesis (Dasari and Tchounwou, 2014; Longley et al., 2003). Of note, S-phase requires 10-12 hours to complete, which constitutes a relatively larger proportion of a cell cycle as compared to M-phase that takes less than an hour to complete in mammalian cells (Alberts et al., 2002). As such, it is plausible to speculate that higher amount of drugs are needed for incorporation/saturation into DNA (higher abundancy) at a longer S-phase, while lower amount of drugs to inhibit the mitosis machinery which is effective at a shorter M-phase.

Based on SI, Dox and Vin appeared superior to Cis and 5FU by displaying higher SI (Table 3.10). Due to lower IC_{50} values of Dox and Vin, the selectivity is higher. However, in the actual clinical setting, chemotherapy has been traditionally administrated at the maximum tolerated dose to ensure the highest therapeutic response, which however has led to toxicity-associated complications and deaths (Chan et al., 2016). Hence, it is of importance to reduce an effective dose required yet with an increase the therapeutic window. As such, prolonged treatment is feasible to ensure complete eradication of cancer cells population. Therefore, these considerations have led to subsequent combined treatment experimental design on studying the dose reduction and selectivity indices of the chemotherapeutic drugs by combinatorial application of δT3 and TRF.

Based on the superior anti-proliferative potency and selectivity of single treatments as described above, δT3 and TRF were selected as tocotrienol agents to be combined with the chemotherapeutic drugs on colorectal and lung cancer cell lines. Sub-effective concentrations of δT3 (10μM) and TRF (5μg/ml) lying within IC_{10}-IC_{20} were chosen, as suggested by several previous studies (Abdul-Rahman et al., 2014; Abubakar et al., 2017, 2016; Shirode and Sylvester, 2011; Tiwari et al., 2015), to combine with varying concentrations of chemotherapeutic drugs with an anticipation that a low amount of tocotrienol could reduce the required effective concentration and improve the cancer selectivity of the chemotherapeutic drugs.

After combining chemotherapeutic drugs with the sub-effective concentration of δT3, a synergism was detected in cancer type-dependent and chemotherapeutic drug-dependent manners. In general, δT3 + Dox combined treatment resulted in mostly synergistic interaction while δT3 + Cis combined treatment was mostly antagonistic (Table 3.13). δT3 + 5FU combined treatment exhibited a strong synergism only in colorectal cancer cell lines (Table 3.13). On the other hand, δT3 + Vin combined treatment gave rise to synergism only in lung cancer cell lines (Table 3.13). These cancer types and drug specific effects were similar in TRF combinations.

The current results suggested that δT3 is more effective than TRF when combined with chemotherapeutic drugs. For instance, δT3 combined treatments showed a total of ten synergistic interactions on various cancer cell lines (Table 3.15 & 3.16). In comparison, TRF only resulted in five combined treatments showing synergistic effects. TRF contains a mixture of tocotrienols and α-tocopherol, which is highly expected to lead to diverse biological and pharmacological responses. Therefore, it is difficult to explicate the potential interactions with chemotherapeutic drugs. Moreover, the presence of α-tocopherol in TRF could be another reason for

reducing the chemosensitising properties. To further illustrate, it was reported that α-tocopherol blocks the multidrug-resistance-reversal activity of chemosensitising agents and preventing the restoration of sensitivity to both Dox and Vin (Van Rensburg et al., 1998). Therefore, TRF combinations were not considered for subsequent investigations in the current work.

Serving as the first line chemotherapeutic drug in lung cancer, Dox showed synergisms in three lung cancer cell lines. However, these combinations did not exhibit a general selectivity (SI<2) (Table 3.19). As such, combined treatments of lung cancer cell lines were ruled out from the current work as well.

Of note, δT3 + 5FU combined treatment resulted synergism in Caco-2 and SW48 cells, in which the IC_{50} values of 5FU were reduced by approximately 16-fold and 4-fold, respectively as compared to individual 5FU single treatment (Table 3.17). Remarkably, the SI was improved by at least 25-fold and 4-fold (Table 3.19), respectively as compared to their individual chemotherapeutic drug treatments (Table 3.10). Considering the clinical relevance of 5FU for colorectal cancer treatment, these combinations warrant a continual investigation.

Additionally, it was reported that Dox treatment is in fact effective against colorectal cancer which can be used clinically provided that the high dose associated toxicities are reduced (Sonowal et al., 2017). In the present study, δT3 + Dox combined treatment showed dose reduction (Table 3.17) and improved selectivity (Table 3.19). Hence, it is prospective to study the potential of δT3 + Dox combined treatment as a second line treatment, providing an alternative treatment if the first line treatment fails. Although δT3 + Dox combined treatment was identified as an antagonistic effect in SW48 cell line (Table 3.13), the combined treatment

demonstrated improvement in selectivity therefore it was taken one step further to evaluate for its anti-survival effect. Collectively, both δT3 + 5FU and δT3 + Dox combined treatments were further investigated in Caco-2 and SW48 cells for exploring their feasibility to be used as primary and alternative treatments for colorectal cancer which combinations are summarised in Table 3.5.

Following that, clonogenic assay was performed to study the survival effect of Caco-2 and SW48 cell lines after receiving the individual single and combined treatments. From the results, it was clearly demonstrated that both the single and combined treatments inhibited cell survival, inferring a cytotoxic rather than cytostatic effect was exerted (Figures 3.6 – 3.9). In the presence of a cytostatic effect, the treated cells may not undergo mitotic death but were temporarily suppressed from proliferating. A withdrawal of treatment followed by prolonged incubation in complete media should foster the regrowth of cancer cells and establishment of visible colonies. On the contrary, the cytotoxic effect renders a reproductive death on the treated cancer cells in such a way that they lose their proliferation capacity to form colonies. Notably, the cytotoxic effects of the combined treatments were significantly stronger even after 4-fold (5FU) and 100-fold (Dox) dilutions (Figures 3.10 & 3.11). The cytotoxic effect in fact is seen as a favourable outcome, as a cytostatic effect could be easily overcome by cancer and reserves a potential of cancer recurrence. It is noteworthy that the combined treatment with tocotrienols were may not necessarily cytotoxic, as it was previously reported that combination of γT3 and statins imparting a cytostatic but not cytotoxic effect (Sylvester, 2012; Wali and Sylvester, 2007). Despite an antagonistic effect was initially suggested for δT3 + Dox combined treatment on SW48 cells, the combined treatment could undeniably improve cytotoxicity than the individual single treatments, which therefore deserves a further

investigation. All together, these combinations (δT3 + 5FU and δT3 + Dox) conferred prospective therapeutic outcomes that are worthwhile to be further investigated in the subsequent chapters.

3.5 Conclusion

In summary, the current study identified that anti-proliferative potencies of tocotrienol isomers are δT3 ≈ γT3 > αT3. In colorectal cancer, δT3 showed a superior selectivity, hence it was chosen for the combined treatment study. Combined treatments of chemotherapeutic drugs with δT3 are more effective than the combinations with TRF. In Caco-2 and SW48 colorectal cancer cell lines, δT3 + 5FU remarkably reduced the effective dose of the chemotherapeutic drug by 16-fold and 4-fold, respectively. This could potentially contribute to the reduction in dose-association toxicities. In addition, the synergistic combined treatments with improved SI as compared to single agent treatment have shown that these combinations were cancer-selective. Besides, δT3 + 5FU and δT3 + Dox combined treatments exerted a cytotoxic rather than cytostatic effect on Caco-2 and SW48 cell lines. Taken together, current work serves as a solid foundation to embark in the subsequent objectives to investigate the apoptotic effects and the underlying mechanisms as described in the next chapters.

Chapter Four: Characterisation of cell death responses induced by individual and combined treatments of δ-tocotrienol and/or chemotherapeutic drugs (5-fluorouracil and doxorubicin)

4.1 Introduction

Green and Evan (2002) proposed that the fundamental alterations for transforming a normal cell into a malignant one are through an increase in cell proliferation and a decrease in cell death. For instance, cancer drives normal cells impervious toward cell death stimuli to be able to undergo uncontrolled cell division. Hence, an effective anti-cancer strategy should be able to reverse the perturbed state by decreasing proliferation and increasing death in cancer cells (Tham et al., 2019). Guided by promising anti-proliferative effects of δ-tocotrienol and 5-fluorouracil (δT3 + 5FU) and δ-tocotrienol and doxorubicin (δT3 + Dox) in Caco-2 and SW48 cells as described in Chapter Three, current chapter further characterises the cell death responses induced by the single and combined treatments.

Elimination of cancer cells via activation of cell death programs remains an attractive and promising approach in cancer therapy. Generally, there are three forms of widely accepted cell death modalities, namely apoptosis, autophagy and necrosis (Galluzzi et al., 2007). Depending on the nature of therapeutic interventions and the underlying molecular identity of cancer cells, cell death can occur through different mechanism(s) leading to differential therapeutic responses.

Literatures widely reported that apoptosis is convened as an anti-cancer mechanism for δ-tocotrienol (δT3), 5-fluorouracil (5FU) and doxorubicin (Dox) in various types of cancer cells such as breast, lung and colon (Loganathan et al., 2013; Park et al., 2010; Phutthaphadoong et al., 2012; Xu et al., 2012). Apoptosis, also known as type II PCD, is a physiological process of cell death. Morphologically, the

manifestation of apoptosis is reflected by cell shrinkage, nuclear chromatin condensation (nuclear pyknosis), nuclear fragmentation (karyorrhexis), plasma membrane blebbing and/or apoptotic bodies formation (Galluzzi et al., 2018, 2007). At biochemical level, externalization of phosphatidylserine (PS) and DNA fragmentation are an early and late event of apoptosis, respectively. Collectively, the morphological and biochemical assessments are important for characterisation of apoptosis, as recommended by the Nomenclature Committee on Cell Death (NCCD) (Galluzzi et al., 2018).

With reference to the morphological and biochemical criteria of apoptosis, current study was designed to encompass the both aspects. Phase-contrast and fluorescence microscopies were adopted to assess morphological changes of treated cells at 24 hours and with an interval up to 72 hours. Phase-contrast microscopy deduces gross morphological changes associated with apoptosis, which include cell shrinkage and membrane blebbing. The supplementary 4, 6-Diamidino-2-phenylindole (DAPI) staining enables observation of nuclear changes while acridine orange/propidium iodide (AO/PI) dual staining differentiates apoptosis at different stages, namely early/late apoptosis or secondary necrosis. On the other hand, flow cytometric detection of PS exposure was conducted to quantify cells undergoing apoptosis. In addition, single-cell gel electrophoresis (comet assay) was performed to study the DNA damage patterns (i.e., DNA single-stranded or double-stranded breaks) caused in the treated cells while cell cycle analysis was conducted to assess potential involvement of DNA-damage induced cell cycle arrest. Moreover, sub-G1 population detection using flow cytometry was performed to quantify the fragmented DNA, which is accepted as a late-stage event of apoptosis.

The apoptosis-inducing capacity and actions of the single and combined treatments were equally important in order to decipher the underlying synergistic actions. Hence, the respective concentrations of single agents applied in the combinations were studied, similar to those previous combined treatment studies involving tocotrienols (Bachawal et al., 2010b; Malaviya and Sylvester, 2014; Prasad et al., 2016; Shirode and Sylvester, 2011). In fact, assessing and quantifying apoptosis at a single time point may underestimate the population of apoptotic cells. Hence, experiments were designed and performed in several time points (24-72 hours in this study) as cell death is a kinetics process (Queiroz et al., 2014); monitoring the changes over an appropriate period of time may help to unveil differential capacity between single and combined treatments.

A correct identification of cell death modality induced by the treatments is crucial for cancer therapy success. Hence, the motivation of the current chapter was to study the kinetic cell death responses on Caco-2 and SW48 colorectal cancer cells after single (δT3, 5FU, Dox) and combined (δT3 + 5FU and δT3 + Dox) treatments. The specific objectives as indicated herein:

i. To morphologically characterise the cell death response induced by the single and combined treatments.
ii. To quantify apoptosis induced by the single and combined treatments.
iii. To evaluate the DNA damage profiles induced by the single and combined treatments.
iv. To study the cell cycle profiles induced by the single and combined treatments.
v. To quantify the DNA fragmentation induced by the single and combined treatments.

4.2 Materials and Methods

Generally, the experimental design of current chapter was divided into two parts. The cell death morphologies induced by single and combined treatments were initially observed under phase-contrast (for unstained cells) and (for DAPI and AO/PI stained cells) fluorescence microscopes. Following the confirmation on apoptosis induction, a series of apoptosis-related evaluations were performed, including Annexin V-FITC/PI apoptosis quantification assay, comet assay, cell cycle analysis and sub-G1 assay (Figure 4.1).

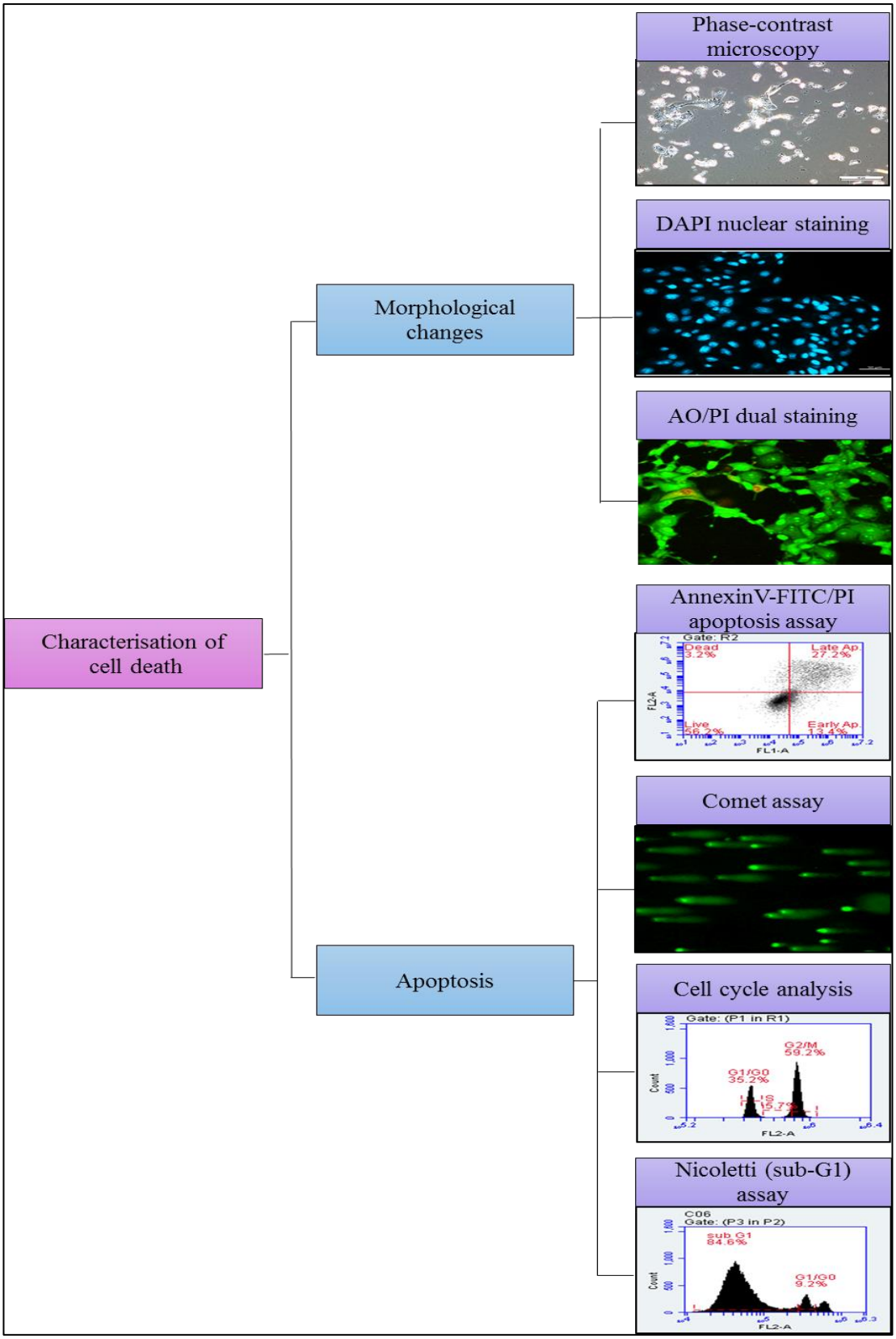

Figure 4.1 An overview of experiments involved in Chapter Four for characterising the induced cell death responses by the single and combined treatments on Caco-2 and SW48 cells.

4.2.1 Cell seeding and experimental treatment

An optimal cell density for 6-well plate (90% confluence by 72 hours) was identified and used in the actual experiment. Six-well plate format was used in experiments throughout this chapter unless otherwise stated. A total 1.5 x 10^5 and 3 x 10^5 cells/well of the respective Caco-2 and SW48 cells were seeded into 6-well plates and incubated overnight to allow cell attachment. Following that, the plates were replaced with the treatment media containing single and combined treatments as presented (see Table 3.5). Untreated wells containing medium and equivalent amount of DMSO were included as a vehicle control.

4.2.2 Microscopy

For more than 150 years, morphological features play a significant role in cell death identification (Ziegler and Groscurth, 2004). Using microscopy, cellular and nuclear morphologies can be appropriately assessed based on the currently available knowledge on cell death.

4.2.2.1 Phase-contrast

Phase-contrast microscopy is an optical microscopy technique that produces high-contrast images of transparent (unstained) specimens. It reveals cellular structure that is not visible under brightfield microscopy. Hence, it was employed to inspect the morphologies of live cells (e.g., adherent/detached, cell size and shape changes). In a 6-well plate, Caco-2 and SW48 colorectal cancer cells were seeded, treated and cell morphologies were captured using the Nikon Eclipse TiU phase-contrast microscope (Nikon, Japan) at 100x and 200x magnifications after 24, 48 and 72 hours of treatment.

4.2.2.2 4′,6-Diamidino-2-phenylindole (DAPI) staining

DAPI is a fluorescent stain that preferentially binds to adenine–thymine rich region of DNA strands. As a result, blue fluorescence is emitted and visualisation of

nuclear changes during apoptosis such as chromatin condensation and nuclear fragmentation (Taatjes et al., 2008). The treated cells were fixed in freshly prepared 3.7% (v/v) formaldehyde (Sigma-Aldrich, USA) for 10 minutes. Next, the cells were washed with 1x phosphate buffered saline (PBS) for three times at 5-minute interval to remove the fixative. Next, the cells were permeabilised with 0.2% (v/v) Triton-X100 (Sigma-Aldrich, USA) in PBS for 5 minutes. Subsequently, the cells were washed as previously mentioned and stained with 20µg/ml of DAPI in PBS for 5 minutes. Lastly, the cells were washed with PBS for three times to remove the unbound DAPI. The cell images were captured by Axio Observer 7 (Zeiss, Germany) with DAPI filter (365/460nm).

4.2.2.3 Acridine orange (AO) and propidium iodide (PI) dual fluorescent staining

AO/PI double stains help to differentiate between viable, apoptotic and necrotic cells. Viable cells are stained green by acridine orange; late apoptotic cells appear orange and necrotic cells are stained red by propidium iodide. Caco-2 and SW48 cells were cultured on sterile gelatin-coated cover slips placed in a 6-well plate and subjected to the respective treatments. A 10µl of AO (10µg/ml) and PI (10µg/ml) mixture at 1:1 ratio was applied as reported previously (Lim et al., 2014a). Using the Nikon Eclipse 80i fluorescence microscope (Nikon, Japan) supplemented with appropriate filter for AO (502/525nm) and PI (535/617nm), morphologies of cells under single and combined treatments were assessed within 20 minutes at the magnification of 200x.

4.2.3 Single cell gel electrophoresis (comet)

Single cell gel electrophoresis or comet assay is commonly used to detect DNA damage at single cell level (Olive and Banáth, 2006). Cells are embedded in agarose onto a microscope slide and lysed with high salt detergent to obtain nucleoids. Comet

assay performed under alkaline condition (pH >13) is capable of detecting DNA single-stranded breaks (SSBs); neutral comet predominantly detects DNA double-stranded DNA breaks (DSBs) (Olive and Banáth, 2006). In the presence of DNA breaks, the DNA will migrate away from the nucleoid 'head' during gel electrophoresis resembling comets. On the other hand, undamaged DNA remains in the 'head' with little/no tail formation. The slides were visualised using the Nikon Eclipse Ti-U fluorescence microscope (Nikon, Japan) upon staining with SYBR™ Safe DNA binding fluorescent stain (Invitrogen, USA). The protocol of this assay was developed from Olive and Banáth (2006) with slight modifications.

4.2.3.1 Alkaline comet

Caco-2 and SW48 cells were treated for 24, 48 and 72 hours. Thereafter, cells were harvested by trypsinisation and washed with PBS. Then, the cells were re-suspended in 0.5ml PBS. The cell suspensions were mixed with 1% (w/v) low-melting agarose at 1:1 ratio and transferred onto a microscopic slide pre-coated with 1% (w/v) normal melting agarose. The slides were immersed in alkaline lysis solution [2.5M NaCl, 100mM EDTA, 1% sodium lauryl sarcosinate (w/v), 10mM Tris, 0.5% Triton X-100 (v/v) and 10% DMSO (v/v)] with pH adjusted to 13 for 2 hours. Following that, the slides were equilibrated in alkaline electrophoresis buffer (300mM NaOH, 1 mM EDTA, pH 13.5) at 4°C for 20 minutes. The slides were subjected to electrophoresis at 20V for 20 minutes. After that, the slides were rinsed with neutralisation buffer (0.4M Tris, pH 7.5) for three times. One hundred microliters of diluted (1:10,000) SYBR Safe (Thermo Scientific, USA) was dropped onto the slide and incubated for 5 minutes. The slides were visualised using the fluorescence microscope. Ten images were captured at different fields for each slide. At least 50 comets were analysed using OpenComet software v1.3.1 (Gyori et al., 2014).

4.2.3.2 Neutral comet

The single cell suspensions were harvested and embedded in agarose on microscope slides as mentioned in the alkaline comet preparation (Section 4.2.3.1). Following that, the cells were lysed in neutral lysis buffer [2.5M NaCl, 1% (w/v) N-lauroylsarcosine sodium, 10mM Na_2EDTA (pH 8), 10mM Tris-HC1 (pH 8), 1% (v/v) Triton X-100] for 2 hours. Following that, the slides were equilibrated in Tris-Boric Acid buffer at 4°C for 20 minutes. The slides were subjected to electrophoresis at 20V for 20 minutes. Next, the slides were stained, visualised and analysed similar to alkaline comet preparation (Section 4.2.3.1)

4.2.4 Flow cytometry

Flow cytometry is a laser-based technology that can be used to analyse the characteristics of cells or particles. Cells stained with fluorochromes are taken by the flow cytometer in a stream of fluid to generate a single cell suspension. A laser module in the flow cytometer excites the fluorochrome labels and the emitted signals are detected by the detectors and converted into digital data for analyses. Hence, it is a powerful method for analysis at a single cell level.

4.2.4.1 Annexin V-fluorescein isothiocyanate (FITC)/PI apoptosis detection assay

PS externalisation to the outer leaflet of plasma membrane due to the loss of lipid symmetry has been widely recognised as a biochemical hallmark of apoptosis (Crowley et al., 2016). Annexin V labelled with fluorescein isothiocyanate (Annexin V-FITC) binds specifically to the PS and emits green fluorescence. On the other hand, PI membrane impermeant dye stains only dead cells with the compromised plasma membrane. Hence, Annexin V-FITC positive cells indicate an early apoptosis, Annexin-V FITC/PI positive cells indicate a late apoptosis whereas PI only positive cells indicate dead cells. After 24, 48 and 72 hours of treatment, the cells were

detached by 0.5ml of 0.05% trypsin (Corning, USA) and centrifuged (Eppendorf, Germany) at the speed of 500x*g* for 5 minutes. The cells were washed with ice-cold PBS for twice and re-suspended in 0.1ml of 1x binding buffer (1.4M NaCl and 25mM $CaCl_2$, pH 7.4). Then, 5µl of Annexin V-FITC and PI were added into each sample respectively. No-stain and single-stained controls (individually with Annexin V-FITC or PI) were included for colour compensation purpose. All the stained samples were incubated for 10 minutes before subjected to data acquisition using BD Accuri C6 flow cytometer (BD Biosciences, USA). The data were collected at FL1 channel (for FITC) and FL2 channel (for PI) and analysed using BD Accuri C6 software.

4.2.4.2 Cell cycle analysis

The cell cycle consists of two specific and distinct phases: interphase, consisting of G1 (Gap 1), S (synthesis), and G2/M (Gap 2/mitosis) phases. Cell cycle analysis by flow cytometry quantifies the cell population at different stages of cell cycle. The corresponding cellular DNA content of the PI-stained cells is reflected in DNA content frequency histogram.

Both floating and attached cells were collected at 800x*g* for 5-minute centrifugation. Briefly, cells were washed twice with 1x PBS and fixed in 70% ice-cold ethanol at -20°C overnight. Subsequently, the cells were suspended in 500µl of 1x PBS then treated with 0.1mg/ml of RNase A (Nacalai Tesque, Japan) for 15 minutes at room temperature. Following that, 50µg/ml of PI (Sigma-Aldrich, USA) was added and incubated for 30 minutes at 37°C. DNA content was acquired and analysed by using BD Accuri C6 flow cytometer (Becton Dickinson, USA). At least 12,000 events were collected after gated out the doublets.

4.2.4.3 Nicoletti (sub-G1) assay

Nicoletti and co-workers (1991) developed a modified protocol of cell cycle analysis to detect DNA fragmentation. During apoptosis, DNA fragmentation results in DNA hypodiploidy owing to the degradation by endonucleases. As a result, nuclei of apoptotic cells will contain lesser DNA than the healthy cells. Under PI staining, the fragmented DNA gives rise to sub-G1 DNA population and was quantified during flow cytometry. The sub-G1 assay was adapted from Riccardi and Nicoletti (2006).

Caco-2 and SW48 cells were treated, detached and washed with PBS as described previously. After washing with ice-cold PBS, 0.5ml of ice-cold 70% (v/v) ethanol was added to re-suspend the cells. The samples were incubated on ice for 30 minutes. Then, the cells were collected at 800x*g* of centrifugation and washed twice with sub-G1 phosphate-citrate buffer (0.2M Na_2HPO_4, 0.1M citric acid, pH 7.8). Subsequently, the cells were re-suspended in 0.5ml of PBS containing 25µg/ml PI and 0.1mg/ml RNase A. The cells were incubated at 37°C for 30 minutes to facilitate staining. The stained cells were analysed using BD Accuri C6 flow cytometer (BD Biosciences, USA). Cells appeared before G1 peak were regarded as sub-G1 fraction.

4.2.5 Statistical analysis

All statistical analyses in this chapter were performed using GraphPad Prism 7 (GraphPad Software, USA). One way analysis of variance (ANOVA) test was followed by Dunnett's multiple comparisons to identify the statistical significance levels between the mean values of treated groups and untreated vehicle control. P-values < 0.0001 (****), $p < 0.001$ (***) $p < 0.01$ (**) and $p < 0.05$ (*) were considered as statistically significant.

4.3 Results

4.3.1 Morphological changes of colorectal cancer cells treated with individual single and combined treatments

4.3.1.1 Phase-contrast microscopy

Under a phase-contrast microscope, morphological changes of live cells including cell size, shape and detachment were observed. Generally, healthy cells possessed a defined cell shape and still attached to the surface of cultureware. In contrast, stressed cells underwent shrinkage (loss of cell volume), rounding up, vacuolisation (vacuole formation in cytoplasm) and eventually detached from the surface of cultureware in response to death stimuli.

Caco-2 cell micrographs portrayed a time-dependent increase in cell rounding and detachment after treatments (Appendices: Figures A4.1 – A4.4). These morphologies found the most prominent at 72-hour treatment, were therefore selected for representation (Figures 4.2 – 4.5). In Figure 4.2c, it shows that 5FU single treatment induced cell detachment as compared to the vehicle control. In comparison, the cell detachment occurred in δT3 + 5FU combined treatment (Figure 4.2d) was greater than that of the individual single treatments. In SW48 cells, δT3 and 5FU single treatments caused cell rounding. In comparison, δT3 + 5FU combined treatment (Figure 4.3d) resulted in a substantial rounding and detachment as compared to vehicle control and the respective individual single treatments (Figure 4.3a,b,c).

On the other hand, δT3 + Dox combined treatment resulted in a prominent cell detachment in Caco-2 cells (Figure 4.4d), as compared to vehicle control and the respective individual single treatments (Figure 4.4a,b,c). Likewise, enhanced cell detachment was observed in SW48 cells receiving δT3 + Dox combined treatment

(Figure 4.5d) when compared to the vehicle control and the respective individual single treatments (Figure 4.5a,b,c).

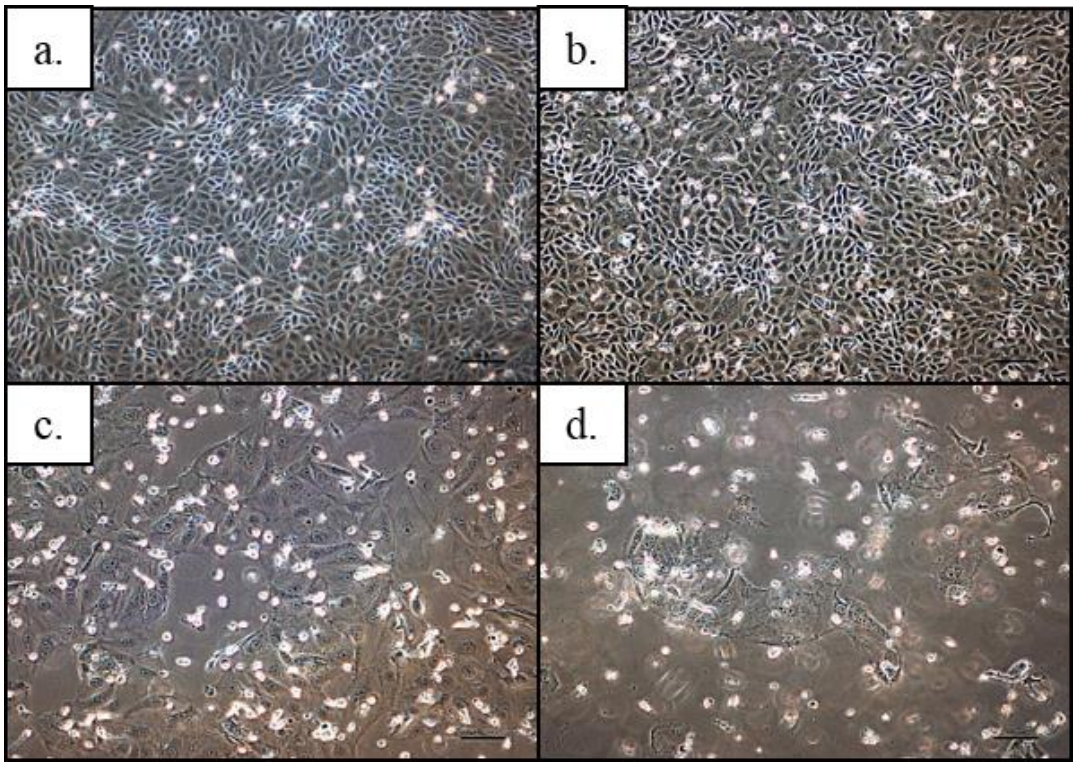

Figure 4.2 Representative phase-contrast micrographs of Caco-2 after receiving 72-hour treatments of δT3, 5FU and the combined treatment. a, vehicle control; b, δT3; c, 5FU; d, δT3 + 5FU. Magnification at 100x. Scale bar represents 100μm.

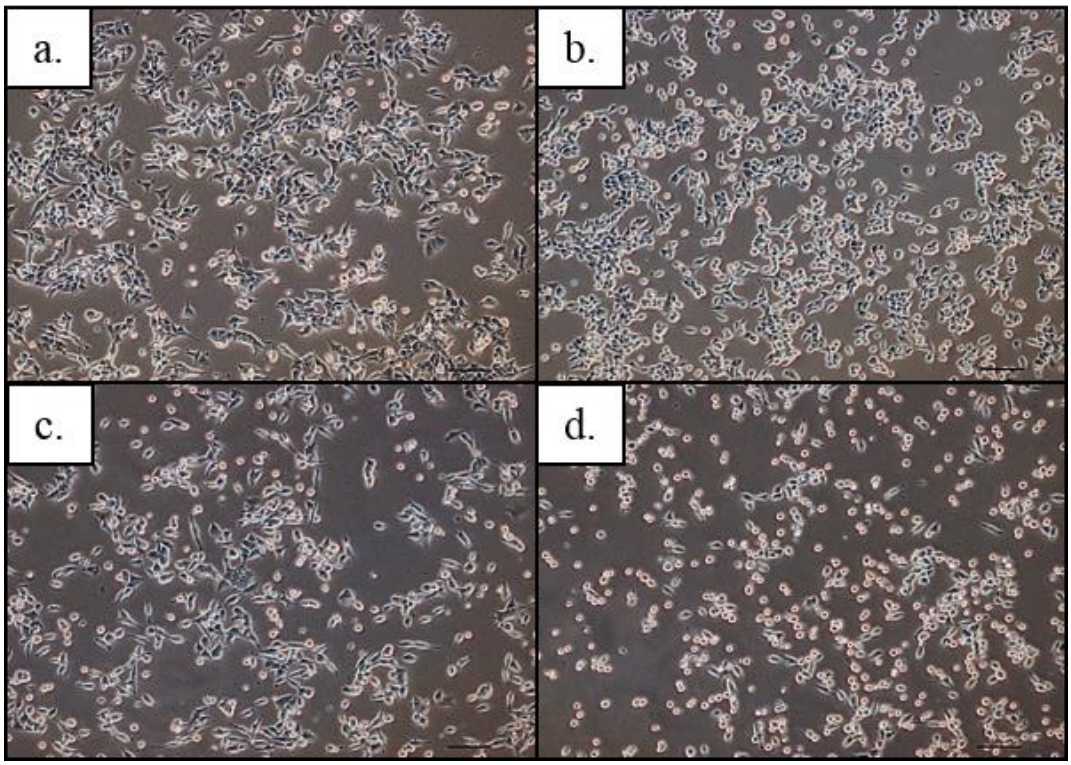

Figure 4.3 Representative phase-contrast micrographs of SW48 after receiving 72-hour treatments of δT3, 5FU and the combined treatment. a, vehicle control; b, δT3; c, 5FU; d, δT3 + 5FU. Magnification at 100x. Scale bar represents 100μm.

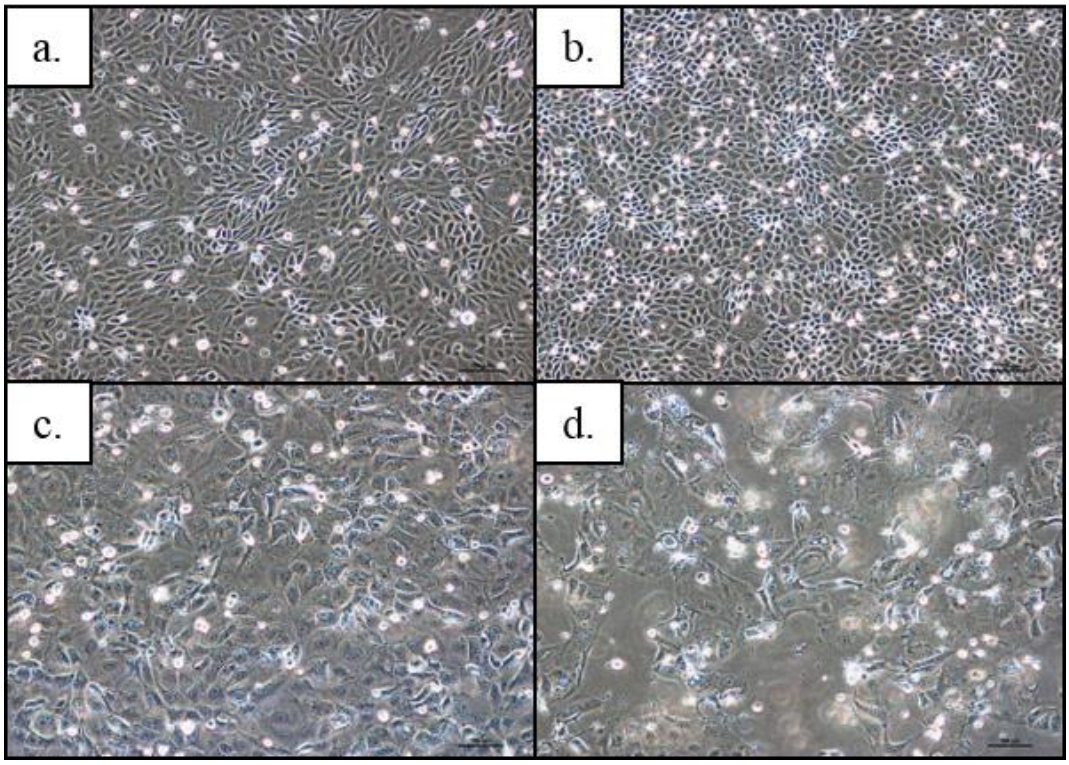

Figure 4.4 Representative phase-contrast micrographs of Caco-2 after receiving 72-hour treatments of δT3, Dox and the combined treatment. a, vehicle control; b, δT3; c, Dox; d, δT3 + Dox. Magnification at 100x. Scale bar represents 100μm.

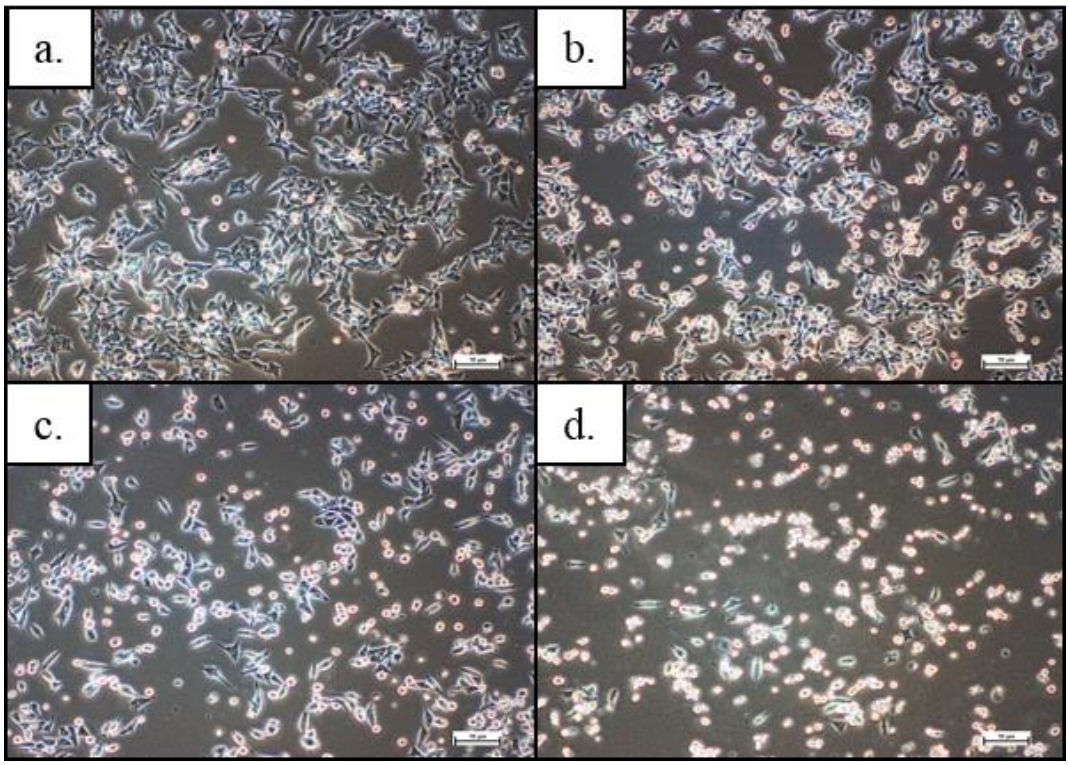

Figure 4.5 Representative phase-contrast micrographs of SW48 after receiving 72-hour treatments of δT3, Dox and the combined treatment. a, vehicle control; b, δT3; c, Dox; d, δT3 + Dox. Magnification at 100x. Scale bar represents 100μm.

At a higher magnification of 200x, it was observed that δT3 + 5FU combined treatment exhibited cell shrinkage in conjunction with cytoplasmic extension in both Caco-2 and SW48 cells after receiving 24-hour treatments. After getting 48- and 72-hour δT3 + 5FU combined treatments, Caco-2 and SW48 exhibited cytoplasmic vacuolisation and cell membrane blebbing (Figure 4.6). Similarly, δT3 + Dox combined treatment also caused cell shrinkage associated with cytoplasmic extension, cytoplasmic vacuolisation and membrane blebbing (Figure 4.7). Taken together, these morphological changes suggest an induction of apoptotic cell death.

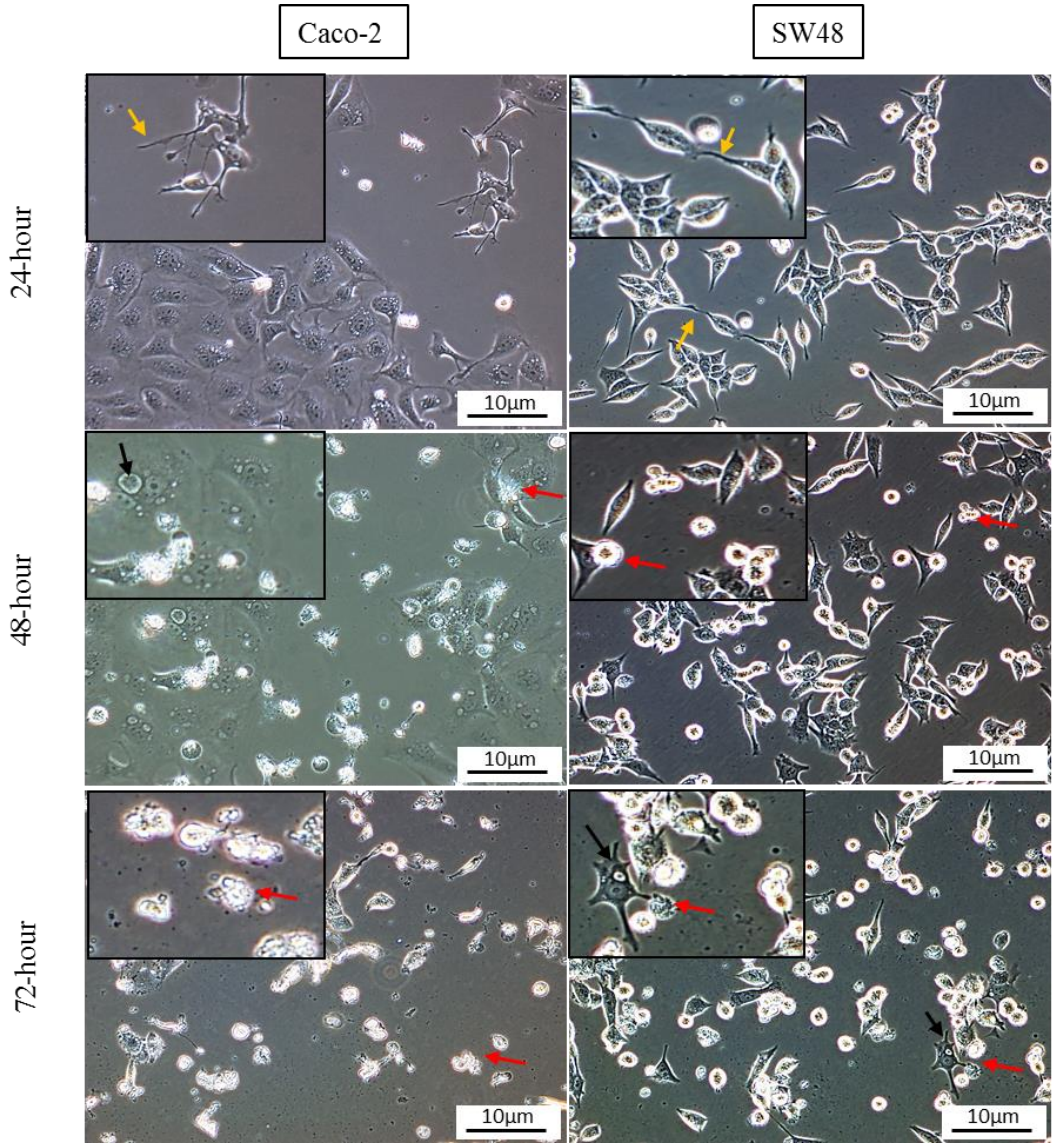

Figure 4.6 Representative phase-contrast micrographs of Caco-2 and SW48 cells receiving δT3 + 5FU combined treatment at various time points. Black box, enlarged images; Yellow arrow, cytoplasmic extension; black arrow, cytoplasmic vacuolisation; red arrow, membrane blebbing. Magnification at 200x. Scale bar represents 10µm.

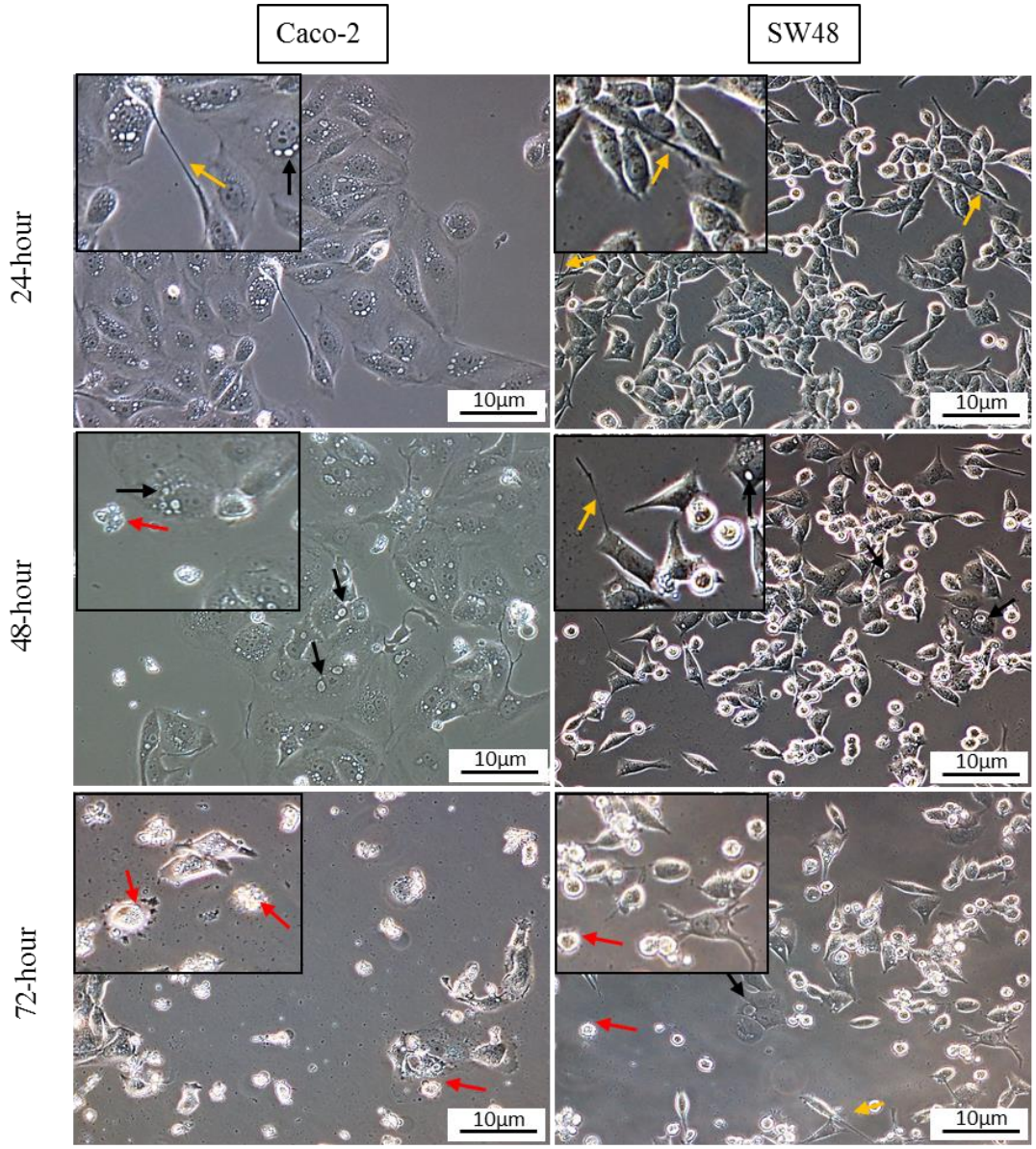

Figure 4.7 Representative phase-contrast micrographs of Caco-2 and SW48 cells receiving δT3 + Dox combined treatment at various time points. Black box, enlarged images; Yellow arrow, cytoplasmic extension; black arrow, cytoplasmic vacuolisation; red arrow, membrane blebbing. Magnification at 200x. Scale bar represents 10µm.

4.3.1.2 DAPI nuclear staining

The DAPI staining was performed after 24-72 hours of treatments (see Appendices: Figure A4.5 – A4.8 for the complete time point profiles). For clearer presentation, only 48-hour profiles are presented in this section. Under DAPI staining, condensed nuclei appeared bright-blue and smaller in size as compared to uncondensed nuclei. It showed that single and combined treatments of δT3 and 5FU

caused nuclear condensation in Caco-2 after 48-hour treatment. Of note, the combined treatment caused an enhanced nuclear fragmentation as compared to the single treatments (Figure 4.8). Similarly, δT3 + 5FU combined treatment exhibited both nuclear condensation and fragmentation in SW48 cells (Figure 4.9).

On the other hand, despite δT3 and Dox single treatments could cause nuclear condensation and fragmentation in Caco-2 and SW48, δT3 + Dox combined treatment had caused more pronounced changes in nuclei (Figures 4.10 & 4.11).

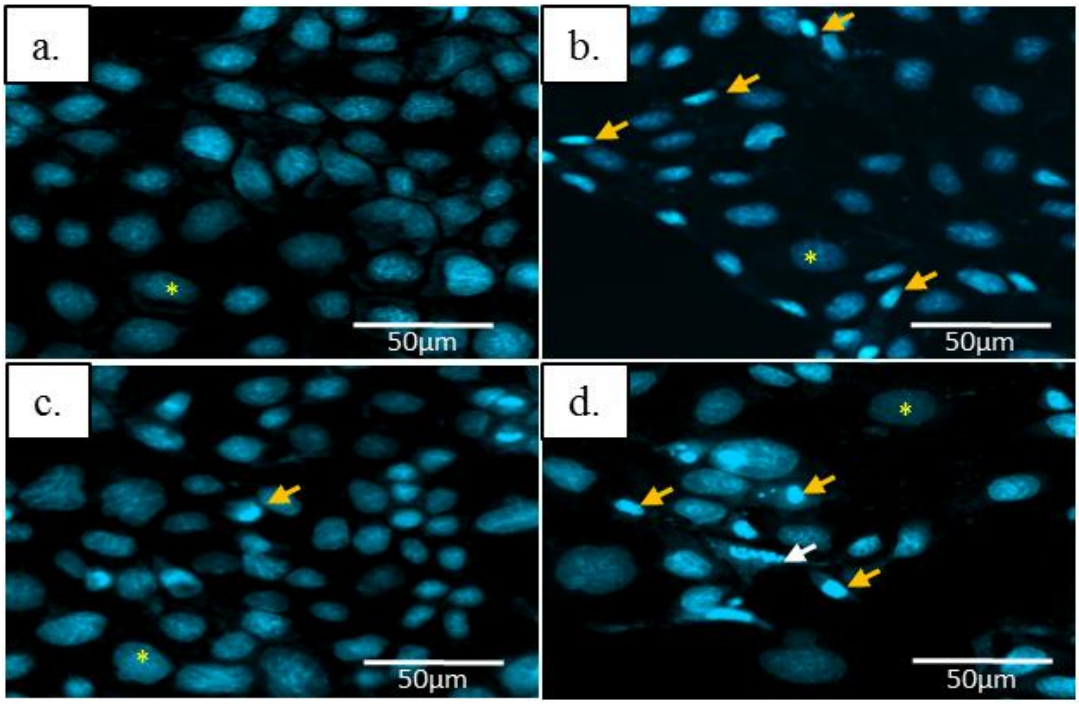

Figure 4.8 Representative nuclear morphologies of Caco-2 after receiving 48-hour treatments of δT3, 5FU and the combined treatment. a, vehicle control; b, δT3; c, 5FU; d, δT3 + 5FU. Yellow arrow, nuclear condensation; white arrow, nuclear fragmentation; * represents uncondensed nucleus. Scale bar represents 50μm.

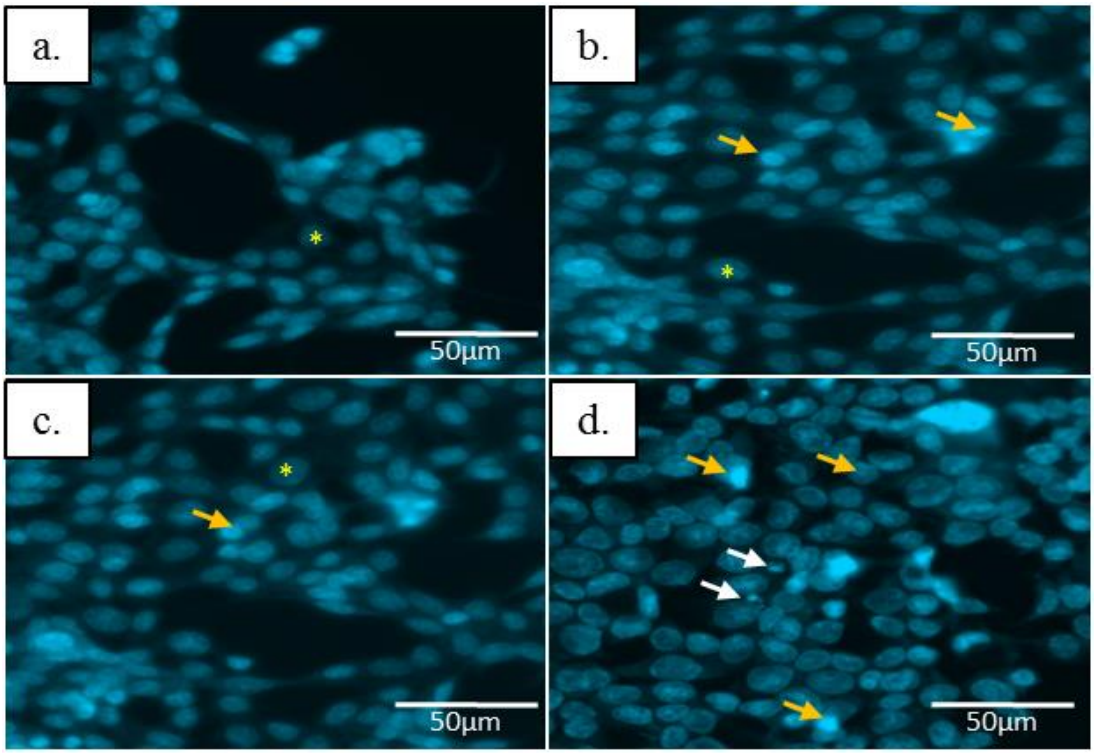

Figure 4.9 Representative nuclear morphologies of SW48 after receiving 48-hour treatments of δT3, 5FU and the combined treatment. a, vehicle control; b, δT3; c, 5FU; d, δT3 + 5FU. Yellow arrow, nuclear condensation; white arrow, nuclear fragmentation. * represents uncondensed nucleus. Scale bar represents 50µm.

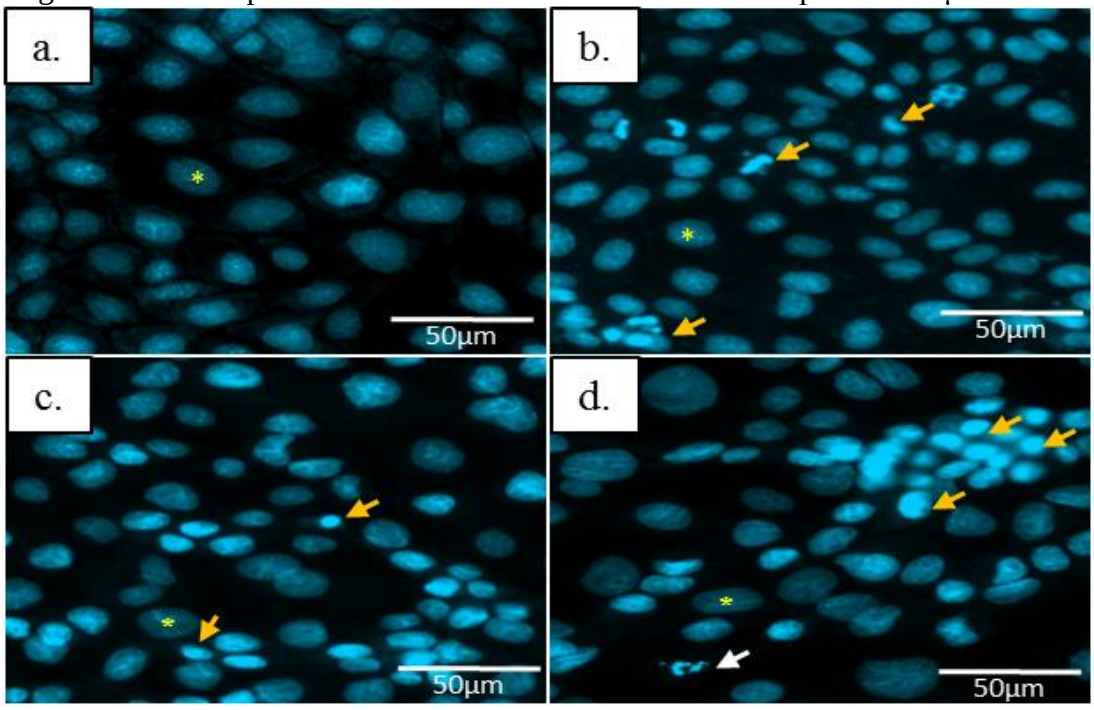

Figure 4.10 Representative nuclear morphologies of Caco-2 after receiving 48-hour treatments of δT3, Dox and the combined treatment. a, vehicle control; b, δT3; c, Dox; d, δT3 + Dox. Yellow arrow, nuclear condensation; white arrow, nuclear fragmentation. * represents uncondensed nucleus. Scale bar represents 50µm.

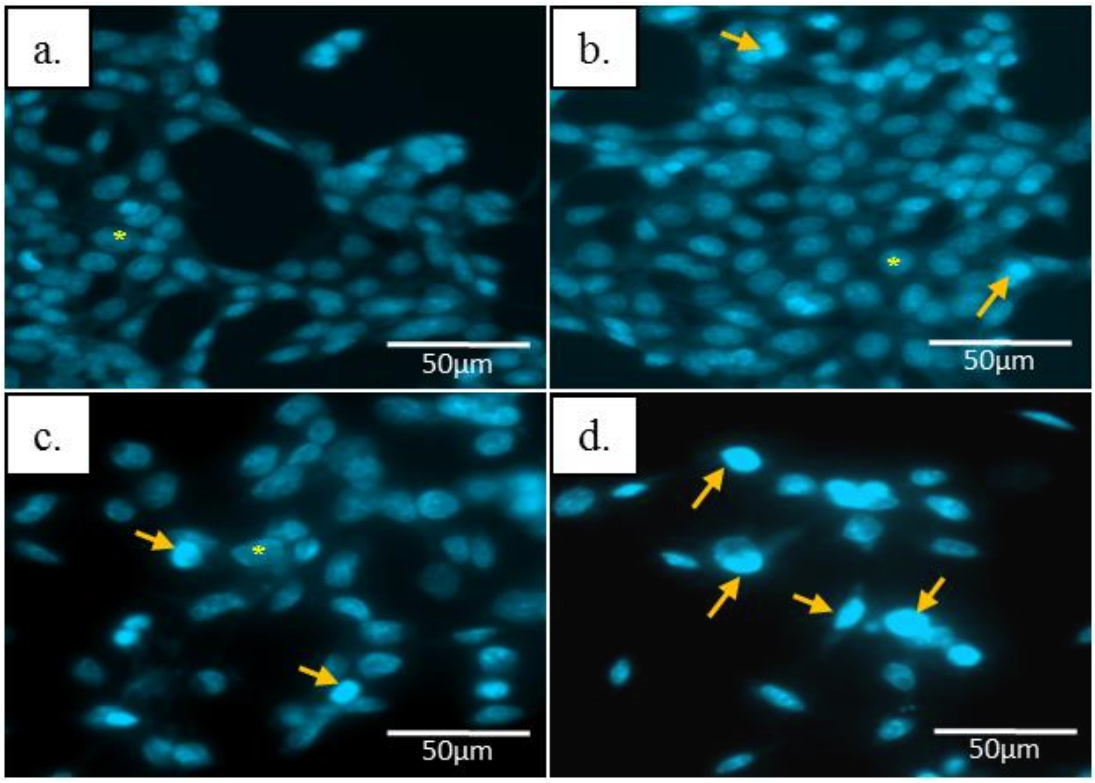

Figure 4.11 Representative nuclear morphologies of SW48 after receiving 48-hour treatments of δT3, Dox and the combined treatment. a, vehicle control; b, δT3; c, Dox; d, δT3 + Dox. Yellow arrow, nuclear condensation. * represents uncondensed nucleus. Scale bar represents 50µm.

4.3.1.3 AO/PI staining

The AO/PI staining reveals apoptotic changes in treated cells by colour and morphology. The control cells displaying green colouration and intact nuclear structure indicate their healthy and viable state. In contrast, treated cells exhibited bright green (nuclear condensation), demonstrating an early apoptosis phase. The orange coloration signifies the presence of late apoptotic cells, meanwhile, a red nucleus suggests dead or secondary necrotic cells (Mai et al., 2014). The membrane blebbing, which is characterised by spherical and bulky "bubble-like" appearance could also be observed.

AO/PI profiles demonstrated that all the treatments groups induced early apoptosis (bright green condensed nucleus) at 24-hour post treatment and an increasing late apoptosis (orange nucleus) after 48-hour treatments on Caco-2 (Figure

4.12) and SW48 cells (Figure 4.13). Notably, membrane blebbing was evident in δT3 + 5FU and δT3 + Dox combined treatments on SW48 cells (Figure 4.13). These observations further conformed to the apoptotic morphological changes as shown in phase-contrast and DAPI micrographs.

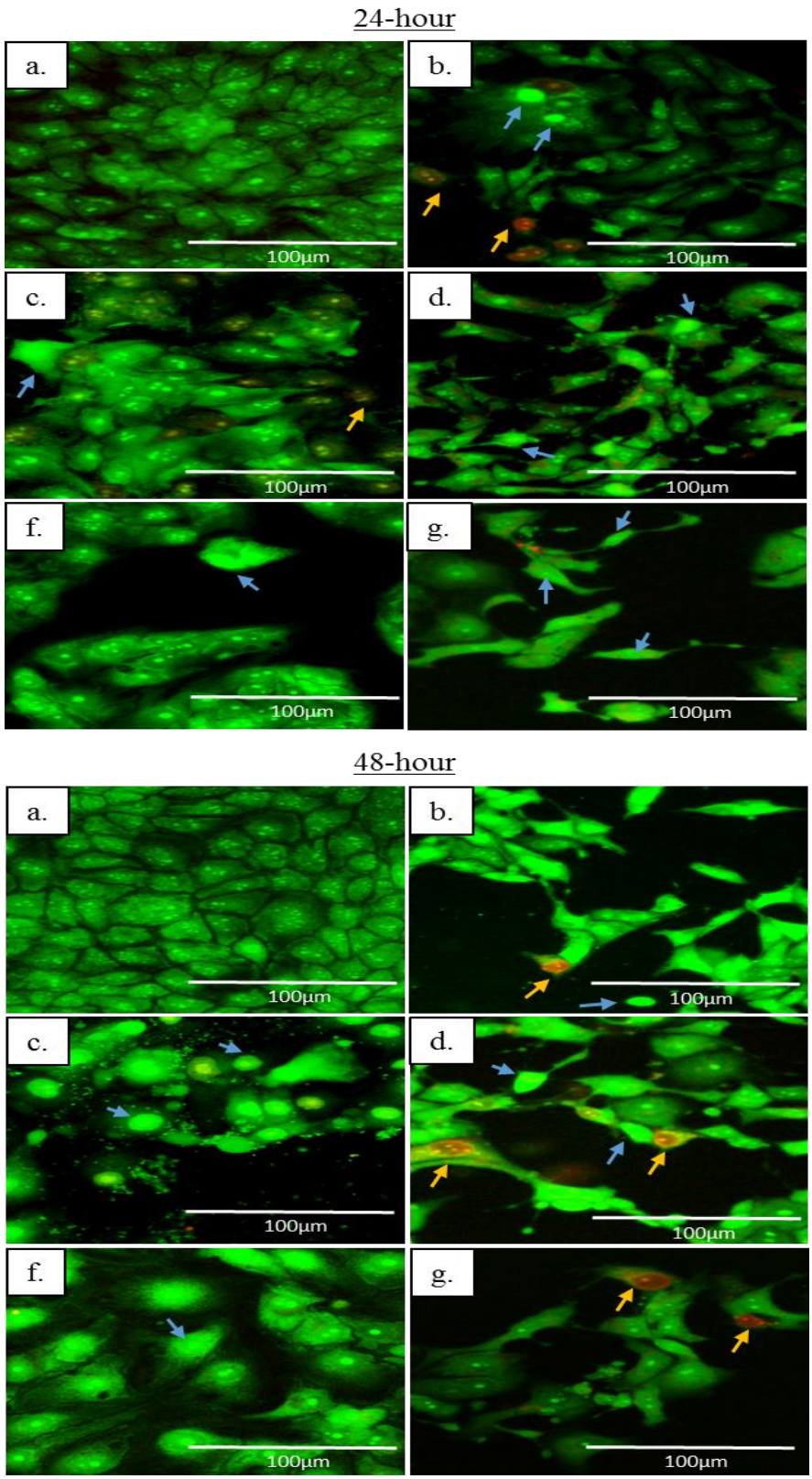

Figure 4.12 Micrographs of Caco-2 under AO/PI staining at various time points after receiving treatments. a, vehicle control; b, δT3; c, 5FU; d, δT3 + 5FU; e, Dox; f, δT3 + Dox. Blue arrow, condensed nucleus; yellow arrow, dead/secondary necrosis; pink arrow, membrane blebbing. Scale bar represents 100µm.

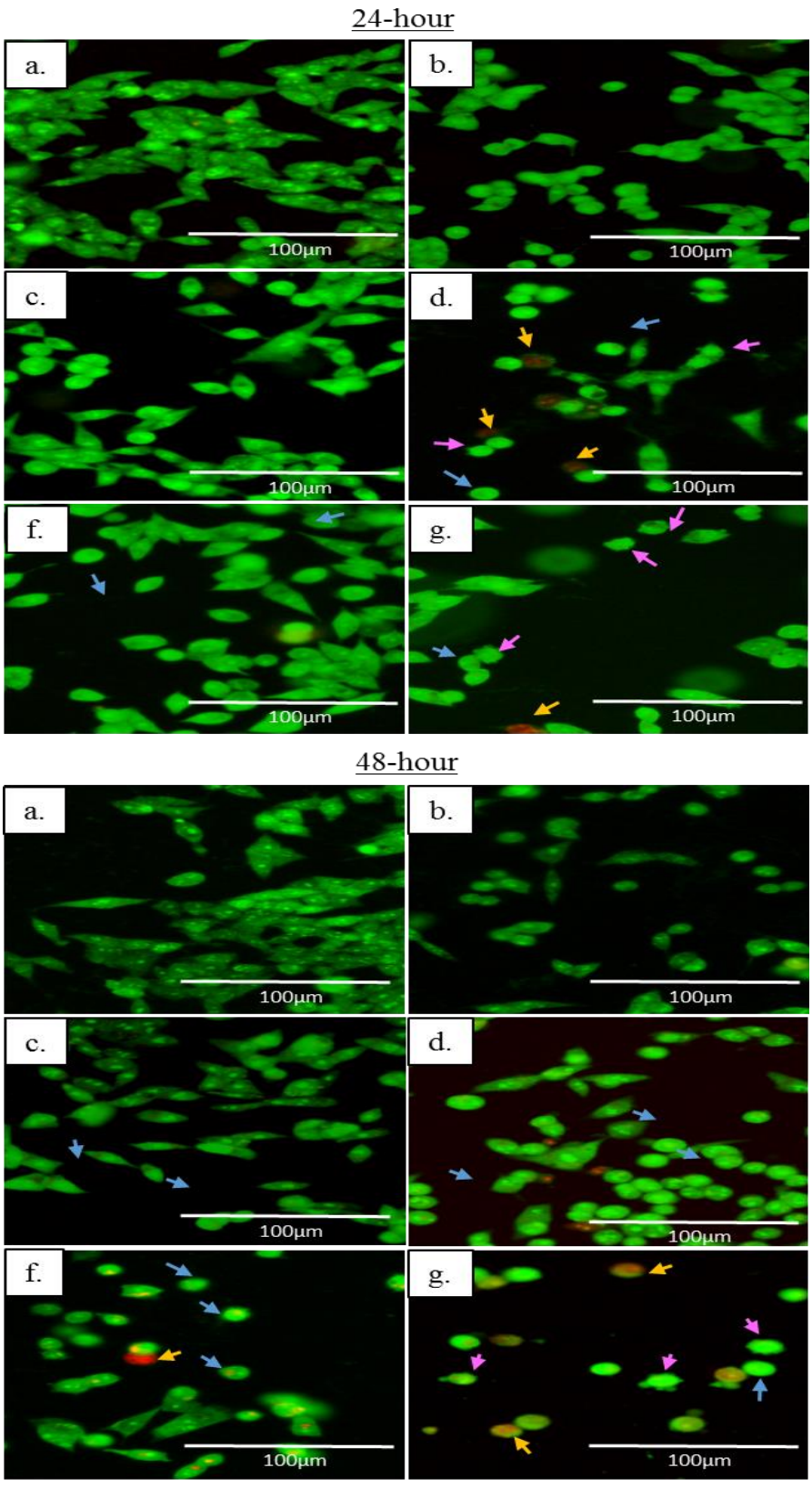

Figure 4.13 Micrographs of SW48 under AO/PI staining at various time points after receiving treatments. a, vehicle control; b, δT3; c, 5FU; d, δT3 + 5FU; e, Dox; f, δT3 + Dox. Blue arrow, condensed nucleus; pink arrow, membrane blebbing; yellow arrow, dead/secondary necrosis. Scale bar represents 100μm.

4.3.2 Quantitative assessment of apoptosis

Morphological profiles demonstrate the presence of apoptosis qualitatively. A flow cytometric approach was employed to detect PS externalisation by Annexin V-FITC and PI to quantify and monitor the progression of apoptosis (Brauchle et al., 2015). A flow cytometry dot plot presents live cells as Annexin V/PI double negative (Annexin V-FITC−/PI−), early apoptotic cells as Annexin V-positive and PI-negative (Annexin V-FITC+/PI−), late (end-stage) apoptotic cells as Annexin V/PI double-positive (Annexin V-FITC+/PI+) (Brauchle et al., 2015). Meanwhile, dead cells are Annexin V-negative and PI-positive (Annexin V-FITC−/PI+). Upon receiving single and combined treatments, Caco-2 and SW48 cells demonstrated a shift toward early apoptosis and/or late apoptosis (Appendix: Figure A4.9), indicating an apoptosis induction. The dot plots were analysed and presented in bar graphs in Figures 4.14 & 4.15.

Albeit the induction of apoptosis by δT3 and 5FU single treatments were non-significant as compared to the vehicle control after receiving 24-hour treatment, δT3 + 5FU combined treatment induced a modest but significant apoptosis in both treated cell lines, over their respective vehicle control ($p < 0.05$) (Figure 4.14). Notably, the combined treatment consistently induced higher apoptotic cell populations than vehicle control, δT3 and 5FU single treatments throughout the three time points tested on Caco-2 and SW48 cells.

On the other hand, δT3 + Dox combined treatment induced a significantly higher apoptosis ($p < 0.0001$) in Caco-2 as early as 24 hours after treatment (Figure 4.15). For SW48, δT3 + Dox combined treatment induced a significant apoptosis ($p < 0.0001$) after 48 hours, and was becoming more prominently after 72 hours of treatment (Figure 4.15)

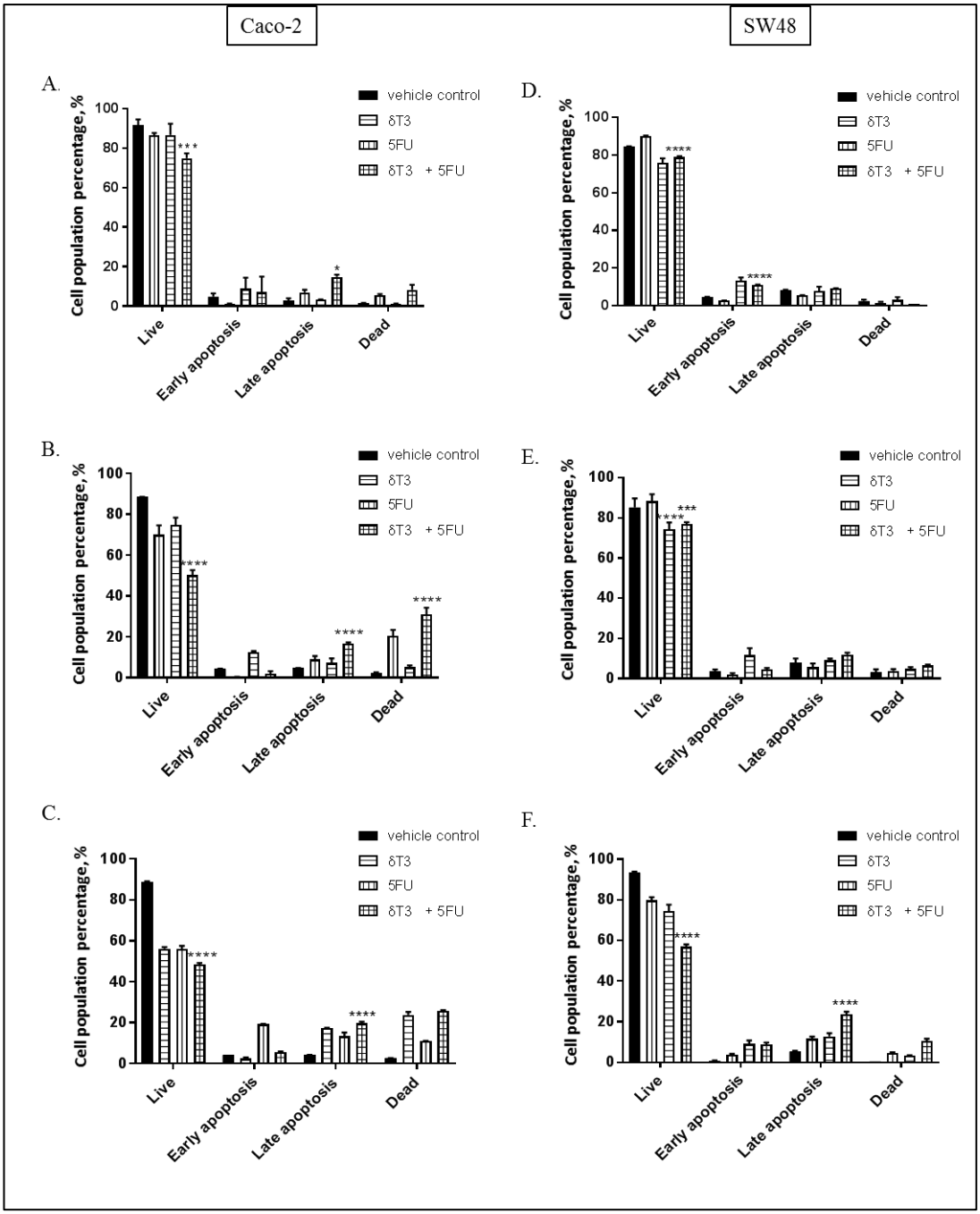

Figure 4.14 Apoptosis profiles of treated colorectal cancer cells at various time points after receiving treatments of δT3, 5FU and the combination. Caco-2 (left); SW48 (right); A&D, 24-hour post treatment; B&E, 48-hour post treatment; C&F, 72-hour post treatment * $p < 0.05$; *** $p < 0.001$; **** $p < 0.0001$.

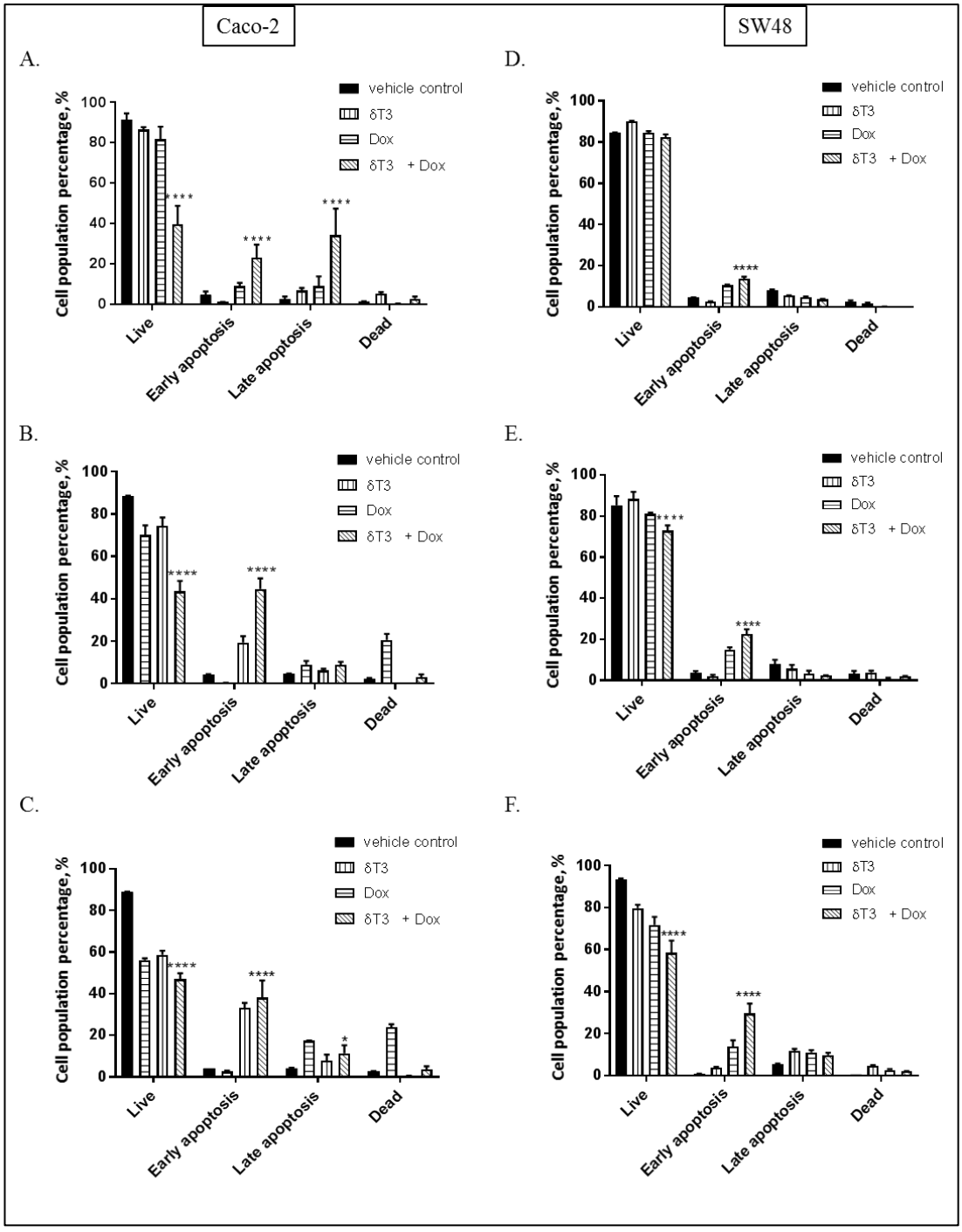

Figure 4.15 Apoptosis profiles of treated colorectal cancer cells at various time points after receiving treatments of δT3, Dox and the combination. Caco-2 (left); SW48 (right); A&D, 24-hour post treatment; B&E, 48-hour post treatment; C&F, 72-hour post treatment. * $p < 0.05$; *** $p < 0.001$; **** $p < 0.0001$.

4.3.3 DNA damage profiles of single and combined treatments

DNA single-stranded breaks (SSBs) will cause migration of DNA to form 'comet' appearance in alkaline condition. The percentage of DNA in the tail showed

a good linearity to magnitude of DNA damage, hence was chosen as the parameter for analysis. It was demonstrated that the combined treatments induced prominent tails in earlier time point, hence the 24-hour profiles and analyses were presented in Figures 4.16 - 4.19 (see Appendices: Figures A4.10 – A4.17 for comet profiles of all time points).

In Caco-2 cells, δT3 and 5FU single treatments did not induce significant SSBs as compared to vehicle control after 24-hour treatment ($p > 0.05$). Tail formation gradually appeared after 48 and 72 hours of δT3 and 5FU single treatments (Appendices: Figures A4.10 & A4.11). In comparison, δT3 + 5FU combined treatment rapidly induced significant SSBs after 24-hour treatment ($p < 0.05$) (Figure 4.16). Dox single treatment and δT3 + Dox combined treatment also induced significant SSBs over the vehicle control ($p < 0.05$) (Figure 4.16). Notably, δT3 + Dox combined treatment displayed an enhanced DNA damage as compared to Dox single treatment.

In SW48 cells, the SSBs induced by 5FU single treatment ($p < 0.05$) and δT3 + 5FU combined treatment ($p < 0.01$) were significantly higher as compared to the vehicle control (Figure 4.17). Meanwhile, Dox single and δT3 + Dox combined treatments induced significant SSBs over the vehicle control ($p < 0.01$) (Figure 4.17), of which the DNA damage in the combined treatment is higher than Dox single treatment.

On the other hand, double-stranded breaks (DSBs) will cause migration of DNA to form 'comet' appearance in a neutral condition. In both cell lines, δT3 and 5FU single, as well as δT3 + 5FU combined treatments were unable to induce significant DSBs (Figure 4.18 & 4.19). However, δT3 + Dox combined treatment caused significant DSBs on Caco-2 and SW48 cells ($p < 0.05$) (Figure 4.18 & 4.19)

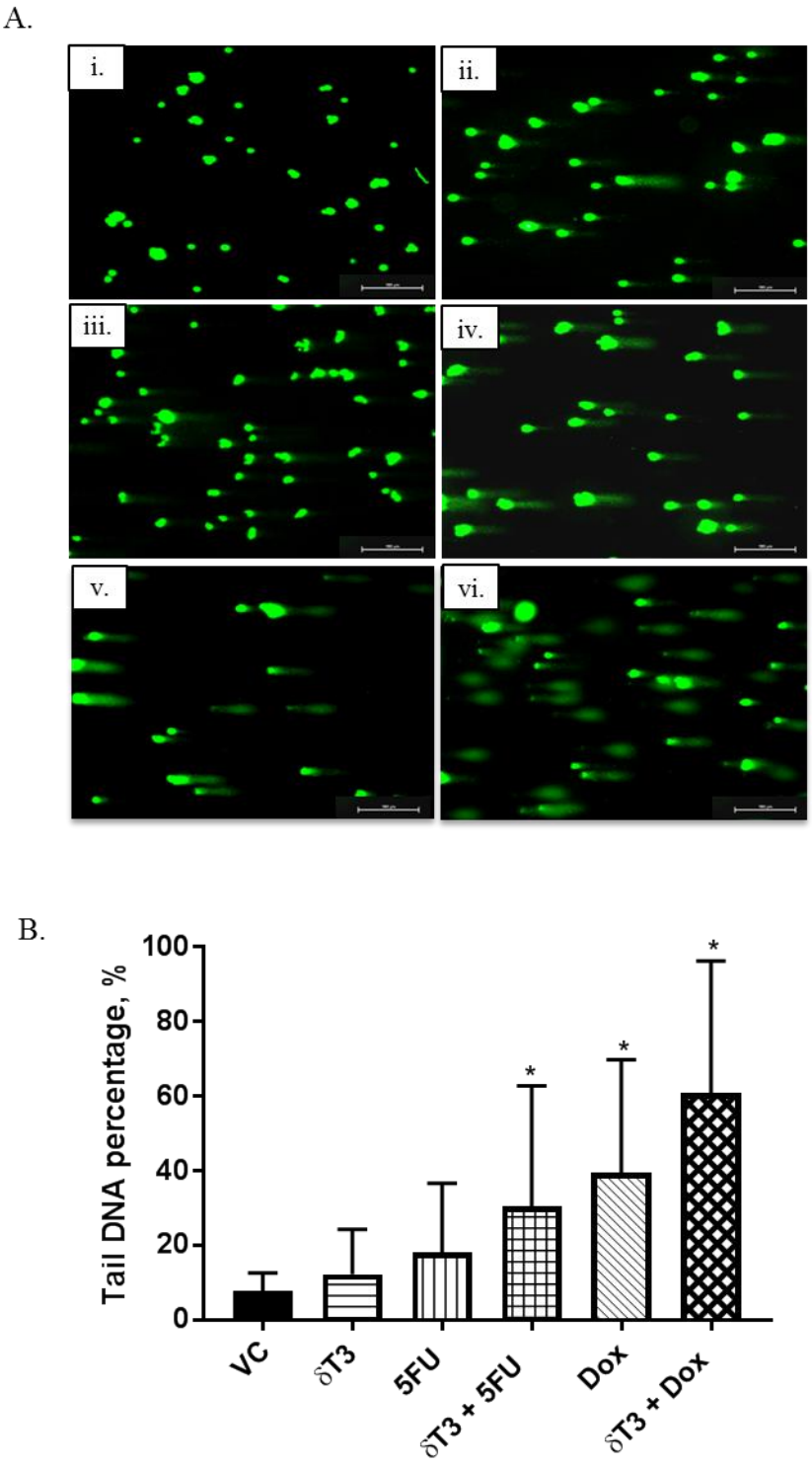

Figure 4.16 Representative alkaline comet images (A) and analysis of alkaline comet profiles (B) of Caco-2 after receiving 24 hours of treatments. i, vehicle control (VC); ii, δT3; iii, 5FU; iv, δT3 + 5FU; v, Dox; vi, δT3 + Dox. Scale bar represents 100μm. * $p < 0.05$.

A.

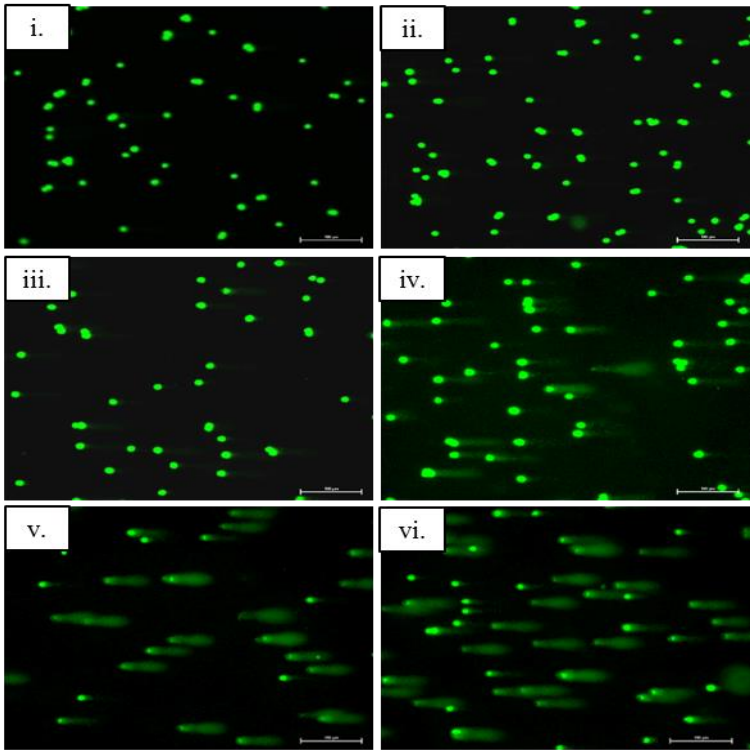

B.

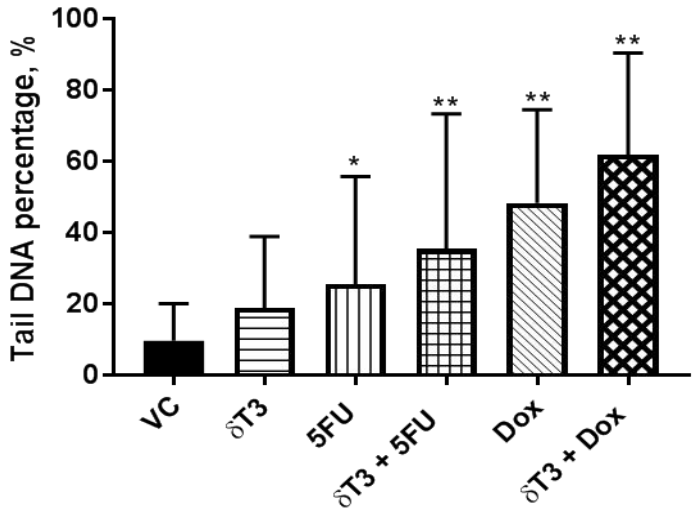

Figure 4.17 Representative alkaline comet images (A) and analysis of alkaline comet profiles (B) of SW48 after receiving 24 hours of treatments. i, vehicle control (VC); ii, δT3; iii, 5FU; iv, δT3 + 5FU; v, Dox; vi, δT3 + Dox. Scale bar represents 100μm. * $p < 0.05$; ** $p < 0.01$.

A.

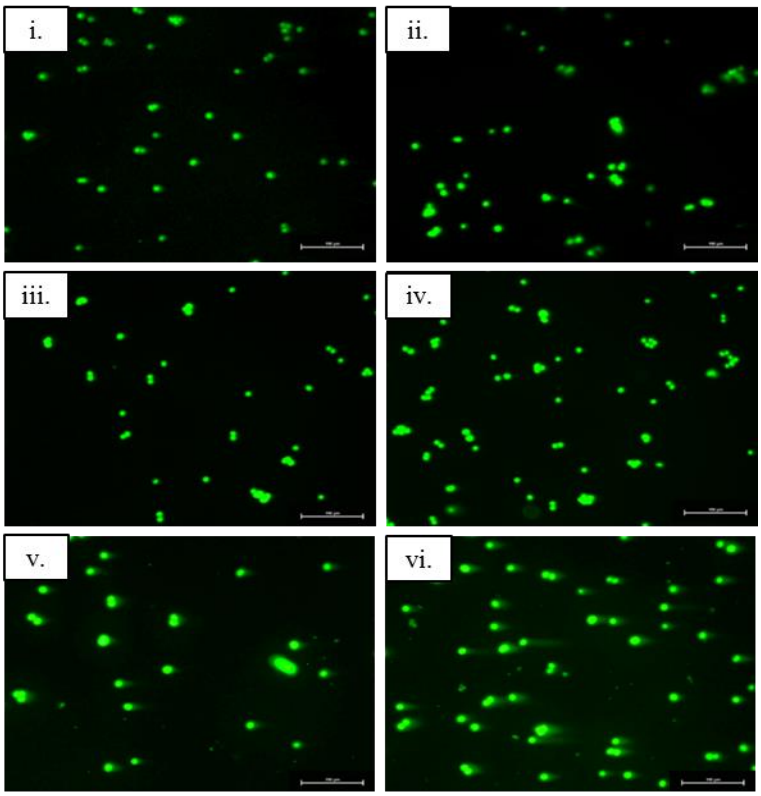

B.

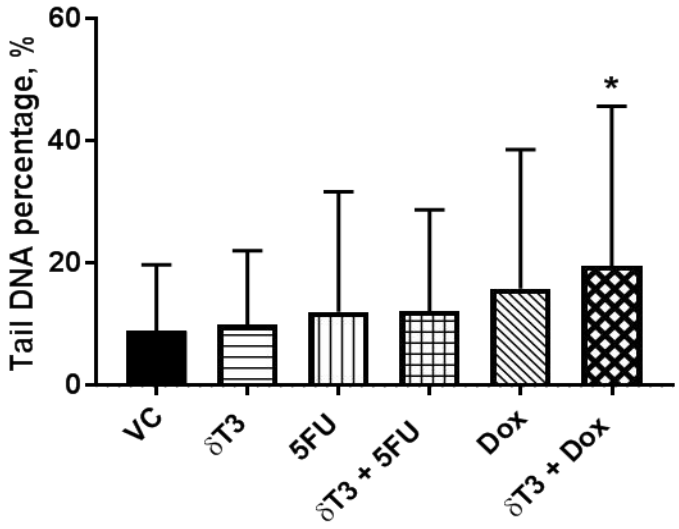

Figure 4.18 Representative neutral comet images (A) and analysis of neutral comet profiles (B) of Caco-2 after receiving 24 hours of treatments. i, vehicle control (VC); ii, δT3; iii, 5FU; iv, δT3 + 5FU; v, Dox; vi, δT3 + Dox. Scale bar represents 100μm. * $p < 0.05$.

A.

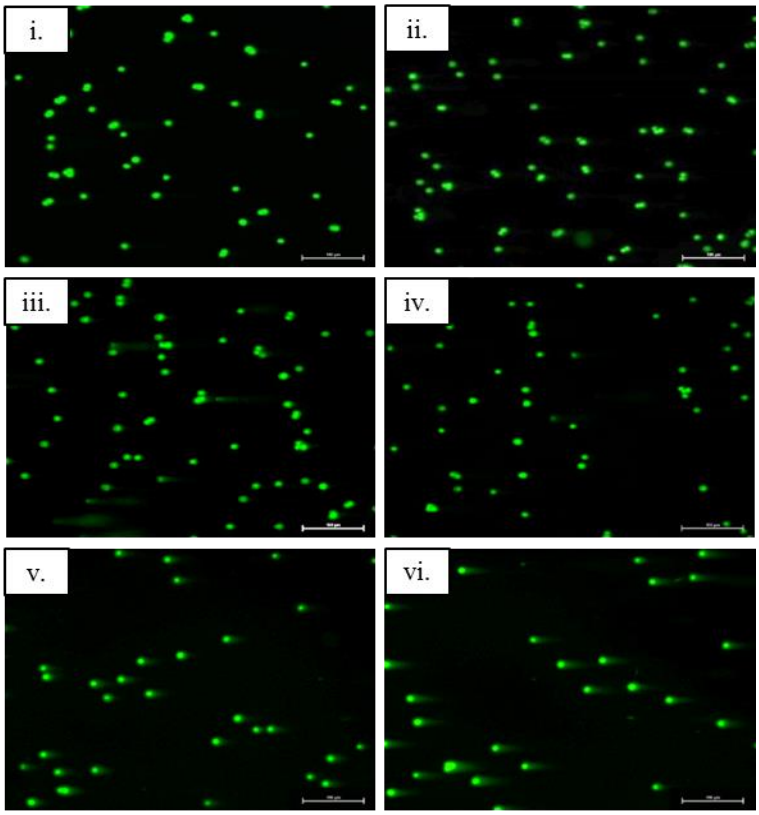

B.

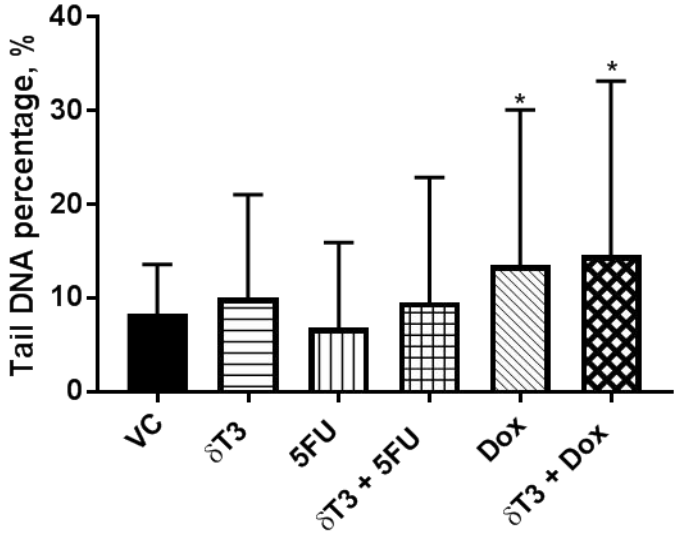

Figure 4.19 Representative neutral comet images (A) and analysis of neutral comet profiles (B) of SW48 after receiving 24 hours of treatments. i, vehicle control (VC); ii, δT3; iii, 5FU; iv, δT3 + 5FU; v, Dox; vi, δT3 + Dox. Scale bar represents 100μm. * $p < 0.05$.

4.3.4 Cell cycle profiles of single and combined treatments

DNA damage induced by cytotoxic agent may halt cell cycle progression, leading to cell cycle arrest at various checkpoints. Cell cycle profiling allows the determination of cell distribution across various phases, namely G0/G1, S and G2/M. The DNA content at post replicative state (G2/M) was found twice higher than cells that were at G1 state as conformed to Darzynkiewicz et al. (2010). Meanwhile, the DNA content in between G1 and G2/M phases was referred to as S-phase as depicted in DNA histograms (see Appendix: Figure A4.18).

Cell cycle analyses demonstrated that distributions of cells treated with δT3 were similar to the vehicle control throughout the study for Caco-2 (Figures 4.20 & 4.22) and SW48 (Figures 4.21 & 4.23). There was a non-significant increase in G0/G1 was observed at 48-hour (Caco-2) and 72-hour's (SW48) profile. Of note, 5FU single and δT3 + 5FU combined treatments resulted in a significant S-phase arrest ($p < 0.0001$) over vehicle control (Figures 4.20 & 4.21). On the other hand, Dox single and δT3 + Dox combined treatments caused a significant G2/M arrest ($p < 0.0001$) over vehicle control on Caco-2 and SW48 cells (Figures 4.22 & 4.23). Notably, the cell cycle arrest induced by the individual chemotherapeutic drugs (5FU and Dox) had no significant difference as compared to the respective combined treatment with δT3.

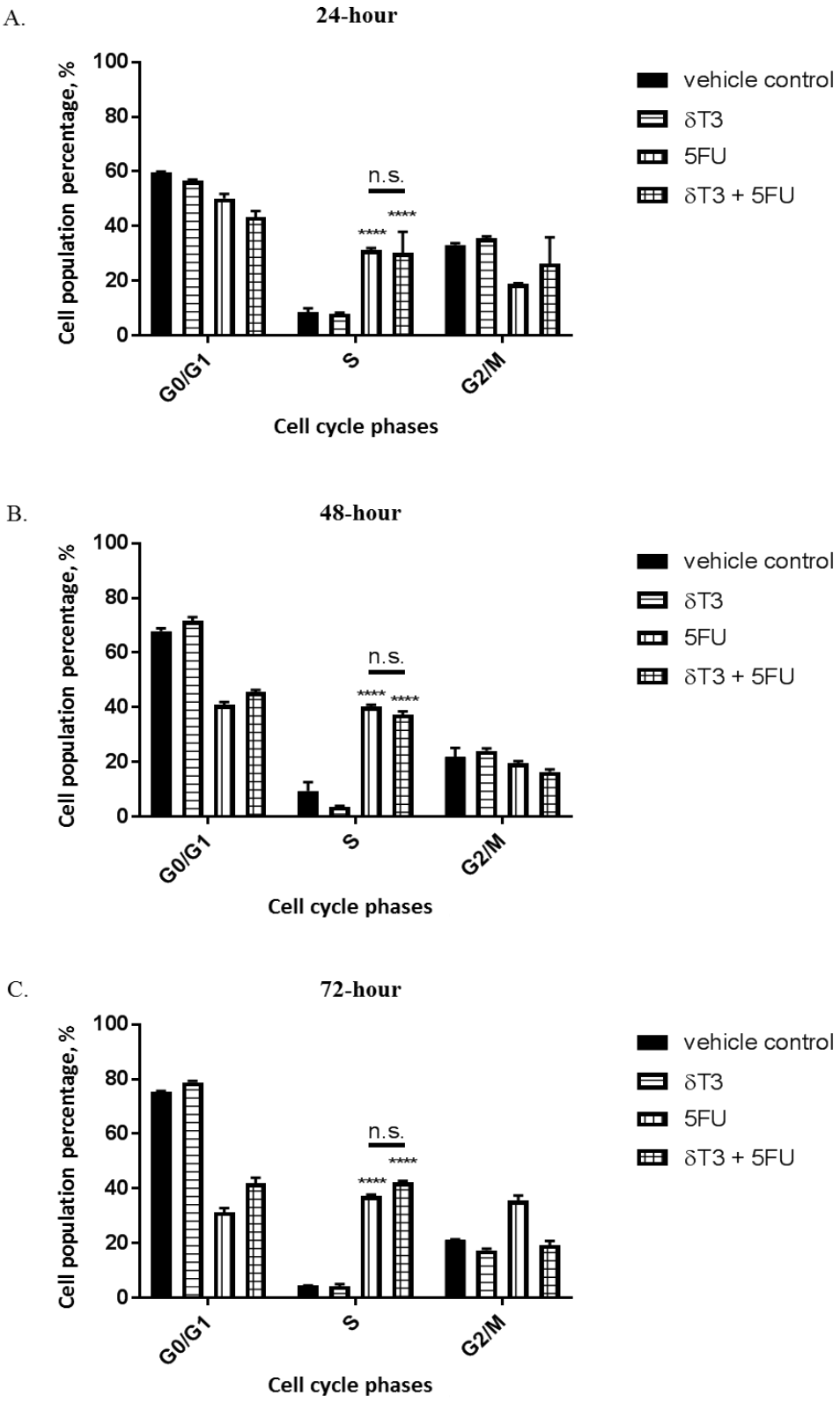

Figure 4.20 Cell cycle profiles of Caco-2 at various time points after receiving treatments of δT3, 5FU and the combination. **** $p < 0.0001$; n.s., not significant.

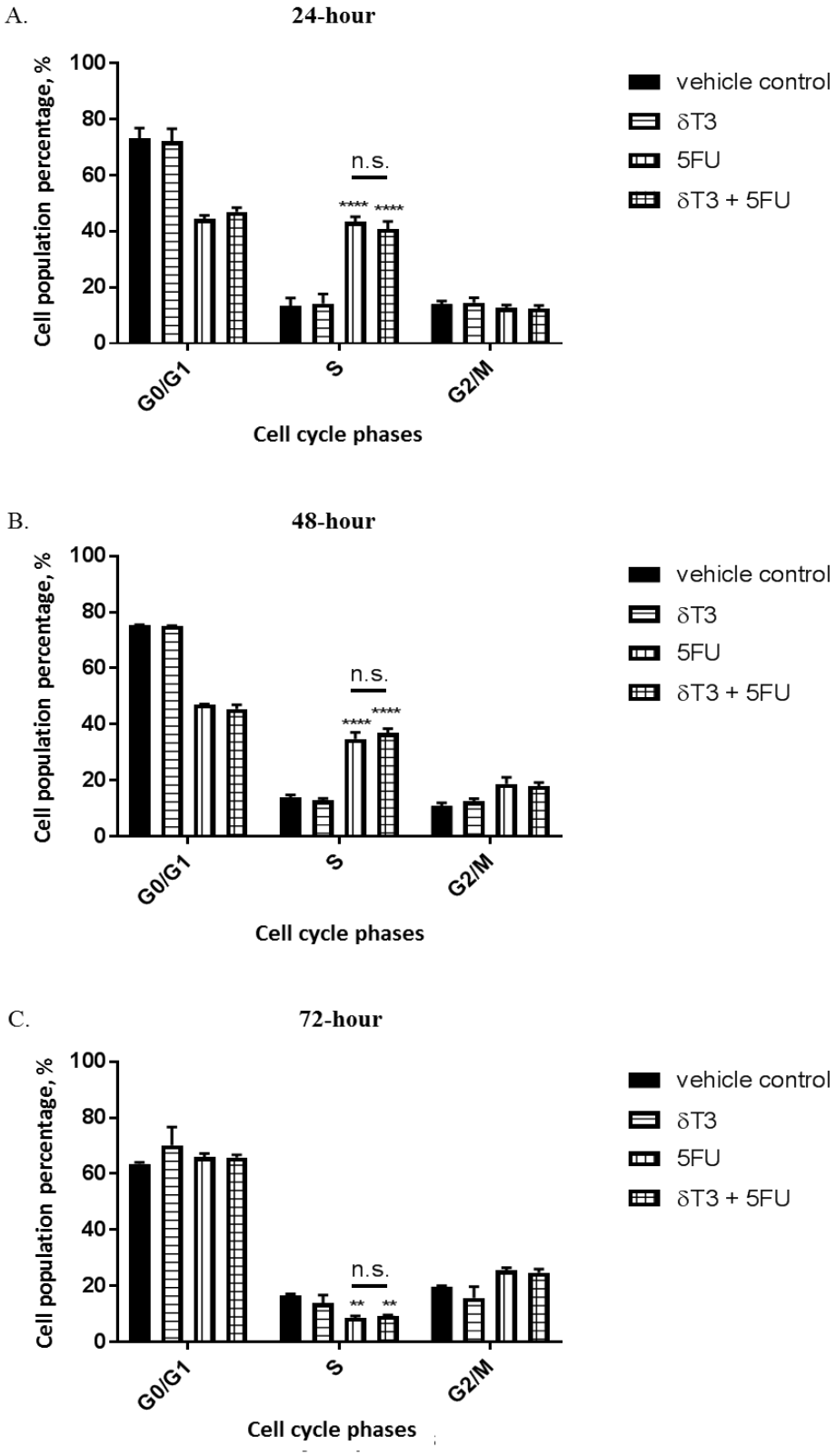

Figure 4.21 Cell cycle profiles of SW48 at various time points after receiving treatments of δT3, 5FU and the combination. ** $p < 0.01$; n.s., not significant.

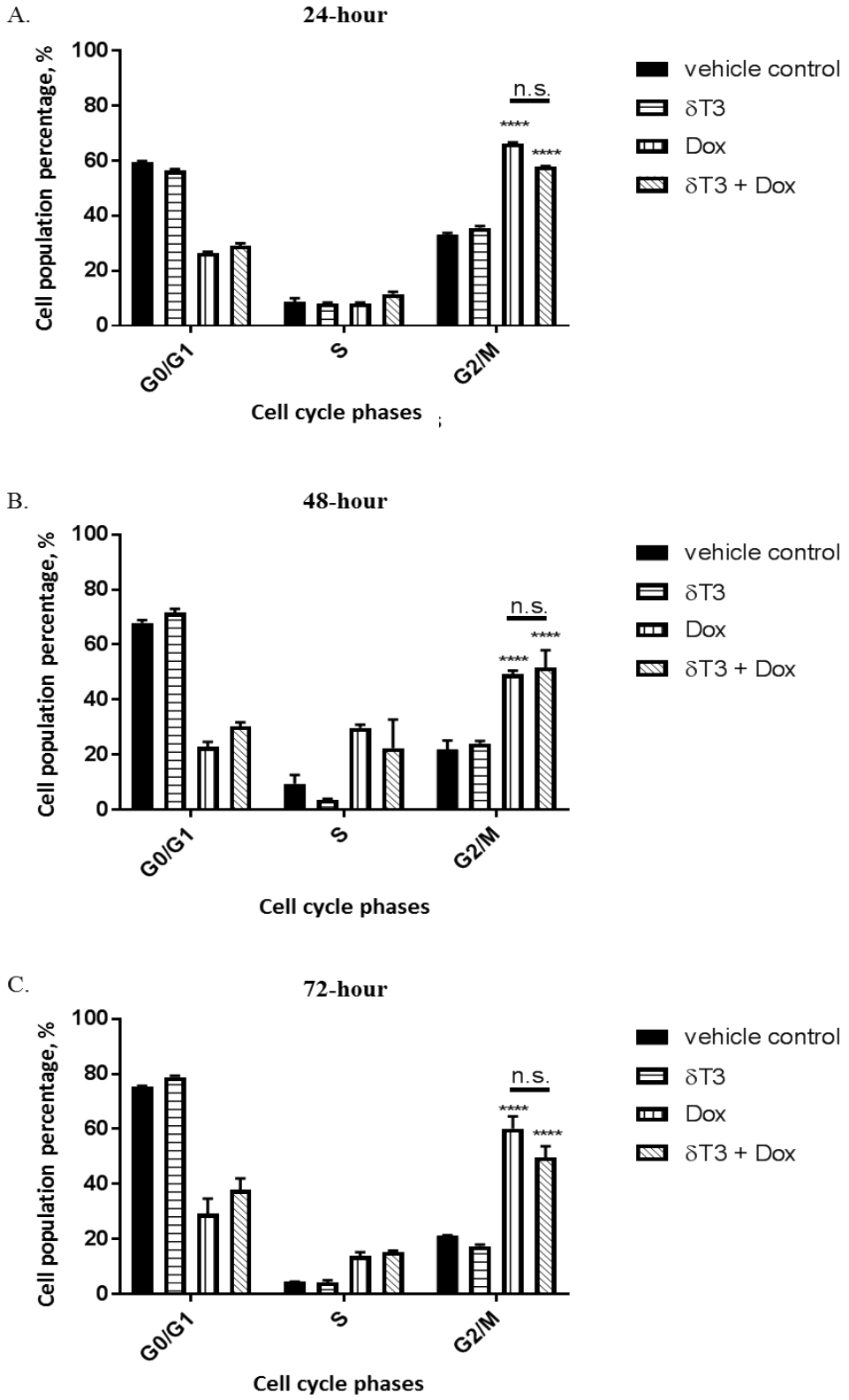

Figure 4.22 Cell cycle profiles of Caco-2 at various time points after receiving treatments of δT3, Dox and the combination. **** $p < 0.0001$; n.s., not significant.

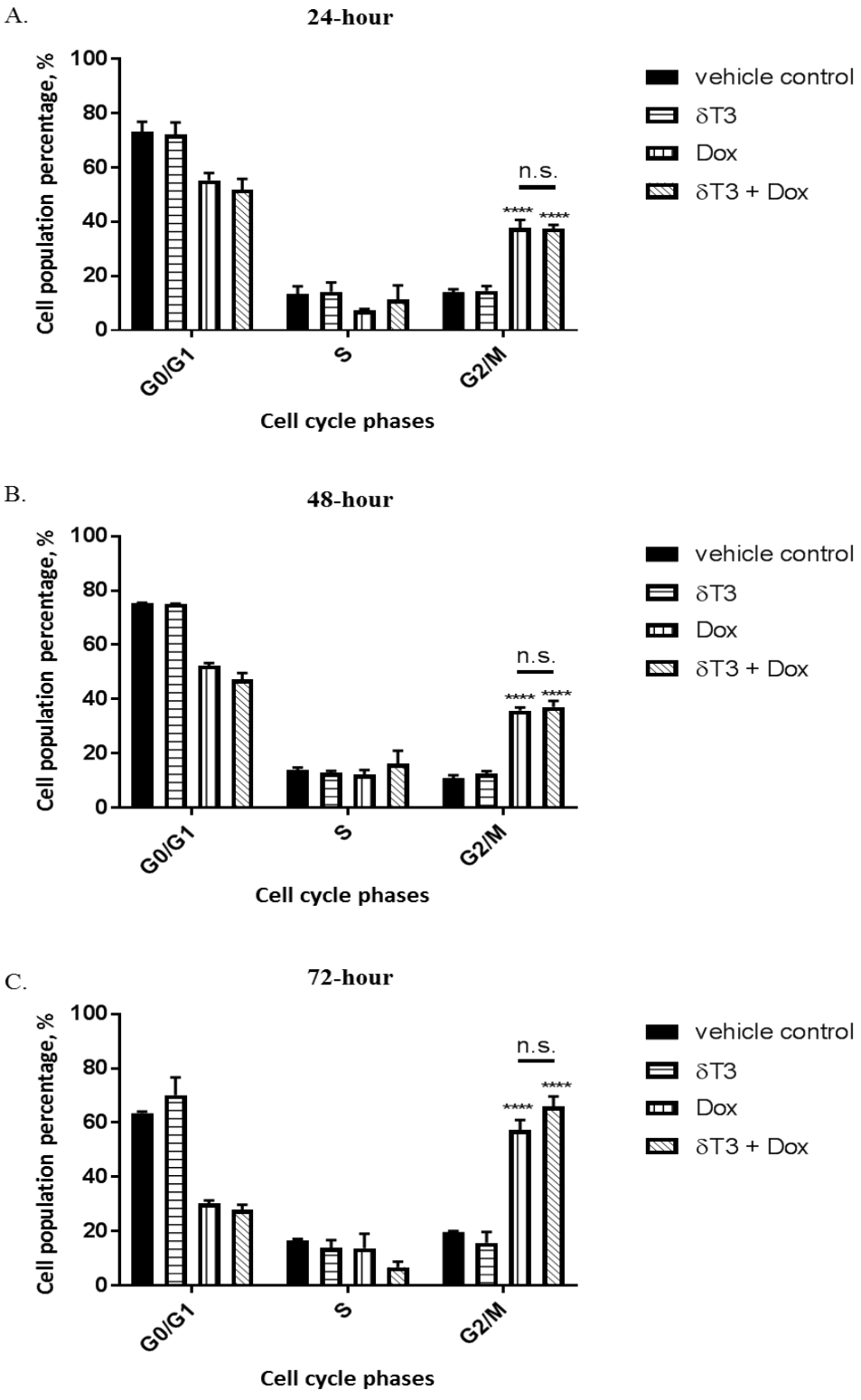

Figure 4.23 Cell cycle profiles of SW48 at various time points after receiving treatments of δT3, Dox and the combination. **** $p < 0.0001$; n.s., not significant.

4.3.5 DNA fragmentation effect of single and combined treatments

DNA fragmentation is a late stage event of apoptosis (Collins et al., 1997). Due to losing a substantial amount of DNA, the fractional DNA appeared as sub-G1 population, which was located to the left of the G1 peak in a DNA histogram (see Appendix: Figure A4.20).

Herein, the result demonstrated that δT3 + 5FU combined treatment caused a time-dependent increase of nuclear fragmentation in Caco-2 (Figure 4.24) and SW48 (Figure 4.25). The fragmentation was most prominent after 72-hour treatment. The effect was significant against the vehicle control, individual δT3 and 5FU single treatments ($p < 0.001$).

On the other hand, combined treatment of δT3 + Dox caused significant DNA fragmentation in Caco-2 throughout the study period of 24 hours to 72 hours ($p < 0.001$), as compared to the vehicle control and single treatments (Figure 4.26). For SW48, δT3 + Dox combined treatment produced a significantly prominent nuclear fragmentation ($p < 0.001$) as compared to the single treatments, at only after 48 hours after treatment (Figure 4.27), correspondingly to apoptosis detection.

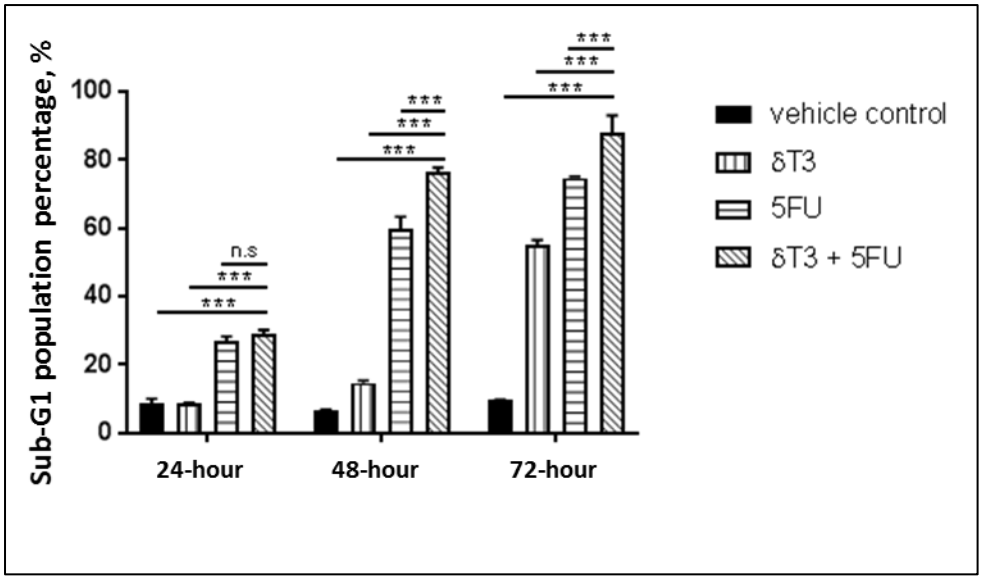

Figure 4.24 Sub-G1 population of treated Caco-2 cells at various time points after receiving treatments of δT3, 5FU and the combination. *** $p < 0.001$; n.s., not significant.

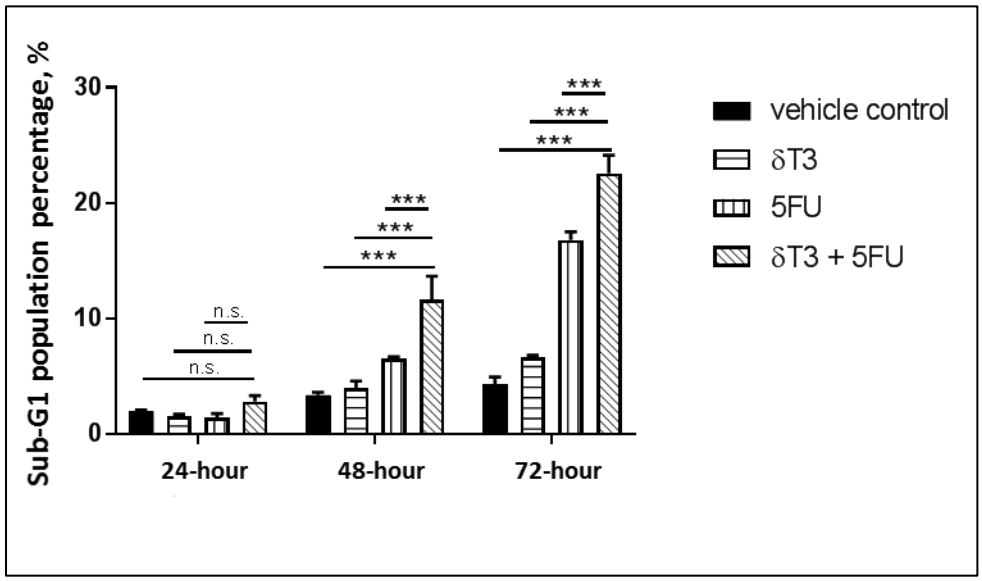

Figure 4.25 Sub-G1 population of treated SW48 cells at various time points after receiving treatments of δT3, 5FU and the combination. *** $p < 0.001$; n.s., not significant.

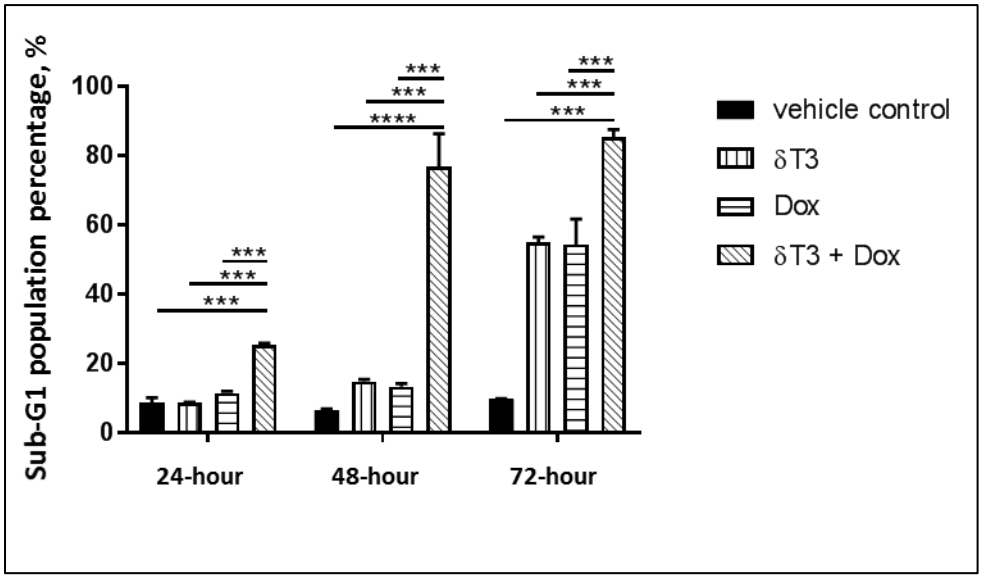

Figure 4.26 Sub-G1 population of treated Caco-2 cells at various time points after receiving treatments of δT3, Dox and the combination. * $p < 0.05$; *** $p < 0.001$; **** $p < 0.0001$; n.s., not significant.

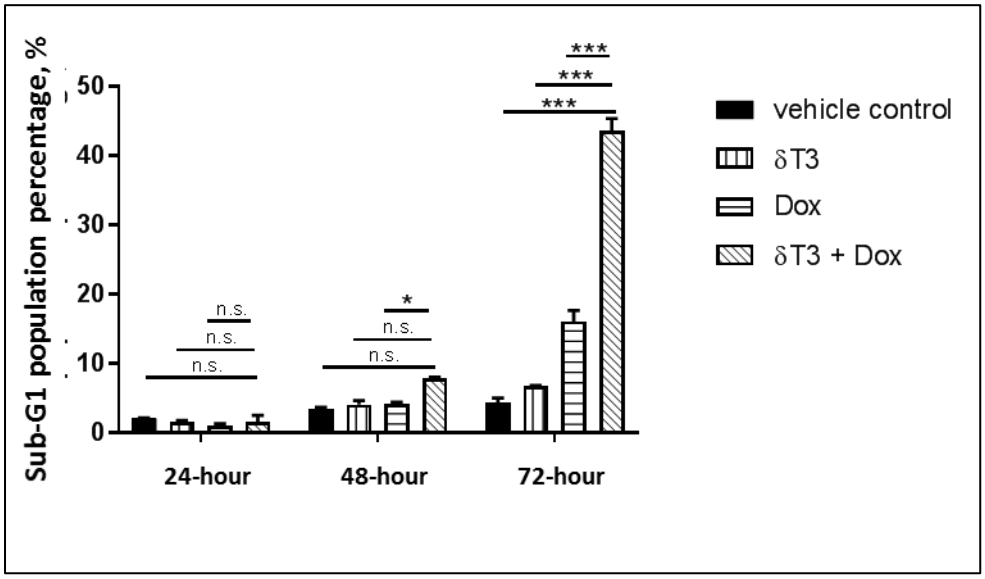

Figure 4.27 Sub-G1 population of treated SW48 cells at various time points after receiving treatments of δT3, Dox and the combination. * $p < 0.05$; *** $p < 0.001$; n.s., not significant.

4.4 Discussion

Human body maintains homeostasis state by keeping the rate of cell proliferation and cell death in the balance. However, the homeostasis is disturbed in cancer, leading to an increased proliferation and reduced cell death (Green and Evan, 2002). Therapeutics that target at reversing the perturbed state leading to decreased proliferation and enhanced cell death, may serve as a promising intervention for cancer management. Following the determination of anti-proliferative and cytotoxic effects of the combined treatments in Chapter Three, current chapter focuses on studying the cell death responses induced by the single and combined treatments. Various aspects of cell death including type(s) and magnitude of cell death, DNA damage patterns, cell cycle arrest profiles and DNA fragmentation percentage were characterised and evaluated. Given that the combinations involved in current study are novel, these parameters are important to shed a light on cell killing effects of the combined treatments.

Morphological changes of cells upon treatments exposure were monitored for a defined period as a kinetic assessment of the drug-induced responses. Current study revealed that the single and combined treatments with 24-hour exposure did not show apparent morphological changes in Caco-2 and SW48 cells. Until 48-hour post treatment, the cells appeared to experience changes in cell morphologies (i.e., cell rounding and detachment), indicating a reflection on cellular stress. These morphological changes were the most remarkable after 72-hour treatments, suggesting a time-dependent increase of cellular stress (Appendices: Figures A4.1 – A4.4). Hence, the selection of study period of 24-72 hours was justifiable for conducting the subsequent assays.

In current study, the Caco-2 and SW48 cells receiving single and combined treatments were apparently smaller in size, rounded and lost adherence as compared to the vehicle control, signifying these cells were undergoing regulated cell death (Figures 4.2 – 4.5). Primarily, loss of cell volume or cellular shrinkage has been a morphological hallmark of apoptosis (Bortner and Cidlowski, 2007). A study demonstrated that a reduction in cytoplasmic volume is necessary and sufficient to trigger apoptotic cell death in human malignant glioma (Ernest et al., 2008) further establish a connection of cell shrinkage to apoptosis. These phenomena could potentially associate with ionic regulation of apoptosis. The cells, which are committed to apoptosis requires K+ and CI- efflux, leading to cell shrinkage that termed apoptotic volume decrease (AVD). As a result, this phenomenon gives rise to a round-up morphology for cells pursuing AVD. Eventually, the cells lose contact with the neighbouring cells and detach from the extracellular matrix (ECM). On the contrary, cells undergoing necrosis will lead to swelling (increase in volume) as a result of Na+ efflux, an active response termed necrotic volume increase (NVI) (Barros et al., 2001). Based on the critical difference between apoptosis and necrosis, the findings shed the *prima facie* evidence in supporting the presence of apoptosis.

It was demonstrated that δT3-treated A549 lung adenocarcinoma appeared bright-green in the nucleus due to chromatin condensation, suggesting an early apoptosis event as revealed by AO/PI staining (Lim et al., 2014a). In addition, the authors also showed that the treated cells underwent membrane blebbing and nuclear margination/fragmentation. In addition, with the aid of DAPI staining, it was reported that 5FU induced nuclear condensation and fragmentation in HCT116, HT29 and LOVO colon cancer cell lines, concluding a significant increment in apoptosis (Das et al., 2014). In another study, Dox-treated T24 bladder carcinoma exhibited apoptotic

morphologies of chromatin condensation and cytoplasm shrinkage (Mizutani et al., 1997). In relation to the current study, the single and combined treatments also displayed similar apoptotic features of cell shrinkage, membrane blebbing, nuclear condensation and fragmentation on Caco-2 and SW48 cells. Hence, the current results inevitably confirmed the induction of apoptosis by single and combined treatments.

Notably, the combined treatments appeared to induce a higher proportion of apoptotic cells when compared to single treatments individually, with greater cellular detachment (Figures 4.2 – 4.5), enhanced nuclear chromatin condensation and fragmentation (Figures 4.8 – 4.11). Correspondingly, the AO/PI profiles demonstrated an enhanced nuclear condensation and/or membrane blebbing (Figures 4.12 & 4.13) in the combined treatments. Collectively, these morphological observations therefore suggested that δT3 + 5FU and δT3 + Dox combined treatments lead to apoptosis enhancement.

The results from apoptosis detection demonstrated a corresponding agreement to morphological changes, which δT3, 5FU and Dox single treatments induced apoptosis increasingly in a time-dependent manner in both Caco-2 and SW48 cells (Figures 4.14 & 4.15). Of note, δT3 + 5FU and δT3 + Dox combined treatments resulted in elevated apoptosis on Caco-2 and SW48 cells, rendering a more effective apoptosis through combinations. The current finding is in agreement with two γ-tocotrienol (γT3) combination studies on colorectal cancer cells (Prasad et al., 2016; Yusof et al., 2015). Of which, a combination of γT3 with 6-gingerol synergistically increased apoptosis in HT-29 and SW837 cell lines (Yusof et al., 2015), whereas a combination of γT3 and capecitabine prominently increased apoptotic cells in HCT-116 cell line (Prasad et al., 2016). Notably, the sub-effective concentrations of γT3 used were 163μM (HT-29), 48μM (SW837) and 25μM (HCT116), which were higher

than the 10μM of δT3 used in the current study. Therefore, the current study suggests that δT3 may be superior to γT3 to be used in drug combinations to enhance apoptosis in colorectal cancer.

Other than the kill-more (effective) apoptotic effect of the combined treatments, the current study also observed a kill-fast (efficient) apoptotic effect in Caco-2. For instance, it is noticeable that δT3 + 5FU and δT3 + Dox combined treatments caused a drastic apoptosis increment at earlier time points (i.e., after 48-hour and 24-hour treatments, respectively) as compared to the individual single treatments, implying a rapid induction of apoptosis in Caco-2 cells. In SW48 cells, the time taken for apoptosis induction was longer (after 72-hour treatments) as compared to Caco-2 cells, suggesting that SW48 cells are more resistant to apoptosis. This observation could be explained by the origin of SW48 (Broder's Grade IV) which was derived from a metastatic site (Abbasi et al., 2012), denoting a more invasive cancer behaviour and therefore less prone to apoptosis. In comparison, Caco-2 cell line was established from a low-grade tumour (Broder's Grade II), indicating a less invasive nature (see Appendix A7.1). Despite a lower apoptosis susceptibility nature of SW48 cells, an augmented apoptotic rate in the combined treatments than that of individual single treatments was noted and therefore highlighting the potential apoptosis-enhancing properties of the combined treatments.

In fact, there is a wide array of external or internal stimuli that can pull the apoptotic trigger. DNA damage (generated by toxic agents or cell-cycle checkpoint defects) is one of the common factors of apoptosis (Lowe and Lin, 2000). Previous studies reported that δT3 induced DSBs in A549 lung adenocarcinoma, U87MG neuroblastoma and HT29 colon adenocarcinoma (Abubakar et al., 2016; Lim et al., 2014a). In addition, Dox and 5FU were widely reported as cytotoxic agents that disturb

DNA replication, potentially leading to DNA damage (Adamsen et al., 2011; De Angelis et al., 2006; Yang et al., 2014). Hence, studying the DNA damage and cell cycle profiles are important to gain insights on actions and targets of the combined treatments.

For DNA damage detection, comet assay was selected over the terminal deoxynucleotidyl transferase dUTP nick end labelling (TUNEL) assay because the latter was intended to detect apoptotic cells that undergo extensive DNA degradation during the late stages of apoptosis (Kyrylkova et al., 2012). The detection of DNA fragmentation by TUNEL assay can be achieved by labelling the 3'hydroxyl termini of DSBs generated during apoptosis. In other words, DNA damage generated by SSBs is unable to be detected. In contrast, comet assay is more appropriate as it can detect both SSBs (alkaline comet) and DSBs (neutral comet) at a single cell level (Collins, 2004; Pu et al., 2015).

The comet profiles demonstrated that δT3 can neither cause a significant SSBs nor DSBs after 24-hour treatment, could be due to its sub-effective concentration used in the current study. However, an enhanced DNA damage was observed in all the combined treatments, suggesting that the application of δT3 in the combination sensitises cancer cells to DNA damage induced by chemotherapeutic drugs. From this perspective, δT3 may provide an additive role/function for enhancing DNA damage in the combination. Notably, 5FU single treatment and δT3 + 5FU combined treatment induced only SSBs in both cell lines (Figures 4.16 – 4.19). Whereas, Dox single treatment and δT3 + Dox combined treatment generated both SSBs and DSBs in Caco-2 (Figures 4.16 & 4.18) and SW48 cells (Figures 4.17 & 4.19). These findings therefore suggest a chemotherapeutic drug-driven effect in the combined treatments.

Contrary to the previous finding of 5FU's capacity in generating SSBs and/or DSBs breaks (Adamsen et al., 2011), only SSBs were detected in the current study. The authors demonstrated a high concentration (380μM, continuously every 4 hours up to 24 hours) of 5FU induced DSBs in HCT116 and HCT15 colon cancer cells. Additionally, a bolus concentration (500μM, two-fold dilution performed at 4-hour interval up to 24 hours) of 5FU induced a sequential induction of SSBs and DSBs in HT29 colon cells (Adamsen et al., 2011). This study therefore implies that 5FU's concentration and duration of exposure are the key determinants to DNA damage patterns. In comparison, the concentrations of 5FU used in current study were considerably lower, i.e., at 3.5μM (Caco-2 cells) and 18μM (SW48 cells). Hence, it is plausible to explain that only SSBs were triggered at low 5FU treatment concentration.

On the other hand, the SSBs and DSBs generated by Dox single and δT3 + Dox combined treatments are likely to be caused by the malfunctioned topoisomerase II. During DNA replication, Dox intercalates into DNA and forms a stable complex with topoisomerase, leading to the collapse of replication forks. As a result, the stalling of replication leaves the DNA backbone broken on the single strand, that can be often converted to DSBs (Zhang et al., 2016). Another line of evidence also suggested that chemotherapeutic agents that poison topoisomerase II are known to induce persistent protein-mediated DSBs (De Campos-Nebel et al., 2010).

In the presence of DNA damage, the DNA damage checkpoints will be activated, causing a delayed cell cycle progression (namely cell cycle arrest) which is awaiting the potential repair to take place (Harrington et al., 1998). In the current study, cell cycle profiles revealed that 5FU induced S-phase arrest while Dox induced G2/M arrest, as early as 24-hour post treatment. In fact, these findings are aligned with several previous studies (Bilim et al., 2000; Focaccetti et al., 2015; Liu et al., 2008).

However, δT3 did not induce a prominent G1 phase arrest as suggested by two previous studies (Fernandes et al., 2010; Ye et al., 2015), albeit a mild increment at G1 phase was observed after 48 hours of treatment in Caco-2 cells. Probably, this is due to the application of a sub-effective concentration of δT3 which causes a delayed action.

In the event of late apoptosis, extensive DNA fragmentation gives rise to fractional DNA that appears as 'sub-G1' population. From this study, it showed that all single and combined treatments caused a time-dependent increase of DNA fragmentation. Notably, DNA fragmentation of combined treatments was considerably higher as compared to the single treatments individually, inferring an enhanced fragmentation caused by combined agents. DNA fragmentation was peaked at 72-hour post treatment, coherently suggests that the cells have entered a final demise of apoptosis following DNA damages and cell cycle arrests.

In fact, literature has suggested DNA damage will induce cell cycle arrest to allow repair of mutations before the commencement of DNA replication (Harrington et al., 1998). Prolonged DNA damage which is unrepairable will eventually lead to apoptosis (Norbury and Zhivotovsky, 2004). Based on the abovementioned findings, it is plausible to propose that the combined treatments have exerted an unrepairable DNA damage (via SSBs and/or DSBs), thereby leading to a prolonged cell cycle arrest which enhances apoptosis with particular weight placed on the late apoptosis DNA fragmentation event as illustrated in Figure 4.28.

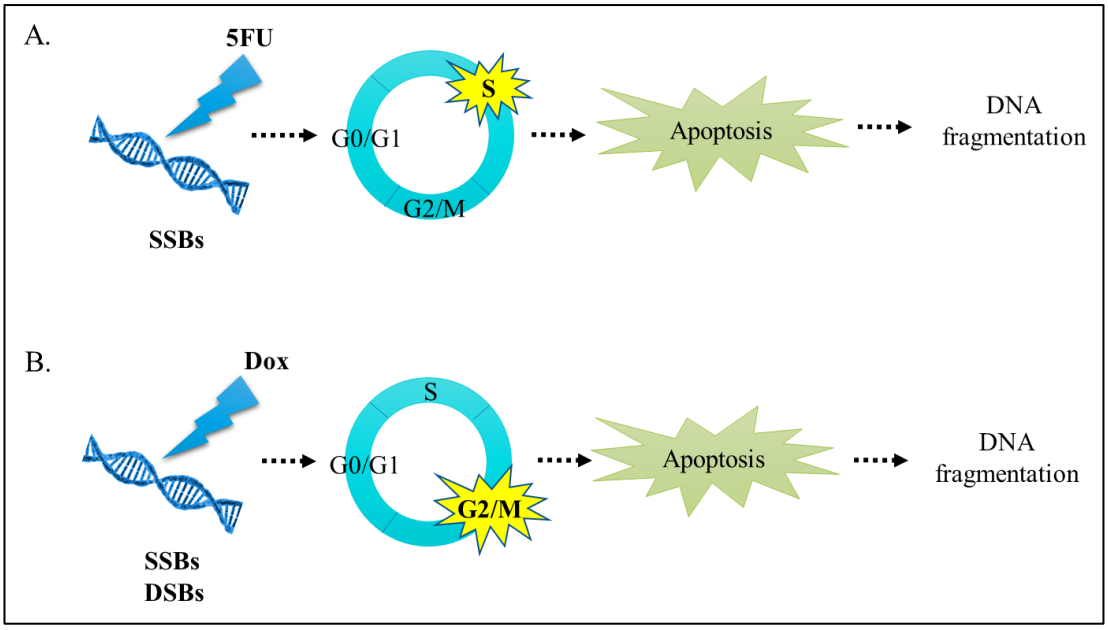

Figure 4.28 A proposed explanation for the chemotherapeutic drug-driven apoptosis effects induced by the combined treatments. A, δ-tocotrienol + 5-fluorouracil (δT3 + 5FU); B, δ-tocotrienol + doxorubicin (δT3 + Dox).

The manifestations of stereotypical apoptotic cell death features induced by the combined treatments such as DNA cell shrinkage, nuclear condensation, DNA fragmentation, blebbing and phosphatidylserine externalization signify a potential involvement of a family of cysteine proteases called caspases (Thornberry and Lazebnik, 1998). This clue has therefore necessitated an investigation on caspase-mediated apoptosis.

Of note, the combined treatments also induced morphological changes, which are not typical features of apoptosis, such as cytoplasmic vacuolisation. Cytoplasmic vacuolisation could indicate a cellular stress response. For instance, autophagic vacuolisation is a common feature of autophagy involving in the stress adaptive response and quality control mechanism (Elmore, 2007; Murrow and Debnath, 2013; Ravanan et al., 2017). On the other hand, cell death could possibly be induced by non-autophagic cytoplasmic vacuolisation. For example, it was reported that curcumin induced endoplasmic reticulum stress with cytoplasmic vacuolisation appearance

mediated by oxidative stress and was independent of autophagy in prostate cancer cells (Lee et al., 2015). Regardless of autophagy or non-autophagy mediated cytoplasmic vacuolisation, this observation suggests that the cells treated with combined treatments experience a greater cellular stress, which may potentially evoke an additional cell death modality other than apoptosis. At this point, the potential involvement of other cell death modalities alongside with apoptosis can neither be ruled out nor confirmed, which definitely necessitates a further investigation.

4.5 Conclusion

In conclusion, the manifestations of cell shrinkage, nuclear condensation, nuclear fragmentation and membrane blebbing upon treatments undoubtedly confirmed an induction of apoptosis in Caco-2 and SW48 colorectal cancer cells. δT3 + 5FU and δT3 + Dox combined treatments exhibited an enhanced apoptosis. In addition, δT3 + 5FU combined treatment only induced SSBs whereas δT3 + Dox combined treatment induced both SSBs and DSBs. Of note, the DNA damage induced by the combined treatments was higher compared to the individual single treatments. 5FU single and δT3 + 5FU combined treatments caused S-phase arrest; Dox single and δT3 + Dox combined treatments resulted G2/M arrest. DNA fragmentation of all treatment groups increased in a time-dependent manner. The DNA fragmentation in combined treatments was significantly higher as compared to that of all single treatments. Collectively, it is suggested that combined treatments caused an enhanced DNA damage, leading to cell cycle arrest and heightened apoptosis. These interesting findings have undeniably exhilarated the next elucidation of mechanisms of action on these combined treatments.

Chapter Five: Investigations on underlying pro-apoptotic mechanisms induced by individual single and combined treatments of δ-tocotrienol and/or chemotherapeutic drugs (5-fluorouracil and doxorubicin)

5.1 Introduction

Previous findings in Chapter Four have demonstrated that single and combined treatments manifested apoptosis, by which the apoptotic response induced by combined treatments were enhanced. Hence, it was hypothesised that combined treatment may differentially regulate the apoptosis pathways. In this regard, investigations on the underlying apoptotic mechanisms triggered by the single and combined treatments are justifiably necessitated.

There are two principal pathways of apoptosis, namely mitochondria-mediated (intrinsic), and death receptor-mediated (extrinsic) pathways. As the names suggest, intrinsic pathway predominantly originates from mitochondria which cognate internal cellular stress to activate apoptosis. Briefly, the intrinsic pathway happens via cytochrome *c* release from mitochondria, which subsequently leads to caspase-9 activation and thus triggers the downstream signalling of apoptosis (Elmore, 2007; Kiraz et al., 2016). Whereas, the extrinsic pathway is stimulated through the transmembrane death receptors in response to external stress. The extrinsic pathway of apoptosis is principally mediated by membrane-bound death receptors under TNF (tumour necrosis factor) receptor superfamily. Upon ligation of death domains to these receptors, caspase-8 is activated to trigger mitochondria-mediated pathway, or, directly activate the executioner caspases (caspase-3 or -7) (Elmore, 2007; Kiraz et al., 2016). Hence, caspase-9 and caspase-8 represent an activation of intrinsic and extrinsic pathways of apoptosis respectively, which take place at the upstream of caspase-3/7 activation.

Previously, it was reported that tocotrienols triggered both caspase-8- and caspase-9-dependent apoptosis in different studies (Lim et al., 2014a; Park et al., 2010; Sun et al., 2009). Additionally, 5FU was reported to engage a TNF-related apoptosis-inducing ligand (TRAIL)-death-inducing signalling complex (DISC)-dependent extrinsic apoptosis pathway axis as well as caspase-9-dependent apoptosis in colon cancer cells (Akpinar et al., 2015; Mhaidat et al., 2014). On the other hand, Dox showed altered Bax/Bcl-xL ratio, caspase-9 as well as caspase-8 levels in breast cancer cells (Sharifi et al., 2015). Overall, these evidences suggested that there is an equal possibility of intrinsic and/or extrinsic pathway(s) engagement. Hence, it is of great importance to identify the apoptotic pathways that are triggered by the combined treatments in this study.

Apoptosis antibody array was adopted as a preliminary approach for concurrent detection of pro-apoptotic and anti-apoptotic protein markers to hope for shedding a light on the potential mechanisms of action. Guided by strong synergism of δT3 + 5FU combined treatment in Caco-2 cells (Table 3.13), this combination was taken as a representative to identify the key molecular changes in apoptosis.

As suggested by the results obtained in apoptosis array, mitochondria-mediated apoptosis pathway was firstly studied in both Caco-2 and SW48 cells. To ascertain the involvement of mitochondria as a target site, it is of importance to detect the mitochondrial membrane permeabilisation (MMP). Current study adopted 5,5',6,6'-tetrachloro-1,1',3,3'-tetraethylbenzimidazolocarbocyanine (JC-1) staining to assess the apoptosis-associated mitochondrial membrane potential (ΔΨm) loss, which is an indicator of inner mitochondrial permeabilisation.

Additionally, mitochondrial outer membrane permeabilisation (MOMP) is also a critical event which leads to the release of many important apoptosis inducing

molecules. MOMP is triggered by pro-apoptotic B cell lymphoma (Bcl)-2 family proteins (e.g., Bax protein), while the integrity of mitochondrial membrane is maintained by anti-apoptotic members of Bcl-2 family (e.g., Bcl-2 protein). In cytosol, cytochrome *c*, apoptotic protease activating factor-1 (Apaf-1) and procaspase-9 form a complex called apoptosome, resulting in activations of caspase-9 and subsequently caspase-3. Therefore, Bax, Bcl-2 and cytochrome *c*, caspase-9 and caspase-3 were studied to identify the activation of mitochondria-mediated apoptosis pathway.

Additionally, serving as the endogenous apoptosis inhibitors, the inhibitor of apoptosis (IAP) proteins play significant roles in blocking apoptosis. It was previously reported that γT3 downregulated the expression of survivin and X-linked inhibitor of apoptosis protein (XIAP) in human gastric cancer cells and enhanced by combined treatment with capecitabine (Manu et al., 2012), suggesting an apoptosis sensitisation effect of the combined treatment. Hence, expressions of IAP proteins, namely XIAP, cellular inhibitor of apoptosis protein-1 (cIAP1), survivin and livin were assessed in this study.

Other than the intrinsic apoptosis pathway, the involvement of the extrinsic pathway was also studied by assessing the caspase-8 activation. Caspase-8 is a cysteine protease that is important in triggering extrinsic apoptotic signalling pathway via death receptors. Unlike caspase-9 which can be activated without proteolytic processing (Stennicke et al., 1999), the full activation of caspase-8 however requires a two-step proteolytic cleavage to i) separate the large and small subunits and ii) to separate the large submit and the prodomain (Chang et al., 2003). Hence, Western blotting was performed to assess the cleavage of caspase-8 and its relation to caspase-3 cleavage at various time points.

Lastly, pharmacological inhibition studies were performed with the aids from several chemical compounds to block the function of proteins/events in various pathways of interest. As such, the treatment associated pathway/process can be identified. In line with this motivation, cyclosporine A was used to block the opening of mitochondrial permeability transition pore (MPTP), while caspase-8 and caspase-3 inhibitors were employed to inhibit the caspase-8 and caspase-3, respectively. In addition, a pan-caspase inhibitor was used as a broad spectrum inhibitor to block 'general' caspases, to cross validate the caspase-8 and caspase-3 inhibitions.

Overall, it is of importance to delineate the apoptotic mechanisms and molecular events in apoptosis of single (δT3, 5FU, Dox) and combined (δT3 + 5FU and δT3 + Dox) treatments in Caco-2 and SW48 colorectal cancer cells. Hence, the study as described in this chapter specifically aimed:

i. To identify the changes of apoptosis-related proteins induced by the single and combined treatments in the representative Caco-2 cells.
ii. To assess the changes of $\Delta\Psi m$ on Caco-2 and SW48 cells induced by the single and combined treatments.
iii. To monitor the kinetic changes of mitochondrial pathway-related proteins, namely Bcl-2, Bax and cytochrome *c* in Caco-2 and SW48 cells induced by the single and combined treatments.
iv. To evaluate the changes of IAP proteins in Caco-2 and SW48 cells upon receiving the single and combined treatments.
v. To evaluate the caspase-9, -3 and -8 activities in Caco-2 and SW48 cells induced by the single and combined treatments.
vi. To examine the dependency of caspase enzymes and mitochondrial permeability transition for apoptosis in conjunction with the cell death

manifestations in Caco-2 and SW48 cells induced by the single and combined treatments.

5.2 Materials and Methods

The experimental design of current chapter can be divided into three parts, namely screening, mitochondrial pathway study and pathway validation (Figure 5.1). Initially, apoptosis array was employed to identify the changes of pro-apoptotic and anti-apoptotic proteins upon treatments. Guided by the indication, the mitochondrial pathway was investigated by i) assessing the mitochondrial membrane potential ($\Delta\Psi m$), ii) identifying changes of mitochondrial pathway-related proteins and iii) caspases activations and level of endogenous caspase inhibitors. Following that, pharmacological inhibitors were employed to identify the dependence of mitochondrial permeability transition or caspases in determining cell death.

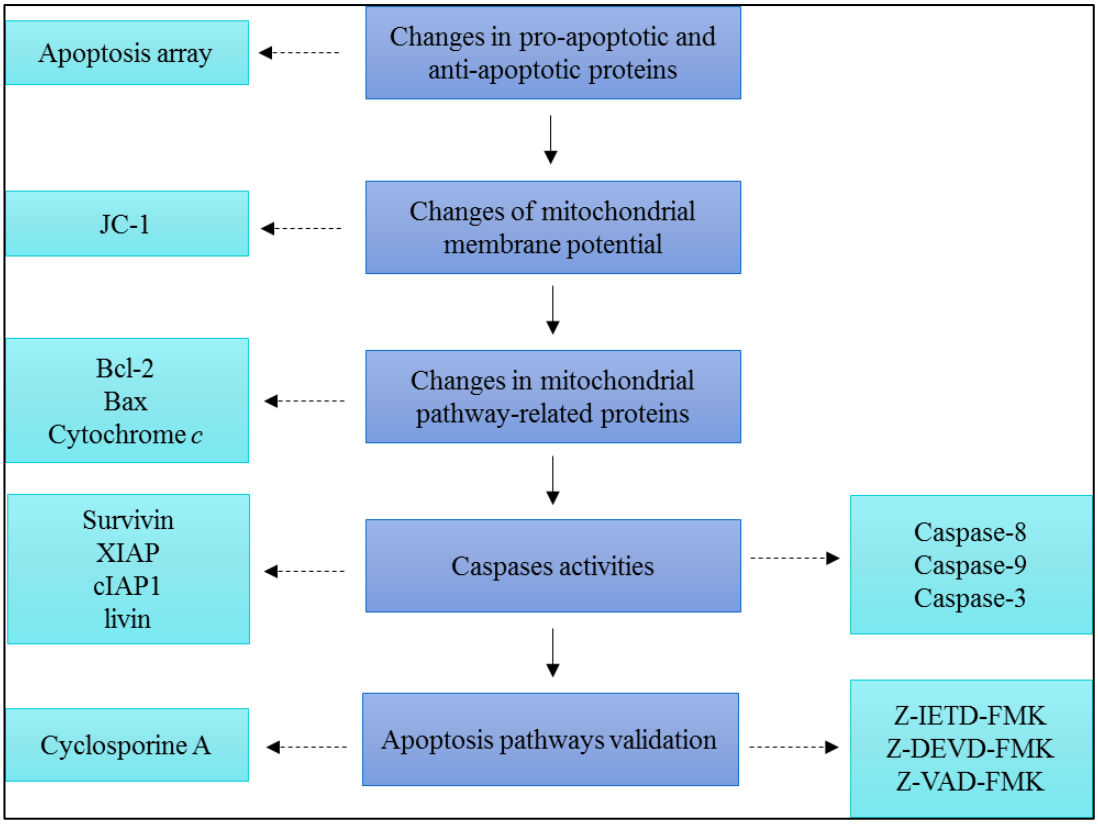

Figure 5.1 An overview of experiments involved in Chapter Five for investigating the underlying pro-apoptotic mechanisms. Dark blue boxes represent the research motivations; light blue boxes represent the approaches taken to address the research motivations.

5.2.1 Apoptosis antibody array

The RayBio® G-Series Human Apoptosis Antibody Array used in the current study adapted the design principle of sandwich enzyme-linked immunosorbent assay (ELISA). Multiple 'sub-arrays' containing apoptosis antibodies pre-printed on a standard-size microscopic glass slide (75mm x 25mm) were supplied. Briefly, the methodical procedures involved non-specific blocking, incubation with samples, washing, incubations with biotinylated detection antibodies and fluorophore conjugated-streptavidin and lastly, detection using a fluorescence laser scanner.

In this study, Caco-2 cells at a density of 1.5 x 10^5 per well were seeded in 6-well plates and incubated overnight to allow cell attachment. After that, the culture media were removed and supplied with the respective treatment media (see Table 3.5)

for 48 hours. Floating cells in the treatment media were harvested and centrifuged at 500x*g* for 5 minutes. The attached and floating cells were washed with PBS to remove traces of trypsin. One time of lysis buffer supplemented with 1x protease inhibitor cocktail (supplied in Human Apoptosis Array G1 kit) was added to the cells (RayBiotech, USA). The lysates were centrifuged at 10,000x*g* for 10 minutes and the supernatants were collected. The protein concentration was determined by Bradford protein assay (Bio-Rad, USA). Two microliters of protein sample was added to 1ml of 1x Bradford reagent in a cuvette. The cuvettes were then subjected to 595nm wavelength reading using Lambda 25 UV/Vis Spectrometer (PerkinElmer, Singapore). The protein lysates were stored at -80°C until further use.

To begin, the array chamber slide (pre-coated with apoptosis antibodies) was equilibrated to room temperature and air-dried for an hour. For blocking, as much as 100µl of 1x blocking buffer was added into each well and incubated at room temperature for 30 minutes. Next, the blocking buffer was decanted and added with 0.5µg of protein samples in appropriate volume into the respective wells. The array chamber slide containing samples was incubated overnight at 4°C to facilitate hybridisation. Next, the samples were removed and washed five times with 150µl of 1x Wash Buffer I at room temperature. Following that, the slide was washed twice with 150µl of 1x Wash Buffer II at room temperature. Subsequently, each well was added with 70µl of Biotin-conjugated Antibody Mix and incubated for 2 hours at room temperature. The washing steps involving Wash Buffer I and II were repeated. After that, each well was added with 70µl of HiLyte Plus™-conjugated streptavidin. Covered with adhesive film to avoid light exposure, the chamber slide was incubated for 2 hours at room temperature. Next, the chamber slide was washed with Wash Buffer I twice. The slide was then disassembled from the chamber and placed into a

50-ml centrifuge tube. Covering with 30ml Wash Buffer I, the slide was gently agitated for 10 minutes. Similar washing steps were repeated once using Wash Buffer I and II again. Ensuing the washing steps, the slide was rinsed with distilled water followed by centrifugation at 180x*g* for 3 minutes to remove excess water droplets. The slide was air-dried for 30 minutes (protected from light). Finally, the slide was sent for signal scanning service using a compatible laser scanner (Genomax Technologies Pte Ltd, Singapore).

The data of apoptosis antibody array were collected from two replicates on Caco-2 cells. The results obtained were plotted in histogram in relative intensity unit from different treatment groups.

5.2.2 Mitochondrial membrane potential (ΔΨm) assay

JC-1 (5,5′,6,6′-tetrachloro-1,1′,3,3′-tetraethylbenzimidazolocarbocyanine iodide) is a potential-dependent fluorochrome which incorporates into mitochondria. In healthy cells, JC-1 forms J-aggregates, emitting red fluorescence at 590nm. By contrast, JC-1 forms monomers in apoptotic cells exhibiting green fluorescence at 527nm. Hence, qualitative estimation of ΔΨm changes can be performed with the aid from fluorescence microscopy by observing the shift from green to red fluorescence in JC-1 (Kroemer et al., 2007; Sivandzade et al., 2019).

Caco-2 and SW48 cells were seeded and treated in 6-well plates as previously discussed. The ΔΨm assay was conducted as described by Soo et al. (2017). Briefly, 2ml staining media containing 5µg/ml of JC-1 (Sigma-Aldrich, USA) was added into each well and incubated for 30 minutes in a CO_2 incubator. Thereafter, the wells were washed with PBS twice at 5 minutes each. The cells were viewed under Nikon Ti-U fluorescence microscope (Nikon, Japan) with the aids of FITC (485/535nm) and

TRITC (590/610nm) filters. At least ten images were captured for each well. The ΔΨm assay was conducted every 24 hours up to 72 hours post treatment.

5.2.3 Caspase activation assays

Caspase-Glo® assay systems were employed in this study to measure activities of different caspases, namely caspase-9, caspase-8 and caspase-3/7. These systems, based on luminescence are less prone to compound interference unlike fluorescent- and calorimetric-based assays. In addition, each system offers a simple "add-mix-measure" workflow. Briefly, addition of the Caspase-Glo® reagent induces cell lysis, followed by caspase cleavage of the luminogenic substrate and generation of luminescence signal, produced by luciferase. The luminescence signal measured is therefore directly proportional to the amount of caspase activity present.

A cell number of 2,000 Caco-2 and SW48 cells were seeded in each well of an opaque 384-well plate (Thermo Scientific, USA) and incubated overnight for cell attachment. After that, the cells were subjected to appropriate single and combined treatments (see Table 3.5), followed by 24 and 48 hours of incubation. At each time point, cells were terminated with Caspase-Glo® 9 Assay Systems, Caspase-Glo® 3/7 Assay Systems and Caspase-Glo® 8 Assay Systems (Promega, USA) by adding an equal volume of the respective caspase reagent to each sample (1:1). Then, the plates were incubated for 30 minutes to induce cell lysis. Next, the luminescence signal was measured using SpectraMax® M3 Multi-Mode Microplate Reader (Molecular Devices, USA). Three independent experiments were conducted to ensure consistency and reproducibility.

5.2.4 Western blotting technique

Western blotting is a crucial technique in cell and molecular biology to identify specific proteins from a complex mixture of proteins. Briefly, the extracted proteins

are firstly separated by size via electrophoresis, then transferred to a solid support (i.e., blotting membrane), followed by the detection of protein band(s) using primary antibody that can recognise the specific protein of interest. Lastly, the secondary antibody conjugated to an enzyme is added to bind to the primary antibody. When an appropriate substrate is added, the chemical reaction takes place and the protein band(s) can be visualised or detected. The chemiluminescent signal intensity of the protein band is proportional to the amount of protein present in the sample. Inclusion of GAPDH as a loading control is important to validate the equal loading of protein samples in each well so that protein expression can be interpreted fairly.

5.2.4.1 Protein harvest and quantification

A total of 1.5 x 10^5 Caco-2 and 3 x 10^5 SW48 cells were seeded in 6-well plates and incubated overnight to allow cell attachment. Following that, the culture media were replaced with the treatment media containing individual concentrations of δ-tocotrienol (δT3), 5-fluorouracil (5FU), doxorubicin (Dox) and the (δT3 + 5FU and δT3 + Dox) combinations (see Table 3.5). Floating cells in the treatment media were pelleted at 500x*g* for 5 minutes. Both the attached and floating cells were washed with ice-cold PBS to remove traces of trypsin. One hundred fifty microliters of 1% NP40 (v/v) lysis buffer supplemented with 1x cOmplete™ Protease Inhibitor Cocktail (Roche, Switzerland), 1x phosphatase inhibitor 1 and 2 (Sigma-Aldrich, USA), was added into each sample in the 6-well plates. The lysis of the cells was facilitated by mechanical scrapping. The lysates were collected and centrifuged at 10,000x*g* for 10 minutes at 4°C. Following that, the supernatants were collected. The protein concentration was determined by Bradford protein assay (Bio-Rad, USA) as previously described in Section 5.2.1. The protein lysates were stored at -80°C until further use.

5.2.4.2 Sodium dodecyl sulphate polyacrylamide gel electrophoresis (SDS-PAGE)

Fifty micrograms of protein samples added with 1x sample buffer (see Appendix: Table A5.1 for recipe) were subjected to denaturation at 95°C for 5 minutes. The samples were loaded into a 4-12% gradient gel (see Appendix: Table A5.2 for recipe). Eight microliters of Spectra™ Multicolour Broad Range Protein Ladder (Thermo Fisher Scientific, USA) was loaded to serve as a molecular weight marker. Then, the polyacrylamide gels were run at a condition of 200V for 45 minutes in 1x Tris-Glycine SDS running buffer (see Appendix: Table A5.3 for recipe).

5.2.4.3 Immunoblotting and immunodetection

Initially, each polyvinylidene difluoride (PVDF) membrane (7cm x 8cm) was activated in methanol for 2 minutes. Then, extra thick blot absorbent filter papers (Bio-Rad, USA) and the activated PVDF membrane were equilibrated in 1x transfer buffer (see Appendix: Table A5.4 for recipe) for 15 minutes. The gel was sandwiched within filter papers and PVDF membrane on the Trans-blot® SD Semi-Dry Transfer Cell (Bio-Rad, USA). Next, the proteins on polyacrylamide gel were transferred/blotted onto the PVDF membrane (Bio-Rad, USA) at 12V for an hour.

Thereafter, the blots were blocked with 5% bovine serum albumin (BSA, w/v) dissolved in phosphate buffered saline-Tween 20 (PBST, see Appendix: Table A5.5 for recipe) for 2 hours. Following that, the blocking buffer was removed and added with the respective primary antibodies (Table 5.1) for overnight incubation at 4°C. Next, the primary antibodies were removed and washed with PBST for three times at 5-minute intervals. Then, horseradish peroxidase (HRP)-linked anti-mouse (1: 5,000) or anti-rabbit (1: 25,000) secondary antibodies (Bio-Rad, USA) were added to the respective blots for 1-hour incubation (Bio-Rad, USA). Lastly, the blots were washed thrice with PBST, each for 5 minutes to remove unbound secondary antibodies. The

blots were added with 200µl of ECL Select™ Western Blotting Detection Reagent (GE Healthcare, USA) and chemiluminescent signals were detected using ChemiDoc™ XRS+ Imaging System (Bio-Rad, USA).

Table 5.1 Various primary antibodies used in the assays described in Chapter Five.

Primary antibody	Molecular weight (kDa)	Dilution	Manufacturer	Host species of primary antibody
Bcl-2	26	1:1,000	Cell Signaling Technology, USA	Rabbit
Bax	21	1:1,000	Cell Signaling Technology, USA	Rabbit
Cytochrome *c*	14	1:1,000	Cell Signaling Technology, USA	Rabbit
Pro-caspase-3	35	1:1,000	Cell Signaling Technology, USA	Rabbit
Cleaved caspase-3	17, 19	1:1,000	Cell Signaling Technology, USA	Rabbit
Pro-caspase-8	57	1:1,000	Cell Signaling Technology, USA	Rabbit
Cleaved caspase-8	43, 41, 18	1:1,000	Cell Signaling Technology, USA	Rabbit
Survivin	16	1:1,000	Cell Signaling Technology, USA	Rabbit
XIAP	55	1:1,000	Cell Signaling Technology, USA	Rabbit
cIAP1	62	1:1,000	Cell Signaling Technology, USA	Rabbit
Livin	36,34	1:1,000	Cell Signaling Technology, USA	Rabbit
GAPDH	37	1:2,500	Santa Cruz Biotechnology, USA	Mouse

5.2.5 Pharmacological inhibition assays

Pharmacological inhibition agents can be used as a research tool to define the role or criticality of biomolecules or an event in culminating apoptosis. Herein, caspase inhibitors were recruited in this study, which could irreversibly bind to the catalytic site of caspase proteases to inhibit apoptosis induction. Meanwhile, cyclosporine A is an agent to block the opening of MPTP, which can attenuate mitochondrial permeability transition.

Approximately 2,000 cells were seeded into each well of 384-well plates and incubated overnight for cell attachment. Thereafter, the culture media were removed and replenished with fresh media containing the pharmacological inhibitors (Table 5.2). The inhibitors were pre-incubated for 2 hours prior to drug treatment. Next, 5µl of treatment solution was added to the respective wells (see Table 5.3). Cell viability was assessed after 24, 48 and 72 hours of treatment using CellTitre-Glo® Luminescent Cell Viability Assay (Promega, USA) as previously described in Section 3.2.5 of Chapter Three. The cell viability was obtained by normalizing luminescence signal of treated samples with an average of luminescence signal of untreated (vehicle) control and multiplying by 100%. The experiment was repeated for three times independently.

Table 5.2 Pharmacological inhibitors used in Chapter Five.

Inhibitor	Peptide sequence	Final concentration	Manufacturer
Caspase-8	Z-IETD-FMK	10µM	R&D Systems, USA
Caspase-3	Z-DEVD-FMK	10µM	R&D Systems, USA
Pan-caspase	Z-VAD-FMK	10µM	R&D Systems, USA
Cyclosporine A	-	1µM	Tocris Bioscience, UK

5.2.6 Statistical analyses

One-way analysis of variance (ANOVA) was performed in Section 5.2.1 (apoptosis antibody array) and Section 5.2.3 (caspase-9, caspase-8 and caspase-3 activations) to compare the differences of means among the experimental groups. Turkey's multiple comparisons test was conducted to identify the statistical significance between the treatment groups while Dunnett's multiple comparisons test was performed to identify statistical significance between treated groups and vehicle control.

Two-way ANOVA was performed to compare the differences of means between treatment groups, with or without the presence of apoptosis inhibitors used (Section 5.2.5). Dunnett's multiple comparisons test was conducted to identify the statistical significance levels between the respective groups with the use of apoptosis inhibitors and those without. The differences were marked as significant when $p < 0.05$ (*), $p < 0.01$ (**), $p < 0.001$ (***), $p < 0.0001$ (****).

5.3 Results

5.3.1 Effects of single and combined treatments on cellular apoptosis markers as detected by apoptosis antibody array

The changes of anti-apoptosis and pro-apoptosis proteins in Caco-2 cells after treatments with δT3 and 5FU single treatments, as well as the δT3 + 5FU combined treatment, were detected using apoptosis array. The signal intensities detected by antibodies on the apoptosis array correspond to the abundancy of the respective proteins. The profiles of anti-apoptotic proteins (Section 5.3.1.1) and pro-apoptotic proteins (Section 5.3.1.2) are presented in the following sections.

5.3.1.1 Evaluation of anti-apoptotic protein expressions

The results demonstrated that δT3 + 5FU combined treatment caused a general downregulation of anti-apoptotic proteins. The affected anti-apoptotic protein families include anti-apoptotic Bcl-2 family (Figure 5.2), IAP family (Figure 5.3), heat shock protein (HSP) family (Figure 5.4) and insulin-like growth factor binding protein (IGFBP) family (Figure 5.5) in Caco-2 cells.

In the Bcl-2 anti-apoptotic proteins, δT3 + 5FU combined treatment caused significant downregulation of Bcl-2 protein expression in Caco-2 cells, as compared to vehicle control ($p<0.01$), and its level was lower than that of δT3 and 5FU single treatments. Although statistically non-significant, it is noteworthy to mention that the Bcl-w protein expression of Caco-2 cells which subjected to combined treatment was the lowest when compared to the individual single treatments (Figure 5.2).

Notably in the IAP family, the lowest expressions in cIAP2, livin, survivin and XIAP were observed Caco-2 cells which were treated with combined treatment. The downregulations were significant in XIAP over vehicle control ($p<0.0001$); livin

(p<0.05) and cIAP2 (p<0.01) were significantly downregulated when compared to δT3 alone (Figure 5.3).

Additionally, δT3 + 5FU combined treatment induced general downregulations in HSP27, HSP60 and HSP70. However, only the downregulation in HSP70 was statistically significant when compared to δT3 (p<0.01) and 5FU (p<0.01) single treatments individually (Figure 5.4).

Moreover, IGF-1 was significantly downregulated in Caco-2 cells which were treated with δT3 + 5FU combined treatment, as compared to vehicle control (p<0.05), δT3 and 5FU single treatments (p<0.001) (Figure 5.5). However, there was no significant difference in other proteins under the same family.

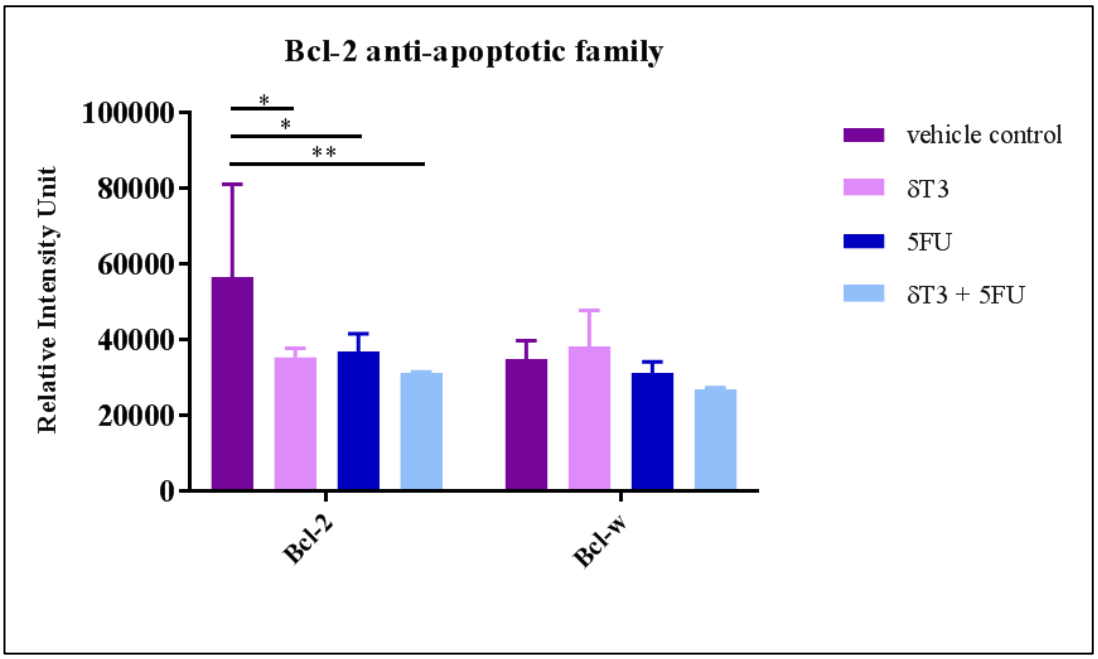

Figure 5.2 Apoptosis array protein expression of Bcl-2 anti-apoptotic proteins in Caco-2 cells. * p < 0.05; ** p < 0.01.

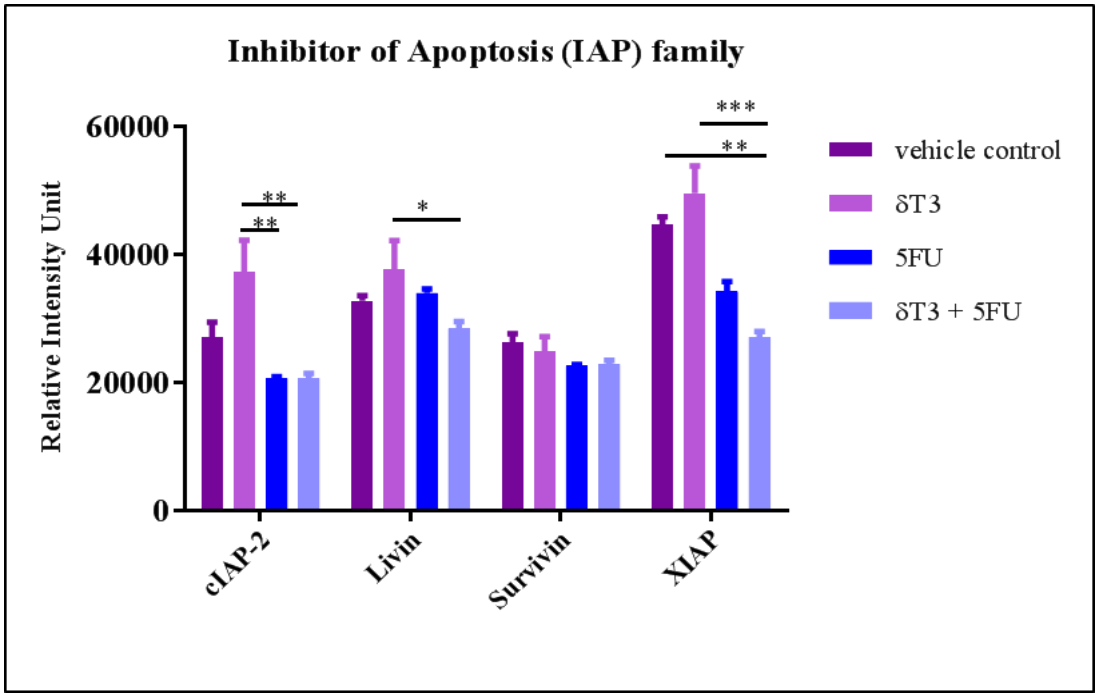

Figure 5.3 Apoptosis array protein expression of IAP family in Caco-2 cells. * $p < 0.05$; ** $p < 0.01$; *** $p < 0.001$; **** $p < 0.0001$.

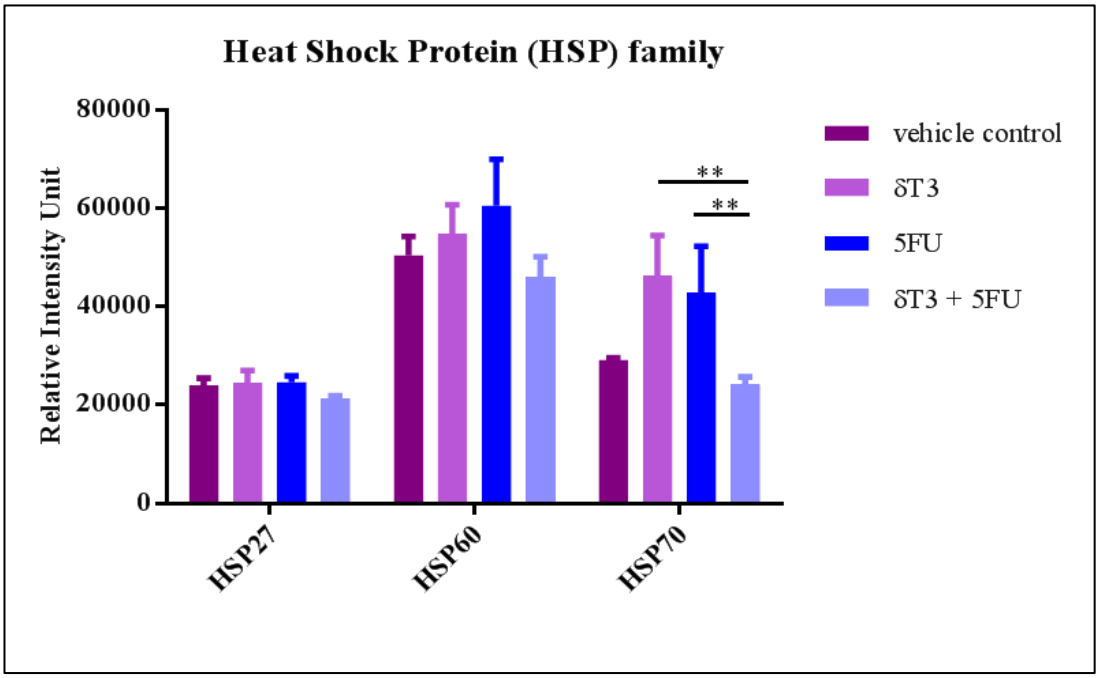

Figure 5.4 Apoptosis array protein expression of HSPs in Caco-2 cells. * $p < 0.05$; ** $p < 0.01$.

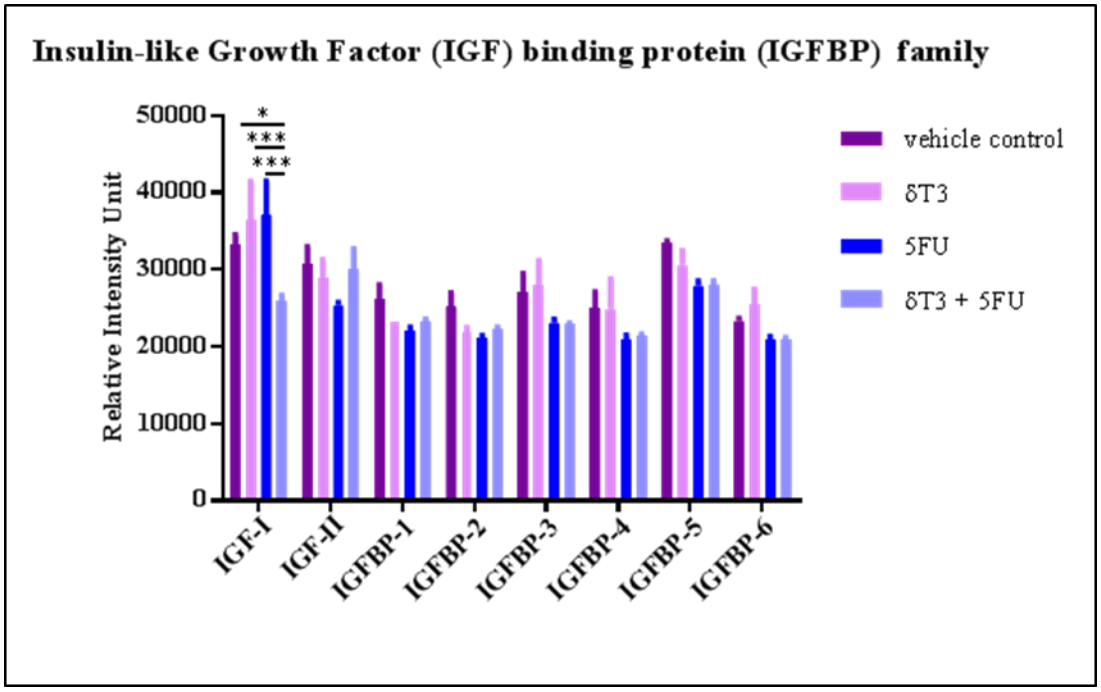

Figure 5.5 Apoptosis array protein expression of IGF and IGFBP proteins in Caco-2 cells. * $p < 0.05$; ** $p < 0.01$; *** $p < 0.001$.

5.3.1.2 Evaluation of pro-apoptotic protein expressions

All the treatment groups displayed non-significant changes in pro-apoptotic proteins family such as pro-apoptotic Bcl-2 family (Figure 5.6), mitochondrial proteins (Figure 5.7) and tumour suppressor proteins (Figure 5.8). Albeit statistically non-significant, there was a consistent trend of showing a slight increase in Bid, Bim, Bax (Figure 5.6), HTRA (Figure 5.7) and p27 (Figure 5.8) in Caco-2 cells subjected to treatments of δT3, 5FU or δT3 + 5FU.

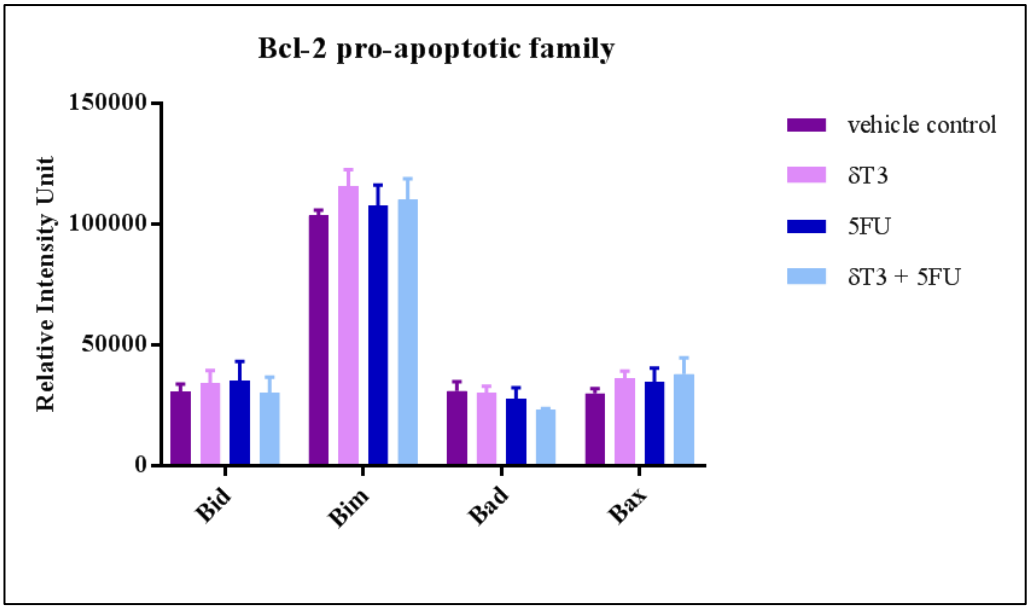

Figure 5.6 Apoptosis array protein expression of Bcl-2 pro-apoptotic family in Caco-2 cells.

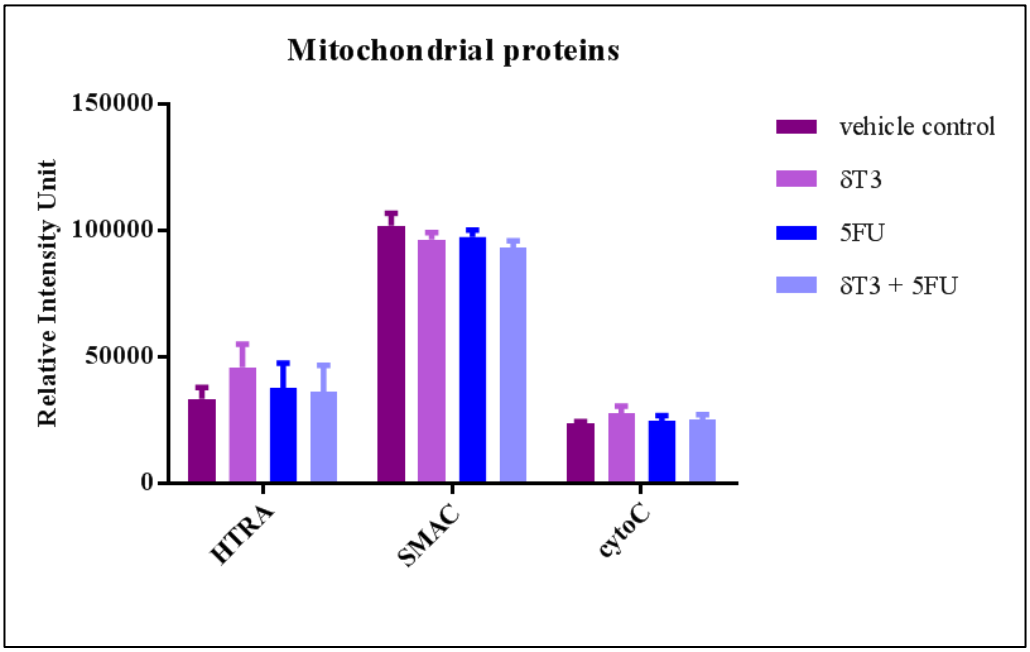

Figure 5.7 Apoptosis array protein expression of mitochondrial proteins in Caco-2 cells.

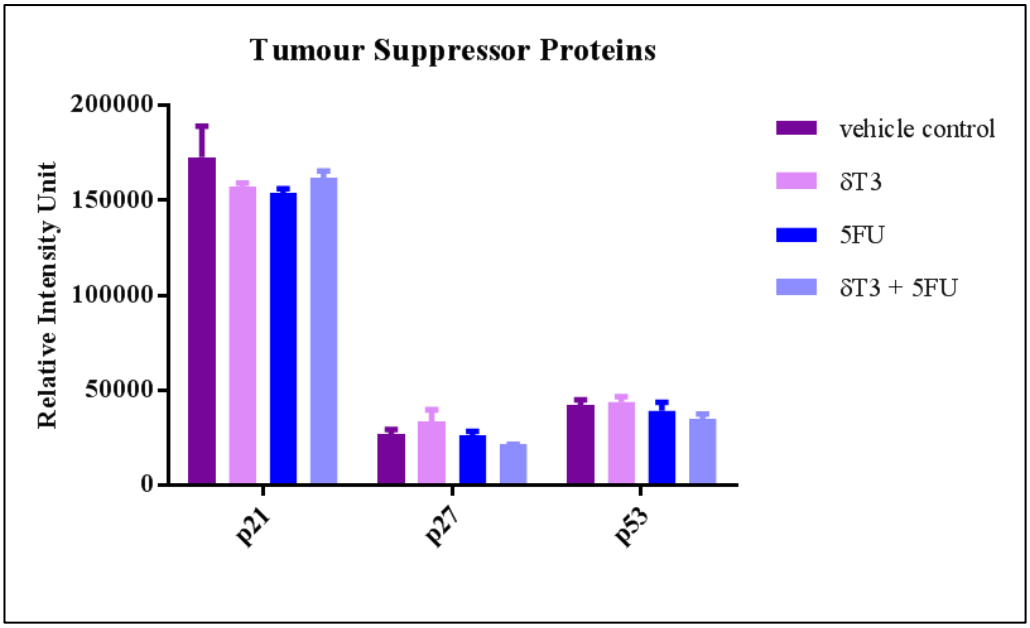

Figure 5.8 Apoptosis array protein expression of tumour suppressor proteins in Caco-2 cells.

5.3.2 Effects of single and combined treatments on mitochondria-mediated apoptosis pathway

In the following sections, the mitochondria-mediated apoptosis pathway was evaluated by from four aspects. In Section 5.3.2.1, the JC-1 profiles that demonstrate changes of mitochondrial membrane potential (ΔΨm) were presented. In Section 5.3.2.2, Western blotting profiles of mitochondrial pathway-related proteins were showed. The activations of caspase-9 and -3, as well as the endogenous caspase inhibitor (IAP family) were exhibited in the Western blotting profiles in Sections 5.3.2.3 & 5.3.2.4 respectively.

5.3.2.1 Qualitative detection of ΔΨm changes

The changes of ΔΨm on Caco-2 and SW48 cells were monitored for 24, 48 and 72 hours after treatment. Generally, there was an increase in green intensity and a decrease in red intensity observed after 48-hour treatments, which indicate a loss of ΔΨm. The ΔΨm profiles upon receiving the single and combined treatments at 48 and 72 hours are represented in Figures 5.19 – 5.12.

In Caco-2 cells, treatments with δT3, 5FU and δT3 + 5FU caused an increase in green signal at 48 hours. At 72 hours, green signal augmentation was obviously observed in δT3 single treatment (Figure 5.9). Based on the upsurge of green signal and a corresponding decline in red signal, the increased green/red ratio in δT3 + 5FU combined treatment signifies a loss of ΔΨm (Figure 5.9). Similarly in SW48 cells, a loss of ΔΨm was resulted in δT3 single treatment and δT3 + 5FU combined treatment due to the noticeable increment of green/red ratio (Figure 5.10).

On the other hand, Dox only disturb ΔΨm after 72 hours of treatments in both Caco-2 and SW48 cells. In comparison, δT3 single treatment and δT3 + Dox combined treatment caused loss of ΔΨm as evidenced by the increase in green signal after 48 and 72 hours of treatments in Caco-2 (Figure 5.11) and SW48 cells (Figure 5.12).

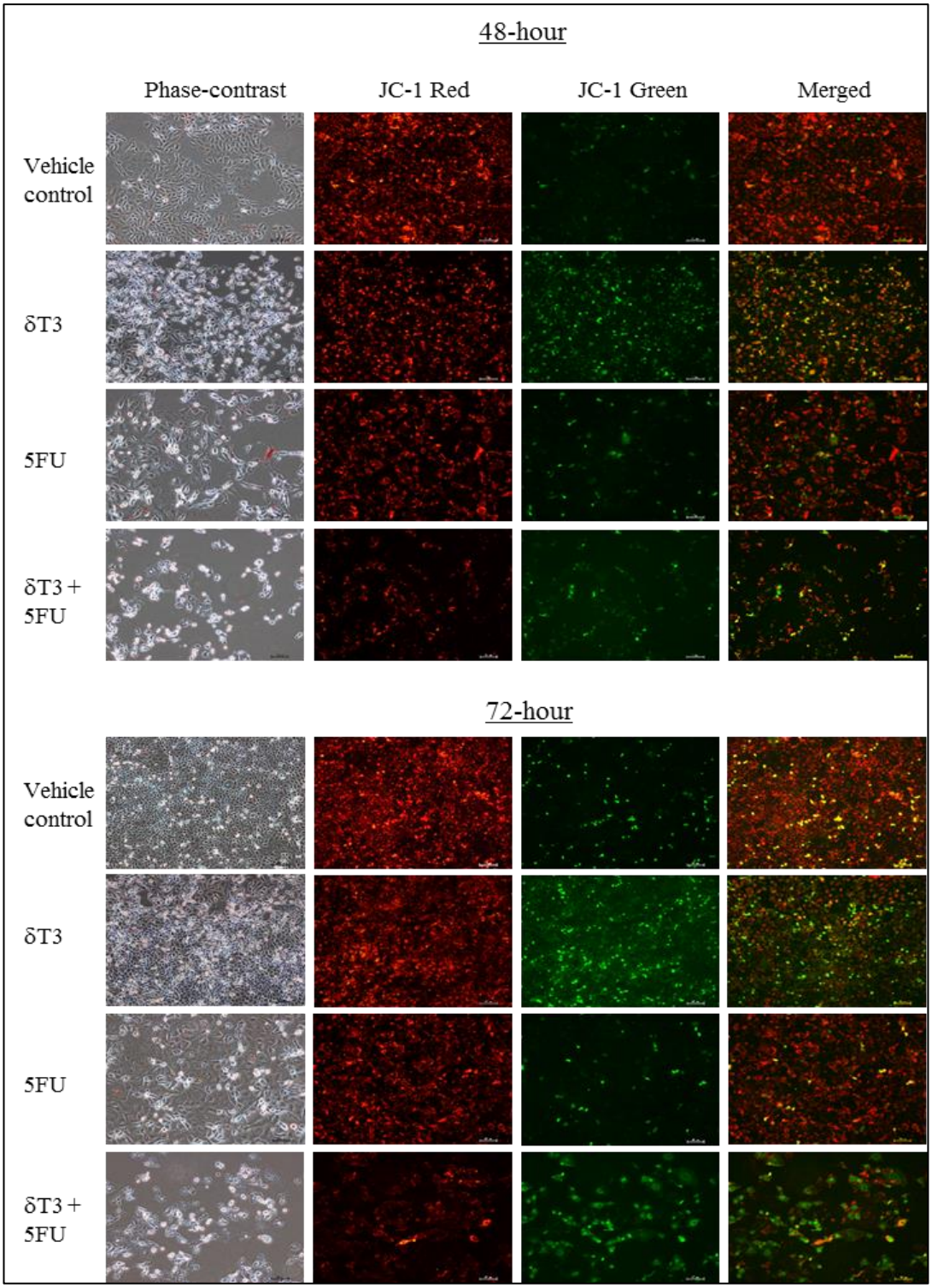

Figure 5.9 Mitochondrial membrane potential (ΔΨm) profiles of Caco-2 cells after receiving 48- and 72-hour treatments from δT3, 5FU and the combination. δT3, δ-tocotrienol; 5FU, 5-fluorouracil; δT3 + 5FU, δ-tocotrienol and 5-fluorouracil combined treatment.

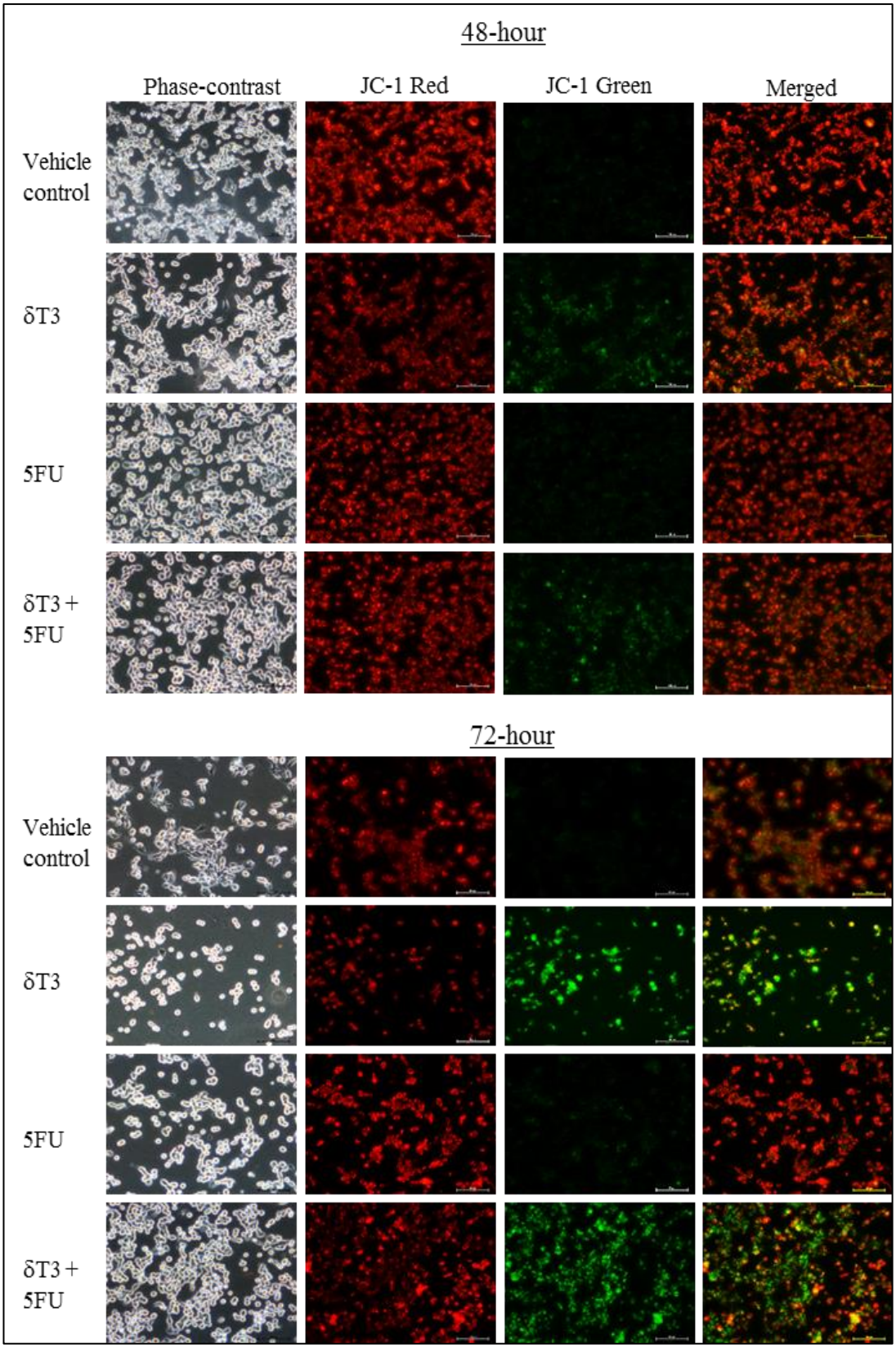

Figure 5.10 Mitochondrial membrane potential (ΔΨm) profiles of SW48 cells after receiving 48- and 72- hour treatments from δT3, 5FU and the combination. δT3, δ-tocotrienol; 5FU, 5-fluorouracil; δT3 + 5FU, δ-tocotrienol and 5-fluorouracil combined treatment.

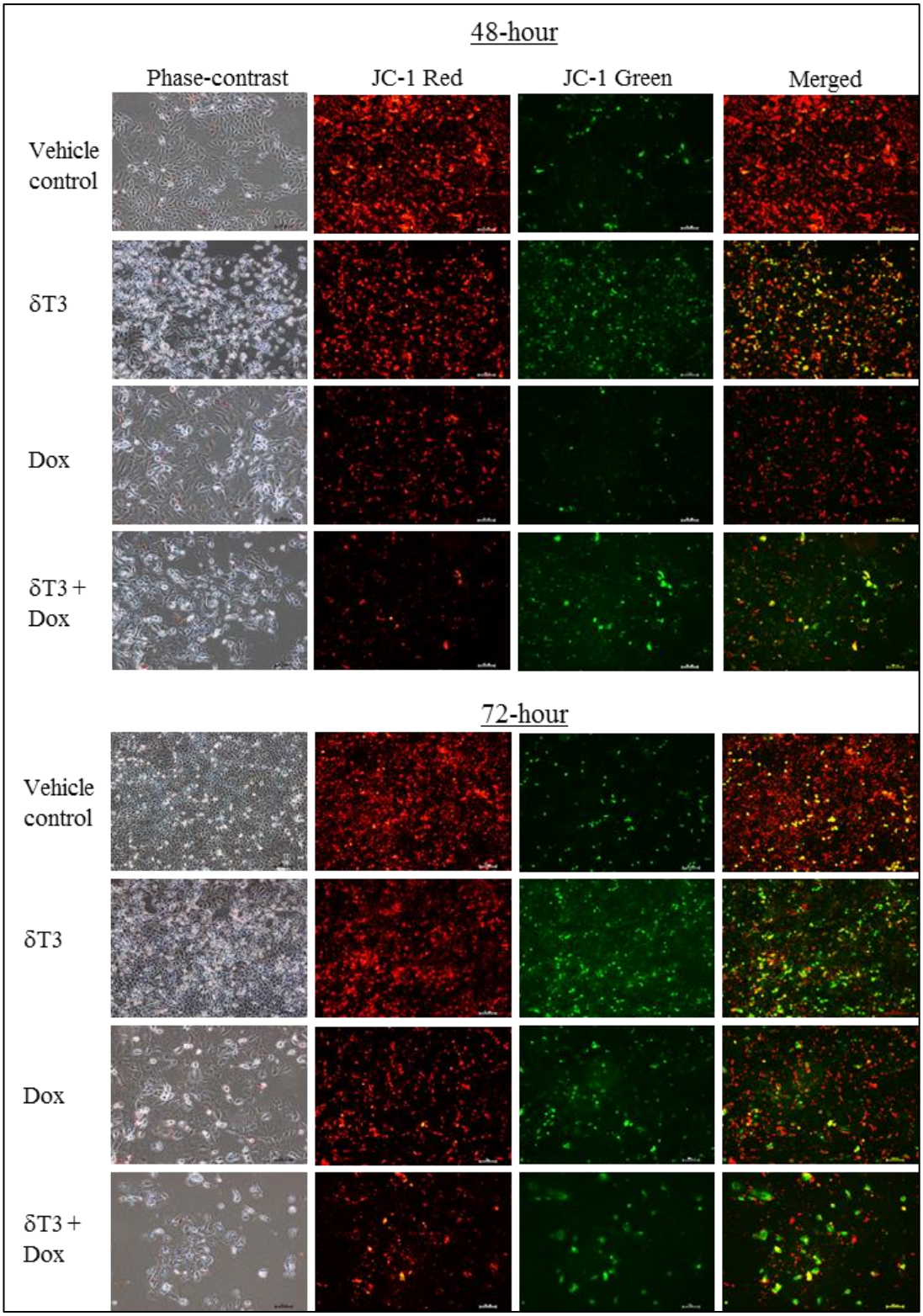

Figure 5.11 Mitochondrial membrane potential (ΔΨm) profiles of Caco-2 cells after receiving 48- and 72-hour treatments from δT3, Dox and the combination. δT3, δ-tocotrienol; Dox, doxorubicin; δT3 + Dox, δ-tocotrienol and doxorubicin combined treatment.

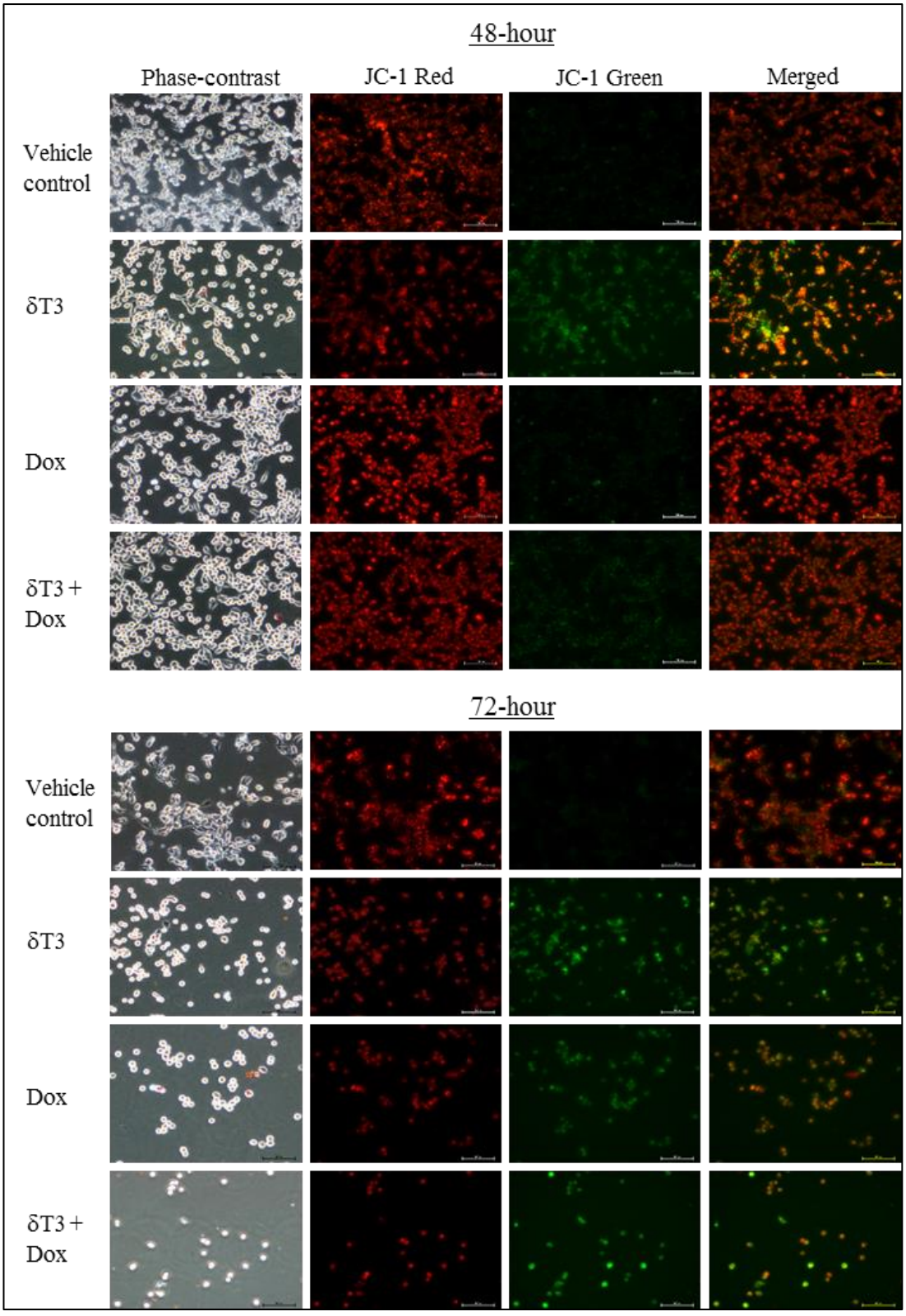

Figure 5.12 Mitochondrial membrane potential (ΔΨm) profiles of SW48 after receiving 48- and 72- hour treatments from δT3, Dox and the combination. δT3, δ-tocotrienol; Dox, doxorubicin; δT3 + Dox, δ-tocotrienol and doxorubicin combined treatment.

5.3.2.2 Western profiling of mitochondrial pathway-related proteins

At 24 hours, Bax was upregulated in Caco-2 cells receiving 5FU single treatment and δT3 + 5FU combined treatment, and a corresponding increase in cytochrome *c* level. After 48 hours of treatments, Bax and cytochrome *c* levels of Caco-2 cells were enhanced in the combined treatment group as compared to those of vehicle control, δT3 and 5FU individually. However, these effects were not observed after 72 hours of treatments (Figure 5.13).

For SW48 cells, a downregulation of Bcl-2 level was detected in 5FU single treatment and δT3 + 5FU combined treatment after 24 and 48 hours, comparing to the expressions in vehicle control and δT3 single treatment. Interestingly, Bax expression of SW48 cells was unable to be detected in this study. Following that, the level of cytochrome *c* of SW48 cells was enhanced after 48 and 72 hours of δT3 + 5FU combined treatment, comparing to the expressions in vehicle control, δT3 and 5FU single treatments (Figure 5.14).

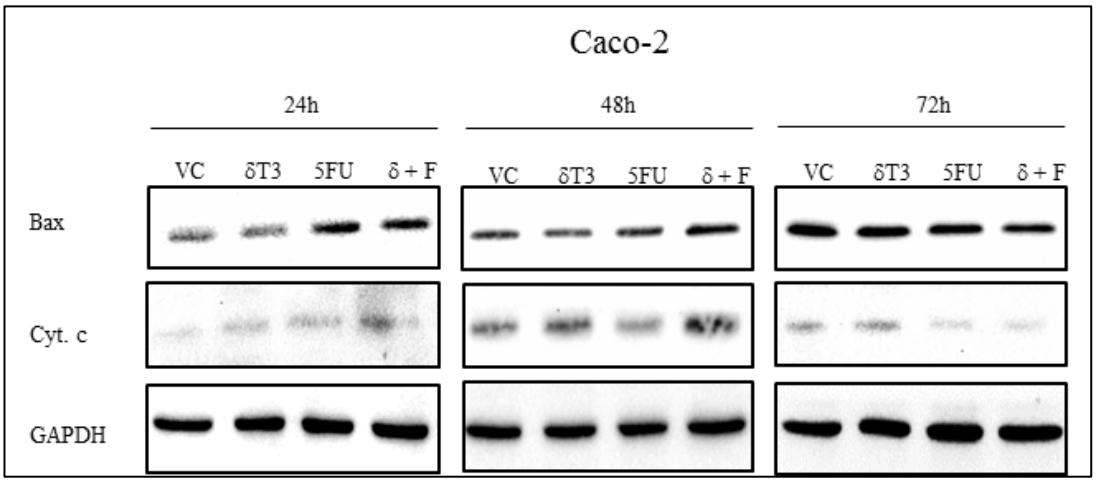

Figure 5.13 Representative Western blotting profiles of mitochondrial pathway-related proteins for Caco-2 cells at various time points after receiving treatments of δT3, 5FU and the combination. GAPDH serves as a loading control. VC, vehicle control; δT3, δ-tocotrienol; 5FU, 5-fluorouracil; δ + F, δ-tocotrienol + 5-fluorouracil.

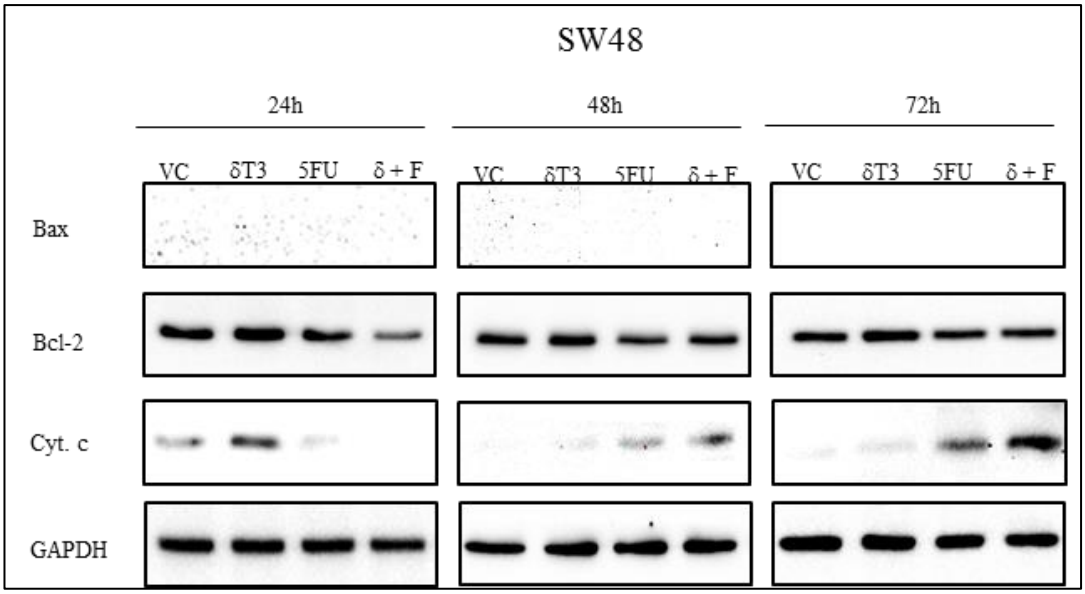

Figure 5.14 Representative Western blotting profiles of mitochondrial pathway-related proteins for SW48 cells at various time points after receiving treatments of δT3, 5FU and the combination. GAPDH serves as a loading control. VC, vehicle control; δT3, δ-tocotrienol; 5FU, 5-fluorouracil; δ + F, δ-tocotrienol + 5-fluorouracil.

In Caco-2 cells, individual Dox single treatment and δT3 + Dox combined treatments caused elevated expressions of Bax and cytochrome *c* after 24- and 48-hour treatments (Figure 5.15). In SW48 cells, a downregulation of Bcl-2 was observed when subjected to δT3 + Dox combined treatment for 24 hours, as compared to vehicle control and δT3 single treatment. However, the Bax expression in SW48 was unable to be detected. An elevated cytochrome *c* expression was also detected after 48-hour treatment with δT3 + Dox. Notably, the cytochrome *c* expression induced by the combined treatment was the highest after 72 hours (Figure 5.16).

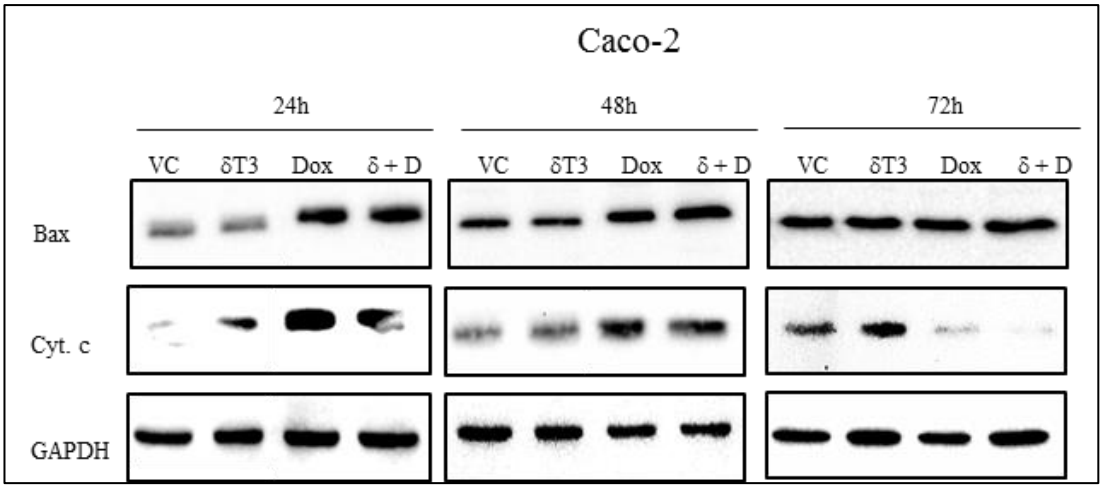

Figure 5.15 Representative Western blotting profiles of mitochondrial pathway-related proteins for Caco-2 cells at various time points after receiving treatments of δT3, Dox and the combination. GAPDH serves as a loading control. VC, vehicle control; δT3, δ-tocotrienol; Dox, doxorubicin; δ + D, δ-tocotrienol + doxorubicin.

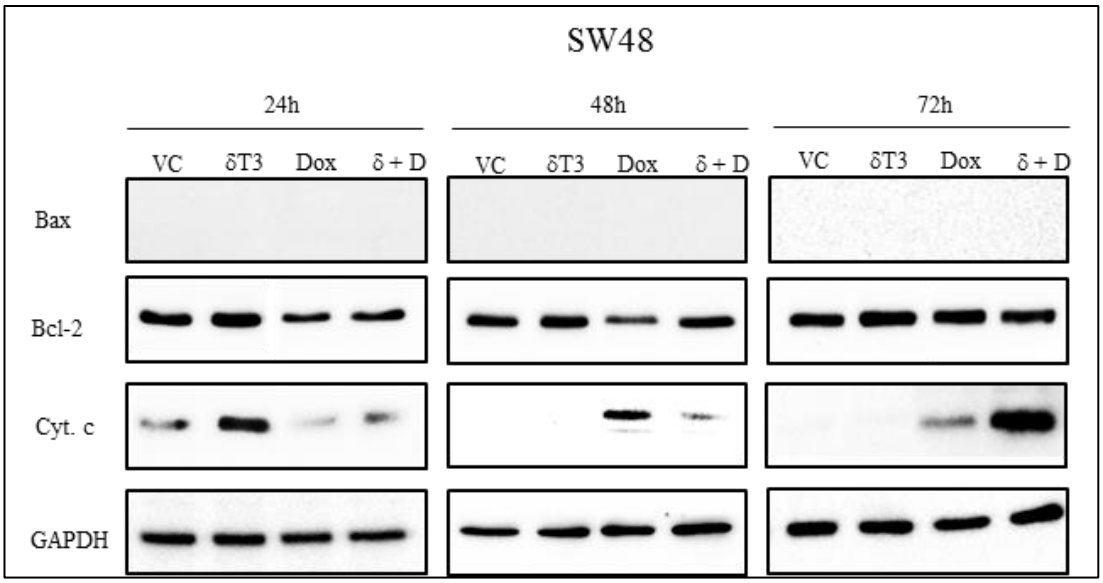

Figure 5.16 Representative Western blotting profiles of mitochondrial pathway-related proteins for SW48 cells at various time points after receiving treatments of δT3, Dox and the combination. GAPDH serves as a loading control. VC, vehicle control; δT3, δ-tocotrienol; Dox, doxorubicin; δ + D, δ-tocotrienol + doxorubicin.

5.3.2.3 Evaluation of caspase-9 and caspase-3/7 activations

In Caco-2 cells, it was demonstrated that individual δT3, 5FU and Dox single treatments did not induce caspase-9 activation. Albeit there was an increase in caspase-9 activity in Caco-2 cells which subjected to δT3 + 5FU combined treatment after 24 and 48 hours, the increment was not statistically significant (Figure 5.17 A & C).

Similarly, δT3 + Dox combined treatment slightly increased the caspase-9 activation over the vehicle control and single treatments in Caco-2 cells after 24 hours, but it was also not statistically significant (Figure 5.17 A & C).

In SW48 cells, all treatment groups did not show a significant difference in caspase-9 activation after 24 hours of treatments (Figure 5.17 B). However, the caspase-9 activation was significantly decreased in 5FU ($p < 0.001$), δT3 + 5FU ($p < 0.01$), Dox ($p < 0.0001$) and δT3 + Dox ($p < 0.0001$) when compared to vehicle control after 48-hour treatment (Figure 5.17 D), suggesting that caspase-9 activation is not involved in SW48 cells.

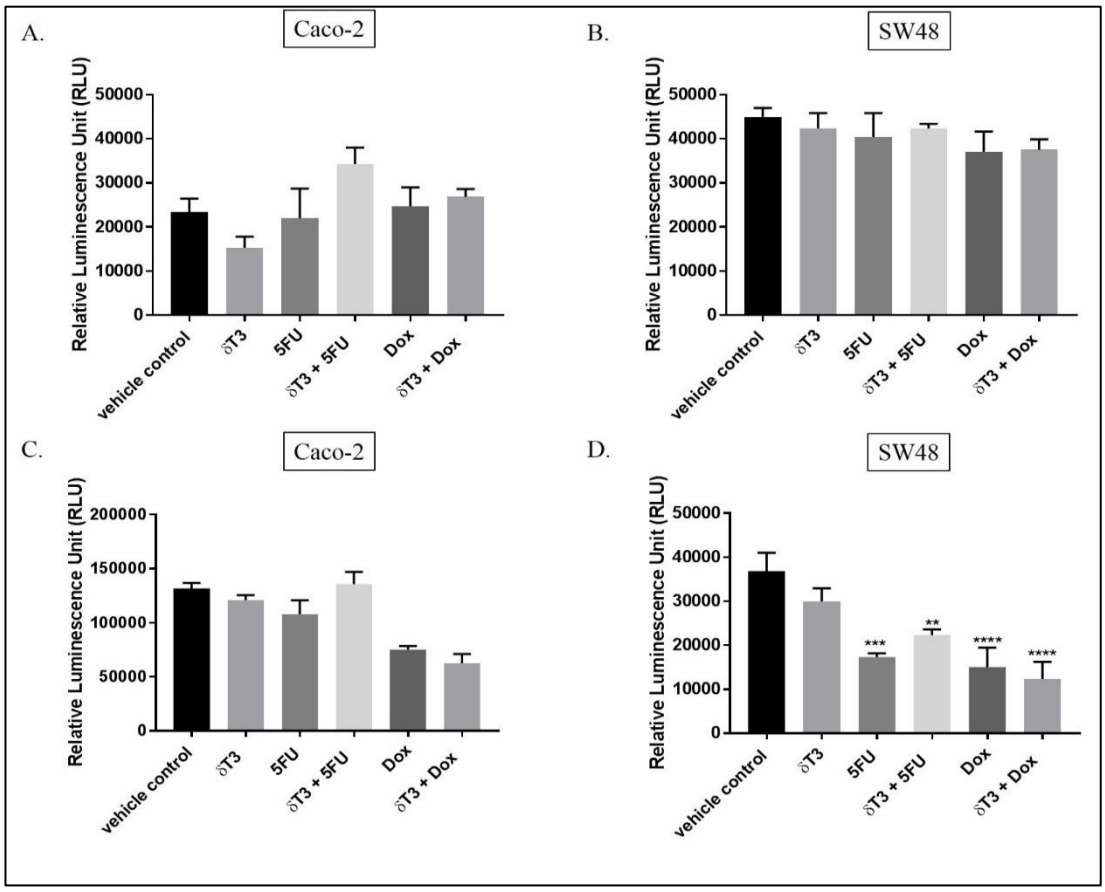

Figure 5.17 Caspase-9 activation profiles of Caco-2 and SW48 cells after 24 hours (A & B) and 48 hours (C & D) of treatments. δT3, δ-tocotrienol; 5FU, 5-fluorouracil; δ + F, δ-tocotrienol + 5-fluorouracil; Dox, doxorubicin; δ + D, δ-tocotrienol + doxorubicin. ** $p < 0.01$; *** $p < 0.001$; *** $p < 0.0001$.

In Caco-2 cells, the increases in caspase-3/7 activation of δT3, 5FU and Dox single treatments were not significant when compared to vehicle control in both 24- and 48-hour treatments. In contrast, δT3 + 5FU and δT3 + Dox combined treatments induced a significantly higher ($p < 0.0001$) caspase-3/7 activation over vehicle control, for both 24- and 48-hour treatments (Figure 5.18 A & C).

In SW48 cells, δT3 and 5FU single treatments did not induce a significant caspase-3/7 activation. On the contrary, δT3 + 5FU combined treatment caused a significantly higher ($p < 0.0001$) caspase-3/7 activation after 24- and 48-hour treatments (Figure 5.18 B & D). Notably, a significantly higher caspase-3/7 activation was observed in SW48 cells receiving Dox single treatment ($p < 0.0001$) and δT3 + Dox combined treatment ($p < 0.01$) over the vehicle control after 24 hour-treatment (Figure 5.18 B). After 48-hour treatment, the capase-3/7 activation was significantly higher in δT3 + 5FU ($p < 0.0001$) and δT3 + Dox combined treatments ($p < 0.05$) when compared to vehicle control (Figure 5.18 D).

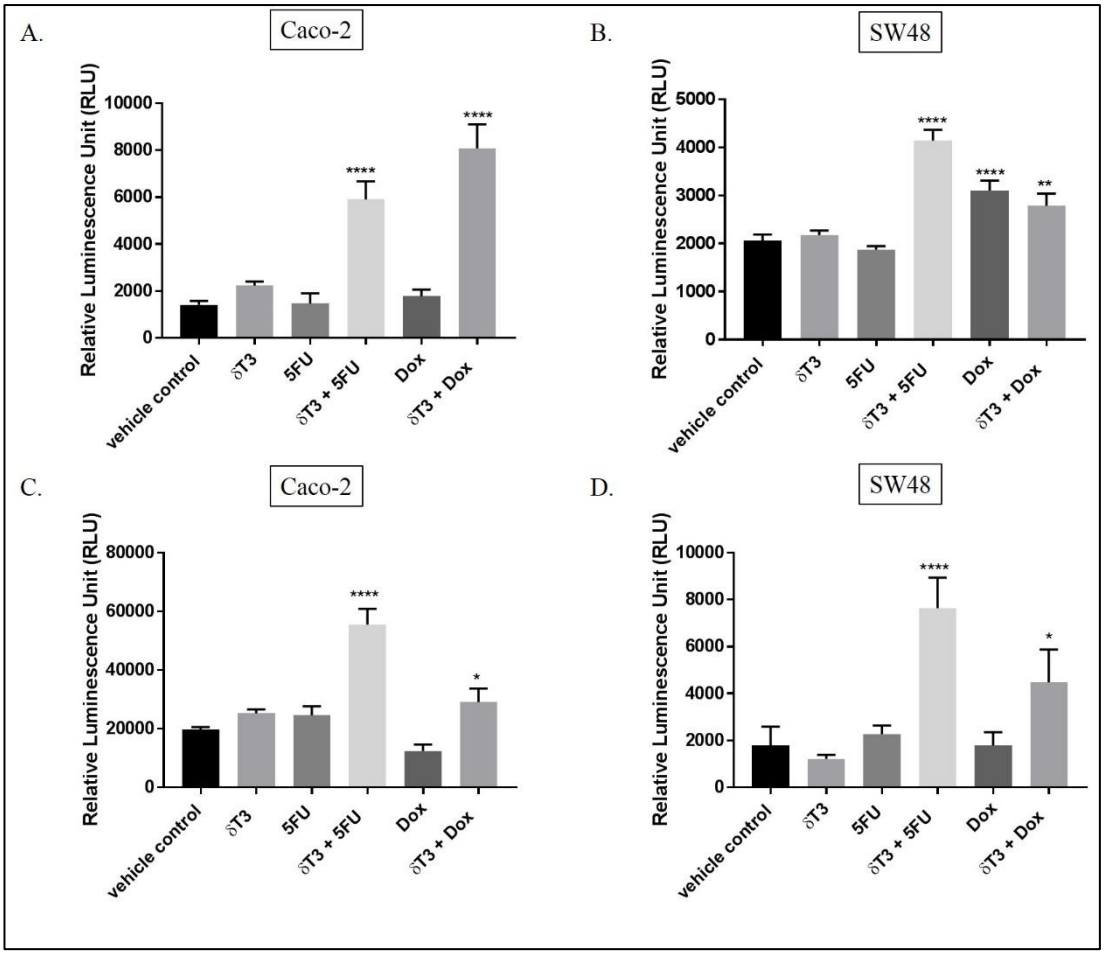

Figure 5.18 Caspase-3/7 activation profiles of Caco-2 and SW48 cells after 24 hours (A & B) and 48 hours (C & D) of treatments. δT3, δ-tocotrienol; 5FU, 5-fluorouracil; δ + F, δ-tocotrienol + 5-fluorouracil; Dox, doxorubicin; δ + D, δ-tocotrienol + doxorubicin. * $p < 0.05$; ** $p < 0.01$; *** $p < 0.001$; *** $p < 0.0001$.

5.3.2.4 Western profiling of IAP family

Western blotting profiles revealed that 5FU single treatment upregulated expression of survivin in Caco-2 cells after 48 and 72 hours of treatment; in comparison, a lower expression of survivin was detected in δT3 + 5FU combined treatment. Of note, the expressions of other proteins in IAP family, namely, XIAP, cIAP1 and livin were found negligible in Caco-2 cells (Figure 5.19).

As compared to Caco-2 cells, the basal expression levels of IAP proteins in SW48 cells were higher. In SW48 cells, lower expressions of survivin, XIAP and

cIAP1 were observed in cells subjected to δT3 + 5FU combined treatment as compared to vehicle control, δT3 and 5FU single treatments after 72 hours (Figure 5.20).

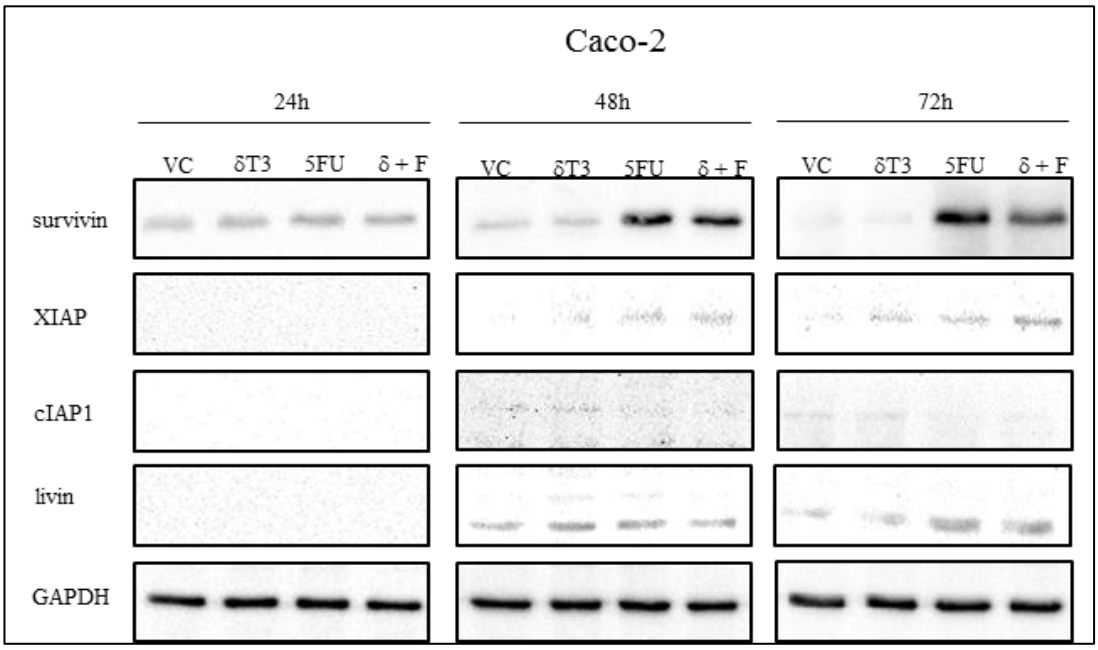

Figure 5.19 Representative Western blotting profiles of IAP proteins for Caco-2 cells after receiving treatments of δT3, 5FU and the combination at various time points. GAPDH serves as a loading control. δ-tocotrienol, 5-fluorouracil and the combined treatment. 5FU, 5-fluorouracil; δ + F, δ-tocotrienol + 5-fluorouracil.

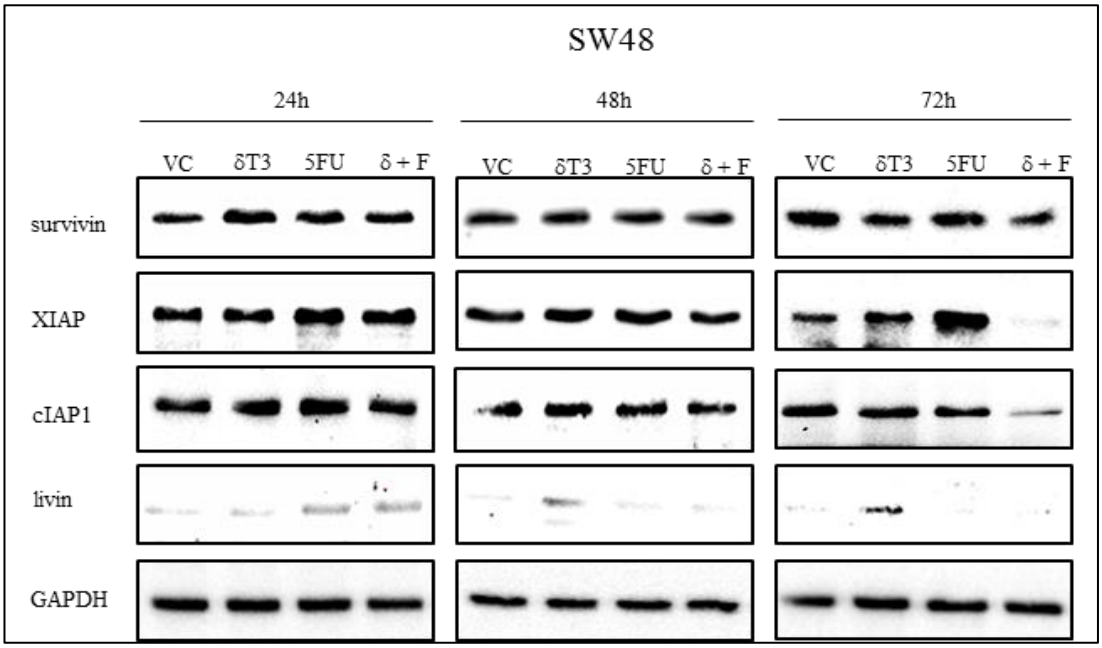

Figure 5.20 Representative Western blotting profiles of IAP proteins for SW48 cells after receiving treatments of δT3, 5FU and their combination at various time points. GAPDH serves as a loading control. δ-tocotrienol, 5-fluorouracil and the combined treatment. 5FU, 5-fluorouracil; δ + F, δ-tocotrienol + 5-fluorouracil.

On the other hand, δT3 + Dox combined treatment showed a lower expression of survivin in Caco-2 cells, as compared to vehicle control after 24 and 48 hours of treatment. As mentioned above, the expressions of XIAP, cIAP1 and livin were found trivial (Figure 5.21).

In SW48 cells, δT3 + Dox combined treatment showed a marked reduction in survivin, XIAP, cIAP1 and livin as compared to vehicle control. Of note, δT3 + Dox combined treatment showed a greater reduction in survivin, XIAP, cIAP1 and livin after 72 hours of treatment, when compared to δT3 and Dox single treatments (Figure 5.22).

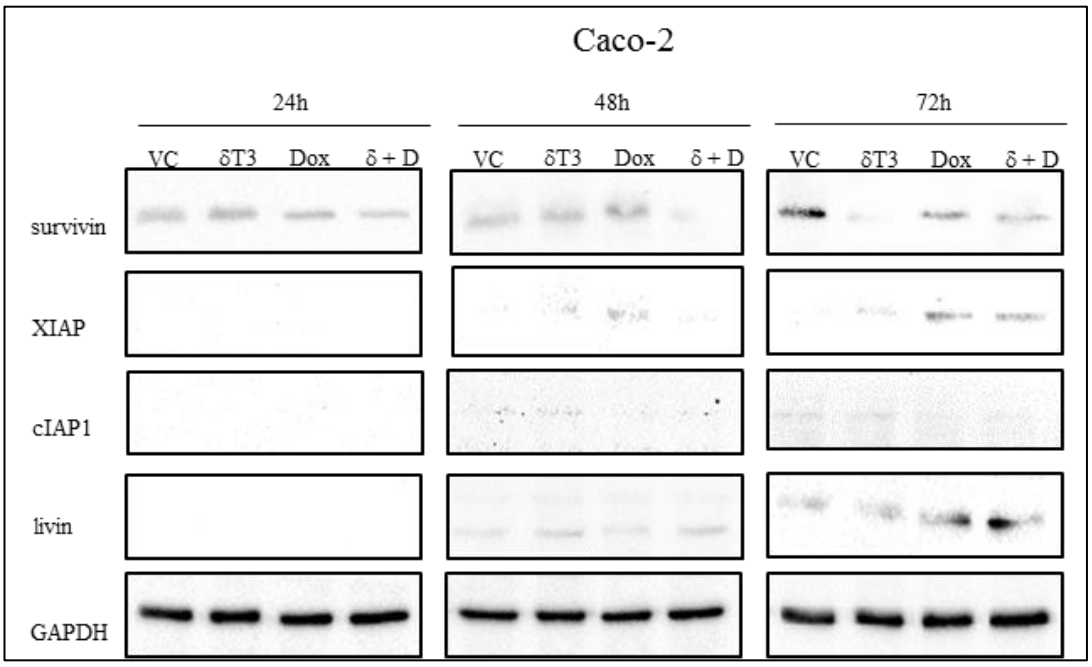

Figure 5.21 Representative Western blotting profiles of IAP proteins for Caco-2 cells after receiving treatments of δT3, Dox and their combination at various time points. GAPDH serves as a loading control. VC, vehicle control; δT3, δ-tocotrienol; Dox, doxorubicin; δ + D, δ-tocotrienol + doxorubicin.

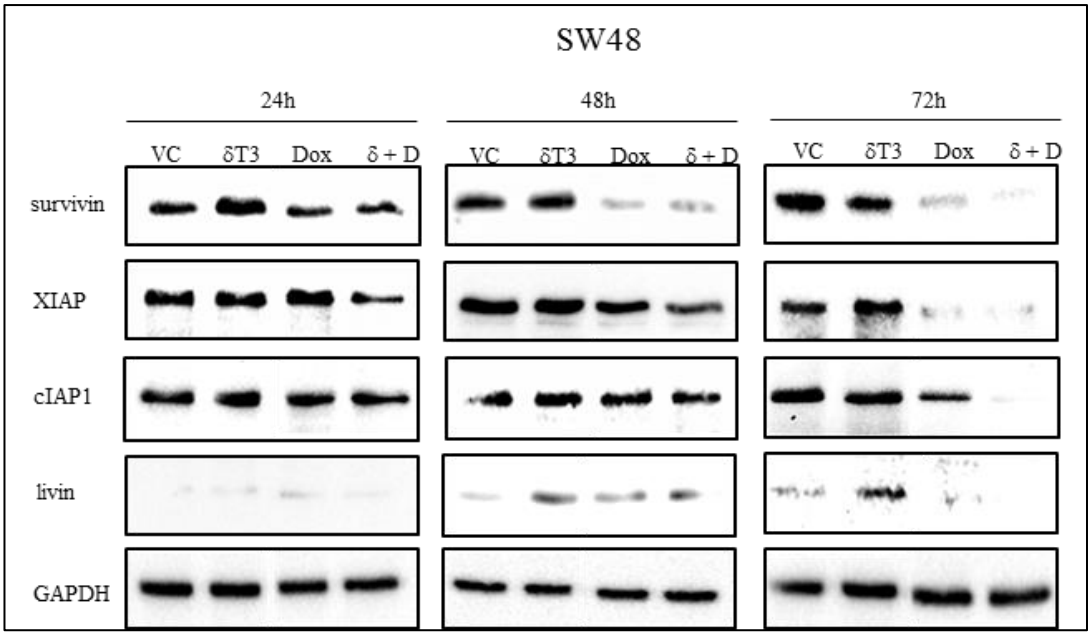

Figure 5.22 Representative Western blotting profiles of IAP proteins for SW48 cells after receiving treatments of δT3, Dox and their combination at various time points. GAPDH serves as a loading control. VC, vehicle control; δT3, δ-tocotrienol; Dox, doxorubicin; δ + D, δ-tocotrienol + doxorubicin.

5.3.3 Effects of single and combined treatments on caspase-8 and caspase-3 activations

After 24 hours of treatment, it was evident that caspase-8 of Caco-2 cells was significantly activated in δT3 + 5FU combined treatment ($p < 0.05$), but not in the respective individual single treatments. Despite an increase in caspase-8 was observed in both Dox single treatment and δT3 + Dox combined treatment, the increment was not statistically significant (Figure 5.23 A). In SW48, all the treatment groups did not result in caspase-8 activation after 24-hour treatments (Figure 5.23 B).

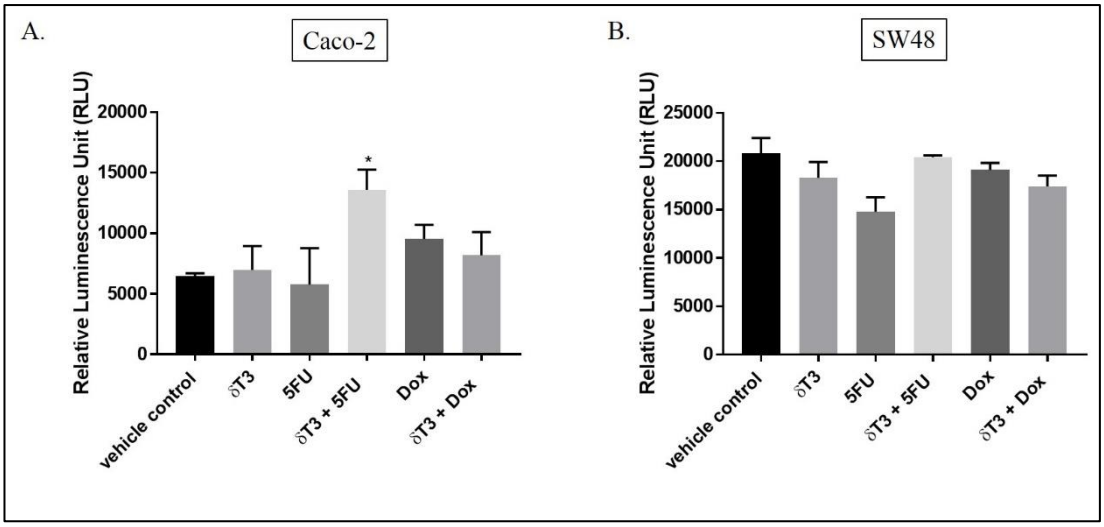

Figure 5.23 Caspase-8 activation profiles in Caco-2 and SW48 cells after 24 hours of single and combined treatments. VC, vehicle control; δT3, δ-tocotrienol; 5FU, 5-fluorouracil; δ + F, δ-tocotrienol + 5-fluorouracil; Dox, doxorubicin; δ + D, δ-tocotrienol + doxorubicin. * $p < 0.05$.

The Western blotting profiles of Caco-2 cells further revealed that caspase-8 was cleaved in all treatment groups, of which more pronounced in δT3 + 5FU combined treatment after 72 hours (Figure 5.24). Correspondingly, the caspase-3 was cleaved, signifying an activation of caspase-3 (Figure 5.24). In SW48 cells, δT3 + 5FU combined treatment demonstrated caspase-8 cleavage after 48-hour treatments. A more prominent caspase-8 cleavage was noticed in δT3 + 5FU combined treatment after 72 hours. Concurrently, caspase-3 was also cleaved (Figure 5.25).

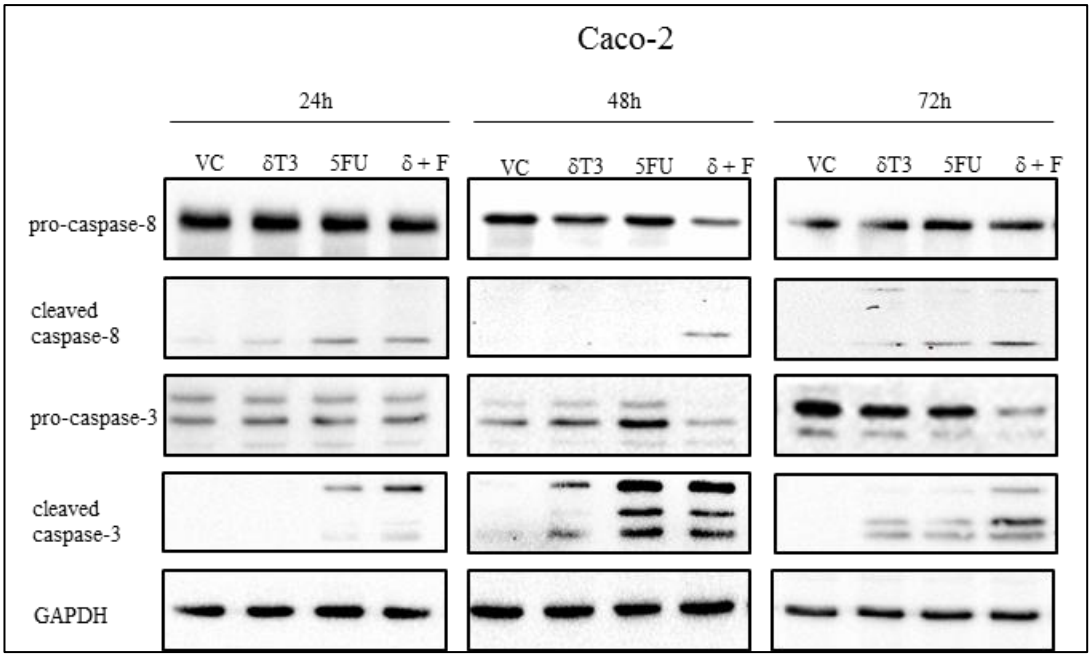

Figure 5.24 Representative Western blotting profiles of caspase-8 and caspase-3 for Caco-2 cells after receiving treatments of δT3, 5FU and their combination at various time points. VC, vehicle control; δT3, δ-tocotrienol; 5FU, 5-fluorouracil; δ + F, δ-tocotrienol + 5-fluorouracil.

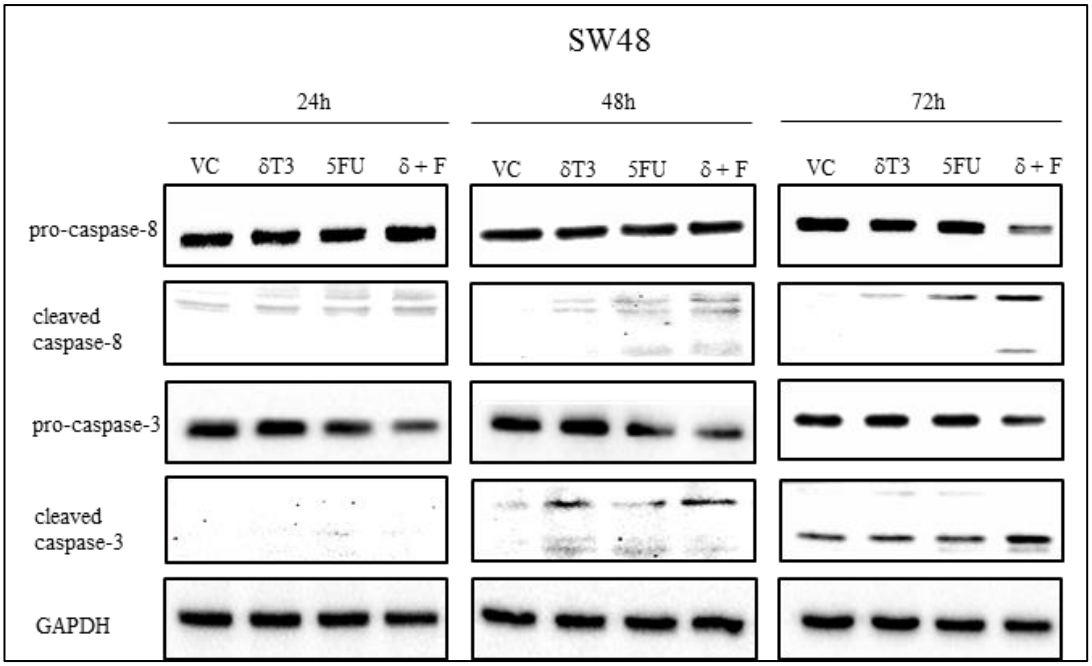

Figure 5.25 Representative Western blotting profiles of caspase-8 and caspase-3 for SW48 cells after receiving treatments of δT3, 5FU and their combination at various time points. VC, vehicle control; δT3, δ-tocotrienol; 5FU, 5-fluorouracil; δ + F, δ-tocotrienol + 5-fluorouracil.

In Caco-2 cells, δT3 + Dox combined treatment caused caspase-8 cleavage, with an increase in caspase-3 cleavage after 48-hour treatment (Figure 5.26),

demonstrating a correlation between the two caspases. In SW48 cells, δT3 + Dox combined treatment resulted in caspase-8 and caspase-3 cleavages after 48- and 72-hour treatments (Figure 5.27).

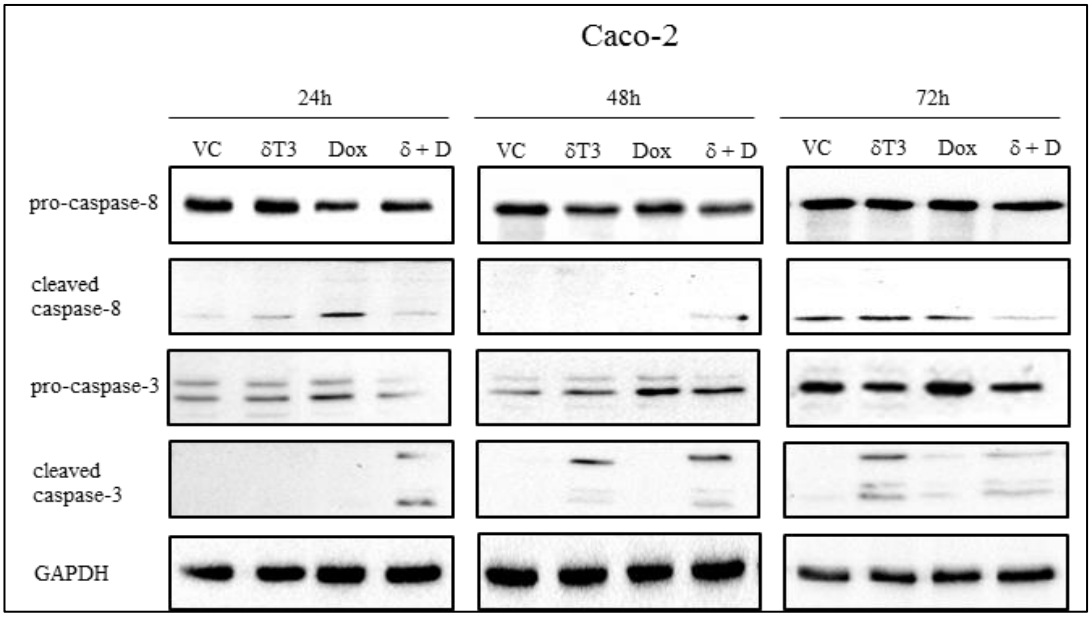

Figure 5.26 Representative Western blotting profiles of caspase-8 and caspase-3 for Caco-2 cells after receiving treatments of δT3, Dox and their combination at various time points. VC, vehicle control; δT3, δ-tocotrienol; Dox, doxorubicin; δ + D, δ-tocotrienol + doxorubicin.

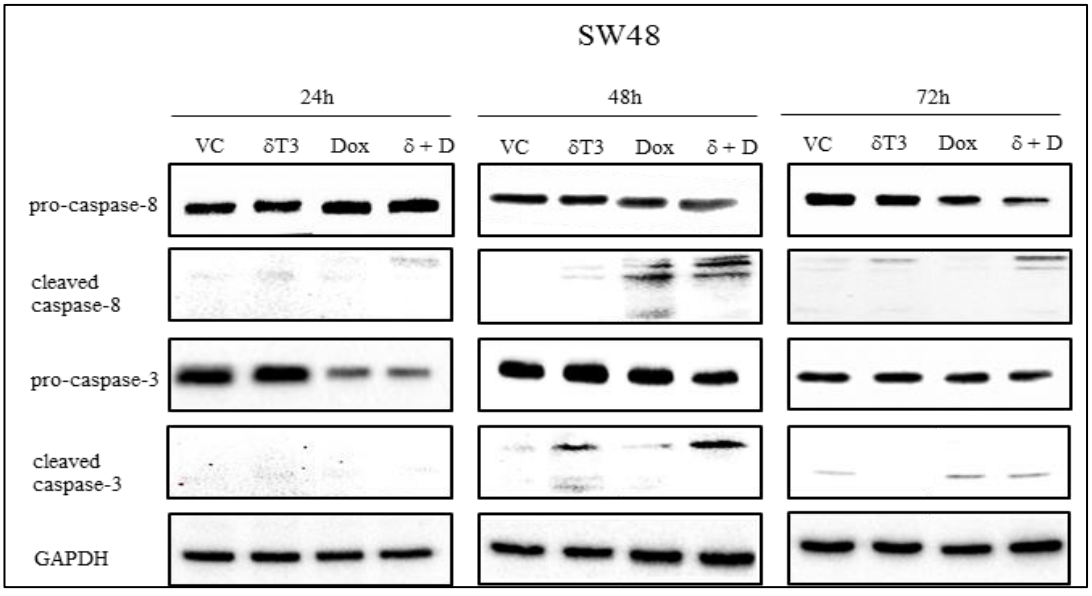

Figure 5.27 Representative Western blotting profiles of caspase-8 and caspase-3 for SW48 cells after receiving treatments of δT3, Dox and their combination at various time points. VC, vehicle control; δT3, δ-tocotrienol; Dox, doxorubicin; δ + D, δ-tocotrienol + doxorubicin.

5.3.4 Cell viabilities of single and combined treatments in reacting with caspases inhibitions

5.3.4.1 Evaluation on cell viability upon caspase-8 inhibition

Caspase-8 inhibitor was used at 10μM, which was guided by some previous studies (Bodur et al., 2013; Wu et al., 2016). Inhibition of caspases-8 activation showed no cell viability improvement on Caco-2 (Figure 5.28) and a slight improvement on cell viability of SW48 (Figure 5.29) cells at all time points attempted in this study. However, the improvements were not statistically significant, demonstrating that inhibition of caspase-8 activation could not completely block the cell death.

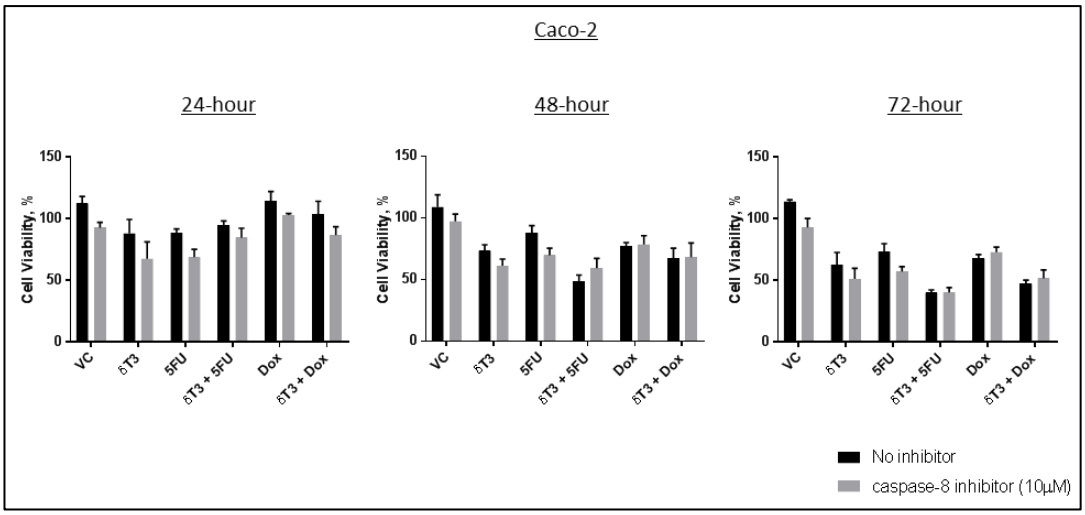

Figure 5.28 Cell viability of Caco-2 cells treated with or without 10μM of caspase-8 (Z-IETD-FMK) inhibitor at various time points. VC, vehicle control; δT3, δ-tocotrienol; 5FU, 5-fluorouracil; δT3 + 5FU, δ-tocotrienol + 5-fluorouracil; Dox, doxorubicin; δT3 + Dox, δ-tocotrienol + doxorubicin.

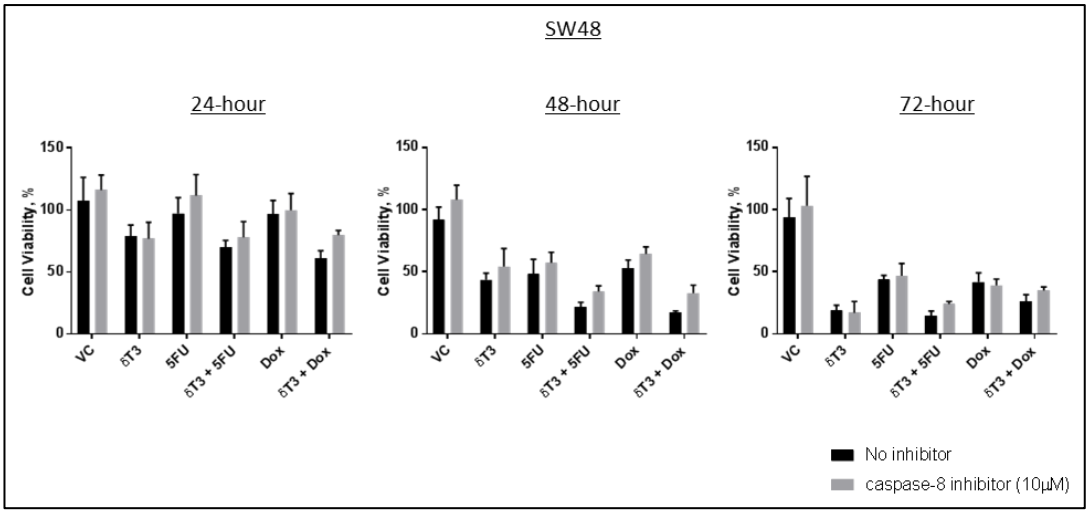

Figure 5.29 Cell viability of SW48 cells treated with or without 10μM of caspase-8 (Z-IETD-FMK) inhibitor at various time points. VC, vehicle control; δT3, δ-tocotrienol; 5FU, 5-fluorouracil; δT3 + 5FU, δ-tocotrienol + 5-fluorouracil; Dox, doxorubicin; δT3 + Dox, δ-tocotrienol + doxorubicin.

5.3.4.2 Evaluation on cell viability upon caspase-3 inhibition

In Caco-2, there was a slight improvement in cell viability for δT3 + Dox and δT3 + 5FU combined treatments via inhibition of caspase-3 activation after 24-hour and 72-hour treatments respectively. However, the improvement was not statistically significant (Figure 5.30).

In SW48 cells, inhibition of caspase-3 activation exhibited a significant increase in cell viability only in δT3 + 5FU combined treatment ($p < 0.05$), indicating that cell death was blocked through caspase-3 inhibition (Figure 5.31). There was a slight improvement in cell viability treated with δT3 + Dox combined treatment for 24 hours although not statistically significant.

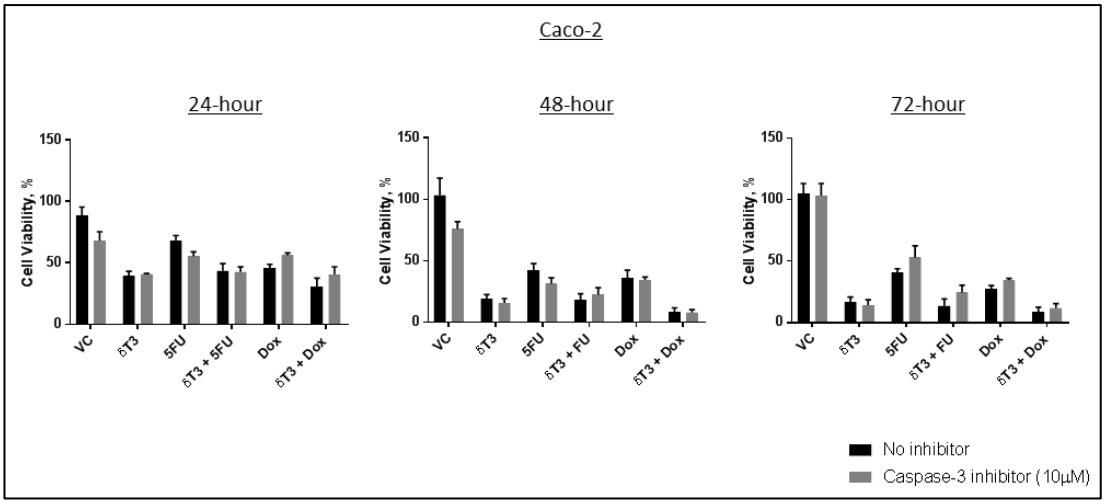

Figure 5.30 Cell viability of Caco-2 cells treated with or without 10μM of caspase-3 (Z-DEVD-FMK) inhibitor at various time points. VC, vehicle control; δT3, δ-tocotrienol; 5FU, 5-fluorouracil; δT3 + 5FU, δ-tocotrienol + 5-fluorouracil; Dox, doxorubicin; δT3 + Dox, δ-tocotrienol + doxorubicin.

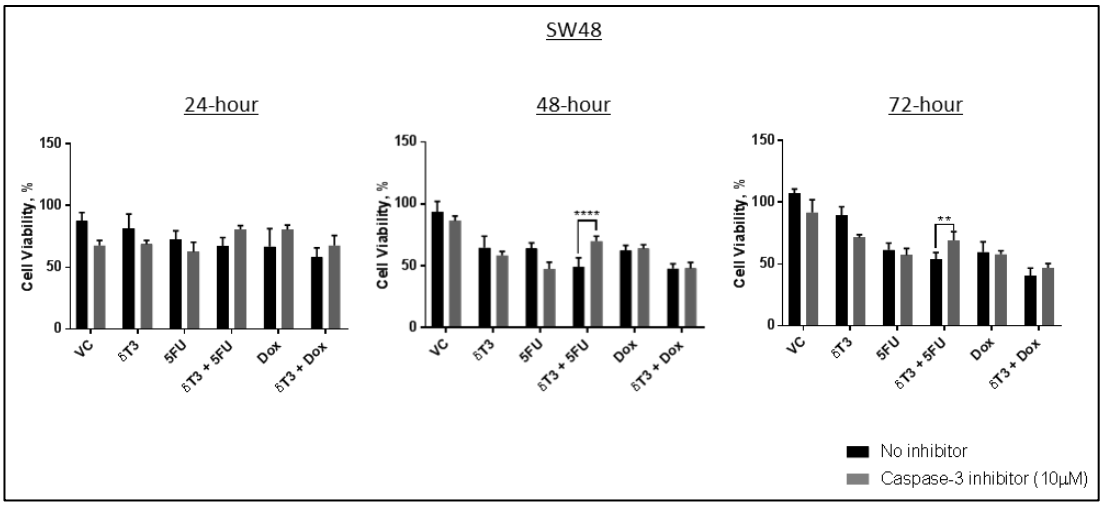

Figure 5.31 Cell viability of SW48 cells treated with or without 10μM of caspase-3 (Z-DEVD-FMK) inhibitor at various time points. VC, vehicle control; δT3, δ-tocotrienol; 5FU, 5-fluorouracil; δT3 + 5FU, δ-tocotrienol + 5-fluorouracil; Dox, doxorubicin; δT3 + Dox, δ-tocotrienol + doxorubicin. ** $p < 0.01$; **** $p < 0.0001$.

5.3.4.3 Evaluation on cell viability upon pan-caspase inhibition

Consistent with the findings from caspase-3 inhibition, pan-caspase inhibitor caused a slight improvement of cell viability in δT3 + 5FU and δT3 + Dox combined treatments after 48- and 72-hour treatments on Caco-2 cells, however it was not statistically significant (Figure 5.32). Of note, a significant improvement in cell viability was observed in SW48 cells subjected to δT3 + 5FU combined treatment (p

< 0.05) and a slight increase in cell viability of δT3 + Dox combined treatment, which is consistent with caspase-3 inhibition study (Figure 5.33).

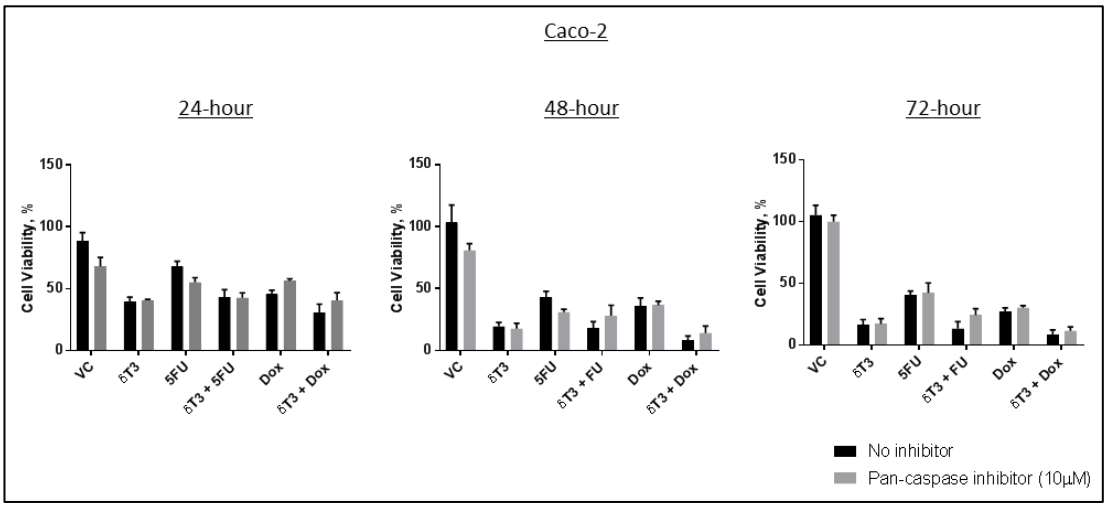

Figure 5.32 Cell viability of Caco-2 cells treated with or without 10μM of pan-specific caspase (Z-VAD-FMK) inhibitor at various time points. VC, vehicle control; δT3, δ-tocotrienol; 5FU, 5-fluorouracil; δ + F, δ-tocotrienol + 5-fluorouracil; Dox, doxorubicin; δ + D, δ-tocotrienol + doxorubicin.

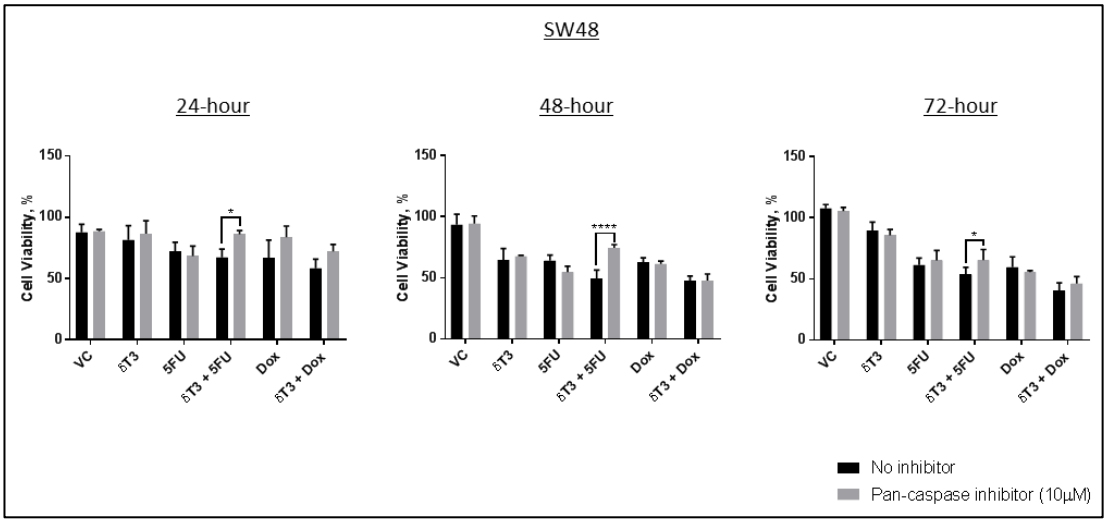

Figure 5.33 Cell viability of SW48 cells treated with or without 10μM of pan-specific caspase (Z-VAD-FMK) inhibitor at various time points. VC, vehicle control; δT3, δ-tocotrienol; 5FU, 5-fluorouracil; δ + F, δ-tocotrienol + 5-fluorouracil; Dox, doxorubicin; δ + D, δ-tocotrienol + doxorubicin. * $p < 0.01$; **** $p < 0.0001$.

5.3.4.4 Evaluation on cell viability upon mitochondrial permeability transition inhibition

Application of cyclosporine A did not affect viability of Caco-2 and SW48 cells as seen in vehicle control group, signifies that 1μM of cyclosporine A is well

tolerated by the cells. The cell viabilities of Caco-2 (Figure 5.34 A) and SW48 (Figure 5.34 B) were significantly ($p < 0.0001$) improved in all the treatment groups by cyclosporine A application, demonstrating a successful abrogated cell death.

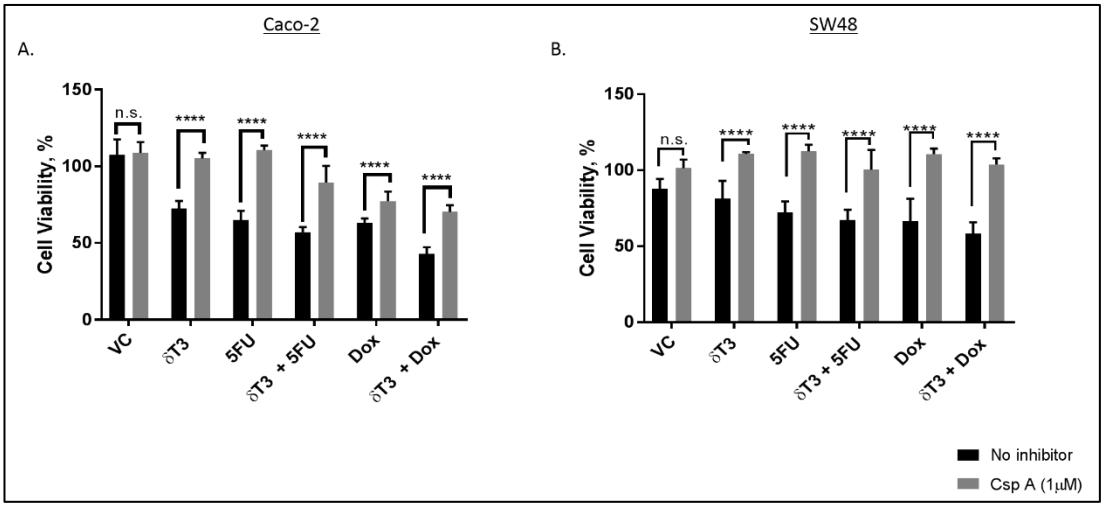

Figure 5.34 Cell viability profiles of Caco-2 and SW48 cells treated with or without 1μM of cyclosporine A. VC, vehicle control; δT3, δ-tocotrienol; 5FU, 5-fluorouracil; δ + F, δ-tocotrienol + 5-fluorouracil; Dox, doxorubicin; δ + D, δ-tocotrienol + doxorubicin. n.s., non-significant; **** $p < 0.0001$.

5.3.5 Summarised effects of combined treatments on mitochondria-mediated apoptosis pathway and caspases activations

The findings gathered from Section 5.3.1 until 5.3.4.4 demonstrated differential actions and responses of δT3 + 5FU and δT3 + Dox combined treatments on Caco-2 and SW48 cells. For a better clarity, the findings of combined treatments were summarised (Table 5.3).

Table 5.3 A summary of findings in Chapter Five.

	δT3 + 5FU		δT3 + Dox	
	Caco-2	SW48	Caco-2	SW48
Loss of ΔΨm	Yes	Yes	Yes	Yes
Cytochrome *c*	↑	↑	↑	↑
Bcl-2	↓	↓	-	↓
Bax	↑	ND	↑	ND
IAP	↓	↓	↓	↓
Caspase 9 activation	↑	No	↑	No
Caspase-3 activation	↑	↑	↑	↑
Caspase-8 activation	↑	↑	↑	↑
Inhibition of cell death (by Caspase-8 inhibitor)	No	Yes	No	No
Inhibition of cell death (by Caspase-3 inhibitor)	No	Yes	No	No
Inhibition of cell death (by pan-caspase inhibitor)	No	Yes	No	No
Inhibition of cell death (by cyclosporine A)	Yes	Yes	Yes	Yes

Note: ↑, upregulation; ↓, downregulation; ND, not detected

5.4 Discussion

Resistance to cell death is considered a hallmark of cancer (Hanahan and Weinberg, 2011) which also represents a major hurdle for an effective cancer treatment. Hence, an understanding of cell death mechanism/pathway mediated by the novel anti-cancer treatments may pave a better understanding of their therapeutic actions. Following the previous identification of enhanced apoptosis induced by δT3 + 5FU and δT3 + Dox combined treatments, current chapter therefore attempted to delineate the underlying apoptotic mechanisms towards an effective therapeutic approach in colorectal cancer.

The apoptotic signalling is tightly orchestrated by a delicate equilibrium between pro-apoptotic and anti-apoptotic proteins. Pro-apoptotic proteins promote apoptosis, while anti-apoptotic proteins inhibit apoptosis; together, these factors determine whether the cell death signalling can activate the apoptotic program (Wei et al., 2008). With respect to that, the apoptosis antibody array platform, which can concurrently detect pro-apoptotic and anti-apoptotic proteins was taken as a preliminary screening approach to study the underlying apoptotic response of δT3 and 5FU in Caco-2 cells, by which δT3 + 5FU combined treatment was previously detected as the most potent synergistic combination in Chapter Three.

The results from apoptosis antibody array demonstrated a consistent downregulation of anti-apoptotic proteins from various proteins family, including Bcl-2, IAP, HSP and IGF families. Particularly, Bcl-2, Bcl-w, cIAP2, survivin, livin, XIAP, HSP70, and IGF-1 were downregulated in response to δT3 + 5FU combined treatment (Figures 5.2 – 5.5). In fact, these anti-apoptotic proteins play distinct roles in apoptosis, which could provide a grounding for speculations in the apoptotic mechanism involved.

Both Bcl-2 and Bcl-w belong to anti-apoptotic proteins of Bcl-2 family which plays a determining role in regulating MOMP. Specifically, Bcl-2 anti-apoptotic protein inhibits Bax/Bak (pro-apoptotic) proteins activation, impeding their oligomerisation to trigger MOMP. Although the role of Bcl-w as an anti-apoptotic mechanism was scarcely reported, a study had suggested that Bcl-w enables mitochondrial membrane insertion to exert its pro-survival role (Kaufmann et al., 2004). Hence, downregulations of Bcl-2 and Bcl-w triggered by δT3 + 5FU combined treatment may serve as an indication that mitochondria is the target.

On the other hand, IAP proteins are endogenous caspase inhibitors. It was demonstrated that IAP proteins such as XIAP, cIAP1, cIAP2 and survivin can inhibit caspase-3, -7 and -9 activities (Deveraux et al., 1997; Roy et al., 1997). The conserved baculoviral IAP repeat (BIR) domain that is involved in protein-protein interactions may directly interact with caspases, rendering IAPs' ability in inhibiting caspases activation (Scott et al., 2005). In relation to this study, apoptosis array revealed downregulations in IAP proteins in Caco-2 cells such as XIAP, survivin and livin, especially in δT3 + 5FU combined treatment group, which may suggest a lower threshold for caspase activations.

HSPs are expressed to facilitate recovery and maintain cell survival in response to internal and external cellular stresses (Beere, 2004). Notably, the same stress signals that trigger apoptosis also stimulate the expression and release of HSPs, which act as repressors of apoptosis via inhibition of pro-apoptotic proteins (e.g., Bid, Bax, p53, Akt and etc.) (Ikwegbue et al., 2017). It was reported that HSP27 interacts with cytochrome *c* to prevent apoptosome formation and caspase-9 activation (Garrido et al., 1999). In addition, several lines of evidence suggested that HSP70 could suppress apoptosis by inhibiting caspase activation, probably in the downstream or upstream of

mitochondrial cytochrome *c* release (Beere et al., 2000; Ikwegbue et al., 2017; Mosser et al., 2000). A downregulated expression of HSP70 in Caco-2 cells receiving δT3 + 5FU combined treatment therefore proposing a connection between the HSPs and mitochondria-mediated apoptosis.

IGF-1 was reported to confer cytoprotective effect associated with mitochondrial protection, via a reduction of free radical generation, oxidative damage and apoptosis as well as increase in ATP production (Puche et al., 2008). Hence, the downregulation of IGF-1 in Caco-2 cells receiving δT3 + 5FU combined treatment may lead to a loss of mitochondrial protection, thereby increasing the cellular susceptibility towards mitochondria-mediated apoptosis.

Collectively, the data from apoptosis antibody array have shed a light on two key areas, namely i) mitochondria as a potential target and ii) potential caspases activation induced by δT3 + 5FU combined treatment. Driven by these indications, the mitochondria-mediated pathway of apoptosis was therefore studied in-depth.

In fact, mitochondrial membrane permeabilisation (MMP) constitutes of inner membrane permeabilisation and outer membrane permeabilisation (Kroemer et al., 2007). In fact, loss of ΔΨm is recognised as an inner membrane permeabilisation event associated with mitochondria-mediated apoptosis (Elmore, 2007; Kroemer et al., 2007; Leytin et al., 2018). The JC-1 dye is a lipophilic cationic dye that used as an indicator for determining ΔΨm. The JC-1 molecules accumulate in healthy mitochondria (high ΔΨm) in a concentration-dependent manner to form J-aggregates and exhibit red fluorescence. On the contrary, JC-1 molecules are unable to form J-aggregates in mitochondria of apoptotic cells due to low ΔΨm, thereby remaining in their monomers state and exhibit green fluorescence. As a result, both increase in green fluorescence and decrease in red fluorescence indicate a loss in ΔΨm. Current results clearly

demonstrated that δT3 + 5FU and δT3 + Dox combined treatments caused ΔΨm loss in Caco-2 and SW48 cells, potentially leading to inner membrane permeabilisation. Apparently, this ΔΨm disruption ability may be contributed by δT3 as increased green fluorescence signal was detected at 48 hours, in both SW48 and Caco-2 cells. This observation was in agreement with previous studies, which reported that tocotrienols indeed possess mitochondrial targeting property. Likewise, γT3-treated MDA-MB-231 breast cancer cells showed a collapse in ΔΨm (Takahashi and Loo, 2004). Additionally, the loss of ΔΨm triggered by αT3, βT3, γT3 and δT3 had also been reported in U87MG neuroblastoma and A549 lung adenocarcinoma (Lim et al., 2014a, 2014b).

The loss of ΔΨm induced by the combined treatments infers an occurrence of mitochondrial permeability transition, a state of long-lasting openings of MPTP complex which leads to inner membrane permeabilisation (Fulda et al., 2010). In response to apoptotic stimuli, mitochondrial permeability transition results in an immediate dissipation of ΔΨm and osmotic swelling of mitochondrial matrix (Fulda et al., 2010). Eventually, the mitochondrial permeability transition may also lead to mitochondrial outer membrane permeabilisation (MOMP) as the surface area of inner membrane exceeds the outer membrane (Fulda et al., 2010).

Alternatively, MOMP can be mediated by the pore-forming activity of pro-apoptotic members such as Bax. With regards to studying the involvement of MOMP, the Bax (pro-apoptotic), Bcl-2 (anti-apoptotic), and cytochrome *c* levels were studied in a timely manner to monitor the proteins' kinetic changes. Notably, δT3 + 5FU and δT3 + Dox combined treatments caused an upregulated Bax expression in Caco-2 cells and a downregulated Bcl-2 expression in SW48 cells as early as 24 hours. Concurrently, there was an increase in cytochrome *c* expression in both Caco-2 and

SW48 cells (Figures 5.13 – 5.16). These results had therefore suggested a commencement of MOMP, potentially leading to cytochrome *c* release.

Activation of caspases represents a crucial step in precipitating (caspase-dependent) apoptosis. It was noticeable that the caspase-3 activation was remarkably higher in δT3 + 5FU and δT3 + Dox combined treatments. One potential reason could be due to lower expression of IAPs in Caco-2 and SW48 cells. In SW48, survivin, XIAP and cIAP1 were downregulated. Notably, XIAP has been exemplified as the main member of IAPs family. It has been widely reported that XIAP directly inhibits caspase-3 activation (Paulsen et al., 2008; Riedl et al., 2001). The BIR2 domain of XIAP tightly binds to caspase-3/7 to prevent its full activation, substrate cleavage and cell death (Riedl et al., 2001). Additionally, cIAP1 was found to inhibit caspase-3/7 and suppress apoptosis (Wadegaonkar and Wadegaonkar, 2012). Hence, it is plausible to postulate that downregulations of IAP proteins, especially XIAP and cIAP1, could lead to an enhanced caspase-3 activation in Caco-2 and SW48 cells.

To determine which activation pathways were involved, the activity of upstream initiator caspases were evaluated. An activation of caspase-9 or caspase-8 signifies a potential engagement in mitochondria-mediated or death receptor-mediated apoptosis pathway, respectively. Surprisingly, despite a remarkable increase in caspase-3/7 activation was detected in δT3 + 5FU and δT3 + Dox combined treatments, a slight activation of caspase-9 was detected in Caco-2 while none was detected in SW48 cells. This phenomenon has then directed the attention towards caspase-8 activation.

To study the involvement of extrinsic pathway, caspase-8 activation via proteolytic cleavage was assessed. Upon activation, caspase-8 undergoes cleavage at Asp391, resulting in p18 (active large subunit) and p43/41 (processed precursor) (Hou

et al., 2010). Current study detected cleavages of caspase-8 in Caco-2 (from 24 hours onwards) and SW48 (from 48 hours onwards) cells, demonstrating a successful activation of caspase-8. Concurrently, cleavage of caspase-3 (resulted in p17 and p19) was also detected (Figure 5.24 – 5.27), showing a good collaboration to caspase-8 activation. These results therefore suggest a potential activation of extrinsic pathway, in which activation of caspase-8 leads to the downstream activation of caspase-3.

In an attempt to identify the reliance of caspases in precipitating apoptosis, caspase inhibitors were employed to inhibit apoptosis. The supplementary of pan-caspase or caspase-3 inhibitor in Caco-2 and SW48 resulted in two distinctive responses. In SW48, the caspase-3 and pan-caspase inhibitor successfully improved cell viability upon δT3 + 5FU combined treatment, indicating a dependency on caspase-dependent cell death. However, the caspase-8 inhibitor was unable to inhibit cell death induced by the combined treatments although caspase-8 was activated. This therefore infers that the cell death was not mediated solely through caspase-8 activation.

Conversely, incompetent halt of the cell death by caspase-3 and pan-caspase inhibitors also suggests a potential participation of caspase-independent cell death (CICD). CICD normally occurs in response to most intrinsic apoptotic cues in the presence of MOMP but is unable to trigger caspase activation (Tait and Green, 2008). Following MOMP and in the absence of caspase activity, mitochondrial intermembrane space proteins such as EndoG, cytochrome *c*, AIF, Smac/Diablo and Htr2A/Omi are released, triggering loss of mitochondrial function eventually and/or actively contributing to cell death (Tait and Green, 2008). In this study, failure to significantly activate caspase-9 in the presence of MOMP further support the presence of CICD.

To verify the dependence of cell death on mitochondrial permeability transition, cyclosporine A was employed. It is a hydrophobic undecapeptide that inhibits MPTP opening via interacting with cyclophilin D, a crucial component of MPTP formation (Kim et al. 2017; Liu et al. 2008). Hence, it was widely employed to block mitochondrial permeability transition. Notably, cyclosporine A successfully blocked the cell death in all treatments in Caco-2 and SW48 cells, clearly demonstrating a determining role of mitochondria in triggering cell death. From the result, mitochondria could be the primary target for stress signal inception, potentially promoting CCID, which is independent of caspase activities.

The differential cell death pathways engaged by Caco-2 and SW48 when subjected to δT3 + 5FU combined treatment could be a cell-line specific or p53-dependent effect. The SW48 cell line expresses a wild-type p53 tumour suppressor protein, whereas Caco-2 cell line consists of a mutant p53 (see Appendix: Figure A5.1). In this study, it was identified that δT3 + 5FU combined treatment and the individual 5FU and Dox single treatments induced an enhanced p53 expression in SW48 cell line. On the contrary, p53 expression in Caco-2 cells was absent even at the basal level, which is in agreement with a previous report (Thant et al., 2008). This dichotomy in Caco-2 and SW48 cells may drive the differential cell death responses, particularly dependence on caspases for apoptosis.

5.5 Conclusions

In conclusion, current study demonstrated that δT3 + 5FU and δT3 + Dox combined treatments induced prominent decrease in IAP proteins and increase in caspase-3 activation, suggesting a lower apoptotic threshold, which may impart a chemosensitisation effect. The extrinsic pathway was potentially activated as evidenced by an enhanced cleaved caspase-8 level. However, blocking of caspase-8

and caspase-3 was unable to prevent cell death in both cells (except δT3 + 5FU combined treatment in SW48), suggesting a potential involvement of additional cell death pathway(s). Both the combined treatments were found to exert cytotoxic effect via mitochondria, which potentially involved permeabilisation of both inner and outer mitochondrial membranes. In addition, the combined treatments induced mitochondrial-dependent cell death without a prominent increase in caspase-9 activation in Caco-2 and SW48 cells has therefore suggested a manifestation of CCID. In brief, these data suggest that concurrent activations of caspase-dependent and caspase-independent cell death have been induced by the combined treatments in Caco-2 and SW48 cells.

Chapter Six: An involvement of autophagy as a cell death mechanism induced by individual single and combined treatments of δ-tocotrienol and/or chemotherapeutic drugs (5-fluorouracil and doxorubicin)

6.1 Introduction

In Chapter Four, morphological observations demonstrated that Caco-2 and SW48 colorectal cancer cells exhibited cytoplasmic vacuolisation upon treatments, which is not a typical feature for apoptosis. A subsequent investigation in Chapter Five learnt that the cell death induced by the combined treatments could not be inhibited by caspase inhibitors. Together, these observations have suggested two possibilities, which are i) induction of caspase-independent cell death and/or ii) presence of an additional cell death modality other than apoptosis. Guided by these clues in previous chapters, special attention was given to autophagy, which is another form of programmed cell death characterised by the presence of autophagic vacuoles in the cytoplasm.

Generally, there are two prominent features of autophagy, namely i) formation of double-membrane-bound organelle known as autophagosome and ii) engagement of a lysosome-dependent pathway for the degradation of damaged cytoplasmic organelles and protein aggregates. During autophagy, the damaged cellular organelles in the cytoplasmic compartments are sequestered into the double-membrane vesicles known as autophagosomes that later fuse with the lysosome to form autophagolysosomes. There are several subtypes of autophagy; current chapter focuses on macroautophagy (hereafter known as autophagy), which is characterized by the engulfment and degradation of cytoplasmic materials in bulk in a selective/nonselective manner.

To date, autophagy has been found to exhibit dual effects in cancer for suppressing tumourigenesis as well as promoting survival of cancer cells under an adverse condition (Maheswari and Sadras, 2018). Equivocal evidences have demonstrated that autophagy is involved as an adaptive response to mitigate cellular stress as well as acts as a stress sensor to engage autophagic cell death pathway (Codogno and Meijer, 2005; Shen and Codogno, 2011). Hence, it is imperative to study and understand the role of autophagy induced by the single and combined treatments in this study. With the motivation, current chapter describes the autophagy induction predominantly at the morphological, molecular and functional aspects of autophagy on Caco-2 and SW48 cells.

Firstly, the presence of autophagy was assessed morphologically by using acridine orange (AO) and quantitatively using monodansylcadaverine (MDC) staining methods. AO is a cell-permeable lysotropic dye that accumulates in acidic vesicular organelles (AVOs), such as autophagolysosomes. On the other hand, MDC is another popular autofluorescent marker that preferentially accumulates in autophagic vacuoles due to ion-trapping mechanism and its special interaction with vacuolar membrane lipids (Pattingre et al., 2004). Hence, both staining methods were employed to cross-validate the presence of autophagosomes.

Secondly, the autophagy markers such as beclin-1 and microtubule-associated protein 1A/1B light chain 3 (LC3) were assessed by Western blotting. Beclin-1 involves the early stage of autophagy for phagophore nucleation (Glick et al., 2010), while LC3 is a marker for autophagosome formation (at mid-late phase). Immunoblotting for endogenous LC3 represents one of the widely used assays to monitor autophagosome synthesis or degradation (Mizushima and Yoshimori, 2007).

In this study, the protein expression levels of beclin-1 and LC3-II were studied to assess for the autophagy induction.

Thirdly, Akt and its activating enzyme, phosphoinositide-dependent kinase-1 (PDK1) were also studied. Autophagy is regulated by PI3K signalling pathway, in which the activation of class I PI3K leads to recruitment and activation of Akt. Eventually, the activated Akt modulates mammalian target of rapamycin (mTOR) that inhibits autophagy. Meanwhile, Akt is a central pathway known to promote cellular growth, proliferation and survival (Manning and Cantley, 2007). Studying Akt and PDK1 proteins could therefore provide a better understanding of the nature of autophagy: pro-survival versus pro-death.

Lastly, pharmacological inhibition of autophagy was performed aiming to delineate the role of autophagy in Caco-2 and SW48 cells upon receiving the single and combined treatments. The two pharmacological inhibitors, namely 3-methyladenine (3-MA) and bafilomycin A1 (Baf-1) were involved in autophagy inhibition. The 3-MA is a PI3K inhibitor that acts on early phase by blocking autophagosomes formation. Meanwhile, Baf-1 acts on late phase by inhibiting the fusion between autophagosomes and lysosomes via blocking the vacuolar H^+ ATPase. Thus, both inhibitors were employed to investigate the dependence on autophagy for cell death.

All together, current chapter aimed to study the autophagic responses induced by single (δT3, 5FU, Dox) and (δT3 + 5FU and δT3 + Dox) combined treatments on Caco-2 and SW48 colorectal cancer cells. The specific objectives were:

i. To evaluate the cellular characteristics of autophagy in Caco-2 and SW48 cells induced by the single and combined treatments via AO and MDC staining methods.

ii. To access the changes of autophagy markers, namely LC3-II, beclin-1, Akt and PDK1 upon receiving the single and combined treatments.

iii. To determine the role of induced autophagy on cell death via pharmacological inhibition.

6.2 Materials and Methods

The experimental design of current chapter is illustrated in Figure 6.1. AO staining was initially performed to detect the presence of autophagy. MDC staining was conducted to quantify the intensity of autophagy induced by the single and combined treatments. Western immunodetection was conducted to assess the expression of autophagy-related proteins LC3-II, beclin-1, Akt and PDK1. Lastly, autophagy was suppressed by 3-MA and Baf-1, the autophagic pharmacological inhibitors in order to validate the potential involvement of autophagy in mediating a putative cell death.

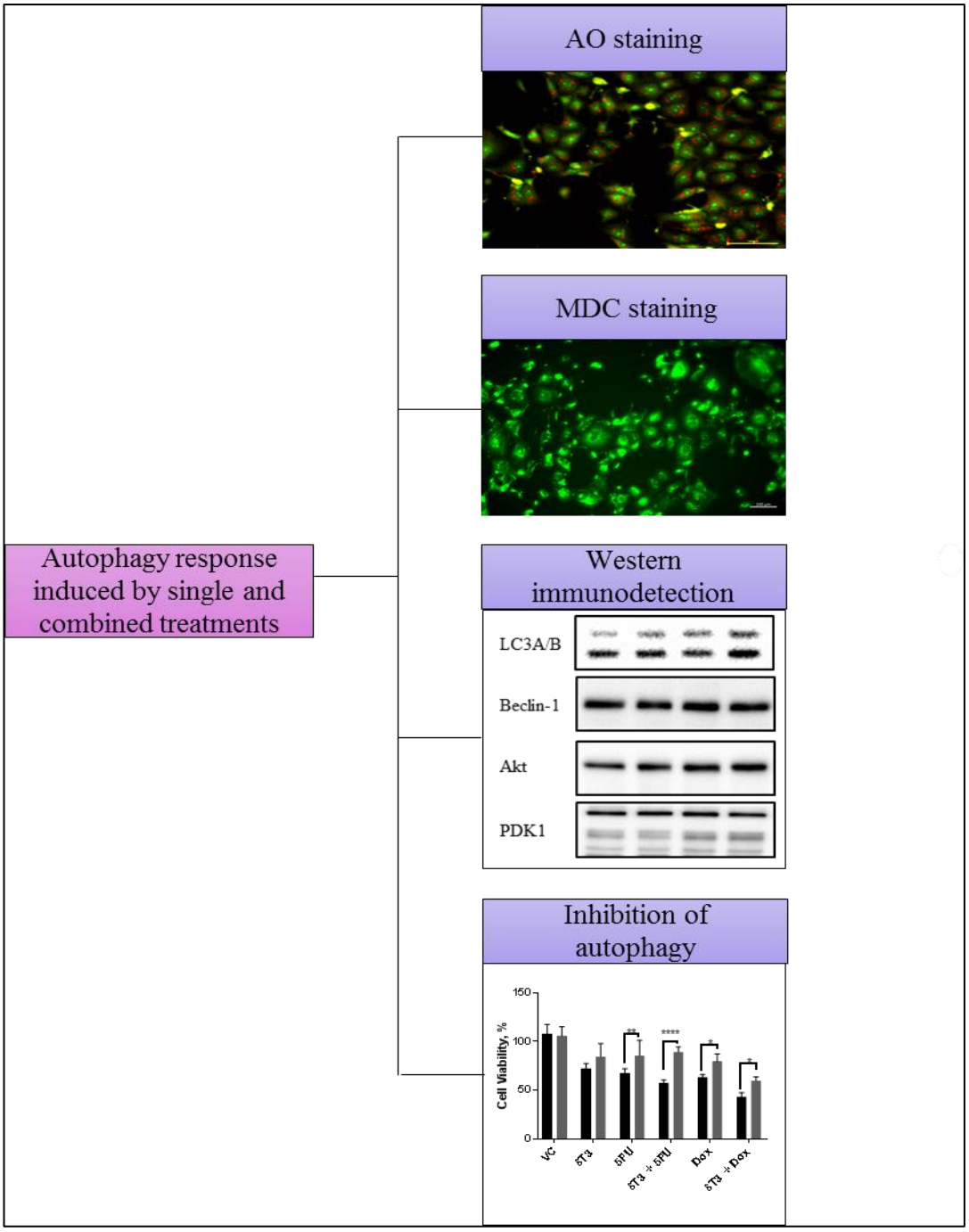

Figure 6.1 An overview of experiments involved in Chapter Six for investigating the autophagy response induced by single and combined treatments.

6.2.1 Acridine orange (AO) staining for autophagy detection

AO is an acidotrophic dye that can be protonated and sequestered in AVOs. It undergoes a metachromatic shift to red fluorescence in a pH-dependent manner. At neutral pH, AO exhibits green fluorescence in cellular compartments such as nucleus and cytoplasm. In contrast, protonated AO aggregates and fluoresces red within AVOs

such as autophagolysosomes. The differential fluorescence makes AO staining a quick, accessible and reliable method to assess AVOs, which increases upon autophagy induction (Thomé et al., 2016).

Caco-2 (1.5 X 10^5) and SW48 (3 X 10^5) cells were seeded in 6-well plates and incubated overnight to allow cell attachment. Following that, the media were replaced with the treatment media containing individual concentrations of δ-tocotrienol (δT3), 5-fluorouracil (5FU), doxorubicin (Dox) and the combinations as previously mentioned (see Table 3.5). AO solution (2μg/ml) was added to each well and incubated for 15 minutes. The cells were viewed under Axio Observer 7 (Zeiss, Germany) fluorescence microscopy. The images were captured at 20x magnifications. The experiment was repeated at least three times.

6.2.2 Monodansylcadaverine (MDC) staining for autophagy detection and quantification

MDC is an autofluorescent compound that can be used as a probe to detect autophagic vacuoles in cultured cells (Munafó and Colombo, 2001). Hence, the intensity of MDC is correlated to the number of autophagolysomes within the cells.

Caco-2 and SW48 cells were seeded and treated in 6-well plates similar to AO staining (Section 6.2.1). Vehicle control consisting of 0.1% of DMSO was included as a negative control to check for the basal degree of autophagy. Fifty micromolars of MDC solution were added into each well and incubated for 10 minutes. The cells were viewed under Axio Observer 7 (Zeiss, Germany) fluorescence microscopy and quantified using Zeiss Zen microscope software. Statistical analyses were performed to identify the intensity difference of treated samples (induced autophagy) over vehicle control (basal autophagy).

6.2.3 Western blotting for autophagy markers detection

Western blotting was performed similar as previously mentioned in Chapter Five (see Section 5.2.4). Following cell seeding and treatments (see Table 3.5), the protein lysates were harvested and subjected to protein quantification, SDS-PAGE and immunoblotting. The primary antibodies used in current chapter are depicted in Table 6.1.

Table 6.1 List of involving antibodies for Western blotting in Chapter Six.

Primary antibody	Molecular weight (kDa)	Dilution	Manufacturer	Host species of primary antibody
Beclin-1	52	1:1,000	Cell Signaling Technology, USA.	Rabbit
LC3-I/II	14, 16	1:1,000	Cell Signaling Technology, USA.	Rabbit
Akt	60	1:1,000	Cell Signaling Technology, USA.	Rabbit
PDK1	58-68	1:1,000	Cell Signaling Technology, USA.	Rabbit
GAPDH	37	1:2,500	Santa Cruz Biotechnology, USA	Mouse

6.2.4 Cell viability and pharmacological inhibition of autophagy

A cell number of 2,000 cells (Caco-2 and SW48) were seeded into each well of 384-well plates and incubated overnight for cell attachment. Thereafter, the media were removed and replenished with fresh media containing 2.5mM of 3-methyladenine (3-MA) and 10nM of bafilomycin A1 (Baf-1) (Tocris Bioscience, UK). The inhibitors were incubated for 4 hours prior to drug treatment. Next, five microliters of treatment solution was added to the respective wells (see Chapter Three, Table 3.5). Cell viability was assessed after 24 hours of treatment using CellTitre-Glo® Luminescent Cell Viability Assay (Promega, USA) as previously described in Section 3.2.5. The cell viability was obtained by normalizing the luminescence signal

of treated samples with the average luminescence signal of untreated (vehicle) control and multiplying with 100%.

6.2.5 Statistical analyses

The average of fluorescence intensity (Section 6.2.2) and cell viability (Section 6.2.4) of various treatment groups from three independent experiments (n=3) were subjected to one-way ANOVA with Dunnett's multiple comparison test using GraphPad Prism 7 software. The differences were marked as significant when $p < 0.0001$ (****), $p < 0.001$ (***), $p < 0.01$ (**), $p < 0.05$ (*).

6.3 Results

6.3.1 Assessments of autophagy by microscopy

6.3.1.1 AO staining profiles

The process of autophagy begins with the autophagosome formation and progresses to autophagolysosomes through the fusion of acidic lysosomes with autophagosomes (Hippert et al., 2006). Under a fluorescence microscope, AO is protonated and emits bright red fluorescence within these acidic vesicles, which the volume of acidic vesicular organelles (AVOs) increases upon autophagy induction (Thomé et al., 2016).

As shown in Figure 6.2, cytoplasm and nucleus appeared green whereas AVOs appeared red in AO-stained Caco-2 cells, which observation indicates an induction of autophagy under nutrient free condition.

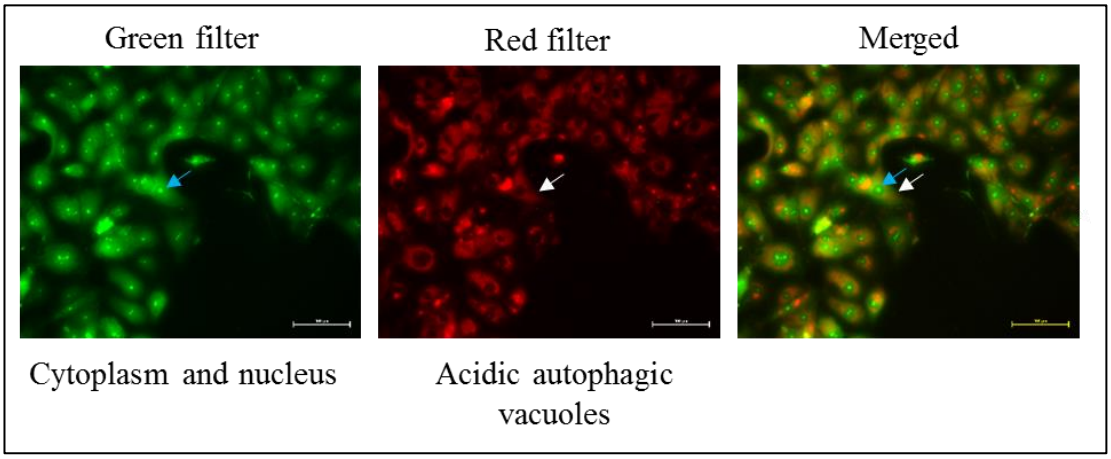

Figure 6.2 Representative morphologies of AO-stained Caco-2 cells under nutrient-free condition (without drug treatment) for 72 hours. Autophagy induction can be exhibited by red AVOs within cytoplasm (white arrow) whereas the nucleus and cytoplasm exhibit bright green (blue arrow) and faint green around the nucleus. Scale bar represents 100μm.

The δT3, 5FU and Dox single treatments, as well as δT3 + 5FU and δT3 + Dox combined treatments were assessed timely from 24-72 hours. The first appearance of

autophagy was observed after 24 hours of treatment, hence, the representative images were selected for a clearer presentation in Figures 6.3 – 6.6.

As shown in Figure 6.3, the AO-stained Caco-2 cells revealed the presence of AVOs after receiving 24-hour combined treatment of δT3 + 5FU, suggesting the autophagolysosomes formation. After 48 to 72 hours of treatments, δT3 single treatment and δT3 + 5FU combined treatment markedly elevated the stained AVOs (Appendices: Figures A6.1 & A6.2), demonstrating a time-course increase in autophagy.

Similarly in SW48 cells, the AVOs were detected in δT3 single treatment and δT3 + 5FU combined treatment after 24 hours (Figure 6.4). The signal intensity continues to increase after 48 hours (Appendix: Figure A6.2) and 72 hours (Appendix: Figure A6.4) of treatments, signifying a time-dependent induction of autophagy.

On the other hand, δT3 + Dox combined treatment also induced the formation of AVOs in Caco-2 (Figure 6.5) and SW48 cells (Figure 6.6) after 24-hour treatment. δT3 + Dox combined treatment exhibited prominent increase of AVOs in 48-hour and 72-hour profiles of Caco-2 (see Appendices: Figures A6.5 & A6.6) and SW48 (see Appendices: Figure A6.7 & A6.8).

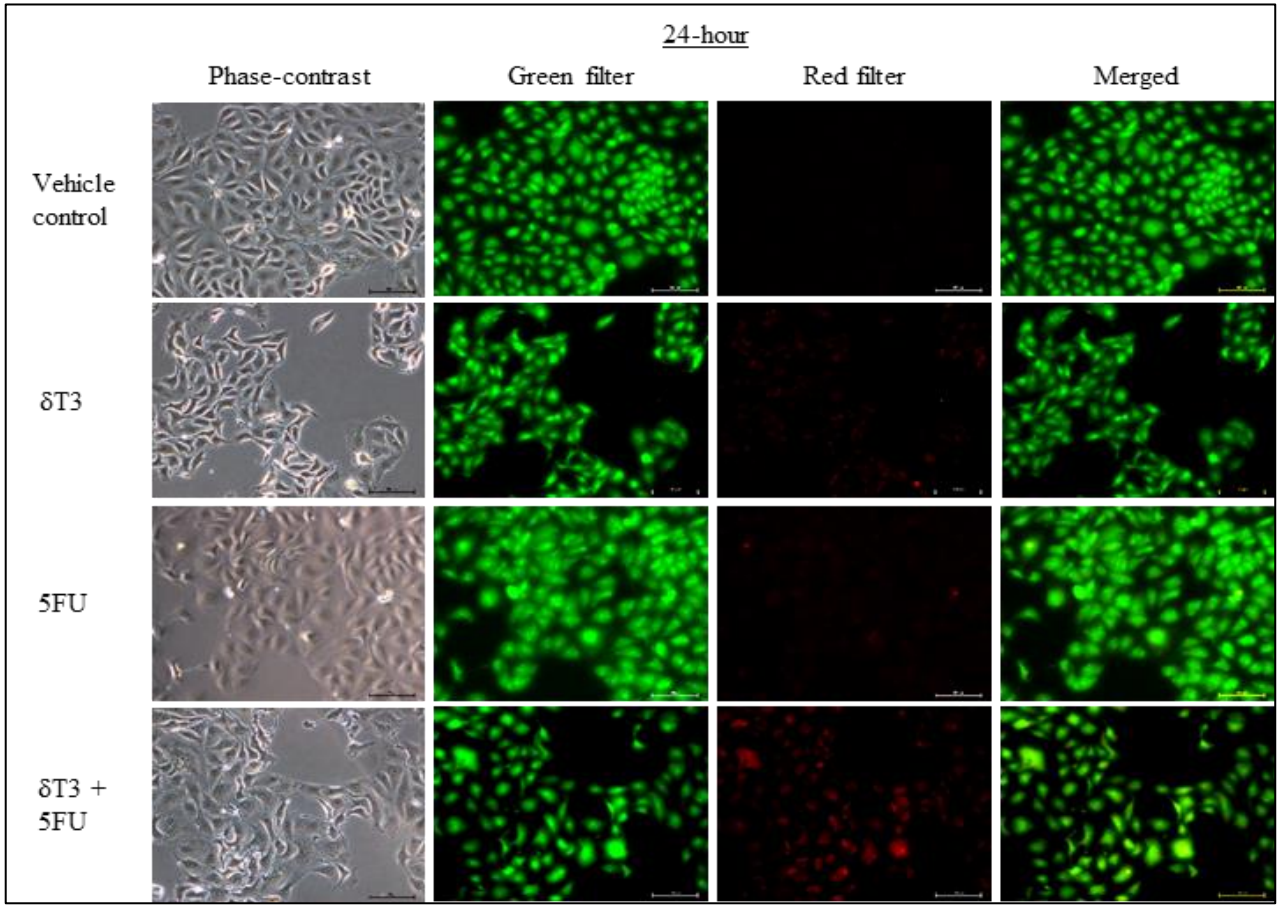

Figure 6.3 Representative AO-stained Caco-2 cells treated for 24 hours with individual δT3 or 5FU and the combined treatments. Vehicle control containing 0.1% of DMSO served as negative control. δT3, δ-tocotrienol; 5FU, 5-fluorouracil; δT3 + 5FU, δ-tocotrienol + 5-fluorouracil. Scale bar represents 100μm.

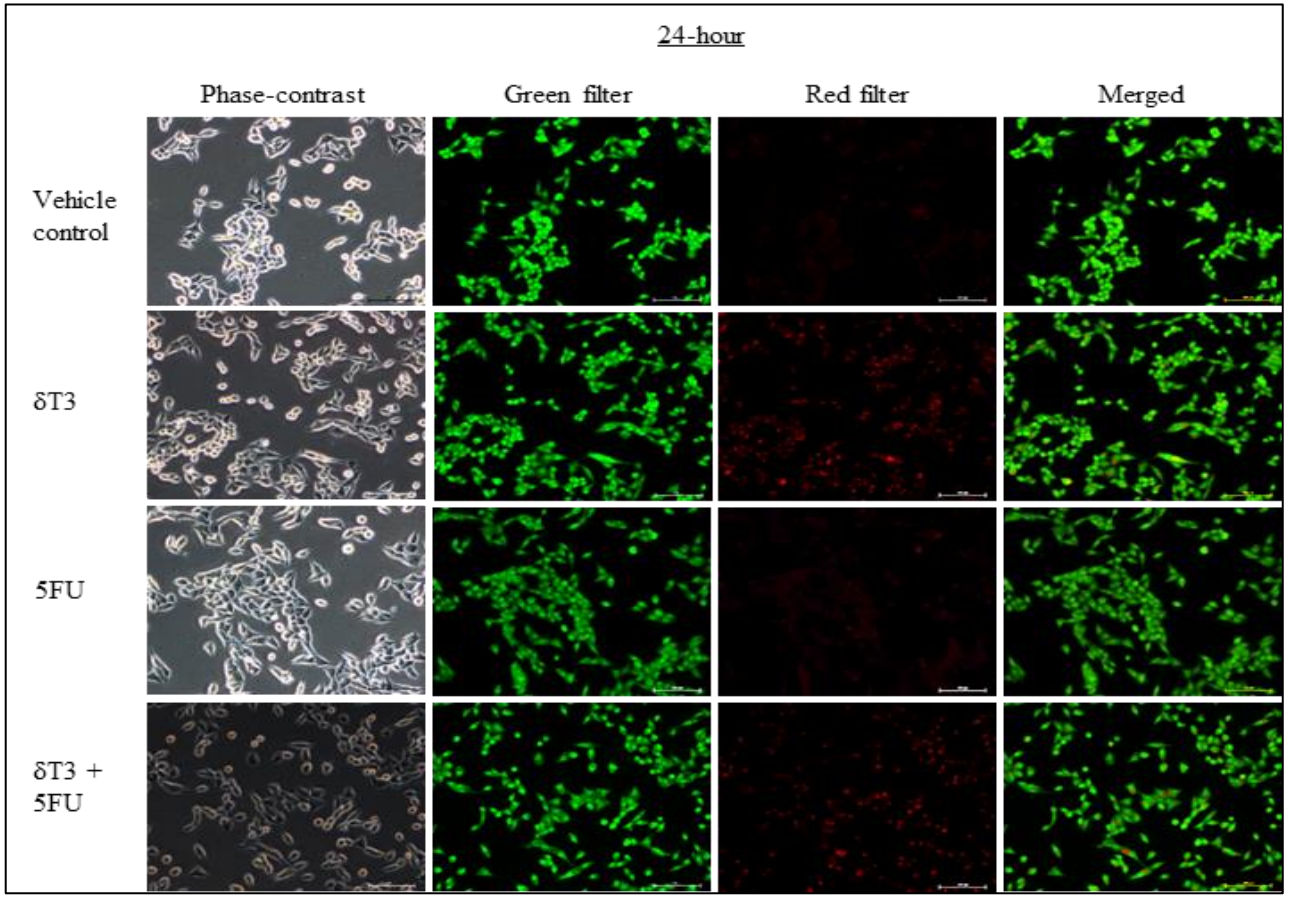

Figure 6.4 Representative AO-stained SW48 cells treated for 24 hours with individual δT3 or 5FU and the combined treatments. Vehicle control containing 0.1% of DMSO served as negative control. δT3, δ-tocotrienol; 5FU, 5-fluorouracil; δT3 + 5FU, δ-tocotrienol + 5-fluorouracil. Scale bar represents 100μm.

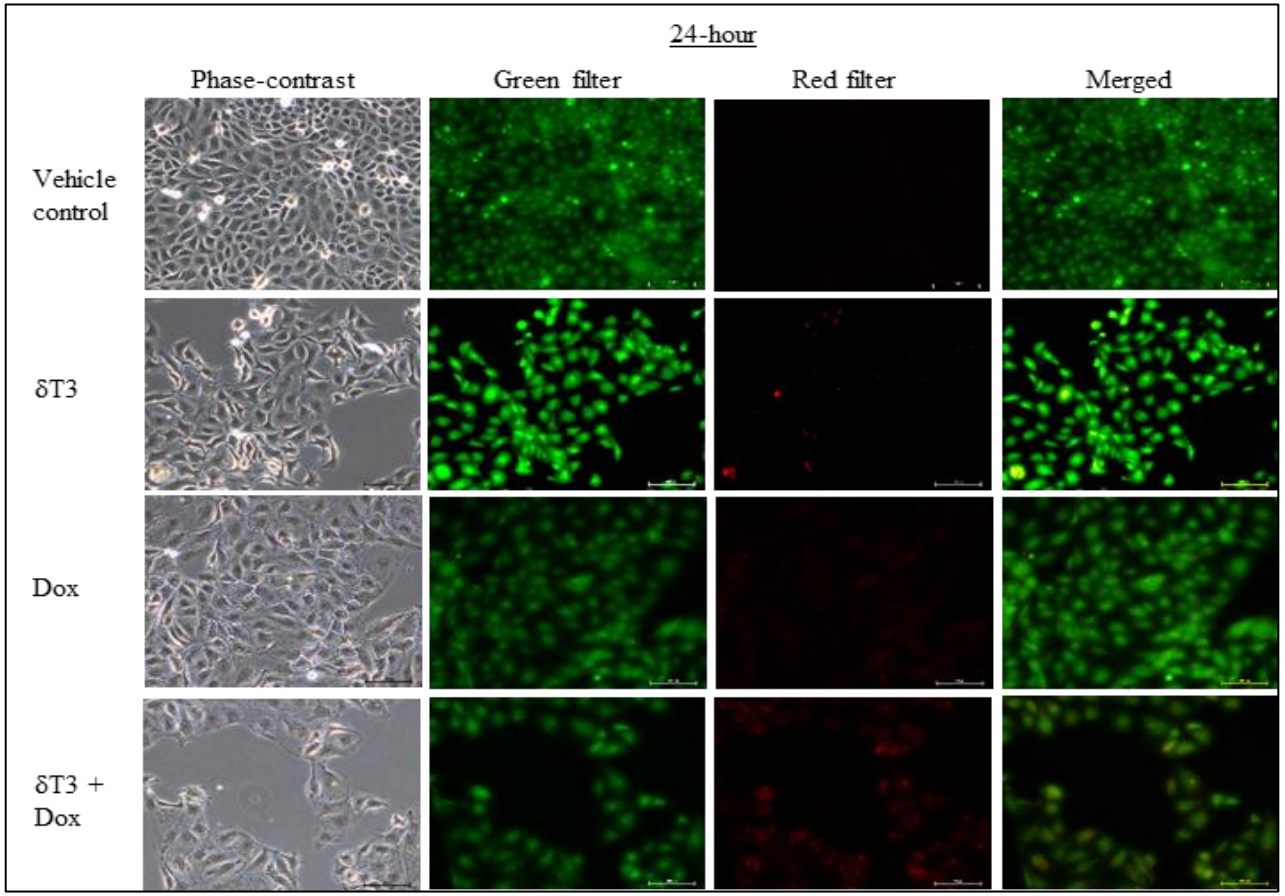

Figure 6.5 Representative AO-stained Caco-2 cells treated for 24 hours with individual δT3 or Dox and the combined treatments. Vehicle control containing 0.1% of DMSO served as negative control. δT3, δ-tocotrienol; Dox, doxorubicin; δT3 + Dox, δ-tocotrienol + doxorubicin. Scale bar represents 100μm.

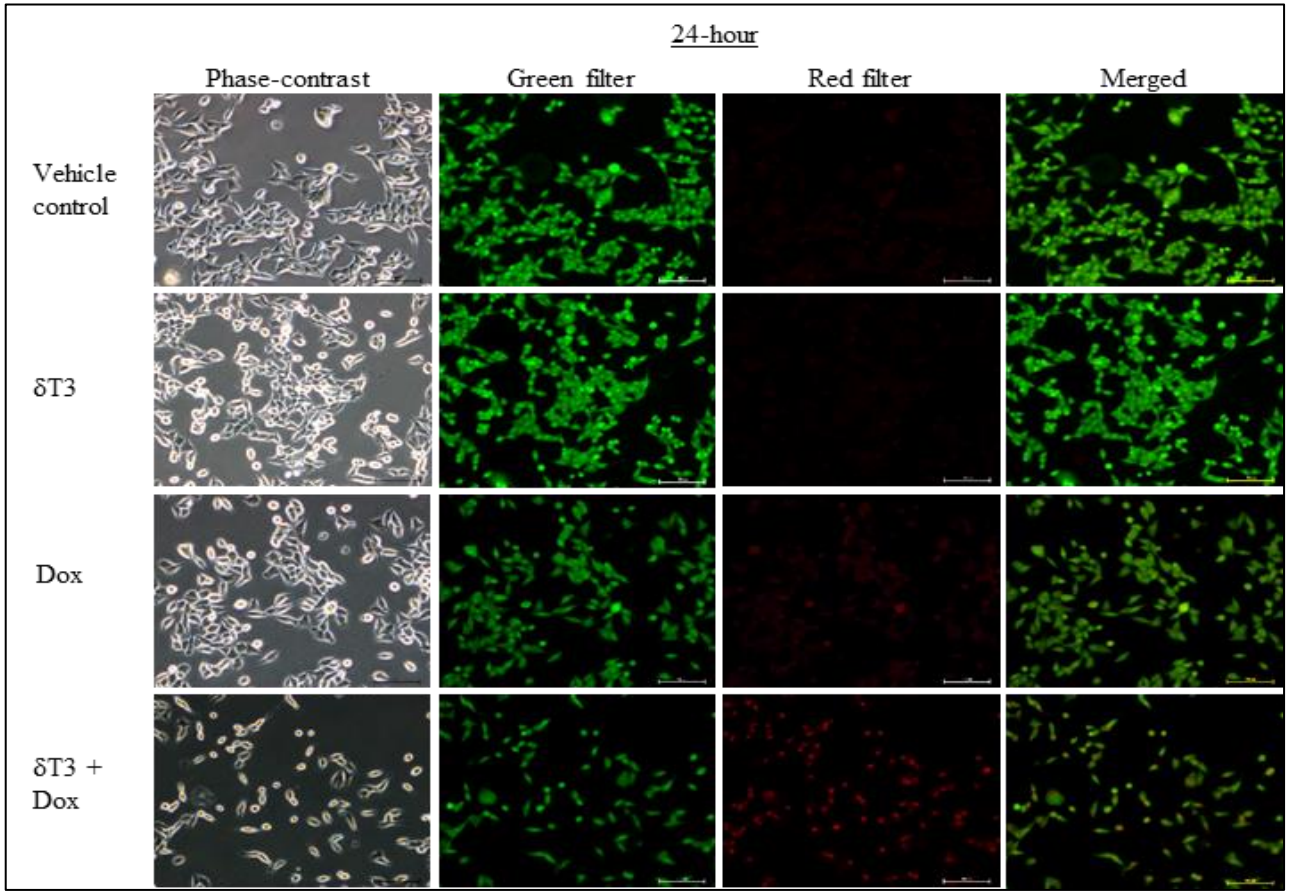

Figure 6.6 Representative AO-stained SW48 cells treated for 24 hours with individual δT3 or Dox and the combined treatments. Vehicle control containing 0.1% of DMSO served as negative control. δT3, δ-tocotrienol; Dox, doxorubicin; δT3 + Dox, δ-tocotrienol + doxorubicin. Scale bar represents100μm.

6.3.1.2 MDC staining profiles

MDC accumulates in mature autophagic vacuoles such as autophagolysosomes, but not in the early endosome compartment (Munafó and Colombo, 2001). Autophagic cells stained by MDC appeared as distinct green fluorescent dot-like structures distributing within the cytoplasm or localizing in the perinuclear regions (Shin et al., 2012). Based on the observation of AO profiles, a clear autophagic induction was identified in Caco-2 cells receiving δT3 + 5FU combined treatment as contrasting to the basal autophagy appearance of vehicle control (Figure 6.7).

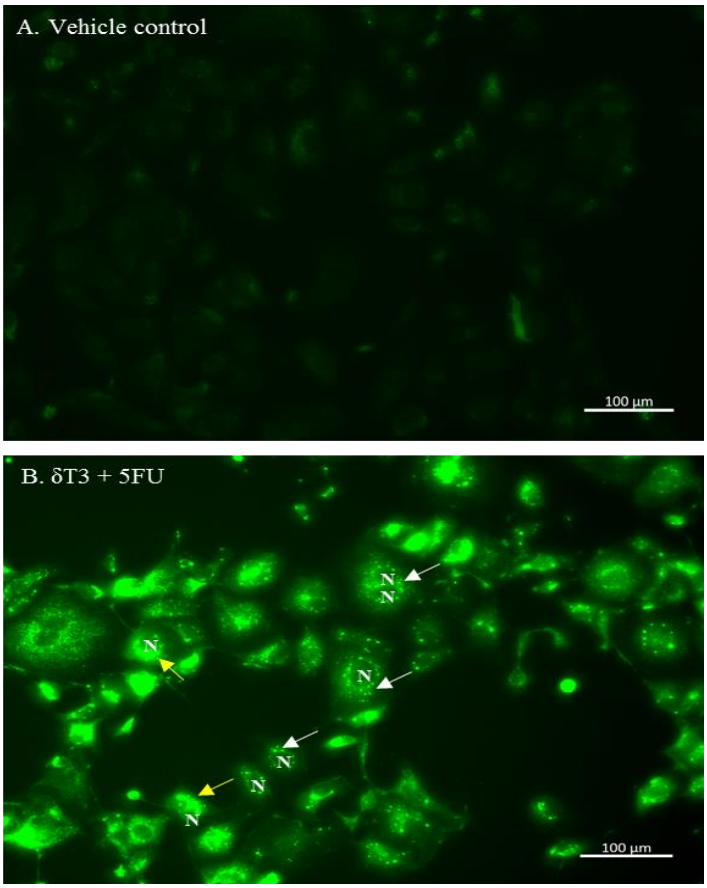

Figure 6.7 Representative comparison of basal autophagy in vehicle control (A) and induced autophagy in Caco-2 cells receiving δT3 + 5FU combined treatment (B). Autophagic morphologies are detected by using MDC. Accumulation of MDC autophagolysomes forming punctate structures as indicated by green dots (white arrow) appearing around N (nucleus). Yellow arrow denotes the dense aggregates of autophagolysomes appearing as bright green clumps. Scale bar represents 100µm.

The MDC staining was conducted at 24, 48 and 72 hours post for Caco-2 cells (Appendices: Figures A6.9 & A6.11) and SW48 (Appendices: Figures A6.10 & A6.12). Only representative images from 24-hour treatment were displayed for a clearer presentation (Figures 6.8 & 6.9); their respective intensity analyses are exhibited in Figures 6.10 & 6.11.

As shown in Figure 6.8, there was a slight increased signal of MDC-labelled vesicles in Caco-2 cells receiving δT3 and 5FU single treatments but a marked increase in those receiving δT3 + 5FU combined treatment after 24 hours. In SW48 cells, increase of MDC signal was also observed in δT3 and 5FU single treatments. Notably, the MDC signal was found to be the highest in SW48 cells receiving δT3 + 5FU combined treatment. Similarly, δT3 + Dox combined treatment induced higher MDC signals in both Caco-2 and SW48 cells (Figure 6.9).

Consistent to the microscopic observation, quantitative assessment of MDC-stained cells demonstrated a significantly higher MDC intensity in δT3 single treatment ($p < 0.01$) and δT3 + 5FU combined treatment ($p < 0.0001$) than that of vehicle control (24 hours) (Figure 6.10). In Caco-2 cells, the autophagy induction by 5FU and Dox single treatments appeared later, which were after 48 and 72 hours of treatment (Figure 6.10). The δT3 single treatment and δT3 + Dox combined treatment also displayed significantly higher MDC intensity in Caco-2 ($p < 0.001$) and SW48 ($p<0.01$) cells after 24-hour treatment (Figure 6.11). The effects of 5FU and Dox single treatments on autophagy induction were not statistically significant in SW48 cells (Figure 6.11).

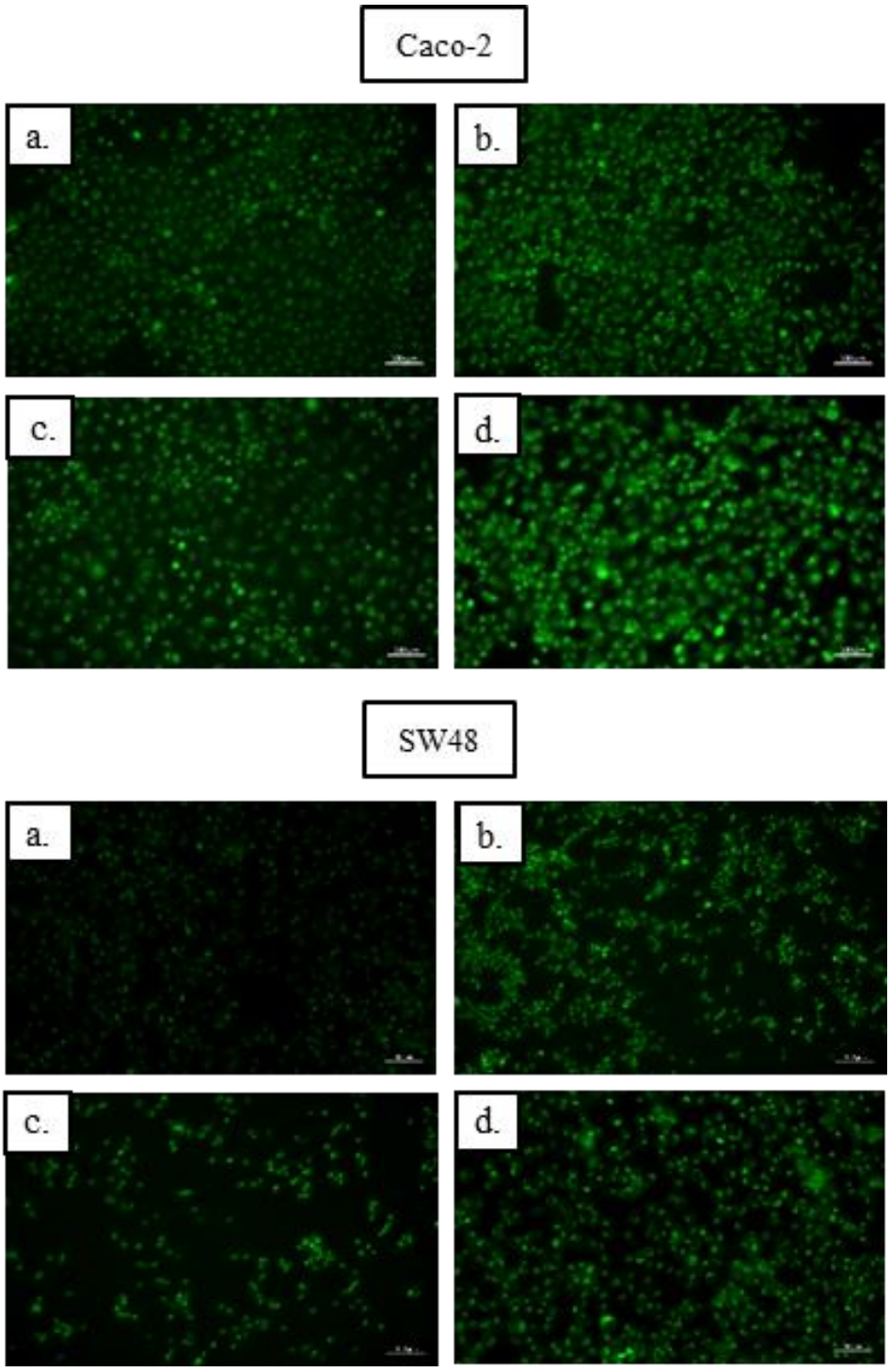

Figure 6.8 Representative MDC profiles of Caco-2 and SW48 cells after 24 hours of receiving treatments of δT3, 5FU and the combined treatment. a, vehicle control; b, δ-tocotrienol; c, 5-fluorouracil; d, δ-tocotrienol + 5-fluorouracil. Scale bar represents 100μm.

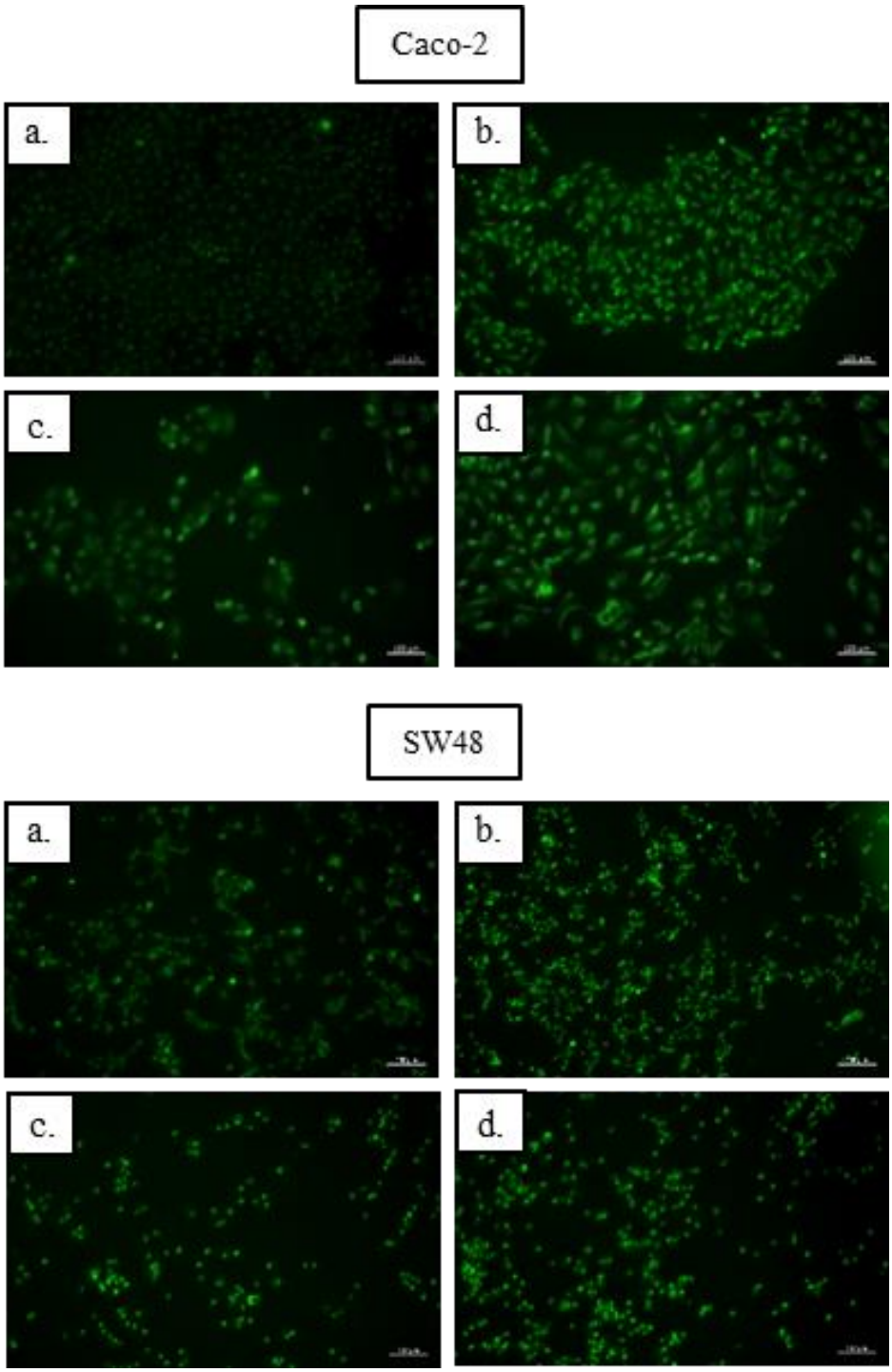

Figure 6.9 Representative MDC profiles of Caco-2 and SW48 cells after 24 hours of receiving treatments of δT3, Dox and the combined treatment. a, vehicle control; b, δ-tocotrienol; c, doxorubicin; d, δ-tocotrienol + doxorubicin. Scale bar represents 100μm.

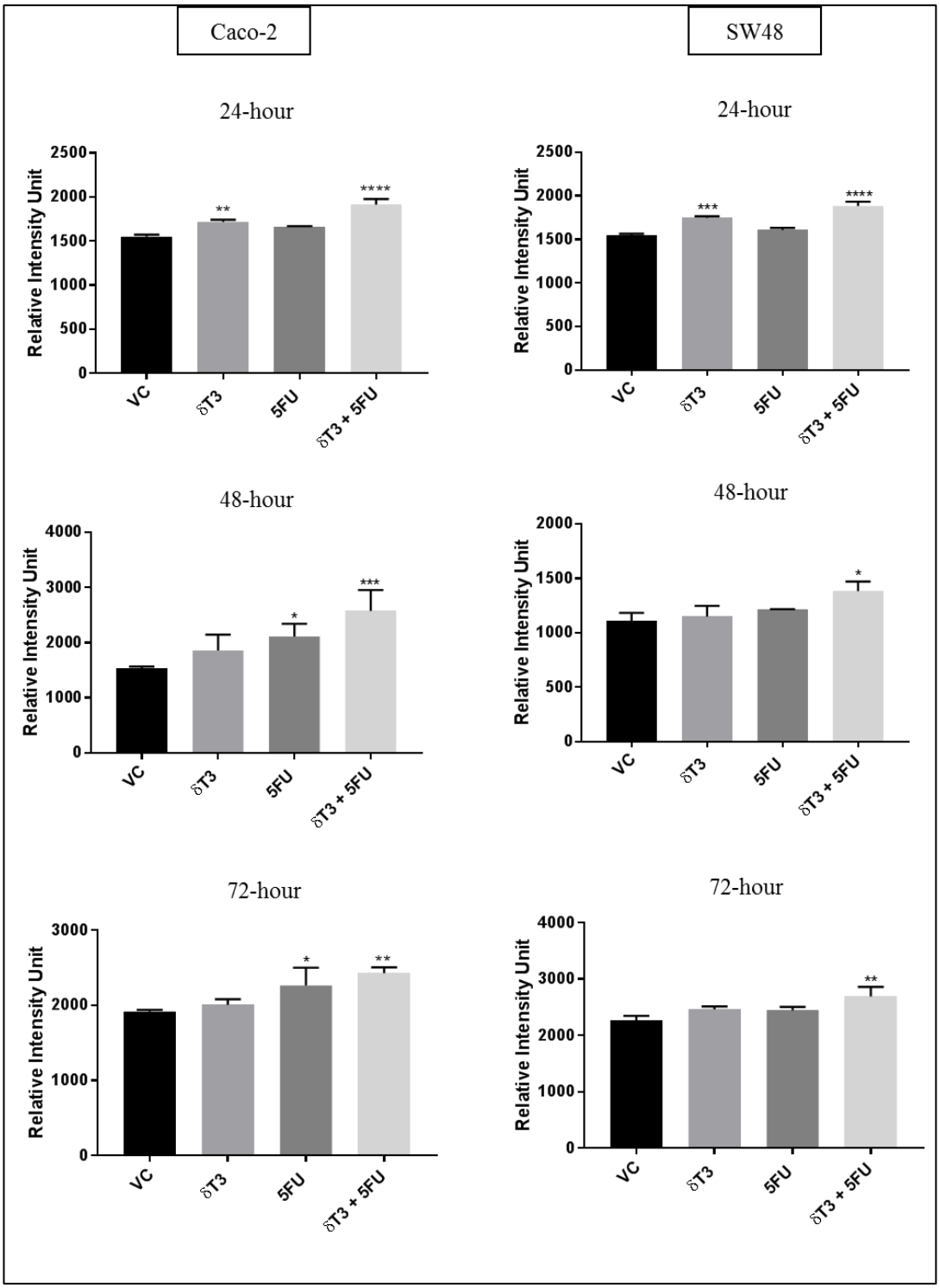

Figure 6.10 Analyses of MDC intensity of Caco-2 and SW48 cells at various time points after receiving treatments from δT3, 5FU and their combination. VC, vehicle control; δT3, δ-tocotrienol; 5FU, 5-fluorouracil; δT3 + 5FU, δ-tocotrienol + 5-fluorouracil. ****p<0.0001; ***p<0.001; **p <0.01; *p <0.05.

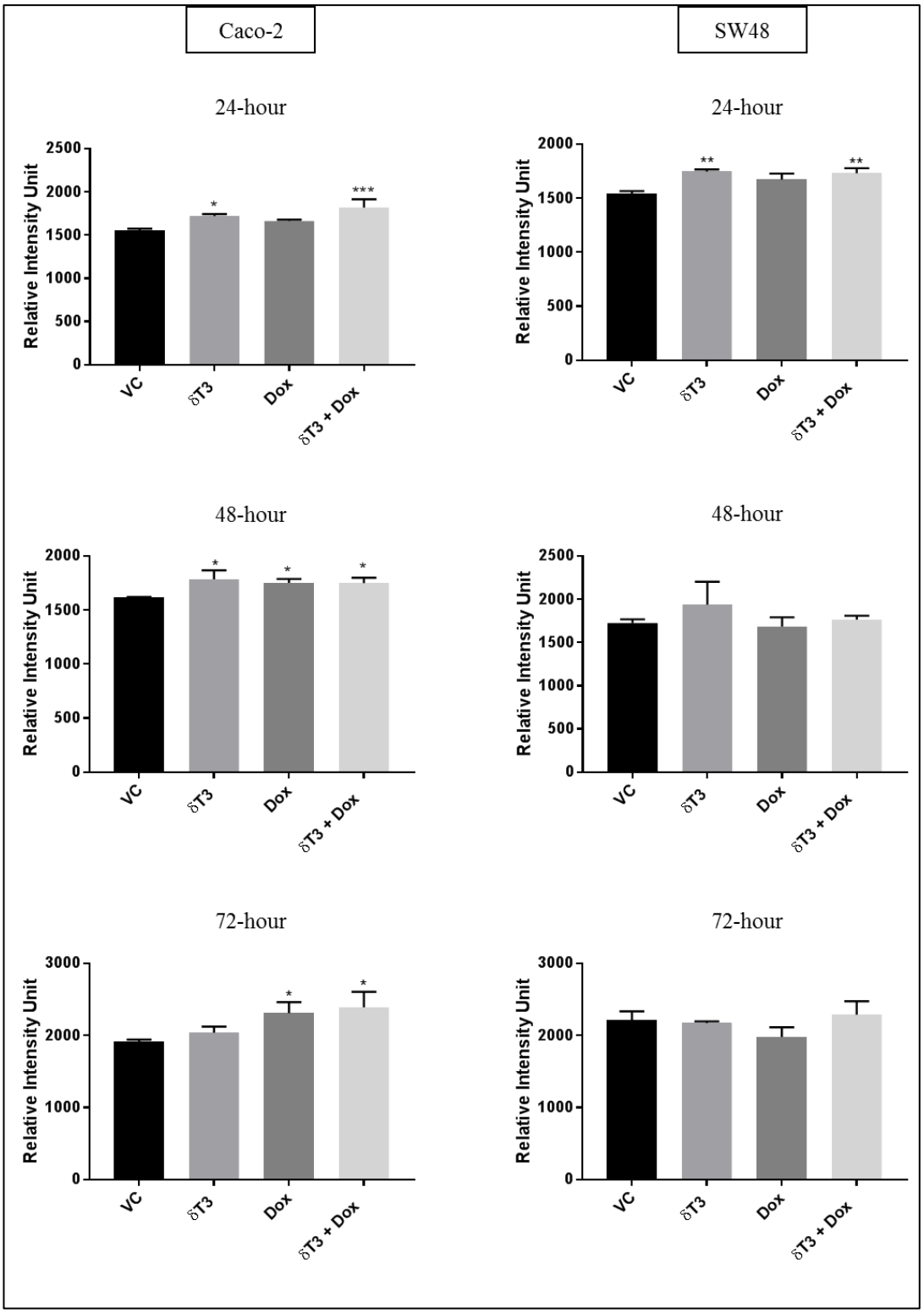

Figure 6.11 Analyses of MDC intensity of Caco-2 and SW48 cells at various time points after receiving treatments from δT3, Dox and their combination. VC, vehicle control; δT3, δ-tocotrienol; Dox, doxorubicin; δT3 + Dox, δ-tocotrienol + doxorubicin. ***p<0.001; **p <0.01; *p <0.05.

6.3.2 Western immunodetection for autophagy markers

As shown in Figure 6.12, the Western profiles demonstrated markedly increased LC3-II and beclin-1 in both Caco-2 and SW48 cells receiving δT3 + 5FU combined treatment. The highest expression of LC-II was found at 72-hour post treatment. On the other hand, beclin-1 expression increased as earlier as 4 hours after treatment. Of note, the expression pattern of beclin-1 and LC3-II appeared to be inversed to each other.

Similarly, δT3 + Dox combined treatment also elicited a time-dependent increase of LC3-II level, by which its highest expression was found at 72 hours in Caco-2 and SW48 cells (Figure 6.13). The temporal expression of beclin-1 exhibited an early but inversely related to the increase of LC3-II.

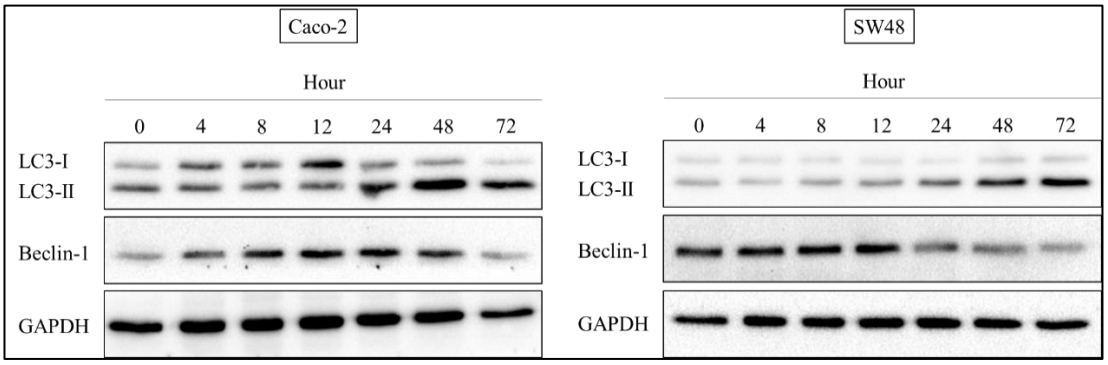

Figure 6.12 Representative Western profiles of LC3-I/II and beclin-1 for Caco-2 and SW48 cells at 0-72 hours after receiving δT3 + 5FU combined treatment. GAPDH serves as a loading control.

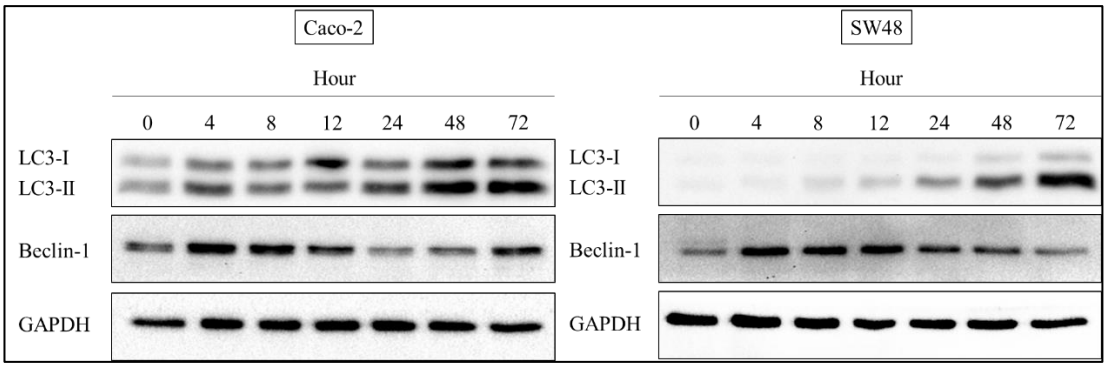

Figure 6.13 Representative Western profiles of LC3-I/II and beclin-1 for Caco-2 and SW48 cells at 0-72 hours after receiving δT3 + Dox combined treatment. GAPDH serves as a loading control.

Since the peaked LC3-II expression was detected at 72 hours, a relative comparison to the respective single treatments was therefore performed at this given time point (Figures 6.14 & 6.15). As shown in Figure 6.14, LC3-II expressions triggered by 5FU single treatment and δT3 + 5FU combined treatment were found the highest in Caco-2 cells. For SW48 cells, the LC3-II expressions were seen the highest induced by δT3 + 5FU combined treatment and the lowest by 5FU single treatment. Notably, the expression levels of beclin-1 were consistently low in treatment groups.

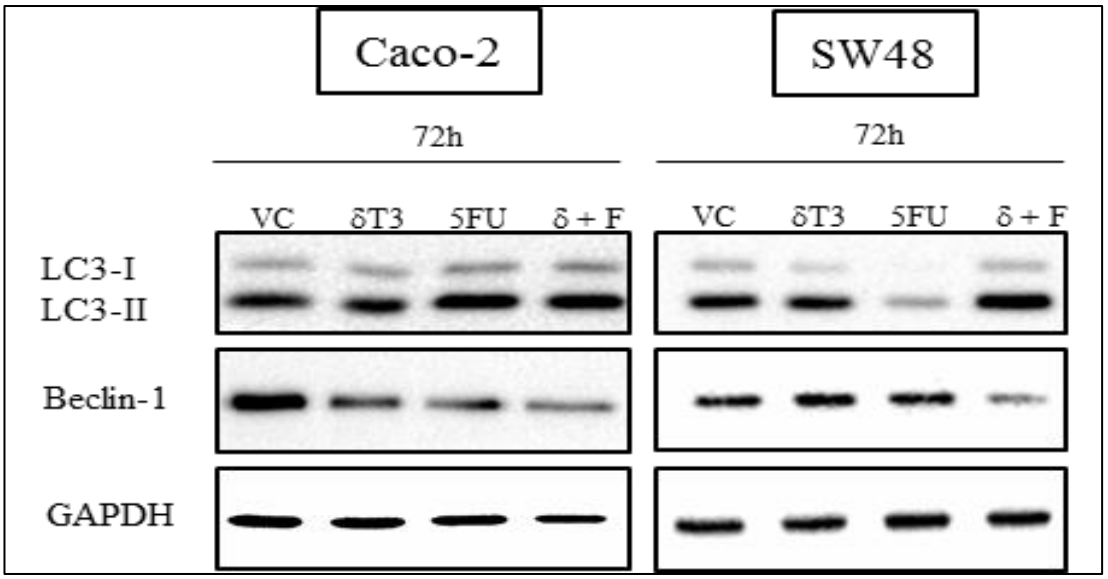

Figure 6.14 Representative Western profiles of LC3-I/II and beclin-1 for Caco-2 and SW48 cells after 72-hour treatments with δT3, 5FU and their combination. GAPDH serves as a loading control. VC, vehicle control; δT3, δ-tocotrienol; 5FU, 5-fluorouracil; δ + F, δ-tocotrienol + 5-fluorouracil.

As shown in Figure 6.15, there was a noticeable increase of LC3-II induced by Dox single treatment and δT3 + Dox combined treatment in Caco-2 cells. In SW48 cells, expression of LC3-II was found the lowest upon receiving Dox single treatment, but the highest in δT3 + Dox combined treatment group. Beclin-1 expression was revealed to be the lowest in both cell lines receiving δT3 + Dox combined treatment.

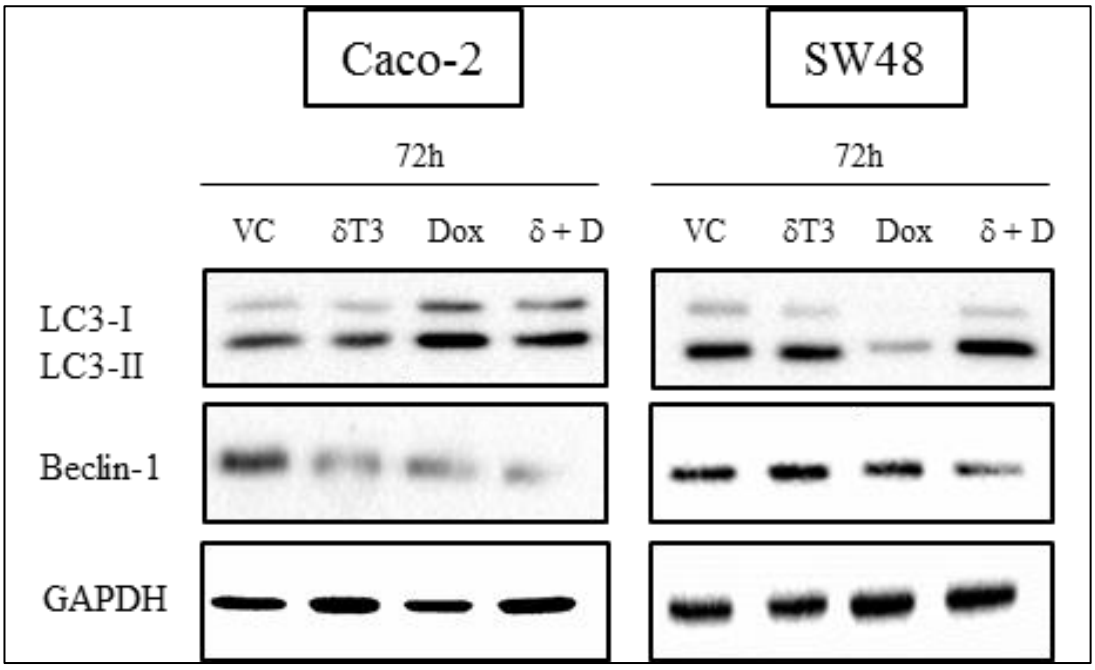

Figure 6.15 Representative Western profiles of LC3-I/II and beclin-1 for Caco-2 and SW48 cells after 72-hour treatments with δT3, Dox and their combination. GAPDH serves as a loading control. VC, vehicle control; δT3, δ-tocotrienol; Dox, doxorubicin; δ + D, δ-tocotrienol + doxorubicin.

It was demonstrated that Akt and PDK1 were downregulated in Caco-2 and SW48 cells upon receiving δT3 + 5FU combined treatment (Figure 6.16) as well as δT3 + Dox combined treatment (Figure 6.17), when compared to vehicle control group.

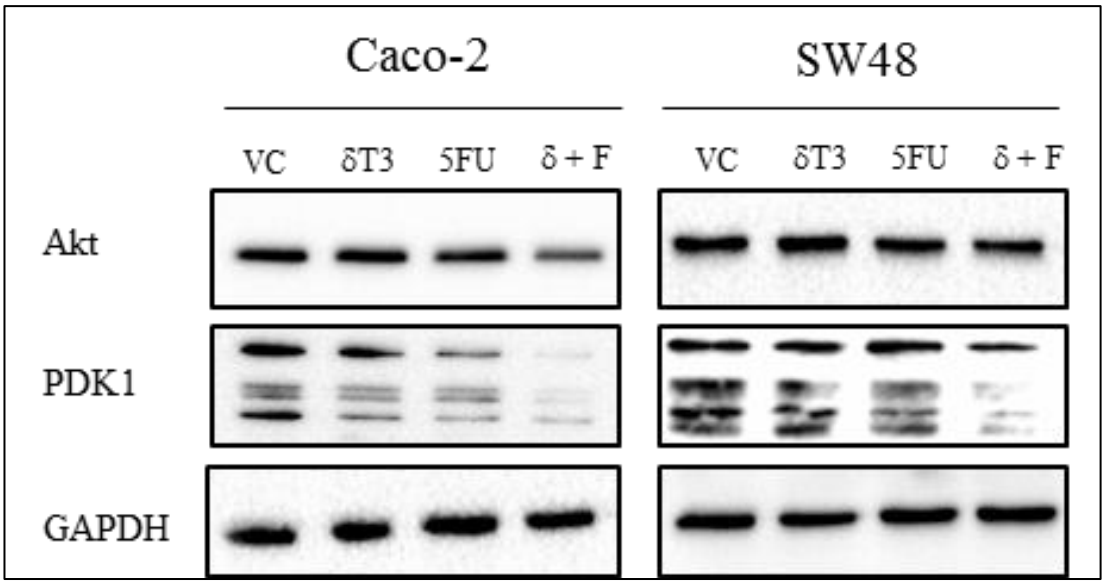

Figure 6.16 Representative Western profiles of Akt and PDK1 for Caco-2 and SW48 cells after 72-hour treatments with δT3, 5FU and their combination. VC, vehicle control; δT3, δ-tocotrienol; 5FU, 5-fluorouracil; δ + F, δ-tocotrienol + 5-fluorouracil.

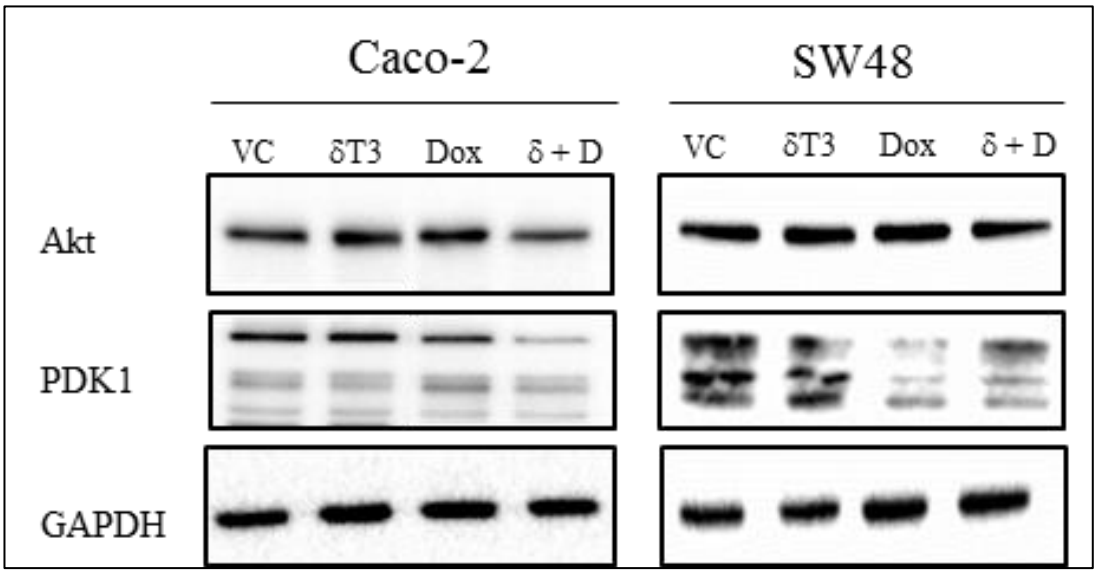

Figure 6.17 Representative Western profiles of Akt and PDK1 for Caco-2 and SW48 cells after 72-hour treatments with δ-tocotrienol, doxorubicin and their combination. VC, vehicle control; δT3, δ-tocotrienol; Dox, doxorubicin; δ + D, δ-tocotrienol + doxorubicin.

6.3.3 Effects of autophagy inhibitors on cell viability

6.3.3.1 Blocking autophagy with 3-methyladenine (3-MA)

Guided by the published study conducted on colorectal cancer cell lines (Guamán Ortiz et al., 2014), pre-treatment of Caco-2 and SW48 cells with 2.5mM of 3-

MA for 4 hours was followed in this experiment. Notably, this concentration was found non-toxic to Caco-2 and SW48 cells based on the non-significant effect of cell viability for vehicle control (Figure 6.18).

In Caco-2 cells, application of 3-MA autophagy inhibitor did not improve the cell viability under δT3 and 5FU single treatments. In contrast, 3-MA significantly reverted (although not completely) the cytotoxic effect of δT3 + 5FU combined treatment ($p < 0.01$). On the other hand, the presence of 3-MA increased cell viability of Caco-2 cells receiving Dox single treatment and δT3 + Dox combined treatment, suggesting a partial prevention of cell death (Figure 6.18 A).

In SW48 cells, application of 3-MA non-significantly improve cell viability of δT3 and 5FU single treatments. In contrast, the cytotoxic effect of Dox single treatment, δT3 + 5FU and δT3 + Dox combined treatments were completely reversed by the application of 3-MA (Figure 6.18 B) in SW48 cells, signifying a complete suppression of cell death.

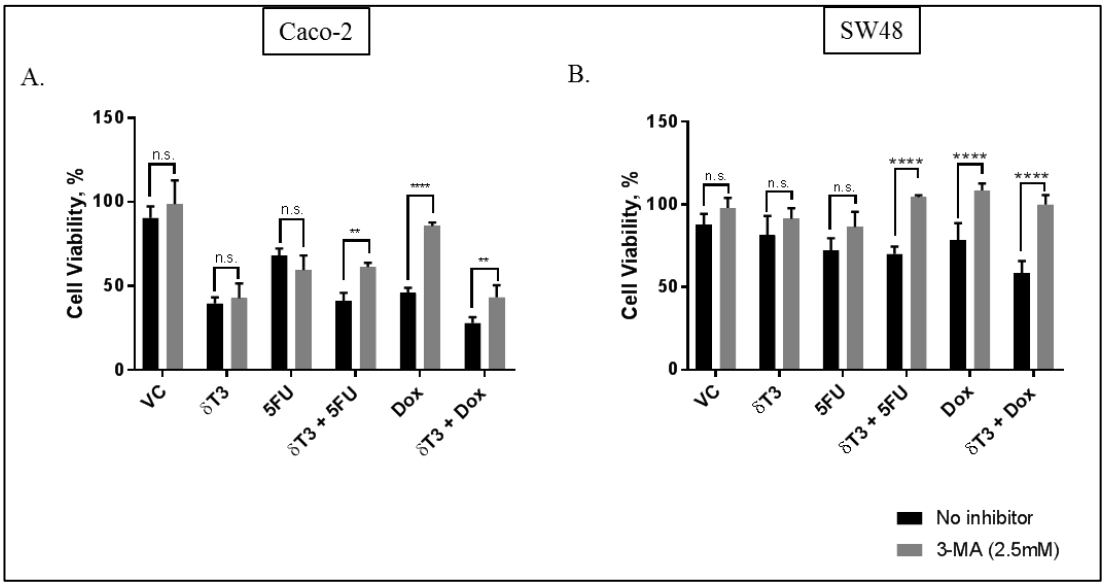

Figure 6.18 Effects of 3-MA on the viability of Caco-2 (A) and SW48 (B) cells after receiving various treatments. VC, vehicle control; δT3, δ-tocotrienol; 5FU, 5-fluorouracil; δT3 + 5FU, δ-tocotrienol + 5-fluorouracil; Dox, doxorubicin; δT3 + Dox, δ-tocotrienol + doxorubicin. ****p<0.0001; ***p<0.001; **p <0.01.

6.3.3.2 Blocking autophagy with bafilomycin A1 (Baf-1)

Baf-1 was used at 10nM in this experiment in reference to several previously published works for studying the autophagy inhibition in colorectal cancer cell lines (Greene et al., 2013; Huang and Sinicrope, 2010; Was et al., 2017). In this study, it was showed that 10nM of Baf-1 did not cause toxicity to the cells.

Corresponding to the results from 3-MA, inhibition of autophagy using Baf-1 was unable to inhibit cell death of Caco-2 from δT3 and 5FU single treatments. However, a significant (although not complete) restore in cell viability was observed in Caco-2 cells subjected to δT3 + 5FU combined treatment in the presence of Baf-1 (Figure 6.19 A), suggesting a partial inhibition of cell death. The application of Baf-1 significantly improved cell viability (although not complete) in Caco-2 cells treated with Dox and δT3 + Dox combined treatment.

In SW48 cells, the presence of Baf-1 significantly and completely improved the cell viability triggered by δT3 and 5FU single treatments and δT3 + 5FU combined treatment (Figure 6.19 B), which demonstrate a complete inhibition of cell death. However, cell viability of SW48 cells was non-significantly restored in the Dox single treatment in the presence of Baf-1. In comparison, Baf-1 could significantly restored cell viability in SW48 cells subjected to δT3 + Dox combined treatment (Figure 6.19 B).

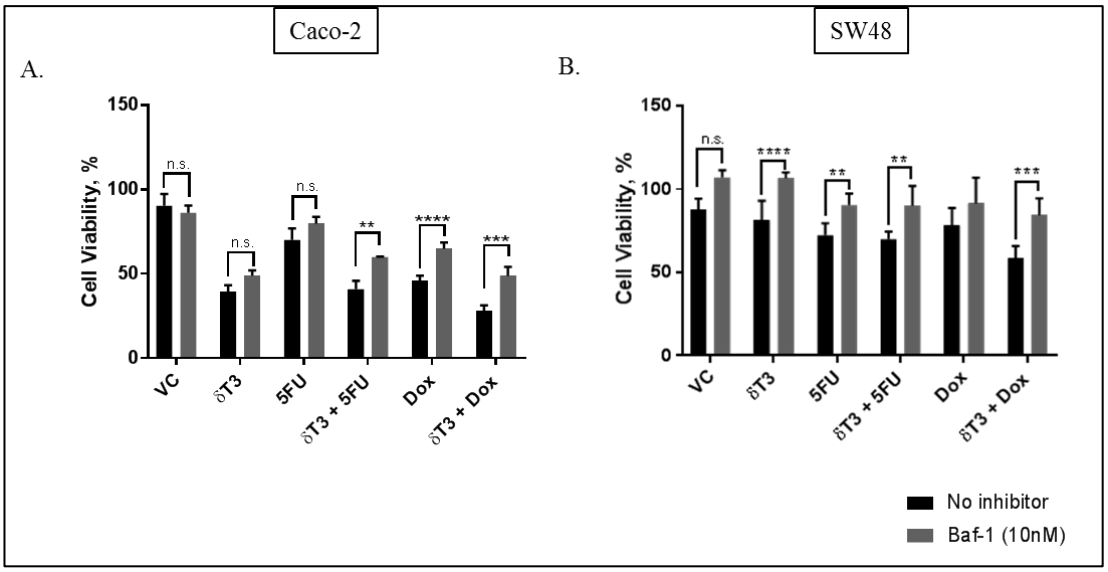

Figure 6.19 Effects of Baf-1 on the viability of Caco-2 (A) and SW48 (B) cells after receiving various treatments. VC, vehicle control; δT3, δ-tocotrienol; 5FU, 5-fluorouracil; δT3 + 5FU, δ-tocotrienol + 5-fluorouracil; Dox, doxorubicin; δT3 + Dox, δ-tocotrienol + doxorubicin. ****p<0.0001; ***p<0.001; **p <0.01.

6.4 Discussion

Guided by the findings as described in Chapter Four and Chapter Five which consensually suggested the potential involvement of autophagy as an additional cell death modality, current study in this chapter was hence conducted to investigate the autophagic responses induced by the treatments on Caco-2 and SW48 cells.

Literally, the term 'autophagy' refers to 'self-eating' in Greek, inclining that autophagy may be a cell suicide process (Codogno and Meijer, 2005; Shen and Codogno, 2016). Autophagy was reported to exhibit dual functions in cell survival and death. Such controversial roles have indeed reflected in at least two previous studies in which tocotrienols exhibited cytoprotective autophagy in MDA-MB-231 breast cancer cells (Tran et al., 2015) and anti-tumour effect in PC-3 prostate cancer cells (Fontana et al., 2019). Hence, it is interesting to explore the roles of autophagy (in relation to cell death) induced by the combined treatments identified in the current study, for exploring new opportunities in novel cancer treatments.

Morphologically, the AO and MDC profiles had clearly demonstrated the formation of acidic vesicular organelles (AVOs, see Figures 6.3 – 6.6) and autophagolysosomes (see Figures 6.8 & 6.9) upon treatments, thereby confirmed the presence of autophagy in Caco-2 and SW48 cells. Notably, an enhanced autophagy triggered by δT3 + 5FU and δT3 + Dox combined treatments was detected at an early time point, i.e., 24 hours and persistently higher thereafter. These observations therefore suggest a rapid and prolonged autophagy induction by the combined treatments.

Since it has been suggested that autophagy activity is a dynamic process in which assessing an autophagy marker at a specific time point could not truly reflect

the presence of autophagy (Yoshii and Mizushima, 2017), hence, current study performed a temporal kinetic study (0-72 hours, Figures 6.12 & 6.13) on LC3-II, a marker of autophagosome formation. Upon activation of autophagy, a cytosolic form of LC3 (LC3-I) is conjugated to phosphatidylethanolamine and generates a lipidated form of LC3 (LC3-II), which is then recruited to produce the autophagosomal membranes (Glick et al., 2010). During the subsequent process of autophagosome maturation, LC3-II is deconjugated from the outer surface while LC3-II that is present within the inner vesicle remains associated with the completed autophagosomes. Therefore, the LC3-II level correlates well with autophagosome number (Loos et al., 2014). Based on this ground, LC3-II is a useful indicator of autophagosome initiation (Gottlieb et al., 2015). Although some groups adopted the LC3-II/ LC3-I ratio as an indication of autophagic activity, however this approach is generally unreliable and discounted (Gottlieb et al., 2015) because antibodies tend to have greater affinity for LC3-II than LC3-I. As such, the signal ratio of LC3-I and LC3-II does not accurately represent the ratio amount of cytosolic and membrane-bound LC3 (Mizushima and Yoshimori, 2007). In relation to this study, a noticeable increase of LC3-II was observed in Caco-2 (Figure 6.12) and SW48 (Figure 6.13) cells receiving δT3 + 5FU and δT3 + Dox combined treatments, which induced autophagy in a time-dependent fashion. A relative comparison between single and combined treatments demonstrated that the latter resulted in earlier and/or persistent autophagic activities (Appendices: Figures A6.13 & A6.14). These results therefore suggest a rapid and/or prolonged autophagic response, which are conforming to the microscopic observations. Potentially, these findings also suggest an immense autophagic stimuli triggered by the combined treatments. In the light of a proposed idea that autophagy acts as a protective mechanism in response to brief stressful episode while sustained autophagy

will lead to an autophagic cell death (Amelio et al., 2011), the result from current study infers an enhanced autophagic cell death induced by the combined treatments.

One the other hand, beclin-1 is another important marker to study autophagy. As opposed to several previous studies reporting a positive correlation between beclin-1 and LC3-II (Kobayashi et al., 2010; Kumari et al., 2012; Lee et al., 2013; Valente et al., 2014), current study demonstrated an inversely proportional expression. One potential explanation of the phenomenon is the involvement of a non-canonical beclin-1-independent autophagy in current study. In contrast to classical or canonical autophagy, the non-canonical autophagy does not require an entire set of autophagy-related protein (ATG), particularly beclin-1 to form autophagosomes (Scarlatti et al., 2008b). This non-canonical autophagy has been gaining attention as an alternative mechanism for therapeutic purposes in cancers (Dupont and Codogno, 2013), especially those cancers with too low expression of beclin-1 for canonical autophagy induction. Albeit it is largely unknown how does the autophagosome is formed without the aid from beclin-1, this form of non-canonical autophagy was in fact reported to associate with cell death (Scarlatti et al., 2008a; Tian et al., 2010; Zhu et al., 2007). The underlined mechanism of current finding is therefore still necessitated to be elucidated by which genetic silencing of beclin-1 may help to answer the question.

An additional line of evidence suggests that not all autophagy is associated with high beclin-1 level. It was reported that upregulation of beclin-1 was only observed in starved-induced autophagy, but not the rapamycin-induced autophagy (Li et al., 2013). Therefore, it could be possible that the combined treatments engage a similar mechanism of the rapamycin-induced autophagy.

On the other hand, Akt signalling representing one of the pathways, which is closely related to autophagy, was also studied. Akt signalling was reported to regulate cell death and survival machineries, hence, it is interesting to examine how its regulation integrates into the cell death and survival through autophagy. In fact, the activation of Akt via PDK1 promotes cell survival (Martelli et al., 2012; Noguchi et al., 2014). As such, the Akt and its activation enzyme, PDK1 were examined. In the current study, it was demonstrated that Akt and its regulatory enzyme, PDK1 were downregulated, especially in the combined treatment (Figures 6.16 & 6.17). This result therefore proposes an inactivation of cell survival mechanism in the presence of autophagy, implying an autophagic cell death.

According to the recommendations from NCCD, autophagic cell death refers to autophagy that mediates cell death and can be suppressed by the inhibition of autophagy pathway (Galluzzi et al., 2018). Hence, pharmacological inhibitors of autophagy, namely 3-methyladenine (3-MA) and bafilomycin A1 (Baf-1) were applied in order to prove that the autophagy induction was associated with cell death but not a cytoprotective mechanism. The caution has been taken towards the selection of pharmacological inhibitors as an increase in autophagosomes (suggested by MDC staining) can be resulted from both upsurge of autophagosome formation and/or blockage of autophagosome maturation (lysosomal fusion and degradation). Hence, the selection of inhibitors was based upon these criteria in which the 3-MA inhibits autophagy by blocking autophagosome formation (early stage) while Baf-1 inhibits autolysosome acidification (late stage) in autophagy process.

In the case when autophagy exerts a cytotoxic action, autophagy inhibition may delay or prevent/inhibit cell death. In contrast, cytoprotective autophagy when it is inhibited would promote or accelerate cell death (Clarke and Puyal, 2012). It is

interesting to note that the 3-MA partially prevented the cell death induced by δT3 + 5FU combined treatment in Caco-2 and SW48 cells (Figure 6.18), but not their individual single treatments, suggesting that the formation of autophagosomes is a crucial process in mediating the cell death in δT3 + 5FU combined treatment. Likewise, autophagosomes formation is crucial in mediating the autophagic cell death for both Dox single treatment and δT3 + Dox combined treatment, as evidenced by the abrogated cell death in the presence of 3-MA (Figure 6.18). In fact, this is in agreement with a previous study which reported that blocking autophagosome formation using 3-MA, silencing beclin-1 or Atg-5, had conferred a protective effect in cardiac cells from doxorubicin toxicity (Koleini and Kardami, 2017). Formation of autophagosome may essentially suggest a quarantine of 'survival factors' in the cells, whereas, blocking of this process confers cell survival.

On the other hand, Baf-1 successfully inhibited cell death of Caco-2 and SW48 subjected to δT3 + 5FU and δT3 + Dox combined treatments (Figure 6.19). In these groups, acidification of autolysosome represents another crucial mechanism in mediating the cell death, further supporting the actions of combined treatment in promoting an autophagic cell death. Despite the actual role of autophagic degradation activity is unknown, it can be speculated that degradation of the sequestered 'survival factors' may take place. For instance, it was reported that the autophagic cell death in malignant peripheral nerve sheath tumour induced by tamoxifen was associated to degradation of Kirsten rat sarcoma viral oncogene homolog (pro-survival proteins) (Kohli et al., 2013). In relation to this study, downregulations of Akt and PDK1 may be involved in precipitating cell death; conversely, inhibition of the degradation machinery can then contribute to cell survival. As compared to Caco-2, the δT3 + Dox combined treatment in SW48 did not downregulate PDK1 level as much as the Dox

single treatment, suggesting that the combined treatment is more effective in Caco-2 cells.

The role of autophagy in cancer cell death is gaining research attention, which tamoxifen represents one of the widely investigated clinical drugs. It is commonly being used as a hormonal therapeutic agent to treat estrogen receptor positive breast cancer. In glioblastoma cells, tamoxifen resulted in a concentration-dependent increase of LC3-II and decrease activated Akt levels, while inhibition of autophagy induction successfully blocked cell death (Graham et al., 2016), which demonstrated the presence of autophagic cell death. Current study is conformed to the previous study in which the combined treatments also caused elevated LC3-II and downregulated Akt while blocking autophagic induction via 3-MA and Baf-1 prevented cell death. Through the combination, the autophagy is enhanced, suggesting a potential therapeutic approach to promote colorectal cancer cell death.

6.5 Conclusions

In conclusion, current study confirmed the presence of induced autophagy in single treatments (i.e., δT3, 5FU and Dox) and combined treatments (i.e., δT3 + 5FU and δT3 + Dox) on both Caco-2 and SW48 cells. Notably, the induction of autophagy was faster and/or prolonged in the combined treatments as compared to the single treatments in both cell lines. In the combined treatments, LC3-II expression was upregulated accompanied by downregulations of Akt and PDK1 cell survival proteins. Application of 3-MA and Baf-1 autophagy inhibitors successfully inhibited cell death. These evidences assertively suggested that δT3 + 5FU and δT3 + Dox combined treatments induced autophagic cell death in Caco-2 and SW48 colorectal cancer cells.

Chapter Seven: General Discussion and Conclusions

7.1 Background

The conventional chemotherapeutic drugs generally display poor cancer selectivity and high dose associated toxicities, which have largely limit their efficacy. Ideally, reducing the doses of chemotherapeutic drugs while getting comparable or higher efficacy could be a solution for cancer management. To attempt addressing this issue, tocotrienols could be an attractive counterpart to chemotherapeutic drugs, attributed by the selective cancer killing and multi-targeted anti-cancer actions. In fact, tocotrienols are recommended to be used at low doses in an adjunct treatment (Abubakar et al., 2018; Sylvester et al., 2011; Wali et al., 2009b), to circumvent the saturable uptake and high metabolic degradation in human body. Therefore, it was hypothesised that synergistic combinations of tocotrienols and chemotherapeutic drugs at low loses, could offer an augmented therapeutic efficacy.

A combination treatment is a feasible approach seeks to provide an immediate, effective and affordable solution to cancer. The conceptualisation was based upon attaining a synergy, in which the effect of two or more agents in combination is greater than the expected additive effect of the single agents (Greco et al., 1996). Through a synergistic interaction, lower doses of their respective constituents could potentially be used in a combination, while still granting improved therapeutic effectiveness and reduced adverse reactions.

Therefore, the current research embarked on investigating the feasibility of combining tocotrienols and conventional chemotherapeutic drugs to attain an enhanced therapeutic outcome in cancers. In line with the aspiration, the current works encompassed identification of synergistic combinations, characterisation of the

induced apoptosis, study on the underlying apoptotic mechanisms and validation of an involvement of autophagic cell death.

In Chapter Three, several synergistic combinations were identified through a high-throughput screening based anti-proliferative assay. The combinatorial application of δ-tocotrienol (δT3) and 5-fluorouracil (5FU) or doxorubicin (Dox) at lower concentrations of the respective single agents demonstrated anti-proliferative effects on colorectal cancer cells. Further examination on the clonogenicity showed that the combined treatments exerted cytotoxic, rather than cytostatic effects.

Since the induction of cell death in cancer is playing a pivotal role in shaping successful treatment, characterisation on the induced cell death responses was conducted in Chapter Four. Essentially, the study was initiated by focusing on apoptosis, which is a primary cell death mechanism in cancer therapy. Morphologically, the single and combined treatments demonstrated apoptotic and non-apoptotic morphologies. The observations of nuclear condensation, nuclear fragmentation and membrane blebbing supported the presence of apoptosis. A quantitative analysis of apoptosis further suggested an enhanced apoptosis as compared to the individual single treatments. An enhanced DNA damage was detected in the combined treatments, inferring a heightened apoptosis stimulus.

Guided by the enhancement of apoptosis, the mechanisms of apoptosis were studied in-depth in Chapter Five. Both the intrinsic and extrinsic apoptosis pathways were attempted. Surprisingly, the study suggested an involvement of caspase-dependent as well as caspase-independent cell death. Notably, downregulations of IAPs suggested a chemosensitisation effect of the combined treatments.

Following that, Chapter Six explored an involvement of autophagic cell death as inspirited by the cytoplasmic vacuolation observed (Chapter Three). Interestingly,

the combined treatments triggered an enhanced autophagy as compared to the individual single treatments. Moreover, the autophagic response was found mediating the cell death and thus inferring an involvement of autophagic cell death.

7.2 Synergistic anti-proliferative and cytotoxic effects of the combined treatments

Current study adopted the method from Lowe Additivity (or dose additivity) for identifying synergism in the combined treatment. It is one of the several common models used to measure drugs interaction in pharmacology. To detect synergism, it is of importance to gather the dose-effect data of the individual drugs (Tallarida, 2011). The individual dose-effect data can provide a ground to estimate the expected effect (known as additivity) to benchmark the observed combination effect, whether a synergism (higher than additive effect) or antagonism (lower than additive effect) has occurred. In fact, the Lowe Additivity method has widely been employed in tocotrienol combination studies (Abubakar et al., 2017, 2016; Shirode and Sylvester, 2011, 2010; Steuber et al., 2016; Wali and Sylvester, 2007). These studies have collectively suggested promising anti-proliferative and apoptosis effects via multiple signalling pathways such as NF-κB pathway inhibition (Shirode and Sylvester, 2010; Steuber et al., 2016), MAPK pathway (Wali and Sylvester, 2007) and Akt pathway (Shirode and Sylvester, 2010). In light of these promising studies, the current study is signified conforming to a universal standard for combined treatment approach and captivates an in-depth investigation of the mechanisms of action.

Of note, the "excess over highest single agent" (EOHSA) synergy model is currently adopted by FDA for drug combination approval under the Code of Federal Regulations Title 21 (21 CRF § 300.55). To further illustrate, a combination of fixed

doses can be referred as synergy in EOHSA if the combined treatment is superior to the highest single agent effect at the corresponding concentration (Borisy et al., 2003). Also, the evaluation of the individual effect of the single agents is important to identify changes (possibly improvement) of single treatment over the combined treatment, which is in line with the synergy in EOHSA. As such, the individual concentrations of δT3, 5FU and Dox used in the combinations (Table 3.5) were included in the subsequent experiments. In current study, it has clearly shown that the combined treatments displayed a synergistic cytotoxic effect but not cytostatic effect (Figures 3.10 & 3.11). These findings inferred that the combined treatments could kill the colorectal cancer cells, rather than suppressing the growth of cells, which may lead to recurrence when the treatment is withdrawn.

Collectively, the Lowe Additivity and/or EOHSA have suggested a promising synergy in the two combined treatments of δT3 + 5FU, and δT3 + Dox on Caco-2 and SW48 cells, which warrant further investigations in the subsequent chapters.

7.3 Combined treatments exert a chemotherapeutic drug-driven cell cycle arrest

Apoptosis plays an important role in treatment of cancer because it is a popular target of many treatment strategies (Wong, 2011). In this study, it has been clearly demonstrated that combined treatments resulted in an enhanced apoptosis (Figures 4.14 & 4.15), drug-driven DNA damage(s) (Figures 4.16 – 4.19), a drug-driven cell cycle arrest (Figures 4.20 – 4.23) and DNA fragmentation (Figures 4.24 – 4.27).

The arrests of cell cycle progression were determined by the respective chemotherapeutic drugs, namely S-phase arrest (5FU) and G2/M-phase arrest (Dox), but not a G1-arrest (δT3) in the combined treatments. Intriguingly, this is in fact opposed to two previous δT3 combination studies which demonstrated a single G1

arrest (Yeganehjoo et al., 2017) and dual arrests at G1 and G2/M (Sato et al., 2017). In fact, the synergistic interactions between tocotrienols and chemotherapeutic drugs can be explained by their potential synergistic interactions proposed by Boik (2001) as illustrated in Figure 7.1. A concurrent inhibition would have resulted if both agents exert at the same cell cycle checkpoint. For example, a combination of δT3 and geranylgeraniol combined treatment showed an enhanced arrest at G1 on prostate cancer cells (Yeganehjoo et al., 2017), postulating a concurrent inhibition has taken place. On the other hand, if concerted cell cycle arrest has taken place, the cell cycle profiles should demonstrate a simultaneous arrest. For instance, it was reported that combination of δT3 and γ-tocopherol caused a simultaneous increase of G1 and G2/M arrest after 24 hours on prostate cancer cells (Sato et al., 2017), suggesting a concerted inhibition in this scenario. Based on the current results, it is clearly demonstrated that the S and G2/M arrests of chemotherapeutic drugs occurred at 24 hours post treatment, were dominant and more rapid over the effect of δT3 (G1 arrest at 48 hours in Caco-2 cells), proposing a sequential action in the cell cycle arrest. The sequential inhibition of cell cycle progression is believed has taken place which the chemotherapeutic drugs arrested most of the colorectal cancer cells, while δT3's action was delayed. Collectively, this proposal suggests that the combined treatments with δT3 may render a differential perturbation in the cell cycle, vary across cancer types and are influenced by the single agents incorporated in the combination.

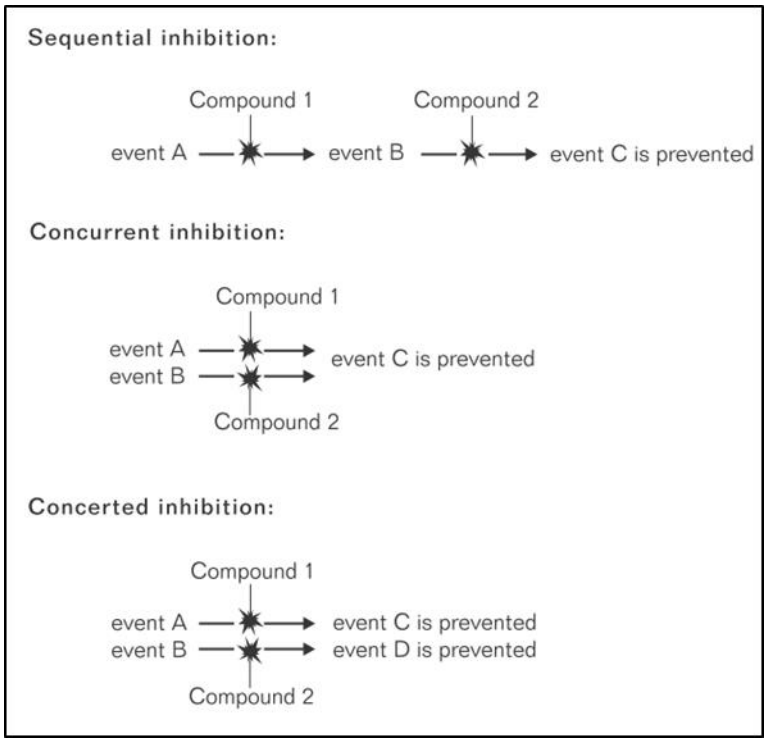

Figure 7.1 Three examples of potential synergistic interactions. Sequential inhibition can be achieved if two compounds act on a linear sequence of events to inhibit cell proliferation (event C). Meanwhile, concurrent inhibition describes two compounds that inhibit two parallel events that simultaneously impede an important event for the cell proliferation. On the other hand, concerted inhibition happens when two compounds inhibit two parallel events, resulting in inhibition of two separate events that are responsible for cell proliferation (Boik, 2001).

Targeting cell cycle checkpoints (e.g., G1, S or G2/M) in cancer can be regarded as an important strategy (Visconti et al., 2016). In response to DNA damage, sensor proteins within the cells detect the damages and signal the downstream effectors, leading to cell cycle arrest and promote repair. The DNA damage triggered in S- and G2/M-phase is likely to be sensed by Ataxia Telangiectasia and Rad3-related (ATR) kinase that activate Checkpoint Kinase 1 (Chk1) (Xiao et al., 2003), contrasting to G1-phase that requires Ataxia Telangiectasia Mutated (ATM) kinase that activates Checkpoint Kinase 2 (Chk2) (Matsuoka et al., 1998). Of note, the G1 checkpoint is critically dependent on p53 (Visconti et al., 2016) while targeting S- and G2/M does not necessarily require a wide type p53 (Arita et al., 1997; Concin et al., 2003). Given

that p53 mutation is common in colorectal cancer, which constitutes about 34% of proximal tumours and 45% of distal tumours (Russo et al., 2005), targeting S- and G2/M phases suggest a p53-independent approach which is more versatile for cancer treatments.

In addition, it appears that the tocotrienol-induced G1 arrest in combined treatment is associated with cytostatic effect. It was previously reported that the synergistic anti-proliferative effect of combined treatments of γT3 and sesamin, statins or tyrosine kinase inhibitors resulted in G1 arrest can neither induce apoptosis nor decrease in cell viability mammary cancer cell lines (Akl et al., 2013; Wali et al., 2009b; Wali and Sylvester, 2007). Hence, the authors concluded that a cytostatic but not cytotoxic effect was resulted. On the contrary, apparent S-phase and G2/M phase induced by the δT3 + 5FU and δT3 + Dox combined treatments respectively, which therefore consensually agreeable to the cytotoxic and apoptotic effects detected in the current study.

7.4 Combined treatments downregulate the inhibitors of apoptosis (IAPs) proteins - a potential chemosensitisation effect

Guided by morphological and biochemical confirmations on apoptosis, Chapter Five studied the underlying apoptosis mechanisms of the combined treatments on Caco-2 and SW48 cells. The δT3 + 5FU combined treatment showed a reduction of IAPs (e.g., survivin, cIAP1, cIAP2, XIAP) in Caco-2 cells (Figure 5.3), suggesting a chemosensitisation effect. For instance, a previous study demonstrated that the downregulation of XIAP led to an enhanced chemosensitivity in human gastric cancer cells (Tong et al., 2005). Additionally, it was previously reported that an overexpression of cIAP2 contributed to 5FU resistance of oral cancer cells (Nagata et

al., 2011); while a downregulation of cIAP2 effectively enhanced the sensitivity of 5FU-resistant DLD-1 colon cancer cells and activation of caspase 3/7 for apoptosis (Karasawa et al., 2009).

On the other hand, overexpression of survivin was evident in Dox-resistant osteosarcoma; an addition of the survivin suppressant YM155 reversed Dox resistance via promoting the elevated caspase-8, -9 and -3 activities (Zhang et al., 2015). Correspondingly in the current study, the combined treatments resulted in the downregulation of IAPs (Figures 5.19 – 5.22) accompanied by upregulation of caspase-3 activity (Figure 5.18) and enhancement of apoptosis (Figures 4.14 & 4.15), all these observations exemplify a chemosenstisation effect through apoptosis.

Notably, the current study revealed a higher basal expression of IAP proteins in SW48 cells than that of Caco-2 cells (Figures 5.19 & 5.20). This phenomenon could potentially be explained by the role of IAP proteins in malignancy progression (LaCasse et al., 1998), as SW48 cell line is comparably more invasive (Broder's Grade IV) than Caco-2 cell line (Broder's Grade II) (see Appendix: Figure A7.1). Previous studies showed that XIAP, livin and cIAP were associated to colorectal tumour progression (Myung et al., 2013; Paschall et al., 2014; Takeuchi et al., 2005), resulting in increased motility and reduced apoptosis. These studies have therefore highlighted an opportunity of targeting IAP proteins for colorectal cancer. The capability of δT3 + 5FU and δT3 + Dox combined treatments in downregulating IAP proteins expression identified in this study may represent an attractive therapeutic approach in colorectal cancer cells, which could block cancer progression.

In addition, a previous study found that 25μM of γT3 and 20μM of capecitabine combined treatment downregulated cIAP1, cIAP2 and survivin in HCT116 colon cancer cells (Prasad et al., 2016). In the current study, lower

concentrations of the combined treatment were used in Caco-2 (i.e., 10μM δT3 + 3.5 μM 5FU or 2μM Dox) and SW48 (i.e., 10μM δT3 + 18μM 5FU or 1μM Dox) to attain a similar outcome. Therefore, the current combined treatments may suggest promising therapeutic interventions for colorectal cancer management.

7.5 Combined treatments activate apoptosis and caspase-independent cell death

In current study, the combined treatments resulted in significantly higher caspase-3/7 activation (Figure 5.18), which is correlated well to the increased apoptosis detected in Chapter Four (Figures 4.14 & 4.15). A further study revealed that the caspase-3 activation could be mediated by caspase-8 (initiator caspase of the extrinsic pathway) in both Caco-2 and SW48 cell lines, and caspase-9 (initiator caspase of the intrinsic pathway) in Caco-2 cells only. Intriguingly, except for δT3 + 5FU combined treatment on SW48 cells, cell death of other combinations could not be blocked by caspase-8, caspase-3 or pan-caspase inhibitors despite clear evidences of caspase-8 and caspase-3 cleavage (activation) were detected. The resultant differential responses therefore suggested a combination- and cell line-specific effects as tabulated in Table 7.1.

In combination group ①, application of caspase-3 and pan-caspase inhibitors successfully prevented cell death, demonstrating a dependency of caspase in executing apoptosis (Table 7.1). In other combination groups (② - ④), caspase-3 and pan-caspase inhibitors were unable to prevent cell death. Hence, it is therefore plausible to speculate that the caspase-dependent apoptosis may not be the sole pathway to provoke the cell death.

Additionally, blockade of mitochondrial permeability transition pore (MPTP) by cyclosporine A successfully inhibited cell death, suggesting that mitochondrial

permeability transition is a crucial event in determining apoptosis induced by the combined treatments (Figure 5.34). An increase in Bax and/or a decrease in Bcl-2 protein levels suggest an occurrence of MOMP. Current study rules out the possibility that the MOMP was mediated by the upstream caspase-8 activation (via Bid), by which otherwise could be blocked by caspase-8 inhibition. Hence, MOMP should be independently triggered in response to the apoptotic cues. In addition, the occurrence of MOMP without a significant caspase-9 activation supported an engagement of caspase-independent cell death (CICD).

Table 7.1 Combination- and cell line-specific effects in apoptosis.

Combined treatments	δT3 + 5FU		δT3 + Dox	
Cell line/ (Combination group)	SW48 (①)	Caco-2 (②)	Caco-2 (③)	SW48 (④)
Caspase activations	Caspase-8 Caspase-3	Caspase-8 Caspase-9 Caspase-3	Caspase-8 Caspase-9 Caspase-3	Caspase-8 Caspase-3
Caspase inhibitor that blocked cell death	Caspase-3 Pan-caspase	-	-	-
Non-caspase inhibitor that blocked cell death	Cyclosporine A	Cyclosporine A	Cyclosporine A	Cyclosporine A
Conclusion	Apoptosis confirmed	Presence of additional cell death mechanism	Presence of additional cell death mechanism	Presence of additional cell death mechanism

CICD is defined as a cell death modality that ensues when apoptotic signal fails to activate caspases (Tait and Green, 2008). However, CICD does share common characteristics with apoptotic cell death, including MOMP, which is an upstream

signalling that takes place for both forms of cell death. Commencement of MOMP leads to the release of a wide array of mitochondrial intermembrane space proteins such as second mitochondria-derived activator of caspase/direct inhibitor of apoptosis-binding protein with low pI (Smac/Diablo), cytochrome *c*, high temperature requirement protein A2/Omi serine protease (HtrA2/Omi), apoptosis inducing factor (AIF) and endonuclease G (EndoG) (see Figure 7.2); these proteins may redundantly constitute both the caspase-dependent or independent cell death (Lorenzo and Susin, 2004).

Although the definite pathway is currently still unknown, special attention may be devoted to endoplasmic reticulum (ER) stress-mediated apoptosis. The ER stress-mediated apoptosis has been proposed to lie upstream mitochondria, and may engage MOMP as a central amplification step to precipitate both caspase-mediated apoptotic pathway and caspase-independent cell death in the situation where caspase activation is insufficient (Gupta et al., 2010). As a result, both caspase-dependent and caspase-independent pathways are activated in parallel upon MOMP (Kögel and Prehn, 2013). When caspase is inhibited, CICD mechanism can sufficiently induce cell death, albeit in a slower or less effective manner (Kögel and Prehn, 2013). Based on the data gathered from the current study, it is speculated that the combined treatments trigger both caspase-dependent apoptosis and CICD; while blocking of caspase has further shifted the reliance toward CICD.

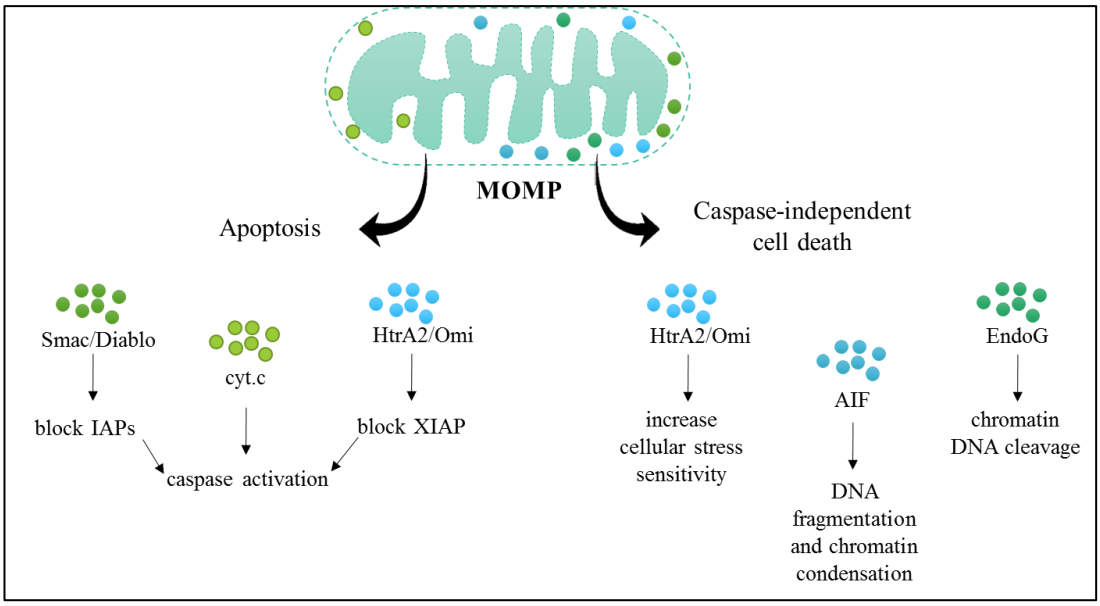

Figure 7.2 Illustrative diagram of apoptosis and caspase-independent cell death at post MOMP. MOMP, mitochondrial outer membrane permeabilisation; Smac/Diablo, Second mitochondria-derived activator of caspase/direct inhibitor of apoptosis-binding protein with low pI; cyt.c, cytochrome *c*; HtrA2/Omi, high temperature requirement protein A2/Omi serine protease; AIF, apoptosis inducing factor; EndoG, endonuclease G.

From this study, the single treatments inferred that δT3 targets mitochondria, not the chemotherapeutic drugs (Figures 5.9 - 5.12). In fact, several events induced by tocotrienols also suggested a potential CICD [Zhang et al. (2013) referred them as caspase-independent programmed cell death, CI-PCD] including a caspase-independent DNA damage (Constantinou et al., 2012), disruption of mitochondria-independent apoptosis markers (Takahashi and Loo, 2004) and autophagy (Jiang et al., 2012; Rickmann et al., 2007). These extra-apoptosis events have correspondingly agreed to the proposed CICD mediated by δT3 in colorectal cancer cells. It was suggested in a separate study that elimination of colorectal cancer via CICD could be a better alternative to apoptosis, because CICD will trigger anti-tumourigenic immune activation to eliminate cancer more effectively (Giampazolias et al., 2017). Current study represents the first study reporting on δT3 + 5FU and δT3 + Dox combined

treatments with the involvement of CICD, may potentially lead to securing better benefits in colorectal cancer treatment.

Based upon the evidence gathered in the current study, an integrated overview of apoptosis and caspase-independent cell death mechanisms of single and combined treatments are illustrated (Figures 7.2 – 7.5). As shown in Figure 7.3, 5FU dominantly induced S-phase arrest and activated caspase-8 of the extrinsic pathway, which may probably execute through a TNF superfamily receptor and caused the caspase-3 activation. Whereas, δT3 dominantly induced mitochondrial membrane permeabilisation (MMP) (Figure 7.3). The δT3 + 5FU combined treatment induced S-phase arrest, activated caspase-8, and caused MMP on Caco-2 and SW48 cells (Figure 7.4). Notably, there was a slight caspase-9 activation (intrinsic pathway) evident in the combined treatments (Caco-2 cells only) (Figure 7.4). On the other hand, Dox single treatment induced G2/M arrest and activated caspase-8, while δT3 primarily targeted the mitochondria (Figure 7.5). As shown in Figure 7.6, δT3 + Dox combined treatment caused G2/M arrest, caspase-8 activation and MMP, with a slight increment of caspase-9 activity (Caco-2 cells only), but enhanced caspase-3 activation in both cell lines.

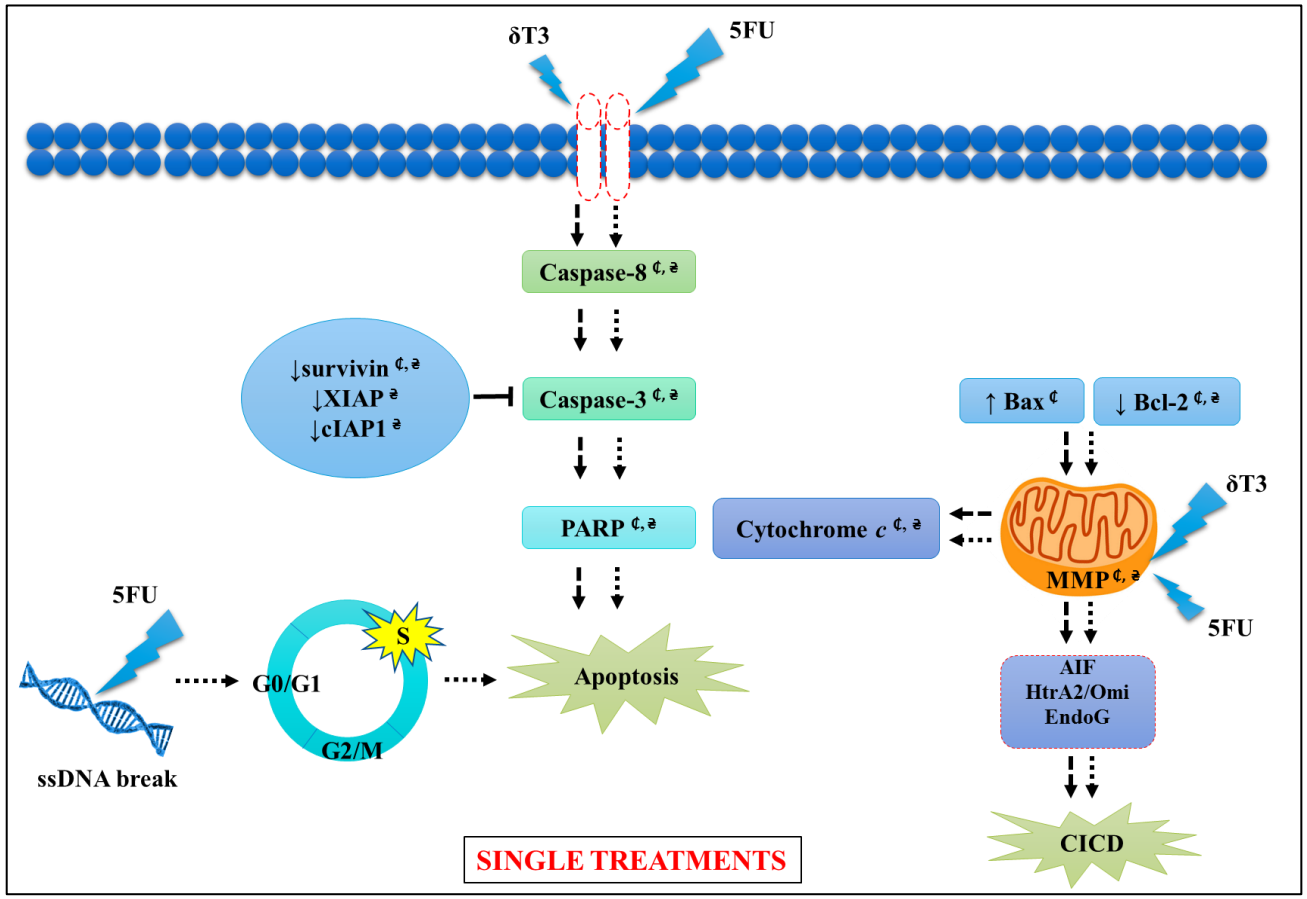

Figure 7.3 Illustrative diagram of apoptosis pathway that is triggered by δT3 and 5FU single treatments. δT3, δ-tocotrienol (➡); 5FU, 5-fluorouracil (⇢); MMP, mitochondrial membrane permeabilisation; CICD, caspase-independent cell death. Dashed red-line box suggests potential involvement. ¢ Caco-2; ƨ SW48.

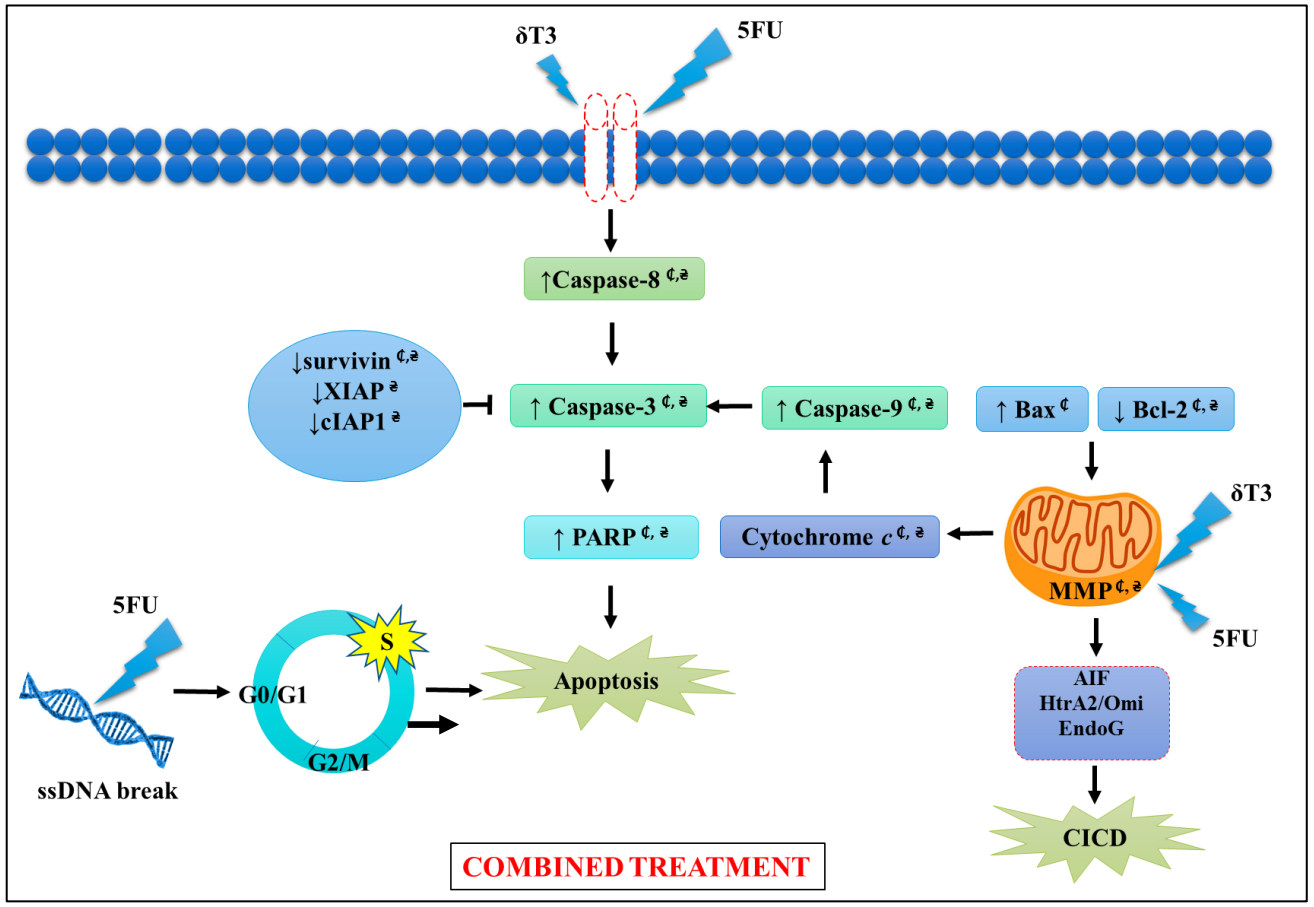

Figure 7.4 Illustrative diagram of apoptosis pathway that is triggered by δT3 + 5FU combined treatment. δT3, δ-tocotrienol; 5FU, 5-fluorouracil; MMP, mitochondrial membrane permeabilisation; CICD, caspase-independent cell death. Dashed red-line box suggests potential involvement. ¢ Caco-2; ₴ SW48.

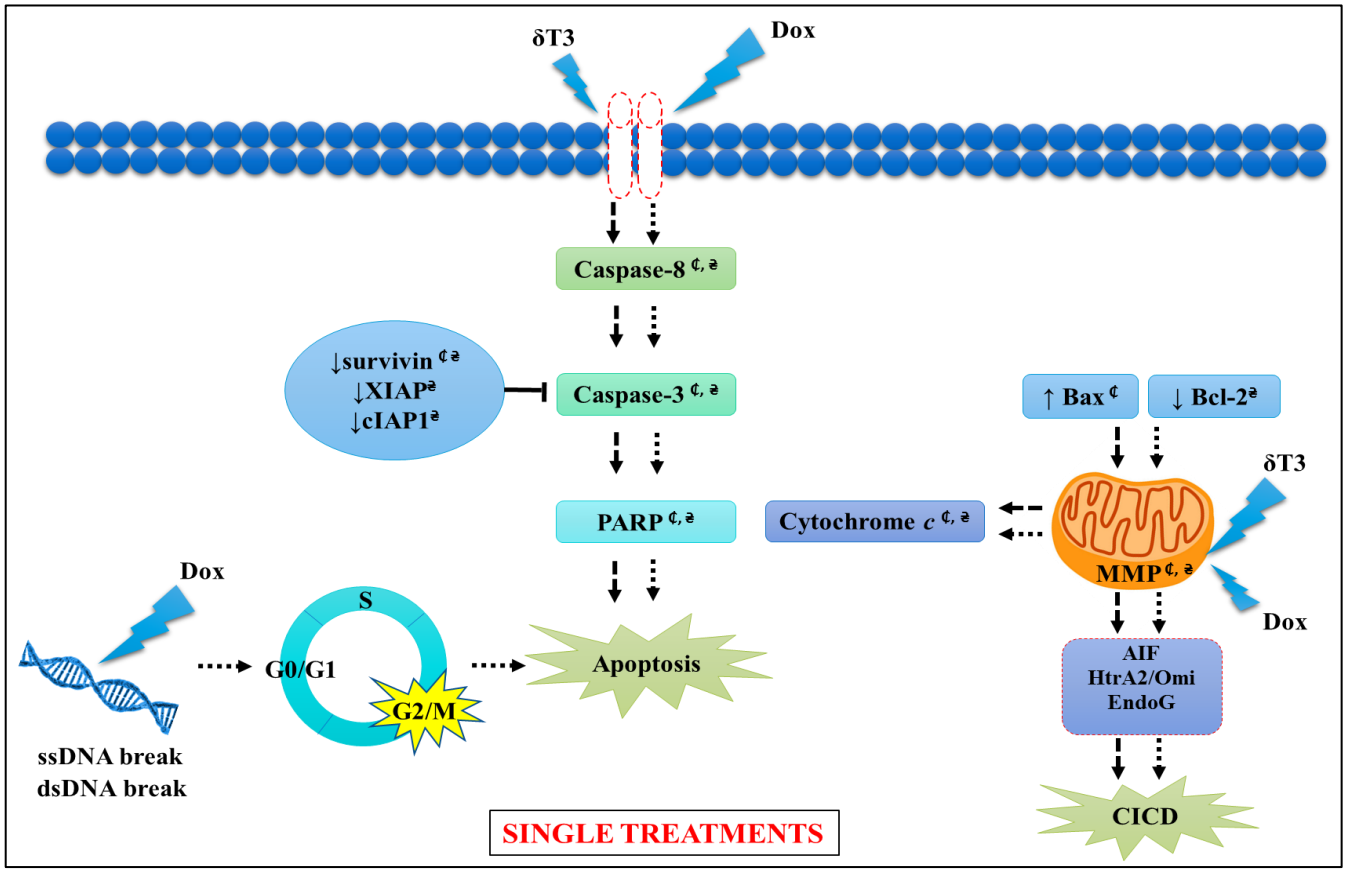

Figure 7.5 Illustrative diagram of apoptosis pathway that is triggered by δT3 and Dox single treatments. δT3, δ-tocotrienol (➡); Dox, doxorubicin (⇢); MMP, mitochondrial membrane permeabilisation; CICD, caspase-independent cell death. Dashed red-line box suggests potential involvement. ¢ Caco-2; ₴ SW48.

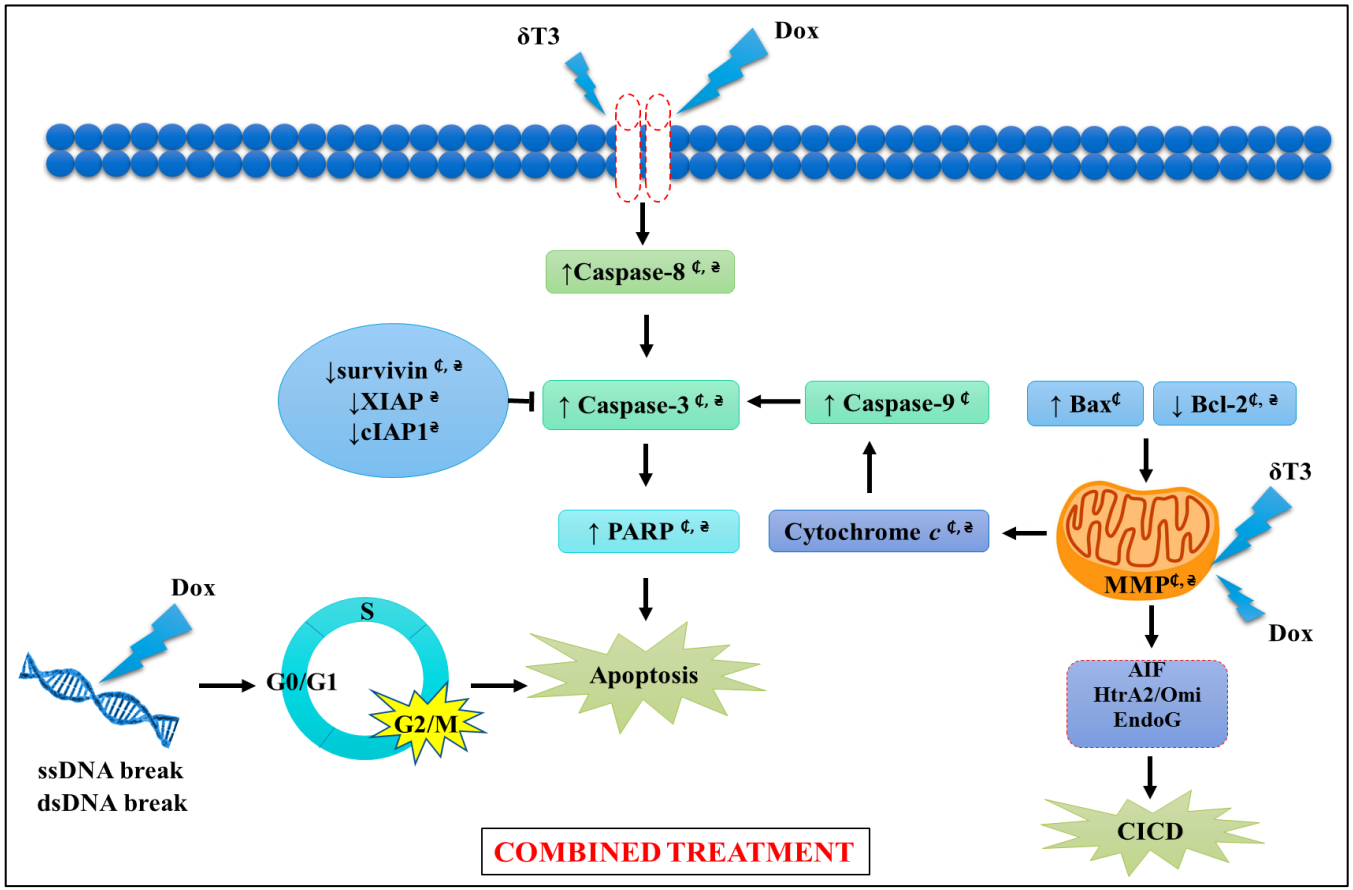

Figure 7.6 Illustrative diagram of apoptosis pathway that is triggered by δT3 + Dox combined treatment. δT3, δ-tocotrienol; Dox, doxorubicin; MMP, mitochondrial membrane permeabilisation; CICD, caspase-independent cell death. Dashed red-line box suggests potential involvement.[¢] Caco-2; [₴] SW48

7.6 Combined treatments induce an autophagic cell death

The autophagy induced by δT3, 5FU and Dox single treatments appeared controversial in terms of promoting cancer cell survival versus cell death. For instance, δT3-induced autophagy in rat pancreatic stellate cells (Rickmann et al., 2007) and prostate cancer cells (Fontana et al., 2019) were reported to participate in cell death. For 5FU, the autophagy induced appeared to confer cancer protection as an inhibition of 5FU-induced autophagy enhanced cell death (Li et al., 2010; Schonewolf et al., 2014). Another report shed light on potential anti-cancer role of autophagy as inhibition of autophagy could lead to resistance development in colorectal cancer cells (Yao et al., 2017), whereas the induction of autophagy facilitated the anti-cancer effect of 5FU (Yang et al., 2018). On the contrary, Dox-induced autophagy appeared to confer survival protection in breast cancer, osteosarcoma, hepatocellular carcinoma and neuroblastoma cells (Chen et al., 2018; Cosan et al., 2010), but none has reported on autophagy function in colorectal cancer type. Given that no study had been performed on the effect of autophagy in the combined treatments, the role of autophagy induced by δT3 + 5FU and δT3 + Dox underline the gap to be answered in this study.

In this study, the presence of autophagy induced by the single and combined treatments on Caco-2 and SW48 cells was clearly demonstrated in AO (Figures 6.3 - 6.6) and MDC (Figure 6.8Figures 6.8 & 6.9) profiles. Notably, the combined treatments showed an enhanced autophagy as supported by a time-dependent increase of LC3-II level, suggesting an accumulation of autophagosomes, which was consistent with AO and MDC profiles. Current study is conformed to several previous studies that demonstrated an induction of autophagy by tocotrienols. For instance, γT3 at

10μM resulted in an elevation of LC3-II, demonstrating an induction of autophagy in both PC-3 and LNCaP prostate cancer cells (Jiang et al., 2012). In addition, autophagy induction was also reported in γT3-treated breast cancer cells with an evidence of increased LC3-II (Sylvester and Tiwari, 2016). δT3 also triggered autophagy in PC3 prostate cancer cells as evidenced by the augmented LC3-II (Fontana et al., 2019). Herein, this is the first report of showing the ability of δT3 single treatment and combined treatments (δT3 + 5FU and δT3 + Dox) for promoting autophagy on colorectal cancer cells.

According to the recommendation from NCCD, autophagic cell death involves an autophagy process that constitutes a lethal function in that cell death can be prevented by a genetic or pharmacological inhibition (Galluzzi et al., 2018). Pertaining to the guideline, the presence of 3-MA (early stage autophagy inhibitor) and Baf-1 (late stage autophagy inhibitor) successfully inhibited cell death of the combined treatments (Figures 6.18 & 6.19), firmly suggests an involvement of autophagic cell death.

In fact, the role of autophagy in cell death, in which 'cell death with autophagy' and 'cell death by autophagy' are still currently under debate in the scientific community. The former indicates an auxiliary role of autophagy before or during the actual cell death (e.g., apoptosis) while the latter suggests a sole dependence of autophagy to initiate or execute the cell death (Kroemer and Levine, 2008). The authors argued that autophagic cell death is mostly 'overclaimed' when inhibition of autophagy cannot completely block or rescue the cell death, and autophagy does not involve as a sole perpetrator but is compliance with other cell death modalities (Kroemer and Levine, 2008). However, another line of argument explained that autophagic cell death can be 'underappreciated' when autophagy is restricted to a

direct connection to cell death (Yonekawa and Thorburn, 2013). Clarke and Puval (2012) also suggested that identification of 'pure' autophagic cell death as a distinct cell death modality independent from apoptosis and necrosis may not happen. An autophagy that triggers apoptosis or necrosis, or occurs parallel with them should be recognised as autophagic cell death if there is a clear connection to cell death (Clarke and Puyal, 2012). In addition, the authors argued that 'pure' autophagic cell death may not exist in rapidly dividing cancer cells due to the underlying genetic defects (Clarke and Puyal, 2012). In the light of this argument, current study represents an additional line of evidence supporting the occurrence of autophagic cell death based on the fact that autophagy is mediating the cell death, not cell survival. Hence, it is reasonable to suggest that autophagic cell death should be valued as a cell death mechanism although more evidences are still needed to elucidate their underlying actions in shaping the putative demise of cancer cells in the future.

7.7 Connection of autophagy with apoptosis - linking now to beyond

In this study, the activations of apoptosis (Chapter Five) and autophagy (Chapter Six) induced by the combined treatments were confirmed. Temporal expressions of caspase-3 (responsible for apoptosis) and LC3-II (responsible for autophagy) were investigated. To illustrate at higher clarity, the evidence has been shown in Table 7.2. Based on the observations, two speculations are derived, namely sequential and concurrent actions.

In combination group ①, the increment level of cleaved caspase-3 (active) was the highest after receiving the 24-hour combined treatments, while LC3-II reached the highest slightly later, i.e., after 48 hours SW48 cells, suggesting an apoptosis activity followed by autophagy (Table 7.2). This could also infer a sequential action

between these two pathways (as illustrated in Figure 7.7 A). Conversely, a similar temporal pattern of apoptosis and autophagy is demonstrated in the combination group ② - ④ (Table 7.2), suggesting a concomitance of the two pathways as depicted in Figure 7.7 B.

To date, the connection between apoptosis and autophagy has yet been fully deduced. Generally, review papers highlighted two potential connections between apoptosis and autophagy, in which i) autophagy precedes apoptosis and ii) autophagy inhibits apoptosis (Fan and Zong, 2013; Gump and Thorburn, 2011; Mariño et al., 2014; Thorburn, 2008). In the first proposal (i), autophagy comes in as a stress regulatory mechanism, in which an autophagy is immense stress triggers apoptosis. However, current study appears suggesting a reverse of the proposal (i). In this study, δT3 + 5FU combined treatment appeared to culminate in apoptosis before the autophagy in SW48 cells. Potentially, a fraction of the cells is sensitised towards (caspase-3 dependent) apoptosis; whereas the left-over cell population is subjected to autophagic cell death. A differential response might be a possible explanation for the sequential action proposed, in which apoptosis may commence ahead of autophagy. This proposal is correspondingly agreed and supported by the successful suppression of cell death via caspase inhibitions in combination group ① (Table 7.2). However, the specific mechanism remains elusive.

Table 7.2 Potential actions of apoptosis and autophagy based upon temporal expressions of LC3-II and cleaved caspase-3.

Combination group	Cell line	Treatment	Kinetics of protein expressions (hours) 0 4 8 12 24 48 72	Speculation
①	SW48	δT3 + 5FU	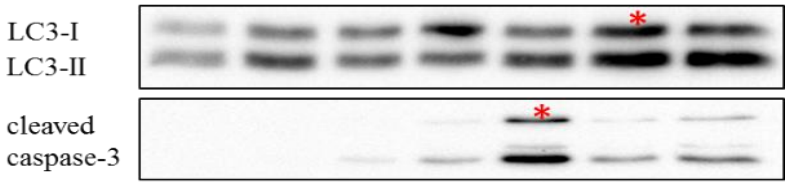	Sequential action
②	Caco-2	δT3 + 5FU	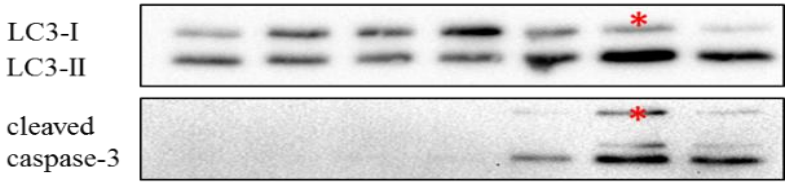	Concurrent action
③	Caco-2	δT3 + Dox	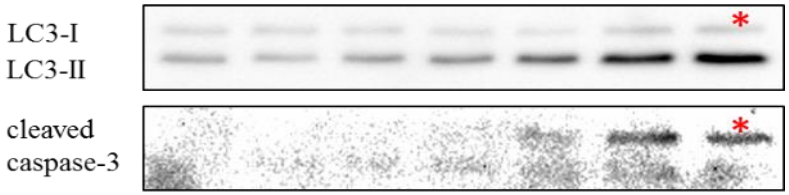	
④	SW48	δT3 + Dox	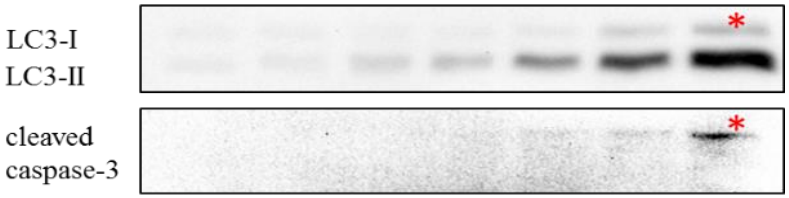	

Note: * marked the time point with the highest protein expression.

In relation to the second proposal (ii), autophagy steps in as a recovery mechanism to prevent unnecessary apoptosis. As a result, inhibition of autophagy often leads to heightened apoptosis as suggested by many previous studies (Liu et al., 2015; Schonewolf et al., 2014; Shin et al., 2012; Tran et al., 2015). The concurrent action of apoptosis and autophagy is in fact opposed to the canonical/paradoxical view on mutually exclusive relationship between apoptosis and autophagy, as stated in proposal (ii). It was proposed that autophagy and apoptosis are not always mutually exclusive and may even occur simultaneously in the same cell type (Ryter et al., 2014). Current results are in fact conformed to the growing body of evidence on concomitant induction of apoptosis and autophagy (Cao et al., 2017; Jeon et al., 2011; Jiang et al., 2012; Zhang et al., 2018) that contributes to an enhanced cell death in cancer. Another recent study reported oxyresveratrol could activate apoptosis and autophagic cell death pathways in neuroblastoma independently and in parallel as opposing to the proposal (ii). Collectively, current study provides an additional line of evidence on parallel and non-exclusive relationships on apoptosis and autophagy.

However, other differential factors underlying Caco-2 and SW48 should also be taken into consideration for future studies, including p53 status and malignancy grade of the cell lines. In fact, Caco-2 carries a mutant p53 tumour suppressor status (see Appendix: Figure A5.1) and classified as Grade II malignancy (see Appendix: Figure A7.1). On the other hand, SW48 has a wild-type p53 and classified as Grade IV malignancy. Additionally, the presence of CICD should also be taken into the consideration when delineating the integrated mechanistic connection of apoptosis and autophagy. These factors may partly if not all affect the differential responses toward autophagy and apoptosis in the combined treatments, which indeed warrant future investigations.

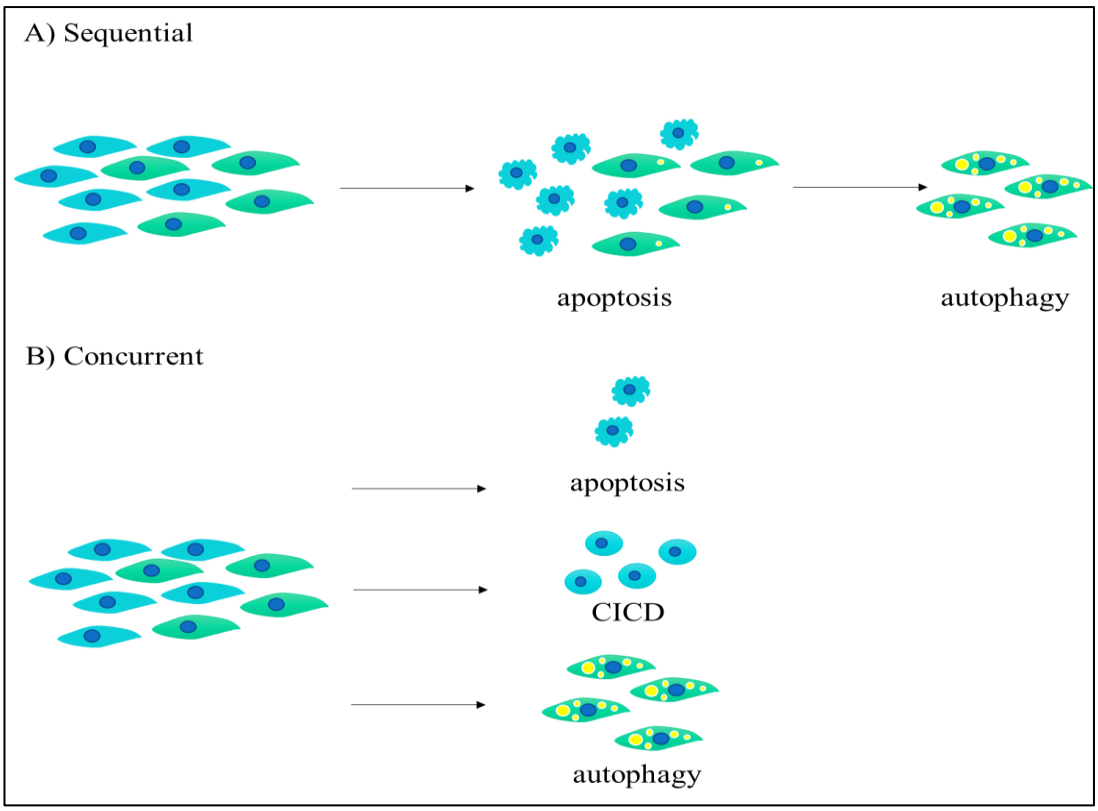

Figure 7.7 Schematic diagrams of proposed cell death actions of the combined treatments. A, sequential action of apoptosis, followed by autophagy. B, concurrent action of apoptosis, caspase-independent cell death (CICD) and autophagy.

Collectively, current study suggests multi-targeted actions of δT3 + 5FU and δT3 + Dox combined treatments, including apoptosis, CICD, and autophagic cell death. Since cancers may acquire cumulative mutations leading to defect(s) in diverse cell death pathways, the multi-targeted actions offer alternative pathways to target cancer more effectively. Combined treatments could possibly offer a therapeutic advantage for reducing the risk of drug resistance development. *In vivo*, inter-tumour and intra-tumour heterogeneity often lead to differential therapeutic responsiveness in cancer (Fisher et al., 2013). The combined treatments identified in current study could possibly target both susceptible and resistant tumour populations (toward cell death), rendering a more effective killing of cancer cells.

7.8 Limitations of current study and recommendations for future investigations

In fact, *in vitro* cell culture model is a rapid and cost-effective platform in cancer drug discovery. Essentially, it enables a high-throughput screening to identify the potential drug combinations and key mechanisms. Despite clear *in vitro* evidences on improved cancer selectivity, enhanced apoptosis and autophagic cell death obtained in the combined treatments, the current study model is lacking interactions with extracellular matrix. Hence, *in vivo* testing using small animals like a mouse model should be considered in the future to study the toxicological and pharmacokinetic profiles of the combined treatments. As such, the research outcomes could accelerate the translation from the bench into clinical application.

In this study, caspase-3 activation and increased in apoptotic cells population have confirmed the caspase-dependent apoptosis involvement in the combined treatments. While major focus has been devoted to the caspase-dependent apoptosis in the present study, the involvement of caspase-independent cell death (CICD) in fact deserves further research attention. Particularly, the effects of the combinations on other mitochondrial effectors in the mitochondrial intermembrane space, such as AIF, Smac/Diablo, HtrA2/Omi and EndoG should be investigated to provide a direct evidence on the engagement of CICD.

It had been confirmed in this study that autophagic cell death was remarkably induced by the combined treatments, concomitantly with apoptosis and CICD. Future investigation of the underlying mechanistic connections should be conducted. In addition, the potential interactions of apoptosis, CICD and autophagy (i.e., sequential, concurrent or concerted) using genetic silencing technologies (after identifying the molecules at the crossroad) could be performed in order to provide an integrated understanding of the pathways in the future.

Besides, encapsulating the combined treatments in nanomedicine using a nano drug delivery platform appears to offer manifold benefits owing to the fact that tocotrienol-based nanoformulation has been proven effective. For instance, PEGlyted of tocotrienol was reported to improve oral bioavailability (Abu-Fayyad et al., 2015). A conjugation of the nanomedicine to a tumour-targeted ligand improved the cancer selectivity while leaving normal cells unharmed (Fu et al., 2009). It was reported that entrapping tocotrienols in transferrin-bearing vesicles showed 3-fold higher uptake and 100-fold higher cytotoxicity *in vitro*. The same study also showed that the tocotrienol entrapment led to improved survival and tumour regression *in vivo* (Fu et al., 2009). Alternatively, a controlled-release nanomedicine which could release the desired amount of drugs over a prolonged period may further improve therapeutic efficacy while minimising the impact on the normal cells. It was previously reported that the controlled release of 5FU and Dox exhibited greater cytotoxicity and selectivity toward cancer cells in comparison to the free drugs (Mo et al., 2015; Nair et al., 2011). Hence, formulating the combinations into nanomedicine appears as a viable approach to unleash the therapeutic potential of the current combined treatments.

7.9 Conclusions

Current study identified the synergistic anti-proliferative and/or cytotoxic combinations on Caco-2 and SW48 colorectal cancer cells, comprising δT3 and 5FU or Dox. The IC_{50} of 5-fluorouracil (a first line chemotherapeutic drug for colorectal cancer), was successfully reduced by approximately 16 and 4 folds in combined treatments on Caco-2 and SW48 cells respectively, suggesting a lower toxicity could be resulted without compromising the therapeutic effectiveness.

Mechanistically, δT3 + 5FU combined treatment resulted in single-stranded DNA break, leading to S-phase cell cycle arrest. On the other hand, δT3 + Dox combined treatment caused single- and double-stranded DNA breaks, leading to G2/M phase arrest. All combined treatments under the study resulted in enhanced apoptosis and DNA fragmentation as compared to the individual single agent treatments.

Additionally, downregulations of IAPs such as survivin, XIAP, and cIAP1 further and enhanced caspase-3 activation suggest a chemosenstisation effect of the combinations. The combined treatments resulted in caspase-8 activation, signifying an engagement of the extrinsic apoptosis pathway. However, except for δT3 + 5FU combined treatment on SW48 cells, the cell death in three other combinations were unable to be prevented by caspase-3 and pan-caspase inhibitors, suggesting additional cell death pathway was involved. Interestingly, ΔΨm disruption had occurred without a significant activation of caspase-9; an inhibition of ΔΨm disruption using cyclosporine A successfully restored cell viability. These data collectively propose a co-activation of caspase-dependent and caspase-independent cell death.

The combined treatments also exhibited an enhanced autophagy. Inhibition of autophagy with 3-MA (early autophagy inhibitor) and Baf-1 (late autophagy inhibitor) improved viability of Caco-2 and SW48 cells. Of note, downregulations of Akt and PDK1 survival-associated proteins were observed. Undeniably, the autophagic cell death induced by the combined treatments has been confirmed.

Collectively, current study represents the first of its kind to understand the combinatorial application of δT3 and 5FU or Dox on colorectal cancer cells. Undeniably, these novel drug combinations have contributed to the advancement of research knowledge in colorectal cancer treatment, despite numerous questions are still awaiting answers. The research outcomes generated from current study have

suggested the potential applications of δT3 + 5FU and δT3 + Dox combined treatments to attain an augmented cancer cell death via multi-targeted actions, which demonstrate a promising and new treatment option for colorectal cancer in the future.

References

Abbas, Z., Rehman, S., 2018. An overview of cancer treatment modalities. In: Hafiz Naveed Shahzad (Ed.), Neoplasm. InTech.

Abbasi, S., Janmaleki, M., Moghadam, M.K., Abdolahad, M., Mohajerzadah, S., Peirovi, H., 2012. Detection of different grade of cancerous cell regarding their impedance. In: Mian, L. (Ed.), World Congress on Medical Physics and Biomedical Engineering. Springer Berlin Heidelberg, pp. 1416–1419.

Abdul-Hafid, S.R., Chakravarthi, S., Nesaretnam, K., Radhakrishnan, A.K., 2013. Tocotrienol-adjuvanted dendritic cells inhibit tumor growth and metastasis: A murine model of breast cancer. PLoS One 8, e74753.

Abdul-Manan, A., Ibrahim-Tamin, N.S., Abdullah, N.H., Zainal-Abidin, A., Wahab, M., 2016. Malaysian National Cancer Registry Report 2007-2011, Ministry of Health Malaysia. Kuala Lumpur.

Abdul-Rahman, A., Jamal, A.R.A., Harun, R., Mohd-Mokhtar, N., Wan-Ngah, W.Z., 2014. Gamma-tocotrienol and hydroxy-chavicol synergistically inhibits growth and induces apoptosis of human glioma cells. BMC Complement. Altern. Med. 14, doi: 10.1186/1472-6882-14-213.

Abe, C., Uchida, T., Ohta, M., Ichikawa, T., Yamashita, K., Ikeda, S., 2007. Cytochrome P450-Dependent Metabolism of Vitamin E Isoforms is a Critical Determinant of Their Tissue Concentrations in Rats. Lipids 42, 637–645.

Abu-Fayyad, A., Behery, F., Sallam, A.A., Alqahtani, S., Ebrahim, H., El Sayed, K.A., Kaddoumi, A., Sylvester, P.W., Carroll, J.L., Cardelli, J.A., Nazzal, S., 2015. PEGylated γ-tocotrienol isomer of vitamin E: Synthesis, characterization, in vitro cytotoxicity, and oral bioavailability. Eur. J. Pharm. Biopharm. 96, 185–195.

Abu-Hassan, M.R., Ismail, I., Mohd-Suan, M.A., Ahmad, F., Wan-Khazim, W.K., Othman, Z., Mat-Said, R., Tan, W.L., Mohammed, S.R.N.S., Soelar, S.A., Nik-Mustapha, N.R., 2016. Incidence and mortality rates of colorectal cancer in Malaysia. Epidemiol. Health 38, doi: 10.4178/epih/e2016007.

Abubakar, I.B., Lim, K.-H., Kam, T.-S., Loh, H.-S., 2018. Jerantinine B enhances the mitochondria-mediated apoptosis by p53 activation in human glioblastoma cells via a combination with δ-tocotrienol. J. Biol. Act. Prod. from Nat. 8, 21–27.

Abubakar, I.B., Lim, K.H., Kam, T.S., Loh, H.S., 2016. Synergistic cytotoxic effects of combined δ-tocotrienol and jerantinine B on human brain and colon cancers. J. Ethnopharmacol. 184, 107–118.

Abubakar, I.B., Lim, K.H., Kam, T.S., Loh, H.S., 2017. Enhancement of apoptotic activities on brain cancer cells via the combination of γ-tocotrienol and jerantinine A. Phytomedicine 30, 74–84.

AbuHammad, S., Zihlif, M., 2013. Gene expression alterations in doxorubicin resistant MCF7 breast cancer cell line. Genomics 101, 213–220.

Adamsen, B.L., Kravik, K.L., De Angelis, P.M., 2011. DNA damage signaling in response to 5-fluorouracil in three colorectal cancer cell lines with different mismatch repair and TP53 status. Int. J. Oncol. 39, 673–682.

Agarwal, M.K., Agarwal, M.L., Athar, M., Gupta, S., 2004. Tocotrienol-rich fraction of palm oil activates p53, modulates Bax/Bcl2 ratio and induces apoptosis independent of cell cycle association. Cell Cycle 3, 205–211.

Aggarwal, B.B., Sundaram, C., Prasad, S., Kannappan, R., 2010. Tocotrienols, the vitamin E of the 21st century: Its potential against cancer and other chronic diseases. Biochem. Pharmacol. 80, 1613–1631.

Akl, M., Ayoub, N.M., Sylvester, P.W., 2012. Mechanisms mediating the synergistic anticancer effects of combined gamma-tocotrienol and sesamin treatment. Planta Med. 78, 1731–1739.

Akl, M.R., Ayoub, N.M., Abuasal, B.S., Kaddoumi, A., Sylvester, P.W., 2013. Sesamin synergistically potentiates the anticancer effects of gamma-tocotrienol in mammary cancer cell lines. Fitoterapia 84, 347–359.

Akpinar, B., Bracht, E. V, Reijnders, D., Safarikova, B., Jelinkova, I., Grandien, A., Vaculova, A.H., Zhivotovsky, B., Olsson, M., 2015. 5-Fluorouracil-induced RNA stress engages a TRAIL-DISC-dependent apoptosis axis facilitated by p53. Oncotarget 6, 43679–97.

Alberts, B., Johnson, A., Lewis, J., Raff, M., Roberts, K., Walter, P., 2002. An overview of the cell cycle. In: Molecular Biology of The Cell. Garland Science, New York: Garland.

Amelio, I., Melino, G., Knight, R.A., 2011. Cell death pathology: Cross-talk with autophagy and its clinical implications. Biochem. Biophys. Res. Commun. 414, 277–281.

American Cancer Society, 2016. Early history of cancer. Available at https://www.cancer.org/cancer/cancer-basics/history-of-cancer/what-is-cancer.html (Accessed: 20 Oct 2019).

Arita, D., Kambe, M., Ishioka, C., Kanamaru, R., 1997. Induction of p53-independent apoptosis associated with G2/M arrest following DNA damage in human colon cancer cell lines. Japanese J. Cancer Res. 88, 39–43.

Arnold, M., Sierra, M.S., Laversanne, M., Soerjomataram, I., Jemal, A., Bray, F., 2016. Global patterns and trends in colorectal cancer incidence and mortality. Gut 1–9.

Ayalew Sisay, E., 2015. Drug related problems in chemotherapy of cancer patients. J. Cancer Sci. Ther. 07, 1–5.

Aykin-Burns, N., Pathak, R., Boerma, M., Kim, T., Hauer-Jensen, M., 2019. Utilization of Vitamin E Analogs to Protect Normal Tissues While Enhancing Antitumor Effects. Semin. Radiat. Oncol. 29, 55–61.

Ayob, A.Z., Ramasamy, T.S., 2018. Cancer stem cells as key drivers of tumour progression. J. Biomed. Sci. 25, doi: 10.1186/s12929-018-0426-4.

Ayoub, N.M., Akl, M.R., Sylvester, P.W., 2013. Combined γ-tocotrienol and Met inhibitor treatment suppresses mammary cancer cell proliferation, epithelial-to-mesenchymal transition and migration. Cell Prolif. 46, 538–553.

Ayoub, N.M., Bachawal, S. V., Sylvester, P.W., 2011. γ-Tocotrienol inhibits HGF-dependent mitogenesis and Met activation in highly malignant mammary tumour cells. Cell Prolif. 44, 516–526.

Bachawal, S. V, Wali, V.B., Sylvester, P.W., 2010a. Enhanced antiproliferative and apoptotic response to combined treatment of gamma-tocotrienol with erlotinib or gefitinib in mammary tumor cells. BMC Cancer 10, doi: 10.1186/1471-2407-10-84.

Bachawal, S. V, Wali, V.B., Sylvester, P.W., 2010b. Combined gamma-tocotrienol and erlotinib/gefitinib treatment suppresses Stat and Akt signaling in murine mammary tumor cells. Anticancer Res. 30, 429–437.

Badisa, R.B., Darling-Reed, S.F., Joseph, P., Cooperwood, J.S., Latinwo, L.M., Goodman, C.B., 2009. Selective cytotoxic activities of two novel synthetic drugs on human breast carcinoma MCF-7 cells. Anticancer Res. 29, 2993–2996.

Bajaj, A., Zheng, Q., Adam, A., Vincent, P., Pumiglia, K., 2010. Activation of endothelial ras signaling bypasses senescence and causes abnormal vascular morphogenesis. Cancer Res. 70, 3803–3812.

Barrett-Lee, P.J., Dixon, J.M., Farrell, C., Jones, A., Leonard, R., Murray, N., Palmieri, C., Plummer, C.J., Stanley, A., Verrill, M.W., 2009. Expert opinion on the use of anthracyclines in patients with advanced breast cancer at cardiac risk. Ann. Oncol. 20, 816–827.

Barros, L.F., Hermosilla, T., Castro, J., 2001. Necrotic volume increase and the early physiology of necrosis. Comp. Biochem. Physiol. Part A Mol. Integr. Physiol. 130, 401–409.

Barve, A., Khor, T.O., Reuhl, K., Reddy, B., Newmark, H., Kong, A.N., 2010. Mixed tocotrienols inhibit prostate carcinogenesis in TRAMP mice. Nutr. Cancer 62, 789–794.

Beere, H.M., 2004. `The stress of dying': the role of heat shock proteins in the regulation of apoptosis. J. Cell Sci. 117, 2641–2651.

Beere, H.M., Wolf, B.B., Cain, K., Mosser, D.D., Mahboubi, A., Kuwana, T., Tailor, P., Morimoto, R.I., Cohen, G.M., Green, D.R., 2000. Heat-shock protein 70 inhibits apoptosis by preventing recruitment of procaspase-9 to the Apaf-1 apoptosome. Nat. Cell Biol. 2, 469–475.

Bell, D.S.H., 2013. Combine and conquer: advantages and disadvantages of fixed-dose combination therapy. Diabetes, Obes. Metab. 15, 291–300.

Bernig, T., Ritz, S., Brodt, G., Volkmer, I., Staege, M.S., 2016. Glutathione-S-transferases and chemotherapy resistance of Hodgkin's lymphoma cell lines. Anticancer Res. 36, 3905–3915.

Bhutia, S.K., Mukhopadhyay, S., Sinha, N., Das, D.N., Panda, P.K., Patra, S.K., Maiti, T.K., Mandal, M., Dent, P., Wang, X.-Y., Das, S.K., Sarkar, D., Fisher, P.B., 2013. Autophagy. In: Advances in Cancer Research. pp. 61–95.

Bilim, V., Kawasaki, T., Takahashi, K., Tomita, Y., 2000. Adriamycin induced G2/M cell cycle arrest in transitional cell cancer cells with wt p53 and p21(WAF1/CIP1) genes. J. Exp. Clin. Cancer Res. 19, 483–488.

Bodur, C., Kutuk, O., Karsli-Uzunbas, G., Isimjan, T.T., Harrison, P., Basaga, H., 2013. Pramanicin analog induces apoptosis in human colon cancer cells: critical roles for Bcl-2, Bim, and p38 MAPK signaling. PLoS One 8, doi: 10.1371/journal.pone.0056369.

Boik, J., 2001. Natural compounds in cancer therapy. Oregon Medical Press.

Borisy, A.A., Elliott, P.J., Hurst, N.W., Lee, M.S., Lehar, J., Price, E.R., Serbedzija, G., Zimmermann, G.R., Foley, M.A., Stockwell, B.R., Keith, C.T., 2003. Systematic discovery of multicomponent therapeutics. Proc. Natl. Acad. Sci. 100, 7977–7982.

Bortner, C.D., Cidlowski, J.A., 2007. Cell shrinkage and monovalent cation fluxes: role in apoptosis. Arch. Biochem. Biophys. 462, 176–188.

Bray, F., Ferlay, J., Soerjomataram, I., Siegel, R.L., Torre, L.A., Jemal, A., 2018. Global cancer statistics 2018: GLOBOCAN estimates of incidence and mortality worldwide for 36 cancers in 185 countries. CA. Cancer J. Clin. 68, 394–424.

Brentnall, M., Rodriguez-Menocal, L., De Guevara, R.L., Cepero, E., Boise, L.H., 2013. Caspase-9, caspase-3 and caspase-7 have distinct roles during intrinsic apoptosis. BMC Cell Biol. 14, doi: 10.1186/1471-2121-14-32.

Brigelius-Flohé, R., 2005. Induction of drug metabolizing enzymes by vitamin E. J. Plant Physiol. 162, 797–802.

Calderón-Montaño, J.M., Martínez-Sánchez, S.M., Burgos-Morón, E., Guillén-Mancina, E., Jiménez-Alonso, J.J., García, F., Aparicio, A., López-Lázaro, M., 2018. Screening for selective anticancer activity of plants from Grazalema natural park, Spain. Nat. Prod. Res. 1–5.

Cao, B., Bray, F., Beltrán-Sánchez, H., Ginsburg, O., Soneji, S., Soerjomataram, I., 2017. Benchmarking life expectancy and cancer mortality: global comparison with cardiovascular disease 1981-2010. BMJ 357, doi: https://doi.org/10.1136/bmj.j2765.

Cao, Z.J., Zhang, H.N., Cai, X.Y., Fang, W., Chai, D., Wen, Y., Chen, H.S., Chu, F.J., Zhang, Y.L., 2017. Luteolin promotes cell apoptosis by inducing autophagy in hepatocellular carcinoma. Cell. Physiol. Biochem. 43, 1803–1812.

Chan, T.S., Hsu, C.C., Pai, V.C., Liao, W.Y., Huang, S.S., Tan, K.T., Yen, C.J., Hsu, S.C., Chen, W.Y., Shan, Y.S., Li, C.R., Lee, M.T., Jiang, K., Chu, J.M., Lien, G.S., Weaver, V.M., Tsai, K.K., 2016. Metronomic chemotherapy prevents therapy-induced stromal activation and induction of tumor-initiating cells. J. Exp. Med. 213, 2967–2988.

Chang, C.-H., Liu, W.-T., Hung, H.-C., Gean, C.-Y., Tsai, H.-M., Su, C.-L., Gean, P.-W., 2017. Synergistic inhibition of tumor growth by combination treatment with drugs against different subpopulations of glioblastoma cells. BMC Cancer 17, 905.

Chang, D.W., Xing, Z., Capacio, V.L., Peter, M.E., Yang, X., 2003. Interdimer processing mechanism of procaspase-8 activation. EMBO J. 22, 4132–4142.

Chang, P.N., Yap, W.N., Lee, D.T.W., Ling, M.T., Wong, Y.C., Yap, Y.L., 2009. Evidence of gamma-tocotrienol as an apoptosis-inducing, invasion-suppressing, and chemotherapy drug-sensitizing agent in human melanoma cells. Nutr. Cancer 61, 357–366.

Chen, C., Lu, L., Yan, S., Yi, H., Yao, H., Wu, D., He, G., Tao, X., Deng, X., 2018. Autophagy and doxorubicin resistance in cancer. Anticancer. Drugs 29, 1–9.

Chen, C.C., Liu, T.Y., Huang, S.P., Ho, C.T., Huang, T.C., 2015. Differentiation and apoptosis induction by lovastatin and γ-tocotrienol in HL-60 cells via Ras/ERK/NF-κB and Ras/Akt/NF-κB signaling dependent down-regulation of glyoxalase 1 and HMG-CoA reductase. Cell. Signal. 27, 2182–2190.

Chen, D.-H., Zhang, X.-S., 2015. Targeted therapy: resistance and re-sensitization. Chin. J. Cancer 34, 496–501.

Citrin, D.E., 2016. Short-term screening assays for the identification of therapeutics for cancer. Cancer Res. 76, 3443–3445.

Clarke, P.G.H., Puyal, J., 2012. Autophagic cell death exists. Autophagy 8, 867–869.

Codogno, P., Meijer, A.J., 2005. Autophagy and signaling: their role in cell survival and cell death. Cell Death Differ. 12, 1509–1518.

Collins, A.R., 2004. The comet assay for DNA damage and repair: principles, applications, and limitations. Mol. Biotechnol. 26, 249–261.

Collins, J.A., Schandl, C.A., Young, K.K., Vesely, J., Willingham, M.C., 1997. Major DNA fragmentation is a late event in apoptosis. J. Histochem. Cytochem. 45, 923–934.

Comitato, R., Ambra, R., Virgili, F., 2017. Tocotrienols: A family of molecules with

specific biological activities. Antioxidants 6, doi: 10.3390/antiox6040093.

Comitato, R., Guantario, B., Leoni, G., Nesaretnam, K., Ronci, M.B., Canali, R., Virgili, F., 2016. Tocotrienols induce endoplasmic reticulum stress and apoptosis in cervical cancer cells. Genes Nutr. 11, doi: 10.1186/s12263-016-0543-1.

Comitato, R., Leoni, G., Canali, R., Ambra, R., Nesaretnam, K., Virgili, F., 2010. Tocotrienols activity in MCF-7 breast cancer cells: Involvement of ERβ signal transduction. Mol. Nutr. Food Res. 54, 669–678.

Concin, N., Stimpfl, M., Zeillinger, C., Wolff, U., Hefler, L., Sedlak, J., Leodolter, S., Zeillinger, R., 2003. Role of p53 in G2/M cell cycle arrest and apoptosis in response to gamma-irradiation in ovarian carcinoma cell lines. Int. J. Oncol. 22, 51–57.

Constantinou, C., Hyatt, J.A., Vraka, P.S., Papas, A., Papas, K.A., Neophytou, C., Hadjivassiliou, V., Constantinou, A.I., 2009. Induction of caspase-independent programmed cell death by vitamin E natural homologs and synthetic derivatives. Nutr. Cancer 61, 864–874.

Constantinou, C., Neophytou, C.M., Vraka, P., Hyatt, J.A., Papas, K.A., Constantinou, A.I., 2012. Induction of DNA damage and caspase-independent programmed cell death by vitamin E. Nutr. Cancer 64, 136–152.

Cosan, D., Soyocak, A., Tekedereli, I., Gacar, G., Karaoz, E., Ozpolat, B., 2010. Abstract 5109: Doxorubicin-induced autophagy functions as a pro-survival pathway in breast cancer cells. Cancer Res. 70, 5109–5109.

Crowley, L.C., Marfell, B.J., Scott, A.P., Waterhouse, N.J., 2016. Quantitation of apoptosis and necrosis by annexin V binding, propidium iodide uptake, and flow cytometry. Cold Spring Harb. Protoc. 2016, doi: 10.1101/pdb.prot087288.

Das, D., Preet, R., Mohapatra, P., Satapathy, S.R., Siddharth, S., Tamir, T., Jain, V., Bharatam, P. V, Wyatt, M.D., Kundu, C.N., 2014. 5-Fluorouracil mediated anti-cancer activity in colon cancer cells is through the induction of Adenomatous Polyposis Coli: Implication of the long-patch base excision repair pathway. DNA Repair (Amst). 24, 15–25.

Das, G., Shravage, B. V, Baehrecke, E.H., 2012. Regulation and function of autophagy during cell survival and cell death. Cold Spring Harb. Perspect. Biol. 4, doi: 10.1101/cshperspect.a008813.

Dasari, S., Tchounwou, B.P., 2014. Cisplatin in cancer therapy: Molecular mechanisms of action. Eur. J. Pharmacol. 740, 364–378.

Davis, C., Naci, H., Gurpinar, E., Poplavska, E., Pinto, A., Aggarwal, A., 2017. Availability of evidence of benefits on overall survival and quality of life of cancer drugs approved by European Medicines Agency: retrospective cohort study of drug approvals 2009-13. BMJ 359, doi: 10.1101/cshperspect.a008813.

De Angelis, P.M., Svendsrud, D.H., Kravik, K.L., Stokke, T., 2006. Cellular response to 5-fluorouracil (5-FU) in 5-FU-resistant colon cancer cell lines during treatment and recovery. Mol. Cancer 5, doi: 10.1186/1476-4598-5-20.

De Campos-Nebel, M., Larripa, I., González-Cid, M., 2010. Topoisomerase II-mediated DNA damage is differently repaired during the cell cycle by non-homologous end joining and homologous recombination. PLoS One 5, doi: 10.1371/journal.pone.0012541.

De Silva, L., Chuah, L.H., Meganathan, P., Fu, J.-Y., 2016. Tocotrienol and cancer metastasis. Biofactors 42, 149–162.

Deveraux, Q.L., Takahashi, R., Salvesen, G.S., Reed, J.C., 1997. X-linked IAP is a

direct inhibitor of cell-death proteases. Nature 388, 300–304.

Dienstmann, R., Rodon, J., Serra, V., Tabernero, J., 2014. Picking the point of inhibition: A comparative review of PI3K/AKT/mTOR pathway inhibitors. Mol. Cancer Ther. 13, 1021–1031.

Dobson, J.M., Hohenhaus, A.E., Peaston, A.E., 2008. Cancer chemotherapy, second. ed, Small Animal Clinical Pharmacology. Saunders Elsevier.

Dupont, N., Codogno, P., 2013. Non-canonical autophagy: Facts and prospects. Curr. Pathobiol. Rep. 1, 263–271.

Eitsuka, T., Nakagawa, K., Miyazawa, T., 2006. Down-regulation of telomerase activity in DLD-1 human colorectal adenocarcinoma cells by tocotrienol. Biochem. Biophys. Res. Commun. 348, 170–175.

Eitsuka, T., Tatewaki, N., Nishida, H., Kurata, T., Nakagawa, K., Miyazawa, T., 2014. Synergistic inhibition of cancer cell proliferation with a combination of delta-tocotrienol and ferulic acid. Biochem. Biophys. Res. Commun. 453, 606–611.

Eitsuka, T., Tatewaki, N., Nishida, H., Nakagawa, K., Miyazawa, T., 2016. A combination of delta-tocotrienol and ferulic acid synergistically inhibits telomerase activity in DLD-1 human colorectal adenocarcinoma cells. J Nutr Sci Vitaminol 62, 281–287.

Elmore, S., 2007. Apoptosis: a review of programmed cell death. Toxicol. Pathol. 35, 495–516.

Ernest, N.J., Habela, C.W., Sontheimer, H., 2008. Cytoplasmic condensation is both necessary and sufficient to induce apoptotic cell death. J. Cell Sci. 121, 290–297.

Evans, H.M., Bishop, K.S., 1922. On the existence of a hitherto unrecognized dietary

factor essential for reproduction. Science 56, 650–651.

Fan, Y.-J., Zong, W.-X., 2013. The cellular decision between apoptosis and autophagy. Chin. J. Cancer 32, 121–129.

Fernandes, N. V, Guntipalli, P.K., Mo, H., 2010. δ-Tocotrienol-mediated cell cycle arrest and apoptosis in human melanoma cells. Anticancer Res. 30, 4937–4944.

Fisher, R., Pusztai, L., Swanton, C., 2013. Cancer heterogeneity: implications for targeted therapeutics. Br. J. Cancer 108, 479–485.

Focaccetti, C., Bruno, A., Magnani, E., Bartolini, D., Principi, E., Dallaglio, K., Bucci, E.O., Finzi, G., Sessa, F., Noonan, D.M., Albini, A., 2015. Effects of 5-fluorouracil on morphology, cell cycle, proliferation, apoptosis, autophagy and ROS production in endothelial cells and cardiomyocytes. PLoS One 10, doi: 10.1371/journal.pone.0115686.

Fontana, F., Moretti, R.M., Raimondi, M., Marzagalli, M., Beretta, G., Procacci, P., Sartori, P., Montagnani Marelli, M., Limonta, P., 2019. δ-Tocotrienol induces apoptosis, involving endoplasmic reticulum stress and autophagy, and paraptosis in prostate cancer cells. Cell Prolif. e12576.

Franzen, C.A., Blackwell, R.H., Todorovic, V., Greco, K.A., Foreman, K.E., Flanigan, R.C., Kuo, P.C., Gupta, G.N., 2015. Urothelial cells undergo epithelial-to-mesenchymal transition after exposure to muscle invasive bladder cancer exosomes. Oncogenesis 4, e163–e163.

Fu, J.Y., Blatchford, D.R., Tetley, L., Dufès, C., 2009. Tumor regression after systemic administration of tocotrienol entrapped in tumor-targeted vesicles. J. Control. Release 140, 95–99.

Fulda, S., 2013a. Regulation of cell death in cancer-possible implications for immunotherapy. Front. Oncol. 3, doi: 10.3389/fonc.2013.00029.

Fulda, S., 2013b. The mechanism of necroptosis in normal and cancer cells. Cancer Biol. Ther. 14, 999–1004.

Fulda, S., Galluzzi, L., Kroemer, G., 2010. Targeting mitochondria for cancer therapy. Nat. Rev. Drug Discov. 9, 447–464.

Gabay, M., Li, Y., Felsher, D.W., 2014. MYC activation is a hallmark of cancer initiation and maintenance. Cold Spring Harb. Perspect. Med. 4, doi: 10.1101/cshperspect.a014241.

Galluzzi, L., Kepp, O., Chan, F.K.-M., Kroemer, G., 2017. Necroptosis: Mechanisms and relevance to disease. Annu. Rev. Pathol. Mech. Dis. 12, 103–130.

Galluzzi, L., Maiuri, M.C., Vitale, I., Zischka, H., Castedo, M., Zitvogel, L., Kroemer, G., 2007. Cell death modalities: classification and pathophysiological implications. Cell Death Differ. 2007 147.

Galluzzi, L., Vitale, I., Aaronson, S.A., Abrams, J.M., Adam, D., Agostinis, P., Alnemri, E.S., Altucci, L., Amelio, I., Andrews, D.W., Annicchiarico-Petruzzelli, M., Antonov, A. V., Arama, E., Baehrecke, E.H., Barlev, N.A., Bazan, N.G., Bernassola, F., Bertrand, M.J.M., Bianchi, K., Blagosklonny, M. V., Blomgren, K., Borner, C., Boya, P., Brenner, C., Campanella, M., Candi, E., Carmona-Gutierrez, D., Cecconi, F., Chan, F.K.-M., Chandel, N.S., Cheng, E.H., Chipuk, J.E., Cidlowski, J.A., Ciechanover, A., Cohen, G.M., Conrad, M., Cubillos-Ruiz, J.R., Czabotar, P.E., D'Angiolella, V., Dawson, T.M., Dawson, V.L., De Laurenzi, V., De Maria, R., Debatin, K.-M., DeBerardinis, R.J., Deshmukh, M., Di Daniele, N., Di Virgilio, F., Dixit, V.M., Dixon, S.J., Duckett, C.S., Dynlacht,

B.D., El-Deiry, W.S., Elrod, J.W., Fimia, G.M., Fulda, S., García-Sáez, A.J., Garg, A.D., Garrido, C., Gavathiotis, E., Golstein, P., Gottlieb, E., Green, D.R., Greene, L.A., Gronemeyer, H., Gross, A., Hajnoczky, G., Hardwick, J.M., Harris, I.S., Hengartner, M.O., Hetz, C., Ichijo, H., Jäättelä, M., Joseph, B., Jost, P.J., Juin, P.P., Kaiser, W.J., Karin, M., Kaufmann, T., Kepp, O., Kimchi, A., Kitsis, R.N., Klionsky, D.J., Knight, R.A., Kumar, S., Lee, S.W., Lemasters, J.J., Levine, B., Linkermann, A., Lipton, S.A., Lockshin, R.A., López-Otín, C., Lowe, S.W., Luedde, T., Lugli, E., MacFarlane, M., Madeo, F., Malewicz, M., Malorni, W., Manic, G., Marine, J.-C., Martin, S.J., Martinou, J.-C., Medema, J.P., Mehlen, P., Meier, P., Melino, S., Miao, E.A., Molkentin, J.D., Moll, U.M., Muñoz-Pinedo, C., Nagata, S., Nuñez, G., Oberst, A., Oren, M., Overholtzer, M., Pagano, M., Panaretakis, T., Pasparakis, M., Penninger, J.M., Pereira, D.M., Pervaiz, S., Peter, M.E., Piacentini, M., Pinton, P., Prehn, J.H.M., Puthalakath, H., Rabinovich, G.A., Rehm, M., Rizzuto, R., Rodrigues, C.M.P., Rubinsztein, D.C., Rudel, T., Ryan, K.M., Sayan, E., Scorrano, L., Shao, F., Shi, Y., Silke, J., Simon, H.-U., Sistigu, A., Stockwell, B.R., Strasser, A., Szabadkai, G., Tait, S.W.G., Tang, D., Tavernarakis, N., Thorburn, A., Tsujimoto, Y., Turk, B., Vanden Berghe, T., Vandenabeele, P., Vander Heiden, M.G., Villunger, A., Virgin, H.W., Vousden, K.H., Vucic, D., Wagner, E.F., Walczak, H., Wallach, D., Wang, Y., Wells, J.A., Wood, W., Yuan, J., Zakeri, Z., Zhivotovsky, B., Zitvogel, L., Melino, G., Kroemer, G., 2018. Molecular mechanisms of cell death: recommendations of the Nomenclature Committee on Cell Death 2018. Cell Death Differ. 25, 486–541.

Garrido, C., Bruey, J.M., Fromentin, A., Hammann, A., Arrigo, A.P., Solary, E., 1999. HSP27 inhibits cytochrome c-dependent activation of procaspase-9. FASEB J.

13, 2061–2070.

Giacinti, C., Giordano, A., 2006. RB and cell cycle progression. Oncogene 25, 5220–5227.

Giampazolias, E., Zunino, B., Dhayade, S., Bock, F., Cloix, C., Cao, K., Roca, A., Lopez, J., Ichim, G., Proïcs, E., Rubio-Patiño, C., Fort, L., Yatim, N., Woodham, E., Orozco, S., Taraborrelli, L., Peltzer, N., Lecis, D., Machesky, L., Walczak, H., Albert, M.L., Milling, S., Oberst, A., Ricci, J.-E., Ryan, K.M., Blyth, K., Tait, S.W.G., 2017. Mitochondrial permeabilization engages NF-κB-dependent anti-tumour activity under caspase deficiency. Nat. Cell Biol. 19, 1116–1129.

Glick, D., Barth, S., Macleod, K.F., 2010. Autophagy: cellular and molecular mechanisms. J. Pathol. 221, 3–12.

Gopalan, A., Yu, W., Sanders, B.G., Kline, K., 2013. Eliminating drug resistant breast cancer stem-like cells with combination of simvastatin and gamma-tocotrienol. Cancer Lett. 328, 285–296.

Gottlieb, R.A., Andres, A.M., Sin, J., Taylor, D.P.J., 2015. Untangling autophagy measurements: all fluxed up. Circ. Res. 116, 504–514.

Graham, C.D., Kaza, N., Klocke, B.J., Gillespie, G.Y., Shevde, L.A., Carroll, S.L., Roth, K.A., 2016. Tamoxifen induces cytotoxic autophagy in glioblastoma. J. Neuropathol. Exp. Neurol. 75, 946–954.

Greco, W.R., Faessel, H., Levasseur, L., 1996. The search for cytotoxic synergy between anticancer agents: a case of Dorothy and the ruby slippers? J. Natl. Cancer Inst. 88, 699–700.

Green, D.R., Evan, G.I., 2002. A matter of life and death. Cancer Cell 1, 19–30.

Greene, L.M., Nolan, D.P., Regan-Komito, D., Campiani, G., Williams, D.C., Zisterer, D.M., 2013. Inhibition of late-stage autophagy synergistically enhances pyrrolo-1,5-benzoxazepine-6-induced apoptotic cell death in human colon cancer cells. Int. J. Oncol. 43, 927–935.

Griffiths, M., Sundaram, H., 2011. Drug design and testing: Profiling of antiproliferative agents for cancer therapy using a cell-based methyl-[3H]-thymidine incorporation assay. In: Methods in Molecular Biology (Clifton, N.J.). pp. 451–465.

Gu, W., Prasadam, I., Yu, M., Zhang, F., Ling, P., Xiao, Y., Yu, C., 2015. Gamma tocotrienol targets tyrosine phosphatase SHP2 in mammospheres resulting in cell death through RAS/ERK pathway. BMC Cancer 15, doi: 10.1186/s12885-015-1614-1.

Guamán Ortiz, L.M., Tillhon, M., Parks, M., Dutto, I., Prosperi, E., Savio, M., Arcamone, A.G., Buzzetti, F., Lombardi, P., Scovassi, A.I., 2014. Multiple effects of berberine derivatives on colon cancer cells. Biomed Res. Int. 2014, doi: 10.1155/2014/924585.

Gump, J.M., Thorburn, A., 2011. Autophagy and apoptosis: what is the connection? Trends Cell Biol. 21, 387–392.

Gupta, S., Cuffe, L., Szegezdi, E., Logue, S.E., Neary, C., Healy, S., Samali, A., 2010. Mechanisms of ER stress-mediated mitochondrial membrane permeabilization. Int. J. Cell Biol. 2010, 170215.

Gupta, S.C., Kannappan, R., Reuter, S., Kim, J.H., Aggarwal, B.B., 2011. Chemosensitization of tumors by resveratrol. Ann. N. Y. Acad. Sci. 1215, 150–160.

Guthrie, N., Gapor, A., Chambers, A.F., Carroll, K.K., 1997. Inhibition of proliferation of estrogen receptor-negative MDA-MB-435 and -positive MCF-7 human breast cancer cells by palm oil tocotrienols and tamoxifen, alone and in combination. J. Nutr. 127, 544S-548S.

Gyori, B.M., Venkatachalam, G., Thiagarajan, P.S., Hsu, D., Clement, M.-V., 2014. OpenComet: an automated tool for comet assay image analysis. Redox Biol. 2, 457–465.

Hanahan, D., Weinberg, R.A., 2011. Hallmarks of cancer: the next generation. Cell 144, 646–674.

Har, C.H., Keong, C.K., 2005. Effects of tocotrienols on cell viability and apoptosis in normal murine liver cells (BNL CL.2) and liver cancer cells (BNL 1ME A.7R.1), in vitro. Asia Pac. J. Clin. Nutr. 14, 374–380.

Harrington, E.A., Bruce, J.L., Harlow, E., Dyson, N., 1998. pRB plays an essential role in cell cycle arrest induced by DNA damage. Proc. Natl. Acad. Sci. U. S. A. 95, 11945–11950.

Harris, M.H., Thompson, C.B., 2000. The role of the Bcl-2 family in the regulation of outer mitochondrial membrane permeability. Cell Death Differ. 7, 1182–1191.

Hasani, N.A., Bak, K., Wan Ngah, W.Z., 2011. The anti proliferative effect of palm oil γ-tocotrienol involves alterations in MEK-2 and ERK-2 protein expressions in CaSki cells. Asian Biomed. 5, 601–609.

Hasani, N.A., Yusoff, P.A., BAK, K., MT, A.G., WZ, W.N., 2008. The possible mechanism of action of palm oil γ-tocotrienol and α- tocopherol on the cervical carcinoma CaSki cell apoptosis. Biomed. Res. 19.

He, B., Lu, N., Zhou, Z., 2009. Cellular and nuclear degradation during apoptosis. Curr. Opin. Cell Biol. 21, 900–912.

He, L., Kulesskiy, E., Saarela, J., Turunen, L., Wennerberg, K., Aittokallio, T., Tang, J., 2018. Methods for high-throughput drug combination screening and synergy scoring. In: Methods in Molecular Biology (Clifton, N.J.). pp. 351–398.

Hippert, M.M., O'Toole, P.S., Thorburn, A., 2006. Autophagy in cancer: Good, bad, or both? Cancer Res. 66, 9349–9351.

Hiura, Y., Tachibana, H., Arakawa, R., Aoyama, N., Okabe, M., Sakai, M., Yamada, K., 2009. Specific accumulation of γ- and δ-tocotrienols in tumor and their antitumor effect in vivo. J. Nutr. Biochem. 20, 607–613.

Hodul, P.J., Dong, Y., Husain, K., Pimiento, J.M., Chen, J., Zhang, A., Francois, R., Pledger, W.J., Coppola, D., Sebti, S.M., Chen, D.-T., Malafa, M.P., 2013. Vitamin E δ-tocotrienol induces p27Kip1-dependent cell-cycle arrest in pancreatic cancer cells via an E2F-1-dependent mechanism. PLoS One 8, doi: 10.1371/journal.pone.0052526.

Hosomi, A., Arita, M., Sato, Y., Kiyose, C., Ueda, T., Igarashi, O., Arai, H., Inoue, K., 1997. Affinity for alpha-tocopherol transfer protein as a determinant of the biological activities of vitamin E analogs. FEBS Lett. 409, 105–108.

Hou, W., Han, J., Lu, C., Goldstein, L.A., Rabinowich, H., 2010. Autophagic degradation of active caspase-8: a crosstalk mechanism between autophagy and apoptosis. Autophagy 6, 891–900.

Housman, G., Byler, S., Heerboth, S., Lapinska, K., Longacre, M., Snyder, N., Sarkar, S., 2014. Drug resistance in cancer: An overview. Cancers (Basel). 6, 1769–1792.

Hsieh, T.C., Wu, J.M., 2008. Suppression of cell proliferation and gene expression by combinatorial synergy of EGCG, resveratrol and gamma-tocotrienol in estrogen receptor-positive MCF-7 breast cancer cells. Int. J. Oncol. 33, 851–859.

Huang, S., Sinicrope, F., 2010. Celecoxib-induced apoptosis is enhanced by ABT-737 and by inhibition of autophagy in human colorectal cancer cells. Autophagy 6, 256–269.

Husain, K., Centeno, B.A., Chen, D.-T., Fulp, W.J., Perez, M., Guo, Z.L., Luetteke, N., Hingorani, S.R., Sebti, S.M., Malafa, M.P., 2013. Prolonged survival and delayed progression of pancreatic intraepithelial neoplasia in LSL-Kras ;Pdx-1-Cre mice by vitamin E δ-tocotrienol. Carcinogenesis 34, 858–863.

Husain, K., Centeno, B.A., Coppola, D., Trevino, J., Sebti, S.M., Malafa, M.P., 2017. δ-Tocotrienol, a natural form of vitamin E, inhibits pancreatic cancer stem-like cells and prevents pancreatic cancer metastasis. Oncotarget 8, 31554–31567.

Husain, K., Francois, R.A., Yamauchi, T., Perez, M., Sebti, S.M., Malafa, M.P., 2011. Vitamin E -tocotrienol augments the antitumor activity of gemcitabine and suppresses constitutive NFk-B activation in pancreatic cancer. Mol. Cancer Ther. 10, 2363–2372.

Husain, K., Zhang, A., Shivers, S.C., Davis-Yadley, A.H., Coppola, D., Yang, C.S., Malafa, M.P., 2019. Chemoprevention of azoxymethane-induced colon carcinogenesis by delta-tocotrienol. Cancer Prev. Res. (Phila). canprevres.0290.2018.

Ikwegbue, P., Masamba, P., Oyinloye, B., Kappo, A., 2017. Roles of heat shock proteins in apoptosis, oxidative stress, human inflammatory diseases, and cancer. Pharmaceuticals 11, doi: 10.3390/ph11010002.

Inoue, A., Takitani, K., Koh, M., Kawakami, C., Kuno, T., Tamai, H., 2011. Induction of apoptosis by γ -tocotrienol in human cancer cell lines and leukemic blasts from patients: Dependency on Bid, cytochrome c , and caspase pathway. Nutr. Cancer 63, 763–770.

Jeon, J.H., Park, E.J., Lee, C.R., Chun, J.N., Cho, N.H., Kim, I.-G., Lee, S., Kim, T.W., Park, H.H., So, I., Jeon, J.H., 2011. Geraniol induces cooperative interaction of apoptosis and autophagy to elicit cell death in PC-3 prostate cancer cells. Int. J. Oncol. 40, 1683–1690.

Ji, X., Wang, Z., Sarkar, F.H., Gupta, S. V., 2012. Delta-tocotrienol augments cisplatin-induced suppression of non-small cell lung cancer cells via inhibition of the Notch-1 pathway. Anticancer Res. 32, 2647–2656.

Jiang, Q., Rao, X., Kim, C.Y., Freiser, H., Zhang, Q., Jiang, Z., Li, G., 2012. Gamma-tocotrienol induces apoptosis and autophagy in prostate cancer cells by increasing intracellular dihydrosphingosine and dihydroceramide. Int. J. Cancer 130, 685–693.

Jiang, W.G., Sanders, A.J., Katoh, M., Ungefroren, H., Gieseler, F., Prince, M., Thompson, S.K., Zollo, M., Spano, D., Dhawan, P., Sliva, D., Subbarayan, P.R., Sarkar, M., Honoki, K., Fujii, H., Georgakilas, A.G., Amedei, A., Niccolai, E., Amin, A., Ashraf, S.S., Ye, L., Helferich, W.G., Yang, X., Boosani, C.S., Guha, G., Ciriolo, M.R., Aquilano, K., Chen, S., Azmi, A.S., Keith, W.N., Bilsland, A., Bhakta, D., Halicka, D., Nowsheen, S., Pantano, F., Santini, D., 2015. Tissue invasion and metastasis: Molecular, biological and clinical perspectives. Semin. Cancer Biol. 35, S244–S275.

Kale, J., Osterlund, E.J., Andrews, D.W., 2018. BCL-2 family proteins: changing

partners in the dance towards death. Cell Death Differ. 25, 65–80.

Kaneko, S., Sato, C., Shiozawa, N., Sato, A., Sato, H., Virgona, N., Yano, T., 2018. Suppressive effect of delta-tocotrienol on hypoxia adaptation of prostate cancer stem-like cells. Anticancer Res. 38, 1391–1399.

Kani, K., Momota, Y., Harada, M., Yamamura, Y., Aota, K., Yamanoi, T., Takano, H., Motegi, K., Azuma, M., 2013. γ-tocotrienol enhances the chemosensitivity of human oral cancer cells to docetaxel through the downregulation of the expression of NF-κB-regulated anti-apoptotic gene products. Int. J. Oncol. 42, 75–82.

Kantari, C., Walczak, H., 2011. Caspase-8 and Bid: Caught in the act between death receptors and mitochondria. Biochim. Biophys. Acta - Mol. Cell Res. 1813, 558–563.

Karasawa, H., Miura, K., Fujibuchi, W., Ishida, K., Kaneko, N., Kinouchi, M., Okabe, M., Ando, T., Murata, Y., Sasaki, H., Takami, K., Yamamura, A., Shibata, C., Sasaki, I., 2009. Down-regulation of cIAP2 enhances 5-FU sensitivity through the apoptotic pathway in human colon cancer cells. Cancer Sci. 100, 903–913.

Karjalainen, E., Repasky, G.A., 2016. Molecular changes during acute myeloid leukemia (AML) evolution and identification of novel treatment strategies through molecular stratification. Prog. Mol. Biol. Transl. Sci. 144, 383–436.

Kaufmann, T., Schinzel, A., Borner, C., 2004. Bcl-w(edding) with mitochondria. Trends Cell Biol. 14, 8–12.

Kiraz, Y., Adan, A., Kartal Yandim, M., Baran, Y., 2016. Major apoptotic mechanisms and genes involved in apoptosis. Tumor Biol. 37, 8471–8486.

Kobayashi, S., Volden, P., Timm, D., Mao, K., Xu, X., Liang, Q., 2010. Transcription factor GATA4 inhibits doxorubicin-induced autophagy and cardiomyocyte death. J. Biol. Chem. 285, 793–804.

Kögel, D., Prehn, J., 2013. Caspase-independent cell death mechanisms, Madame Curie Bioscience Database. Landes Bioscience, Austin (TX).

Kohli, L., Kaza, N., Coric, T., Byer, S.J., Brossier, N.M., Klocke, B.J., Bjornsti, M.-A., Carroll, S.L., Roth, K.A., 2013. 4-Hydroxytamoxifen induces autophagic death through K-Ras degradation. Cancer Res. 73, 4395–4405.

Koleini, N., Kardami, E., 2017. Autophagy and mitophagy in the context of doxorubicin-induced cardiotoxicity. Oncotarget 8, 46663–46680.

Komiyama, K., Iizuka, K., Yamaoka, M., Watanabe, H., Tsuchiya, N., Umezawa, I., 1989. Studies on the biological activity of tocotrienols. Chem. Pharm. Bull. (Tokyo). 37, 1369–1371.

Kroemer, G., Galluzzi, L., Brenner, C., 2007. Mitochondrial Membrane Permeabilization in Cell Death. Physiol. Rev. 87, 99–163.

Kroemer, G., Levine, B., 2008. Autophagic cell death: the story of a misnomer. Nat. Rev. Mol. Cell Biol. 9, 1004–1010.

Kumar, A., Gautam, B., Dubey, C., Tripathi, P.K., 2014. A Review: role of doxorubicin in treatment of cancer. Int. J. Pharm. Sci. Res. 4117–4128.

Kumari, S., Mehta, S.L., Li, P.A., 2012. Glutamate induces mitochondrial dynamic imbalance and autophagy activation: Preventive effects of selenium. PLoS One 7, doi: 10.1371/journal.pone.0039382.

Kunnumakkara, A.B., Sung, B., Ravindran, J., Diagaradjane, P., Deorukhkar, A., Dey,

S., Koca, C., Yadav, V.R., Tong, Z., Gelovani, J.G., Guha, S., Krishnan, S., Aggarwal, B.B., 2010. Gamma-tocotrienol inhibits pancreatic tumors and sensitizes them to gemcitabine treatment by modulating the inflammatory microenvironment. Cancer Res. 70, 8695–8705.

Kwang, S.A., Sethi, G., Krishnan, K., Aggarwal, B.B., 2007. γ-tocotrienol inhibits nuclear factor-κB signaling pathway through inhibition of receptor-interacting protein and TAK1 leading to suppression of antiapoptotic gene products and potentiation of apoptosis. J. Biol. Chem. 282, 809–820.

Kyrylkova, K., Kyryachenko, S., Leid, M., Kioussi, C., 2012. Detection of apoptosis by TUNEL assay. In: Methods in Molecular Biology (Clifton, N.J.). pp. 41–47.

LaCasse, E.C., Baird, S., Korneluk, R.G., MacKenzie, A.E., 1998. The inhibitors of apoptosis (IAPs) and their emerging role in cancer. Oncogene 17, 3247–3259.

Lee, J.-W., Kim, K.-S., An, H.-K., Kim, C.-H., Moon, H.-I., Lee, Y.-C., 2013. Dendropanoxide induces autophagy through ERK1/2 activation in MG-63 human osteosarcoma cells and autophagy inhibition enhances dendropanoxide-induced apoptosis. PLoS One 8, doi: 10.1371/journal.pone.0039382.

Lee, W.-J., Chien, M.-H., Chow, J.-M., Chang, J.-L., Wen, Y.-C., Lin, Y.-W., Cheng, C.-W., Lai, G.-M., Hsiao, M., Lee, L.-M., 2015. Nonautophagic cytoplasmic vacuolation death induction in human PC-3M prostate cancer by curcumin through reactive oxygen species -mediated endoplasmic reticulum stress. Sci. Rep. 5, doi: 10.1038/srep10420.

Leytin, V., Gyulkhandanyan, A. V., Freedman, J., 2018. Role of mitochondrial membrane permeabilization and depolarization in platelet apoptosis. Br. J. Haematol. 181, 281–285.

Li, H., Huang, K., Gao, L., Wang, L.X., Niu, Y., Liu, H., Wang, Z., Wang, L., Wang, G., Wang, J., 2016. TES inhibits colorectal cancer progression through activation of p38. Oncotarget 7, 45819–45836.

Li, J., Hou, N., Faried, A., Tsutsumi, S., Kuwano, H., 2010. Inhibition of autophagy augments 5-fluorouracil chemotherapy in human colon cancer in vitro and in vivo model. Eur. J. Cancer 46, 1900–1909.

Li, X., Prescott, M., Adler, B., Boyce, J.D., Devenish, R.J., 2013. Beclin 1 is required for starvation-enhanced, but not rapamycin-enhanced, LC3-associated phagocytosis of Burkholderia pseudomallei in RAW 264.7 cells. Infect. Immun. 81, 271–277.

Li, Y., Sun, W.-G., Liu, H.-K., Qi, G.-Y., Wang, Q., Sun, X.-R., Chen, B.-Q., Liu, J.-R., 2011. γ-Tocotrienol inhibits angiogenesis of human umbilical vein endothelial cell induced by cancer cell. J. Nutr. Biochem. 22, 1127–1136.

Lim, G., 2006. Clinical oncology in Malaysia: 1914 to present. Biomed. Imaging Interv. J. 2, doi: 10.2349/biij.2.1.e18.

Lim, S.-W., Loh, H.-S., Ting, K.-N., Bradshaw, T.D., Allaudin, Z.N., 2015. Reduction of MTT to purple formazan by vitamin E isomers in the absence of cells. Trop. life Sci. Res. 26, 111–120.

Lim, S.-W., Loh, H.-S., Ting, K.-N., Bradshaw, T.D., Zeenathul, N.A., 2014a. Cytotoxicity and apoptotic activities of alpha-, gamma- and delta-tocotrienol isomers on human cancer cells. BMC Complement. Altern. Med. 14, doi: 10.1186/1472-6882-14-469.

Lim, S.-W., Loh, H.-S., Ting, K.N., Bradshaw, T.D., Zeenathul, N.A., 2014b. Antiproliferation and induction of caspase-8-dependent mitochondria-mediated

apoptosis by β-tocotrienol in human lung and brain cancer cell lines. Biomed. Pharmacother. 68, 1105–1115.

Liu, D., Gao, M., Yang, Y., Qi, Y.U., Wu, K., Zhao, S., 2015. Inhibition of autophagy promotes cell apoptosis induced by the proteasome inhibitor MG-132 in human esophageal squamous cell carcinoma EC9706 cells. Oncol. Lett. 9, 2278–2282.

Liu, H.-K., Wang, Q., Li, Y., Sun, W.-G., Liu, J.-R., Yang, Y.-M., Xu, W.-L., Sun, X.-R., Chen, B.-Q., 2010. Inhibitory effects of γ-tocotrienol on invasion and metastasis of human gastric adenocarcinoma SGC-7901 cells☆☆☆. J. Nutr. Biochem. 21, 206–213.

Liu, H.C., Chen, G.G., Vlantis, A.C., Tong, M.C.F., Chan, P.K.S., van Hasselt, C.A., 2008. Induction of cell cycle arrest and apoptosis by 5-fluorouracil in laryngeal cancer cells containing HPV16 E6 and E7 oncoproteins. Clin. Biochem. 41, 1117–1125.

Liu, J., Lau, E.Y.-T., Chen, J., Yong, J., Tang, K.D., Lo, J., Ng, I.O.-L., Lee, T.K.-W., Ling, M.-T., 2014. Polysaccharopeptide enhanced the anti-cancer effect of gamma-tocotrienol through activation of AMPK. BMC Complement. Altern. Med. 14, 303.

Loganathan, R., Selvaduray, K.R., Nesaretnam, K., Radhakrishnan, A.K., 2013. Tocotrienols promote apoptosis in human breast cancer cells by inducing poly(ADP-ribose) polymerase cleavage and inhibiting nuclear factor kappa-B activity. Cell Prolif. 46, 203–213.

Longley, D.B., Harkin, D.P., Johnston, P.G., 2003. 5-Fluorouracil: mechanisms of action and clinical strategies. Nat. Rev. Cancer 3, 330–338.

Loos, B., Toit, A. du, Hofmeyr, J.-H.S., 2014. Defining and measuring autophagosome flux—concept and reality. Autophagy 10, doi: 10.4161/15548627.2014.973338.

Lowe, S.W., Lin, A.W., 2000. Apoptosis in cancer. Carcinogenesis 21, 485–495.

Luk, S.U., Yap, W.N., Chiu, Y.-T., Lee, D.T., Ma, S., Lee, T.K.W., Vasireddy, R.S., Wong, Y.-C., Ching, Y.P., Nelson, C., Yap, Y.L., Ling, M.-T., 2011. Gamma-tocotrienol as an effective agent in targeting prostate cancer stem cell-like population. Int. J. Cancer 128, 2182–2191.

Maeda, H., Khatami, M., 2018. Analyses of repeated failures in cancer therapy for solid tumors: poor tumor-selective drug delivery, low therapeutic efficacy and unsustainable costs. Clin. Transl. Med. 7, doi: 10.1186/s40169-018-0185-6.

Maheswari, U., Sadras, S.R., 2018. Mechanism and regulation of autophagy in cancer. Crit. Rev. Oncog. 23, 269–280.

Mahipal, A., Klapman, J., Vignesh, S., Yang, C.S., Neuger, A., Chen, D.-T., Malafa, M.P., 2016. Pharmacokinetics and safety of vitamin E δ-tocotrienol after single and multiple doses in healthy subjects with measurement of vitamin E metabolites. Cancer Chemother. Pharmacol. 78, 157–165.

Mai, C.W., Yaeghoobi, M., Abd-Rahman, N., Kang, Y.B., Pichika, M.R., 2014. Chalcones with electron-withdrawing and electron-donating substituents: anticancer activity against TRAIL resistant cancer cells, structure–activity relationship analysis and regulation of apoptotic proteins. Eur. J. Med. Chem. 77, 378–387.

Malaviya, A., Sylvester, P.W., 2014. Synergistic antiproliferative effects of combined γ-tocotrienol and PPAR γ antagonist treatment are mediated through PPAR γ-

independent mechanisms in breast cancer cells. PPAR Res. 2014, doi: 10.1155/2014/439146.

Manning, B.D., Cantley, L.C., 2007. AKT/PKB signaling: navigating downstream. Cell 129, 1261–1274.

Manu, K.A., Shanmugam, M.K., Ramachandran, L., Li, F., Fong, C.W., Kumar, A.P., Tan, P., Sethi, G., 2012. First evidence that gamma-tocotrienol inhibits the growth of human gastric cancer and chemosensitizes it to capecitabine in a xenograft mouse model through the modulation of NF-kappaB pathway. Clin Cancer Res 18, 2220–2229.

Marchi, S., Patergnani, S., Pinton, P., 2014. The endoplasmic reticulum–mitochondria connection: One touch, multiple functions. Biochim. Biophys. Acta - Bioenerg. 1837, 461–469.

Marelli, M.M., Marzagalli, M., Moretti, R.M., Beretta, G., Casati, L., Comitato, R., Gravina, G.L., Festuccia, C., Limonta, P., 2016. Vitamin E δ-tocotrienol triggers endoplasmic reticulum stress-mediated apoptosis in human melanoma cells. Sci. Rep. 6, doi: 10.1038/srep30502.

Margosio, B., Marchetti, D., Vergani, V., Giavazzi, R., Rusnati, M., Presta, M., Taraboletti, G., 2003. Thrombospondin 1 as a scavenger for matrix-associated fibroblast growth factor 2. Blood 102, 4399–4406.

Mariño, G., Niso-Santano, M., Baehrecke, E.H., Kroemer, G., 2014. Self-consumption: the interplay of autophagy and apoptosis. Nat. Rev. Mol. Cell Biol. 15, 81–94.

Martelli, A.M., Tabellini, G., Bressanin, D., Ognibene, A., Goto, K., Cocco, L., Evangelisti, C., 2012. The emerging multiple roles of nuclear Akt. Biochim. Biophys. Acta - Mol. Cell Res. 1823, 2168–2178.

Marzagalli, M., Moretti, R.M., Messi, E., Marelli, M.M., Fontana, F., Anastasia, A., Bani, M.R., Beretta, G., Limonta, P., 2018. Targeting melanoma stem cells with the Vitamin E derivative δ-tocotrienol. Sci. Rep. 8, doi: 10.1038/s41598-017-19057-4.

Matsuoka, S., Huang, M., Elledge, S.J., 1998. Linkage of ATM to cell cycle regulation by the Chk2 protein kinase. Science 282, 1893–1897.

McAnally, J.A., Gupta, J., Sodhani, S., Bravo, L., Mo, H., 2007. Tocotrienols potentiate lovastatin-mediated growth suppression in vitro and in vivo. Exp. Biol. Med. (Maywood). 232, 523–31.

Melisi, D., Piro, G., Tamburrino, A., Carbone, C., Tortora, G., 2013. Rationale and clinical use of multitargeting anticancer agents. Curr. Opin. Pharmacol. 13, 536–542.

Menyhárt, O., Harami-Papp, H., Sukumar, S., Schäfer, R., Magnani, L., de Barrios, O., Győrffy, B., 2016. Guidelines for the selection of functional assays to evaluate the hallmarks of cancer. Biochim. Biophys. Acta - Rev. Cancer 1866, 300–319.

Mhaidat, N.M., Alzoubi, K.H., Khabour, O.F., Alawneh, K.Z., Raffee, L.A., Alsatari, E.S., Hussein, E.I., Bani-Hani, K.E., 2016. Assessment of genotoxicity of vincristine, vinblastine and vinorelbine in human cultured lymphocytes: a comparative study. Balkan J. Med. Genet. 19, 13–20.

Mhaidat, N.M., Bouklihacene, M., Thorne, R.F., 2014. 5-Fluorouracil-induced apoptosis in colorectal cancer cells is caspase-9-dependent and mediated by activation of protein kinase C-δ. Oncol. Lett. 8, 699–704.

Mitchell, E.P., 2012. Colorectal cancer in the young. Color. Cancer 1, 355–358.

Miyazawa, T., Shibata, A., Nakagawa, K., Tsuzuki, T., 2008. Anti-angiogenic function of tocotrienol. Asia Pac. J. Clin. Nutr. 17 Suppl 1, 253–256.

Mizushima, N., Yoshimori, T., 2007. How to interpret LC3 immunoblotting. Autophagy 3, 542–525.

Mizutani, Y., Okada, Y., Yoshida, O., Fukumoto, M., Bonavida, B., 1997. Doxorubicin sensitizes human bladder carcinoma cells to Fas-mediated cytotoxicity. Cancer 79, 1180–1189.

Mo, Y., Wang, H., Liu, J., Lan, Y., Guo, R., Zhang, Yi, Xue, W., Zhang, Yuanming, 2015. Controlled release and targeted delivery to cancer cells of doxorubicin from polysaccharide-functionalised single-walled carbon nanotubes. J. Mater. Chem. B 3, 1846–1855.

Mokhtari, R.B., Homayouni, T.S., Baluch, N., Morgatskaya, E., Kumar, S., Das, B., Yeger, H., Mokhtari, R.B., Homayouni, T.S., Baluch, N., Morgatskaya, E., Kumar, S., Das, B., Yeger, H., 2017. Combination therapy in combating cancer. Oncotarget 8, 38022–38043.

Mosser, D.D., Caron, A.W., Bourget, L., Meriin, A.B., Sherman, M.Y., Morimoto, R.I., Massie, B., 2000. The chaperone function of hsp70 is required for protection against stress-induced apoptosis. Mol. Cell. Biol. 20, 7146–7159.

Muller, P.A.J., Vousden, K.H., Norman, J.C., 2011. p53 and its mutants in tumor cell migration and invasion. J. Cell Biol. 192, 209–218.

Munafó, D.B., Colombo, M.I., 2001. A novel assay to study autophagy: regulation of autophagosome vacuole size by amino acid deprivation. J. Cell Sci. 114, 3619–3629.

Murrow, L., Debnath, J., 2013. Autophagy as a stress-response and quality-control mechanism: implications for cell injury and human disease. Annu. Rev. Pathol. 8, 105–137.

Myung, D.-S., Park, Y.-L., Chung, C.-Y., Park, H.-C., Kim, J.-S., Cho, S.-B., Lee, W.-S., Lee, K.-H., Lee, J.-H., Joo, Y.-E., 2013. Expression of livin in colorectal cancer and its relationship to tumor cell behavior and prognosis. PLoS One 8, e73262.

Nagata, M., Nakayama, H., Tanaka, T., Yoshida, R., Yoshitake, Y., Fukuma, D., Kawahara, K., Nakagawa, Y., Ota, K., Hiraki, A., Shinohara, M., 2011. Overexpression of cIAP2 contributes to 5-FU resistance and a poor prognosis in oral squamous cell carcinoma. Br. J. Cancer 105, 1322–1330.

Nair K, L., Jagadeeshan, S., Nair, S.A., Kumar, G.S.V., 2011. Biological evaluation of 5-fluorouracil nanoparticles for cancer chemotherapy and its dependence on the carrier, PLGA. Int. J. Nanomedicine 6, 1685–1697.

Nakashima, K., Virgona, N., Miyazawa, M., Watanabe, T., Yano, T., 2010. The tocotrienol-rich fraction from rice bran enhances cisplatin-induced cytotoxicity in human mesothelioma H28 cells. Phyther. Res. 24, 1317–1321.

Nasr, M., Nafee, N., Saad, H., Kazem, A., 2014. Improved antitumor activity and reduced cardiotoxicity of epirubicin using hepatocyte-targeted nanoparticles combined with tocotrienols against hepatocellular carcinoma in mice. Eur. J. Pharm. Biopharm. 88, 216–225.

Natrah, M., Ezat WP, S., Syed, M., Rizal, M.A., Saperi, S., Ismail, S., Fuad, I., Azrif, M.M., 2012. Economic evaluation of monoclonal antibody in the management of colorectal cancer in Malaysia. BMC Health Serv. Res. 12, doi: 10.1186/1472-

6963-12-S1-P3.

Nesaretnam, K., Khor, H.T., Ganeson, J., Chong, Y.H., Sundram, K., Gapor, A., 1992. The effect of vitamin e tocotrienols from palm oil on chemically-induced mammary carcinogenesis in female rats. Nutr. Res. 12, 63–75.

Nesaretnam, K., Meganathan, P., 2011. Tocotrienols: inflammation and cancer. Ann. N. Y. Acad. Sci. 1229, 18–22.

Nesaretnam, K., Meganathan, P., Veerasenan, S.D., Selvaduray, K.R., 2012. Tocotrienols and breast cancer: the evidence to date. Genes Nutr. 7, 3–9.

Nesaretnam, K., Selvaduray, K.R., Abdul Razak, G., Veerasenan, S.D., Gomez, P.A., 2010. Effectiveness of tocotrienol-rich fraction combined with tamoxifen in the management of women with early breast cancer: a pilot clinical trial. Breast Cancer Res. 12, doi: 10.1186/bcr2726.

Ng, L.T., Lin, L.T., Chen, C.L., Chen, H.W., Wu, S.J., Lin, C.C., 2014. Anti-melanogenic effects of δ-tocotrienol are associated with tyrosinase-related proteins and MAPK signaling pathway in B16 melanoma cells. Phytomedicine 21, 978–983.

Nicoletti, I., Migliorati, G., Pagliacci, M.C., Grignani, F., Riccardi, C., 1991. A rapid and simple method for measuring thymocyte apoptosis by propidium iodide staining and flow cytometry. J. Immunol. Methods 139, 271–279.

Noguchi, M., Hirata, N., Suizu, F., 2014. The links between AKT and two intracellular proteolytic cascades: Ubiquitination and autophagy. Biochim. Biophys. Acta - Rev. Cancer 1846, 342–352.

Norbury, C.J., Zhivotovsky, B., 2004. DNA damage-induced apoptosis. Oncogene 23,

2797–2808.

Olive, P.L., Banáth, J.P., 2006. The comet assay: a method to measure DNA damage in individual cells. Nat. Protoc. 1, 23–29.

Oren, M., Rotter, V., 2010. Mutant p53 gain-of-function in cancer. Cold Spring Harb. Perspect. Biol. 2, doi: 10.1101/cshperspect.a001107.

Palozza, P., Verdecchia, S., Avanzi, L., Vertuani, S., Serini, S., Iannone, A., Manfredini, S., 2006. Comparative antioxidant activity of tocotrienols and the novel chromanyl-polyisoprenyl molecule FeAox-6 in isolated membranes and intact cells. Mol. Cell. Biochem. 287, 21–32.

Palumbo, M.O., Kavan, P., Miller, W.H., jr., Panasci, L., Assouline, S., Johnson, N., Cohen, V., Patenaude, F., Pollak, M., Jagoe, R.T., Batist, G., 2013. Systemic cancer therapy: achievements and challenges that lie ahead. Front. Pharmacol. 4, doi: 10.3389/fphar.2013.00057.

Parajuli, P., Tiwari, R.V., Sylvester, P.W., 2015a. Anti-proliferative effects of γ-tocotrienol are associated with suppression of c-Myc expression in mammary tumour cells. Cell Prolif. 48, 421–435.

Parajuli, P., Tiwari, R.V., Sylvester, P.W., 2015b. Anticancer effects of γ-tocotrienol are associated with a suppression in aerobic glycolysis. Biol. Pharm. Bull. Pharm. Bull. 38, 1352–1360.

Park, J.-I., Venteicher, A.S., Hong, J.Y., Choi, J., Jun, S., Shkreli, M., Chang, W., Meng, Z., Cheung, P., Ji, H., McLaughlin, M., Veenstra, T.D., Nusse, R., McCrea, P.D., Artandi, S.E., 2009. Telomerase modulates Wnt signalling by association with target gene chromatin. Nature 460, 66–72.

Park, S.K., Sanders, B.G., Kline, K., 2010. Tocotrienols induce apoptosis in breast cancer cell lines via an endoplasmic reticulum stress-dependent increase in extrinsic death receptor signaling. Breast Cancer Res. Treat. 124, 361–375.

Parker, R.A., Pearce, B.C., Clark, R.W., Gordon, D.A., Wright, J.J., 1993. Tocotrienols regulate cholesterol production in mammalian cells by post-transcriptional suppression of 3-hydroxy-3-methylglutaryl-coenzyme A reductase. J. Biol. Chem. 268, 11230–11238.

Paschall, A. V, Zimmerman, M.A., Torres, C.M., Yang, D., Chen, M.R., Li, X., Bieberich, E., Bai, A., Bielawski, J., Bielawska, A., Liu, K., 2014. Ceramide targets XIAP and cIAP1 to sensitize metastatic colon and breast cancer cells to apoptosis induction to suppress tumor progression. BMC Cancer 14, doi: 10.1186/1471-2407-14-24.

Patacsil, D., Tran, A.T., Cho, Y.S., Suy, S., Saenz, F., Malyukova, I., Ressom, H., Collins, S.P., Clarke, R., Kumar, D., 2012. Gamma-tocotrienol induced apoptosis is associated with unfolded protein response in human breast cancer cells. J. Nutr. Biochem. 23, 93–100.

Pattingre, S., Petiot, A., Codogno, P., 2004. Analyses of Gα-interacting protein and activator of G-protein-signaling-3 functions in macroautophagy. Methods Enzymol. 390, 17–31.

Paulsen, M., Ussat, S., Jakob, M., Scherer, G., Lepenies, I., Schütze, S., Kabelitz, D., Adam-Klages, S., 2008. Interaction with XIAP prevents full caspase-3/-7 activation in proliferating human T lymphocytes. Eur. J. Immunol. 38, 1979–1987.

Peh, H.Y., Tan, W.S.D., Liao, W., Wong, W.S.F., 2016. Vitamin E therapy beyond

cancer: Tocopherol versus tocotrienol. Pharmacol. Ther. 162, 152–169.

Peinado, H., Marin, F., Cubillo, E., Stark, H.-J., Fusenig, N., Nieto, M.A., Cano, A., 2004. Snail and E47 repressors of E-cadherin induce distinct invasive and angiogenic properties in vivo. J. Cell Sci. 117, 2827–2839.

Pemovska, T., Bigenzahn, J.W., Superti-Furga, G., 2018. Recent advances in combinatorial drug screening and synergy scoring. Curr. Opin. Pharmacol. 42, 102–110.

Phutthaphadoong, S., Yodkeeree, S., Chaiyasut, C., Limtrakul, P., 2012. Anti-cancer activities of α-and γ-tocotrienol against the human lung cancer. African J. Pharm. Pharmacol. 6, 620–629.

Pierpaoli, E., Viola, V., Pilolli, F., Piroddi, M., Galli, F., Provinciali, M., 2010. γ- and δ-tocotrienols exert a more potent anticancer effect than α-tocopheryl succinate on breast cancer cell lines irrespective of HER-2/neu expression. Life Sci. 86, 668–675.

Prasad, S., Gupta, S.C., Tyagi, A.K., Aggarwal, B.B., 2016. γ-Tocotrienol suppresses growth and sensitises human colorectal tumours to capecitabine in a nude mouse xenograft model by down-regulating multiple molecules. Br. J. Cancer 115, 814–824.

Prasad, V., Mailankody, S., 2017. Research and development spending to bring a single cancer drug to market and revenues after approval. JAMA Intern. Med. 177, doi: 10.1001/jamainternmed.2017.3601.

Pu, X., Wang, Z., Klaunig, J.E., 2015. Alkaline comet assay for assessing DNA damage in individual cells. In: Current Protocols in Toxicology. John Wiley & Sons, Inc., Hoboken, NJ, USA, pp. 3.12.1-3.12.11.

Puche, J.E., García-Fernández, M., Muntané, J., Rioja, J., González-Barón, S., Castilla Cortazar, I., 2008. Low doses of insulin-like growth factor-I induce mitochondrial protection in aging rats. Endocrinology 149, 2620–2627.

Queiroz, E.A.I.F., Puukila, S., Eichler, R., Sampaio, S.C., Forsyth, H.L., Lees, S.J., Barbosa, A.M., Dekker, R.F.H., Fortes, Z.B., Khaper, N., 2014. Metformin induces apoptosis and cell cycle arrest mediated by oxidative stress, AMPK and FOXO3a in MCF-7 breast cancer cells. PLoS One 9, doi: 10.1371/journal.pone.0098207.

Qureshi, A.A., Burger, W.C., Peterson, D.M., Elson, C.E., 1986. The structure of an inhibitor of cholesterol biosynthesis isolated from barley. J. Biol. Chem. 261, 10544–10550.

Rajasinghe, L.D., Gupta, S. V, 2017. Tocotrienol-rich mixture inhibits cell proliferation and induces apoptosis via down-regulation of the Notch-1/NF-κB pathways in NSCLC cells. Nutr. Diet. Suppl. Volume 9, 103–114.

Rajasinghe, L.D., Pindiprolu, R.H., Gupta, S.V., 2018. Delta-tocotrienol inhibits non-small-cell lung cancer cell invasion via the inhibition of NF-κB, uPA activator, and MMP-9. Onco. Targets. Ther. 11, 4301–4314.

Rajendran, P., Li, F., Manu, K.A., Shanmugam, M.K., Loo, S.Y., Kumar, A.P., Sethi, G., 2011. γ-Tocotrienol is a novel inhibitor of constitutive and inducible STAT3 signalling pathway in human hepatocellular carcinoma: Potential role as an antiproliferative, pro-apoptotic and chemosensitizing agent. Br. J. Pharmacol. 163, 283–298.

Ramdas, P., Radhakrishnan, A.K., Abdu Sani, A.A., Abdul-Rahman, P.S., 2019. Tocotrienols Modulate Breast Cancer Secretomes and Affect Cancer-Signaling

Pathways in MDA-MB-231 Cells: A Label-Free Quantitative Proteomic Analysis. Nutr. Cancer 1–9.

Ravanan, P., Srikumar, I.F., Talwar, P., 2017. Autophagy: The spotlight for cellular stress responses. Life Sci. 188, 53–67.

Riccardi, C., Nicoletti, I., 2006. Analysis of apoptosis by propidium iodide staining and flow cytometry. Nat. Protoc. 1, 1458–1461.

Rickmann, M., Vaquero, E.C., Malagelada, J.R., Molero, X., 2007. Tocotrienols induce apoptosis and autophagy in rat pancreatic stellate cells through the mitochondrial death pathway. Gastroenterology 132, 2518–2532.

Riedl, S.J., Renatus, M., Schwarzenbacher, R., Zhou, Q., Sun, C., Fesik, S.W., Liddington, R.C., Salvesen, G.S., 2001. Structural basis for the inhibition of caspase-3 by XIAP. Cell 104, 791–800.

Riss, T.L., Moravec, R.A., Niles, A.L., Duellman, S., Benink, H.A., Worzella, T.J., Minor, L., 2016. Cell viability assays, Assay Guidance Manual. Eli Lilly & Company and the National Center for Advancing Translational Sciences.

Roy, N., Deveraux, Q.L., Takahashi, R., Salvesen, G.S., Reed, J.C., 1997. The c-IAP-1 and c-IAP-2 proteins are direct inhibitors of specific caspases. EMBO J. 16, 6914–6925.

Russo, A., Bazan, V., Iacopetta, B., Kerr, D., Soussi, T., Gebbia, N., 2005. The TP53 colorectal Cancer international collaborative study on the prognostic and predictive significance of p53 mutation: Influence of tumor site, type of mutation, and adjuvant treatment. J. Clin. Oncol. 23, 7518–7528.

Ryter, S.W., Mizumura, K., Choi, A.M.K., 2014. The impact of autophagy on cell

death modalities. Int. J. Cell Biol. 2014, doi: 10.1155/2014/502676.

Sailo, B.L., Banik, K., Padmavathi, G., Javadi, M., Bordoloi, D., Kunnumakkara, A.B., 2018. Tocotrienols: The promising analogues of vitamin E for cancer therapeutics. Pharmacol. Res. doi: 10.1016/j.phrs.2018.02.017.

Sajó, I., 1977. Vinblastine inhibition of microtubule assembly in vitro. Acta Biochim. Biophys. Acad. Sci. Hung. 12, 259–261.

Sakai, M., Okabe, M., Tachibana, H., Yamada, K., 2006. Apoptosis induction by gamma-tocotrienol in human hepatoma Hep3B cells. J. Nutr. Biochem. 17, 672–676.

Samant, G. V., Sylvester, P.W., 2006. γ -Tocotrienol inhibits ErbB3-dependent PI3K/Akt mitogenic signalling in neoplastic mammary epithelial cells. Cell Prolif. 39, 563–574.

Samant, G. V., Wali, V.B., Sylvester, P.W., 2010. Anti-proliferative effects of gamma-tocotrienol on mammary tumour cells are associated with suppression of cell cycle progression. Cell Prolif. 43, 77–83.

Sato, C., Kaneko, S., Sato, A., Virgona, N., Namiki, K., Yano, T., 2017. Combination effect of δ-tocotrienol and γ-tocopherol on prostate cancer cell growth. J. Nutr. Sci. Vitaminol. (Tokyo). 63, 349–354.

Scarlatti, F., Maffei, R., Beau, I., Codogno, P., Ghidoni, R., 2008a. Role of non-canonical beclin 1-independent autophagy in cell death induced by resveratrol in human breast cancer cells. Cell Death Differ. 15, 1318–1329.

Scarlatti, F., Maffei, R., Beau, I., Ghidoni, R., Codogno, P., 2008b. Non-canonical autophagy: An exception or an underestimated form of autophagy? Autophagy 4,

1083–1085.

Schauss, A., Endres, J., Clewell, A., 2008. Safety of unsaturated vitamin E tocotrienols and their isomers, Tocotrienols: Vitamin E Beyond Tocopherols. Taylor & Francis.

Schonewolf, C.A., Mehta, M., Schiff, D., Wu, H., Haffty, B.G., Karantza, V., Jabbour, S.K., 2014. Autophagy inhibition by chloroquine sensitizes HT-29 colorectal cancer cells to concurrent chemoradiation. World J. Gastrointest. Oncol. 6, 74–82.

Scott, F.L., Denault, J.-B., Riedl, S.J., Shin, H., Renatus, M., Salvesen, G.S., 2005. XIAP inhibits caspase-3 and -7 using two binding sites: evolutionarily conserved mechanism of IAPs. EMBO J. 24, 645–655.

Sen, C.K., Khanna, S., Roy, S., 2006. Tocotrienols: Vitamin E beyond tocopherols. In: Life Sciences. pp. 2088–2098.

Serbinova, E., Kagan, V., Han, D., Packer, L., 1991. Free radical recycling and intramembrane mobility in the antioxidant properties of alpha-tocopherol and alpha-tocotrienol. Free Radic. Biol. Med. 10, 263–275.

Shah, S., Sylvester, P.W., 2004. Tocotrienol-induced caspase-8 activation is unrelated to death receptor apoptotic signaling in neoplastic mammary epithelial cells. Exp. Biol. Med. (Maywood). 229, 745–755.

Shah, S.J., Sylvester, P.W., 2005. Gamma-tocotrienol inhibits neoplastic mammary epithelial cell proliferation by decreasing Akt and nuclear factor kappaB activity. Exp. Biol. Med. (Maywood). 230, 235–241.

Sharifi, S., Barar, J., Hejazi, M.S., Samadi, N., 2015. Doxorubicin changes Bax /Bcl-

xL ratio, caspase-8 and 9 in breast cancer cells. Adv. Pharm. Bull. 5, 351–359.

Shen, H.-M., Codogno, P., 2011. Autophagic cell death: Loch Ness monster or endangered species? Autophagy 7, 457–465.

Shen, S., Codogno, P., 2016. The role of autophagy in cell death. Autophagy Cancer, Other Pathol. Inflammation, Immunity, Infect. Aging 139–154.

Shibata, A., Nakagawa, K., Sookwong, P., Tsuduki, T., Asai, A., Miyazawa, T., 2010. α-Tocopherol attenuates the cytotoxic effect of δ-tocotrienol in human colorectal adenocarcinoma cells. Biochem. Biophys. Res. Commun. 397, 214–219.

Shin-Kang, S., Ramsauer, V.P., Lightner, J., Chakraborty, K., Stone, W., Campbell, S., Reddy, S.A.G., Krishnan, K., 2011. Tocotrienols inhibit AKT and ERK activation and suppress pancreatic cancer cell proliferation by suppressing the ErbB2 pathway. Free Radic. Biol. Med. 51, 1164–1174.

Shin, S.W., Kim, S.Y., Park, J.-W., 2012. Autophagy inhibition enhances ursolic acid-induced apoptosis in PC3 cells. Biochim. Biophys. Acta - Mol. Cell Res. 1823, 451–457.

Shirode, A.B., Sylvester, P.W., 2010. Synergistic anticancer effects of combined gamma-tocotrienol and celecoxib treatment are associated with suppression in Akt and NFkappaB signaling. Biomed. Pharmacother. 64, 327–332.

Shirode, A.B., Sylvester, P.W., 2011. Mechanisms mediating the synergistic anticancer effects of combined gamma-tocotrienol and celecoxib treatment. J. Bioanal. Biomed. 3, 1–7.

Shun, M.-C., Yu, W., Gapor, A., Parsons, R., Atkinson, J., Sanders, B.G., Kline, K., 2004. Pro-apoptotic mechanisms of action of a novel vitamin E analog (α-TEA)

and a naturally occurring form of vitamin E (δ-Tocotrienol) in MDA-MB-435 human breast cancer cells. Nutr. Cancer 48, 95–105.

Sivandzade, F., Bhalerao, A., Cucullo, L., 2019. Analysis of the Mitochondrial Membrane Potential Using the Cationic JC-1 Dye as a Sensitive Fluorescent Probe. Bio-protocol 9.

Sonowal, H., Pal, P.B., Wen, J.-J., Awasthi, S., Ramana, K. V., Srivastava, S.K., 2017. Aldose reductase inhibitor increases doxorubicin-sensitivity of colon cancer cells and decreases cardiotoxicity. Sci. Rep. 7, doi: 10.1038/s41598-017-03284-w.

Soo, H.-C., Chung, F.F.-L., Lim, K.-H., Yap, V.A., Bradshaw, T.D., Hii, L.-W., Tan, S.-H., See, S.-J., Tan, Y.-F., Leong, C.-O., Mai, C.-W., 2017. Cudraflavone C induces tumor-specific apoptosis in colorectal cancer cells through inhibition of the phosphoinositide 3-kinase (PI3K)-AKT pathway. PLoS One 12, doi: 10.1371/journal.pone.0170551.

Springett, G.M., Husain, K., Neuger, A., Centeno, B., Chen, D.T., Hutchinson, T.Z., Lush, R.M., Sebti, S., Malafa, M.P., 2015. A Phase I Safety, Pharmacokinetic, and Pharmacodynamic Presurgical Trial of Vitamin E delta-tocotrienol in Patients with Pancreatic Ductal Neoplasia. EBioMedicine 2, 1987–1995.

Srivastava, J.K., Gupta, S., 2006. Tocotrienol-rich fraction of palm oil induces cell cycle arrest and apoptosis selectively in human prostate cancer cells. Biochem. Biophys. Res. Commun. 346, 447–453.

Stennicke, H.R., Deveraux, Q.L., Humke, E.W., Reed, J.C., Dixit, V.M., Salvesen, G.S., 1999. Caspase-9 can be activated without proteolytic processing. J. Biol. Chem. 274, 8359–8362.

Steuber, N., Vo, K., Wadhwa, R., Birch, J., Iacoban, P., Chavez, P., Elbayoumi, T.A.,

2016. Tocotrienol nanoemulsion platform of curcumin elicit elevated apoptosis and augmentation of anticancer efficacy against breast and ovarian carcinomas. Int. J. Mol. Sci. 17, doi:10.3390/ijms17111792.

Stewart, D.J., Stewart, A.A., Wheatley-Price, P., Batist, G., Kantarjian, H.M., Schiller, J., Clemons, M., Bradford, J.-P., Gillespie, L., Kurzrock, R., 2018. The importance of greater speed in drug development for advanced malignancies. Cancer Med. 7, 1824–1836.

Sun, W., Wang, Q., Chen, B., Liu, J., Liu, H., Xu, W., 2008. γ-Tocotrienol-induced apoptosis in human gastric cancer SGC-7901 cells is associated with a suppression in mitogen-activated protein kinase signalling. Br. J. Nutr. 99, 1247–1254.

Sun, W., Xu, W., Liu, H., Liu, J., Wang, Q., Zhou, J., Dong, F., Chen, B., 2009. γ-Tocotrienol induces mitochondria-mediated apoptosis in human gastric adenocarcinoma SGC-7901 cells. J. Nutr. Biochem. 20, 276–284.

Sylvester, P.W., 2012. Synergistic anticancer effects of combined γ-tocotrienol with statin or receptor tyrosine kinase inhibitor treatment. Genes Nutr. 7, 63–74.

Sylvester, P.W., Nachnani, A., Shah, S., Briski, K.P., 2002. Role of GTP-binding proteins in reversing the antiproliferative effects of tocotrienols in preneoplastic mammary epithelial cells. Asia Pac. J. Clin. Nutr. 11 Suppl 7, S452-9.

Sylvester, P.W., Shah, S.J., 2005. Mechanisms mediating the antiproliferative and apoptotic effects of vitamin E in mammary cancer cells. Front. Biosci. 10, 699–709.

Sylvester, P.W., Tiwari, R. V., 2016. Role of autophagy in mediating the anticancer effects of tocotrienols. In: Autophagy in Current Trends in Cellular Physiology

and Pathology. InTech, p. doi: 10.5772/64131.

Sylvester, P.W., Wali, V.B., Bachawal, S. V, Shirode, A.B., Ayoub, N.M., Akl, M.R., 2011. Tocotrienol combination therapy results in synergistic anticancer response. Front. Biosci. (Landmark Ed. 16, 3183–3195.

Taatjes, D.J., Sobel, B.E., Budd, R.C., 2008. Morphological and cytochemical determination of cell death by apoptosis. Histochem. Cell Biol. 129, 33–43.

Tait, S.W.G., Green, D.R., 2008. Caspase-independent cell death: leaving the set without the final cut. Oncogene 27, 6452–6461.

Takahashi, K., Loo, G., 2004. Disruption of mitochondria during tocotrienol-induced apoptosis in MDA-MB-231 human breast cancer cells. Biochem. Pharmacol. 67, 315–324.

Takano, H., Momota, Y., Kani, K., Aota, K., Yamamura, Y., Yamanoi, T., Azuma, M., 2015. γ-tocotrienol prevents 5-FU-induced reactive oxygen species production in human oral keratinocytes through the stabilization of 5-FU-induced activation of Nrf2. Int. J. Oncol. 46, 1453–1460.

Takeuchi, H., Kim, J., Fujimoto, A., Umetani, N., Mori, T., Bilchik, A., Turner, R., Tran, A., Kuo, C., Hoon, D.S.B., 2005. X-linked inhibitor of apoptosis protein expression level in colorectal cancer is regulated by hepatocyte growth factor/c-met pathway via Akt Signaling. Clin. Cancer Res. 11, 7621–7628.

Tallarida, R.J., 2011. Quantitative methods for assessing drug synergism. Genes Cancer 2, 1003–1008.

Tang, K.D., Liu, J., Russell, P.J., Clements, J.A., Ling, M.-T., 2019. Gamma-Tocotrienol Induces Apoptosis in Prostate Cancer Cells by Targeting the Ang-

1/Tie-2 Signalling Pathway. Int. J. Mol. Sci. 20, 1–12.

Tham, S.-Y., Loh, H.-S., Mai, C.-W., Fu, J.-Y., 2019. Tocotrienols modulate a life or death decision in cancers. Int. J. Mol. Sci. 20, doi: 10.3390/ijms20020372.

Thant, A.A., Wu, Y., Lee, J., Mishra, D.K., Garcia, H., Koeffler, H.P., Vadgama, J. V, 2008. Role of caspases in 5-FU and selenium-induced growth inhibition of colorectal cancer cells. Anticancer Res. 28, 3579–3592.

Thirumaran, R., Gilman, P.B., 2007. Cytotoxic chemotherapy in clinical treatment of cancer. Cancer Immunother. 101–116.

Thomé, M.P., Filippi-Chiela, E.C., Villodre, E.S., Migliavaca, C.B., Onzi, G.R., Felipe, K.B., Lenz, G., 2016. Ratiometric analysis of acridine orange staining in the study of acidic organelles and autophagy. J. Cell Sci. 129, 4622–4632.

Thomsen, C.B., Andersen, R.F., Steffensen, K.D., Adimi, P., Jakobsen, A., 2019. Delta tocotrienol in recurrent ovarian cancer. A phase II trial. Pharmacol. Res. 141, 392–396.

Thorburn, A., 2008. Apoptosis and Autophagy: regulatory connections between two supposedly different processes. Apoptosis 13, 1–9.

Thorburn, A., Thamm, D.H., Gustafson, D.L., 2014. Autophagy and cancer therapy. Mol. Pharmacol. 85, 830–838.

Thorn, C.F., Oshiro, C., Marsh, S., Hernandez-Boussard, T., McLeod, H., Klein, T.E., Altman, R.B., 2011. Doxorubicin pathways: pharmacodynamics and adverse effects. Pharmacogenet. Genomics 21, 440–446.

Thornberry, N.A., Lazebnik, Y., 1998. Caspases: enemies within. Science 281, 1312–1316.

Thun, M.J., DeLancey, J.O., Center, M.M., Jemal, A., Ward, E.M., 2010. The global burden of cancer: priorities for prevention. Carcinogenesis 31, 100–110.

Tian, S., Lin, J., Zhou, J., Wang, X., Li, Y., Ren, X., Yu, W., Zhong, W., Xiao, J., Sheng, F., Chen, Y., Jin, C., Li, S., Zheng, Z., Xia, B., 2010. Beclin 1-independent autophagy induced by a Bcl-X L /Bcl-2 targeting compound. Landes Biosci. 1032 Autophagy 18, 1032–1041.

Tiwari, R. V., Parajuli, P., Sylvester, P.W., 2015. Synergistic anticancer effects of combined γ-tocotrienol and oridonin treatment is associated with the induction of autophagy. Mol. Cell. Biochem. 408, 123–137.

Tiwari, R. V, Parajuli, P., Sylvester, P.W., 2013. γ-Tocotrienol-induced autophagy in malignant mammary cancer cells. Exp. Biol. Med. 239, 33–44.

Tran, A.T., Ramalinga, M., Kedir, H., Clarke, R., Kumar, D., 2015. Autophagy inhibitor 3-methyladenine potentiates apoptosis induced by dietary tocotrienols in breast cancer cells. Eur. J. Nutr. 54, 265–272.

Tuerdi, G., Ichinomiya, S., Sato, H., Siddig, S., Suwa, E., Iwata, H., Yano, T., Ueno, K., 2013. Synergistic effect of combined treatment with gamma-tocotrienol and statin on human malignant mesothelioma cells. Cancer Lett. 339, 116–127.

Valente, G., Morani, F., Nicotra, G., Fusco, N., Peracchio, C., Titone, R., Alabiso, O., Arisio, R., Katsaros, D., Benedetto, C., Isidoro, C., 2014. Expression and clinical significance of the autophagy proteins BECLIN 1 and LC3 in ovarian cancer. Biomed Res. Int. 2014, doi: 10.1155/2014/462658.

Van Norman, G.A., 2016. Drugs, devices, and the FDA: Part 1: An overview of approval processes for drugs. JACC Basic to Transl. Sci. 1, 170–179.

Van Rensburg, C.E., Jooné, G., Anderson, R., 1998. Alpha-tocopherol antagonizes the multidrug-resistance-reversal activity of cyclosporin A, verapamil, GF120918, clofazimine and B669. Cancer Lett. 127, 107–112.

Vanamee, É.S., Faustman, D.L., 2018. Structural principles of tumor necrosis factor superfamily signaling. Sci. Signal. 11, doi: 10.1126/scisignal.aao4910.

Viola, V., Ciffolilli, S., Legnaioli, S., Piroddi, M., Betti, M., Mazzini, F., Pierpaoli, E., Provinciali, M., Galli, F., 2013. Mitochondrial-dependent anticancer activity of δ-tocotrienol and its synthetic derivatives in HER-2/neu overexpressing breast adenocarcinoma cells. BioFactors 39, 485–493.

Viola, V., Pilolli, F., Piroddi, M., Pierpaoli, E., Orlando, F., Provinciali, M., Betti, M., Mazzini, F., Galli, F., 2012. Why tocotrienols work better: insights into the in vitro anti-cancer mechanism of vitamin E. Genes Nutr. 7, 29–41.

Visconti, R., Monica, R. Della, Grieco, D., 2016. Cell cycle checkpoint in cancer: a therapeutically targetable double-edged sword. J. Exp. Clin. Cancer Res. 35, doi: 10.1186/s13046-016-0433-9.

Wada, S., 2009. Chemoprevention of tocotrienols: The mechanism of antiproliferative effects. In: Food Factors for Health Promotion. KARGER, Basel, pp. 204–216.

Wada, S., Naito, Y., Matsushita, Y., Nouchi, M., Kawai, M., Minami, E., Aoi, W., Ikeda, S., Higashi, A., Yoshikawa, T., 2017. δ-Tocotrienol suppresses tumorigenesis by inducing apoptosis and blocking the COX-2/PGE2 pathway that stimulates tumor–stromal interactions in colon cancer. J. Funct. Foods 35, 428–435.

Wadegaonkar, V.P., Wadegaonkar, P.A., 2012. Withaferin A targets apoptosis inhibitor cIAP1: A potential anticancer candidate. J. Appl. Pharm. Sci. 2, 154–307

157.

Wali, V.B., Bachawal, S. V., Sylvester, P.W., 2009a. Suppression in mevalonate synthesis mediates antitumor effects of combined statin and gamma-tocotrienol treatment. Lipids 44, 925–934.

Wali, V.B., Bachawal, S. V., Sylvester, P.W., 2009b. Combined treatment of gamma-tocotrienol with statins induce mammary tumor cell cycle arrest in G1. Exp. Biol. Med. (Maywood). 234, 639–650.

Wali, V.B., Sylvester, P.W., 2007. Synergistic antiproliferative effects of γ-tocotrienol and statin treatment on mammary tumor cells. Lipids 42, 1113–1123.

Wang, C., Husain, K., Zhang, A., Centeno, B.A., Chen, D.-T., Tong, Z., Sebti, S.M., Malafa, M.P., 2015a. EGR-1/Bax pathway plays a role in vitamin E δ-tocotrienol-induced apoptosis in pancreatic cancer cells. J. Nutr. Biochem. 26, 797–807.

Wang, C., Ju, H., Shen, C., Tong, Z., 2015b. miR-429 mediates δ-tocotrienol-induced apoptosis in triple-negative breast cancer cells by targeting XIAP. Int. J. Clin. Exp. Med. 8, 15648–15656.

Was, H., Barszcz, K., Czarnecka, J., Kowalczyk, A., Bernas, T., Uzarowska, E., Koza, P., Klejman, A., Piwocka, K., Kaminska, B., Sikora, E., 2017. Bafilomycin A1 triggers proliferative potential of senescent cancer cells in vitro and in NOD/SCID mice. Oncotarget 8, 9303–9322.

Weber, K., Roelandt, R., Bruggeman, I., Estornes, Y., Vandenabeele, P., 2018. Nuclear RIPK3 and MLKL contribute to cytosolic necrosome formation and necroptosis. Commun. Biol. 1, doi: 10.1038/s42003-017-0007-1.

Wei, Y., Fan, T., Yu, M., 2008. Inhibitor of apoptosis proteins and apoptosis. Acta Biochim Biophys Sin 40, 278–288.

White Al-Habeeb, N., Kulasingam, V., Diamandis, E.P., Yousef, G.M., Tsongalis, G.J., Vermeulen, L., Zhu, Z., Kamel-Reid, S., 2016. The use of targeted therapies for precision medicine in oncology. Clin. Chem. 62, 1556–1564.

White, M.C., Holman, D.M., Boehm, J.E., Peipins, L.A., Grossman, M., Henley, S.J., 2014. Age and cancer risk: a potentially modifiable relationship. Am. J. Prev. Med. 46, S7-15.

Wilankar, C., Khan, N.M., Checker, R., Sharma, D., Patwardhan, R., Gota, V., Sandur, S.K., Devasagayam, T.P.A., 2011. γ-Tocotrienol induces apoptosis in human T cell lymphoma through activation of both intrinsic and extrinsic pathways. Curr. Pharm. Des. 17, 2176–2189.

Wong, R.S.Y., 2011. Apoptosis in cancer: from pathogenesis to treatment. J. Exp. Clin. Cancer Res. 30, doi: 10.1186/1756-9966-30-87.

Workman, P., Draetta, G.F., Schellens, J.H.M., Bernards, R., 2017. How much longer will we put up with $100,000 cancer drugs? Cell 168, 579–583.

World Cancer Research Fund/American Institute for Cancer Research, 2018. Diet, Nutrition, Physical Activity and Cancer: a Global Perspective A summary of the Third Expert Report. London.

Wu, S.-J., Ng, L.-T., 2010. Tocotrienols inhibited growth and induced apoptosis in human HeLa cells through the cell cycle signaling pathway. Integr. Cancer Ther. 9, 66–72.

Wu, Y., Zhao, D., Zhuang, J., Zhang, F., Xu, C., 2016. Caspase-8 and caspase-9

functioned differently at different stages of the cyclic stretch-induced apoptosis in human periodontal ligament cells. PLoS One 11, doi: 10.1371/journal.pone.0168268.

Xiao, Z., Chen, Z., Gunasekera, A.H., Sowin, T.J., Rosenberg, S.H., Fesik, S., Zhang, H., 2003. Chk1 mediates S and G2 arrests through Cdc25A degradation in response to DNA-damaging agents. J. Biol. Chem. 278, 21767–21773.

Xiong, A., Yu, W., Liu, Y., Sanders, B.G., Kline, K., 2016. Elimination of ALDH+ breast tumor initiating cells by docosahexanoic acid and/or gamma tocotrienol through SHP-1 inhibition of Stat3 signaling. Mol. Carcinog. 55, 420–430.

Xu, W.-L., Liu, J.-R., Liu, H.-K., Qi, G.-Y., Sun, X.-R., Sun, W.-G., Chen, B.-Q., 2009. Inhibition of proliferation and induction of apoptosis by gamma-tocotrienol in human colon carcinoma HT-29 cells. Nutrition 25, 555–566.

Xu, W., Du, M., Zhao, Y., Wang, Q., Sun, W., Chen, B., 2012. γ-Tocotrienol inhibits cell viability through suppression of β-catenin/Tcf signaling in human colon carcinoma HT-29 cells. J. Nutr. Biochem. 23, 800–807.

Xu, W., Mi, Y., He, P., He, S., Niu, L., 2017. γ-Tocotrienol inhibits proliferation and induces apoptosis via the mitochondrial pathway in human cervical cancer HeLa cells. Molecules 22, doi: 10.3390/molecules22081299.

Yamasaki, M., Nishimura, M., Sakakibara, Y., Suiko, M., Morishita, K., Nishiyama, K., 2014. Delta-tocotrienol induces apoptotic cell death via depletion of intracellular squalene in ED40515 cells. Food Funct. 5, 2842–2849.

Yang, F., Teves, S.S., Kemp, C.J., Henikoff, S., 2014. Doxorubicin, DNA torsion, and chromatin dynamics. Biochim. Biophys. Acta - Rev. Cancer 1845, 84–89.

Yang, J., Zhang, Q., Liu, T., 2018. Autophagy facilitates anticancer effect of 5-fluorouracil in HCT-116 cells. J. Cancer Res. Ther. 14, S1141–S1147.

Yang, Z., Xiao, H., Jin, H., Koo, P.T., Tsang, D.J., Yang, C.S., 2010. Synergistic actions of atorvastatin with γ-tocotrienol and celecoxib against human colon cancer HT29 and HCT116 cells. Int. J. Cancer 126, 852–863.

Yao, C.W., Kang, K.A., Piao, M.J., Ryu, Y.S., Fernando, P.M.D.J., Oh, M.C., Park, J.E., Shilnikova, K., Na, S.-Y., Jeong, S.U., Boo, S.-J., Hyun, J.W., 2017. Reduced autophagy in 5-fluorouracil resistant colon cancer cells. Biomol. Ther. (Seoul). 25, 315–320.

Yap, W.N., Chang, P.N., Han, H.Y., Lee, D.T.W., Ling, M., Wong, Y.., Yap, Y.L., 2008. Gamma-tocotrienol suppresses prostate cancer cell proliferation and invasion through multiple-signalling pathways. Br. J. Cancer 99, 1832–1841.

Yap, W.N., Zaiden, N., Luk, S., Lee, D.T.W., Ling, M.-T., Wong, Y.-C., Yap, Y.L., 2010a. In vivo evidence of γ-tocotrienol as a chemosensitizer in the treatment of hormone-refractory prostate cancer. Pharmacology 85, 248–258.

Yap, W.N., Zaiden, N., Tan, Y.L., Ngoh, C.P., Zhang, X.W., Wong, Y.C., Ling, M.T., Yap, Y.L., 2010b. Id1, inhibitor of differentiation, is a key protein mediating anti-tumor responses of gamma-tocotrienol in breast cancer cells. Cancer Lett. 291, 187–199.

Ye, C., Zhao, W., Li, M., Zhuang, J., Yan, X., Lu, Q., Chang, C., Huang, X., Zhou, J., Xie, B., Zhang, Z., Yao, X., Yan, J., Guo, H., 2015. δ-tocotrienol induces human bladder cancer cell growth arrest, apoptosis and chemosensitization through inhibition of STAT3 pathway. PLoS One 10, doi: 10.1371/journal.pone.0122712.

Yeganehjoo, H., DeBose-Boyd, R., McFarlin, B.K., Mo, H., 2017. Synergistic Impact

of δ-tocotrienol and geranylgeraniol on the growth and HMG CoA reductase of human DU145 prostate carcinoma cells. Nutr. Cancer 69, 682–691.

Yonekawa, T., Thorburn, A., 2013. Autophagy and Cell Death. Essays Biochem. 55, 105.

Yoshida, Y., Niki, E., Noguchi, N., 2003. Comparative study on the action of tocopherols and tocotrienols as antioxidant: chemical and physical effects. Chem. Phys. Lipids 123, 63–75.

Yoshii, S.R., Mizushima, N., 2017. Monitoring and measuring autophagy. Int. J. Mol. Sci. 18, doi: 10.3390/ijms18091865.

Yu, W., Jia, L., Park, S.-K., Li, J., Gopalan, A., Simmons-Menchaca, M., Sanders, B.G., Kline, K., 2009. Anticancer actions of natural and synthetic vitamin E forms: RRR-alpha-tocopherol blocks the anticancer actions of gamma-tocopherol. Mol. Nutr. Food Res. 53, 1573–1581.

Yusof, K.M., Makpol, S., Jamal, R., Harun, R., Mokhtar, N., Ngah, W.Z.W., 2015. γ-Tocotrienol and 6-gingerol in combination synergistically induce cytotoxicity and apoptosis in HT-29 and SW837 human colorectal cancer cells. Molecules 20, 10280–10297.

Zhang, H.-W., Hu, J.-J., Fu, R.-Q., Liu, X., Zhang, Y.-H., Li, J., Liu, L., Li, Y.-N., Deng, Q., Luo, Q.-S., Ouyang, Q., Gao, N., 2018. Flavonoids inhibit cell proliferation and induce apoptosis and autophagy through downregulation of PI3Kγ mediated PI3K/AKT/mTOR/p70S6K/ULK signaling pathway in human breast cancer cells. Sci. Rep. 8, doi: 10.1038/s41598-018-29308-7.

Zhang, J.-S., Li, D.-M., He, N., Liu, Y.-H., Wang, C.-H., Jiang, S.-Q., Chen, B.-Q., Liu, J.-R., 2011. A paraptosis-like cell death induced by δ-tocotrienol in human

colon carcinoma SW620 cells is associated with the suppression of the Wnt signaling pathway. Toxicology 285, 8–17.

Zhang, J.-S., Li, D.-M., Ma, Y., He, N., Gu, Q., Wang, F.-S., Jiang, S.-Q., Chen, B.-Q., Liu, J.-R., 2013. γ-Tocotrienol Induces Paraptosis-Like Cell Death in Human Colon Carcinoma SW620 Cells. PLoS One 8, doi: 10.1371/journal.pone.0057779.

Zhang, J.-S., Zhang, S.-J., Li, Q., Liu, Y.-H., He, N., Zhang, J., Zhou, P.-H., Li, M., Guan, T., Liu, J.-R., 2015. Tocotrienol-rich fraction (TRF) suppresses the growth of human colon cancer xenografts in Balb/C nude mice by the Wnt pathway. PLoS One 10, doi: 10.1371/journal.pone.0122175.

Zhang, J., Dai, Q., Park, D., Deng, X., 2016. Targeting DNA replication stress for cancer therapy. Genes (Basel). 7, doi: 10.3390/genes7080051.

Zhang, Z., Zhang, Y.F., Lv, J.Y., Wang, J.C., 2015. The survivin suppressant YM155 reverses doxorubicin resistance in osteosarcoma. Int. J. Clin. Exp. Med. 8, 18032–18040.

Zhao, L., Au, J.L.-S., Wientjes, M.G., 2010. Comparison of methods for evaluating drug-drug interaction. Front. Biosci. (Elite Ed). 2, 241–249.

Zhou, C., Tabb, M.M., Sadatrafiei, A., Grün, F., Blumberg, B., 2004. Tocotrienols activate the steroid and xenobiotic receptor, SXR, and selectively regulate expression of its target genes. Drug Metab. Dispos. 32, 1075–1082.

Zhu, J., Horbinski, C., Guo, F., Watkins, S., Uchiyama, Y., Chu, C.T., 2007. Regulation of autophagy by extracellular signal-regulated protein kinases during 1-methyl-4-phenylpyridinium-induced cell death. Am. J. Pathol. 170, 75–86.

Ziegler, U., Groscurth, P., 2004. Morphological features of cell death. Physiology 19,

124–128.

Appendices for Chapter Four (A4)

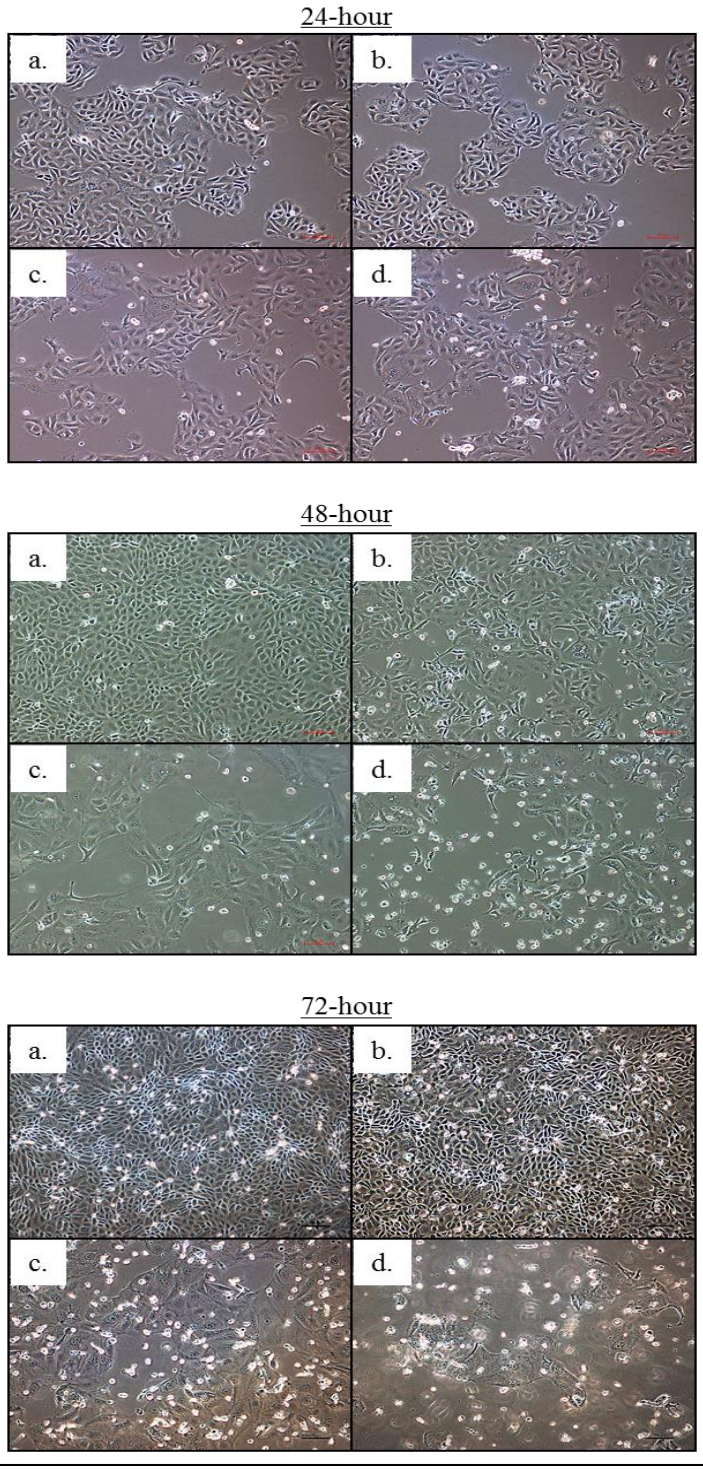

Figure A4.1 Phase-contrast micrographs of Caco-2 at various time points after receiving treatments of δT3, 5FU and the combined treatment. a, vehicle control; b, δT3; c, 5FU; d, δT3 + 5FU. Scale bar represents 100μm.

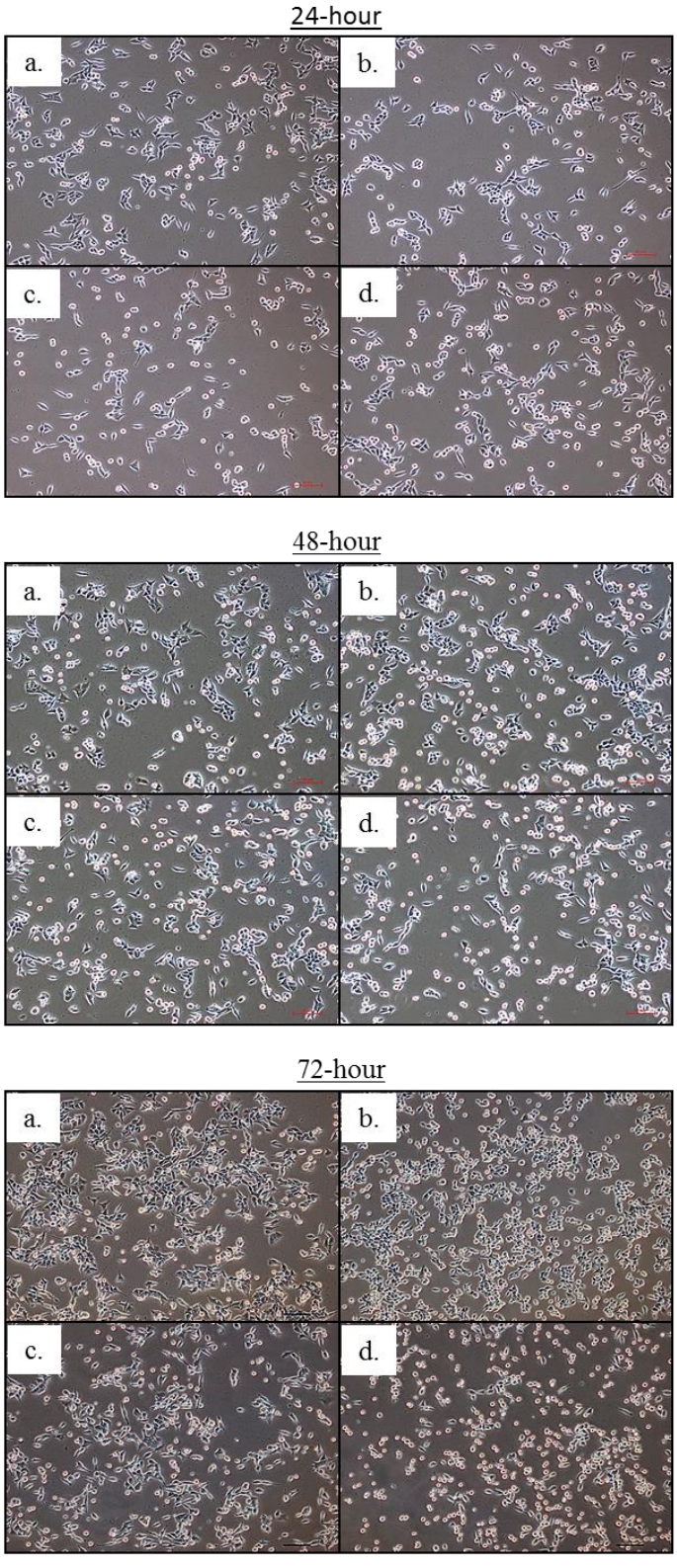

Figure A4.2 Phase-contrast micrographs of SW48 at various time points after receiving treatments of δT3, 5FU and the combined treatment. a, vehicle control; b, δT3; c, 5FU; d, δT3 + 5FU. Scale bar represents 100μm.

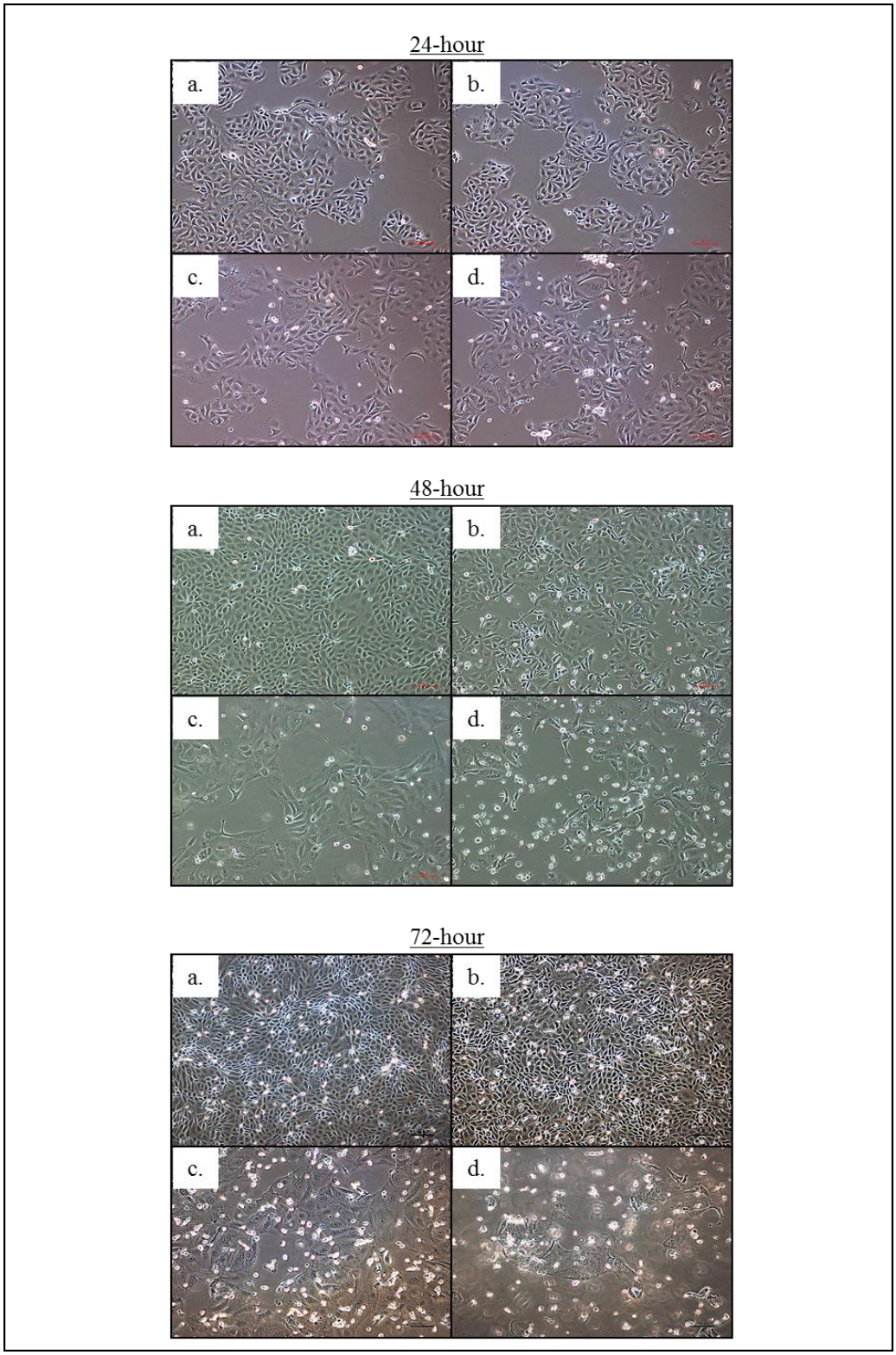

Figure A4.3 Phase-contrast micrographs of Caco-2 at various time points after receiving treatments of δT3, Dox and the combined treatment. a, vehicle control; b, δT3; c, Dox; d, δT3 + Dox. Scale bar represents 100μm.

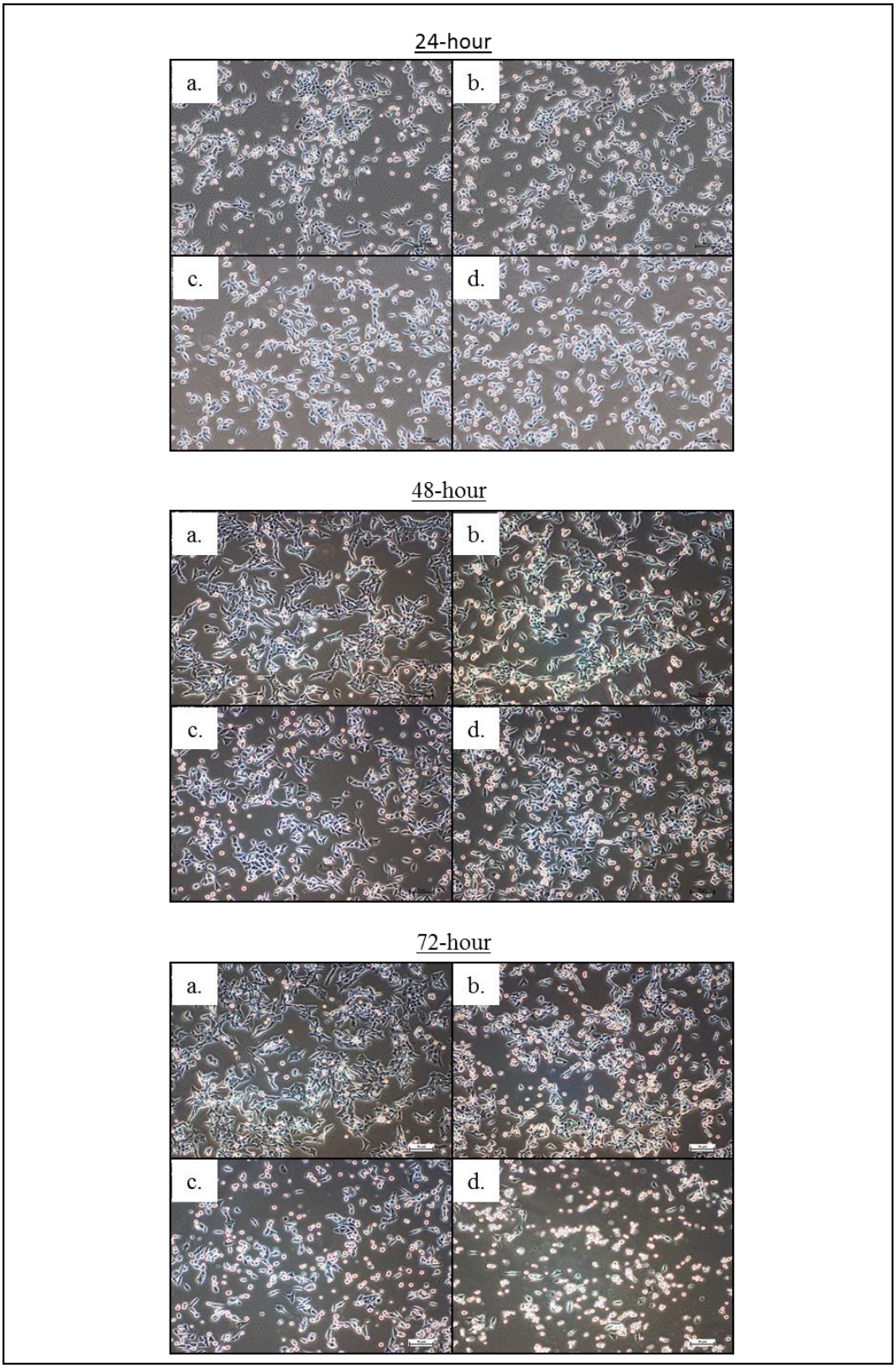

Figure A4.4 Phase-contrast micrographs of SW48 at various time points after receiving treatments of δ-tocotrienol, doxorubicin and the combined treatment. a, vehicle control; b, δT3; c, Dox; d, δT3 + Dox. Scale bar represents 100μm.

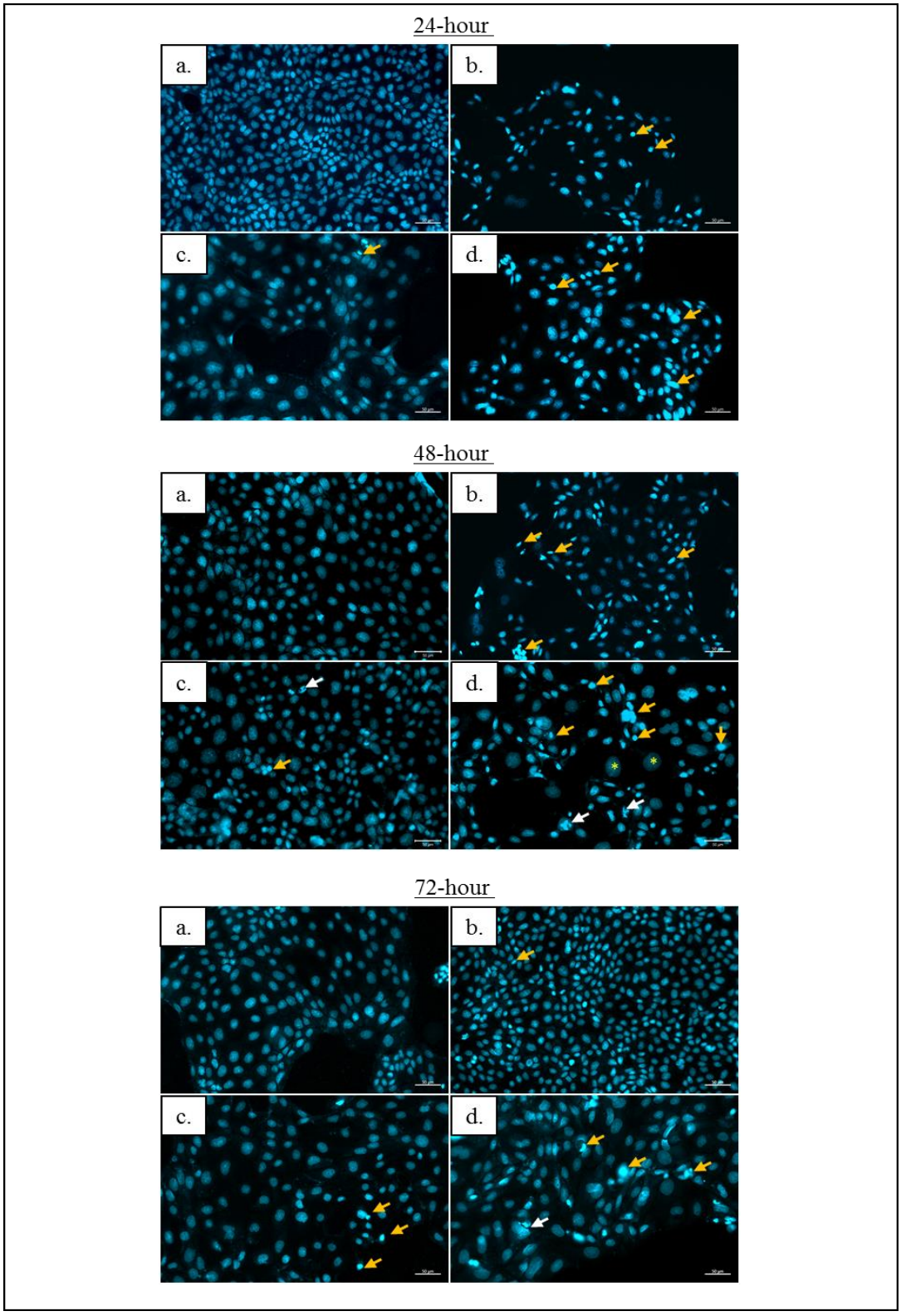

Figure A4.5 Nuclear profiles of Caco-2 at various time points after receiving treatments of δT3, 5FU and the combined treatment. a, vehicle control; b, δT3; c, 5FU; d, δT3 + 5FU. Yellow arrow, nuclear condensation; white arrow, nuclear fragmentation; Scale bar represents 50μm.

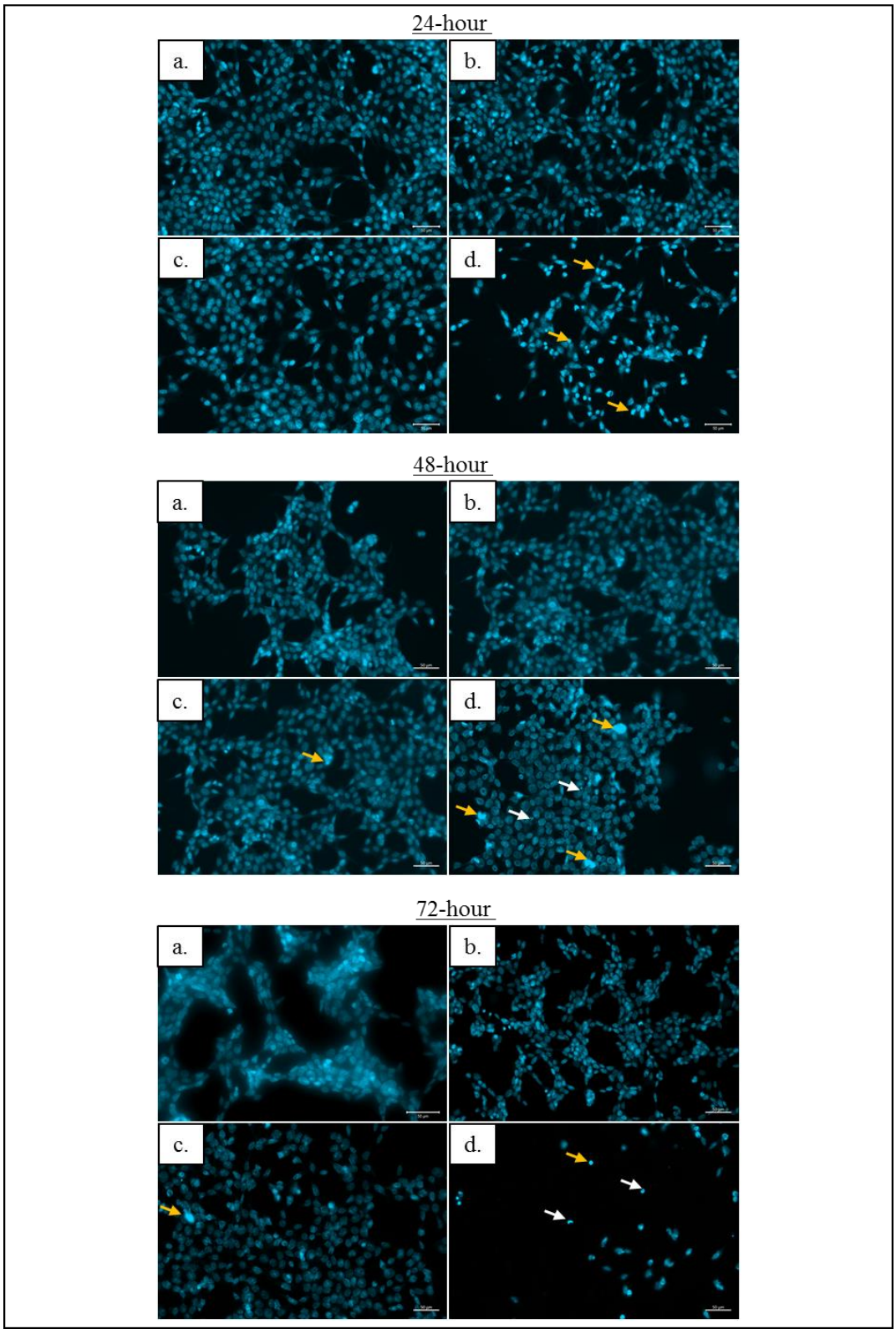

Figure A4.6 Nuclear profiles of SW48 at various time points after receiving treatments of δT3, 5FU and the combined treatment. a, vehicle control; b, δT3; c, 5FU; d, δT3 + 5FU. Yellow arrow, nuclear condensation; white arrow, nuclear fragmentation; Scale bar represents 50μm.

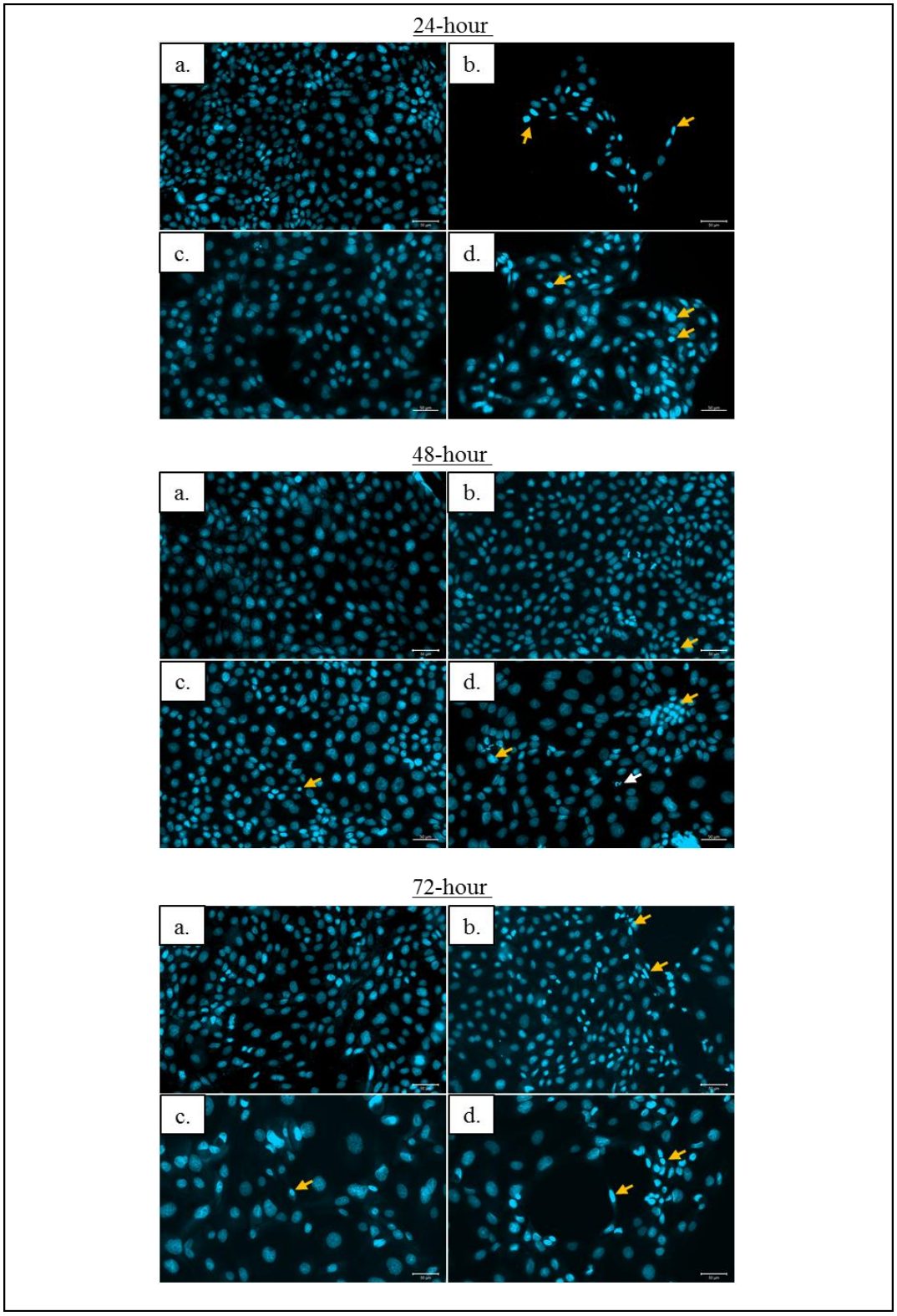

Figure A4.7 Nuclear profiles of Caco-2 at various time points after receiving treatments of δT3, Dox and the combined treatment. a, vehicle control; b, δT3; c, 5FU; d, δT3 + Dox. Yellow arrow, nuclear condensation; white arrow, nuclear fragmentation; Scale bar represents 50 μm.

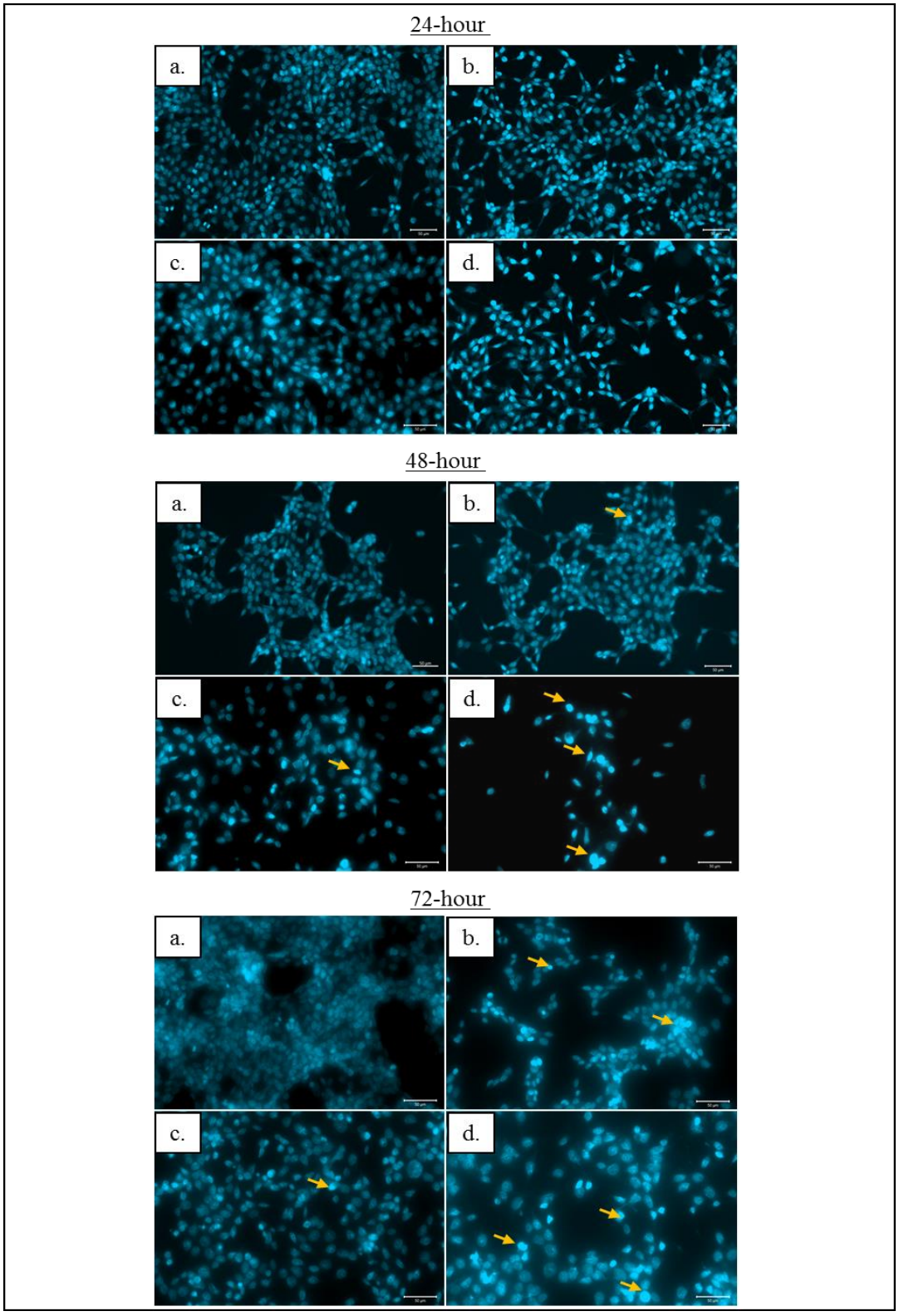

Figure A4.8 Nuclear profiles of SW48 at various time points after receiving treatments of δT3, Dox and the combined treatment. a, vehicle control; b, δT3; c, Dox; d, δT3 + Dox. Yellow arrow, nuclear condensation; white arrow, nuclear fragmentation; Scale bar represents 50μm.

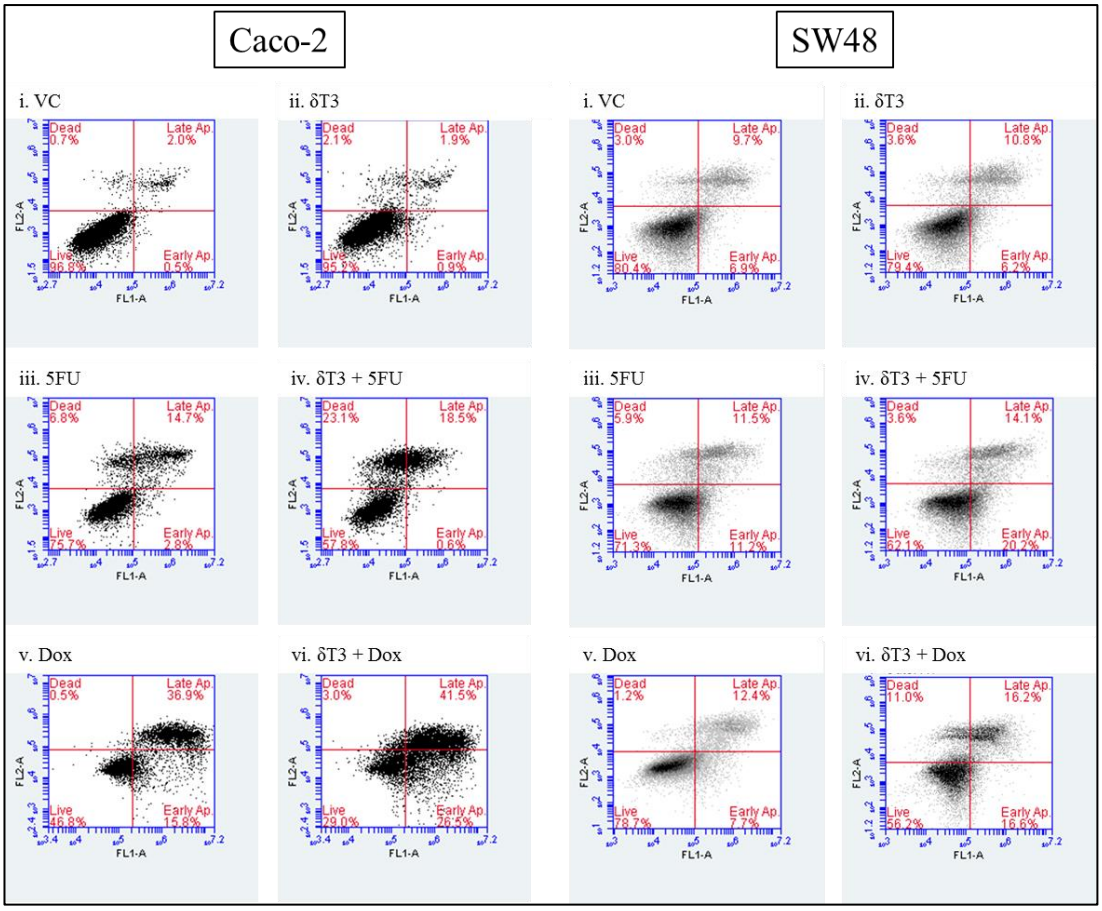

Figure A4.9 Representative dot plots of Annexin V-FITC/PI apoptosis detection assay for Caco-2 and SW48 cells. VC, vehicle control; δT3, δ-tocotrienol; 5FU, 5-fluorouracil; δT3 + 5FU, δ-tocotrienol + 5-fluorouracil; Dox, doxorubicin; δT3 + Dox, δ-tocotrienol + doxorubicin.

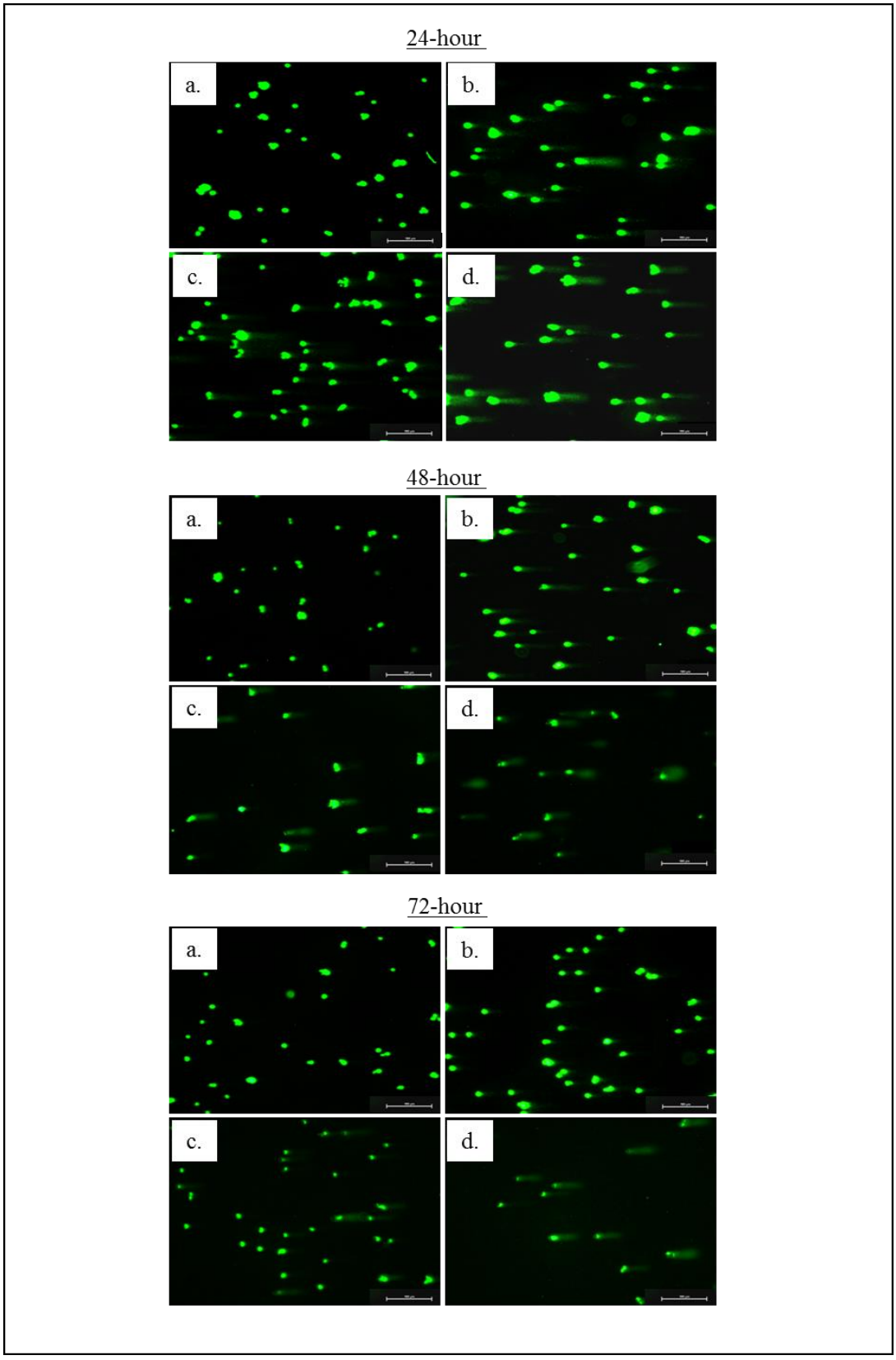

Figure A4.10 Representative alkaline comet profiles of Caco-2 at various time points after receiving treatments of δT3, 5FU and the combined treatment. a, vehicle control; b, δT3; c, 5FU; d, δT3 + 5FU. Scale bar represents 100μm.

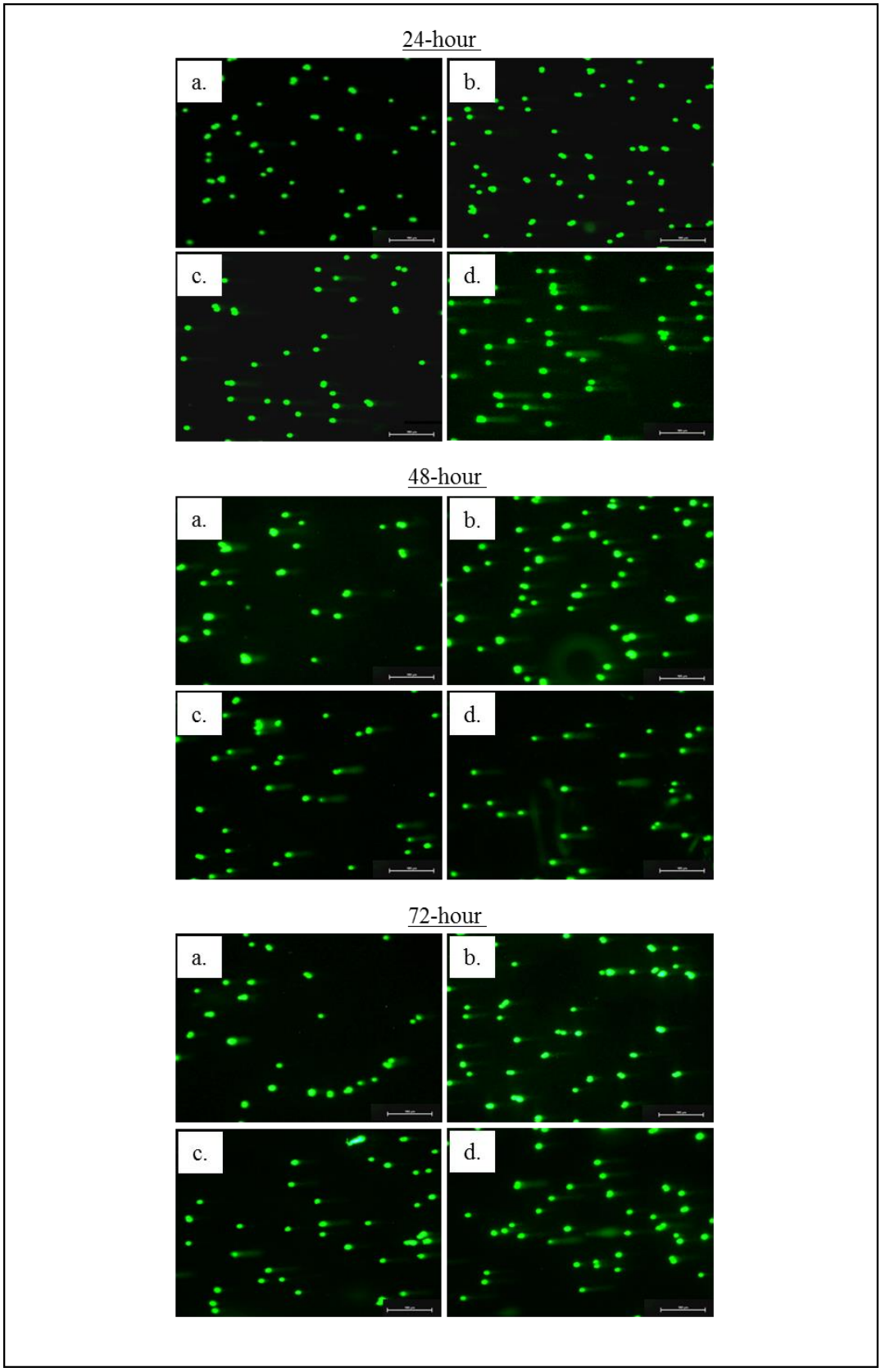

Figure A4.11 Representative alkaline comet profiles of SW48 at various time points after receiving treatments of δT3, 5FU and the combined treatment. a, vehicle control; b, δT3; c, 5FU; d, δT3 + 5FU. Scale bar represents 100μm.

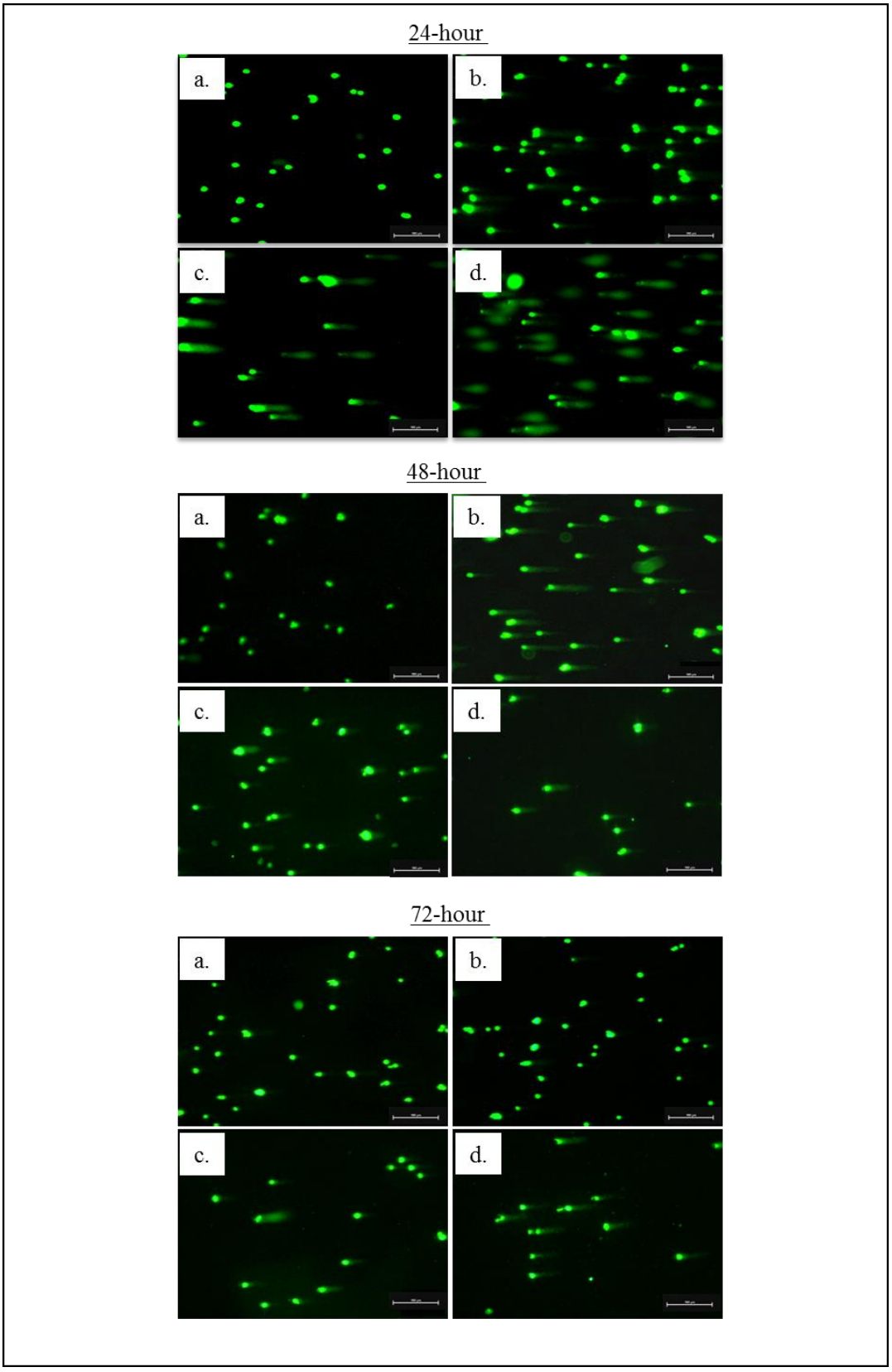

Figure A4.12 Representative alkaline comet profiles of Caco-2 at various time points after receiving treatments of δT3, Dox and the combined treatment. a, vehicle control; b, δT3; c, Dox; d, δT3 + Dox. Scale bar represents 100μm.

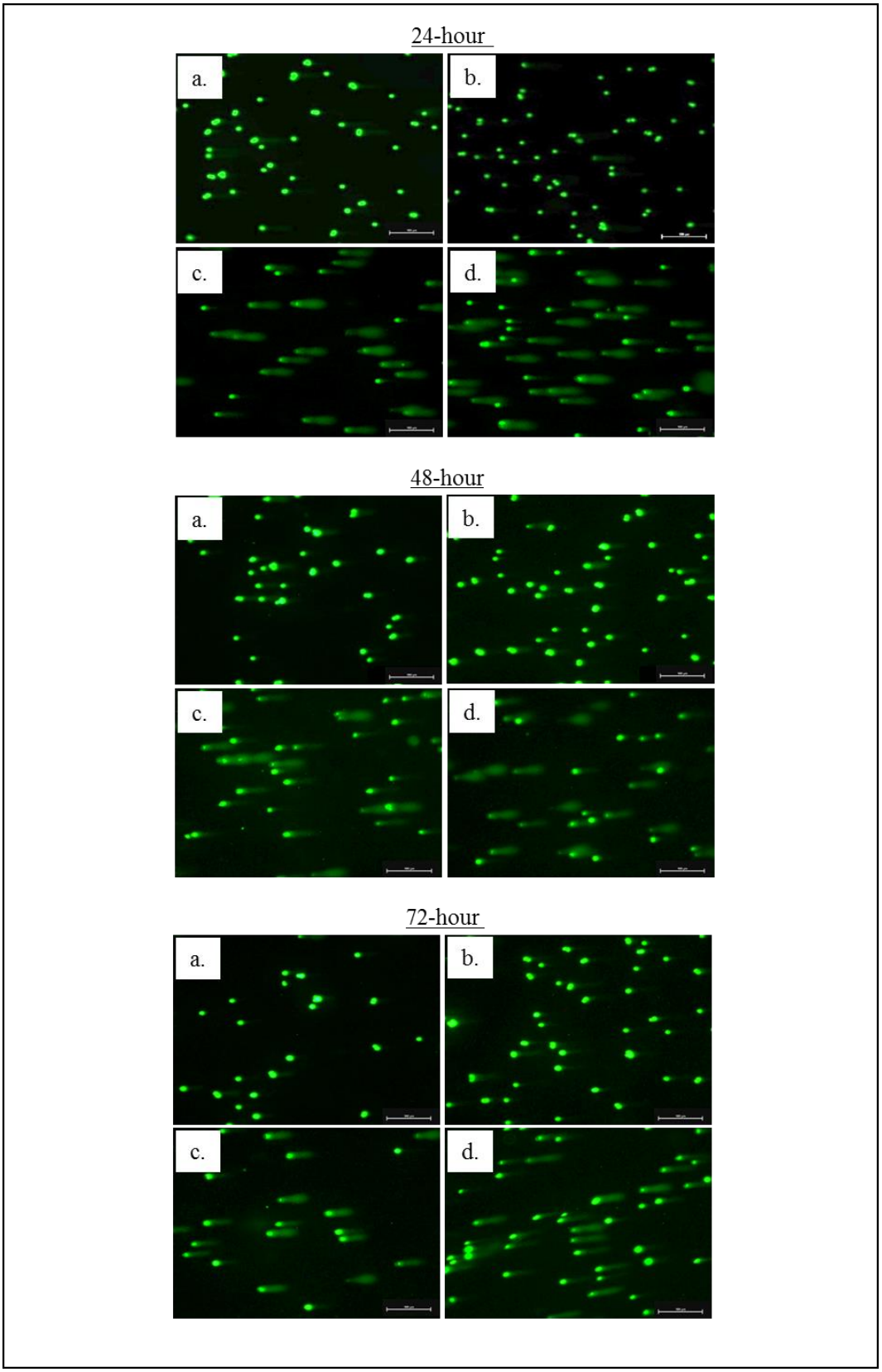

Figure A4.13 Representative alkaline comet profiles of SW48 at various time points after receiving treatments of δT3, Dox and the combined treatment. a, vehicle control; b, δT3; c, Dox; d, δT3 + Dox. Scale bar represents 100μm.

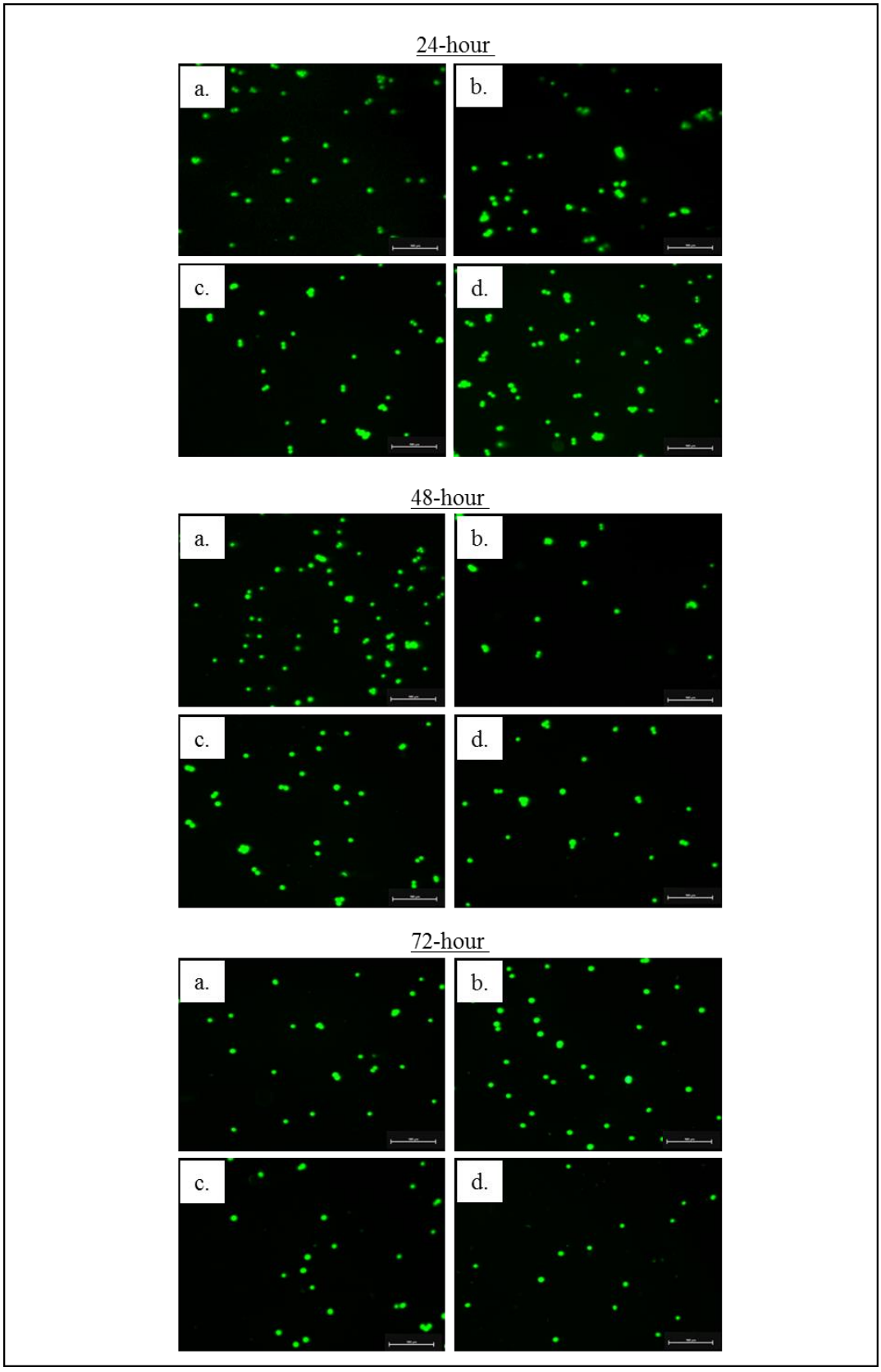

Figure A4.14 Representative neutral comet profiles of Caco-2 at various time points after receiving treatments of δT3, 5FU and the combined treatment. a, vehicle control; b, δT3; c, 5FU; d, δT3 + 5FU. Scale bar represents 100μm.

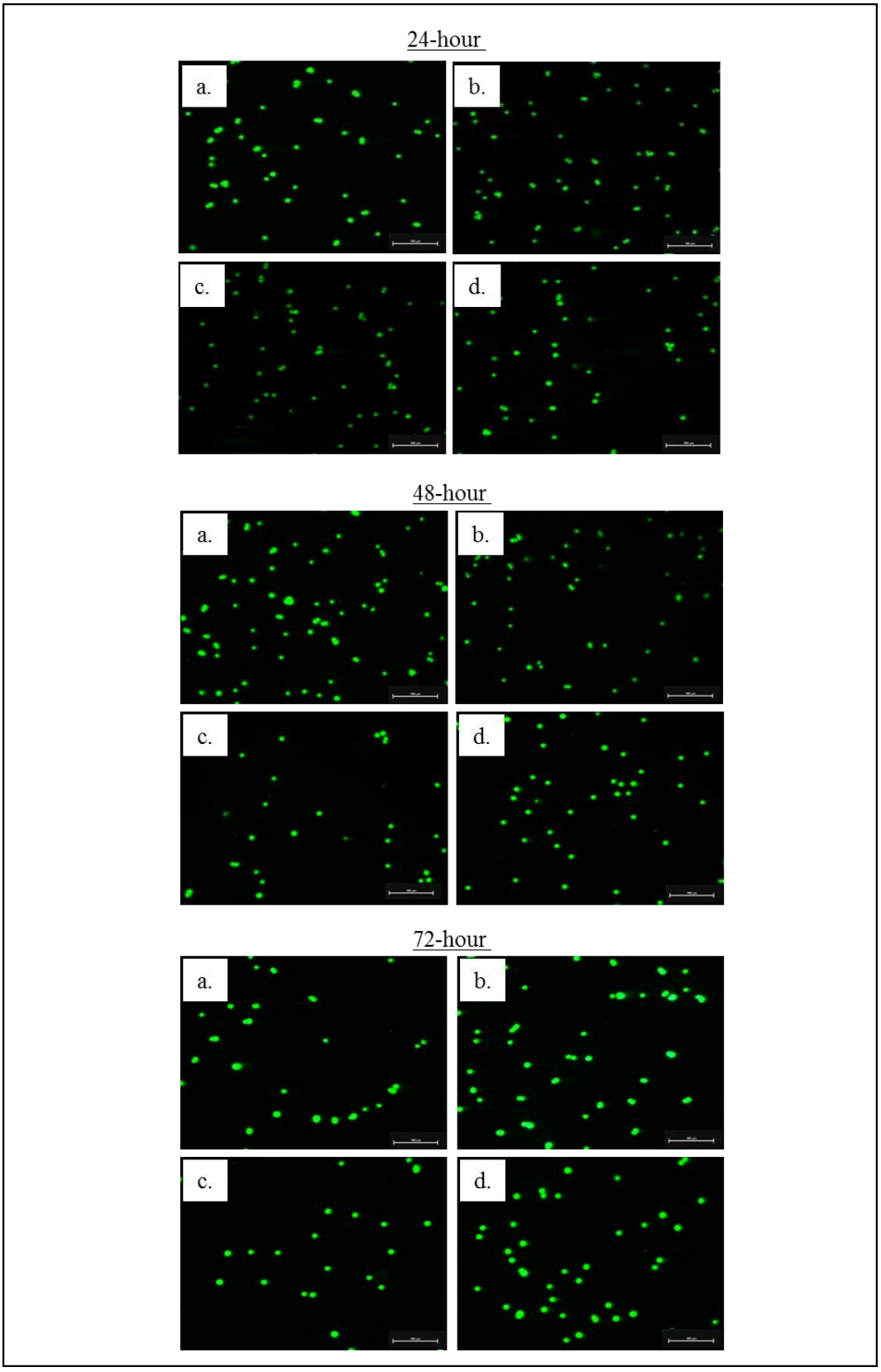

Figure A4.15 Representative neutral comet profiles of SW48 at various time points after receiving treatments of δT3, 5FU and the combined treatment. a, vehicle control; b, δT3; c, 5FU; d, δT3 + 5FU. Scale bar represents 100μm.

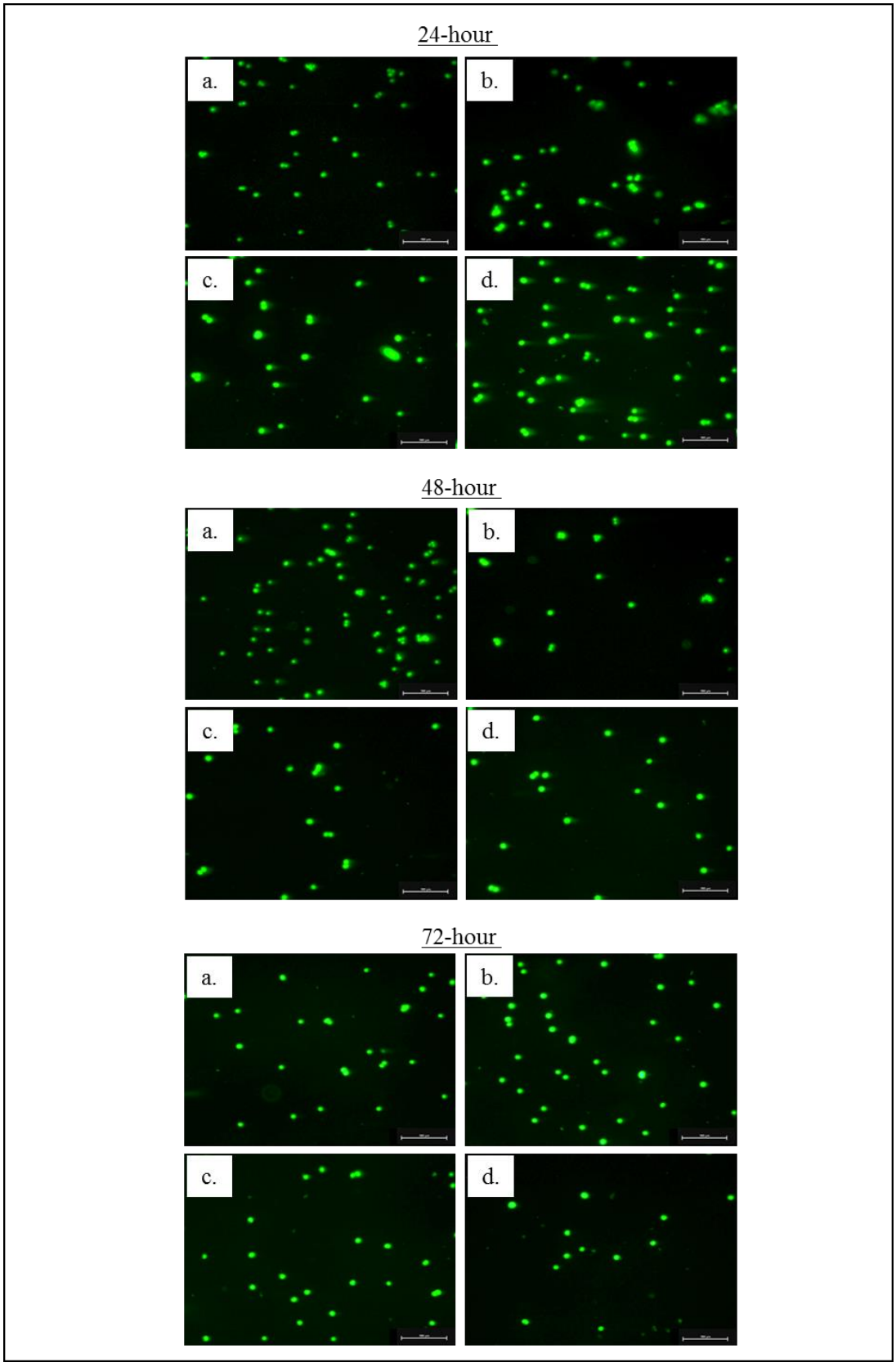

Figure A4.16 Representative neutral comet profiles of Caco-2 at various time points after receiving treatments of δT3, Dox and the combined treatment. a, vehicle control; b, δT3; c, Dox; d, δT3 + Dox. Scale bar represents 100μm.

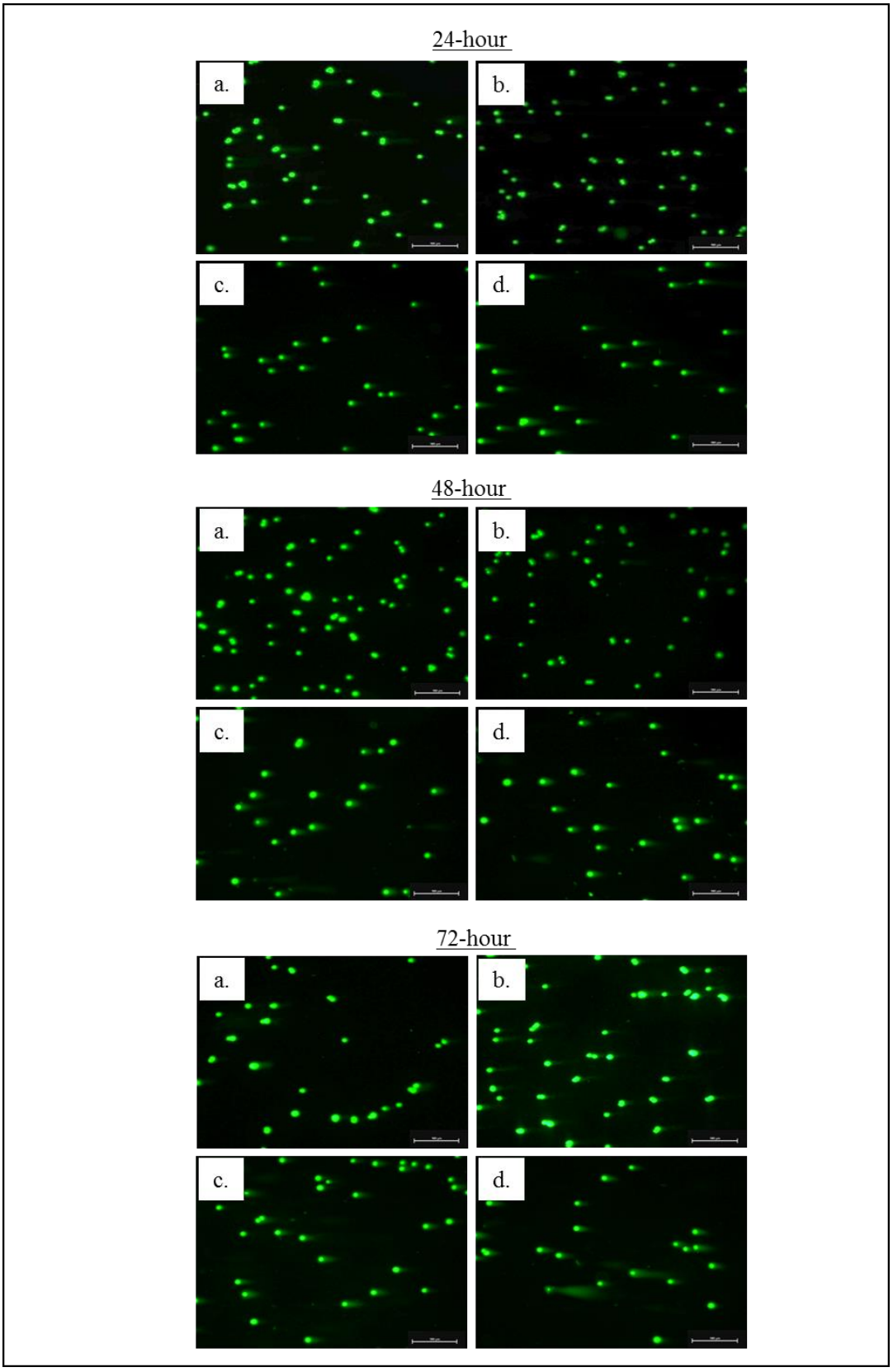

Figure A4.17 Representative neutral comet profiles of SW48 at various time points after receiving treatments of δT3, Dox and the combined treatment. a, vehicle control; b, δT3; c, Dox; d, δT3 + Dox. Scale bar represents 100μm.

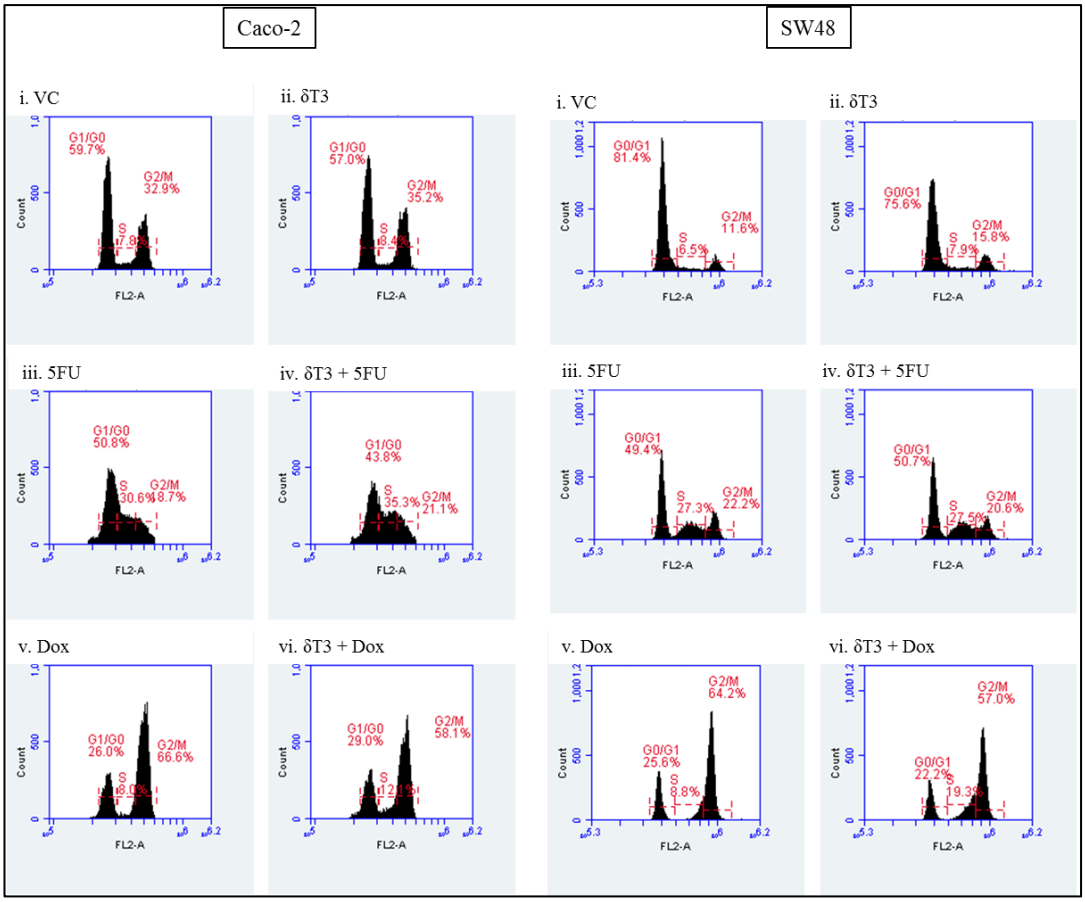

Figure A4.18 Representative DNA histograms illustrating cell cycle profiles of Caco-2 and SW48 cells. VC, vehicle control; δT3, δ-tocotrienol; 5FU, 5-fluorouracil; δT3 + 5FU, δ-tocotrienol + 5-fluorouracil; Dox, doxorubicin; δT3 + Dox, δ-tocotrienol + doxorubicin.

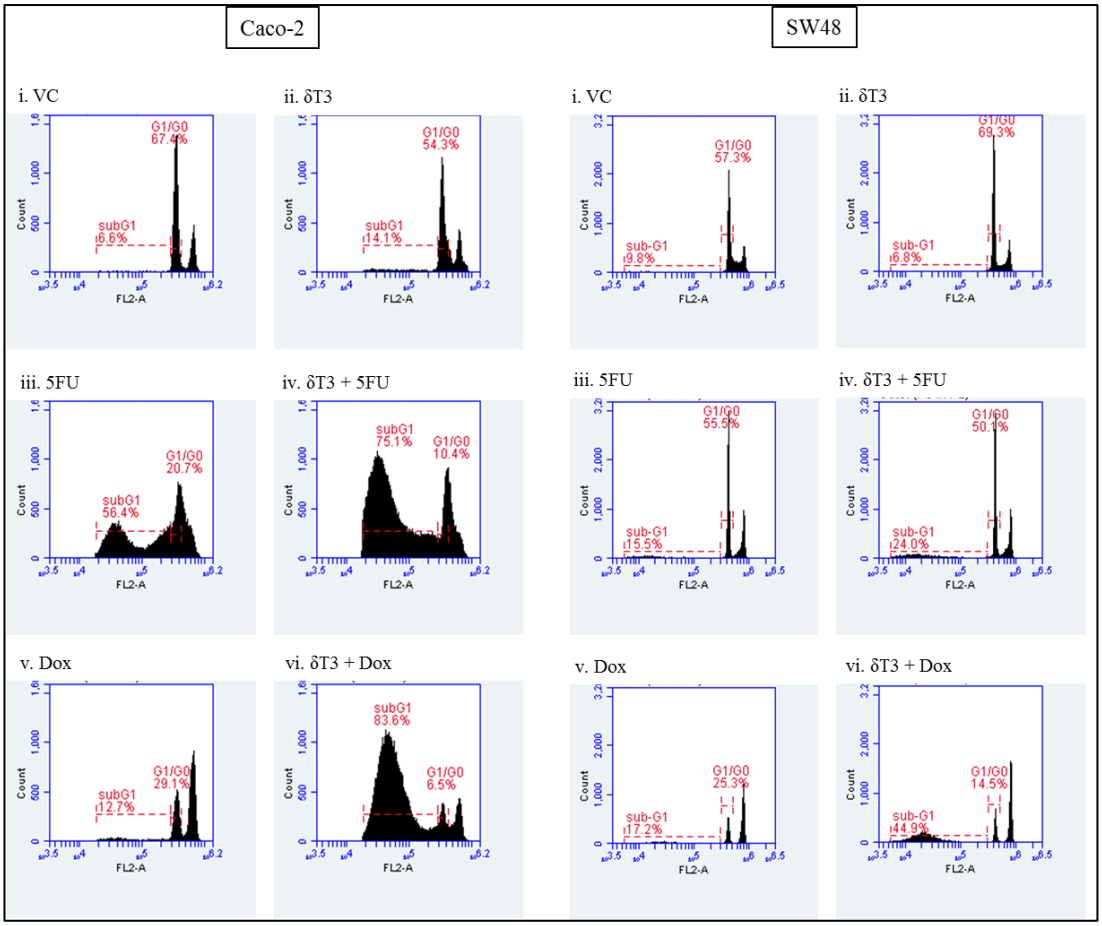

Figure A4.19 Representative DNA histograms illustrating sub-G1 populations of Caco-2 and SW48 cells. VC, vehicle control; δT3, δ-tocotrienol; 5FU, 5-fluorouracil; δT3 + 5FU, δ-tocotrienol + 5-fluorouracil; Dox, doxorubicin; δT3 + Dox, δ-tocotrienol + doxorubicin.

Appendices for Chapter Five (A5)

Table A5.1 Recipe of 6x protein sample buffer.

Reagent	Quantity (for 8ml)
SDS	1.2g
0.5M Tris, pH 6.8	1.2ml
Glycerol	4.7ml
Bromophenol blue	6mg
DTT	0.93g
dH_2O	Adjusted to 8ml

Note: SDS binds to hydrophobic regions of the protein to unfold and gives it a negative charge. DTT breaks disulfide bonds and destroys residual secondary structures. Addition of glycerol is aimed to ensure protein samples to be remained in the gel wells after loading. SDS, sodium dodecyl sulphate; DTT, dithiothreitol.

Table A5.2 Recipe of 10x SDS-PAGE running buffer.

Reagent	Quantity	Final concentration in 1x
Tris base	30g	25mM
Glycine	144g	192mM
Sodium Dodecyl Sulphate (SDS)	10g	0.1% (w/v)
dH_2O	Top up to 1 L	-

Note: ddH_2O denotes distilled water. Running buffer is stored at room temperature and diluted to 1x with ddH_2O before use. ddH_2O, distilled water.

Table A5.3 Recipe of 10x transfer buffer.

Reagent	Quantity	Final concentration in 1x
Tris base	58.2g	48mM
Glycine	29.3g	39mM
dH_2O	Top up to 1 L	-

Note: Running buffer is stored at room temperature. The running buffer is diluted to 1x with ddH_2O containing 20% (v/v) methanol before use. ddH_2O, distilled water.

Table A5.4 Recipe of a 4-12% gradient gel.

Reagent	4% stacking gel	12% separating gel
	Quantity	Quantity
dH_2O	3.15ml	3.45ml
40% acrylamide	0.5ml	2.4ml
0.5M Tris, pH 6.8	1.25ml	-
1.5M Tris, pH8.8	-	2ml
10% SDS (w/v)	50µl	80µl
10% APS (w/v)	50µl	80µl
TEMED	5µl	8µl

Note: This volume is calculated based upon Mini-PROTEAN® Tetra Handcast Systems of 1.5mm thickness. ddH_2O, distilled water; APS, Ammonium persulfate; TEMED, Tetramethylethylenediamine.

Table A5.5 Recipe of PBST buffer.

Reagent	Quantity
Sodium chloride (NaCl)	8g
Potassium chloride (KCl)	0.2g
Disodium hydrogen phosphate (Na_2HPO_4)	1.44g
Potassium dihydrogen phosphate (KH_2PO_4)	0.24g
dH_2O	1L
0.05% Tween-20 (v/v)	0.5ml

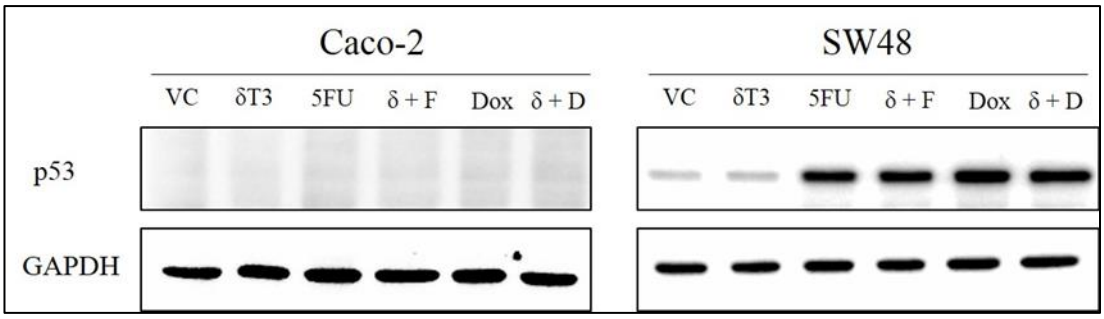

Figure A5.1 p53 expression profiles of Caco-2 and SW48 cells. Note: VC, vehicle control; δT3, δ-tocotrienol; 5FU, 5-fluorouracil; δ + F, δ-tocotrienol + 5-fluorouracil; Dox, doxorubicin; δ + D, δ-tocotrienol + doxorubicin.

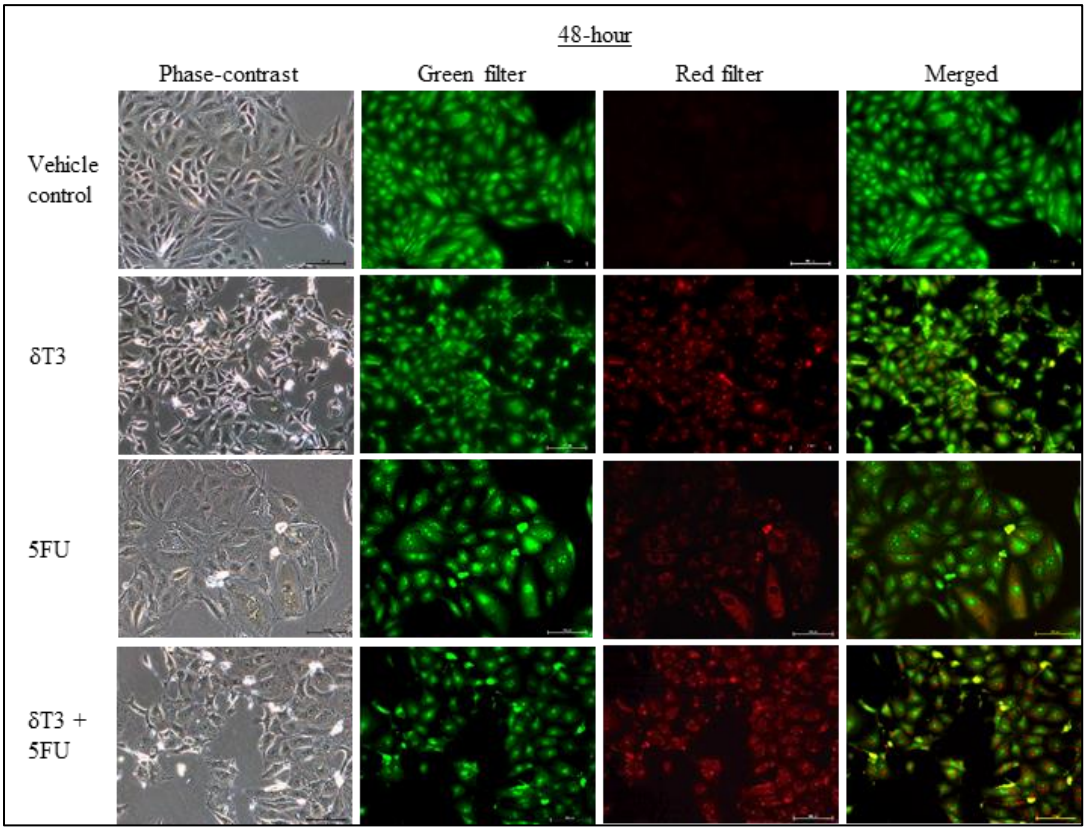

Figure A6.1 Representative AO-stained Caco-2 cells treated for 48 hours with the individual single δT3 or 5FU and the combined treatment. Vehicle control containing 0.1% of DMSO served as negative control. δT3, δ-tocotrienol; 5FU, 5-fluorouracil; δT3 + 5FU, δ-tocotrienol + 5-fluorouracil.

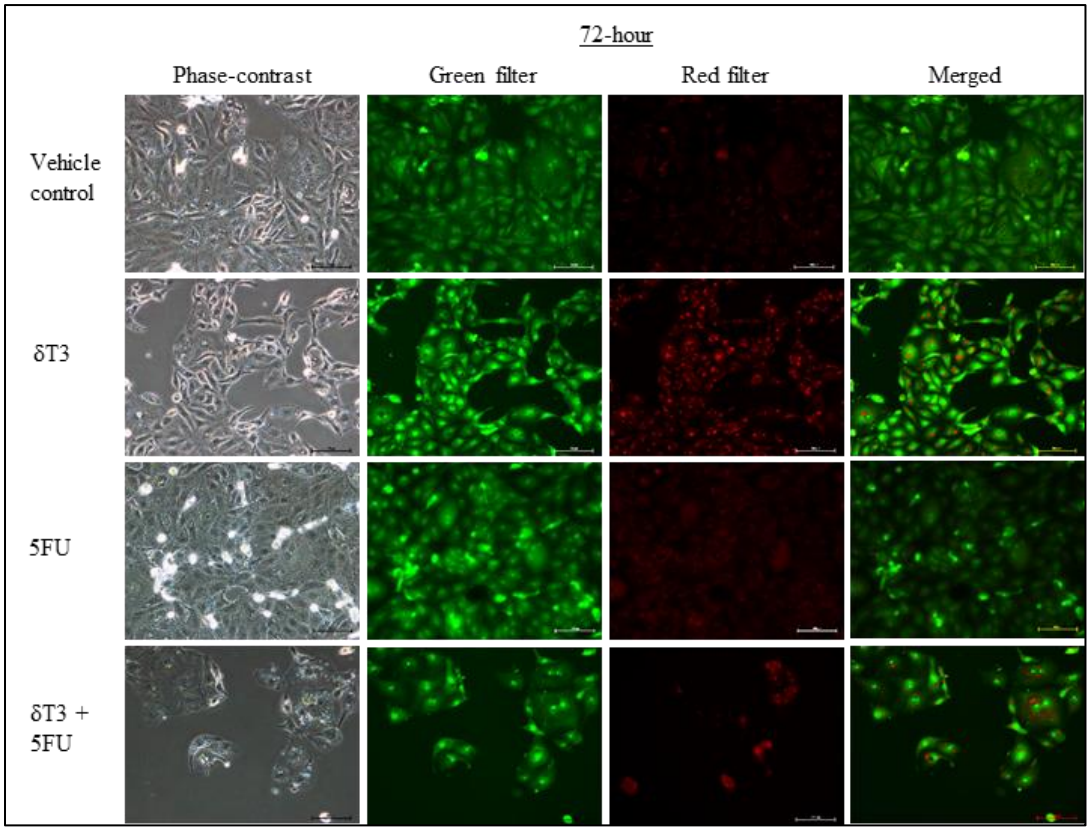

Figure A6.2 Representative AO-stained Caco-2 cells treated for 72 hours with the individual single δT3 or 5FU and the combined treatment. Vehicle control containing 0.1% of DMSO served as negative control. δT3, δ-tocotrienol; 5FU, 5-fluorouracil; δT3 + 5FU, δ-tocotrienol + 5-fluorouracil.

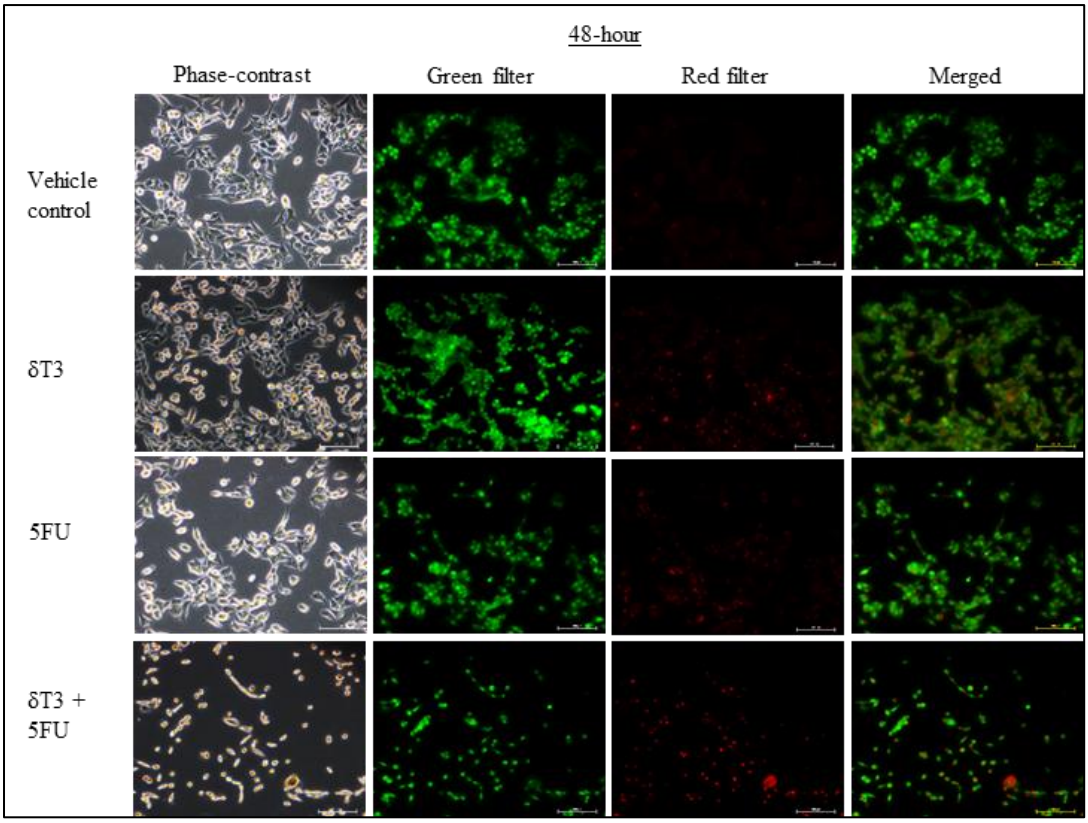

Figure A6.3 Representative AO-stained SW48 cells treated for 48 hours with the individual single δT3 or 5FU and the combined treatment. Vehicle control containing 0.1% of DMSO served as negative control. δT3, δ-tocotrienol; 5FU, 5-fluorouracil; δT3 + 5FU, δ-tocotrienol + 5-fluorouracil.

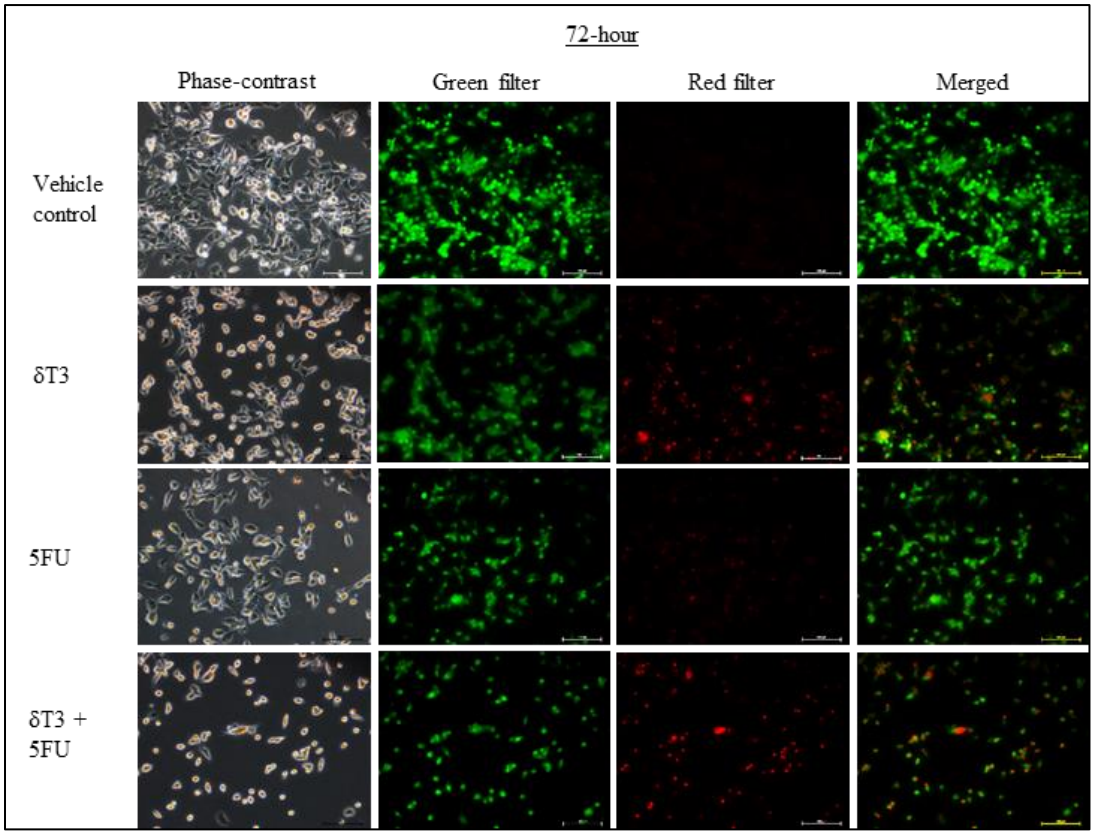

Figure A6.4 Representative AO-stained SW48 cells treated for 72 hours with the individual single δT3 or 5FU and the combined treatment. Vehicle control containing 0.1% of DMSO served as negative control. δT3, δ-tocotrienol; 5FU, 5-fluorouracil; δT3 + 5FU, δ-tocotrienol + 5-fluorouracil.

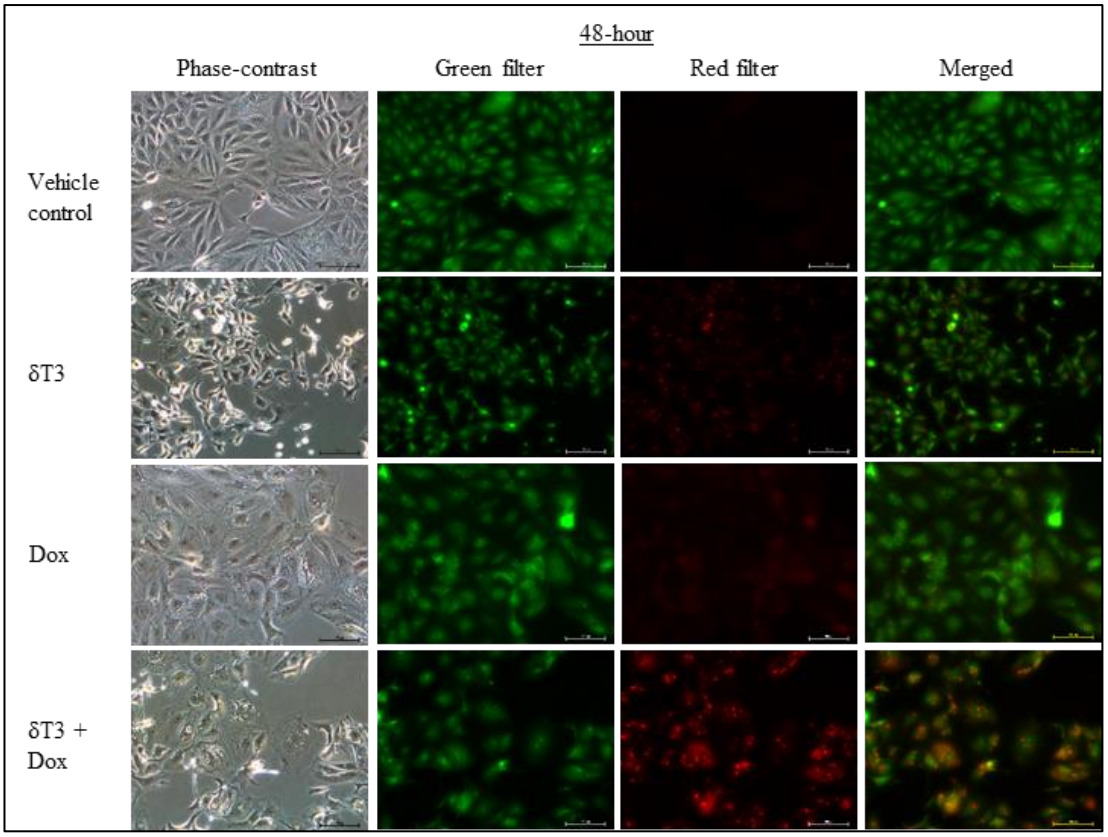

Figure A6.5 Representative AO-stained Caco-2 cells treated for 48 hours with the individual single δT3 or Dox and the combined treatment. Vehicle control containing 0.1% of DMSO served as negative control. δT3, δ-tocotrienol; Dox, doxorubicin; δT3 + Dox, δ-tocotrienol + doxorubicin.

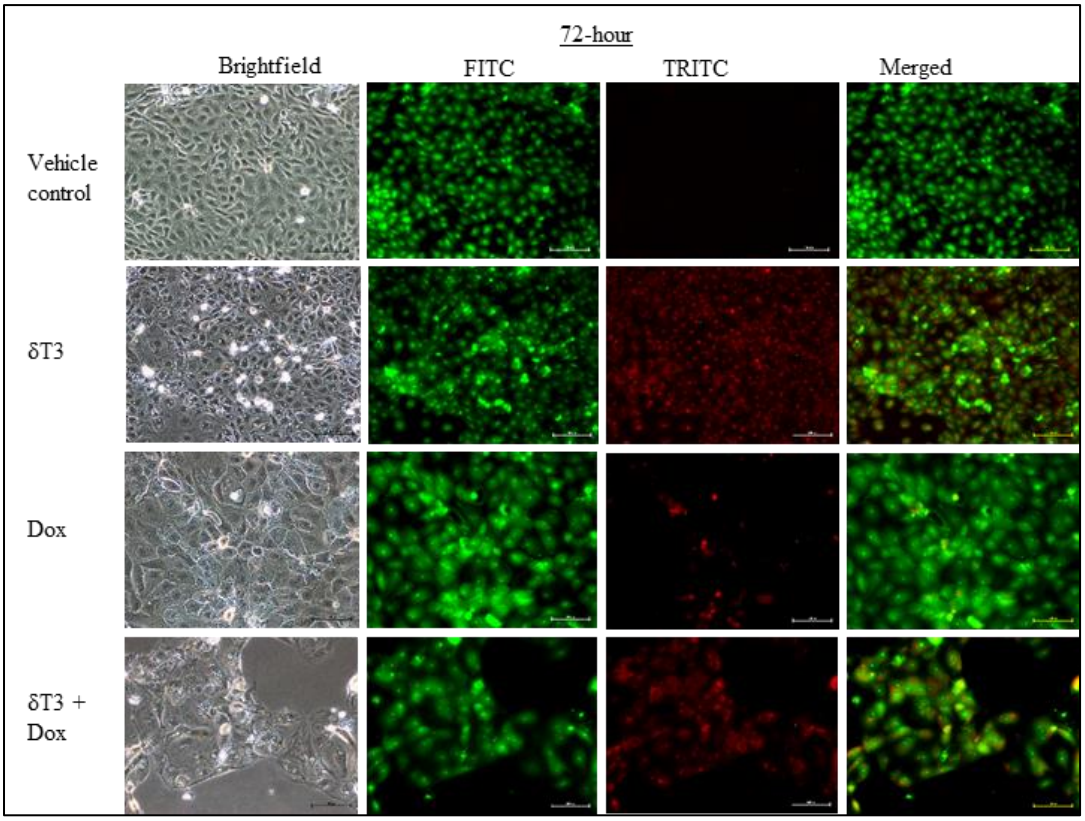

Figure A6.6 Representative AO-stained Caco-2 cells treated for 72 hours with the individual single δT3 or Dox and the combined treatment. Vehicle control containing 0.1% of DMSO served as negative control. δT3, δ-tocotrienol; Dox, doxorubicin; δT3 + Dox, δ-tocotrienol + doxorubicin.

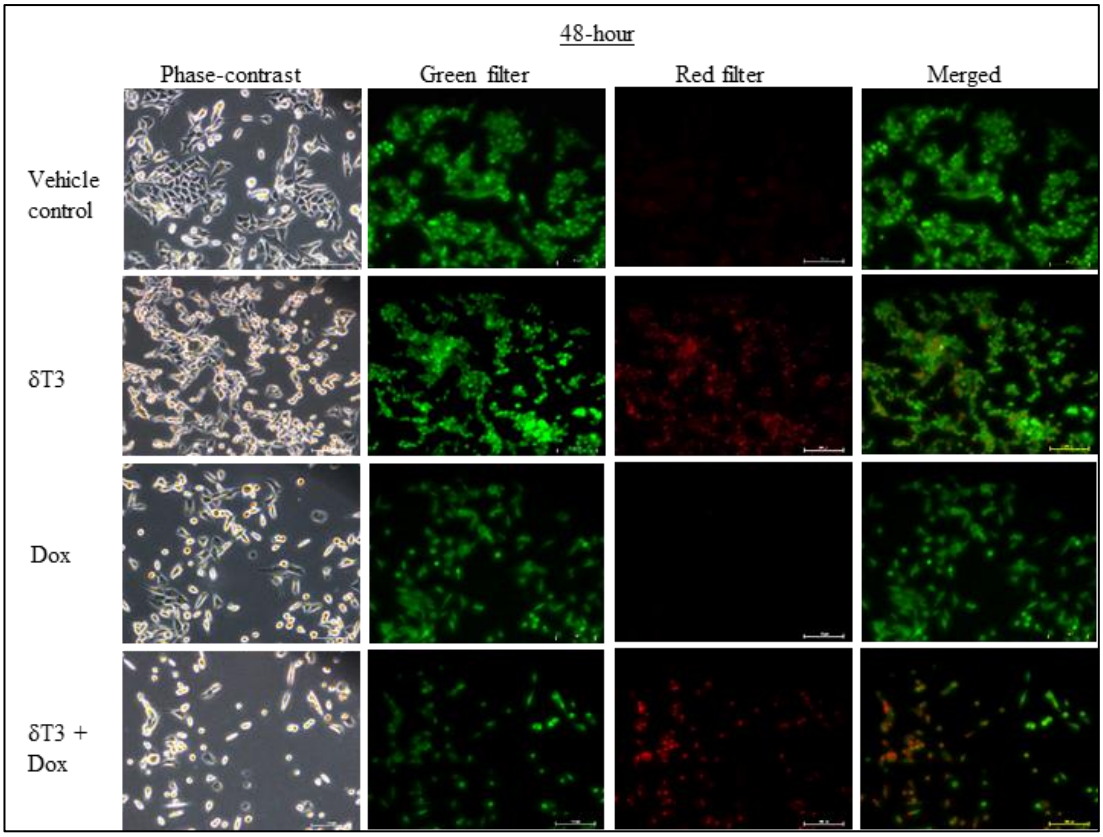

Figure A6.7 Representative AO-stained SW48 cells treated for 48 hours with the individual single δT3 or Dox and the combined treatment. Vehicle control containing 0.1% of DMSO served as negative control. δT3, δ-tocotrienol; Dox, doxorubicin; δT3 + Dox, δ-tocotrienol + doxorubicin.

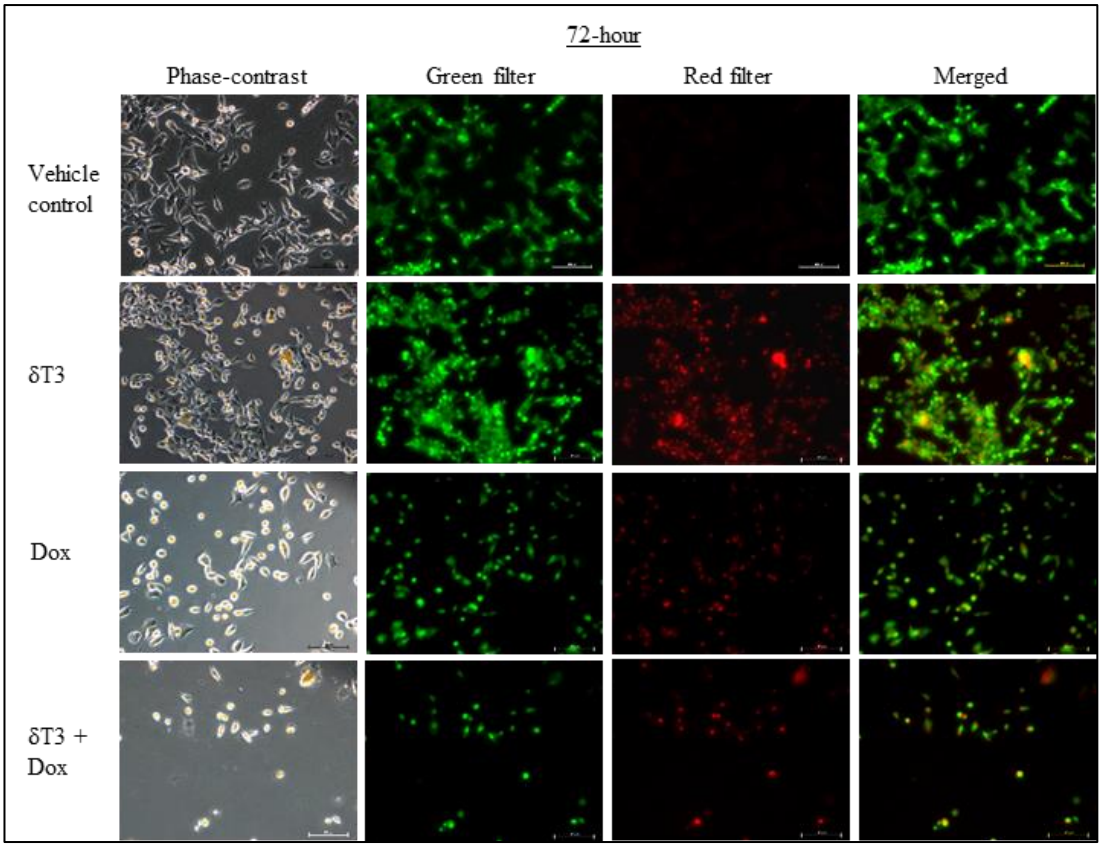

Figure A6.8 Representative AO-stained SW48 cells treated for 72 hours with the individual single δT3 or Dox and the combined treatment. Vehicle control containing 0.1% of DMSO served as negative control. δT3, δ-tocotrienol; Dox, doxorubicin; δT3 + Dox, δ-tocotrienol + doxorubicin.

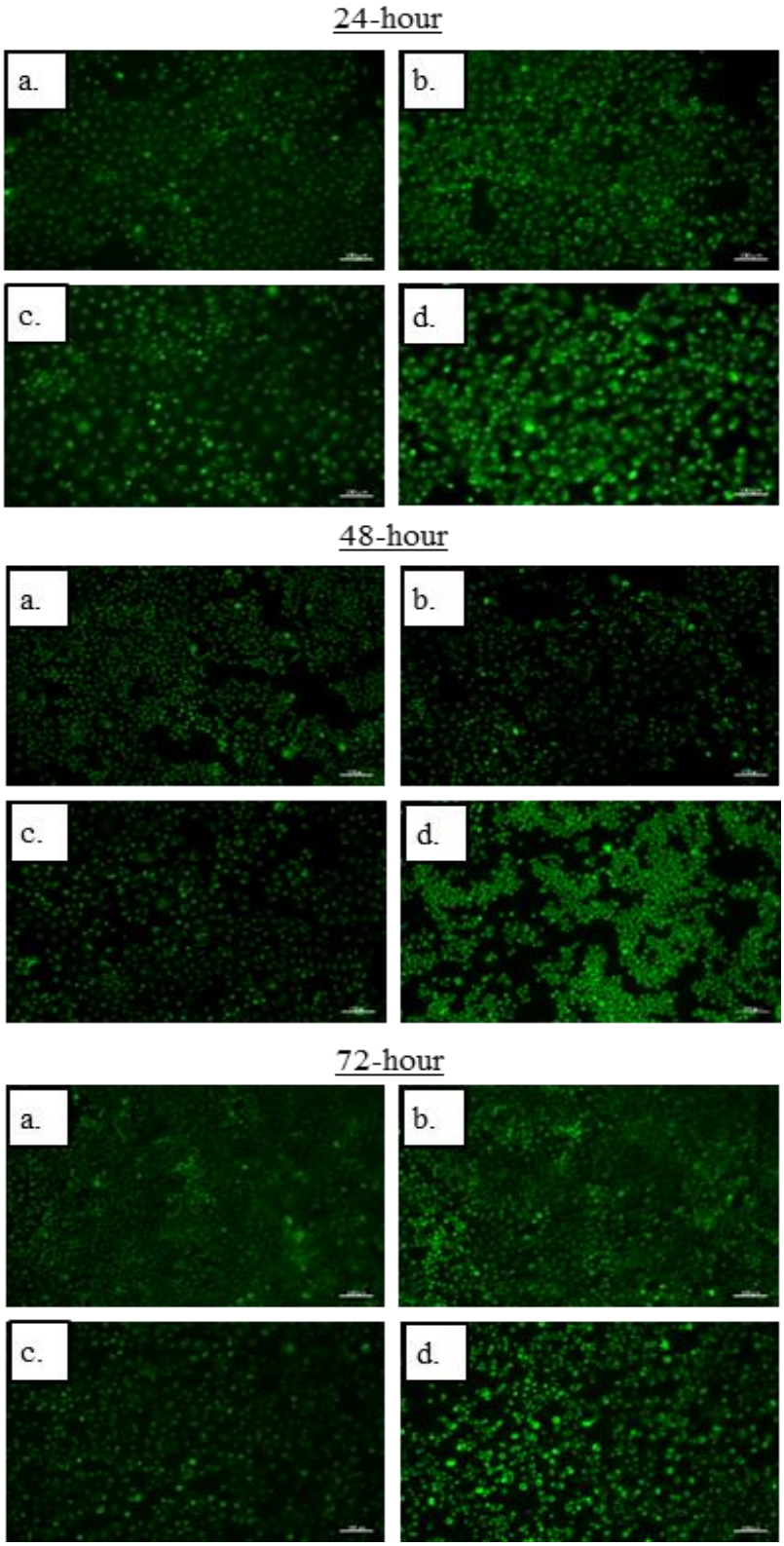

Figure A6.9 Representative MDC profiles of Caco-2 cells at various time points after receiving treatments of δT3, 5FU and the combined treatment. a, vehicle control; b, δT3; c, 5FU; d, δT3 + 5FU.

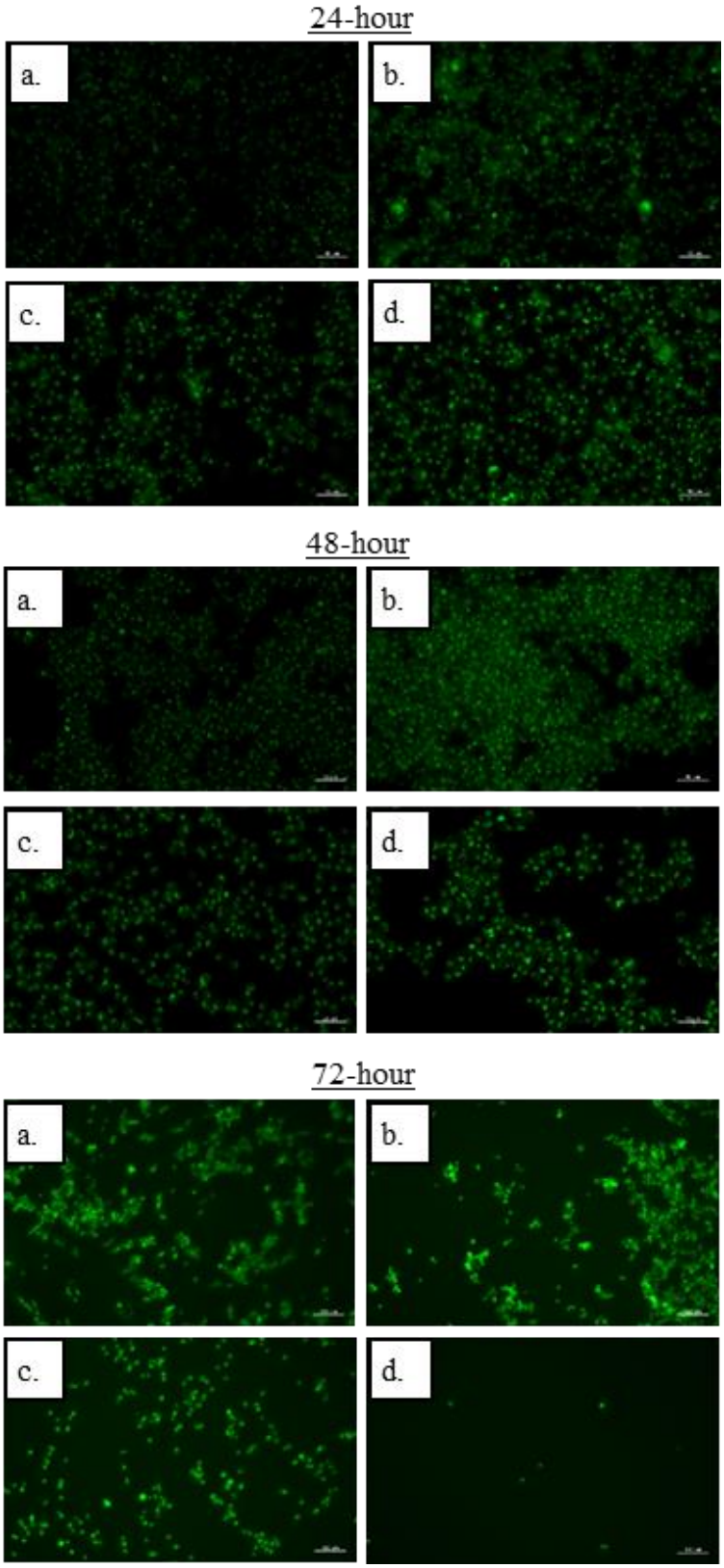

Figure A6.10 Representative MDC profiles of SW48 cells at various time points after receiving treatments of δT3, 5FU and the combined treatment. a, vehicle control; b, δT3; c, 5FU; d, δT3 + 5FU.

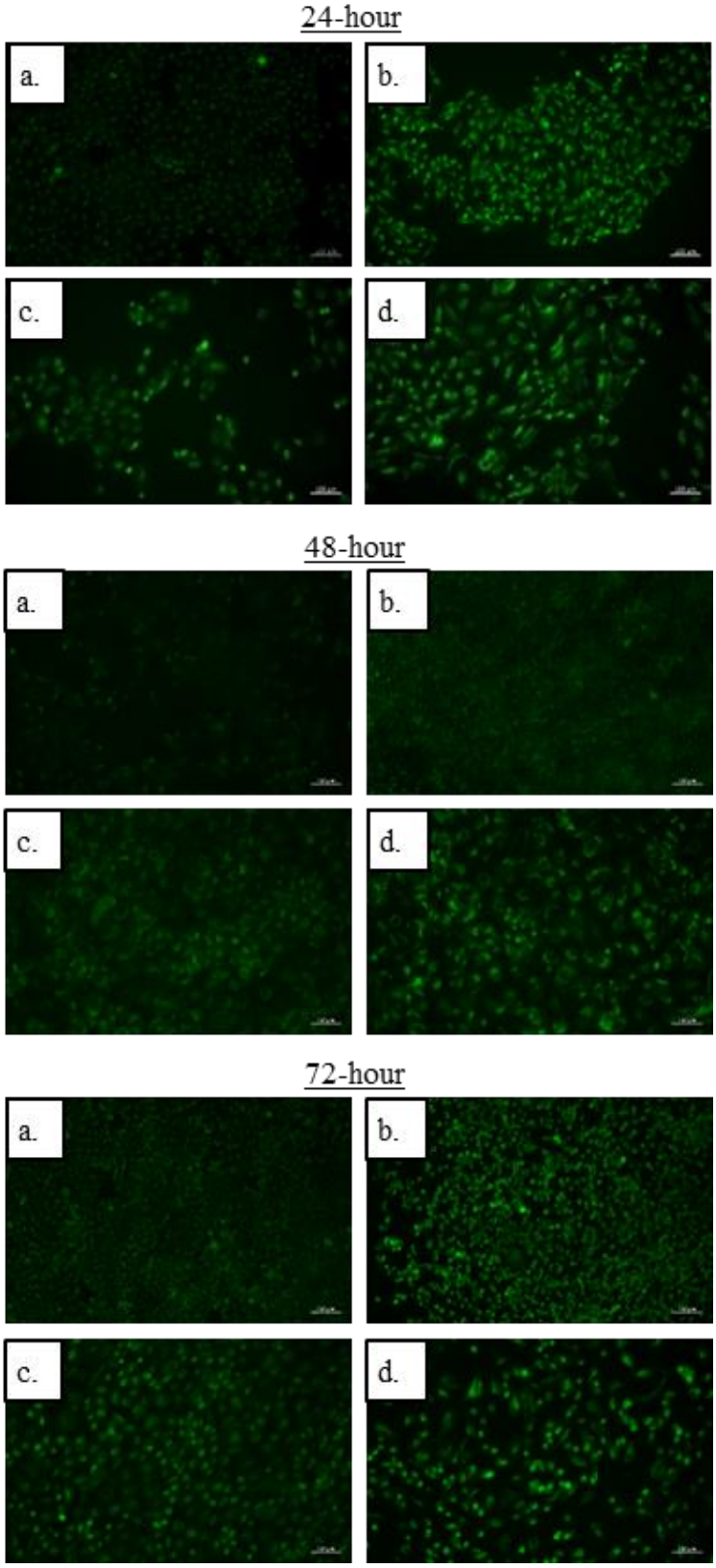

Figure A6.11 Representative MDC profiles of Caco-2 cells at various time points after receiving treatments of δT3, Dox and the combined treatment. a, vehicle control; b, δT3; c, Dox; d, δT3 + Dox.

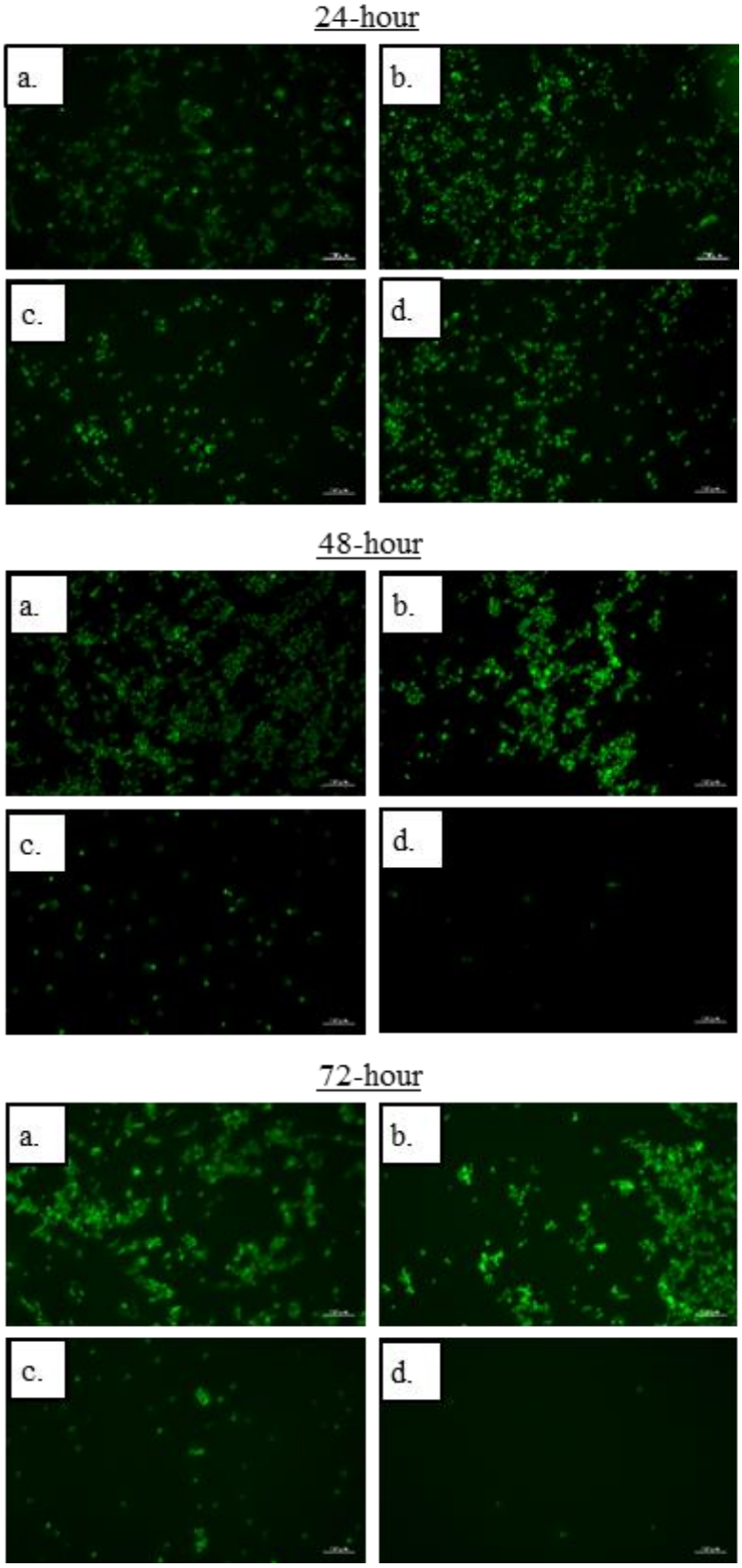

Figure A6.12 Representative MDC profiles of SW48 cells at various time points after receiving treatments of δT3, Dox and the combined treatment a, vehicle control; b, δT3; c, Dox; d, δT3 + Dox.

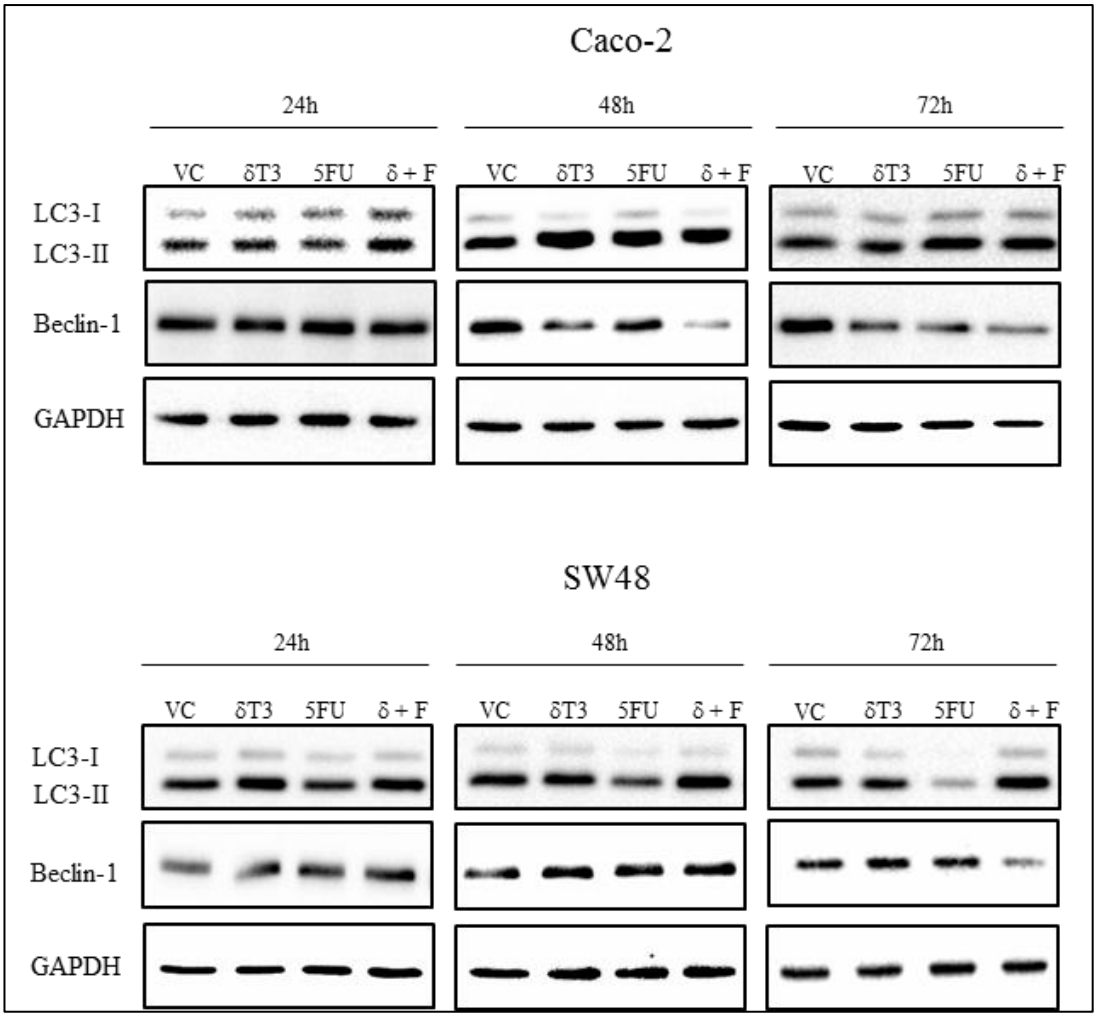

Figure A6.13 Representative Western blotting profiles of LC3-I/II and beclin-1 for Caco-2 and SW48 at 24-72 hours after receiving the δT3 and/or 5FU treatments. VC, vehicle control; δT3, δ-tocotrienol; 5FU, 5-fluorouracil; δ + F, δ-tocotrienol + 5-fluorouracil.

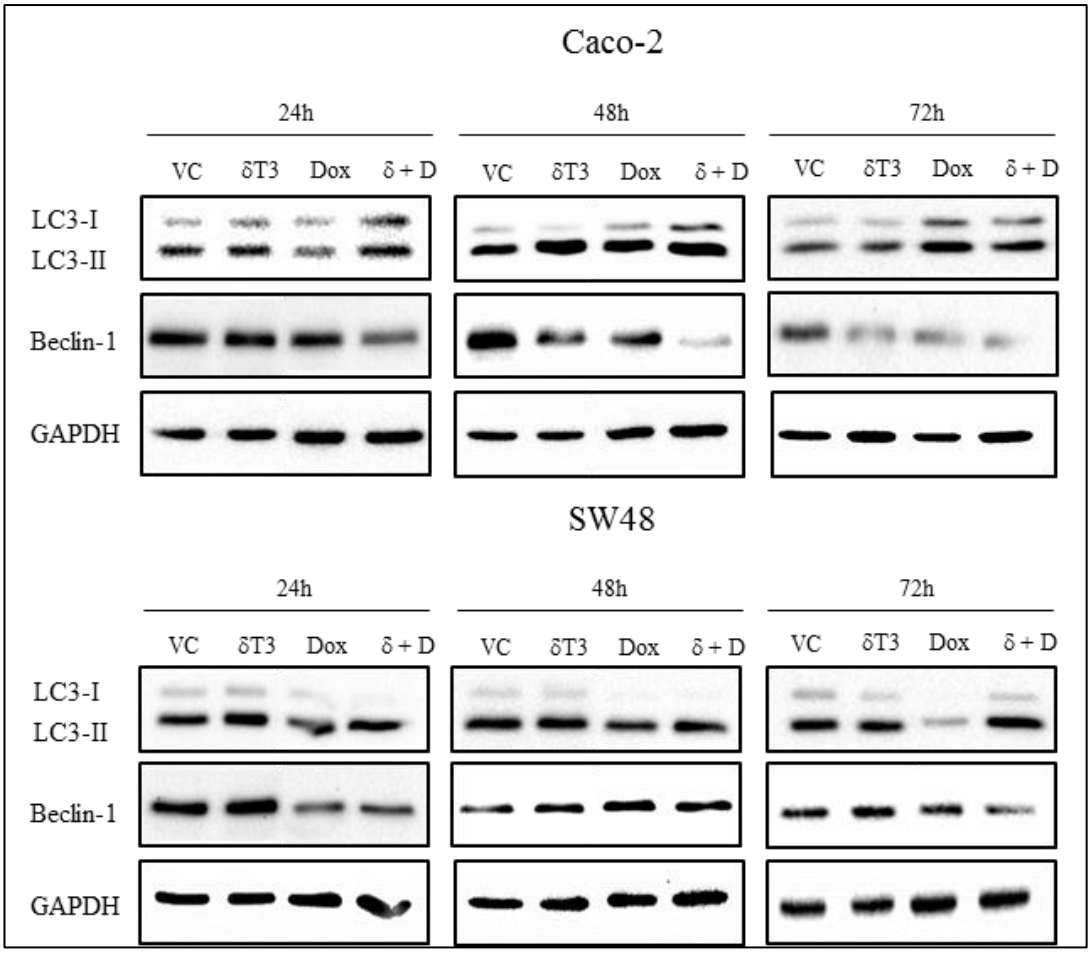

Figure A6.14 Representative Western blotting profiles of LC3-I/II and beclin-1 for Caco-2 and SW48 at 24-72 hours after receiving the δT3 and/or Dox treatments. VC, vehicle control; δT3, δ-tocotrienol; Dox, doxorubicin; δ + D, δ-tocotrienol + doxorubicin

www.impactjournals.com/oncotarget/ Oncotarget, Supplementary Materials 2016

Supplementary Table S2: The Broder's grade and Duke's classification of the original tumors and TES levels of the CRC cell lines

Cell line	Duke's stage	Broder's grade	Differentiation of xenograft	Histological grades
HCT116	ND	III/IV	Poor	High-grade
Caco-2	ND	II	Moderate	Low-grade
HT-29	ND	I	Moderately well	Low-grade
SW48	C	IV	Poor	High-grade
SW480	B	IV	Poor	High-grade
SW620	C	IV	Poor	High-grade
DLD-1	C	III/IV	Poor	High-grade
LoVo	C	IV	Poor/ Moderate	High-grade
RKO	ND	III/IV	Poor	High-grade

ND: not determined

Figure A7.1 Information of Caco-2 and SW48 colorectal cancer cell lines used in the current study. Adapted from the supplementary data of a published article (Li et al., 2016).

Biography

Ms. Tham Shiau Ying graduated from University of Nottingham Malaysia Campus with a first-class honours in Plant Biotechnology in 2013 by virtue of a full scholarship awarded by Public Service Department Malaysia (JPA). She excelled in her undergraduate study in which her diligence earned her the Syngenta Plant Science Prize for scoring the highest aggregates in second year. Winning the 'Top Ten Best Poster Award' in the 24th Intervarsity Biochemistry Seminar where she presented her final year project to a scientific community for the first time was an early indication of her scientific aptitude.

Her interest in cancer research has stemmed from her final year project (FYP) in which she studied Apoptin (an anti-cancer cancer candidate) and concurrently inspired by her supervisor, Prof. Dr Sandy Loh Hwei San. In 2014, she was given the opportunity to work under Dr Jeff Tan Kuan Onn as a research assistant in Sunway University to study modulator in apoptosis 1 (MOAP-1), which had further expanded her knowledge in cancer especially in apoptosis. Having been awarded the MyPhD scholarship by Ministry of Higher Education, she joined her alma mater as a PhD student under the supervision of Prof. Sandy a year later. She is optimistic that her project to employ tocotrienols in the combined treatment approach can help to solve some of the problems challenging chemotherapy. Her great interest in tocotrienols and cancer had led her to publish her first peer-reviewed article entitled "Tocotrienols Modulate a Life or Death Decision in Cancers".

As a PhD student, Shiau Ying took active participations in technical workshops, academic trainings, poster/grant competitions as well as local & international conferences during her four-year study. She again displayed her academic excellence in various academic categories that she participated and was duly awarded for her

achievements which included research grant, poster, travel and best paper awards. In 2016, Shiau Ying won the 'Most Recommended Paper for Oral Presentation' Award from International Conference of Translational Molecular Imaging & Aero-space Medicine & Physiology Showcase (iCT-MIPs 16) where she was honoured to present her work at the plenary session of the conference. In the same year, she was awarded with Cancer Research Priority Area (RPA) travel fund for a research visit to UK campus in order to seek for technical inputs and initiate research collaboration. In 2017, Shiau Ying was honoured to receive a Science & Technology Research Grant from Malaysia Toray Science Foundation that worth RM 20,000 through a highly competitive selection process. Shiau Ying was also the receiver of two awards, namely 'Best Poster Award' and 'Overall Winner Award' in Research Showcase 2017 organised by Graduate School as well as the runner-up in Faculty of Science Postgraduate Research Student Conference Support Poster Competition. In 2018, Shiau Ying won a Meeting Bursary Award from European Association for Cancer Research to attend 'A Matter of Life of Death' Conference in Amsterdam, Netherlands. In the same year, she stood out as one of the three PhD candidates to receive the Best Postgraduate Prize awarded by the university. All of the accolades cement her reputation as an adept researcher in her early scientific journey.

List of Publications and Presentations

i. Tham, S.-Y., Loh, H.-S., Mai, C.-W. and Fu, J.-Y., 2019. Tocotrienols modulate a life or death decision in cancers. *International Journal of Molecular Sciences* 20 (2), 372; https://doi.org/10.3390/ijms20020372

ii. Tham, S.-Y., Mai, C.-W., Fu, J.-Y. and Loh, H.-S., 2018. Combined treatment of 5-fluorouracil and delta-tocotrienol induces apoptosis and autophagy in colorectal cancer cells. In: World Cancer Congress 2018. Kuala Lumpur, Malaysia. *Journal Of Global Oncology* , No. 4_Suppl_2

iii. Tham, S.-Y., Mai, C.-W., Fu, J.-Y. and Loh, H.-S., 2018. Cell death enhancement and chemosensitisation effect of 5-fluorouracil in colorectal cancer cells via the combination with delta-tocotrienol. In: A Matter of Life or Death 2018: From Basic Cell Death Mechanisms to Novel Cancer Treatments [European Association for Cancer Research (EACR) conference series]. Amsterdam, Netherlands.

iv. Tham, S.-Y., Mai, C.-W., Fu, J.-Y. and Loh, H.-S., 2017. δ-Tocotrienol enhances cell death in colorectal cancer cells via modulation of chemosensitivity towards 5-fluorouracil. In: The 1st FOS PGR Student Research Showcase. Selangor, Malaysia.

v. Tham, S.-Y., Mai, C.-W., Fu, J.-Y. and Loh, H.-S., 2017. Beyond the magic bullet: Multitargeted novel drugs cocktails. In: UNMC Research Showcase 2017. Selangor, Malaysia.

vi. Tham, S.-Y., Fu, J.-Y., Mai, C.-W. and Loh, H.-S., 2016. High-throughput screening of prospective combinations of tocotrienols and chemotherapeutic drugs on cancer cells. In: International Conference of Translational Molecular Imaging & Aeorospace Medicine & Physiology (iCT-MIPs 2016). Sepang, Malaysia.